

University of Trento
University of Brescia
University of Padova
University of Trieste
University of Udine
University IUAV of Venezia

JUNQING XUE

RETROFIT OF EXISTING BRIDGES WITH CONCEPT OF INTEGRAL ABUTMENT BRIDGE

– Static and Dynamic Parametric Analyses

Advisor:

Prof. Enzo Siviero
Università IUAV di Venezia, Venice, Italy

Co-Advisors:

Prof. Bruno Briseghella, Prof. Baochun Chen
Fuzhou University, Fuzhou, China
Prof. Tobia Zordan
Tongji University, Shanghai, China

2013

UNIVERSITY OF TRENTO

Engineering of Civil and Mechanical Structural Systems

Ph.D. Head: Prof. Davide Bigoni

15 / April / 2013

Board of Examiners

Prof.ssa Maria Paola Gatti	(Università degli Studi di Trento)
Prof. Giovanni Scudo	(Politecnico di Milano)
Prof. Alessandro De Stefano	(Politecnico di Torino)
Prof. Fabio Biondini	(Politecnico di Milano)

SUMMARY

The integral abutment bridge (IAB) constituted by the superstructure and the substructure can achieve a composite action responding as a single structural unit by eliminating or reducing expansion joints and bearings. Accordingly, the construction and maintenance costs can be reduced. Therefore, the IAB concept has recently become a topic of remarkable interest among bridge engineers, not only for newly built bridges but also during refurbishment processes. The research topic concerns the retrofit of existing bridges with the IAB concept.

In order to investigate the retrofitting technique with the IAB concept, the literature survey on the practical applications of this approach in worldwide was carried out firstly, including retrofitting motivations, detailed processes and structural performance after retrofitting. Besides, another literature review on the critical issues of analysis on the IAB, such as soil-structure interactions, modelling approaches and plastic hinge simulations, was conducted in order to find out the most suitable method in modelling.

The case study of a simply supported prestressed concrete bridge (named Viadotto Serrone) with three spans constructed in 1972 was analyzed, which has some durability problems nowadays. The finite element model was built, involving soil-structure interactions, non-linear behaviors and retrofitting processes. The original and updated Italian design codes are compared through static analysis and seismic analysis. Another investigation was conducted to prove the necessity of considering soil-structure interactions in the IAB.

Based on the appropriate finite element model, a large number of static sensitive analyses were carried out, taking thermal actions; bridge types; soil conditions and substructure heights as parameters. Through analysing the responses of girders, piers, abutment stems and piles, some important factors and the corresponding influence were found, which could be adopted to guide the retrofitting technique with the IAB concept. Then, the verification was conducted in order to check if the existing sections could be reused without any changes and point out the most critical components, which need to be repaired or replaced. Moreover, the dynamic performance of bridge before and after retrofitting was investigated preliminarily through modal analysis and response spectrum analysis.

SOMMARIO

I ponti integrali (IAB) sono recentemente diventati una tipologia di grande interesse fra i progettisti di ponti, non solo nel caso delle nuove realizzazioni ma anche applicati all'adeguamento del patrimonio infrastrutturale esistente. L'eliminazione dei giunti di dilatazione e degli appoggi può costituire infatti un grande vantaggio in termini di costi di gestione e di durabilità dell'opera.

Lo studio presentato in questa tesi riguarda in particolare la possibilità di applicare il concetto del ponte integrale alla riabilitazione dell'esistente.

A questo fine nella prima parte della tesi viene presentato e analizzato criticamente lo stato dell'arte relativo alle applicazioni di questa tipologia di ponti a livello Internazionale.

Viene inoltre affrontata la problematica della simulazione numerica dei ponti integrali considerando in particolare l'interazione terreno-struttura, la formulazione delle cerniere plastiche sulle pile e l'effetto della soletta di transizione.

La Ricerca poi si concentra sulla possibilità di utilizzare la tecnologia dei ponti integrali all'adeguamento del patrimonio infrastrutturale italiano. Questo trae spunto da una reale necessità messa recentemente in evidenza da ANAS, e si sviluppa prendendo in considerazione un tipico viadotto con travi prefabbricate precomprese in semplice appoggio su tre campate realizzato negli anni 70.

Il comportamento del ponte prima e dopo la trasformazione in IAB è stato studiato attraverso modelli implementati in SAP2000 considerando le varie non linearità e l'effetto dell'interazione terreno-struttura e verificando l'affidabilità delle simulazioni effettuate.

Successivamente, vengono presentate una serie di analisi parametriche per verificare la sensibilità del comportamento strutturale del ponte alla tipologia di intervento utilizzato, alle caratteristiche del suolo e alle caratteristiche geometriche delle pile individuando i parametri più importanti e alcune prime indicazioni su come procedere nell'intervento.

Infine, il lavoro si conclude con una dettagliata analisi della risposta strutturale del ponte a intervento eseguito, considerando sia le azioni statiche che quelle sismiche, e ponendo in evidenza i vantaggi e le criticità della metodologia di adeguamento proposta.

DEDICATION

*to my parents
and
my wife*

ACKNOWLEDGEMENTS

*Grateful thanks to Prof. Enzo Siviero and Prof. Baochun Chen
for their deep insights and supports
during my study in Italy.*

*Grateful thanks to Prof. Bruno Briseghella and Prof. Tobia Zordan
for their great kindest helps and advices
not only in my studies but also in my livings,
to make this research work possible.*

*Grateful thanks to Dr. Cheng Lan and Dr. Enrico Mazzarolo
for exchanging opinions and assistances
as a good partner and friend.*

*Special thanks to ANAS
for providing all the materials and drawings
on the bridge studied.*

Sincere thanks to all my dear friends.

CONTENTS

CHAPTER 1

1. INTRODUCTION	1
1.1. DURABILITY PROBLEMS IN SIMPLY SUPPORTED BRIDGES	1
1.2. RETROFITTING METHODS BY ELIMINATING EXPANSION JOINTS AND BEARINGS.....	5
1.2.1 <i>Retrofit of superstructure-pier connection</i>	5
1.2.2 <i>Retrofit of superstructure-abutment connection</i>	12
1.3. INTRODUCTION OF INTEGRAL ABUTMENT BRIDGE	15
1.3.1 <i>Concept of integral abutment bridge</i>	15
1.3.2 <i>Application of integral abutment bridge</i>	18
1.3.3 <i>Attributes and opening issues of IAB</i>	30
1.4. CRITICAL ISSUES AND SOLUTIONS	35
1.4.1 <i>Critical issues</i>	35
1.4.2 <i>Solutions</i>	36
1.5. LAYOUT OF THE THESIS	37

CHAPTER 2

2. STATE-OF-ART: RETROFIT WITH IAB CONCEPT	39
2.1 APPLICATIONS IN NORTH AMERICA	39
2.1.1 <i>USA</i>	39
2.1.2 <i>Canada</i>	49
2.2 APPLICATIONS IN EUROPE	62
2.2.1 <i>Italy</i>	62
2.2.2 <i>Switzerland</i>	70
2.2.3 <i>Germany</i>	70
2.2.4 <i>Austria</i>	71
2.3 APPLICATIONS IN ASIA	71
2.3.1 <i>China</i>	71
2.3.2 <i>Singapore</i>	73
2.4 ADVANTAGES AND OPENING ISSUES OF RETROFIT WITH IAB CONCEPT	76
2.4.1 <i>Advantages</i>	76
2.4.2 <i>Opening issues</i>	77

CHAPTER 3

3. KEY ISSUES IN IAB ANALYSIS	79
--	-----------

3.1 SOIL-STRUCTURE INTERACTION	79
3.1.1 <i>Soil-abutment interaction</i>	80
3.1.2 <i>Soil-pile interaction</i>	107
3.1.3 <i>Numerical software for soil-structure interaction</i>	135
3.2 IAB MODELING APPROACH.....	137
3.2.1 <i>Simplified model</i>	137
3.2.2 <i>Finite element model</i>	139
3.3 PLASTIC HINGE MODELING	143
3.3.1 <i>General modeling approach</i>	143
3.3.2 <i>Moment-rotation curve</i>	145
3.3.3 <i>Plastic hinge length</i>	147
3.3.4 <i>Acceptance criteria</i>	149
CHAPTER 4	
4. PROPOSED RETROFITTING METHODS WITH FIAB CONCEPT	151
4.1 RETROFIT OF SUPERSTRUCTURE-PIER CONNECTION	152
4.1.1 <i>Hinged connection</i>	152
4.1.2 <i>Rigid connection</i>	154
4.2 RETROFIT OF SUPERSTRUCTURE-ABUTMENT CONNECTION	155
4.2.1 <i>Hinged connection</i>	155
4.2.2 <i>Rigid connection</i>	157
CHAPTER 5	
5. CASE STUDY.....	159
5.1 VIADOTTO SERRONE	159
5.2 FINITE ELEMENT MODEL.....	162
5.2.1 <i>Modeling method and elements information</i>	166
5.2.2 <i>Material</i>	171
5.2.3 <i>Modeling of soil-structure interaction</i>	174
5.2.4 <i>Modeling of plastic hinge</i>	180
5.2.5 <i>Modeling of retrofitting process</i>	190
5.3 LOAD CASE	193
5.3.1 <i>Permanent load</i>	194
5.3.2 <i>Deformation</i>	194
5.3.3 <i>Highway live load</i>	195
5.3.4 <i>Seismic load</i>	198
5.3.5 <i>Loads combination</i>	201
5.3.6 <i>Comparison between original and updated codes</i>	202
5.4 MODEL VERIFICATION	209

5.4.1 Finite element model verification	209
5.4.2 Retrofitting process modeling verification	212
5.4.3 Necessity of soil-structure interaction simulation in IAB	214

CHAPTER 6

6. STATIC SENSITIVE ANALYSIS	219
6.1 DIFFERENT BRIDGE TYPES	219
6.1.1 Load case	220
6.1.2 Girder	221
6.1.3 Pier	227
6.1.4 Abutment stem	230
6.1.5 Pile	233
6.1.6 Summary	237
6.2 DIFFERENT SOIL CONDITIONS	238
6.2.1 Soil-structure interaction	239
6.2.2 Vertical load case	244
6.2.3 Horizontal load case	245
6.2.4 Summary	263
6.3 DIFFERENT SUBSTRUCTURE HEIGHTS	264
6.3.1 Research cases definition	264
6.3.2 Girder	265
6.3.3 Pier	270
6.3.4 Abutment stem	277
6.3.5 Pile	282
6.3.6 Summary	289

CHAPTER 7

7. STATIC PERFORMANCE CHECK AFTER RETROFITTING	293
7.1 FORCE-MOMENT INTERACTION DIAGRAM ANALYSIS	293
7.1.1 F_A - M domain	293
7.1.2 F_A - M interaction diagram check	296
7.2 CONSIDERATION OF APPROACH SLAB	320

CHAPTER 8

8. SEISMIC SENSITIVE ANALYSIS	329
8.1 LITERATURE REVIEW	329
8.2 FINITE ELEMENT MODEL	331
8.3 MODAL ANALYSIS	333
8.3.1 Mode shape and vibration period	334

8.3.2 <i>Different bridge types</i>	335
8.3.3 <i>Different soil conditions</i>	336
8.3.4 <i>Different substructure heights</i>	336
8.4 RESPONSE SPECTRUM ANALYSIS	337
8.4.1 <i>Response spectrum</i>	338
8.4.2 <i>Different bridge types</i>	340
8.4.3 <i>Different soil conditions</i>	367
CONCLUSIONS	375
MAIN FINDINGS	375
CONCLUSIONS	383
RECOMMENDATIONS FOR FUTURE INVESTIGATIONS	384
REFERENCES	385

1. INTRODUCTION

Many simply supported bridges have been constructed all over the world, in which expansion joints and bearings are installed in order to absorb cyclic thermal expansion and contraction, creep and shrinkage, and differential settlement. The majority of them have some durability problems during their service life (Arockiasamy et al., 2004; Wolde-Tinsae et al., 1988a). Among them, damaged expansion joints and bearings can be considered as the most common durability problems, which can produce some other bridge diseases, such as the corrosion in girder ends and bearings due to de-icing salt water passing through damaged expansion joints (Loveall, 1985; Shah, 2007), unexpected supernumerary forces caused by debris accumulation, discomfort driving sense and so on. Moreover, frequent retrofit or replacements will cost a lot of money and time (Wasserman & Walker, 1996). In addition, any interruptions or limitations of traffic due to retrofit would lead to serious environmental and social impacts (Briseghella & Zordan, 2006; Feldmann et al., 2010).

Some retrofitting methods, which can reduce the influence of damaged expansion joints and bearings, have been proposed. For road administrations, proposing a retrofitting technique that can resolve these durability problems fundamentally is of greater importance. In order to achieve this requirement, the IAB concept came out.

1.1. Durability problems in simply supported bridges

The simply supported beam is the simplest beam type described by how it is supported. It is supported vertically at each end, horizontally on only one to withstand friction, and is able to rotate at the supports. The simply supported bridge (as illustrated in Fig. 1) is the most basic type of bridge with single or multiple simply supported spans. Consequently, it is the easiest static scheme for engineers and has proved to be very successful in applications. All simply supported spans are supported by bearings, which can transfer vehicular loads and other environmentally imposed loads from the superstructure to the substructure. The expansion joints installed between two adjacent spans or between end spans and pavements can carry loads and provide safety to the traffic over gaps in a way that all bridge

displacements can take place with very low resistance or with no resistance at all. Consequently, the simply supported bridge is able to take up the deformations due to creep and shrinkage, to allow thermal movements and to accommodate differential settlement (Arockiasamy et al., 2004; Fédération internationale du béton, 2004; Ramberger, 2002).

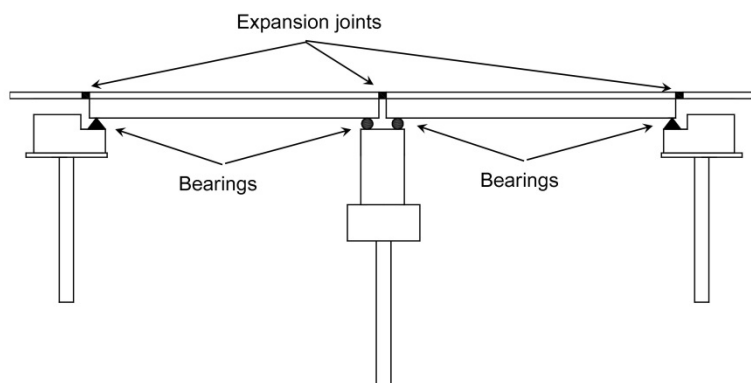


Fig. 1 Simply supported bridge

Many simply supported bridges have maintenance problems, such as damaged expansion joints and bearings, spalling of concrete, corroded reinforcements, deteriorated concrete due to leaking water, corroded prestressing tendon anchorages and so on. Among them, the damaged expansion joints and bearings can be considered as the most common durability problems, based on the following statistics.

1. In 1986, a statistic on the service conditions of the existing bridges in USA (Wolde-Tinsae & Klinger, 1987) was conducted, which indicated that about 248500 out of 570000 of total bridges had durability problems. Among them, more than 50% had damaged expansion joints.
2. Another survey on approximately 200 concrete highway bridges in UK was carried out by the Department of Transport. It could be found that damaged expansion joints should be considered as a serious source of costly and disruptive maintenance works (Wallbank, 1989).
3. In 1995, a survey on the motivation of steel bridge refurbishment was conducted in USA and Canada. The statistical results as shown in Fig. 2 indicated that approximately 91% of the responding agencies in USA and Canada would like to eliminate expansion joints (Tsiatas & Boardman, 2002).

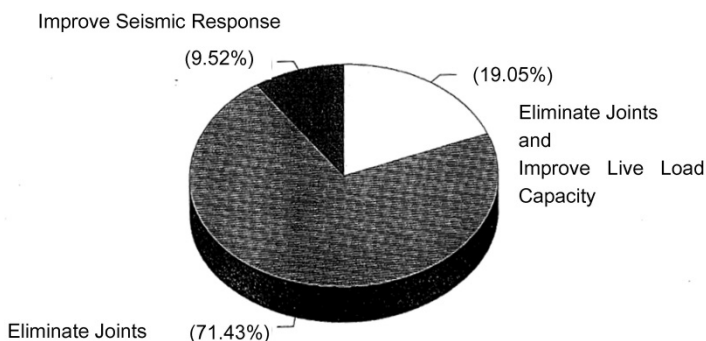


Fig. 2 Motivation of steel bridge refurbishment in USA and Canada (Tsiatas & Boardman, 2002)

4. The investigation on approximately 556 existing bridges, located in thirteen cities in China, including Beijing, Tianjin and so on, indicated that 48.7% of them had damaged expansion joints (Li et al., 1997).

5. The statistical data listed in '2011 Shanghai Bridges Technical Analysis Report' (Shanghai Municipal Engineering Administration Bureau & College of Traffic and Transportation Engineering of Tongji University, 2011) indicated that damaged expansion joints could be found in 23.3% of existing bridges.

6. An investigation on damaged expansion joints was conducted in Taiwan. It could be found that the rubber expansion joint is the most easily damaged (more than 41.4%), and the quantities of the damaged expansion joints located at girder-abutment connections (about 63.4%) is much higher than those located at girder-pier connections (about 4.7%) (Lin, 2004).

Moreover, many of the maintenance problems associated with existing bridges relate to damaged expansion joints and bearings (Washington State Department of Transportation, 2012). For example, girder ends, bearings and pier caps would be significantly corroded by the run-off water containing corrosive de-icing salts leaking through damaged expansion joints (Kaufmann & Alvarez, 2011; Loveall, 1985; Shah, 2007; Wasserman, 1987). This problem is particularly serious in the regions with low seasonal temperatures and an abundance of snow and freezing rain. In these regions, a large amount of de-icing salt application are commonly used to control the icing of bridge decks (Aktan et al., 2008; Dreier et al., 2011; Krier, 2009b). Additionally, expansion joints can be obstructed by debris accumulation, which would effect deck movements and produce additional forces. Besides that,

RETROFIT OF EXISTING BRIDGES WITH CONCEPT OF INTEGRAL ABUTMENT BRIDGE

expansion joints are discomfort to traffic and sometimes can be a very dangerous road hazard when the expansion joints separate from their concrete embedment and become protruding devices out of decks toward high-speed traffic. These problems occur more and more frequently with the fast increment of traffic speed, volume and weight. In addition, expansion joints and bearings are very expensive to buy, install, maintain and repair. The repair cost can run as high as the replacement cost. Moreover, the expansion joints and bearings require maintenance works even if they are designed and constructed correctly (Wasserman & Walker, 1996). Once refurbishment starts, the traffic has to be interrupted or restricted, which will cost a lot of money and time.

The vulnerability of expansion joints and bearings is mainly due to their inherent properties and external cyclic loads. Some typical failure modes are illustrated in Fig. 3.



Fig. 3 Typical failure modes of expansion joints and bearings

The failure mechanisms of different types of expansion joints are different. For example, the modular expansion joint, which has multiple mobile parts, is prone to fatigue fracture, especially on some critical components such as welds and support bars. Dynamic effects can amplify these fatigue problems. For the seal expansion joint, the predominant failure mechanism is the loss of the material elasticity over time. In addition, the seal can be separated from the deck and anchorage at the deck, which could produce some other maintenance problems. For the finger joint, the failure mechanism is due to debris accumulation inside the joint (Caicedo et al., 2011). Considering different types of bearings, the corresponding failure mechanisms are also varied, for example the steel bearing may be ineffective due to loss of lubrication or buildup of corrosion as time goes on, and the elastomeric bearing can split and rupture due to unanticipated movements which may produce overstress and subsequent structural damage (Wasserman & Walker, 1996). Some commonly used types of expansion joints and bearings, and their failure modes, failure mechanisms, conventional repairing approaches, costs and expected life are summarized by the Ohio Department of Transportation (Ohio Department of

Transportation).

1.2. Retrofitting methods by eliminating expansion joints and bearings

As described above, damaged expansion joints and bearings in simply supported bridges can produce a large number of durability problems during their service life. For road administrations, repetitive refurbishment will cost a lot of money and time. Moreover, frequent interruptions or restrictions of traffic will lead to additional environmental and social costs. Although, the service life of expansion joints and bearings can be increased by improving their inherent mechanical properties and using some other auxiliary techniques. The auxiliary techniques include seeking the advice of the manufacturer at the time of installation to avoid incorrect installations, implementing a proactive maintenance program; using deck joint blockouts; positioning seals to match ambient temperature; installing the joint after placing the overlay, and so on (Caicedo et al., 2011; Purvis, 2003). However, these approaches cannot resolve the problems of damaged expansion joints and bearings fundamentally. The idea of 'The only good joint is no joint' was articulated almost 40 years ago by Henry Detrick, who was the former Engineer of Structures for the Tennessee Department of Transportation (Burdette et al., 2005). According to this philosophy, the retrofitting method of eliminating expansion joints and bearings is proposed. This approach is based on the theory of "Moment Distribution" created by Cross in the 1930s (Cross, 1932), which gives bridge engineers an opportunity to adopt continuous construction. Many researchers try to propose some retrofitting methods, including the retrofit of the superstructure-pier connection and the retrofit of the superstructure-abutment connection.

1.2.1 Retrofit of superstructure-pier connection

Three different methods can be adopted to eliminate or reduce the expansion joints and bearings in superstructure-pier connections during refurbishment, including the continuous slab method, the continuous diaphragm method and the integral pier method.

The continuous slab method is a partial continuity approach that only provides continuity of deck slabs; however, girders remain simply supported (Fédération internationale du béton, 2004), as shown in Fig. 4. Several connection methods were proposed by different researchers (Fédération internationale du béton, 2004; Highways Agency, 2001). This method can eliminate the expansion joints in superstructure-pier connections; however, the bearings remain unchanged. It can be

considered as a 'softer' and less challenging solution compared to full continuity at piers (Briseghella & Zordan, 2006).

The continuous diaphragm method can connect adjacent simply supported spans by integrating both deck slabs and girder ends into a continuous diaphragm connection (Fédération internationale du béton, 2004; Miller et al., 2004), as illustrated in Fig. 5. The state scheme of bridges would change from simply supported to continuous. Once the deck slabs and girder ends integrate, a compressive base would be provided at the bottom of girders. The connection segments should be designed to resist the negative bending moment and the tension stress. Based on many experimental and theoretical studies, several design approaches were proposed (Miller et al., 2004; Newhouse, 2005), such as the Portland Cement Association (PCA) method (Freyermuth, 1969), Construction Technology Laboratories method (CTL) suggested in NCHRP Report 322 (Oesterle et al., 1989), the method proposed in BA57/01 (Highways Agency, 2001) and so on. Many different detailed construction configurations of the connections were suggested (Fédération internationale du béton, 2004; Fu, 2001; Fu & Kudsi, 2000; Newhouse, 2005). As a result, the long-term durability of girders could be improved by reducing water and salt that would potentially damage the concrete of girder ends and pier caps, and bearings. On the other hand, the elimination of expansion joints can provide a smooth driving surface (Kaar et al., 1960). Furthermore, this method can reduce the bearings at each pier from double lines to single line.

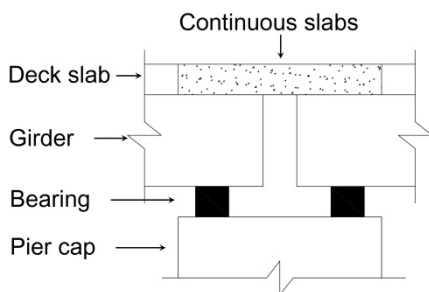


Fig. 4 Continuous slab method

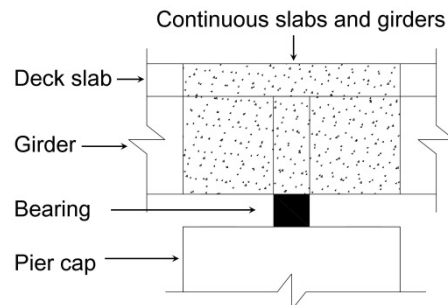


Fig. 5 Continuous diaphragm method

The integral pier method also integrates both deck slabs and girder ends into a continuous diaphragm connection, which is similar to the continuous diaphragm method. Besides, the bearings on piers should be eliminated by casting concrete to integrate the superstructure and piers together (Burke, 2009; Maruri & Petro, 2005), as illustrated in Fig. 6.



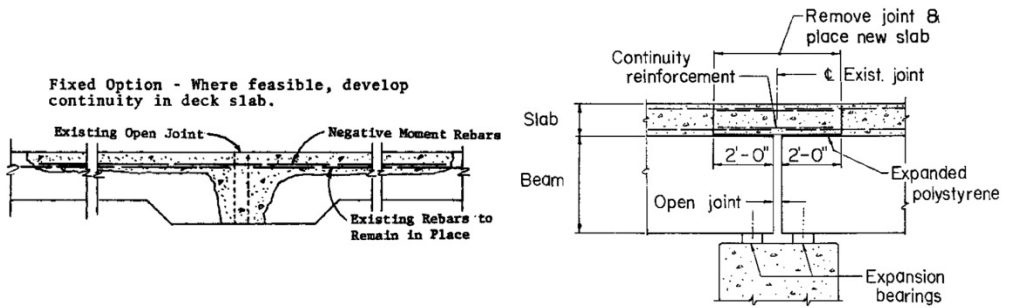
Fig. 6 Integral pier method

All three retrofitting methods introduced above have been used worldwide. In the 1960s, the superstructure conversion in existing steel bridges from simply supported to continuous or semi-continuous was begun in Wisconsin and Massachusetts (Tsiatas & Boardman, 2002). In 1980, a Technical Advisory was proposed by Federal Highway Administration concerning the refurbishment of expansion joints (Leathers, 1980). According to a survey, it indicated that 11 of 30 departments of transportation in USA transformed the static scheme of bridges from multi-span simply supported to continuous-span by using the continuous diaphragm method (Burke, 1990). Another survey carried out in 1995 by the Rhode Island Department of Transportation found that 22 Departments of Transportation in USA and Canada adopted the integral pier method and all 64 agencies responded to express an interest in learning more (Tsiatas & Boardman, 2002). The investigation carried out in 2004 indicated that 49% of the responded states in USA had a policy to retrofit existing bridges by eliminating expansion joints in the superstructure whenever possible (Maruri & Petro, 2005).

The continuous slab method is proposed by some departments of transportation in USA, such as Texas, Utah, New Mexico, and so on. The corresponding detailed retrofitting procedures are introduced respectively in the following. The process adopted in Texas can transform the static scheme from multi-span simply supported to continuous-span only at the slab part though several steps, as illustrated in Fig. 7(a). Remove the concrete of existing slabs as necessary to eliminate existing armoring. Then, add sufficient negative moment rebar to resist transverse cracking. Finally, cast concrete of the same grade as the original deck slabs. However, the girders after retrofitting remain simply supported. In order to use this procedure, it is important to ensure that the bearings after retrofitting are capable of allowing horizontal movements. Providing for such movement will prevent large horizontal

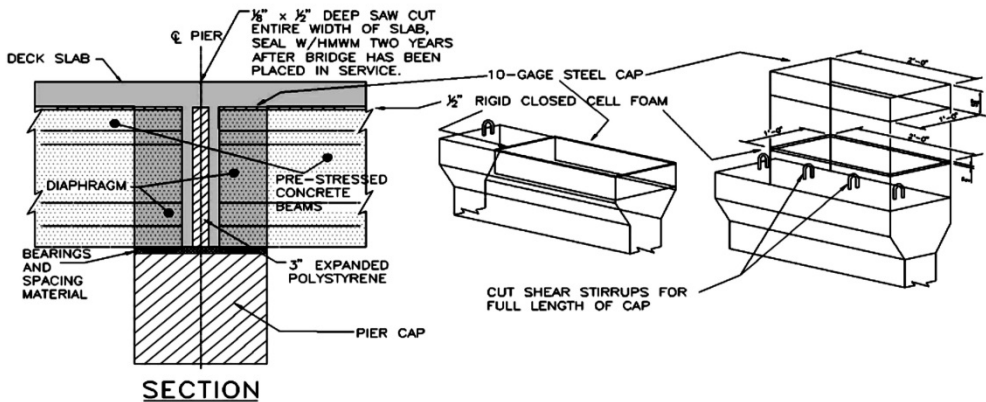
forces from being imposed on bearings due to the rotations of adjacent spans and the continuity of deck slabs (Leathers, 1980). For the procedures in Utah as illustrated in Fig. 7(b), expansion joints should be removed firstly, and then new deck slabs can be casted with continuity rebar and an elastomeric type of membrane that can be used under the overlay to waterproof the new deck slabs. Moreover, the deck slabs would be exposed to longitudinal flexure due to the rotations of girder ends under traffic load. Using this method, some cracks would occur on the deck slabs. However, for short and medium span bridges, it can be accepted compared to the long-term durability problems produced by expansion joints (Burke, 2009). Using the procedures in New Mexico as illustrated in Fig. 7(c), expanded polystyrene can be embedded in the diaphragm over each pier that can allow girder ends to rotate. The rigid foam encased and protected by steel caps can be used to spread cracks over a greater distance and change from one wide crack into some narrow cracks. Some saw cuts are applied to deck slabs for the consideration of expansion. The bearing types are usually changed in order to satisfy additional thermal movements after retrofitting and to eliminate existing deterioration (Maberry et al., 2005). Some advantages of using this retrofitting method can be achieved in New Mexico, including low maintenance costs and long bridge service life. Therefore, it has been used in many projects, such as the retrofit of Interstate-25 over Rio Grande South of Albuquerque and a jointed bridge "Rio Grande Bridge" constructed in 1971 with 12 spans.

Several successful retrofitting projects by using the link slab method to eliminate the expansion joints in superstructure-pier connections were conducted in Ontario, Canada and Michigan, USA and in Australia (Aktan et al., 2008; Connal, 2004; Ho & Lukashenko, 2011; Lam et al., 2008; Patel & Lai, 2001). The detailed configuration of link slab method is illustrated in Fig. 8. There are three different retrofitting approaches. Semi-continuous deck system can convert simply supported spans into a semi-continuous deck system by encasing girder ends in a monolithic transverse concrete diaphragm. Flexible link slab system can connect adjacent simple spans by a thin concrete slab spanned between haunched girder sections on either side of link slab while keeping the girders discontinuous. Debonded Link Slab System uses the similar method as Flexible link slab system, except that the link slab is debonded from girders for a longer length at each end. All structures after retrofitting have performed well to date.



(a) Texas Department of Public Transportation in USA (Leathers, 1980)

(b) Utah Department of Transportation in USA (Burke, 2009)



(c) New Mexico Department of Transportation in USA (Maberry et al., 2005)

Fig. 7 Retrofit with continuous slab method

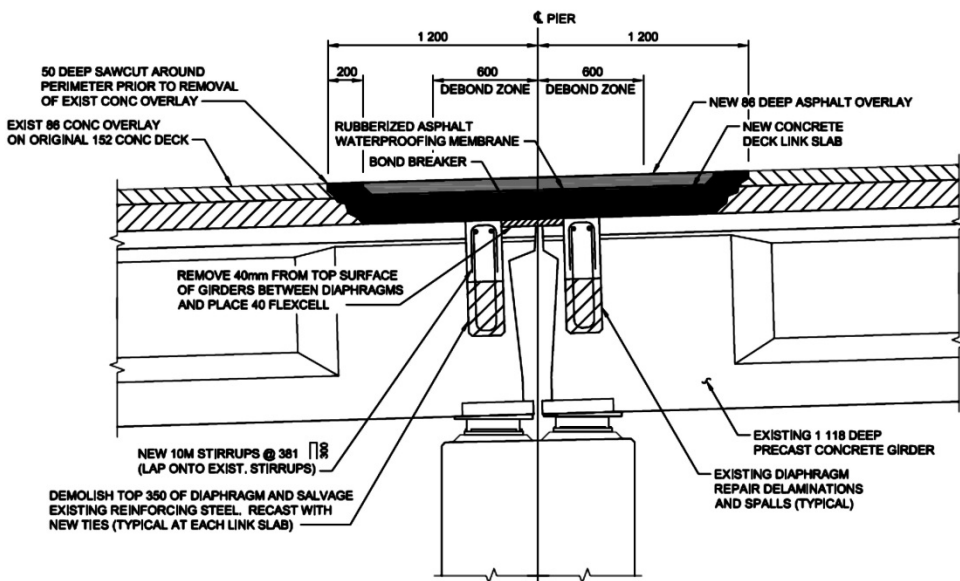
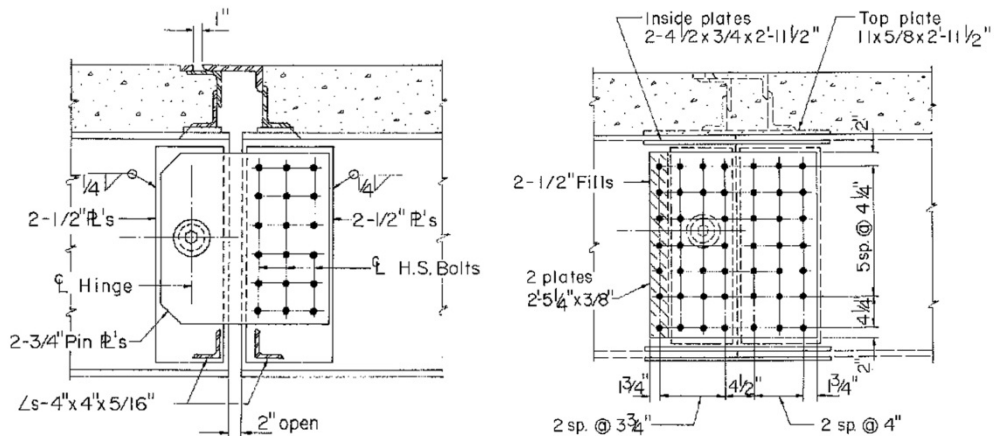


Fig. 8 Link slab method (Ho & Lukashenko, 2011)

RETROFIT OF EXISTING BRIDGES WITH CONCEPT OF INTEGRAL ABUTMENT BRIDGE

The continuous diaphragm method has been widely used by many departments of transportation in USA. The detailed procedure proposed by the Ohio Department of Transportation which can convert the superstructure of the steel girder bridge with expansion joints to the fully continuous superstructure are illustrated in Fig. 9. The expansion joints between adjacent concrete deck slabs and steel girders over each pier are replaced by continuous deck slabs and bolted splices, respectively.

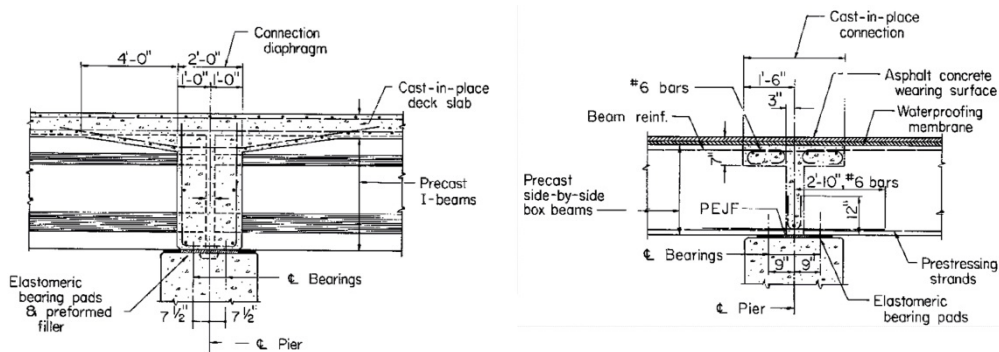


(a) Existing structures

(b) After retrofitting

Fig. 9 Retrofit with continuous diaphragm method, Ohio Department of Transportation in USA (Burke, 2009)

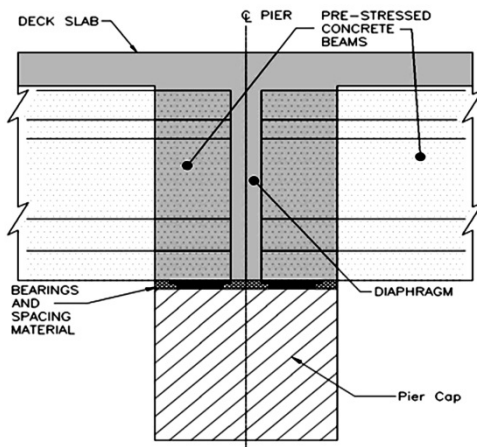
Some other procedures of making decks and girders continuous, which are usually adopted in the original construction, can be also applied to retrofitting projects. Several detailed configurations proposed by some departments of transportation in USA, such as Wisconsin, Ohio and New Mexico, are illustrated respectively in Fig. 10(a), (b) and (c) (Burke, 2009; Maberry et al., 2005).



(a) Wisconsin Department of Transportation

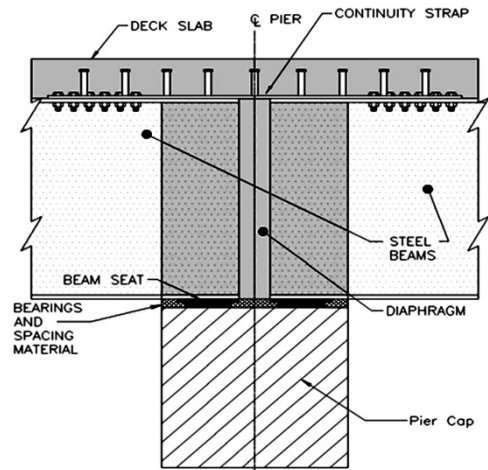
(b) Ohio Department of Transportation in

in USA (Burke, 2009)



Concrete girder

USA (Burke, 2009)



Steel girder

(c) New Mexico Department of Transportation in USA (Maberry et al., 2005)

Fig. 10 Retrofit with continuous diaphragm method

An investigation on the retrofit of a standard Italian simply supported flyover by using the continuous diaphragm method was carried out (Briseghella & Zordan, 2006). Firstly, the expansion joints in superstructure-pier connections can be removed, and the existing bearings can be made inactive by incorporating within expansive concrete mortar. Then, a large number of concrete-to-concrete shear connectors can be installed on the internal web faces of the prefabricated beams and several steel beams can be embedded in the girder-pier connections in order to transmit axial forces and shear forces between the superstructure and piers, as demonstrated in Fig. 11. Finally, the concrete is casted in situ.

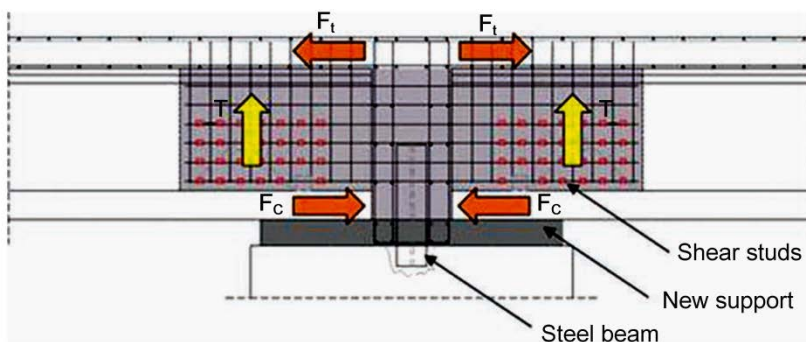


Fig. 11 Structural behaviors of superstructure-pier connection (Briseghella & Zordan, 2006)

Both continuous slab method and continuous diaphragm method are proposed in

Japan (Road Management Technology Center, 1995). Two approaches, 'Buried Type No Joint Method' and 'Connection Type No Joint Method' are suggested. The first method can be used in short span (less than 30m) concrete or prestressed concrete bridges with light traffic load. The second one can be applied to long span steel or concrete bridges with heavy traffic load (Fujiwara et al., 1992; Takano, 1994).

1.2.2 Retrofit of superstructure-abutment connection

There are several different methods which can be used to eliminate or reduce the expansion joints and bearings in superstructure-abutment connections during retrofitting, such as the deck extension method, the fully integral abutment method and the semi-integral abutment method (Maruri & Petro, 2005).

The deck extension method can be used to resolve the durability problem related to expansion joints by allowing the deck slab to slide over the abutment backwall or allowing the deck-backwall combined system to slide over the abutment. As a result, the deck movements can be transferred to the ends of approach slabs (Aktan et al., 2008).

According to different configurations of abutment backwalls, two kinds of deck extension methods are suggested. One method can make the approach slab and deck slab continuous and allow the deck slab to slide over the abutment backwall, which is proposed by the Michigan Department of Transportation and the New York State Department of Transportation in USA (Aktan et al., 2008; Alampalli & Yannotti, 1998). Two detailed drawings are illustrated respectively in Fig. 12(a) and (b). This method can be called as "independent backwall configuration" because the abutment backwall is independent of the superstructure in this case. In order to adapt the superstructure movements, hinged connection can be set between the abutment backwall and abutment. Therefore, when the approach slab or deck slab expand, the abutment backwall can have small movements at the top, which can reduce the forces in both approach slab and abutment backwall.

The other approach proposed only by the Michigan Department of Transportation in USA (Aktan et al., 2008), can be called as 'dependent backwall configuration' because the abutment backwall is dependent on the superstructure. The deck-backwall monolithic system can move together and slide over the abutment when the approach slab or deck slab expand. All movements can be absorbed by abutment backfill. The detailed configuration of this approach is illustrated in Fig. 13.

The integral abutment method can eliminate or reduce the expansion joints and bearings in superstructure-abutment connections (Burke, 2009). According to different connection configurations between the superstructure and abutments, two detailed approaches can be proposed, which are the fully integral abutment method and the semi-integral abutment method, respectively. The fully integral abutment method can eliminate all expansion joints and bearings in superstructure-abutment connections, as illustrated in Fig. 15(a). The semi-integral abutment method can eliminate the expansion joints in superstructure-abutment connections; however retain the original bearings after retrofitting, as illustrated in Fig. 15(b) (Kaufmann & Alvarez, 2011; Maruri & Petro, 2005). Different departments of transportation and standards propose many typical configurations of these two methods. Among them, the proposals of the Precast/Prestressed Concrete Institute and the West Virginia Department of Transportation in USA are chosen as examples and illustrated respectively in Fig. 14 and Fig. 15.

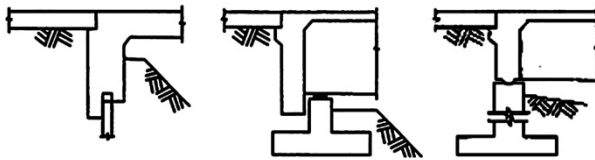
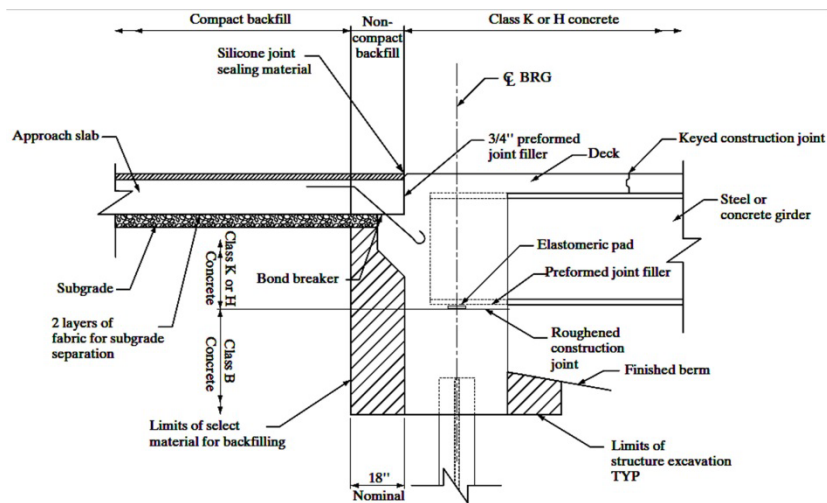
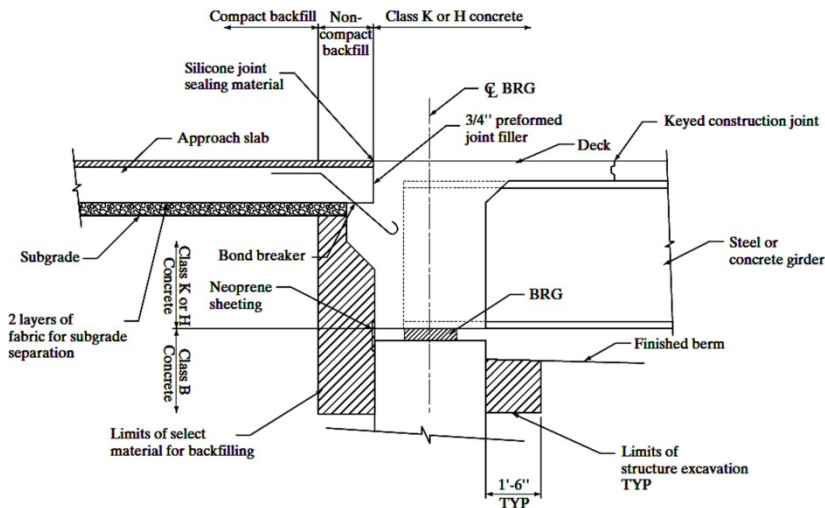


Fig. 14 Fully integral and semi-integral abutment configurations, Precast/Prestressed Concrete Institute (Precast/Prestressed Concrete Institute (PCI), 2001)



(a) Fully integral abutment detail



(b) Semi-integral abutment detail

Fig. 15 Integral abutment configurations, West Virginia Department of Transportation in USA (West Virginia Department of Transportation Division of Highways, 2004)

Both fully integral abutment method and semi-integral abutment method can be also used in retrofitting projects, which will be discussed in detail in Chapter 2.

1.3. Introduction of integral abutment bridge

1.3.1 Concept of integral abutment bridge

Bridges without expansion joints are ages old. In ancient times, the most celebrated were natural stone beam bridges and stone arch bridges carved from bedrock by water and wind. For man-made bridges, there were also some excellent examples, such as stone masonry arch bridges by the Romans, reinforced concrete arch bridges constructed in the early decades of last century, rigid frame bridges constructed from the middle of last century, and so on (Burke, 2009). In the last few years, one type of single- or multi-span bridge without expansion joints and bearings has attracted more and more attention. This kind of bridge can be divided into several subtypes according to different configurations of superstructure-abutment and superstructure-pier connections.

However, it is still in arguing what the right name and suitable definitions for this kind of bridge and its subtypes are. Through summing up several names proposed by different researchers and codes (Burke, 2009; Kaufmann & Alvarez, 2011; Maruri &

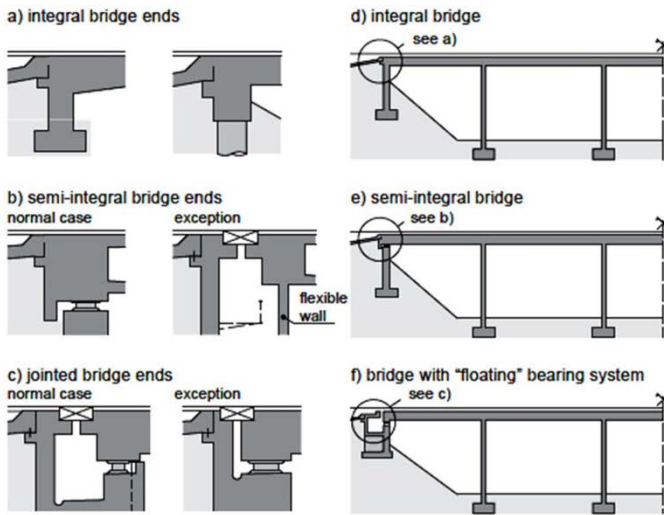
RETROFIT OF EXISTING BRIDGES WITH CONCEPT OF INTEGRAL ABUTMENT BRIDGE

Petro, 2005; White, 2007; White et al., 2010), the full names and abbreviations of different bridge types used in this paper are listed in Table 1.

Simply supported bridge(s) (SSB(s))	
Integral abutment bridge(s) (IAB(s))	Semi-integral abutment bridge(s) (SIAB(s))
	Fully integral abutment bridge(s) (FIAB(s))

Table 1
Names and abbreviations of different bridge types

In order to give the suitable definitions for this kind of bridge and its subtypes, several proposals by different researchers and codes are summarized (Bakeer et al., 2005; Burke, 2009; Iles, 2006; Kaufmann & Alvarez, 2011; White, 2007). Among them, the definitions proposed in revised Federal Roads Office (FEDRO) Guidelines as shown in Fig. 16 (Kaufmann & Alvarez, 2011) can be chosen as the basis of the definitions of the IAB and its subtypes (SIAB and FIAB) used in this paper.



detailing of deck and piers	deck monolithic (jointless)		deck with joint(s)
	all piers monolithic with deck or no piers	pier(s) with bearings or joints (top/bottom)	('gerber'-type joint, joint over piers, ...)
detailing of bridge ends			
both bridge ends integral	integral bridge		jointed bridge
one bridge end semi-integral, other bridge end integral or semi-integral	semi-integral bridge		
at least one bridge end jointed (= with expansion joint)	"floating" bearing system (1)		

(1) both bridge ends with expansion joint and sliding bearings (longitudinally movable).

Fig. 16 Definitions of IAB and its subtypes proposed in (Swiss) Federal Roads Office (FEDRO) Guidelines (Kaufmann & Alvarez, 2011)

Furthermore, when designing an excellent retrofitting process, existing bridge components should be reused as many as possible, and the complete replacement during refurbishment is not easily constructed and economical. Therefore, there should be no specified types of bridge components (girders, abutments, piers and piles) in the definitions. According to different connection flexibility between the superstructure and the substructure, the detailed definitions of the subtypes of SIAB and FIAB are listed in Table 2, Generally, the connection flexibility in real applications can be simulated as a rotational spring with certain rotational resistances provided by vertical pressure and horizontal friction (Lan, 2012). In this paper, the pure hinged connection and pure rigid connection are chosen.

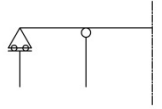
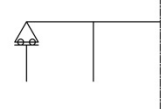
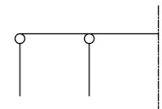
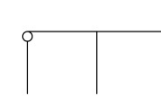
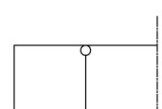

Superstructure-Substructure connection		Superstructure-Pier connection			
		Hinged connection		Rigid connection	
Superstructure- Abutment connection	Movable bearing	SIAB1		SIAB2	
	Hinged connection	FIAB1		FIAB2	
	Rigid connection	FIAB3		FIAB4	

Table 2

Detailed definitions and abbreviations of subtypes of SIAB and FIAB

The structural elements of a typical IAB are illustrated in Fig. 17, including the bridge system consisting of the continuous superstructure, integral abutments, piles or foundations, piers if of multi-span and the approach system that is optional.

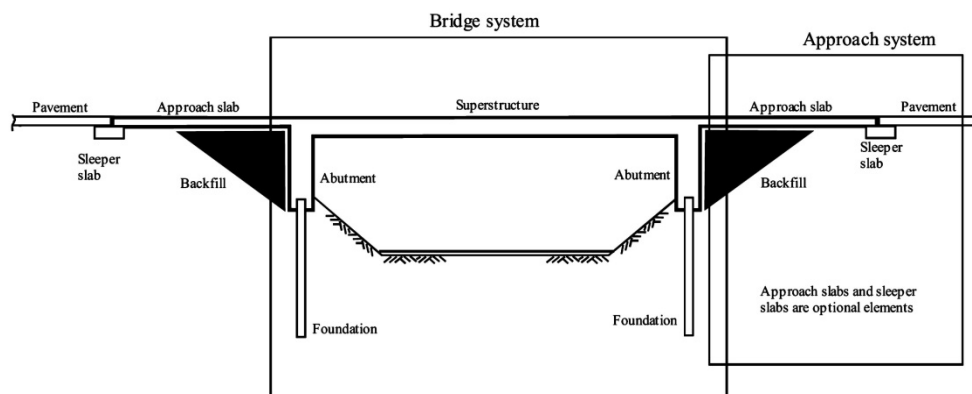


Fig. 17 Simplified geometry of an IAB (Arsoy, 2000)

1.3.2 Application of integral abutment bridge

1.3.2.1 North American

The state of Colorado pioneered to use the IAB concept in USA from 1920, followed by Massachusetts in 1930, and Kansas with Ohio in 1935 (Paraschos & Amde, 2011). The 'Teens Run Bridge' built in 1938 near Eureka in Gallia County, Ohio, which consists of five continuous reinforced concrete slab spans supported by capped pile piers and abutments, can be considered as the first IAB in USA (Burke, 2009; Card & Carder, 1993). From then on, the IAB construction has spread throughout USA and abroad (Wasserman, 2007). An investigation on the service conditions of IABs was performed in 1999. Although some minor problems such as cracking and settlement of bridge approaches are experienced, bridge owners from USA and Canada rated their in-service performance is at least equal to or better than conventional bridges, (Kunin & Alampalli, 1999, 2000). The National Bridge Inventory database noted that 80% of existing bridges in USA had a total length less than 55m, which are well within the maximum length limit of the IAB. At least 40 states in USA would like to choose the IAB when conditions allow (Mistry, 2005). According to a survey conducted in 2004 (Maruri & Petro, 2005), about 13000 IABs have been designed and built in USA from 1995 and in-service, of which approximately 9000 are FIABs and 4000 are SIABs. Moreover, according to another survey conducted by the University of Maryland in 2009, The IAB has been used in 41 states in USA, among which eight states; such as Missouri, Tennessee, California, Iowa, Illinois, Kansas, Washington, and Wyoming, have more than 1000 IABs in their inventories. Many design guidelines and construction details have been proposed by different departments of transportation in USA, which are mainly involving structural limitations, seismic resistance, design of approach slab and

wingwall, effects of earth pressure behind abutments, pile stresses due to the longitudinal movements of bridges, and so on.

In Canada, the IAB concept was used in Ontario with the first application in 1960 (Husain & Bagnariol, 2000). Nova Scotia and Quebec built their first IABs in 1986 and 1988, respectively. Nowadays, several provinces, such as Alberta, Quebec, Nova Scotia, and Ontario, have accepted the IAB. Most of them have reported satisfactory experiences (Bakeer et al., 2005; Kunin & Alampalli, 2000). Three reports, which get positive experience, were published respectively in 1993, 1996 and 2000 by the Ministry of Transportation of Ontario, Canada to establish a general guideline that can be used to conduct the IAB plan, design, construction and health monitoring. The suitable maximum length limits for the FIAB and SIAB are 100m and 150m, respectively (Husain & Bagnariol, 1996, 1999, 2000; Husain & Farago, 1993). The number of IABs has reached approximately 60% of all bridges built in Ontario until 2005 (Husain et al., 2005). The investigation on the retrofit of existing bridges with the SIAB concept was also conducted by the Ministry of Transportation of Ontario (Husain, 2004; Husain & Bagnariol, 1999), which will be introduced in detail in Chapter 2. A new specified design code 'Alberta transportation bridge structures design criteria v. 7.0 Appendix A: integral abutment design guidelines' was proposed by the Alberta Ministry of Transportation, Canada, which indicates that many prestressed concrete bridges up to 60m with pin connected semi-integral abutments perform very well in Alberta. The maximum length limits in Alberta are 90m and 120m for the symmetrical IAB with steel girder and concrete girder, respectively (Alberta Ministry of Transportation, 2012).

The maximum length of constructed IABs and skew angle limits in different states in USA and provinces in Canada are listed in Table 3, of which the information was summarized from several references (Bakeer et al., 2005; Husain & Bagnariol, 1996; Kunin & Alampalli, 2000; Liu et al., 2005; Olson et al., 2009; Paraschos & Amde, 2011). If the values are different, the maximum one is chosen.

State/Province	First Year Built	Maximum length of constructed IABs (m)	Skew Angle Limit (°)
USA			
Alaska	1975	41 (PCG)	30
Arizona	1975	Discontinued in 1996	
Arkansas	1996	91 (SG)	33

RETROFIT OF EXISTING BRIDGES WITH CONCEPT OF INTEGRAL ABUTMENT BRIDGE

California	1950	122 (CG)	45
Colorado	1905	318 (SG) 339 (PCG) 290 (CG)	No limit
Connecticut	1995	NA	NA
Florida	1989	Discontinued in 1998	
Georgia	1975	92 (SG) 125 (CG)	40
Hawaii	NA	76	NA
Illinois	1983	61 (SG) 92 (PCG) 37 (CG)	30
Indiana	1978	92	30
Idaho	1970	122	30
Iowa	1962	82 (SG) 153 (PCG) 41 (CG)	45
Kansas	1935	137 (SG) 126 (PCG) 178 (CG)	No limit
Kentucky	1970	89 (SG) 122 (PCG) 32 (CG)	30
Louisiana	1989	305	0
Maine	1983	57 (SG) 46 (PCG) 29 (CG)	30
Maryland	1986	16 (PCG)	30
Massachusetts	1930	107 (SG) 85 (PCG) 44 (CG)	30
Michigan	1990	148 (PCG)	30
Minnesota	1958	53 (SG) 53 (PCG) 31 (CG)	20
Mississippi	1945	Discontinued in 1953	
Missouri	1969	183	45
Montana	1970	NA	NA
Nebraska	1977	NA	NA
North Dakota	1960	122 (SG) 122 (PCG) 49 (CG)	30
Nevada	1978	78 (SG) 34 (PCG) 84 (CG)	45
New Hampshire	1992	46 (SG) 24 (PCG)	10
New Jersey	1988	NA	30
New Mexico	1955	NA	NA
New York	1980	93 (SG) 68 (PCG)	45
North Carolina	2006	NA	NA
Ohio	1935	114	30
Oklahoma	1980	92 (PCG)	0
Oregon	1940	336 (PCG)	45
Pennsylvania	1946	122 (SG) 183 (PCG)	20
Rhode Island	2004	NA	NA
South Dakota	1948	113 (SG) 209 (PCG) 107 (CG)	35
South Carolina	2001	153	30
Tennessee	1965	175 (SG) 358 (PCG) 189 (CG)	No limit

Texas	1994	Discontinued	
Utah	1984	92	20
Vermont	1975	24 (SG)	20
Virginia	1982	98 (SG) 236 (PCG)	30
Wyoming	1957	100 (SG) 1227 (PCG) 99 (CG)	45
Washington	1965	183 (PCG)	40
West Virginia	1994	98 (SG) 137 (PCG) 34 (CG)	30
Wisconsin	1960	92	30
Canada			
Nova Scotia	1986	38 (PCG)	NA
Quebec	1988	78 (PCG)	20
Ontario	1960	83	30

Table 3

Information of IAB in USA and Canada

SG: Steel girder; PCG: Precast-concrete girder; CG: Cast-in-place concrete girder

1.3.2.2 Europe

The applications of IABs in Europe are significantly less than those in North American. In order to improve the IAB design and construction, many research works have been started in Europe. For example, the European R&D project “Economic and Durable Design of Bridges with Integral Abutments (INTAB)” was started in 2005 with participants from Germany, Sweden, Belgium and Luxembourg. The object of this research project is to investigate the critical issues of IABs experimentally and theoretically, such as soil-structure interactions, pile systems, approach slabs and so on. Based on the research results, a design guideline for IABs with small and medium spans was proposed (Feldmann et al., 2010). Besides, an international workshop on the IAB was held in Stockholm, Sweden in 2006 in order to share the experience from eight countries and to develop the knowledge of the IAB design, construction, and maintenance (Collin et al., 2006). At the same time, the application conditions and design criteria of IABs in European countries, such as England, Finland, Ireland, Germany, and Sweden, were investigated through a survey conducted in 2007 (White, 2007). Since the IAB is a relatively new concept in Europe, design methods and construction procedures in each country are also different. However, the experience gained from existing IABs indicates that the applications of IABs in European countries are successful. As a result, the trend is toward making the IAB a larger percentage of all newly constructed bridges across Europe (White et al., 2010).

RETROFIT OF EXISTING BRIDGES WITH CONCEPT OF INTEGRAL ABUTMENT BRIDGE

UK started to give efforts on the research on the IAB in the 1970s. An advice note for the IAB “BA 42/96: The Design of Integral Bridges” was published in 1996 and modified in 2003 (Highways Agency, 2003), which described the movements and loads which can be used in design, and provided requirements for some design details. It proposed that the bridges with decks up to 60 meters in length and with skew angles not exceeding 30° are generally required to be continuous over intermediate supports and integral with their abutments. The thermally induced cyclic movements of each abutment should not exceed $\pm 20\text{mm}$. Six typical types of integral abutments can be found in this advice note. Steel Construction Institute proposed another composite highway bridge guideline with a section for the IAB in 2010. In this guideline, the maximum length limit of the composite IAB is 80m. Three different types of integral abutments are proposed for composite bridges, including fully integral framed abutments, fully integral bank pad abutments and semi-integral abutments (Steel Construction Institute, 2010a). A multi-girder two-span IAB was taken as an example to introduce the design process (Steel Construction Institute, 2010b). According to the summary of bridge types in UK by 2005, it indicated that the proportion of IABs increased from about 20% of total bridges in 2000 to more than 50% in 2005. Besides, another survey showed that the total length of the IAB up to 80m is common in UK and a few cases have lengths over 100m.

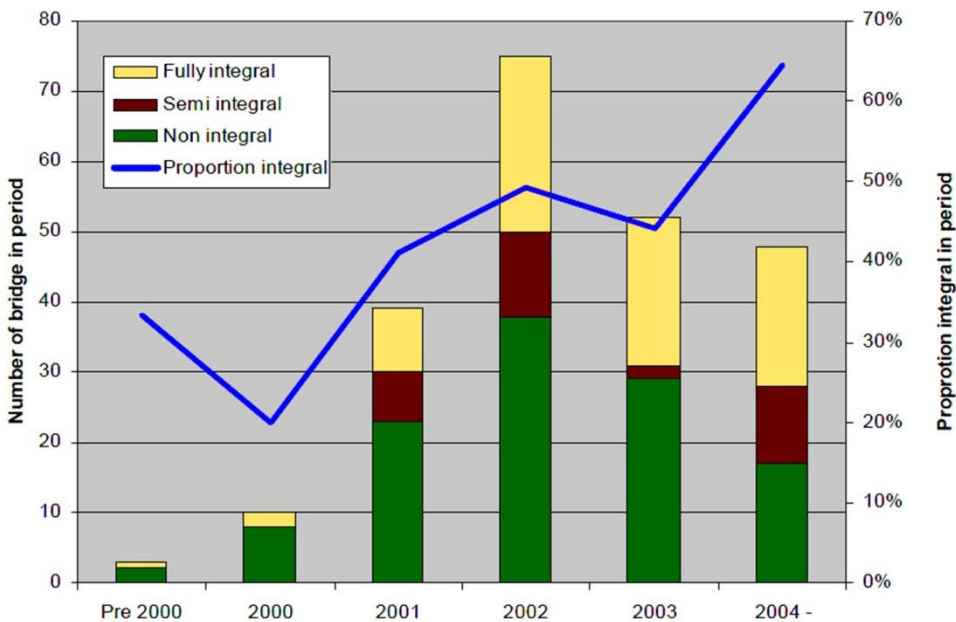


Fig. 18 Summary of bridge types in UK by 2005 (Iles, 2006)

The IAB can be also found in Ireland. A series of fifteen FIABs were built along the

M50 highway in the west of Dublin, Ireland which is one of the most critical elements of the country infrastructure (Wagle & Watt, 2011). The construction of the fully integral abutment adopted the proposed configurations in UK advice note “BA 42/96: The Design of Integral Bridges”.

In 1999, a list of ten single-span prototype bridges was published and recommended by the German Federal Ministry of Transport, Building and Urban Affairs (BMVBS). Eight of them were FIABs with a maximum span length of 45m. However, many of the BMVBS recommendations were withdrawn and replaced by the Eurocode based DIN Fachbericht 101 to 104 in 2003, where no specific rules concerning the IAB can be found. As a result, the IAB design only depends on the experience of designers, which leads to the fact that just a small group of engineering companies have specialized in the FIAB in Germany (Feldmann et al., 2010). The usual slenderness of girder in the FIAB for road and railway is shown in Fig. 19 (Braun et al., 2006b).

Type of bridge	L/h Abutment	L/h Field	L/h without taper
Road Bridges			
Concrete	12-18	20-25	18-21
Prestressed Concrete	15-19	24-30	20-25
Composite	15-19	25-35	21-25
Railway Bridges			
Concrete	10-15	20-25	16-18
Prestressed Concrete	not common		
Composite	15-18	25-30	18-21

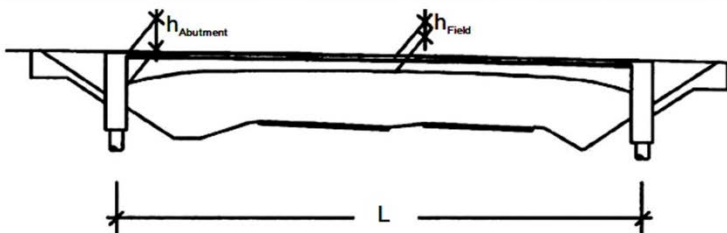


Fig. 19 Usual slenderness of girder in FIAB in Germany (Feldmann et al., 2010)

A survey indicated that IABs in Germany are usually medium or short span bridges. Only 2.1% of the highway bridges with large span, which exist in state of Bavaria, were FIABs or SIABs. However, 78% of them were built in the last ten years, which means that the IAB is becoming more and more important in Germany (Schiefer et al., 2006). Another investigation on the bridge types in Germany from 1840 to 2000 is illustrated in Fig. 20, which indicated that the FIAB construction started from 1960 and its applications increased quite fast from 1960 to 2000 (Marx & Seidl, 2011).

RETROFIT OF EXISTING BRIDGES WITH CONCEPT OF INTEGRAL ABUTMENT BRIDGE

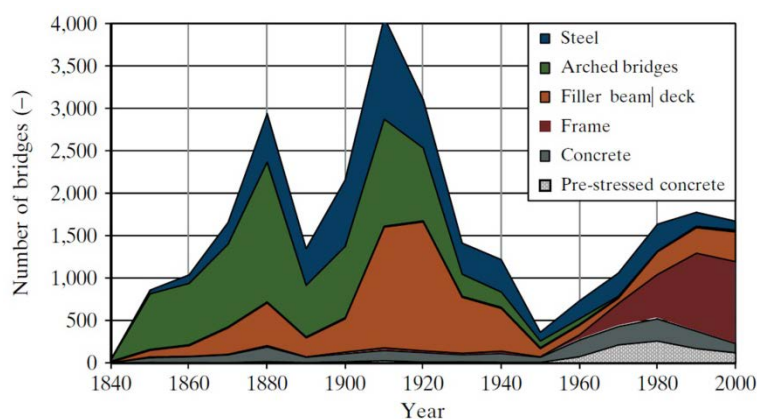


Fig. 20 Bridge types in Germany from 1840 to 2000 (Marx & Seidl, 2011)

The IAB concept has also become more and more important in Austria. However, due to different climatic conditions, regulations and empirical values, the international concepts and guidelines of IABs might not be applied directly in Austria. Some research projects were carried out experimentally and numerically in order to understand the performance of the IAB and propose the specified Austrian guideline for the IAB. Among them, a research project supported by the Austrian Ministry for traffic Information and Technology (BMVIT) and Autobahn and high way financing stock corporation (ASFINAG) was carried out which is focus on the loading bearing capacity of the IAB (Geier, 2010).

The concrete IAB have a long-lasting tradition in Switzerland (Kaufmann & Alvarez, 2011). Most of them were constructed during the main construction period of the national motorway network (1960–1985) with reinforced concrete or prestressed concrete girders. The first specific provision for the IAB ends was proposed in Swiss Federal Roads Office Guidelines (edition 1990). It specified the maximum length limit of the FIAB which can be up to a range of 30–60m depending on the road type and other factors, and the maximum length limit of the SIAB which can be up to 100m according to some specific provisions proposed by different Swiss cantons. Nowadays, the concrete IAB has become well-established construction types in Switzerland and more than 40% of the existing bridges on the Swiss Federal Roads Office network are IABs. Moreover, many existing IABs have exceeded the stipulated maximum length limit. The experience obtained from the usage of these bridges is mainly positive from both construction and maintenance points of view. The Swiss Federal Roads Office Guidelines was revised in 2010, which summarizes the performance of the IAB, provides detailed abutment configurations for the FIAB and the SIAB, and gives comprehensive advices on the selection of the appropriate abutment type. The definitions of the IAB and its subtypes proposed in revised

guidelines are shown in Fig. 16 (p.16).

The IAB came into use in Poland quite early, which can date back to the 1930s. However, due to the limited knowledge of this bridge type at the beginning, engineers did not consider soil-structure interactions and drainage systems in the design, which produced many problems. Nowadays, the applications of IABs in Poland are still limited. Moreover, there are neither length limitations nor recommendations (Feldmann et al., 2010).

The IAB is also used in North Europe. In Sweden, the integral reinforced concrete slab frame bridge has been constructed frequently for over 70 years. It can be considered as one of the most common bridge types with the number of 8000 out of 14000 of total bridges owned by the Swedish Road Administration. Bridges with integrated breast walls are also commonly used with the maximum length limits up to 80m for reinforced concrete bridges and up to 60m for composite bridges (Flener, 2004). In Finland, according to the statistic by the Finnish Road Administration in January 2004, the percentage of IABs in all bridges increased from only 3.6% before 1984 to 17.6% from 2000 to 2004, as listed in Table 4. The maximum length limits for the IAB are 70m and 90m in the case of normal symmetrical and light symmetrical road bridge, respectively (Kerokoski, 2006).

Year of Construction	Number	Percentage of all bridges (%)
Before 1984	279	3.6
1985-1989	130	15.3
1990-1994	201	16.1
1995-1999	111	14.4
2000-2004	75	17.6

Table 4

IABs owned by Finnish Road Administration until 2004 (Kerokoski, 2006)

As mentioned above, the IAB concept is usually used in short or medium span bridges in North Europe. In Finland, according to the Finish bridge design guideline, the maximum length limits for the IAB are 35m in the case of a normal road bridge and 45m in the case of a light traffic bridge (Kerokoski, 2006). In Sweden, the FIAB are usually with short spans and the SIAB are used in the bridges with medium span (Feldmann et al., 2010). According to a survey on the IAB conducted in 1991, the appropriate length limits for concrete and steel-concrete composite integral bridges with end screens in Sweden are up to 90m and 60m in warmest region and 60m and 40m in coldest region, respectively, as listed in Table 5 (Flener, 2004; Hambly, 1997).

	Concrete	Steel-concrete composite
Warmest region	90m	60m
Coldest region	60m	40m

Table 5

Appropriate length limits for integral bridges with end screens in Sweden (Hambly, 1997)

Due to the contributions of researchers and engineers from Luleå University of Technology, Sweden, a specified guideline for the IAB has been developed, which can simplify the conventional design process and be applied in practice (Collin et al., 2006; Feldmann et al., 2010; Hällmark, 2006; Nilsson, 2008; Pétursson et al., 2011; Tlustochowicz, 2005).

The IAB was also constructed in Spain (Kovac, 2010). A guideline for the IAB design and construction was published in Spain called “Guía para la concepción de puentes integrales en carreteras” in 2000. This guideline presents several applications, constructed examples and design procedures of IABs in worldwide (Fomento, 2000). The horizontal displacement limit of abutment is up to 30mm, which means that the corresponding maximum length limit is up to about 100 m and the skew angle limit is 60 degrees (Rodriguez et al., 2011). Some engineers apply the IAB concept to high-speed railway viaducts in Spain. Though a series of numerical and experimental analyses, it outlines that the FIAB is a suitable design for the high-speed railway viaduct (Rodriguez et al., 2011; Rui-Wamba et al., 2011).

The applications of IABs in Italy are in primary stage and there is still no specified design or construction code for the IAB. However, some researchers and engineers start to apply the IAB concept not only to newly constructed bridges, but also to the retrofit of existing bridges. The newly constructed IABs included the new steel-concrete composite integral bridge over the A22 motorway at the new tollbooth of southern Trento (Briseghella et al., 2004; Briseghella & Zordan, 2004), and two FIABs at Milano Malpensa Airport which have a peculiar geometry (transverse width of the deck is much higher than the span) and are subjected to an unusual magnitude of service loads (Airbus 380 Class aircrafts) (Gherardi, 2010; Malerba & Comaita, 2011; Malerba & Comaita, 2012). According to the analysis by Torricelli et al. (2012), some advantages in using integral scheme for Italian highway overpasses were evaluated. Based on two different span organizations of IABs provided for Italian highway overpasses, as illustrated in Fig. 21, a procedure for structural analysis of the IAB was proposed which can simplify the IAB by separating it to two subsystems, which are the deck and the soil-abutment wall. Then, a

comparison between IABs and traditional bridges has been carried out and the main results highlight the benefits in using integral configurations.

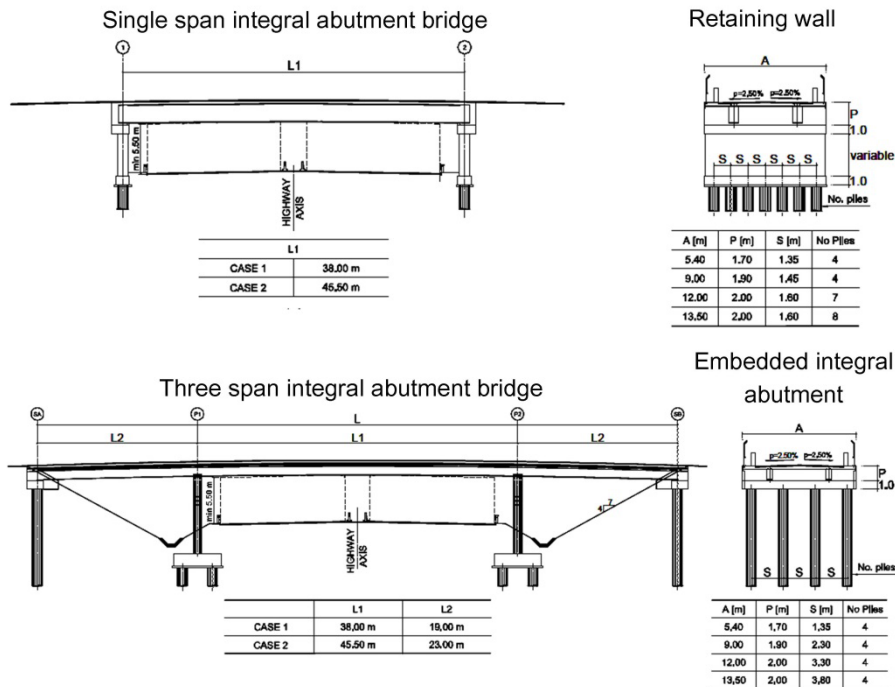


Fig. 21 Selected IAB configurations for Italian highway overpasses (Torricelli et al., 2012)

For the retrofit of existing bridges, the 'Isola della Scala Bridge' in Verona is the most excellent example, which is the longest FIAB in the world up to now with 13 spans and total length of approximately 400m (Zordan & Briseghella, 2007; Zordan et al., 2011a, b). The other example is a SIAB "Treviso Bridge" transformed from a prestressed concrete beam bridge by using the approach of micro-pier groups (Russo et al., 2009). The detailed information of these two bridges will be described in Chapter 2.

1.3.2.3 Asia and Oceania

China began to build IABs at the end of the 1990s. The first application was a SIAB in Hunan constructed in 1998 (Zhang & Ning, 1998). The first FIAB 'Sijiu Bridge' was built in 1999, in Guangdong, with the total length of 75.48m and skew angle of 15 degrees (Ma & Jin, 2002). In 2004, the longest FIAB 'Shangban Bridge' in China was constructed in Fujian with 4 spans and the total length of 137.1m (Hong & Peng, 2004). Besides, the SIAB concept was applied to a retrofitting project 'Longtan Bridge' in 2005, which will be introduced in Chapter 2 (Jin et al., 2005). Although,

RETROFIT OF EXISTING BRIDGES WITH CONCEPT OF INTEGRAL ABUTMENT BRIDGE

there are many IABs designed and constructed in China (as listed in Table 6) (Hong & Peng, 2004; Jin et al., 2005; Jin et al., 2004; Ma & Jin, 2002; Qian, 2002; Zhang & Ning, 1998; Zhang, 2002), there is still no specified design or construction guideline for the IAB.

Name	Location	Year	Length (m)	skew angle (°)	abutment type
Overpass	Hunan	1998	56m (11.4+33.2+11.4)	NA	Semi-integral abutments
Changsha City Viaduct	Hunan	1999	171m (14+2X20+25+4X20+12)	Curved bridge	one fully integral abutment and one abutment with expansion joint
Baozhengang bridge	Shanghai	1999	68 (2X12+20+2X12)	10	Semi-integral abutments
Sijiu Bridge	Guangdong	2000	52m (10+2X16+10)	15°	Fully integral abutments
Liguanhe Bridge	Henan	2000	48m (3X16)	15°	Semi-integral abutments
Shilonghe Bridge	Henan	2000	64m (4X16)	15°	Semi-integral abutments
Shangban Bridge	Fujian	2004	120m (4X30)	0°	Fully integral abutments
Najiao Bridge	Guangxi	2005	80m (4X20)	NA	Semi-integral abutments
Dashuiting Bridge	Henan	2005	64m (4X16)	35°	Semi-integral abutments
Dapu D-Ramp Bridge	Henan	2005	75m (3X25)	Curved bridge	Semi-integral abutments
Longtan Bridge	Guangdong	2006	109.2m (2X11.4+11.1+11.65+4X9.15+13.55+13.5)	NA	Semi-integral abutments

Table 6
Information of IAB in China

The applications of integral bridges and composite bridges which can eliminate

expansion joints were developed after World War II in Japan (Takano, 1994). However, compared with UK and North America, the IAB in Japan is not popular, due to its uncertain mechanical behaviors during a strong earthquake and no specified design code (Iwasaki et al., 2011). However, the number of IABs is increasing, because of its cost efficiency and maintenance friendliness (Akiyama, 2008; Nakamura et al., 2002). Based on two surveys on bridges without expansion joints conducted respectively in 1991 and 1993, the design and construction manual which can be used to eliminate expansion joints in existing bridges was published in 1995 (Road Management Technology Center, 1995). From then on, many single-span IABs, so-called portal rigid frame bridges, were designed and constructed in Japan. NEXCO companies (East, Central and West Nippon Expressway Corporation) specify this bridge type in their design guidelines. In addition, the Public Works Research Centre and Nippon Steel Corporation are proposing a guideline which can be used to plan steel integral bridges with not only single span, but also multiple spans (Akiyama, 2008).

The applications of IABs can be also found in Australia. Since 1963, 41 IABs have been built in New South Wales, of which most were constructed by widening or duplicating the existing short concrete bridges built between 1930 and 1960. The maximum lengths are 54m for precast concrete girder, 27m for cast-in-place concrete girder, and 19m for steel girder (Franco, 1999). One special kind of IAB, in which superstructure-abutment spaces are filled with compressible material, girder-girder spaces are filled with cement mortar and superstructure-pier joints connected by anchor bolts, was built by the Queensland Main Roads Department. According to a survey, it could be found that approximately 200 IABs of this type have been constructed since 1975. The design of this bridge type become standardized in Queensland, with the typical length of 40–70m. Based on observed behaviors of existing bridges and publications that outline experiences from USA, the maximum length limit can be increased to 100m (Franco, 1999). However, there is still no particular section for the IAB in the Australian Bridge Design Code. Designers must refer to the general design requirements contained in the code and relevant specialized literatures (Connal, 2004).

New Zealand's experience with the IAB began in the 1930s through building some short concrete IABs. By the 1950s, the IAB was commonly used in New Zealand. The New Zealand Ministry of Works and Development (NZMWD) developed some standardized design configurations for concrete IABs. The prestressing approach was used by the NZMWD to strengthen several existing concrete IABs for exceptionally heavy loads. In the 1960s, New Zealand started to construct the SIAB.

RETROFIT OF EXISTING BRIDGES WITH CONCEPT OF INTEGRAL ABUTMENT BRIDGE

The maximum length limit of the SIAB is usually 70m, except the 'Kauaeranga Bridge' that has a total length of 136m. The performance of the 'Kauaeranga Bridge' was monitored by the NZMWD in order to check the feasibility of length limit increasing. The results indicated that both SIAB and FIAB are very economical due to the simplicity of abutment construction and the elimination of expansion joints (Franco, 1999).

There are also some applications of IABs in other Asian countries, such as India, Malaysia, Singapore and South Korea (Jayaraman & Merz, 2001; Masrilayanti & Weekes, 2012; Tandon, 2005; Tandon, 2006).

1.3.3 Attributes and opening issues of IAB

According to the applications of IABs mentioned above, it proves that the IAB is becoming a popular structure because it has much more attributes and fewer limitations than conventional bridges with joints, as listed in the following (Alberta Ministry of Transportation, 2012; Burke, 2009; Geier, 2010; Tlustochowicz, 2005).

1.3.3.1 Advantages

Primarily, the IAB can eliminate many problems associated with expansion joints and bearings, such as low construction and maintenance costs, easy construction based on less tolerance restrictions, improved vehicular riding quality due to continuous paving, few unconformable feeling caused by damaged expansion joints, limited traffic interruptions or restrictions due to refurbishment, and so on.

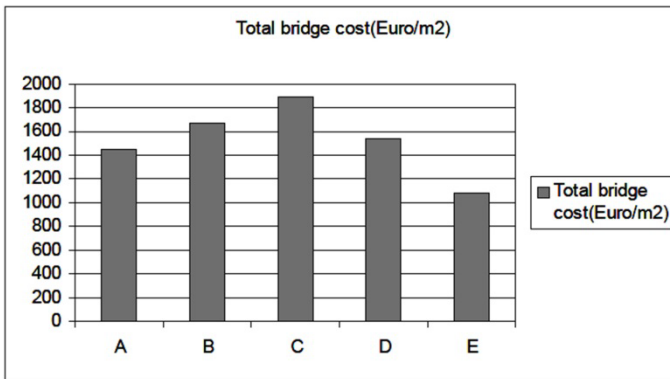
The economics of the IAB can be proved through some experience from real applications as introduced in the following.

Taking the SIAB 'Shilonghe Bridge' in China as example, the economic analysis was carried out. Comparing the SIAB with a conventional bridge with joints, it indicated that the initial construction costs of both solutions are nearly the same; however, the maintenance cost of the SIAB would be significant less than those of the conventional bridge with joints. Considering the bridge service life as 50 years, the maintenance cost of the SIAB can save approximate 600000¥ (Zhang, 2002).

According to the experience in Germany and Austria, approximately 1-3% of the construction cost need to be spent for the retrofit of existing structures every year (Geier, 2010). Choosing the IAB can save the maintenance cost of expansion joints,

bearings and approach structures, which is at least 12% of the annual maintenance cost. Furthermore, the high cost produced by water entering into superstructures, bearings and bridge seats, and traffic interruptions which are difficult to evaluate can be avoided (Braun et al., 2006a).

An investigation on the total costs of bridges with five optional foundations is shown in Fig. 22 (Pétursson & Collin, 2006). The comparison results indicated that the bridge with integral abutments could be considered as the most economical solution.



*A is Bridge founded above ground water level,
B is Bridge founded under ground water level
concrete cast in the water
C is Sheet pile wall and unreinforced bottom layer of concrete preventing water intrusion
D is Elevated foundation
E is Integral abutments*

Fig. 22 Investigated total costs of bridges with different optional foundations in Northern Sweden (Pétursson & Collin, 2006)

The economic analysis of the IAB is also conducted in Sweden. Two different solutions of a bridge constructed across the 'Leduån' river in the north of Sweden are compared. The first one is a two-span concrete bridge with one internal support in the river and concrete piles driven into the ground. The second one is a single-span composite IAB, with vertical steel piles. Based on a life cycle approach that can consider the estimated overall performance of both bridge solutions, the comparison analysis was carried out. It indicated that both construction and maintenance costs of the first solution are larger than those of the second one. The detailed maintenance costs of both solutions are listed in Table 7 (Nilsson et al., 2008).

Maintenance activity	Unit cost	Start year	End year	Frequency
One-span composite IAB				
Inspection of bridge	320 €	6	96	6
Painting of steel structure	37800 €	30	90	30
Replacement of edge beams	51320 €	30	90	30
Two-span concrete bridge				

RETROFIT OF EXISTING BRIDGES WITH CONCEPT OF INTEGRAL ABUTMENT BRIDGE

Inspection of bridge	375 €	6	96	6
Painting of steel structure	1260 €	30	90	30
Replacement of edge beams	60710 €	30	90	30
Cleaning of joint	100 €	1	99	1
Replacement of rubber band	2625 €	10	90	10
Replacement of steel profile	11025 €	20	80	20

Table 7

Maintenance costs of IAB and conventional bridge (Nilsson et al., 2008)

The economic analysis of a steel-concrete composited bridge with single span of 38m and width of 13.5m was conducted in Italy (Torricelli et al., 2012). Two different bridge types are considered, which are the traditional bridge and IAB, respectively. The comparison listed in Table 8 indicated that the weight of steel beams in the IAB is lighter (about 15%) than those in the traditional bridge; however, the concrete slabs in the IAB require more steel reinforcements (about 58%) than those in the traditional bridge. The abutments in the IAB can be designed as slender as well; however, they also require to be strongly reinforced. Moreover, the piles in the IAB are less and smaller than those in the traditional bridge, but they need a greater amount of steel reinforcements. In conclusion, choosing the IAB can totally save about 30% comparing to the traditional bridge.

Comparison		IAB	Traditional bridge
Deck	Steel beam	190kg/m ²	220kg/m ²
	Concrete slab	155m ³	150m ³
	slab steel reinforcement	135kg/m ²	85kg/m ²
Abutment	Concrete	80m ³	160m ³
	Formworks	230m ²	180m ²
	Steel reinforcement	610kg/m ³	415kg/m ³
Pile wall	Concrete	195m ³	495m ³
	Steel reinforcement	110kg/m ³	80kg/m ³

Table 8

Comparison between traditional bridge and IAB in terms of steel and concrete design amounts.

According to a statistic in USA, 30 of 35 response states responded that the construction cost of IABs are not higher than those of conventional bridges, and all response states indicated that the maintenance cost of IABs are less than those of conventional bridges (Paraschos & Amde, 2011).

From the structural point of view, the IAB has many attributions. The reserved load capacity can be increased because it can resist potentially damaging overloads by distributing loads along the continuous and full depth diaphragm at bridge ends. The live load distribution can be optimized. The service load stresses of the superstructure by connecting integrally with abutments and piers can be reduced. The risk of abutments instability can be avoided by using integral abutments. The number of foundation piles can be reduced. The slender and aesthetically appealing superstructure can be constructed due to the restraint in the abutments. The interior span to end span ratio can be increased to allow longer interior spans.

In addition, the construction of IAB is faster, because of the combination effect of few parts, simple members, few materials, broad tolerances, few construction joints, avoidance of labor-intensive practices, simple beam seats, the dry construction (most concrete work is done above stream water levels), and so on. All these features make the completion of such structure in a single short construction season, as illustrated in Fig. 23.

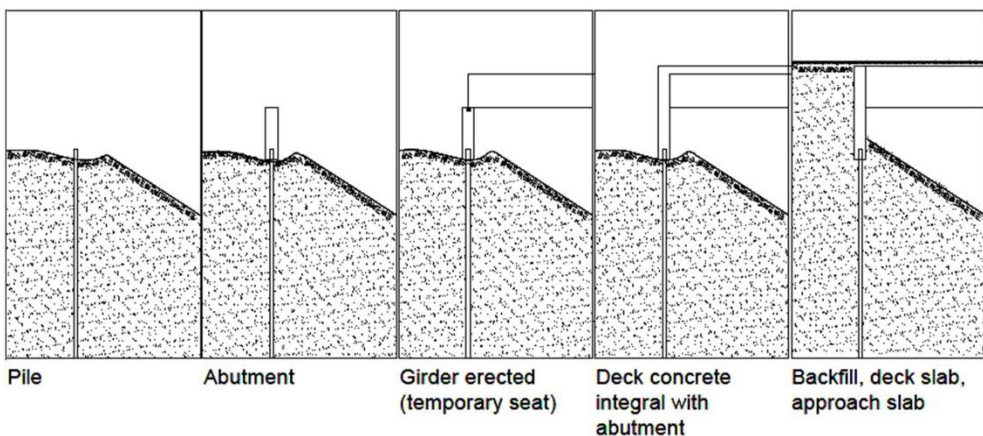


Fig. 23 Typical construction phases of IAB (Lan, 2012)

The widening and replacement of the IAB are simple, because of not only its rapid construction, but also the fact that some components can be reused. For example, the substructure can be recapped or, if necessary, they can be withdrawn or left in place.

The earthquake resistant can be improved, because the superstructure in the IAB is connected to abutments and embankments, which can become one part of the earth and move with the earth during earthquakes. The most common cause of damage to SSBs in seismic events that is loss of girder support can be eliminated in IABs.

From the environmental point of view, the influence of bridge can be reduced by choosing the IAB. A bridge designed for a service life of 120 years in Sweden was chosen to conduct the environmental Life Cycle Analysis (LCA) by Nilsson et al. (2008). Two bridge types were considered, including the composite IAB and the concrete conventional bridge with joints. The normalized results of the life cycle analysis using three damage categories for each solution are illustrated in Fig. 24, which indicated that the composite IAB have a better environmental performance in every damage category than the concrete conventional bridge with joints.

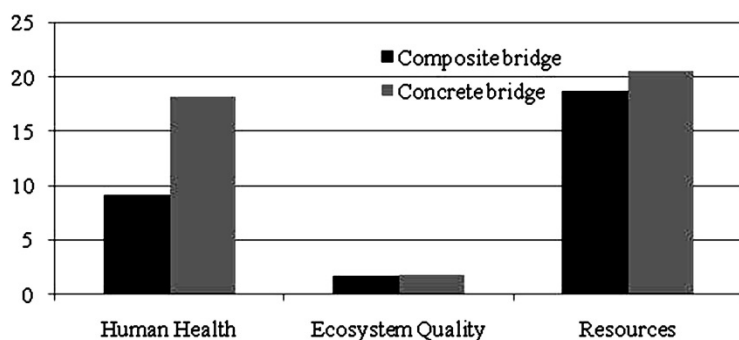


Fig. 24 Total damage analysis per bridge solution (Nilsson et al., 2008)

1.3.3.2 Opening issues

Despite the significant attributes of the IAB mentioned above, there are still some limitations and uncertainties that need to be resolved and recognized, as listed in the following.

One of the most critical limitations of the IAB is the soil-structure interaction. The IAB is fundamentally geotechnical in nature and needs to be analyzed by both structural and geotechnical engineers. Current IAB design mostly depends on the idealized or simplified soil-structure interaction relationships, which probably cannot accurately reflect the true interaction between abutments or piles and soil, especially the long-term behavior, cyclic behavior due to temperature variations and dynamic behavior caused by earthquakes. The IAB cannot be constructed on weak embankments or subsoil

The expansion joints are eliminated or reduced in the IAB. Therefore, the secondary stresses in superstructure caused by shrinkage, creep, thermal gradients, differential settlement, differential deflections, and earth pressure in the IAB are

larger than those in the conventional bridge with joints. These secondary stresses can create some cracks that need to be paid more attention to. Consequently, the maximum length and skewed angle are limited

Except for piles and abutment wingwalls, the other components in the IAB are subjected to stress at the same level. The cyclic elongation and contraction of the bridge structure due to temperature variations may create high stresses in piles. These stresses can form the plastic hinges in the piles and may reduce their axial load capacities. The abutment wingwalls may crack due to the rotation and contraction of the superstructure.

The approach slab is another weakest element in the IAB constructed between bridge ends and pavements. Due to cyclic lengthen and shorten in response to temperature and moisture variations and the backfill settlement, the approach slab is easy to fracture or crack progressively or abruptly.

The construction sequence should be controlled, such as the sequence of embankment placement and pile driving, the sequence of continuity connection placement and deck slab casting, and the sequence of continuity connection placement and approach slab casting.

1.4. Critical issues and solutions

1.4.1 Critical issues

As introduced above, the newly constructed IAB has been used all over the world. Furthermore, it has numerous attributes and few limitations. However, whether this excellent bridge type can be applied to the retrofit of existing bridges and how to do it need to be investigated.

The soil-structure interaction, which does not need to be considered in the existing SSB, should be considered in the IAB. What is the real soil-structure interaction and how to simulate it in the IAB have remained largely unknown.

Different connection approaches between the superstructure and the substructure in the IAB, as listed in Table 2, will correspondingly produce different levels of the connection flexibility. Which one is the most suitable solution is a critical problem worth studying.

In order to design a reasonable and economical retrofitting process, existing bridge components should be reused as many as possible to reduce retrofitting difficulties, periods and costs. Whether the existing bridge components can be reused after retrofitting is a critical issue, especially the substructure.

To maximize benefits from the IAB, the simple and direct way is to apply it not only in newly constructed bridges, but also in the retrofit of existing bridges. Before that, the stated structural problems need to be resolved.

1.4.2 Solutions

In order to resolve the critical issues listed above, some solutions are listed in following.

1. Survey on the retrofitting projects with the IAB concept in worldwide, including the retrofitting motivations, detailed processes and the structural performance after retrofitting.
2. Conduct the literature review on the critical issues of analysis on the IAB, such as soil-structure interactions, modeling approaches and plastic hinge simulations, was conducted in order to find out the most suitable method that can be used to model both bridges before and after retrofitting.
3. Propose the approximate finite element model, which involves soil-structure interactions, non-linear behaviors and retrofitting processes.
4. Compare the original and updated Italian design codes through static analysis and seismic analysis in order to find the suitable design code.
5. Perform a large number of parametric analyses taking thermal actions; bridge types; soil conditions and substructure heights as parameters. Analyze the responses of girders, piers, abutment stems and piles in order to find some important factors and the corresponding influence, which could be adopted to guide the retrofitting technique with the IAB concept.
6. Conduct the verification in order to check if the existing sections can be reused without any changes and point out the most critical components that need to be repaired or replaced.

7. Investigate the dynamic performance of bridge before and after retrofiting through modal analysis and response spectrum analysis.

1.5. Layout of the thesis

Besides this chapter, in the main body of the thesis, it consists of seven chapters, from Chapter 2 to Chapter 8 that introduced as following:

Chapter 2 states a literature survey on the real retrofiting projects with the IAB concept in worldwide. The retrofiting motivations, detailed processes and the structural performance after retrofiting are summarized.

Chapter 3 conducts another literature review on the critical issues of analysis on the IAB, such as soil-structure interactions, modeling approaches and plastic hinge simulations, in order to find out the most suitable method in modeling.

Chapter 4 proposes the detailed retrofiting processes with the FIAB concept used in this paper. Four different subtypes of FIAB can be obtained by choosing different techniques to form the flexibility of superstructure-pier and superstructure-abutment connections, including hinged connections and rigid connections.

Chapter 5 introduces a case study on the performance of an existing simply supported bridge, which can be retrofitted with the FIAB concept. The finite element model of this bridge is built, involving the critical issues analyzed in Chapter 3. The original and updated design codes are compared firstly in order to find the suitable one. The necessity of considering soil-structure interactions in the IAB is verified.

Chapter 6 presents a large number of sensitive analyses using the finite element model introduced in Chapter 5. The influence of different thermal actions, bridge types, soil conditions and substructure heights is analyzed. Some important factors and the corresponding influence can be found, which could be adopted in the guideline for retrofiting existing simply supported bridges with the IAB concept.

Chapter 7 conducts the static performance check of different bridge components after retrofiting using F_A -M domain. Some components that cannot be reused without any changes after retrofiting are pointed out. The horizontal displacement in the IAB transferring from bridge ends to approach slabs is estimated, which can help

engineers choose the appropriate approach slab.

Chapter 8 investigates seismic performance of bridges before and after retrofitting through modal analysis and response spectrum analysis. The most important factors and their influence corresponding to the seismic load can be found.

At the end, the main findings and conclusions drawn from the research and the recommendations for the future investigation will be presented.

2. STATE-OF-ART: RETROFIT WITH IAB CONCEPT

The IAB is an advantaged bridge type which is less expensive to construct, easier to maintain and more economical to retrofit over its service life. Due to these advantages, the IAB concept has been applied to many newly constructed bridges all over the world and is becoming highly attractive to designers, constructors and road administrations (Feldmann et al., 2010). Moreover, the IAB concept could be used not only in the construction of new bridges, but also in the retrofit or replacement of existing bridges (Burke, 2009; Mistry, 2005). To the author's knowledge, some existing jointed bridges have been retrofitted or replaced with the IAB concept in worldwide, which will be introduced in this chapter. Based on these real applications, the advantages of using the IAB concept in the retrofit of existing bridges are summarized. Simultaneously, some opening problems are also proposed which need to be paid attention to.

2.1 Applications in North America

2.1.1 USA

The trend of transforming existing bridges with non-integral abutments to SIABs or FIABs has begun in USA, due to the increasingly substantial damages caused by pavement growth and pressure, de-icing chemical deterioration, or both. The idea of using the IAB concept instead of repairing or replacing damaged expansion joints, bearings or bridge seats has been widely accepted by many departments of transportation in an effort to resolve durability problems, reduce the maintenance cost and remain the service life of existing bridges (Burke, 2009; Mistry, 2005). A survey on the elimination of expansion joints in existing steel bridges in USA and Canada was conducted by the Rhode Island Department of Transportation in 1995, which indicated that the IAB concept is applied to retrofit existing steel bridges in Colorado, Tennessee, Kansas in USA and Ontario in Canada (Tsiatas & Boardman, 2002). Another survey was conducted by Kunin & Alampalli (2000). The results showed that the retrofitting method, which can convert conventional non-integral abutments into integral abutments has been carried out in Colorado, Tennessee,

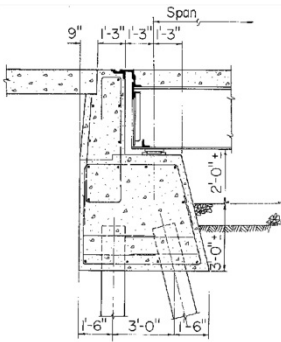
RETROFIT OF EXISTING BRIDGES WITH CONCEPT OF INTEGRAL ABUTMENT BRIDGE

Illinois, Kansas, Oklahoma, South Dakota, Wyoming and North Dakota; however, in Massachusetts, new integral abutments are constructed behind existing abutments, which remain in place to retain fill. According to the statistic in 2004, it could be found that 39% of the states in USA had a policy of transforming non-integral abutment bridges into IABs during retrofitting phases. Many states declared that the IAB shall be considered as the first choice in designing new bridges or retrofitting existing bridges (Maruri & Petro, 2005). Missouri noted that the retrofitting method with the IAB concept could be only considered on bridges with short spans and small skew angles. Virginia and South Dakota tried to incorporate this retrofitting approach with major superstructure replacement projects such as deck replacement or if there are severe problems at abutments. New Mexico indicated that the retrofitting method with the SIAB concept is very common and the bearing selection is a critical issue (Maberry et al., 2005). Through a large number of studies, Burke (2009) found that the SIAB concept has been used most often to retrofit existing single- or multi-span moderate length continuous bridges with expansion joints over rigid abutments.

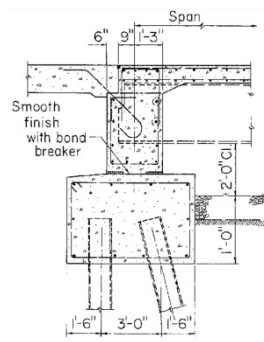
In order to find some suitable candidates which can be retrofitted with the IAB concept, the following considerations should be determined, including continuity methods, curved bridge alignment, skew angles, symmetry of forces, rotational tendencies of semi-integral superstructures, wingwall orientations, stability, secondary forces and so on (Dickson et al., 1996). Among them, some considerations were introduced in detail. For the superstructure continuity, the following issues should be noted. For example, the expansion joints over piers should be eliminated, bolted splices can be used to replace the original pins in existing bridges during deck retrofitting, and integral deck slabs seems to be not a good idea for long bridges. Moreover, the existing foundation type is quite important. When the existing abutments is supported by multi-row piles or a spread footing on soil or rock, the SIAB concept can be considered as the most suitable retrofitting method or the existing foundation can be replaced by single-row piles. The fully integral pier should be avoided in order to achieve the stability of the IAB. Mr. Tom Bolte from Burgess & Niple, Ltd. described some examples of retrofitting existing bridges to SIABs or FIABs.

The retrofitting method, which can by convert conventional non-integral abutments into integral abutments is suggested by the Ohio Department of Transportation to resolve the bridge diseases caused by expansion joints and bearings (Ohio Department of Transportation). Some detailed retrofitting configurations using the IAB concept are illustrated in Fig. 25(a), (b) and (c) (Burke, 2009). Fig. 25(a) and (b) show two retrofitting procedures, which can transform existing very short or normal

continuous bridges with non-integral abutments to FIABs. Fig. 25 (c) illustrates the retrofitting procedure, which can convert single- or multi-span continuous with non-integral abutments to SIABs.

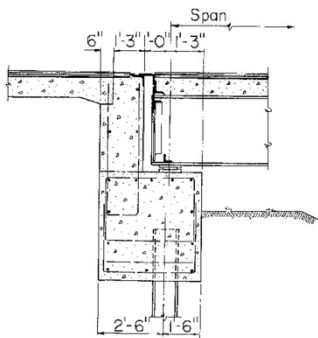


Existing structure

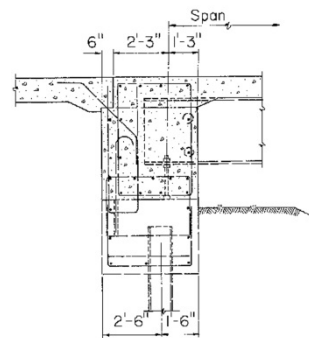


After rehabilitation

(a) Conversion of existing very short continuous bridges with non-integral abutments to FIABs

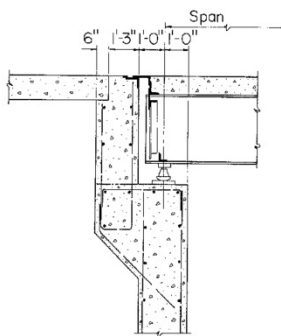


Existing structure

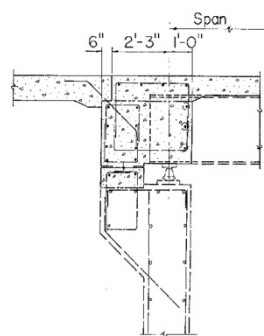


After rehabilitation

(b) Conversion of existing normal continuous bridges with non-integral abutments to FIABs



Existing structure



After rehabilitation

(c) Conversion of existing continuous bridges with non-integral abutments to SIABs

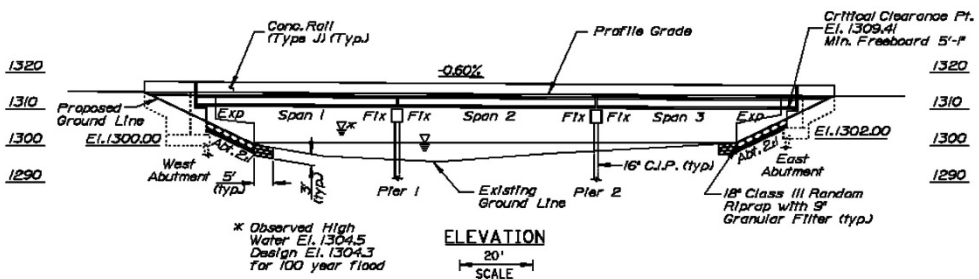
Fig. 25 Conversion of existing continuous bridges with non-integral abutments into IABs by Ohio Department of Transportation in USA (Burke, 2009)

The retrofitting approach with the IAB concept has been applied to many real projects in Ohio. For example, the 'USR I-77, SR 18 Bridge' built originally in 1957 was widened and retrofitted with the FIAB concept in 1972, and the 'SR 771, Big Branch Creek Bridge', which was a single-span bridge with expansion joints over abutments, has been transformed into a SIAB (Burke, 2009). Another two retrofitting projects with the SIAB concept were carried out, which are the "FRA-270-3.09 Bridge" and the "OTT-Lightner Road Bridge" (Bakare).

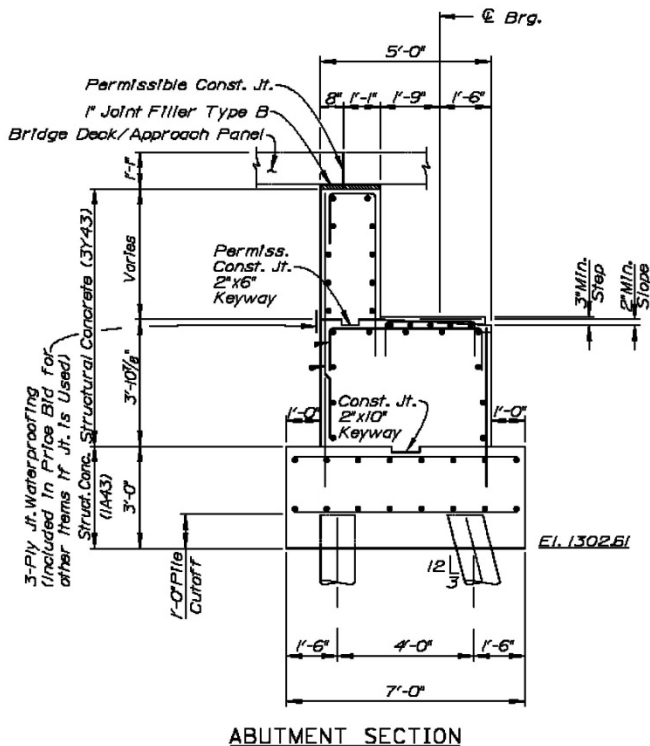
In Minnesota, the IAB concept was used in a special retrofitting case study (Wetmore & Peterson, 2005). The existing bridge 'Bridge Number 04519' needed to be replaced because the narrow bridge and approach slabs are narrow; the profile cannot meet the sight distance requirements and so on. Through comparing several design schemes, the solution of a prestressed concrete beam bridge with pile bent piers, semi-tall parapet abutments and expansion joints over abutments, was chosen. The proposed bridge has three spans with the total length of 51m. The bridge elevation and the abutment details are illustrated in Fig. 26.

After the final design, the 'Bridge Number 04519' was requested to make a change by the Beltrami County Engineer. They want to eliminate the expansion joints over abutments in order to reduce the maintenance cost. Several methods could be to achieve this requirement. The first method is to revise the bridge length to accommodate the usual length for the IAB with short abutments. In this case, all abutment drawings needed to be redesigned which would cost much time and expense, and abutment wingwalls could be changed to a more flexible type that needed to re-grade approach embankments and resulted in additional wetland impacts. Consequently, this solution was denied. The second method is to change semi-tall parapet abutments to stiff parapet abutments, and then integrated the abutments with the superstructure to form a FIAB, which is usually used in Tennessee. However, due to the temperature variations in Minnesota is more extreme than those in Tennessee and the limited experience of the IAB in Minnesota, this solution was considered to be too risky. Finally, the solution of using the design details of existing superstructure, bearings, abutments, piers and approach slabs, while moving the expansion joints over abutments to the ends of approach slabs, was proposed. This solution was chosen because it can eliminate the expansion joints over abutments, while minimizing the cost and time of such a significant design change. As a result, the Minnesota 'Bridge Number 04519' adopted a seldom-used approach that takes the advantages of existing bridge elements in developing a SIAB. Through analyzing, the original design of the superstructure and

piers can be reused. The detailed drawing of the semi-integral abutment is illustrated in Fig. 27. The 1-inch layer of joint filler should be placed on the top of abutment backwalls to soften the abutment backwalls and lengthen the distance between differential vertical movement points, which could avoid the cracking on approach slabs. The vertical joints were installed between approach slabs and abutment wingwalls by mounting barriers on the abutment wingwalls. The original design of approach slabs needed to be modified to add small lips and under-drain systems to prevent backfill from water.



(a) Elevation layout



(b) Semi-tall parapet abutment details

Fig. 26 Proposed prestressed concrete beam bridge for 'Bridge Number 04519' (Wetmore & Peterson, 2005)

RETROFIT OF EXISTING BRIDGES WITH CONCEPT OF INTEGRAL ABUTMENT BRIDGE

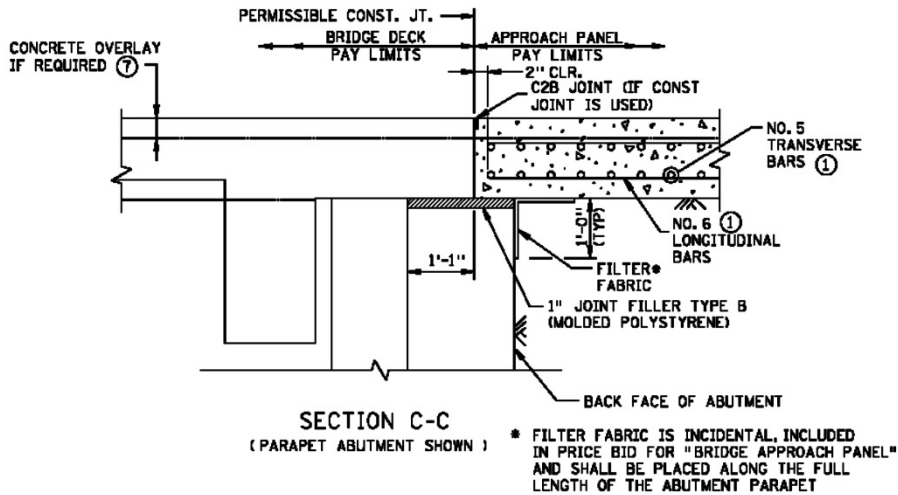


Fig. 27 Semi-integral abutment in 'Bridge Number 04519' (Wetmore & Peterson, 2005)

After opening to public, several field inspections were carried out. The results indicated that the bridge performs as intended. However, some noted deficiencies should be paid attention to. Some cracks radiated from the top flange edge of the beam to the corner of the overhang, as shown in Fig. 28(a). It is because the deck slab changes width to fit the distance between abutment wingwalls, which would behave as a reentrant corner. The other deficiency found in 2001 is the bituminous pavements adjacent to approach slabs require patching, as shown in Fig. 28(b). This problem has been resolved during the investigation in 2002 and works well as indicated in later inspections.



(a) Deck cracking



(b) Approach slab-pavement joint

Fig. 28 Deficiencies of Bridge Number 04519 (Wetmore & Peterson, 2005)

The New York State Department of Transportation in USA also uses the retrofitting method with the IAB concept. The best example is the 'Belt Parkway Bridge' (Jayakumaran et al., 2005). The existing bridge built in 1941 is a two-span simply supported bridge with one wall type pier and two full height abutments. The span length is 21.82m each and the full length is 43.64m. The width is 23.92m with three traffic lanes in each direction. Due to the rapid traffic increment, which is at least 166000 vehicles per day and heavy deterioration of the existing bridge, such as severe corrosion, deck deterioration, bearing failure and timber blocking shoring, the existing bridge was planned to be replaced in 1999. The new bridge should be longer and wider in order to add acceleration/deceleration lanes at the entrance and exit points. The existing outdated cloverleaf interchange should be reconfigured into a modified tight diamond interchange. After a comprehensive consideration, a three-span SIAB with the total length of 65.8m and the width of 40.7m was proposed, as shown in Fig. 29. The superstructure-pier continuity methods for two piers are different, including the integral pier method and the continuous diaphragm method. As a result, very high seismic force will be produced in the fixed pier. The semi-integral abutments with monolithic backwalls, which can transfer the seismic force from abutment backwalls to embankments and mitigate the seismic force in the fixed pier, can resolve this problem.

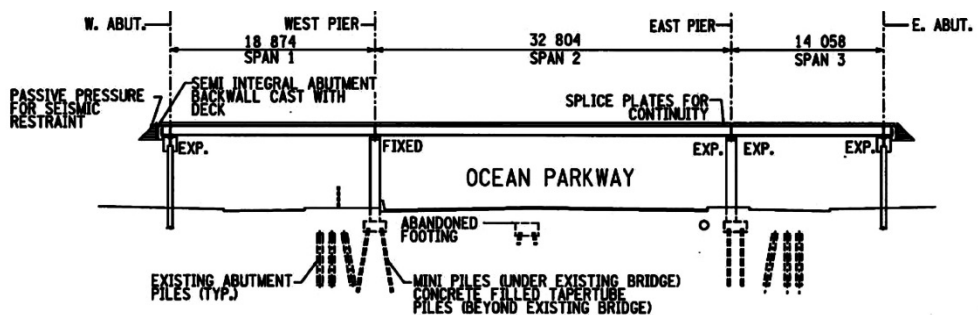


Fig. 29 South elevation of 'Belt Parkway Bridge', in USA (Jayakumaran et al., 2005)

The expansion joints over piers can be eliminated by connecting the top and bottom of adjacent steel girders by steel splice plates, as illustrated in Fig. 30. The adjacent concrete decks can be integrated by casting concrete in situ. In order to eliminate the expansion joints over abutments, the typical semi-integral abutment proposed by the New York State Department of Transportation bridge design guidelines can be chosen, as shown in Fig. 31. With this configuration, the backwall should be cast together with the deck that extended over the abutment cap-beam. The approach slab is placed on a ledge at the deck-backwall interface.

RETROFIT OF EXISTING BRIDGES WITH CONCEPT OF INTEGRAL ABUTMENT BRIDGE

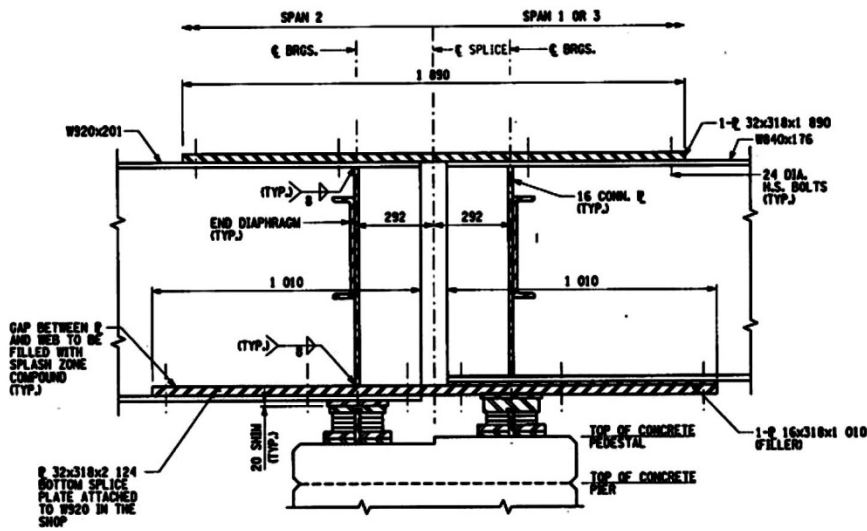
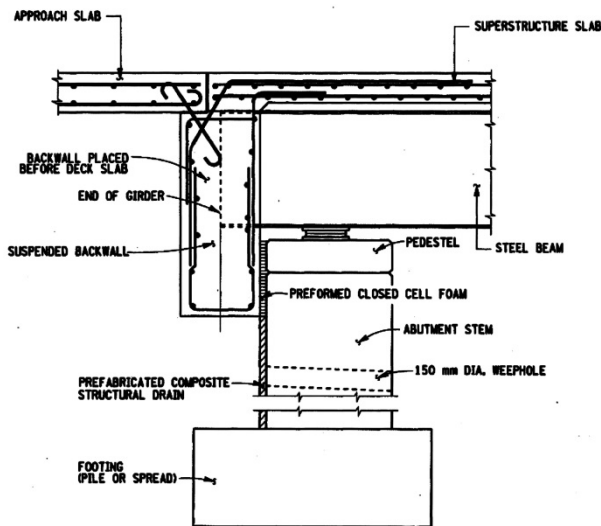


Fig. 30 Steel girders continuity solution of 'Belt Parkway Bridge', in USA (Jayakumaran et al., 2005)



(a) Typical semi-integral abutment with approach slab in New York State, USA (Yannotti et al., 2005)

(b) Construction of semi-integral abutment (Jayakumaran et al., 2005)

Fig. 31 Semi-integral abutment in 'Belt Parkway Bridge'

The new SIAB replaced the existing bridge in 2004. The superstructure were constructed and tested in the other place and then assembled and casted on site. Substructures were constructed on site. From Fig. 29, it could be found that the new bridge did not reuse the foundations and piles of the existing bridge; however, they

were just left in place, which can shorten the retrofit period. The onsite installation of each half of the new bridge took only a few nights in each of two weeks, which is significantly less than the construction period of a conventional bridge. Usually, the cost and the social influence of traffic interruptions due to replacement are quite high. In order to reduce these effects, the replacement construction was divided in two stages. During the first stage, half of the existing bridge was demolished and replaced by the new section with six traffic lanes that was similar to the total traffic lines of the existing bridge. At the same time, the other side of the existing bridge and a temporary bridge could maintain six traffic lines, which would not influence the traffic flow. Once the first half replacement completed, all six lanes on the new bridge were opened to traffic and the remainder of the existing bridge was demolished and replaced. The new bridge performs very well. From this real project, it could be found that the construction of IABs can save the cost and shorten the retrofit period. Using the IAB concept to retrofit the existing bridges in congested areas which need very high maintenance cost shall be encouraged (Jayakumaran et al., 2005).

Another example was the retrofit of the 'Rt.20 Bridge' over an inlet to beautiful Skaneateles Lake in New York, USA, as shown in Fig. 32 (The Fort Miller Co.). A single span integral-abutment-supported superstructure replaced the existing superstructure. The existing stone abutments and adjacent walls were reused.

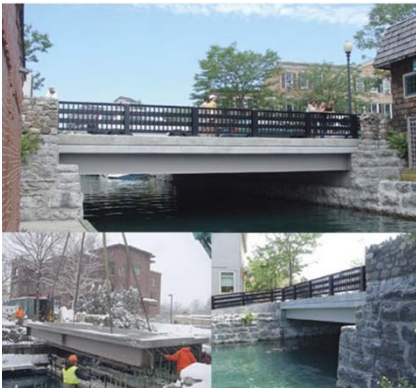
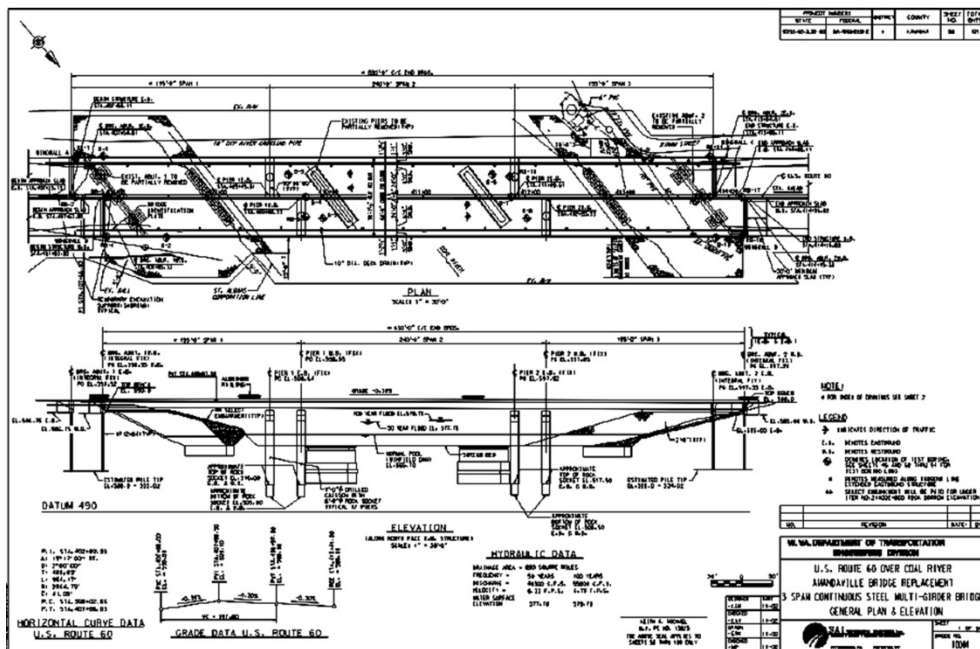


Fig. 32 Rt.20 bridge over Skaneateles Lake in New York, USA (The Fort Miller Co.)

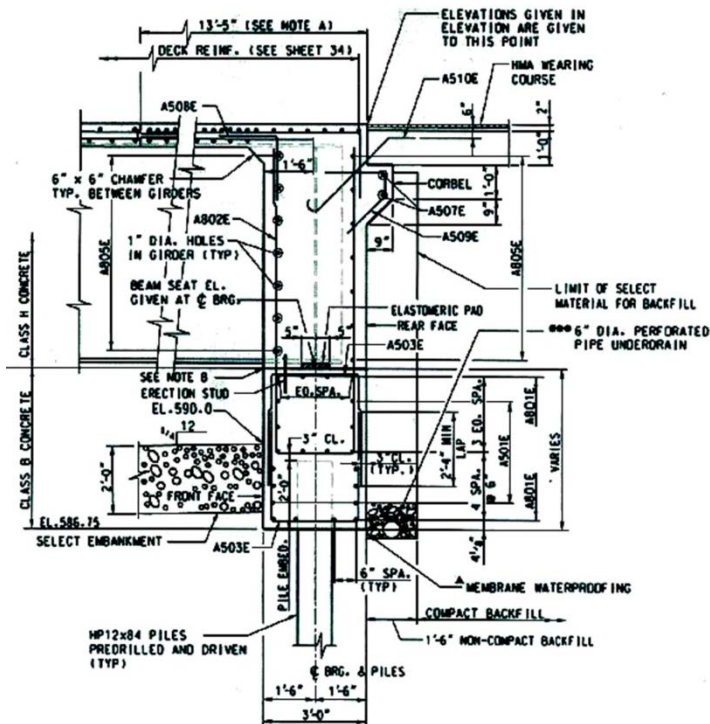
From the economical point of view, a study carried out by the New York State Department of Transportation in 1992 indicated that the retrofitting approach with the IAB concept can be used with minimal material and construction costs, and save an estimated 0.5~1.25 million US dollars every year (Farahani, 2010).

RETROFIT OF EXISTING BRIDGES WITH CONCEPT OF INTEGRAL ABUTMENT BRIDGE

Another retrofitting project, which replaced the existing bridge by an IAB, was conducted over Coal River in West Virginia, USA. The existing bridge is a five-span steel girder bridge with the total length of 174m and the skew angle of 38 degrees. The substructure in the existing bridge is composed of two concrete abutments supported on timber piles and four multi-column piers with solid web walls. Bridge owners decided to replace the existing bridge because the expansion joints were damaged and many accompanying problems arose, such as water infiltration, movement restrictions and so on. Two different replacement solutions with semi-integral abutment or fully integral abutment were proposed. Finally, a three-span steel girder FIAB with the total length of 190m and without skewed angle was chosen, as shown in Fig. 33(a). The steel girders were fixed to the piers. The foundations of the existing bridge, including piles beneath piers and abutments, were decided to left in place. The new substructure is composed of four piers with drilled shaft foundations and four fully integral abutments with single-row pre-drilled and driven HP 12x84 piles, as illustrated in Fig. 33(b).



(a) Plan and elevation layouts



(b) Fully integral abutment

Fig. 33 Detailed drawings of replacement project in West Virginia, USA (Perkun & Micheal, 2005)

2.1.2 Canada

The IAB concept has also been used in the retrofit of existing bridges in Canada, especially the SIAB concept. In Alberta, the Ministry of Transportation has encouraged converting existing bridges with conventional abutments into SIABs where the cost can be justified. Approximately 90% of all bridges in Alberta are shorter than 100m which means that many of them have the potential to be converted into SIABs through retrofitting (Alberta Ministry of Transportation, 2012).

The research on the retrofit of existing bridges with the IAB concept was conducted by the Ontario Ministry of Transportation in 1999 (Husain & Bagnariol, 1999). It indicated that there are only some retrofitting applications of transforming non-integral abutments into fully integral or semi-integral abutments; however, this trend would take place at an increased pace in the future. All existing jointed bridges with the length up to 25m or 150m have the potential to be transformed respectively into FIABs or SIABs. The design of this retrofitting process requires some careful considerations. The flexible or unrestrained abutment, which can rotate freely, is

suggested, such as the abutment with single-row piles or the abutment with hinges at the footing and at the substructure-superstructure interface. Besides, the elimination of the expansion joints over piers should be considered, because the continuous superstructure can not only eliminate the troublesome expansion joints, but also obtain a slightly higher load capacity. The positive moments due to live loads can be reduced by continuity.

Based on the analysis mentioned above, an in-depth research on the retrofit of the existing bridges with joints to SIABs was conducted by the Ontario Ministry of Transportation in 2004 (Husain, 2004). In this study, the retrofit of existing bridges with the FIAB concept is considered to be not usually feasible because rigid foundations are almost used in the existing bridges. However, the SIAB can be used. A guideline for the retrofitting process with the SIAB concept was proposed with some detailed drawings. It proposed that the feasibility of converting existing bridges with joints to SIABs must be considered at the time of retrofitting planning. The expansion joints over piers and abutments should be eliminated. However, this retrofitting method is not feasible for every case, due to some limitations. It should only be considered where it would not adversely influence the design and the integrity of the structure or its components, or where these impacts can be mitigated by using new or enhanced techniques. In order to check if existing bridges can be retrofitted with the SIAB concept, six factors listed in the following should be considered.

1. The expansion length limits of existing bridges are set as 75m, which means the total length of 150m for symmetric bridges. The movement caused by seasonal temperature variations, superstructure types and movement system capacity mainly determines this length.
2. Seven superstructure types are listed as follows.
 - a. Steel I-girders with concrete deck
 - b. Steel box girders with concrete deck
 - c. Canadian Prestressed Concrete Institute (CPCI) girders with concrete deck
 - d. Prestressed precast box girders with concrete deck
 - e. Post-tensioned thick deck slabs
 - f. Post-tensioned circular voided deck slabs
 - g. Post-tensioned trapezoidal deck slabs
3. Once the cantilevered length of abutment wingwalls in existing bridges exceeds 7m, these existing bridges should not be converted into SIABs, unless new wingwalls are planned.
4. There is no limit on the skew angle of existing bridges using this retrofitting approach.

5. The elimination methods of expansion joints over piers should be designed case by case. However, the complete elimination of expansion joints over piers, which can result in the continuous superstructure, is suggested.

6. The substructures of existing bridges should be able to resist lateral loads and can also withstand increased vertical loads from deck diaphragms and end block after retrofitting.

The SIAB design is similar to the design of conventional bridges with joints, which does not require special design considerations except soil-structure interactions and cantilevered wingwall design. In general, the following aspects should be paid more attention to by designers during retrofitting design, including joints and bearings, material applications, wingwall and approach slab treatment, and drainage and water leakage management. The soil-structure interaction may have a little adverse influence on the superstructure, such as slabs and girders. In this guideline, the movable bearings are used for semi-integral abutments. After conversion, the loads on bearings would increase. Therefore, the existing bearings should be evaluated and the replacement of bearings should be considered if necessary. Besides the inherent longitudinal resistance of bearings, additional positive restraint should be provided for long multi-span bridges, skewed bridges and where roadway grade or earthquake considerations warrant it. The partial or full elimination of the ballast wall in abutments can change the behavior and design of wingwalls. Therefore, it is important to check if the existing abutment wall can satisfy the requirement of semi-integral abutment after retrofitting. The existing deck details and reinforcing configurations also need to be reviewed carefully, especially in the case of the prestressed cast-in-place girder deck.

From the seismic point of view, the seismic design of SIABs is similar to that of conventional bridges with joints. Moreover, the SIAB can have additional advantages due to the soil-structure interaction at bridge ends. These advantages can be attested by the results of the Northridge Earthquake in California in 1994, whereas portions of conventional bridges with joints collapsed (Burke, 2009).

Some attentions of construction are also proposed in this guideline (Husain, 2004), as listed in the following.

1. Diaphragms should be cast integrally with the deck;
2. Joint forming materials such as expanded polystyrene should be removed.
3. The requirements for when placing backfill against the superstructure must be satisfied. Backfill should be placed against end diaphragms simultaneously at both ends when the deck has reached more than 75% of its specified concrete

RETROFIT OF EXISTING BRIDGES WITH CONCEPT OF INTEGRAL ABUTMENT BRIDGE

compressive strength. The difference in the height of backfill should not be greater than 0.5m.

4. Special considerations should be required for when to remove the formwork after retrofitting construction.

Some detailed conversion process from conventional abutments with joints into semi-integral abutments are proposed in this guideline (Husain, 2004). The success of a semi-integral abutment design depends largely on the detailing of joints, the use of appropriate bearings and the arrangement of wingwalls, diaphragms and approach slabs. For the existing concrete bridges using CPCI girders and concrete decks with the expansion length less than 50m, the corresponding proposed semi-integral abutment configuration is shown in Fig. 34, and the detailed drawings of removal and retrofitting are illustrated in Fig. 35. The expansion joints, abutment ballast walls, barrier systems, approach slabs, and surfaces of concrete decks and diaphragms in existing bridges should be removed. New integral superstructure-end diaphragms, approach slabs and barrier systems can be cast during retrofitting process. The bearings on abutments can be replaced or maintained according to the real situation of each case. Drainage systems and other ancillary facilities can be added during retrofitting.

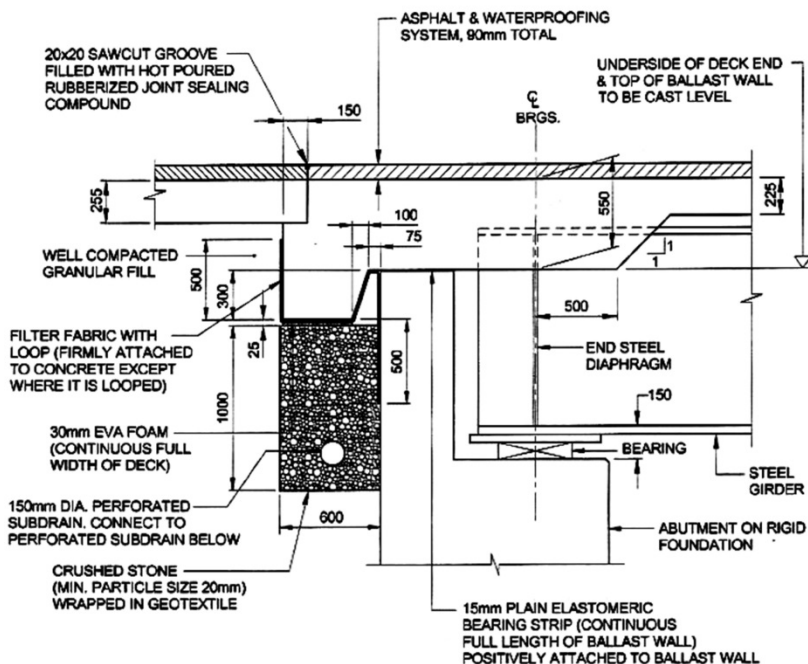
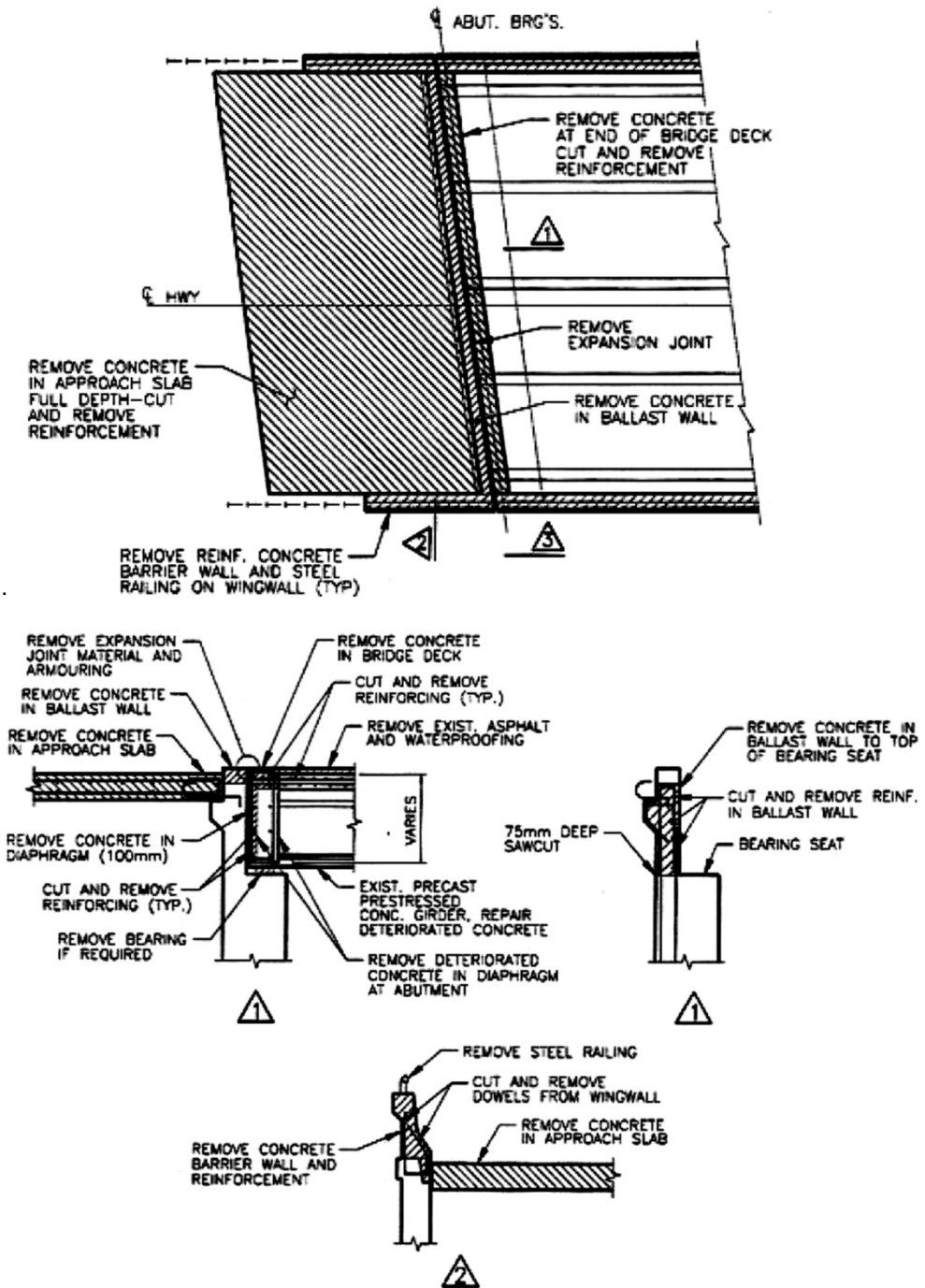
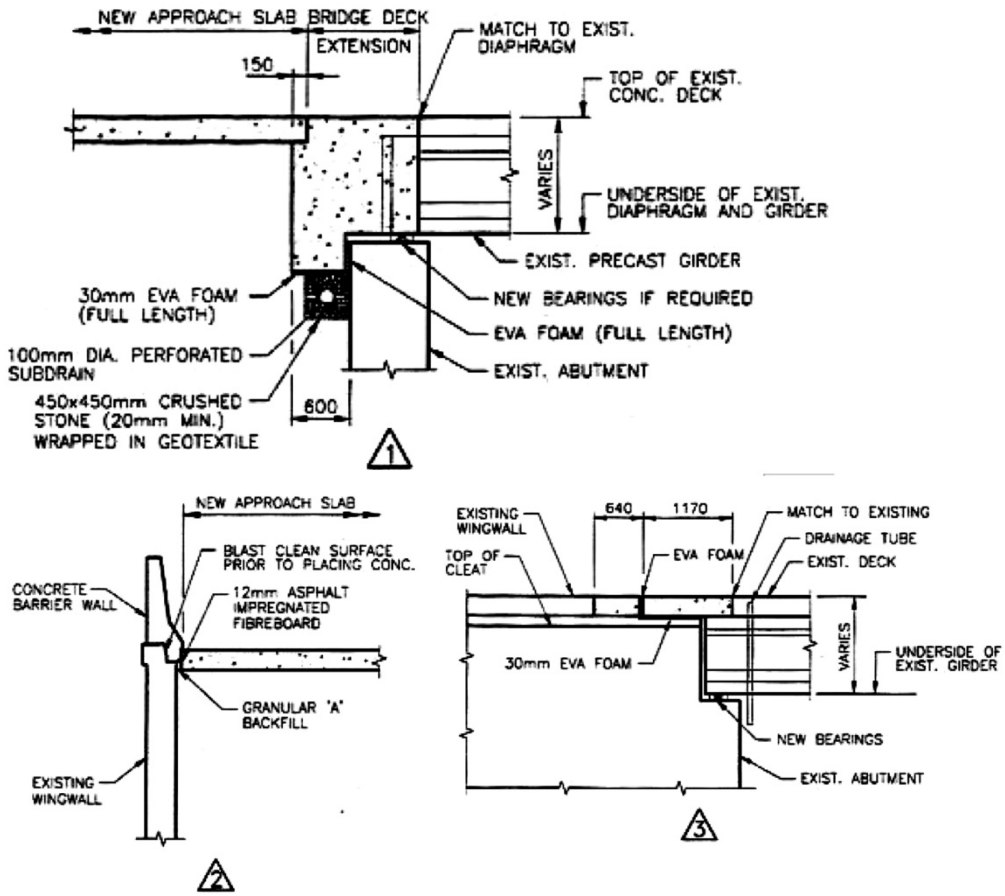


Fig. 34 Semi-integral abutment configuration: CPCI girder with concrete deck and end diaphragm (expansion length less than 50m) (Husain, 2004)



(a) Removal details

RETROFIT OF EXISTING BRIDGES WITH CONCEPT OF INTEGRAL ABUTMENT BRIDGE



(b) Retrofitting details

Fig. 35 Retrofitting process details of existing concrete bridges using CPCI girders and concrete decks with the expansion length less than 50m (Husain, 2004)

For the existing composite bridges using steel girders and concrete decks with the expansion length less than 40m, the responding proposed semi-integral abutment configuration and detailed drawings of removal and retrofitting are illustrated respectively in Fig. 36 and Fig. 37. The expansion joints, barrier systems, approach slabs, backfill, and surfaces of concrete decks in existing bridges should be removed. The abutment ballast walls should be removed partly. New integral concrete deck-end diaphragms, approach slabs and barrier systems can be cast during retrofitting process. The bearings on abutments can be replaced or maintained according to the real situation of each case. A new plain elastomeric bearing strip should be arranged full-length between the integral concrete deck-end diaphragms and remained abutment ballast walls. Drainage systems and other ancillary facilities can be added during retrofitting. The granular backfill can be placed back after retrofitting.

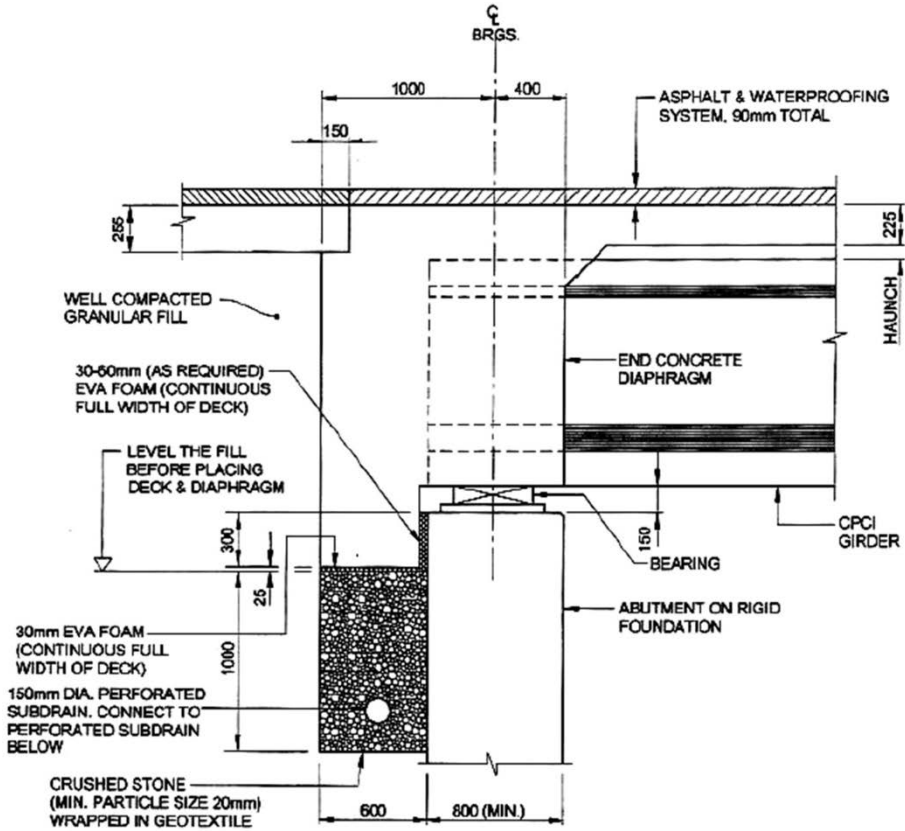
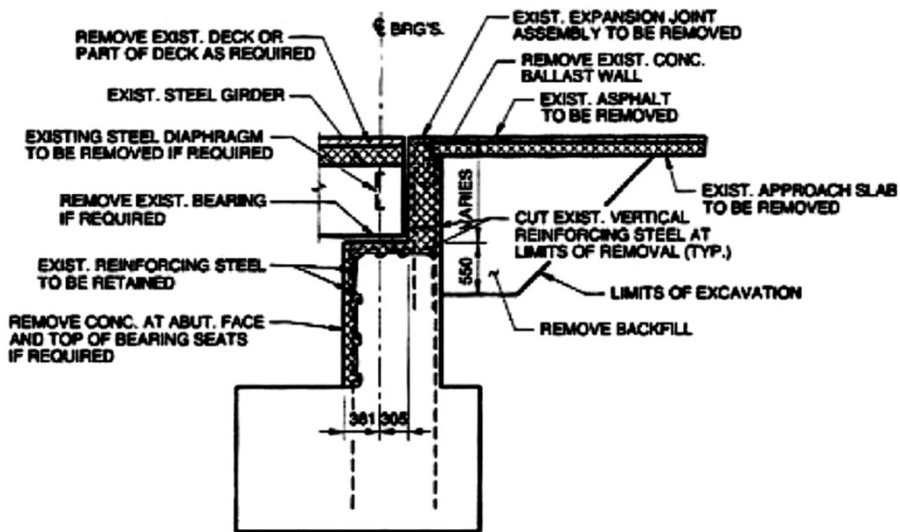
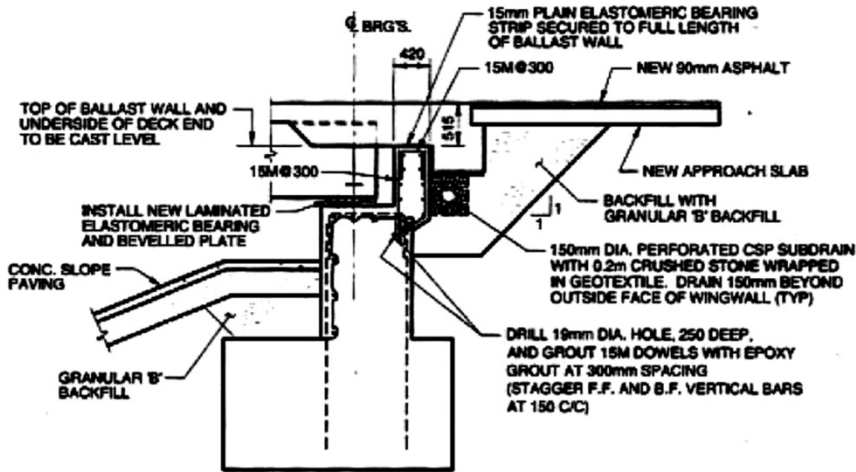


Fig. 36 Semi-integral abutment configuration: steel girder with concrete deck and deck overhanging the ballast wall (expansion length less than 40m) (Husain, 2004)



(a) Removal details

RETROFIT OF EXISTING BRIDGES WITH CONCEPT OF INTEGRAL ABUTMENT BRIDGE



(b) Retrofitting details

Fig. 37 Retrofitting process details of existing composite bridges using steel girders and concrete deck with the expansion length less than 40m (Husain, 2004)

The deep sawcut filled with hot poured rubberized joint sealing compound shown in Fig. 38 should be used in conjunction with the semi-integral abutment retrofitting in two types of existing bridges described above.

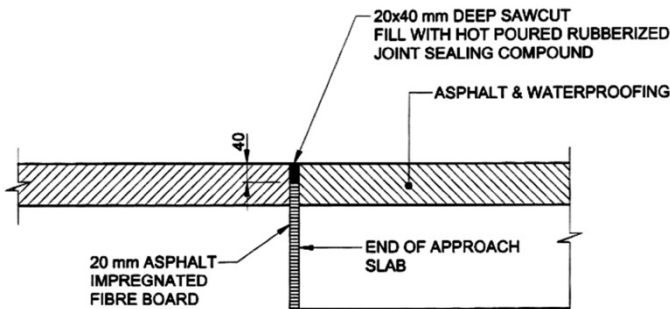


Fig. 38 Expansion joint at the end of approach slab for concrete bridge shorter than 100m and steel bridge shorter than 75m (Husain, 2004)

For the existing concrete bridges using CPCI girders and concrete decks with the length longer than 50m and composite bridges using steel girders and concrete decks with the length longer than 40m, the corresponding proposed semi-integral abutment configurations are illustrated in Fig. 39 and Fig. 40, which are similar to the configurations illustrated in Fig. 34 and Fig. 36. The differences are that the geo-textile and the fill around it should be carefully placed during construction and the expansion joints illustrated in Fig. 41 should be installed at the ends of approach slabs.

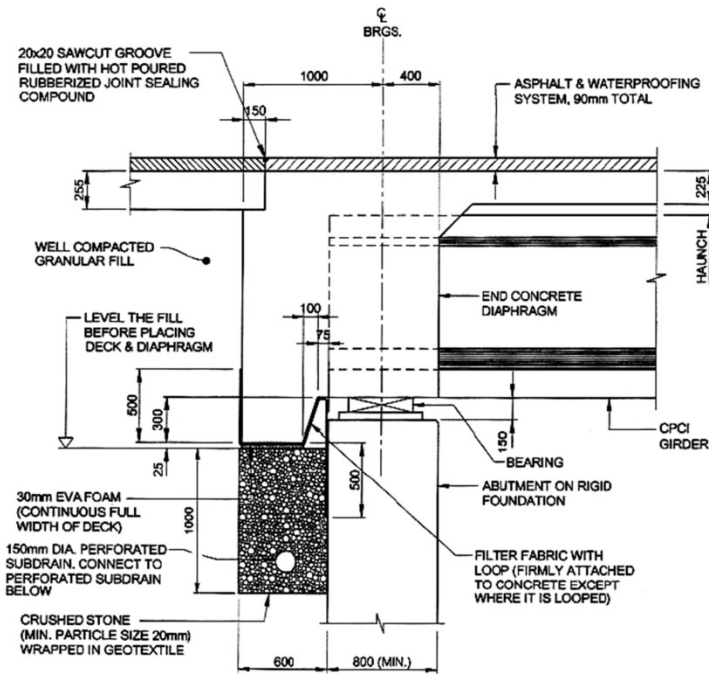


Fig. 39 Semi-integral abutment configuration: CPCI girder with concrete deck and end diaphragm (expansion length greater than 50m) (Husain, 2004)

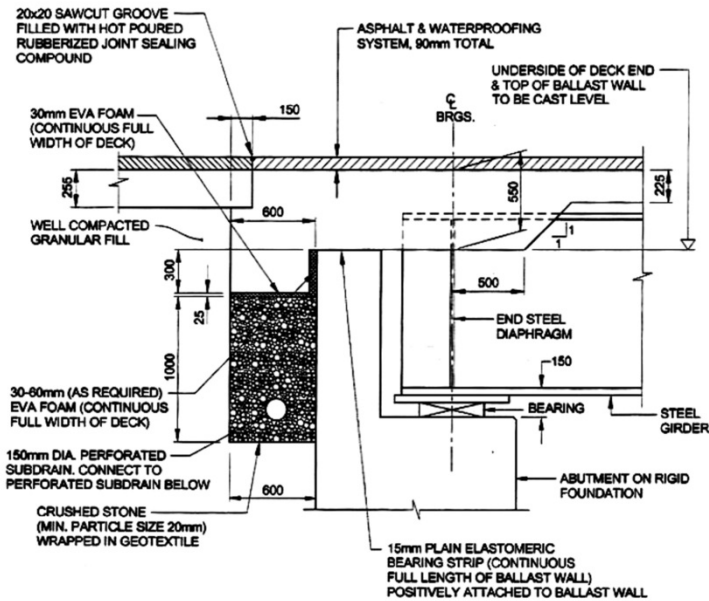


Fig. 40 Semi-integral abutment configuration: steel girder with concrete deck and deck overhanging the ballast wall (expansion length greater than 40m) (Husain, 2004)

RETROFIT OF EXISTING BRIDGES WITH CONCEPT OF INTEGRAL ABUTMENT BRIDGE

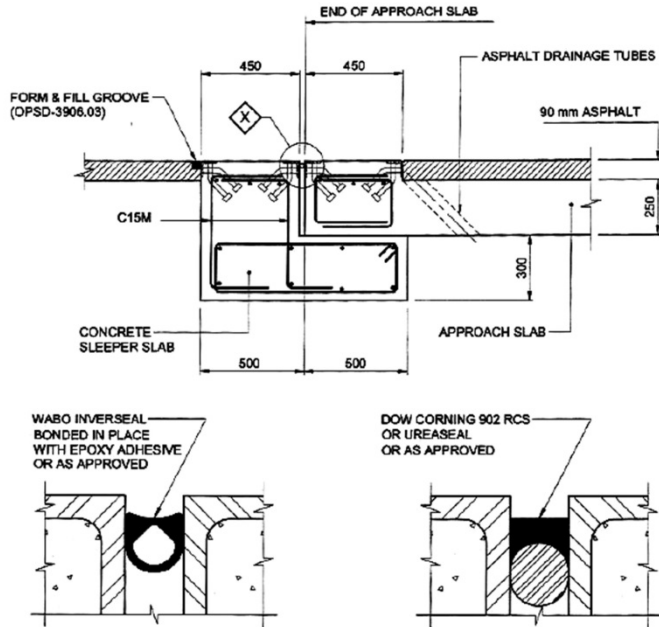
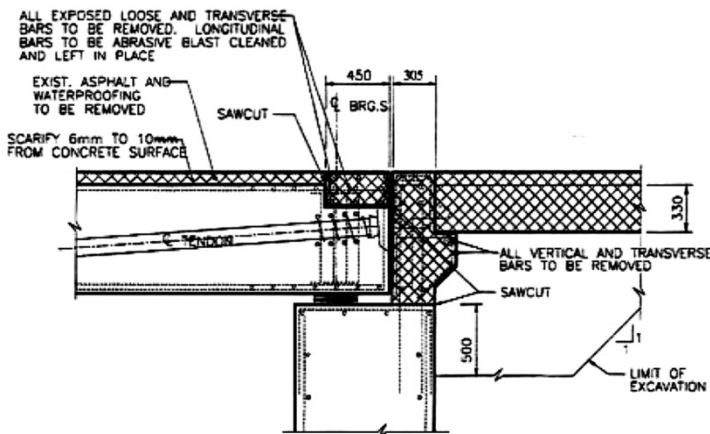
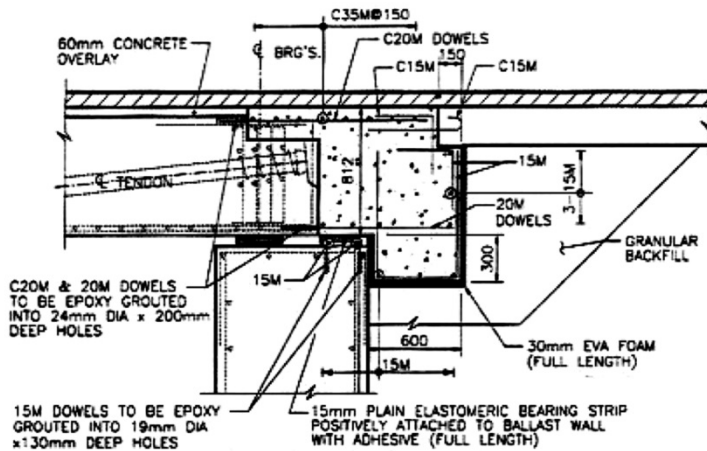


Fig. 41 Expansion joint at the end of approach slab for concrete bridge longer than 100m and steel bridge longer than 75m (Husain, 2004)

A special attention should be paid to the transformation of existing post-tensioned deck bridges into semi-integral abutment, because of the congested anchorage zone areas at girder ends. Therefore, the concrete and reinforcing steel in existing girder ends should be removed minimally. Moreover, a special protection should be applied to the anchorages. It should ensure that new concrete is adequately attached and bonded to old concrete. The detailed configurations of removal and retrofitting of existing post-tensioned deck bridges are illustrated in Fig. 42.



(a) Removal details

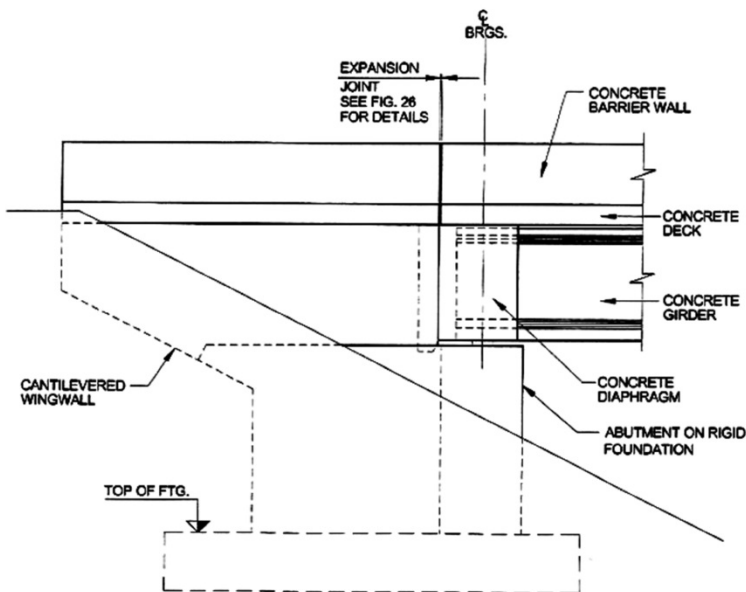


(b) Retrofitting details

Fig. 42 Retrofitting process details of existing post-tensioned deck bridges (Husain, 2004)

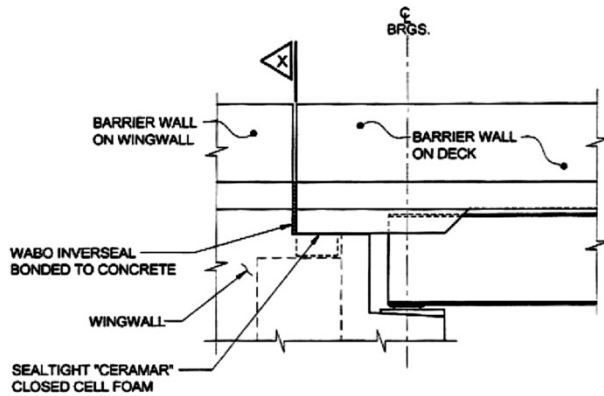
The relative position arrangements and interface design of abutment wingwalls, approach slabs and deck slabs should be considered carefully to ensure a durable design. Some solutions were proposed in this guideline (Husain, 2004).

1. Using fixed wingwalls, integral approach slabs and overhanging decks (Fig. 43).
2. Extending approach slabs over the top of wingwalls with filler material between the undersides of approach slabs and the top of the wingwalls (Fig. 44).
3. Extending approach slabs over to decks with filler material between the undersides of approach slabs and the top of ballast walls (Fig. 45).



(a) CPCI girder with concrete deck and end diaphragm

RETROFIT OF EXISTING BRIDGES WITH CONCEPT OF INTEGRAL ABUTMENT BRIDGE



(b) Steel girder with concrete deck

Fig. 43 Fixed wingwalls, integral approach slab and the overhanging deck (Husain, 2004)

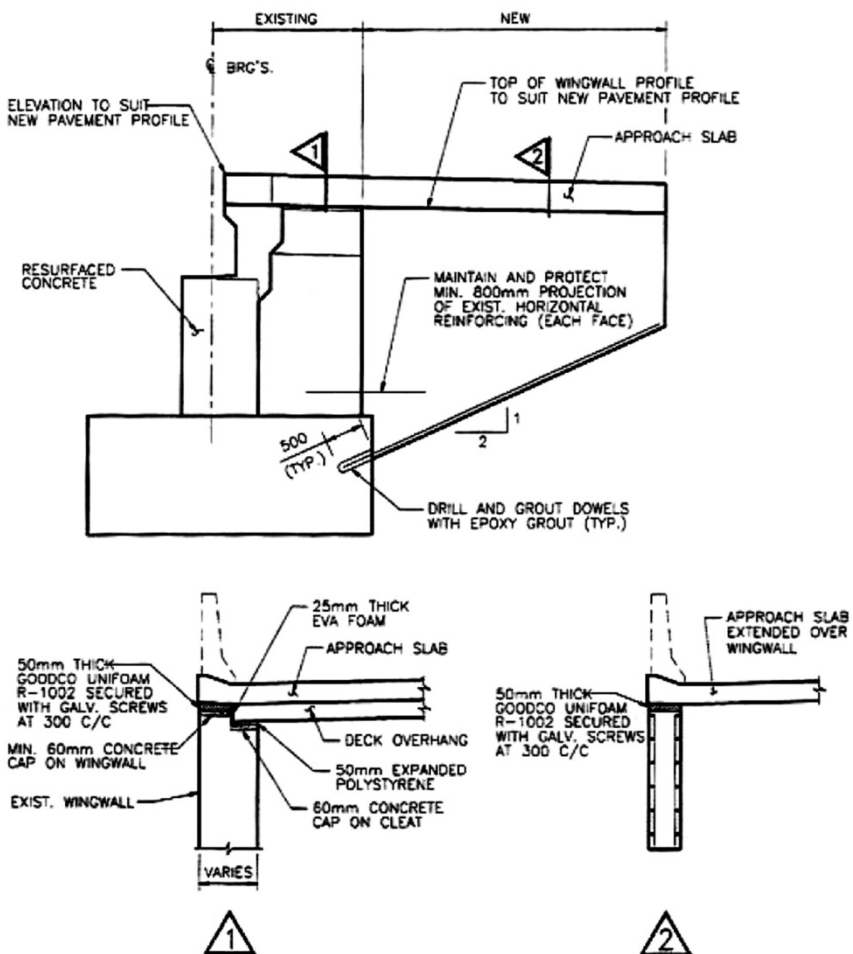
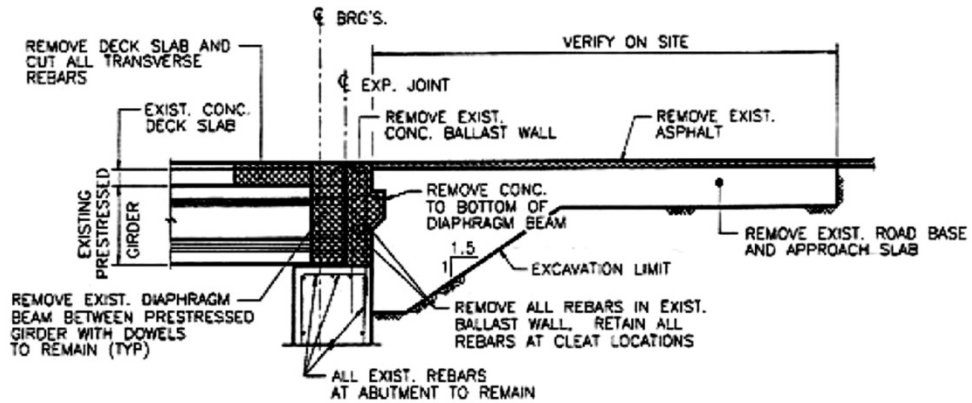
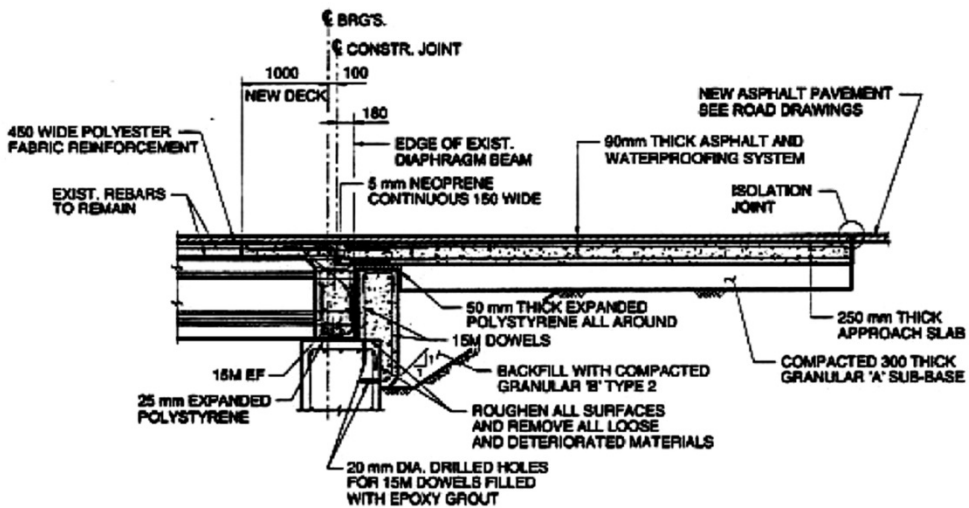


Fig. 44 Approach slab extending over the top of the wingwall (Husain, 2004)



(a) Removal details



(b) Retrofitting details

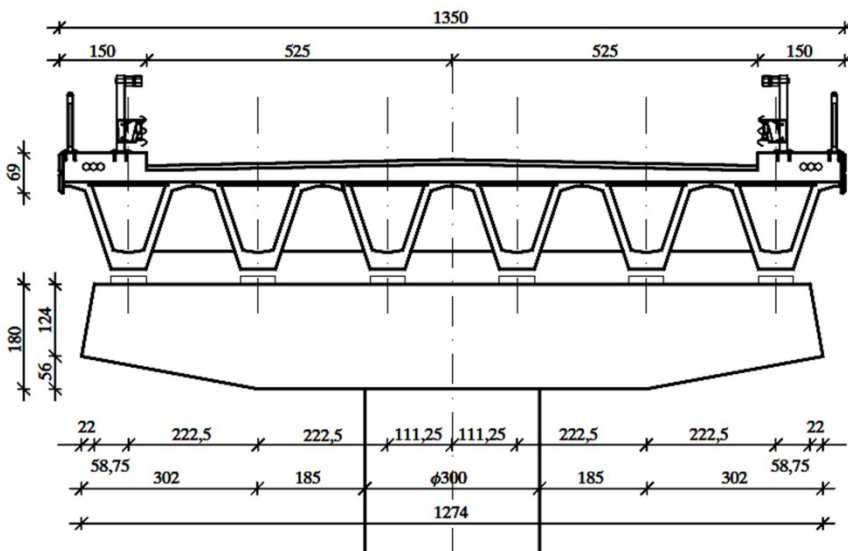
Fig. 45 Approach slab extending over to the deck

The retrofitting solution with the SIAB concept was applied to the 'Bridgeport Bridge' in Kitchener, Ontario, Canada. The existing bridge is a five-span concrete tied-arch bridge with the total length of 124.4m and the width of 10.8m. It was constructed in 1934 and subjected to serious durability problems, such as spalling of concrete, corrosion of rebar, deterioration at expansion joints and so on. Therefore, in order to eliminate original design details that can drive deterioration, conventional non-integral abutments should be converted into semi-integral abutments, the expansion joints over piers should be eliminated and the fascia and soffit should be protected from the corrosion of water. In addition, the robust and durable concrete was chosen to repair the concrete spalling and the FRP reinforcement was chosen to strengthen the exposed concrete (Stephenson, 2009).

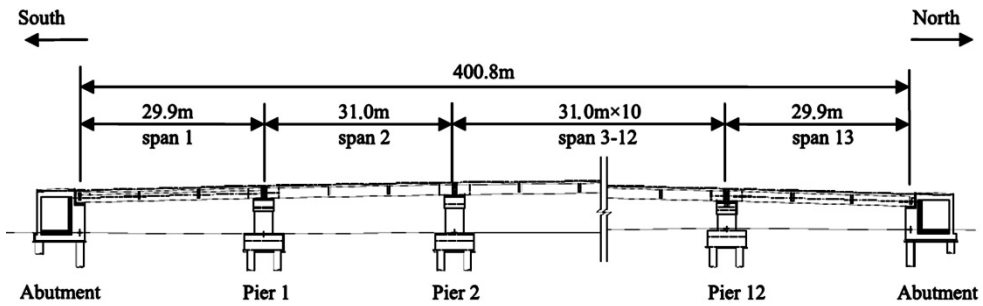
2.2 Applications in Europe

2.2.1 Italy

The most important application of using the FIAB concept to retrofit existing bridges in Italy is the 'Isola della Scala Bridge' (Briseghella & Zordan, 2006; Briseghella et al., 2012; Lan, 2012; Zordan & Briseghella, 2007; Zordan et al., 2011a, b). The existing flyover is located in Verona, Italy with the prestressed concrete simply supported superstructure. The construction of the flyover was started in 2001. However, it was interrupted after two years because of economic problems. Before the interruption, abutments and piers had been built and all prestressed concrete girders and main prefabricated elements had been purchased. At the beginning of 2006, the construction was restarted and the client would like to improve the structure quality without modifying those constructed parts. Moreover, the new design phase should avoid an increase in overall costs. As a result, a new proposal changing the existing bridge type from the simply supported bridge to the FIAB was considered as the best retrofitting solution. This bridge has 13 spans with the total length of approximately 400m and the deck width of 13.5m. The typical cross section and elevation layout of the 'Isola della Scala Bridge' are illustrated in Fig. 46. The main information is listed in Table 9. It is the longest IAB ever built all over the world (Zordan et al., 2011a, b).



(a) Typical cross section



(b) Elevation layout

Fig. 46 Typical cross section and elevation layout of 'Isola della Scala Bridge' (Zordan et al., 2011b)

Bridge type (before and after retrofiting):	Simply supported bridge to Semi-integral abutment bridge
Spans length (m):	$29.9+11 \times 31+29.9= 400.8$
Deck width/height (m):	$13.5/(1.50+0.30)$
Piers column cross section diameter (m):	3
Piers height (cap + column + footing) (m)	$1.80+(3.775-5.385)+2.50$
Piles type:	Reinforcement concrete friction
Piles cross section circular (m)	1.2
Piles length (m):	15~20
Piles number	6 for each pier and abutment

Table 9

Main features of 'Isola della Scala Bridge'

The main retrofiting phases used in 'Isola della Scala Bridge' are listed in the following (Briseghella & Zordan, 2006; Zordan & Briseghella, 2007; Zordan et al., 2011a, b).

1. Partially demolish the wearing surfaces of slabs and girders to create the spaces for concrete casting (Fig. 47(a)).
2. Prepare the internal surfaces of girders to eliminate existing damages and increase the roughness by sandblasting (Fig. 47(b)). Make bearings inactive with expansive concrete mortar before concrete casting.
3. Install shear connectors on existing girder surfaces to strengthen the connectivity between existing concrete and new concrete. Install some steel beams on existing pier caps or abutments, which can transfer forces between the superstructure and the substructure after retrofiting. Position rebar in new superstructure-pier connections and superstructure-abutment connections (Fig. 47(c)).
4. Cast concrete inside the V-shaped girders for a length of 2m and the spaces

RETROFIT OF EXISTING BRIDGES WITH CONCEPT OF INTEGRAL ABUTMENT BRIDGE

between adjacent girders or between girders and abutments to obtain new concrete diaphragms over piers and fully integral abutments. Cast concrete to complete new slabs and approach slabs (Fig. 47(d)).



(a) Demolish concrete surfaces of slabs and girders



(b) Prepare internal surface and make bearings inactive



(c) Install steel beams and position rebar





(d) Cast concrete to complete joints, new slabs and approach slabs

Fig. 47 Retrofitting construction phases (Briseghella & Zordan, 2006; Zordan & Briseghella, 2007)

The average air temperature during retrofitting remained approximately 10–15°C. The conversion sequence of connections started from the central pier and proceeded symmetrically towards two abutments. The construction of 'Isola della Scala Bridge' was completed and opened to traffic in 2007 (Zordan et al., 2011b).

In order to check the service performance of this bridge after retrofitting, some field inspections were carried out. No mentionable damage has been noticed until now, except some uniformly distributed cracks on approach slabs (Zordan et al., 2011b). In addition, two dynamic tests were carried out respectively at Sep. 2010 and Feb. 2011, in order to understand the time-dependent behavior of this bridge, considering the combined effect of temperature variations and concrete deterioration (Zordan et al., 2011c). Through comparing the data of these two tests, it could be found that the main mode shapes are substantially unvaried; however, the frequencies corresponding to different mode shapes increase slightly from the first test to the second one. Nevertheless, due to the limited number of test data, this trend is insignificant and must be further investigated with other dynamic tests, which will be carried out in the future.

Besides the field investigations on the bridge, some numerical analyses were also carried out to study the mechanical behaviors of this super-long IAB. A three-dimensional finite element model was implemented firstly by Briseghella & Zordan (2006). The results indicated that, the Italian standard prefabricated concrete bridges built with the typical type and dimension of girders, piers, abutments and piles are compatible with the increment of vertical reactions caused after retrofitting. Moreover, with reference to a wide number of bridges with commonly used dimensions of piers and foundation piles, the maximum total length of 120m (four spans) can be achieved. Then, some other numerical analyses were conducted

through two finite element models built by finite element programs STRAND 7 (three-dimensional model) and ANSYS (two-dimensional model). The consistency of the results obtained from both models was checked firstly (Zordan et al., 2011b). Moreover, the dynamic test data were also compared with the results of the finite element model built in ANSYS by using the Absolute Frequency Discrepancy method and the Modal Assurance Criterion method. Two comparisons were indicated that the simplified two-dimensional model is able to describe the main features of the dynamic response of the bridge and is suitable to do the further researches (Zordan et al., 2011c). The stiffness of superstructure-pier connections in the finite element model was updated according to the dynamic test results. Using the verified finite element model, a parametric analysis was conducted. A wide number of parameters were considered, such as soil-structure interactions, temperature variations and so on. Some useful results were found. The influence of temperature variations on the axial forces in girders and piles are significant, which can be considered as the key parameters to evaluate the bridge response. Different soil conditions greatly affect the bending moments near abutments and axial forces along girders. Moreover, the influence of negative temperature variations is found to be more significant than the influence of positive ones, because the passive soil reactions are always larger than the active ones (Briseghella et al., 2010; Zordan et al., 2011b). Because existing abutments and piers are reused after retrofitting, the stiffness of abutments is quite large. The analysis revealed that the deformations of the piles beneath piers are negligible and significant bending moments are present at abutments. Comparing to the other parts of the bridge, the internal force distribution at abutments is more greatly influenced by temperature variations, which implies that the stiffness of abutments in this kind of bridge should be thoroughly investigated as one of the key factors. In order to analyze the influence of abutment stiffness on internal force distribution, the temperature pushover analysis was conducted. It could be found that when temperature varies, the respond of slender abutments is more predictable and uniform than the respond of normal abutments. The temperature pushover analysis was also used to analyze the failure pattern of the structure due to temperature variations (Zordan et al., 2011b).

Using the same mechanical properties of construction materials and geometric data of 'Isola Della Scala Bridge', a general finite element model with slender abutments was implemented. It indicated flexible abutments or semi-integral abutments should be considered as the preferred solution. An analytical formulation related by span length, girder sections and pier stiffness was proposed to assess the thermal induced displacement of an idealized IAB, based on conservatively assumption on the earth pressure on abutments and the reactions of pile heads. Through

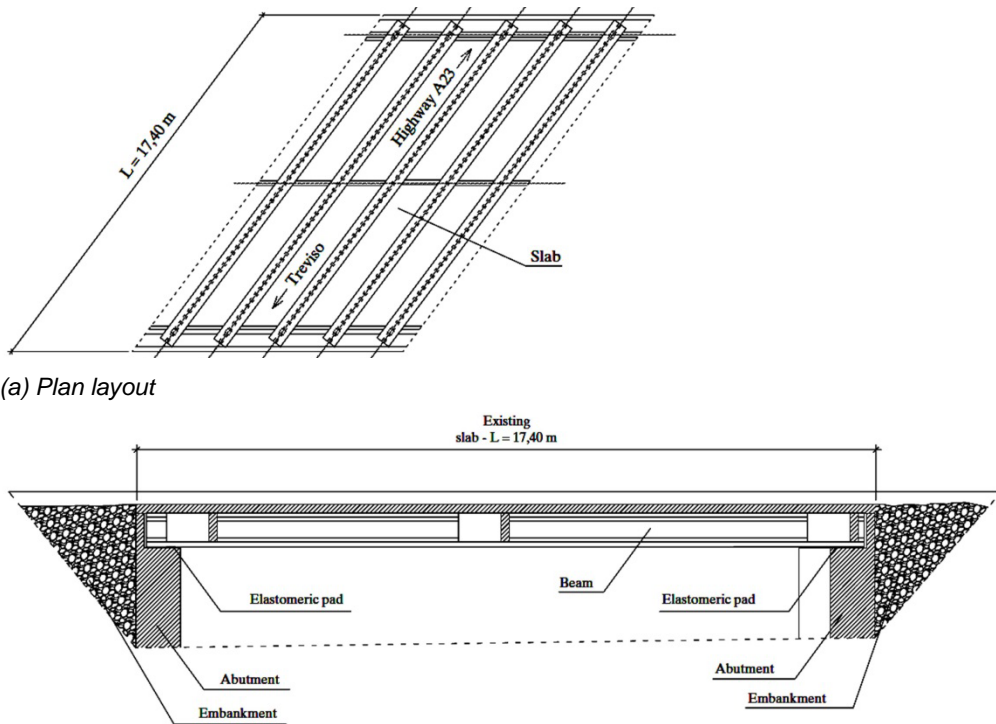
comparing with the finite element model, this formulation was updated by modifying the pier stiffness to consider the non-linearity in the bridge. Moreover, this formulation is still under development because the overall length limit will change case by case due to different bridge characteristics and variable boundary conditions. Nevertheless, the calculation using the modified formulation and considering the pier rotation and abutment capacities indicates that the IAB with the length up to 540m (30mX18 spans) could be built on the same conditions of the studied bridge. If the fatigue effects on the materials are considered in the bridge, the IAB with the length up to 450m (30mX15 spans) could be built. Furthermore, if the durability of approach slabs with the maximum thermal induced displacement is taken into account, the maximum IAB length can reach 430 m (Lan, 2012; Zordan et al., 2011a).

Based on the 'Isola Della Scala Bridge', an optimization procedure of pile design which can not only ensure the pile displacement capacity for super-long IABs, but also provide an application example of this design optimization procedure in general structural analysis, was proposed (Lan, 2012). The optimization method that associates the finite element method with global optimization algorithm was used in this pile design optimization procedure. Using the proposed design optimization procedure, the pile can be designed with less materials and more load capacities to displacements. Simultaneously, the stress level increment is absolutely reasonable and acceptable. Two different optimal design approaches of the pile were considered. One is the pile with two varying sections and the other is the pile with one uniform section and the pre-hole treatment. The lateral displacements at the pile head, stress levels in concrete and reinforcement of these two different optimal design approaches can get nearly the same value. By comparison, the pile with varying sections can reduce more volume than the pile with one uniform section; however, the construction of the pile with varying sections is more difficult than that of the pile with one uniform section.

The 'Treviso Bridge' is another retrofitting application in Italy with the SIAB concept. The existing bridge is a simply supported bridge built in 1980 with the single span of 17.4m and the skew angle of 37°. The cross section is composed of five double T prestressed concrete beams with a deck width of 9m and thickness of 0.2m. There is no approach slab in this bridge. The plan drawing of the existing bridge is illustrated in Fig. 48. The main features are summarized in Table 10. In order to improve its seismic behaviors, the existing bridge needed to be retrofitted because this bridge was designed initially without the consideration of seismic influence. Moreover, the retrofitting cost cannot exceed 60% of the replacement ones. According to these

RETROFIT OF EXISTING BRIDGES WITH CONCEPT OF INTEGRAL ABUTMENT BRIDGE

requirements, the retrofitting approach of transforming the existing bridge to a SIAB with two groups of micro-piers on the bridge ends was proposed (Russo et al., 2009).



(a) Plan layout

(b) Elevation layout

Fig. 48 Existing 'Treviso Bridge' (Russo et al., 2009)

Bridge type (before and after retrofitting):	Simply supported bridge to Semi-integral abutment bridge with micro-piers
Spans length (m):	17.4
Girder type:	5 double T prestressed concrete girders
Deck width/height (m):	9/0.2
Skew angle (°C):	37
Bearing type (before and after retrofitting):	Elastomeric bearing to isolation bearing
Micro-pier type:	Steel tube with the thickness of 8mm
Micro-pier length (m):	16
Micro-pier number:	18 for each group with 2 lines at each side
Approach system:	Connection slab, plinth and approach slab
Approach system length (m):	7 for each one at each side

Table 10

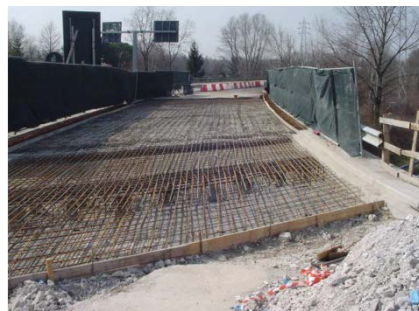
Main features of 'Treviso Bridge'

The retrofitting phases of existing 'Treviso bridges' to a SIAB with micro-piers are listed in the following.

1. Demolish 20mm of the slab by sandblasting in order to eliminate damaged parts.
 2. Excavate the spaces for new approach systems.
 3. Drill two groups of micro-piers in both sides of the bridge (Fig. 49(a)). Each one has 18 micro-piers arranged in two lines. All the micro-piers are steel tubes with the length of 16m and tube thickness of 8mm.
 4. Position reinforcements on embankments and fix them to the reinforcements in existing slabs by connectors (Fig. 49(b)). Cast concrete to form two new approach systems with the length of 7m and thickness of 0.2m at both sides of the bridge. Each approach system is consisted of an approach slab with the length of 3m, a connection slab with the length of 3.12m and a concrete plinth with the length of 1.88m. Two groups of micro-piers drilled before should integrally connect to the concrete plinths. Finally, cast a new integral slab with the thickness of 70mm over the existing bridge slab and approach systems.
 5. Replace the isolation bearings by elastomeric bearings during retrofitting.
- The elevation layout of the new SIAB with two groups of micro-piers and approach systems is illustrated in Fig. 50.



(a) Drill micro-piers



(b) Position reinforcements

Fig. 49 Retrofitting procedure of 'Treviso Bridge' (Russo et al., 2009)

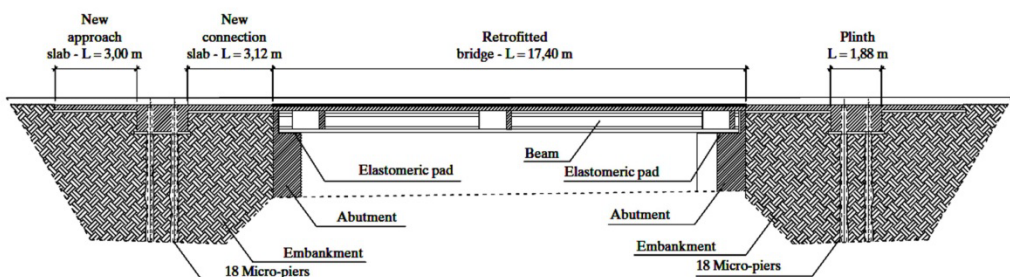


Fig. 50 Elevation layout of 'Treviso Bridge' after retrofitting (Russo et al., 2009)

In order to check whether this retrofitting approach can improve the seismic performance, the numerical analyses were conducted through a finite element model based on Eurocode 8. The results indicated that the retrofitting method could reduce 81.4% of the longitudinal forces on the slab and 55.3% of the vertical forces at the base of abutments. It is because that the micro-piers can not only reinforce the embankments near abutments, but also allow the plastic hinges appeared at their heads. From the static point of view, the new bridge keeps the same static scheme as the old one. Moreover, from the seismic point of view, the micro-piers can form a new system to absorb a considerable rate of horizontal forces, transmit it directly to the ground and reduce the loads on abutments. From the economical point of view, this retrofitting method is acceptable. The costs of the existing bridge and the retrofitted bridge are 650000 € and 95000 €, respectively. The additional cost is only 15% of the replacement cost which is obvious less than the standard value (60% of the replacement cost) (Russo et al., 2009).

2.2.2 Switzerland

According to the revised version of Swiss Federal Roads Office Guidelines in 2010 (Kaufmann & Alvarez, 2011), the elimination of existing expansion joints should be always checked firstly during retrofitting existing bridges. In many cases, expansion joints and bearings can be replaced by monolithic connections. Using the SIAB concept, which is particularly appropriate for the retrofit of existing jointed bridges, is also suggested.

2.2.3 Germany

An one-span FIAB was chosen to replace an existing bridge over River Saale in Germany during retrofitting in order to obtain a low-maintenance, long-lasting structure without expansion joints or bearings (Weizenegger, 2003). The elevation of new bridge is shown in Fig. 51. The superstructure of the new bridge is composed of four steel I-beams and one concrete deck slab, which are prefabricated in the factory, then transported to the bridge site and finally assembled monolithically to abutments. Two reinforced concrete abutments based on single-row piles with the diameter of 1.2m were constructed on site. The low-lying drag plates can be installed behind the abutments to replace the expansion joints between bridge ends and pavements.

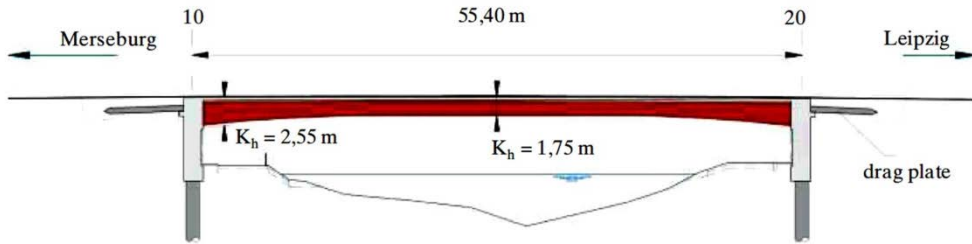


Fig. 51 Elevation layout of a FIAB in Germany (Weizenegger, 2003)

2.2.4 Austria

In Austria, the research on transforming existing bridges into IABs during retrofitting was begun (Geier, 2010). An existing reinforced concrete arch bridge with one span of 26m needed to be retrofitted or replaced, because it has quite poor conversation and limited clearance which cannot satisfy the new requirement of the heavy floods that have occurred in recent years. The bridge administration decided to construct a new bridge, which is able to resolve some problems, such as increasing the flow section of the 'Perschling' channel, reducing the maintenance cost and passing directly without sealing and extra pavements. Based on these demands, a FIAB 'Perschling Bridge' with one span of 32m and the extremely slender superstructure of only 0.8m thickness in the middle was proposed (Geier, 2011), as illustrated in Fig. 52.

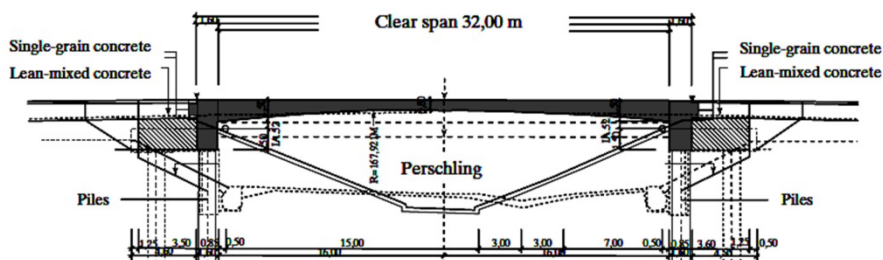


Fig. 52 Elevation layout of fully integral abutment bridge 'Perschling Bridge' (Geier, 2011)

2.3 Applications in Asia

2.3.1 China

A modified type of semi-integral abutment was proposed in China by Jin et al. (2005).

RETROFIT OF EXISTING BRIDGES WITH CONCEPT OF INTEGRAL ABUTMENT BRIDGE

This improved abutment type has been used in many IABs in China, not only the newly constructed IABs, but also the retrofit of existing bridges, due to many advantages.

The first retrofitting application by using the improved semi-integral abutment in China was the 'Longtan Bridge' (Tang et al., 2007). The existing simply supported bridge was constructed in 1966 and subjected to a large number of durability problems. The total length of the existing bridge is 109.2m with 10 unequal spans and the width of deck slab is 6.7m. The superstructure of the existing bridge is composed of four reinforced concrete I-beams and one deck slab. Nine gravity piers and two gravity abutments with splayed wingwalls was constructed in the existing bridge. The elevation layout of the "Longtan Bridge" is shown in Fig. 53 and the detailed information can be found in Table 11.

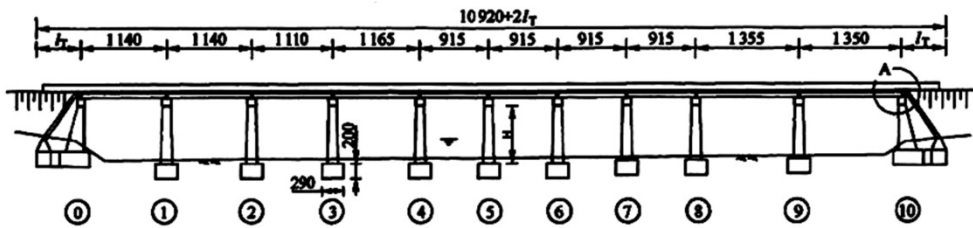


Fig. 53 Elevation layout of "Longtan Bridge" in China (Unit: cm) (Tang et al., 2007)

Bridge type (before and after retrofiting):	SSB to SIAB
Spans length (m):	109.2 (2X11.4+11.1+11.65+4X9.15+13.55+13.5)
Girder Type:	Four reinforced concrete I-beams
Deck width (m): (before and after retrofiting)	6.7 to 8
Abutment type:	Gravity abutments with splayed wingwalls
Pier type:	Gravity piers

Table 11

Main features of "Longtan Bridge" in China

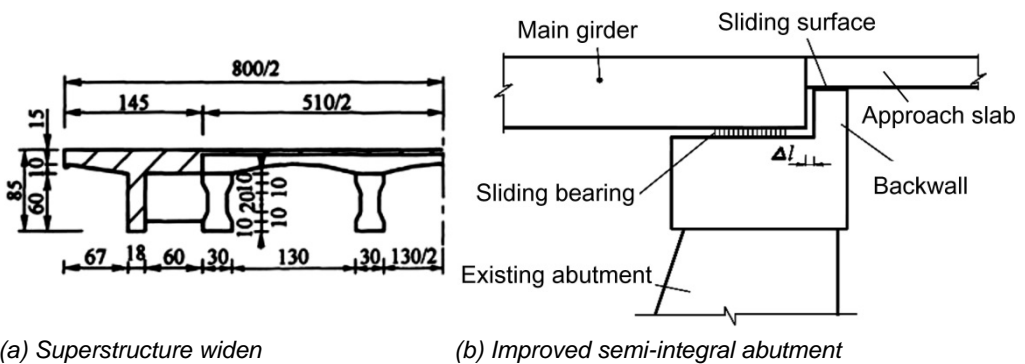
In order to resolve the durability problems and widen the deck slab, the existing bridge was retrofitted using the following procedures.

1. Demolish deck slabs and flange slabs of side girders. Cast concrete to new side girders and deck slabs. In this case, the deck slabs can be widened from 6.7m to 8m (Fig. 54(a)).
2. Convert conventional abutments into improved semi-integral abutments (Fig. 54(b)). Most parts of conventional abutments can be reused; however, the height of

abutment backwalls should be shortened to provide the spaces for approach slabs. The approach slabs with the length of 5.5m are connected directly to girder ends without expansion joints and supported by the abutment backwalls with sliding surfaces and backfill. Sliding bearings should be installed to replace existing bearings.

3. Position the reinforcements of new deck slabs, which should be connected to existing girders by post-embedded rebar. Install steel plates between the ribs of adjacent girders over piers. Add more longitudinal reinforcements for the deck slabs over piers. Position the reinforcements of pavements, which should be connected to approach slabs.

4. Cast concrete to complete the connections of adjacent girders, new deck slabs and approach slabs.



(a) Superstructure widen

(b) Improved semi-integral abutment

Fig. 54 Retrofitting procedure of 'Longtan Bridge' in China (Jin et al., 2005)

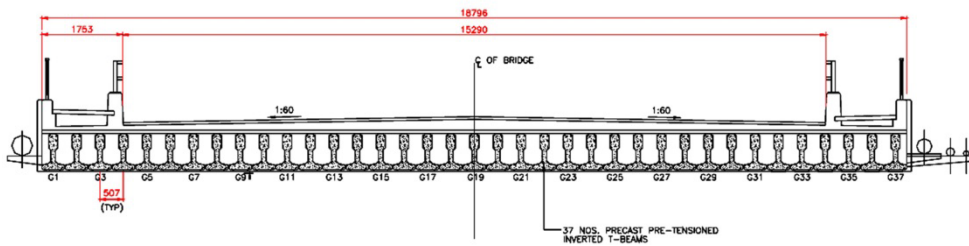
The retrofitted bridge was opened to traffic at 2006. A large number of GHB-2 concrete strain gauges were embedded in the bridge and pavement in order to check the service performance. It could be found that the pavement is always subjected to compression because the temperature during construction is quite low. With the rising of temperatures, the compression forces in the pavement increase and vice versa. The deformations of the bridge and pavement are both elastic and recoverable. All measured values are less than calculated ones. No mentionable damage in the bridge and approach system has been noticed until now (Tang et al., 2007).

2.3.2 Singapore

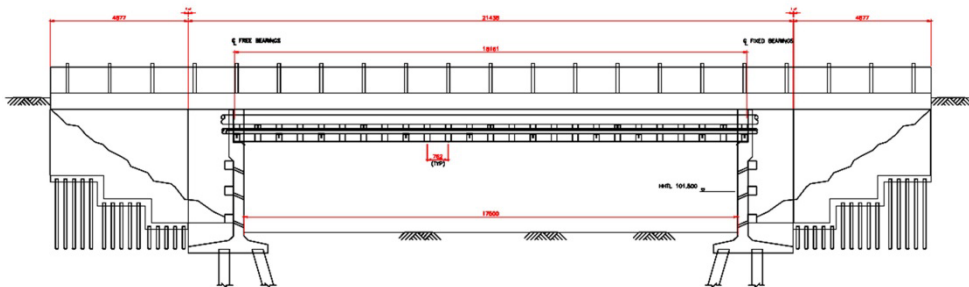
In Singapore, the retrofitting approach with the IAB concept was applied to an existing prestressed concrete bridge with a single span 18.16m constructed in 1968-70. It needed to be upgraded due to the enhanced vehicular load (Jayaraman

RETROFIT OF EXISTING BRIDGES WITH CONCEPT OF INTEGRAL ABUTMENT BRIDGE

& Merz, 2001). The total width of the superstructure is 18.8m, which is composed of 4-lane undivided carriageway with the clear width of 15.3m and two footpaths with the clear width of 1.5m each, as shown in Fig. 55(a). The existing superstructure is made of 37 precast pre-tensioned inverted T-beams connected by casting in-situ reinforced concrete diaphragms and one deck slab. Elastomeric bearings were installed on reinforced concrete cantilever wall type abutments. Precast reinforced concrete square piles were used in the existing bridge. The elevation layout of the existing bridge is illustrated in Fig. 55(b) and the main features are listed in Table 12.



(a) Cross section layout



(b) Elevation layout

Fig. 55 Existing one-span SSB in Singapore (Jayaraman & Merz, 2001)

Bridge type (before and after retrofiting):	Simply supported bridge to Fully integral abutment bridge
Spans length (m):	18.16
Girder Type:	37 Precast pre-tensioned inverted T-beams
Deck width (m):	18.8 with 4-lane undivided carriageway and 2 footpaths
Abutment type:	Reinforced concrete cantilever wall type abutments
Pile type:	Precast reinforced concrete square piles

Table 12

Main features of a retrofitted bridge in Singapore

Three retrofiting approaches were proposed initially, including installing externally

bonded steel plates or composite materials, applying external prestressing and converting the SSB to the IAB. Comparing with the other two retrofitting methods, the retrofitting method with the FIAB concept is found to be the best choice, which can suit the real conditions on site where heavy vehicular and container traffic have to be maintained during retrofitting. The main retrofitting procedures are summarized in the following.

1. Demolish the wearing surfaces of the deck slabs near abutments and the top parts of abutments. Prepare the spaces for reinforcements and approach slabs.
2. Clean the exposed steel plates of elastomeric bearings through high-pressure water jet and apply protective coatings before encasing them with concrete
3. Retrofit existing abutments by diverting canal flow (Fig. 56). Add rebar on the front face of abutment walls. Cast concrete to form the new front face of abutment walls. Reinstate the canal flow.
4. Cast concrete to complete new deck slabs, approach slabs and fully integral connections between the superstructure and abutments. Restore backfill.

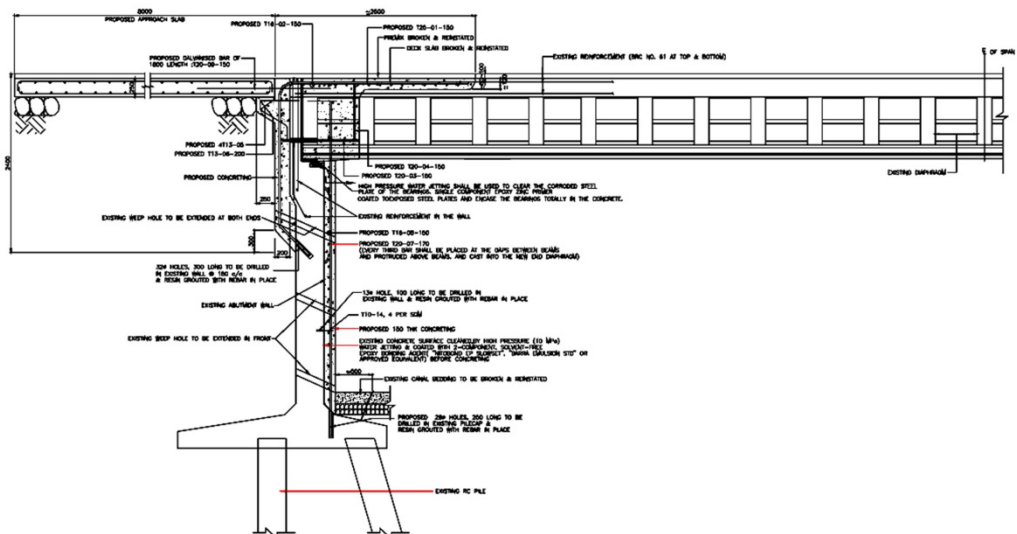


Fig. 56 Abutment retrofitting in a retrofitted bridge in Singapore (Jayaraman & Merz, 2001)

The vibration test and health monitoring were conducted on the bridge before and after retrofitting in order to investigate the improvements of structural performance. The results showed that the frequency corresponding to the first mode shape before and after retrofitting increases from 5Hz to 8.8Hz, and the maximum deck deflection subjected to live load decreases from 17.6mm to 13.2mm. Therefore, it indicated that the transformation from the SSB to the FIAB is effective in flexural strengthening of the deck (Jayaraman & Merz, 2001).

2.4 Advantages and opening issues of retrofit with IAB concept

2.4.1 Advantages

As introduced above, there are many retrofitting applications with the IAB concept all over the world. In addition to the attributes of using the IAB concept in newly constructed bridges, as introduced in Section 1.3.3, applying the IAB concept to retrofit existing bridges has some more advantages, as listed in the following.

1. Creep and shrinkage in existing bridges, which are more than 20 years old, can be neglected. As a result, the secondary stresses caused by creep and shrinkage and the longitudinal deformations of girders in existing bridges after retrofitting should be less than those in newly constructed IABs.
2. The deformation and uneven settlement of bridge foundations in existing bridges are nearly finished. Therefore, the secondary stress caused by foundation settlement can be neglected.
3. The differential deformations among different bridge components are almost completed in existing bridges. Consequently, connecting the superstructure and the substructure and eliminating existing expansion joints will not produce extra forces.
4. Girders and deck slabs are all constructed in existing bridges. Therefore, the cracking problem of connections, which usually happen in newly constructed IABs due to the construction procedure of girders and deck slabs, can be eliminated in retrofitting projects.
5. The validity of drainage systems and other ancillary facilities in existing bridges has been checked. If there are some problems, they can be retrofitted together with bridges.
6. Temperature variations, soil conditions and other in-service performance of existing bridges are understood well. Furthermore, the detailed field investigation could be also carried out, which is beneficial to choose an approximate retrofitting approach.

2.4.2 Opening issues

Although, the conversion from existing bridges into IABs has many additional advantages, by comparing with the newly constructed IABs, engineers should also recognize some opening issues.

1. The retrofitting plan varies for different cases, because it is severely restricted by the design and construction of existing bridges.
2. The retrofitting construction must consider the influence of traffic flow on existing bridges.

3. KEY ISSUES IN IAB ANALYSIS

Although the IAB concept will give a lot benefits and avoid many difficulties in structure, there are still some uncertainties in the analysis and design of an IAB, such as soil-structure interactions, modeling approaches for IAB and plastic hinge simulation. In order to build the reasonable finite element model for the IAB, these key issues should be investigated firstly, as summarized in this chapter.

3.1 Soil-structure interaction

As is well known, most of the civil engineering structures contact directly with ground. Therefore, when the structure moves according to external forces or internal forces, Structural displacements and ground displacements are dependent of each other. This interaction process is termed as soil-structure interaction. The soil-structure interaction in bridges can be usually divided into two aspects, which are the soil-abutment interaction and the soil-pile interaction.

For the existing SSB, the influence of soil-structure interactions can be neglected which is reasonable for light structures in relatively stiff soil. The piles beneath abutments and piers are often designed to carry vertical loads. However, the retrofitting with the IAB concept will let the bridge become stiff in relatively light soil. Consequently, the IAB can be considered as a fundamental example of soil-structure interactions which requires the coordinated attention of both structural and geotechnical engineers working as a multidisciplinary team (Horvath, 2005). The thermal load produced by daily and annual temperature variations, creep and shrinkage, and seismic loads in IABs are associated with the soil-structure interactions. They can create the lateral movements of piles and abutments, which will not present in SSBs due to the function of expansion joints and bearings. On the other hand, the lateral soil reaction is inherently nonlinear and depends on the magnitude of the abutment and pile movements. Therefore, in the analysis and design of the IAB, the soil-structure interactions should be considered as the biggest uncertainty (Faraji et al., 2001; Greimann et al., 1986; Shah, 2007; Zordan et al., 2011b).

Some widely used relationships of lateral soil-abutment interactions and soil-pile interactions obtained experimentally or theoretically are introduced in the following.

3.1.1 Soil-abutment interaction

3.1.1.1 Classical theories on lateral earth pressure

The lateral earth pressure is the pressure that soil exerts against a structure mainly in horizontal direction. It can be calculated using the earth pressure coefficient (K) defined according to the assumption that the horizontal earth pressure (σ_h) is directly proportional to the vertical pressure (σ_v) at any given point in the soil profile ($\sigma_h = K\sigma_v$) (Coduto, 2001; Shamsabadi, 2011), as illustrated in Fig. 57. The earth pressure coefficient can be divided into three categories according to the soil stress history, which are the at-rest earth pressure coefficient (K_0), the active earth pressure coefficient (K_a), and the passive earth pressure coefficient (K_p). These three different earth pressure coefficients can be predicted using many theories, including empirically based and analytically derived.

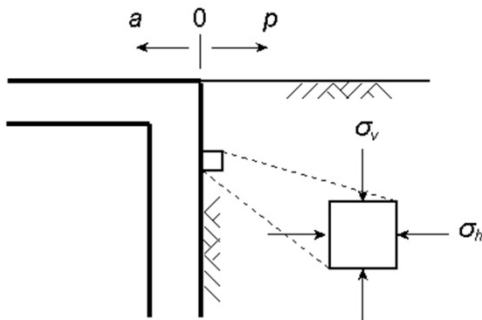


Fig. 57 Stress state of soil behind abutment

At-rest earth pressure coefficient

The at-rest earth pressure is acted on the abutment for a zero abutment lateral movement condition. The K_0 depends mainly on different soil types, loading-unloading histories and relative soil densities. The predicting formulae of K_0 in different cases are shown in the following.

1. For a zero lateral strain condition, horizontal and vertical stresses are related by the Poisson's ratio (μ).

$$K_o = \frac{\mu}{1 - \mu} \quad (1)$$

2. For normally consolidated soil and level backfill with different internal friction angles of soil (ϕ) (Jaky, 1948):

$$K_o = 1 - \sin\phi \quad (2)$$

3. For normally consolidated soil and sloping backfill with different slope angles of backfill (i) (Danish Geotechnical Institute, 1978):

$$K_o = (1 - \sin\phi)(1 + \sin i) \quad (3)$$

4. For overconsolidated soil with different over consolidation ratios (OCR) (Mayne & Kulhawy, 1982):

$$K_o = (1 - \sin\phi)(OCR)^{\sin\phi} \quad (4)$$

Active and passive earth pressure coefficients

The earth pressure decreases when the abutment wall moves outward from soil, until it reaches a minimum value which is the active earth pressure ($\sigma_h = K_a \sigma_v$); on the contrary, when the abutment wall moves toward soil, the earth pressure increases until it reaches a maximum value which is the passive earth pressure ($\sigma_h = K_p \sigma_v$).

The problem of lateral earth pressure on retaining structures was first studied by Coulomb (1776), which was extended by Mayniel (1808) and Müller-Breslau (1906) to account for the soil-structure friction angle (δ) and the slope of stem face (β), respectively. The Coulomb's theory is based on the limit equilibrium approach with an assumed planer wedge-shaped mass of soil bounded by the back of the wall, the backfill surface and the soil-sliding surface. It can be used for cohesionless soil. Formulae (5) and (6) can be used to calculate the active and passive earth pressure coefficients in Coulomb's theory.

$$K_a = \frac{\cos^2(\phi - \beta)}{\cos^2 \beta \cos(\beta + \delta) \left[1 + \sqrt{\frac{\sin(\phi + \delta) \sin(\phi - i)}{\cos(\beta + \delta) \cos(\beta - i)}} \right]^2} \quad (5)$$

$$K_p = \frac{\cos^2(\phi + \beta)}{\cos^2 \beta \cos(\beta - \delta) \left[1 + \sqrt{\frac{\sin(\phi + \delta) \sin(\phi + i)}{\cos(\beta - \delta) \cos(\beta - i)}} \right]^2} \quad (6)$$

where, δ is the soil-structure friction angle (degree). β is the slope of stem face (degree). ϕ is the internal friction angle of soil (degree). i is the slope angle of backfill (degree).

The Rankine's theory is the simplest solution which can predict active and passive earth pressure (Rankine, 1857) with some assumptions that the soil is cohesionless, and the wall is frictionless and vertical. The failure wedge is also assumed as planer, which is a function of soil internal friction and the backfill slope angle. Formulae (7) and (8) are corresponding to the active and passive earth pressure coefficients in Rankine's theory.

$$K_a = \cos i \frac{\cos i - \sqrt{\cos^2 i - \cos^2 \phi}}{\cos i + \sqrt{\cos^2 i - \cos^2 \phi}} \quad (7)$$

$$K_p = \cos i \frac{\cos i + \sqrt{\cos^2 i - \cos^2 \phi}}{\cos i - \sqrt{\cos^2 i - \cos^2 \phi}} \quad (8)$$

where, ϕ is the internal friction angle of soil (degree) and i is the slope angle of backfill (degree).

When the slope angle of backfill (i) is zero, which means the ground surface is horizontal, equations (7) and (8) can be simplified to formulae (9) and (10).

$$K_a = \tan^2 \left(45 - \frac{\phi}{2} \right) = \frac{1 - \sin \phi}{1 + \sin \phi} \quad (9)$$

$$K_p = \tan^2 \left(45 + \frac{\phi}{2} \right) = \frac{1 + \sin \phi}{1 - \sin \phi} \quad (10)$$

where, ϕ is the internal friction angle of soil (degree).

Neither the Coulomb's theory nor the Rankine's theory focuses on cohesionless soil. A modified Rankine's theory, which is usually called as Bell's relation, was proposed in order to calculate the lateral earth pressure of cohesion soil, which uses the square root of the earth pressure coefficient to predict the contribution of cohesion to the overall resulting pressure (Bell, 1915). Formulae (11) and (12) represent the active and passive lateral earth pressure of Bell's relation. In some cases of

cohesive backfill, a negative σ_a will be produced which means that there will be a height of the tension zone. In this case, the tension zone should be ignored and a simplified lateral earth pressure distribution would be acted along the entire wall height (Canadian Geotechnical Society, 2006; Shamsabadi, 2011) or the hydrostatic pressure would be exerted on the tension zone (Barker et al., 1991).

$$\sigma_a = \gamma H K_a - 2c\sqrt{K_a} \quad (11)$$

$$\sigma_p = \gamma H K_p + 2c\sqrt{K_p} \quad (12)$$

where, γ is the unit weight of soil (N/m^3). H is the height of pressure surface on the wall (m). c is the cohesion of soil (N/m^2).

The lateral earth pressure calculated using the Coulomb's theory or the Rankine's theory varies linearly with depth, and the resultant lateral earth load which is equal to the area of the load diagram ($P = 0.5\gamma H^2 K$), is assumed to act at a height of $H/3$ from the base. The direction of lateral earth pressure in Rankine's theory acts parallel to the slope of backfill; however, in the Coulomb's theory, the direction of lateral earth pressure acts at an angle (δ) to the normal line of the wall. For the Bell's solution, the lateral earth pressure distribution acts along the entire wall height.

There are many stable slopes in nature even though the backfill slope angle is larger than the soil internal friction angle due to presence of cohesion, which cannot be calculated by using the earth pressure theories introduced above. Formulae (13) to (16) can be used to solve this problem (Shamsabadi, 2011).

$$\sin i \leq \sin \phi + \frac{C}{l} \cos \phi \quad (13)$$

$$l = \frac{1}{\cos \phi^2} \left[\sigma_x + \frac{1}{2} \sin(2\phi) - \sqrt{\sigma_v (\cos^2 i - \cos^2 \phi) + \sigma_x [C \sin(2\phi)] + C^2 \cos^2 \phi} \right] \quad (14)$$

$$\sigma_v = \gamma(H \cos i) \quad (15)$$

$$\sigma_x = \gamma(H \cos^2 i) \quad (16)$$

where, C is the cohesion of soil (N/m^2) and ϕ is the internal friction angle of soil (degree).

For irregular backfill sloping ground, the trial wedge method can be used (Shamsabadi, 2011). For any assumed soil failure wedges, the maximum values of

active and passive earth pressure can be determined using formulae (17) and (18) based on the limiting equilibrium. The trial wedge method is an iterative process; therefore, a convenient graphical solution was developed (Culmann, 1866).

$$P_a = \frac{W[\tan(\alpha - \phi)] - C_o L_c [\sin \alpha \tan(\alpha - \phi) + \cos \alpha] - C_a L_a [\tan(\alpha - \phi) \cos(-\beta) + \sin \beta]}{[1 + \tan(\delta - \beta) \tan(\alpha - \phi)] \cos(\delta + \beta)} \quad (17)$$

$$P_p = \frac{W[\tan(\alpha + \phi)] + C_o L_c [\sin \alpha \tan(\alpha - \phi) + \cos \alpha] + C_a L_a [\tan(\alpha - \phi) \cos(-\beta) + \sin \beta]}{[1 - \tan(\delta + \beta) \tan(\alpha + \phi)] \cos(\delta + \beta)} \quad (18)$$

where, δ is the soil-structure friction angle (degree). β is the slope of stem face (degree). α is the failure plane angle (degree). ϕ is the internal friction angle of soil (degree). W is the weight of soil (N). L is the length of the failure plane surface (m).

The theory with planer failure surface is simple to use; however, many experiment results showed that the sliding surface is not a plane, but a curved surface. Moreover, there are many application limitations of the theory with the planer failure surface. For example, the Rankine's theory for passive pressure can be only used correctly when the backfill slope angle is not more than zero, and it is not correct and will give unsafe results when the soil-structure friction value is large. When the Coulomb's theory is used, it can only provide the approximate active pressure coefficient, because the soil-structure friction requires a curved sliding surface to satisfy equilibrium, and with the depth increases, the accuracy diminishes. For passive earth pressure, the Coulomb's theory can give overestimated results, especially when the soil-structure friction angle exceeds (0.33–0.5) ϕ (Clough & Duncan, 1991; Cole & Rollins, 2006; Duncan & Mokwa, 2001; Shamsabadi, 2011).

Due to the unrealistic earth pressure obtained by theories assuming a straight planer failure surface, the Log spiral theory was developed. Many numerical analyses were conducted to calculate the passive earth pressure coefficient based on the plasticity theory, and all results showed that the logarithmic spiral failure surface has a close agreement (Cole & Rollins, 2006; Duncan & Mokwa, 2001; Kumar & Subba Rao, 1997; Martin & Yan, 1995; Rollins & Sparks, 2002; Soubra, 2000; Zhu & Qian, 2000). There are two different Log Spiral failure surface types. One is the failure surface combining a logarithmic spiral and a straight line suggested by Terzaghi (1943). Another type uses one single arc of the logarithmic spiral to represent the failure surface proposed by Morrison Jr & Ebeling (1995). Many researches have been conducted using this method, especially on passive earth pressure. The most general method applying the Log Spiral theory is the graphical calculation procedure.

Its accuracy is very high; however, the calculation process is also very complex (Terzaghi, 1943; Terzaghi et al., 1996). In order to use it simply, the logarithmic spiral method with charts was proposed by Caquot & Kerisel (1948), which was also suggested in some literatures and codes (Barker et al., 1991; Shamsabadi, 2011; US Navy, 1986). Due to the fast development of the computer technology, some researchers applied the Log Spiral theory in numerical analyses, such as computer program PYCAP by Duncan & Mokwa (2001), and LSH process by Shamsabadi et al. (2005) and Shamsabadi et al. (2007).

Equivalent fluid pressure method

The equivalent fluid pressure method use some empirical charts, which can predict lateral earth pressure with the consideration of only the soil classification and slope angle of backfill, were developed by Terzaghi et al. (1996). The benefit of this method is that it typically creates an easily understood minimum design loading regardless of structure geometry and soil properties. Typical values for equivalent fluid densities of soil can be found in 'AASHTO LRFD Bridge Design Specifications' (American Association of State Highway and Transportation Officials, 2007)

3.1.1.2 Soil-abutment interaction for IAB

General recommendations for IAB

According to an investigation on the soil-abutment interaction of the IAB design (Kunin & Alampalli, 2000), it could be found that at least two Departments of Transportation in USA neglect earth pressure consideration in smaller IABs and three agencies neglect earth pressure in all their designs. Some researchers also indicated that, neglecting the effects of passive earth pressure may be acceptable for single-span IABs and short IABs with two or three spans (Burke, 1993a).

However, the consideration of earth pressure cannot be neglected for most IABs. It was demonstrated by many researchers and some codes that the passive earth pressure caused by the thermal expansion should be considered as more important factor in the IAB design, compared with the active earth pressure caused by the thermal contraction, live loads surcharge on backfill, and creep and shrinkage (Feldmann et al., 2010; Highways Agency, 2003; Imbsen, 2007). The investigation by Kunin & Alampalli (2000) also showed that most Departments of Transportation in USA consider only passive earth pressure in the IAB design.

The magnitude and distribution of Rankine's passive pressure were widely used by many researchers (Wasserman, 2001). A passive pressure envelope, which combines Rankine's passive pressure coefficients in the upper third of the wall and Rankine's active pressure coefficients towards the base of the abutment, has been proposed in the IAB design. This method is based on the premise that higher lateral earth pressure develops at the top of the wall, and lower pressure at the bottom because the movement of the wall subsides at its base (Broms & Ingelson, 1971).

According to the research by Burke (1993), the idealized formula of the ultimate passive earth pressure, which can be used to design integral abutment bridges with capped pile stub-type abutments, is shown in the equation (19).

$$p_p = \gamma \tan^2 \left(45 + \frac{\phi}{2} \right) H + 2C \tan^2 \left(45 + \frac{\phi}{2} \right) \quad (19)$$

where, γ is the unit weight of soil (N/m^3). H is the height of the pressure surface on the wall (m). ϕ is the internal friction angle of soil (degree). C is the cohesion of soil (N/m^2).

However, some researcher found that using full passive earth pressure is not conservative because it reduces the flexural effects of dead and live loads in bridge girders (Arsoy, 2000; Burke, 1993a). In order to resolve this problem, a method using 2/3 of full passive earth pressure, was suggested by some researchers (Burke, 1993a; Chen, 1997).

Besides the ultimate earth pressure, the lateral earth pressure distributions behind abutments proposed by different researchers are also varied. The abutment movement has some typical modes, such as the lateral translation, the rotation around the top, the rotation around the bottom and their combinations. According to the results of many tests, in-field monitoring and numerical analyses, the typical lateral earth pressure distributions along the abutment height according to different modes of abutment movements are summarized as follows.

For the lateral translation (Lawver et al., 2000), the distribution of lateral earth pressure is triangular which means that the lateral earth pressure can increase linearly with the maximum value at the bottom of the abutment (Fang et al., 1994; Hassiotis & Xiong, 2007; Thompson, 1999). Some empirical or numerical relationships between lateral earth pressure coefficients and abutment movements were proposed. In these relationships, the lateral earth pressure coefficients along the abutment height are always uniform. When the abutment rotates around the top,

the lateral earth pressure distribution is parabolic increasing obviously near the bottom (Fang et al., 1994; Thompson, 1999). The position of lateral earth constant force was proposed as $0.18H$ above the bottom by Fang et al. (1994). For rotation around the bottom, the lateral earth pressure distribution is parabolic with the maximum value towards the upper half of the abutment height (Broms & Ingelson, 1971; England et al., 2000; Fang et al., 1994; Lehane, 2011; Thompson, 1999). According to different test results, the region which has the maximum lateral earth pressure is usually from $H/4$ to $H/2$ calculating from the top (Thompson, 1999). From another test, Fang et al. (1994) indicated that the position of the constant lateral earth force could be proposed as $0.55H$ calculating from the bottom. Based on the monitoring results of an IAB, the lateral earth pressure at the abutment mid-height is larger than those at the top or bottom (Broms & Ingelson, 1971). Some special lateral earth pressure distributions considering the combination of the translation and rotation were proposed by some researchers (Krizek, 2011; Thompson, 1999). For example, Thompson (1999) found that the earth pressure distribution increases from the top to a depth of approximately $0.38H$, and then remains constant. The constant lateral earth pressure distribution along the abutment height can be also used for simplified analysis. The full-scale testing of the IAB 'Scotch Road' and other tests demonstrated that the abutment rotation is relatively small compared with the lateral translation (Hassiotis & Xiong, 2007).

Lateral earth pressure-abutment movement relationship for IAB

As known, the earth pressure is dependent to the abutment movement into or away from backfill. Therefore, considering how the lateral abutment movement develops as a function of the earth pressure changing from the active value to the passive value is very important. Many experiments were conducted by bridge engineers and geologists to study this relationship (Duncan & Mokwa, 2001; England et al., 2000; Fang et al., 1994; Lehane et al., 1999; Narain et al., 1969; Rollins & Sparks, 2002; Rowe & Peaker, 1965; Terzaghi, 1943; Thompson, 1999; Tschebotarioff & Johnson, 1953). Several empirical or numerical curves and formulae, which can simulate the relationships between lateral earth pressure and abutment movements, have been proposed in some codes and literatures. These curves can be linear or nonlinear.

Relationship with constant soil stiffness

The cyclic loading test results of sands suggested that using constant soil stiffness to simulate soil-abutment interactions in IABs is reasonably realistic (Springman et al., 1996). A simple elastic finite element model with equivalent abutment height and

a single translational spring was used to analyze a single-span IAB (Lehane et al., 1999). It indicated that using linear stiffness to simulate the cohesionless backfill-abutment interaction is sufficient for design. Furthermore, based on some test results, it could be found that the stiffness of linear soil springs can be chosen as 40% of the small-strain stiffness of backfill materials which can be measured using standard geophysical techniques (Lehane, 2011). Some researchers used a series of linear spring elements along the abutment height to simulate soil-abutment interactions of IABs in finite element models. For example, the typical stiffness of different soil types proposed in some codes were chosen as the spring stiffness in the finite element model of an IAB in Malaysia to analyze the performance of this bridge subjected to different traffic load combinations (Thanoon et al., 2011). Moreover, the stiffness obtained from the lateral earth pressure-abutment movement relationship proposed by Barker et al. (1991) was adopted as the spring stiffness in the finite element models of IABs (Abendroth & Greimann, 2005; Dicleli & Erhan, 2008, 2009, 2010; Erhan & Dicleli, 2009a, b). The soil-abutment spring stiffness can be also estimated based on the experimental results or field investigation (Talbot, 2008).

Some researchers used an iterative equivalent linear approach, which can obtain the suitable stiffness of soil through multiple iterations (Hong, 2006; Jayaraman & Merz, 2001; Shah, 2007).

Relationship proposed by Tschebotarioff & Johnson (1953)

The lateral earth pressure coefficient-abutment rotation relationship curves for different sand types was proposed by Tschebotarioff & Johnson (1953), as illustrated in Fig. 58. This relationship is adopted in some codes (Canadian Geotechnical Society, 1978; US Navy, 1986). The magnitudes of rotation around the bottom (Ratio of Δ (displacement at the top) to H (abutment height)) corresponding to the minimum active and maximum passive earth pressures for different soil types are listed in Table 13. The Rankine's theory or log spiral charts for uniform and regular backfill configurations and the Coulomb's trial failure wedge method for irregular backfill configurations are proposed to obtain lateral earth pressure coefficients (US Navy, 1986). By comparing with some test results, including tests conducted by Thompson (1999) and some full scale wall tests of MassHighway's standard compacted gravel borrow performed by the University of Massachusetts in USA (Thompson & Lutenegger, 1998), this relationship for dense sand shows a good agreement. In this relationship, the lateral earth pressure distribution along the abutment height is triangular, as illustrated in Fig. 58. The stiffness of the

relationship is nonlinear.

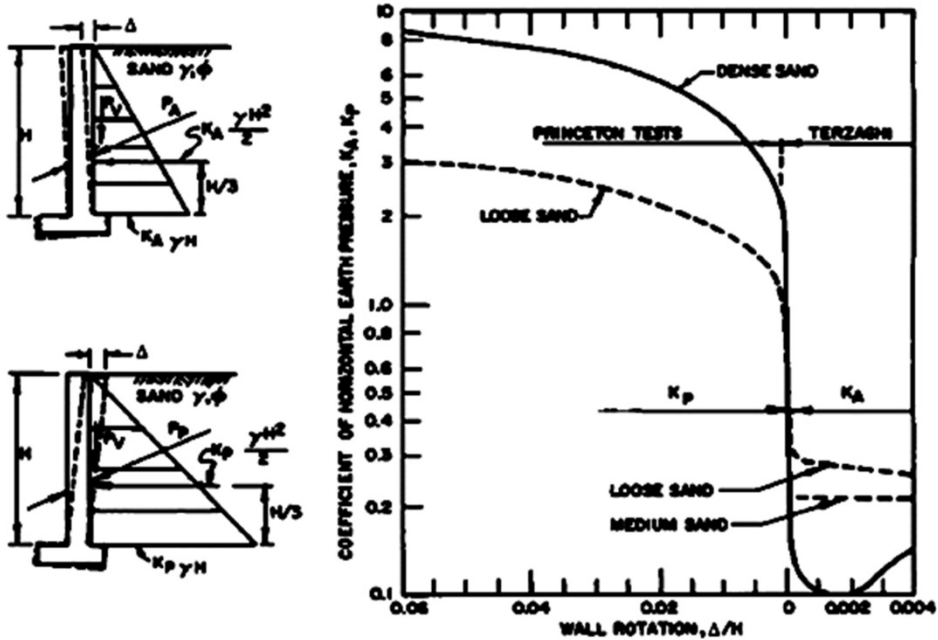


Fig. 58 Lateral earth pressure coefficient-abutment rotation relationship curve (Tschebotarioff & Johnson, 1953)

Soil type and condition	Rotation Δ/H	
	Active	Passive
Dense cohesionless	0.0005	0.002
Loose cohesionless	0.002	0.006
Stiff cohesive	0.01	0.02
Soft cohesive	0.02	0.04

Table 13

Magnitudes of abutment rotation around the bottom for different soil types (Tschebotarioff & Johnson, 1953)

Relationship proposed by Hambly & Burland (1979)

The lateral earth pressure coefficient-abutment movement relationship curves for dense and loose sands are illustrated in Fig. 59 (Hambly & Burland, 1979). The abutment movement includes both lateral translation and rotation around the bottom. In this relationship, the lateral earth pressure distribution along the abutment height is triangular and the stiffness of the relationship is nonlinear.

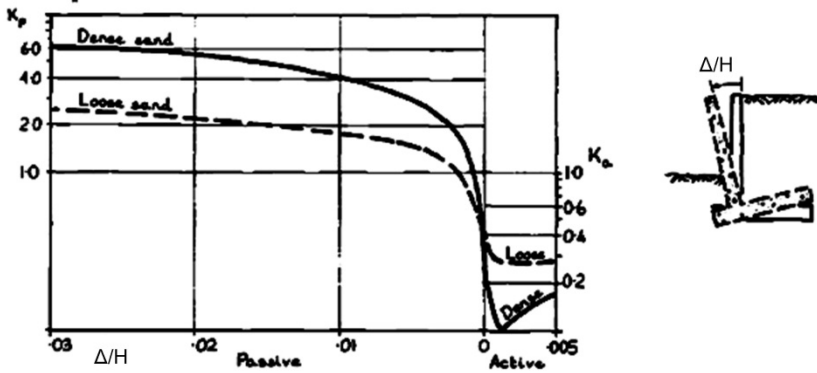
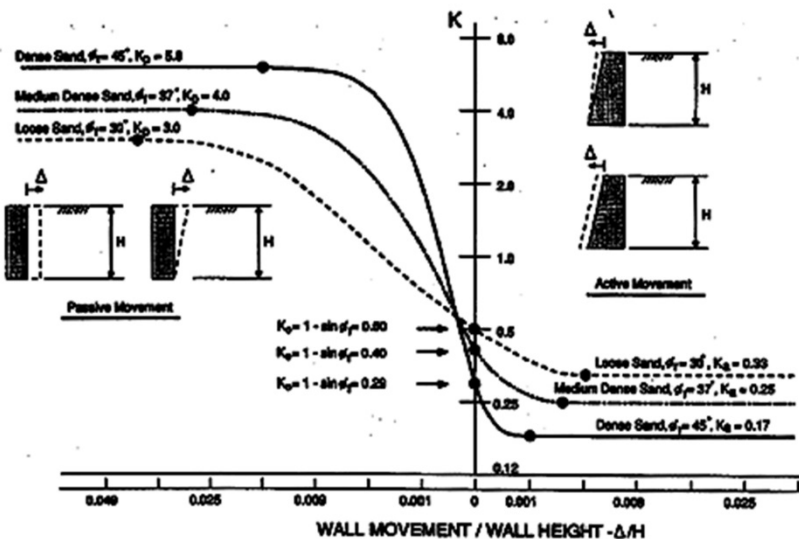


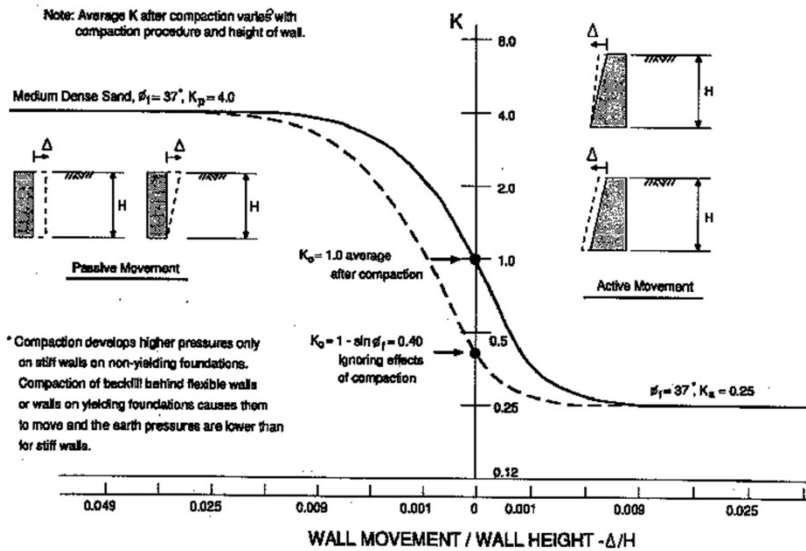
Fig. 59 Lateral earth pressure coefficient-abutment rotation relationship curve (Hambly & Burland, 1979)

Relationship proposed by Clough & Duncan (1991)

Based on finite element analyses, a series of lateral earth pressure coefficient-abutment movement relationship curves were proposed by Clough & Duncan (1991). The curves for normal backfill and compacted backfill are illustrated respectively in Fig. 60(a) and (b). The abutment movement includes both lateral translation and rotation around the bottom. The typical ratios of Δ (displacement at the top of the abutment) to H (abutment height) for different soil types including sands and clays, corresponding to the minimum active and maximum passive earth pressure, are listed in



(a) Normal backfill



(b) Compacted backfill

Fig. 60 Lateral earth pressure coefficient-abutment movement relationship curve (Barker et al., 1991)

Type of backfill	Value of Δ/H	
	Active	Passive
Dense sand	0.001	0.01
Medium dense sand	0.002	0.02
Loose sand	0.004	0.04
Compacted slit	0.002	0.02
Compacted lean and fat clay	0.01	0.05

Table 14

Ratios of lateral displacement to wall height for different soil types (Clough & Duncan, 1991)

This relationship has been adopted in several literatures and design manuals (American Association of State Highway and Transportation Officials, 2007; Barker et al., 1991; Fang, 1991; Shamsabadi, 2011). For determining the lateral earth pressure coefficient, 'Manuals for the Design of Bridge Foundations' (NCHRP) (Barker et al., 1991) suggested to use the Rankine's theory or log spiral charts for uniform and regular backfill configurations and the Coulomb's trial failure wedge method for irregular backfill configurations. In this relationship, the lateral earth pressure distribution along the abutment height is triangular and the stiffness of the relationship is nonlinear.

The curves for normal backfill illustrated in Fig. 60(a) was also chosen by Husain &

RETROFIT OF EXISTING BRIDGES WITH CONCEPT OF INTEGRAL ABUTMENT BRIDGE

Bagnariol (1996) to simulate the lateral soil-abutment interaction in IABs, considering the cohesionless soil as backfill. Different ratios of Δ to H corresponding to the minimum active and maximum passive earth pressure for different modes of abutment movements are listed in Table 15.

Value of Δ/H				
Active		Passive		
Lateral translation	Rotation around bottom	Lateral translation	Rotation around bottom	Rotation around top
0.001	0.002	0.05	0.1	0.02

Table 15

Ratios of lateral displacement to wall height for cohesionless soil (Husain & Bagnariol, 1996)

Based on the relationship proposed by Clough & Duncan (1991), a modified relationship curve was proposed for the IAB (Dicleli, 2000a, b), which can be calculated using the formula (20). For practice purpose, the lateral earth pressure coefficient corresponding to the wall movement of the IAB changes linearly from the at-rest coefficient to the passive earth pressure coefficient, as illustrated in Fig. 61.

$$K = K_o + \varphi \cdot \Delta \tag{20}$$

where, Δ is the abutment displacement towards backfill and φ is the slope of the earth pressure variation. The typical value of φ varies as a function of the backfill soil type based on the stipulations in NCHRP (Barker et al., 1991).

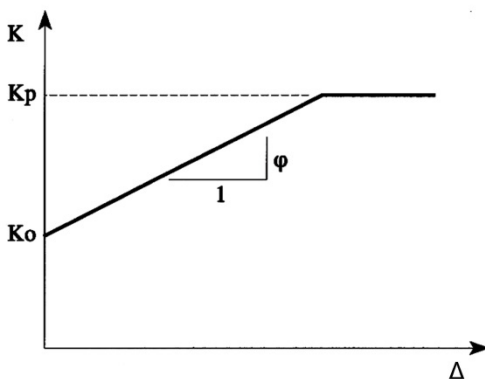


Fig. 61 Passive pressure coefficient-relative wall displacement relationship curve (Dicleli, 2000a, b)

The relationship proposed in NCHRP (Barker et al., 1991) has been compared with

some test results and bridge monitoring data. The results from some full scale wall tests performed by the University of Massachusetts in USA (Thompson & Lutenegger, 1998) showed a reasonable agreement can be found between the curve for dense sand and the predicted average passive earth pressure response of MassHighway's standard compacted gravel borrow. By comparing with some test results of the IAB (Ting & Faraji, 1998), the curve for loose sand can provide an accurate representation of the test data. A triangular soil pressure distribution along the wall height is suggested to represent the soil pressure distribution if the wall rotates around its base. The monitoring data of an IAB 'Scotch Road Bridge' was compared with the curve and the passive earth pressure coefficient (K_p) proposed in NCHRP (Barker et al., 1991) (Hassiotis & Xiong, 2007). It could be found that in the first two years, the earth pressure is low; however, it is larger than that in NCHRP for the loose sand. In the fourth year, the K_p is closer to the predicted value in NCHRP for the dense sand. For small displacements, the coefficients increase with displacements increase and can be predicted by the NCHRP proposed K_p for the dense sand. However, for large displacements, the coefficients decrease a little as the bridge overcomes the original resistance of the soil and the maximum K_p is smaller than the NCHRP proposed K_p for the dense sand. It is because that during summer months, the shear resistance is overcome and the retained soil acts more like the loose sand.

The relationship proposed in NCHRP (Barker et al., 1991) has been widely adopted by many researchers to simulate soil-abutment interactions in IABs. For example, it was used in the finite element model (ANSYS) based on a real 400-metre-long FIAB to carry out several analyses, such as thermal pushover analysis, maximum length estimation and so on (Briseghella et al., 2010; Zordan et al., 2011a, b; Zordan et al., 2011c). Shoukry et al. (2006) used this relationship as the nonlinear spring properties to simulate soil-abutment interactions in the finite element model (ADINA) of a three-span IAB located in Evansville, West Virginia, to study the axial effect of backfill pressure against the expansion of the IAB with steel girders. Civjan et al. (2007) used it in a nonlinear finite element model (GTSTRUDL) to conduct the parametric analysis. It was also used this relationship as the nonlinear spring properties in a finite element model of an IAB (Bemis Road Bridge: F-4-20) located in Fitchburg, Mass with the length of 45.7m (Faraji et al., 2001; Ting & Faraji, 1998). The NCHRP relationship was also adopted by some researchers to analyze several IABs by the nonlinear spring elements in SAP2000 (Dicleli, 2005; Dicleli & Albhaisi, 2003, 2004b, c, 2005; Kalayci et al., 2009; Kalayci et al., 2012; Kalayci et al., 2011).

Relationship proposed by German researchers (1994)

The lateral earth pressure coefficient-abutment movement relationship curves illustrated in Fig. 62 was proposed by a group of German researchers (Forschungsgesellschaft für Straßen- und Verkehrswesen, 1994). In this relationship, the displacement corresponding to the active earth pressure coefficient (Δ_a) is the key factor. Using two different Δ_a , three modes of abutment movements can be taken into account. For rotation around the bottom, the Δ_a is $0.002H$ and for lateral translation or rotation around the top, the Δ_a is $0.0005H$. In this relationship, the lateral earth pressure distribution along the abutment height is triangular and the stiffness of the relationship is nonlinear. This relationship with different friction angles was used by Kerokoski (2006) to model the soil-abutment interaction of a three span IAB 'Haavistonjoki Bridge' in Finland with a length of 50m.

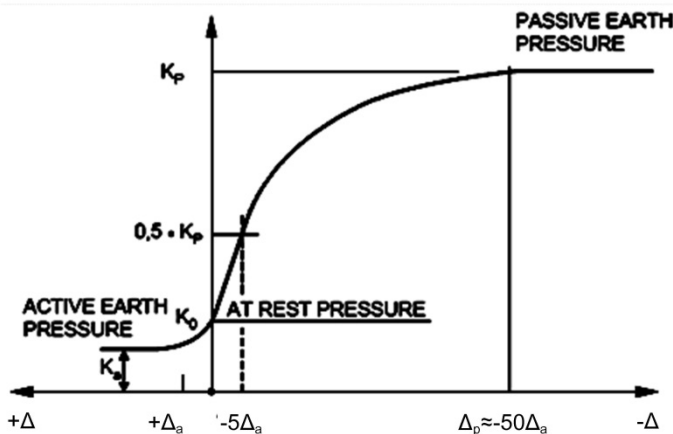


Fig. 62 Lateral earth pressure coefficient-abutment movement relationship curve (Forschungsgesellschaft für Straßen- und Verkehrswesen, 1994)

Relationship proposed by Zhang et al. (1998)

By employing the concept of “intermediate soil wedge” with the planar sliding surface, the lateral earth pressure coefficient-abutment displacement relationship curves was proposed by (Zhang et al., 1998) based on the strain increment ratio, as illustrated in Fig. 63. This relationship can be calculated by formulae (21) to (24). In this relationship, the lateral earth pressure distribution along the abutment height is triangular and the stiffness of the relationship is nonlinear.

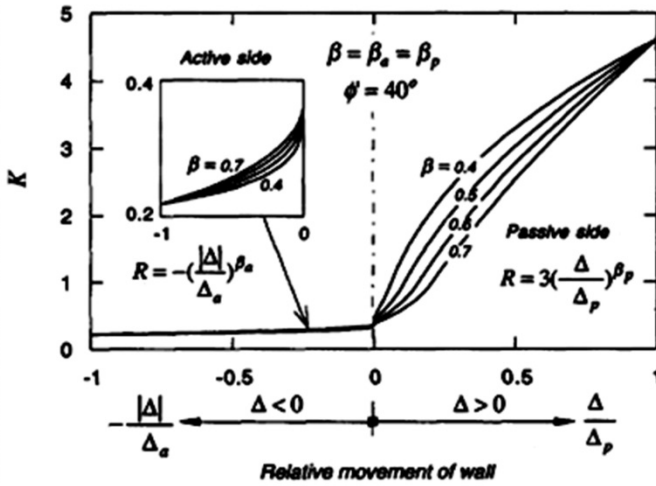


Fig. 63 lateral earth pressure coefficient-abutment movement relationship curve (Zhang et al., 1998)

$$R = \begin{cases} -\left(\frac{|\Delta|}{\Delta_a}\right)^{\beta_a} & (-\Delta_a \leq \Delta \leq 0) \\ -1 & (\Delta < -\Delta_a) \end{cases} \quad (21)$$

$$R = \begin{cases} 3\left(\frac{\Delta}{\Delta_p}\right)^{\beta_p} & (0 \leq \Delta \leq \Delta_p) \\ 3 & (\Delta > \Delta_p) \end{cases} \quad (22)$$

$$K = \frac{K_o}{1 - (1 - K_o)R} \quad (-1 \leq R \leq 1) \quad (23)$$

$$K = 1 + \frac{K_p - 1}{2}(R - 1) \quad (1 \leq R \leq 3) \quad (24)$$

where, R is the soil lateral strain parameter. β_a and β_p are recommended to take around 0.5.

Relationship proposed by Thompson (1999)

A lot of tests were carried out by Thompson (1999). Based on the measured results and other test results (Bros, 1972; Fang et al., 1994; Narain et al., 1969), three calculation formulae (25), (26) and (27) corresponding to three combinations of commonly used abutment types and backfill were proposed (Thompson, 1999). When the abutment movement, the abutment height and the soil depth are fixed, the lateral passive earth pressure coefficient can be predicted by these formulae. It

RETROFIT OF EXISTING BRIDGES WITH CONCEPT OF INTEGRAL ABUTMENT BRIDGE

could be found that the passive earth pressure coefficient obtained by the Coulomb's equation has the closest agreement with the measured results. Using these equations, the lateral earth pressure distribution along the abutment height is irregular, because the lateral earth pressure coefficient varies nonlinearly along the abutment height from the top. The stiffness of the relationship is nonlinear.

For shallow foundations and compacted gravel backfill:

$$K = 0.43 + \left(-18 \frac{Z}{H} + 16\right) \left[1 - e^{-350\Delta/H}\right] \quad (25)$$

For deep foundations and compacted gravel backfill:

$$K = 0.43 + \left(-9.5 \frac{Z}{H} + 16\right) \left[1 - e^{-250\Delta/H}\right] \quad (26)$$

For deep foundations and uncompacted sand zone:

$$K = 0.43 + \left(-8.6 \frac{Z}{H} + 16\right) \left[1 - e^{-250\Delta/H}\right] \quad (27)$$

where, z is the soil depth. H is the abutment height. Δ is the abutment displacement at the top.

Based on formulae (25) to (27), three simplified formulae (28), (29) and (30) using the average earth pressure coefficient along the abutment height were proposed for design. The resultant force locations can be determined by the orientation of abutment wingwalls. Using these equations, the lateral earth pressure distribution along the abutment height is triangular and the stiffness of the relationship is nonlinear.

For shallow foundations and compacted gravel backfill:

$$K = 0.43 + 5.07 \left[1 - e^{-213.52\Delta/H}\right] \quad (28)$$

For deep foundations and compacted gravel backfill:

$$K = 0.43 + 5.70 \left[1 - e^{-190\Delta/H}\right] \quad (29)$$

For deep foundations and uncompacted sand zone:

$$K = 0.43 + 3.82 \left[1 - e^{-140.68\Delta/H}\right] \quad (30)$$

The design guideline of the IAB proposed by the Massachusetts Department of Transportation (2007) adopts the formula (29) to consider the soil-structure interaction. It stipulates that the magnitude of lateral passive earth pressure should depend on the abutment movement subjected to thermal load, whose value is

assumed to be somewhere between at-rest and full passive pressure, as illustrated in Fig. 64. This relationship was used to simulate the soil-abutment interaction in the finite element model of a three-span IAB 'Orange-Wendell Bridge' by some researchers (Bonczar et al., 2005a; Bonczar et al., 2005b).

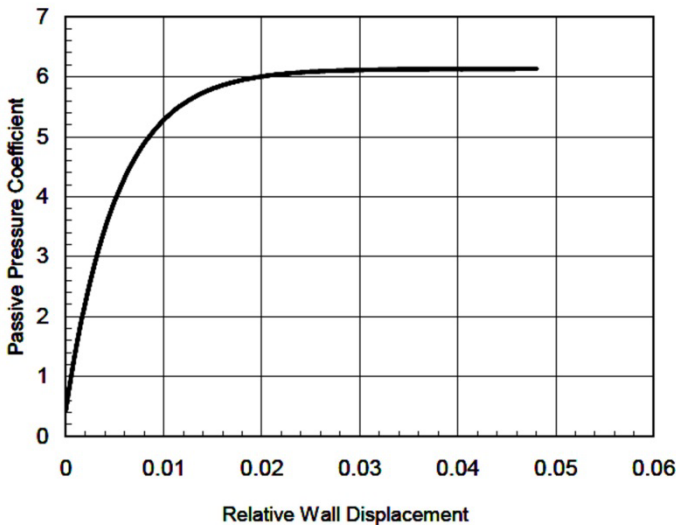


Fig. 64 Passive earth pressure coefficient-relative wall displacement relationship curve (Massachusetts Department of Transportation, 2007)

Relationship proposed by Duncan & Mokwa (2001)

The lateral passive earth pressure depends on several factors, such as the magnitude and direction of the movement, the strength and stiffness of soil, the friction between the abutment and soil, and the geometry of the abutment. Based on the Log Spiral theory and the consideration of 3D influence, the hyperbolic formula (31) was proposed by Duncan & Mokwa (2001), which can be used to calculate the lateral passive earth load-displacement relationship curve, as illustrated in Fig. 65. A value of 0.04 for the maximum displacement normalized by the wall height was recommended. In this relationship, the lateral earth pressure distribution along the abutment height will be constant; however, the stiffness of the relationship is nonlinear. This relationship is found to have a good agreement with the test results (Cole & Rollins, 2006) and has been chosen by some researchers to analyze the IAB (Dicleli & Erhan, 2011; Mokwa & Duncan, 2000)

$$P = \frac{\Delta}{\left[\frac{1}{K_{\max}} + R_f \frac{\Delta}{P_{ult}} \right]} \quad (31)$$

$$R_f = 1 - \frac{P_{ult}}{K_{max} \Delta_{max}} \quad (32)$$

$$P_{ult} = E_p M w \quad (33)$$

where, K_{max} is the initial slope of the relationship curve. R_f is the failure ratio ($P_{ult}/$ hyperbolic asymptote) that is in the range of 0.75~0.95 or can also be estimated using the formula (32) (Cole & Rollins, 2006). E_p is the passive resistance per unit length (N/m), calculated using the Log Spiral theory. M is the Ovesen-Brinch Hansen correction factor for 3D effects (Hansen, 1966; Ovesen, 1964), with a limit of 2. w is the wall width (m). P_{ult} can be calculated by formula (33).

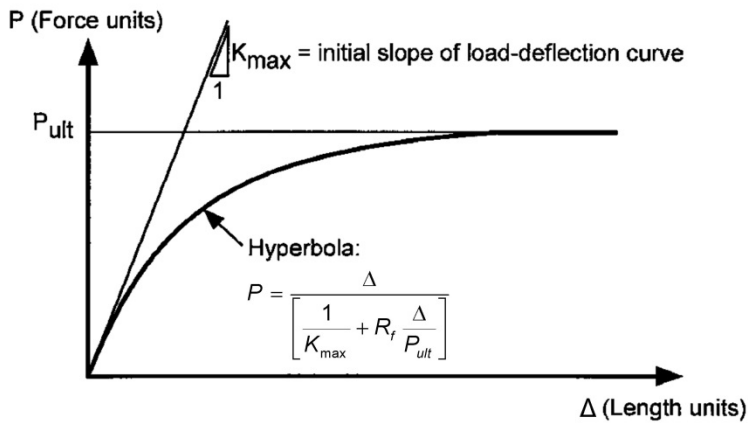


Fig. 65 Hyperbolic lateral passive earth load-displacement relationship curve (Duncan & Mokwa, 2001)

Relationship proposed in Swedish Bridge Code (2002)

An additional lateral earth pressure, which is function of the horizontal movement of the bridge, and the at-rest earth pressure are both taken into account in Swedish design code. It can be divided into two cases (Flener, 2004).

The first case focuses on the reaction pressure on piles, pillars and frame walls. In this case, the lateral earth pressure distribution along the abutment height is combined with the additional pressure (dP) and the at-rest earth pressure, as illustrated in Fig. 66. The stiffness of the relationship is nonlinear.

The formula (34) can be used to estimate the additional lateral earth pressure (dP), which is valid until $H/2$ and approaches to 0 at the bottom.

$$dP = C\gamma z \frac{\Delta}{H} \quad (34)$$

where, C is 300 or 600 depends on the force is advantageous (movement due to breaking forces) or disadvantageous (movement due to thermal variations). γ is the unit weight of soil (N/m^3). z is the soil depth (m). Δ is the horizontal deflection of the abutment (m). H is the abutment height (m).

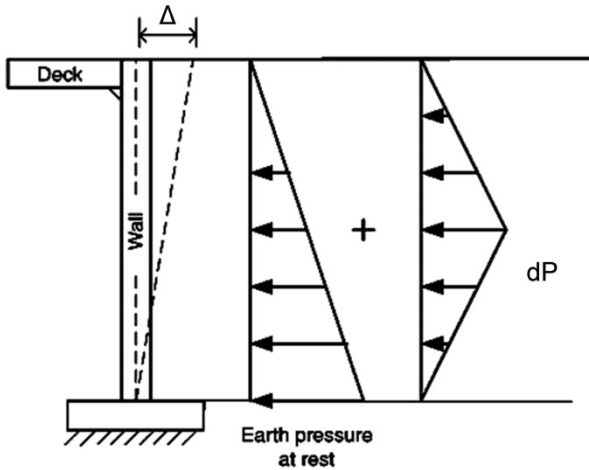


Fig. 66 Design earth pressure proposed in Swedish Bridge Code (Swedish National Road Administration, 2002)

The second case concentrates on the earth pressure on integral abutments with end-screens. In this case, the total lateral earth pressure can be calculated by formula (37). In this relationship, the lateral earth pressure distribution along the abutment height will be triangular; however, the stiffness of the relationship is nonlinear.

$$P = \begin{cases} P_o & \Delta = 0 \\ P_o + C_1 \Delta (200 / H) (P_p - P_o) & 0 < \Delta < H / 200 \\ P_o + C_1 (P_p - P_o) & \Delta > H / 200 \end{cases} \quad (35)$$

where, C_1 is 1 or 0.5 depends on the force is advantageous (movement due to breaking forces) or disadvantageous (movement due to thermal variations). P_o is the at-rest earth pressure (N/m^2). P_p is the passive earth pressure (N/m^2). Δ is the horizontal deflection of the abutment (m). H is the abutment height (m).

The earth pressure coefficients for different soil types are also proposed in Swedish design code (Swedish National Road Administration, 2002), as listed in Table 16.

Material	K_o	K_a	K_p
Crushed stone	0.34	0.17	5.83
Subbase material	0.36	0.22	4.60
Clinker	0.43	0.27	3.70
Plastic cell	0.40	0	-

Table 16

Earth pressure coefficients proposed in Swedish Bridge Code (Swedish National Road Administration, 2002)

Relationship proposed in Highways Agency Design Manual for Roads and Bridges (2003)

In the Highways Agency Design Manual for Roads and Bridges (Department of Transport, 2003), the proposed design earth pressure distributions along the abutment height for three different abutment types are summarized in the following. They are largely based on the findings of centrifuge and analytical studies reported by Springman et al. (1996). The active earth pressure on abutments can be ignored.

1. Shallow height bank pad and end screen abutments

The typical height of a bank pad or end screen abutment is up to 3m and the total force generated by passive excitations is accommodated within the design. The earth pressure coefficient can be calculated by formula (36), when the retained height and thermal displacement at the top are known. For this abutment type, the lateral earth pressure distribution along the abutment height will be triangular and the stiffness of the relationship is nonlinear.

2. Full height frame abutments

For full height frame abutments, the magnitudes of passive pressure acting on the back of the wall are likely to be significant. The lateral earth pressure distribution along the abutment height will be special, which can be divided into three parts, as illustrated in Fig. 67. In the first part, the lateral earth pressure distribution is triangular based on the uniform lateral earth pressure coefficient K^* over the top one-half of the wall height. Then in the second part, the lateral earth pressure distribution remains constant with the depth increases, because the lateral earth pressure coefficient K^* drops towards K_o . Finally, the lateral earth pressure can increase again with the depth increases and obtain the maximum value at the

bottom. According to the lateral earth pressure coefficient falls to K_o , and then keep the same below that depth. The lateral earth pressure coefficient K^* can be obtained by formula (37). For this abutment type, the stiffness of the relationship is nonlinear.

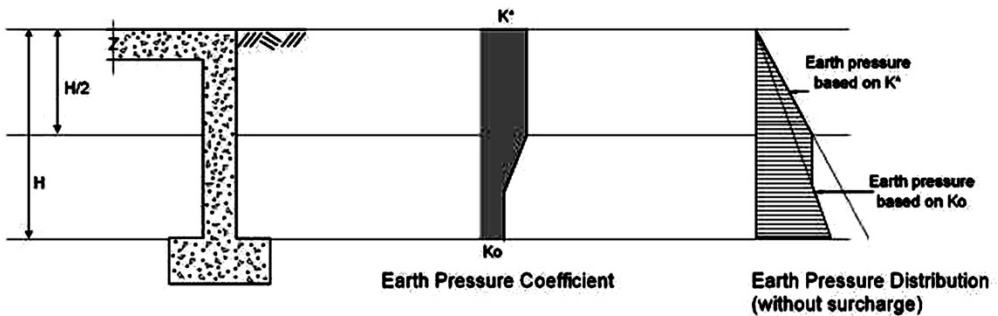


Fig. 67 Earth pressure distribution for frame abutment (Department of Transport, 2003)

However, the formula (37) was modified by England et al. (2000) to the equation (38) because of the incorrect evaluation of K^* . The modified formula is based on a model rigid wall test that was used to study the effects of thermal loads on integral abutments. The model simulated an abutment, which can rotate freely around its base corresponding to cyclic loads at the top. For the modified formula, the lateral earth pressure distribution along the abutment height will be triangular and the stiffness of the relationship is nonlinear. Both formulae (37) and (38) were adopted in the design of two IABs at Milano Malpensa Airport (Gherardi, 2010).

3. Full height embedded wall abutments.

The full height embedded wall abutments are installed in undisturbed ground and are more likely to be used in clayey conditions. In this case, the lateral earth pressure distribution along the abutment height can be also divided into three parts, as illustrated in Fig. 68. In the first part, the lateral earth pressure distribution is triangular based on the uniform lateral earth pressure coefficient K^* over the top two thirds of the wall height. Then in the second part, the lateral earth pressure distribution remains constant with the depth increases, because the lateral earth pressure coefficient K^* drops towards K_o . Finally, the lateral earth pressure can increase again with the depth increase and obtain the maximum value at the bottom. Because the lateral earth pressure coefficient falls to K_o , and then keep the same below that depth. The calculation formula of K^* use the equation (37). The stiffness of force-deflection relationship is nonlinear.

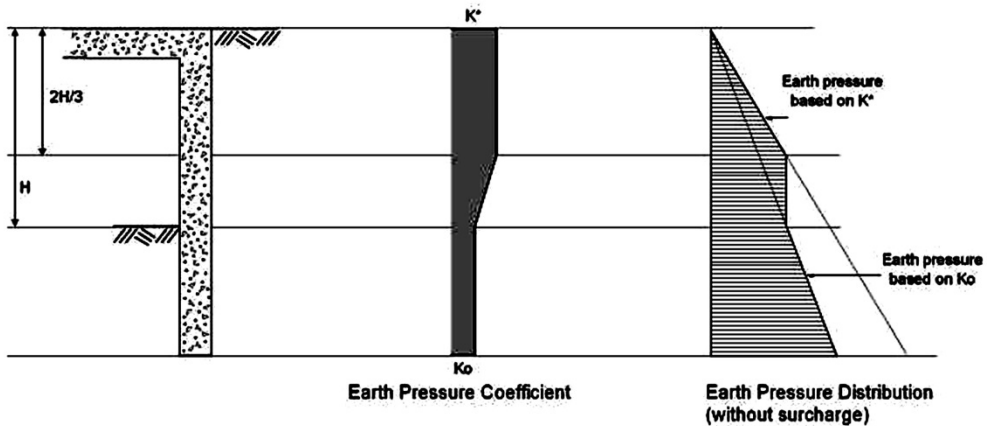


Fig. 68 Earth Pressure Distribution for Full height Embedded Wall Abutments (Department of Transport, 2003)

$$K^* = K_0 + \left(\frac{d}{0.025H}\right)^{0.4} K_p \quad (36)$$

$$K^* = \left(\frac{d}{0.05H}\right)^{0.4} K_p \geq K_0 \quad (37)$$

$$K^* = K_0 + \left(\frac{d}{0.03H}\right)^{0.6} K_p \quad (38)$$

where, H is the wall height. d is thermal displacement at the top. K_0 is the at-rest earth pressure coefficient. K_p is the passive earth pressure coefficient which can be obtained based on $\delta = \Phi/2$ and taken from Eurocode 7.

Relationship proposed in Eurocode 7 (2004)

In Eurocode 7 (Eurocode CEN, 2004b), the active and passive earth pressure can be calculated using the Bell's relation. The linear interpolation is suggested to obtain the intermediate values of active earth pressure between the at-rest state and the limit state, and the parabolic interpolation is suggested to obtain the intermediate values of passive earth pressure between the at-rest state and the limit state, as shown in Fig. 69. The active and passive earth pressure coefficients can be obtained from some figures or numerical procedures in Eurocode 7 (Eurocode CEN, 2004b). The ratio of the abutment movement to the abutment height corresponding to the active and passive limit state in non-cohesive soil (loose and dense sands) are proposed in Eurocode 7 (Eurocode CEN, 2004b), as listed in Table 17. The wall is vertical and the top surface of backfill is horizontal. Several typical modes of abutment movements are considered, as shown in Table 17. In this relationship, the lateral earth pressure distribution along the abutment height is triangular and the

stiffness of the relationship is nonlinear.

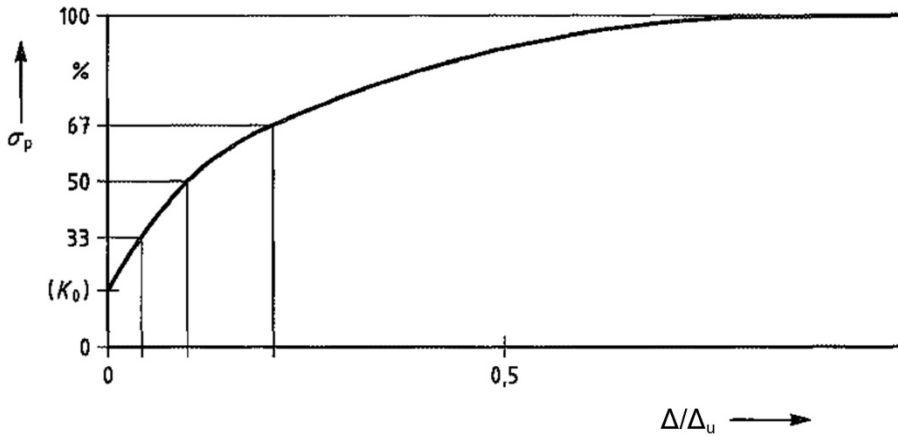


Fig. 69 Mobilization of passive earth pressure of non-cohesive soil versus normalized wall displacement (Eurocode CEN, 2004b)

Kind of wall movement		v_a/h loose soil %	v_a/h dense soil %
a)		0,4 to 0,5	0,1 to 0,2
b)		0,2	0,05 to 0,1
c)		0,8 to 1,0	0,2 to 0,5
d)		0,4 to 0,5	0,1 to 0,2

where:
 v_a is the wall motion to mobilise active earth pressure
 h is the height of the wall

Kind of wall movement		v_p/h loose soil %	v_p/h dense soil %
a)		7 (1,5) to 25 (4,0)	5 (1,1) to 10 (2,0)
b)		5 (0,9) to 10 (1,5)	3 (0,5) to 6 (1,0)
c)		6 (1,0) to 15 (1,5)	5 (0,5) to 6 (1,3)

where:
 v_p is the wall motion to mobilise passive earth pressure
 h is the height of the wall

Table 17

Ratios of abutment movement to abutment height (Eurocode CEN, 2004b)

Relationship proposed by Arsoy (2004)

Based on classical earth pressure theories, a modified passive earth pressure coefficient calculation approach for IAB was proposed by Arsoy (2004), through

RETROFIT OF EXISTING BRIDGES WITH CONCEPT OF INTEGRAL ABUTMENT BRIDGE

using the mobilized friction angle instead of the soil friction at failure. Some charts were constructed to estimate the magnitude and location of the passive earth resultant force for a cohesionless backfill, including both medium-dense and dense granular backfill materials. Both translation and rotation of the abutment are taken into account. In this relationship, the lateral earth pressure distribution along the abutment height is triangular and the stiffness of the relationship is nonlinear.

Relationship proposed in Canadian Foundation Engineering Manual (2006)

The lateral earth pressure coefficient-abutment rotation relationship curves proposed in Canadian Foundation Engineering Manual (Canadian Geotechnical Society, 2006), as illustrated in Fig. 70 is similar to the relationship suggested by Tschebotarioff & Johnson (1953). The magnitudes of rotation around the bottom (Ratio of Δ (displacement at the top) to H (abutment height)) corresponding to the minimum active and maximum passive earth pressure are listed in Table 18, which is different to the values suggested by Tschebotarioff & Johnson (1953). In this relationship, the lateral earth pressure distribution along the abutment height is triangular and the stiffness of the relationship is nonlinear. By comparing with some test results, it could be found that the relationships proposed by in Canadian Foundation Engineering Manual provide an accurate representation of the experimental data for loose and dense sands (Ting & Faraji, 1998).

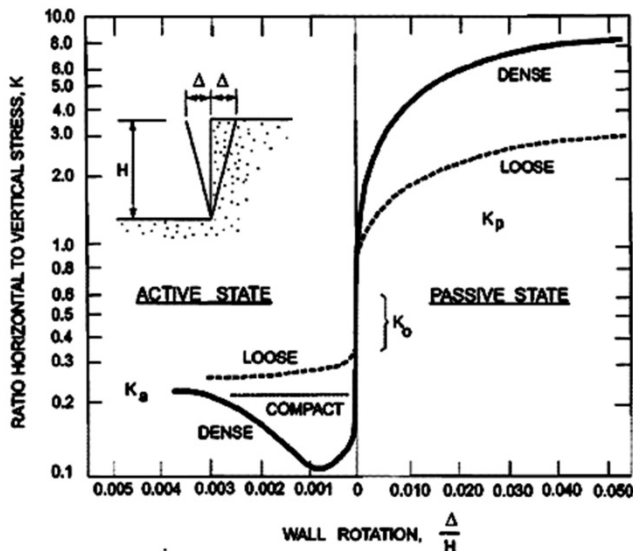


Fig. 70 Lateral earth pressure coefficient-abutment rotation relationship curve (Canadian Geotechnical Society, 2006)

Soil type and condition	Rotation Δ/H	
	Active	Passive
Dense cohesionless	0.001	0.02
Loose cohesionless	0.004	0.06
Stiff cohesive	0.01	0.02
Soft cohesive	0.02	0.04

Table 18

Magnitudes of abutment rotation around the bottom for different soil types (Canadian Geotechnical Society, 2006)

Relationship proposed by Kerokoski (2006)

The passive earth pressure coefficient-abutment movement relationship curve for IABs was suggested by Kerokoski (2006), which is easy for practice. This relationship considers cyclic abutment displacements (quite high pressure after a small displacement) and the wall friction angle. It is adopted in the guideline "Design of Integral Abutment Bridges with small and medium spans" proposed by Feldmann et al. (2010) with the maximum value of earth pressure coefficient and wall movement calculated using Eurocode 7 (Eurocode CEN, 2004b). The continuous line determines the maximum lateral passive earth pressure and the dashed line determines the minimum lateral passive earth pressure, as illustrated in Fig. 71. The active earth pressure may be ignored in general earth pressure calculations for IABs. In this relationship, the lateral earth pressure distribution along the abutment height is triangular and the stiffness of the relationship is nonlinear.

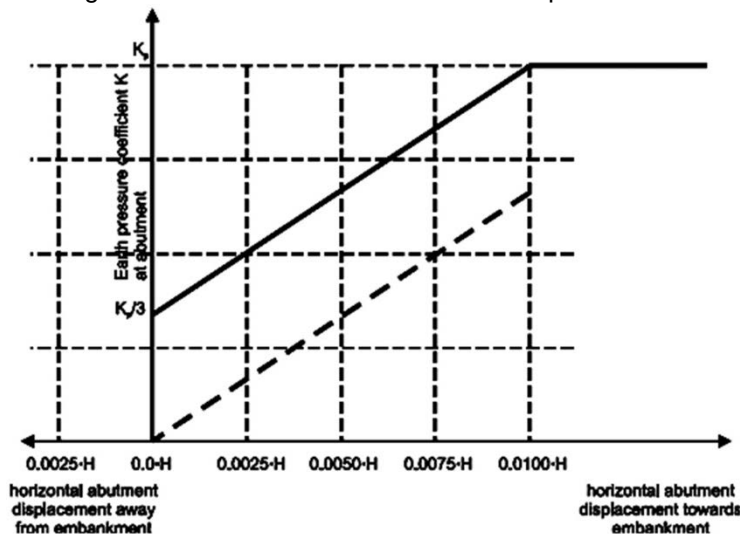


Fig. 71 Recommended earth pressure coefficient based on abutment displacement (Feldmann et al., 2010)

Relationship proposed by Krizek (2011)

The lateral passive earth pressure coefficient-abutment movement relationship proposed by Krizek (2011) can be used to analyze the soil-abutment interaction of IABs. Similar to the classical theories, the lateral earth pressure can be divided into three types corresponding to the abutment movement, which are at-rest earth pressure, active earth pressure and passive earth pressure, respectively. In this case, the passive earth pressure is combined of at-rest earth pressure and an increased earth pressure due to the abutment moving into backfill. The modulus (k_h) of the relationship between the increased earth pressure and the abutment movement can be calculated by formula (39). The stiffness of the relationship is nonlinear.

$$k_h = \frac{AE_{def}u_T}{10^4} + \frac{BE_{def}}{10^2} + \frac{Cu_T}{10^2} + D \quad (39)$$

where, A , B , C and D are the factors depending on the abutment height and the backfill type (sandy materials and gravely materials) that can be calculated through numerical model (Krizek, 2009). E_{def} is the elastic modulus of backfill under drained conditions (MPa). u_T is the horizontal translation at the top (mm).

In this relationship, three different modes of abutment movements, including the lateral translation, the rotation around the bottom and the combination of the translation and rotation, can be considered. Using the approach proposed by Krizek (2011), the lateral earth pressure distribution along the abutment height can be divided into two parts, as illustrated in Fig. 72. It can be calculated based on the abutment movements corresponding to different modes.

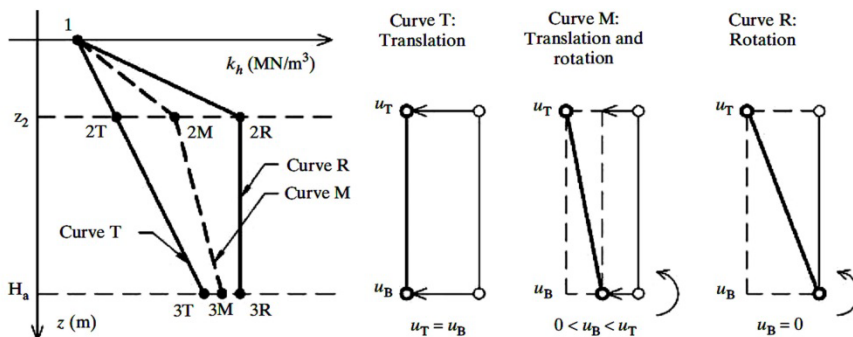


Fig. 72 Distribution of modulus of subgrade reaction along the depth of abutment (Krizek, 2011)

3.1.2 Soil-pile interaction

Piles can be used to resist lateral or uplift forces or to extend the foundation below the depth of scour. Most bridge abutments utilize either spread footings or pile foundations at the bottom of the wall to support bridge loads. The soil-pile interaction can be simulated as the combination of three relationships between earth pressure and the relative pile movement, such as the lateral earth pressure-pile displacement relationship, vertical skin friction-pile settlement relationship and bearing stress-pile settlement relationship, as illustrated in Fig. 73 (Greimann et al., 1987). These three relationships are independent (Parker & Reese, 1970) and the behavior of the soil at a particular depth is independent of the soil behavior at another depth (Desai & Christian, 1977).

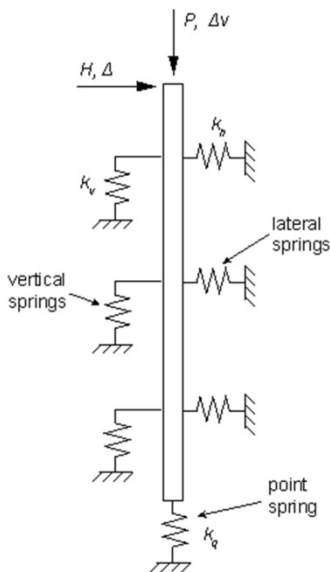


Fig. 73 Design of Soil-Pile System (Greimann et al., 1987)

3.1.2.1 Classical approach

Lateral earth pressure-pile displacement relationship

According to the material mechanics, it could be found that the relationship between the lateral earth pressure distribution (q) and the pile displacement can be present using the formula (40) (Desai & Christian, 1977), as illustrated in Fig. 74.

$$EI \frac{d^4 y}{dz^4} + w\bar{P}(Z, y) = 0 \quad (40)$$

where, y is the lateral displacement of the pile (m). Z is the soil depth (m). w is the pile width (m).

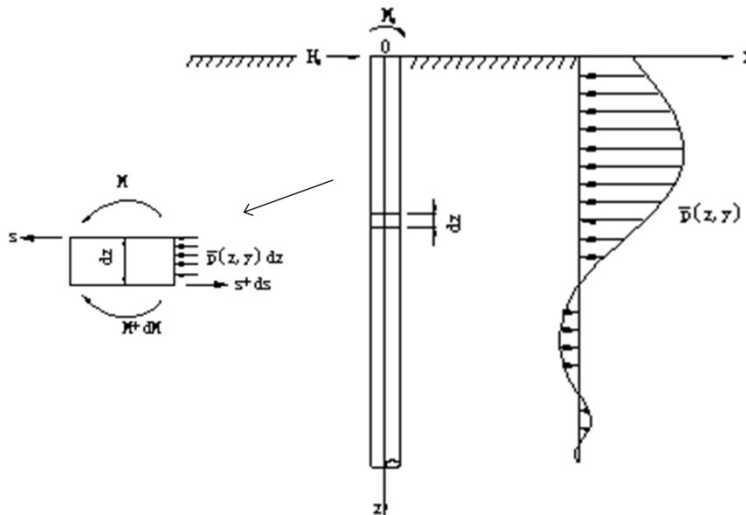


Fig. 74 Lateral earth pressure distribution and pile displacement

The calculation method of lateral subgrade reaction for piles can be divided into several categories: ultimate subgrade reaction method, elastic subgrade reaction method, elastic-plastic method, elastic theory; numerical method and so on.

The ultimate subgrade reaction method is a limit equilibrium method, such as the Brinch Hansen method (Hansen & Christensen, 1961) and the Broms method (Broms, 1964, 1965) which is suitable for the short rigid pile embedded in soil.

The elastic subgrade reaction method is based on the assumption of modeling soil as an elastic medium which obeys Hooke's law (Winkler, 1868). In this case, the deflection at any point of the beam on elastic soil is proportional to the pressure applied at that point and is independent of pressure acting at nearby points. The soil medium should be assumed as a system of identical but mutually independent, closely spaced, discrete and linearly elastic springs. The Winkler soil model can be represented by equation (41).

$$p = K(Z)y^n \quad (41)$$

where, p is the pressure of a certain point on the pile (N/m^2). y is the lateral displacement of the pile (m). If $n=1$, the method is called linear elastic subgrade reaction method; if $n>1$, the method is called nonlinear elastic subgrade reaction method. $K(Z)$ is subgrade reaction modulus or subgrade reaction coefficient (N/m^3) that is the key parameter depending on different soil types (sand or clay). It has been investigated by many researchers and it can be constant, linear varying or nonlinear varying with the depth (Z) increases (Baguelin et al., 1978; Davisson, 1970; Davisson & Gill, 1963; Fan, 1997; Kubo, 1965; Madhav et al., 1971; Prakash & Kumar, 1996; Terzaghi, 1955; Vesic, 1961).

The elastic theory presented by Poulos & Davis (1980) can be adopted to consider the nonlinear behavior of soil, and to provide an approach to determine both immediate and final movements of the pile with the soil represented as an elastic continuum.

In addition to these empirical methods, the numerical method develops very fast in the research on laterally loaded piles, such as resolving differential equations of deflection curve, finite difference method and finite element method (Desai & Christian, 1977; Poulos & Davis, 1980). The strain wedge (SW) model formulation was used by Ashour & Norris (2000).

The elastic-plastic method, so-called p-y curves approach, devised by McClelland & Focht (1958), is most widely used. It set a series of p-y curves along the pile length, as illustrated in Fig. 75.

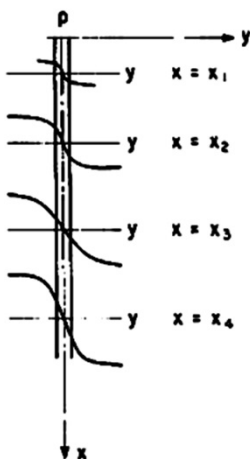


Fig. 75 A series of p-y curves along the length of the pile

There are many empirical p-y curves calculation methods corresponding to different soil types. Some of them, which can be used in the analysis of the IAB, will be introduced in Section 3.1.2.

Based on a large amount of p-y curves, a simplified procedure approach was proposed by Evans & Duncan (1982), which can be used to predict the dimensionless nonlinear behavior of single pile subjected to static lateral load. On the basis of this approach, a modified approach was devised, so-called Characteristic Load Method (CLM), by Duncan et al. (1994). This method is suitable for either fixed head piles or free head piles in both cohesive and cohesionless soil. It has been modified by many researchers in order to obtain good results (Brettmann & Duncan, 1996; Chang, 2003; Wang, 2000).

Based on the p-y curves concept, a semi-empirical and semi-theoretical method called Simple Approach for Lateral Load On Piles (SALLOP), was developed by Smith (1983) and Briaud et al. (1985) to resolve the problem of single pile subjected to lateral load. The essential of this method is because the shear forces in a laterally loaded pile are negligible at some depth named as zero-shear depth. The recommendation of this value was suggested by Briaud (1997).

Vertical earth pressure-pile displacement relationship

Besides the lateral force-displacement relationship, the vertical earth pressure-pile displacement relationship, which consists of the skin friction-pile settlement relationship and the bearing stress-pile settlement relationship, should be also considered. The theoretical skin friction-pile settlement relationship curve, so-called t-z curve, was developed by Kraft et al. (1981). Many numerical and empirical t-z curves can be obtained based on the results of models and full-scale pile load tests (Coyle & Reese, 1966; Coyle & Sulaiman, 1967; Poulos & Davis, 1980; Seed & Reese, 1957; Vijayvergiya, 1977). The bearing stress-pile settlement relationship curve, so-called Q-z curve, was developed by Randolph & Wroth (1978). Some numerical and empirical Q-z curves can be obtained based on the results of models and full-scale pile load tests (Poulos & Davis, 1980; Vijayvergiya, 1977).

3.1.2.2 Soil-pile interaction for IAB

Lateral earth pressure-pile displacement relationship

In this section, some lateral earth pressure-pile displacement relationships, which

can be applied in the analysis of IABs, will be introduced. Some of them use the elastic subgrade reaction method, which consider the linear or nonlinear relationship between lateral earth pressure and pile displacements; however, the lateral earth pressure will not change along the pile length. Others choose the elastic-plastic method, which is nonlinear including the nonlinear relationship between lateral earth pressure and pile displacements, and the nonlinear lateral earth pressure variation along the pile length.

Elastic subgrade reaction method: Relationship proposed by Terzaghi (1943)

The Terzaghi's method is one of the most fundamental elastic subgrade reaction methods. The lateral subgrade reaction coefficient for a vertical beam with width can be determined by formula (42) for sand and formula (43) for clay (Terzaghi, 1943, 1955). The detailed value of lateral subgrade reaction coefficient is listed in Table 19 (Davisson, 1970; Terzaghi et al., 1996).

For sand:

$$p = n_h \frac{Z}{w} y = \frac{A\gamma Z}{1.35w} y \quad (42)$$

For clay:

$$p = \frac{\bar{k}_{s1}}{1.5w} y \quad (43)$$

where, n_h is the factor representing the constant of lateral subgrade reaction for vertical piles (N/m^3). γ is the unit weight of soil (N/m^3). Z is the depth of soil (m) and w is the width of pile (m). A is a coefficient which depends only on the density of sand, of which the adopted values are 200, 600 and 1500 for loose, medium and dense sand, respectively. \bar{k}_{s1} is the vertical subgrade reaction coefficient for a square plate with a width of 0.3048m, which is approximately in proportion to the unconfined compressive strength of clay (N/m^2).

Soil type	Value
Granular soil	$n_h=0.5\sim 50$ kPa/mm (usually from 3~30 kPa/mm and approximately proportional to the relative density)
Normally loaded organic silt	$n_h=0.1\sim 0.8$ kPa/mm
Peat	$n_h=0.05$ kPa/mm
Cohesive soil	$k_h=67S_u$

Table 19

Detailed value of lateral subgrade reaction coefficient (Davisson, 1970; Terzaghi et al., 1996)

Elastic subgrade reaction method: Relationship proposed by Prakash & Kumar (1996) for sand

Based on experimental observations collected from 14 full-scale lateral pile load tests reported by Mwindo (1992), a step-by-step procedure based on the subgrade reaction method was developed for the nonlinear prediction of the load-displacement relationship of single piles subjected to lateral load in the sand with the uniform property. The relationship between lateral earth load on the pile and the deflection subjected to different pile-head fixity conditions can be obtained using the step-by-step procedure and the formulae suggested by Prakash & Sharma (1990). This relationship was applied to springs to simulate the nonlinear properties of soil around the piles of an IAB (Shah, 2007).

Elastic subgrade reaction method: Relationship proposed by Finnish National Road Administration (2000) for steel pipe pile

The subgrade reaction method for steel pipe pile was proposed by the Finnish National Road Administration (2000), which is suitable for both cohesionless and cohesive soil types. The corresponding lateral earth pressure-pile displacement relationship curves are illustrated in Fig. 76 and Fig. 77, which can be calculated by formulae (44) to (48). This nonlinear elastic subgrade reaction method was adopted in the guideline "Design of Integral Abutment Bridges with small and medium spans" proposed by Feldmann et al. (2010). It has been also used by Kerokoski (2006) to model a three-span IAB 'Haavistonjoki Bridge' in Finland.

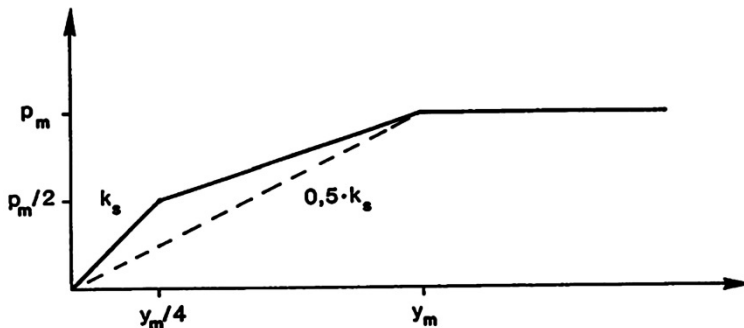
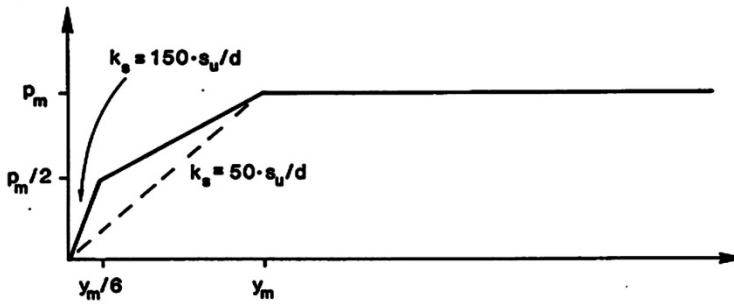
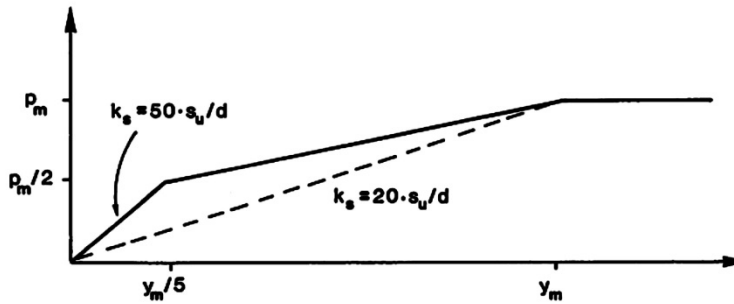


Fig. 76 Lateral earth pressure-pile displacement relationship curve for cohesionless soil (Finnish National Road Administration, 2000).



(a) Short-term load



(b) Long-term load

Fig. 77 Lateral earth pressure-pile displacement relationship curve for cohesive soil (Finnish National Road Administration, 2000).

For cohesionless soil:

$$p_m = (3 \sim 4.4)\gamma ZK_p \quad (44)$$

$$k_s = n_h Z / w \quad (45)$$

For cohesive soil:

$$p_m = (6 \sim 9)S_u \quad (46)$$

Subjected to short-term load:

$$k_s = (50 \sim 150)S_u / w \quad (47)$$

Subjected to long-term load:

$$k_s = (20 \sim 50)S_u / w \quad (48)$$

where, k_s is the lateral subgrade reaction (N/m^3). n_h is the coefficient of subgrade reaction, which can be obtained from Fig. 78 (N/m^3). Φ is the internal friction angle of soil (degree). γ is the unit weight of soil (N/m^3). K_p is the passive earth pressure coefficient. S_u is the undrained shear strength (N/m^2). w is the width of pile (m). Z is

the depth from the ground surface (m). p_m is the ultimate lateral pressure (N/m^2).

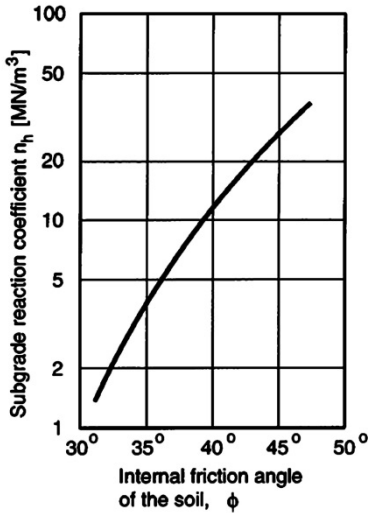
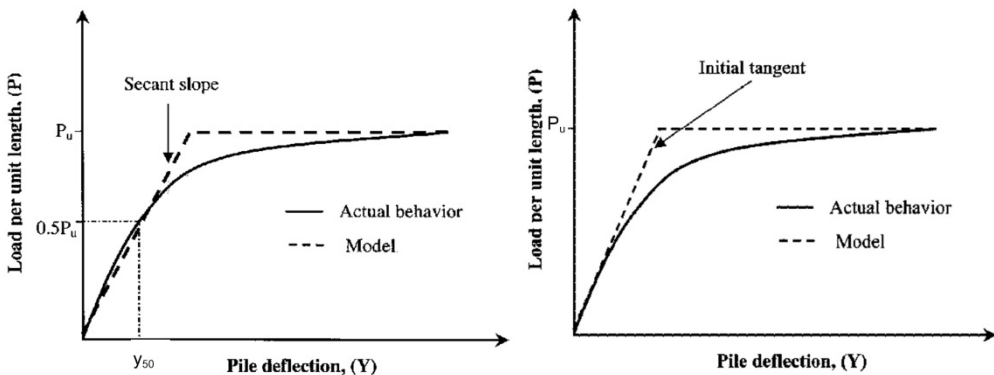


Fig. 78 Relationship between n_h and Φ . Below the ground water level n_h is 60% of values presented (Finnish National Road Administration, 2000).

Elastic-plastic method: p-y curves proposed by Haliburton (1971)

The typical nonlinear lateral p-y curves for sand and clay are illustrated as a solid line in Fig. 79, which can be simplified to the elastic-plastic curve (the dashed line) (Haliburton, 1971). The elastic portion of this simplified relationship can be defined as a slope, which is equal to the secant soil modulus for clay and the initial soil modulus for sand (E_s). Furthermore, the plastic portion can be defined as the ultimate soil resistance per unit length of the pile (P_u).



(a) clay

(b) sand

Fig. 79 p-y curves (Haliburton, 1971)

For clay

$$p_u = 9S_u w \quad (49)$$

$$y_{50} = 2.5\varepsilon_{50} w \quad (50)$$

$$E_s = 0.5P_u / y_{50} \quad (51)$$

For sand

$$p_u = k_a w (\gamma Z + q) (\tan^8 \beta - 1) + k_0 w (\gamma Z + q) \tan^4 \beta \tan \phi \quad (52)$$

$$E_s = kZ \quad (53)$$

where, S_u is the undrained shear strength (N/m^3). w is the pile width (m). ε_{50} is the strain corresponding to 50% the ultimate soil resistance. γ is the unit weight of soil (N/m^3). Z is the depth from the ground surface (m). Φ is the internal friction angle of soil (degree). q is the surcharge pressure (N/m^2). $\beta = 45 + \Phi/2$ (degree). $k_a = \tan^2(45 - \Phi/2)$. $k_0 = 1 - \sin \Phi$.

This family of p-y curves was used in a series of researches on IABs (Dicleli, 2005; Dicleli & Albhaisi, 2003, 2004a, b, c, 2005; Dicleli & Erhan, 2008, 2009, 2010; Erhan & Dicleli, 2009a, b). It can be applied not only to the nonlinear spring element with the elastic-plastic relationship, but also to the linear spring element using the stiffness.

Elastic-plastic method: p-y curves proposed by Reese et al. (1974) for sand

The p-y curves for sand were proposed by Reese et al. (1974) based on the theoretical studies using the following formulae (54)~ (56), which can consider both static and cyclic loads

Ultimate resistance near ground surface:

$$p_{\alpha} = \gamma Z \left[\frac{K_o Z \tan \phi \sin \beta}{\tan(\beta - \phi) \cos \alpha} + \frac{\tan \beta}{\tan(\beta - \phi)} (b + Z \tan \beta \tan \alpha) + K_o Z \tan \beta (\tan \phi \sin \beta - \tan \alpha) - K_a w \right] \quad (54)$$

Ultimate resistance below ground surface:

$$p_{cd} = K_a w \gamma Z (\tan^8 \beta - 1) + K_o w \gamma Z \tan \phi \tan^4 \beta \quad (55)$$

where, Φ is the internal friction angle of soil (degree). $\alpha = \Phi/2$. $\beta = 45 + \Phi/2$. $K_o = 0.4$.

$K_g = \tan^2(45 - \Phi/2)$. The value of Z_R can be obtained when $P_{ct} = P_{cd}$.

The corresponding p-y curve is illustrated in Fig. 80, in which y is divided into four segments.

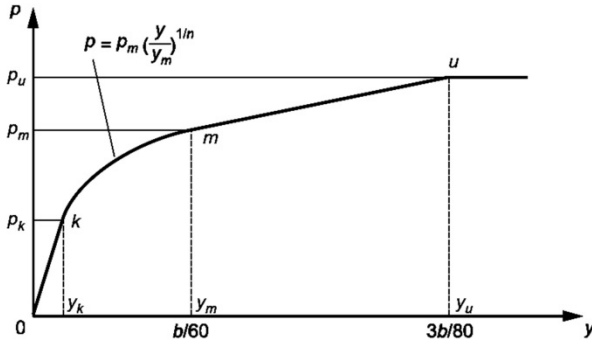


Fig. 80 p-y curves for sand (Reese et al., 1974)

$$p = \begin{cases} k_n y & 0 < y \leq y_k \\ C y^{1/n} & y_k < y < y_m \\ p_m = B p_c & y = y_m \\ m y & y_m < y < y_u \\ p_u = A p_c & y = y_u \end{cases} \quad (56)$$

where, $y_m = w/60$. $y_u = 3w/80$. $y_k = (C/k_n)^{n/(n-1)}$. $m = (p_u - p_m)/(y_u - y_m)$. $n = p_m/(m y_m)$. $C = p_m/(y_m^{1/n})$. k is 5400, 16300 and 34000 kN/m³ for loose, medium and dense sand, respectively. A and B can be obtained from Fig. 81.

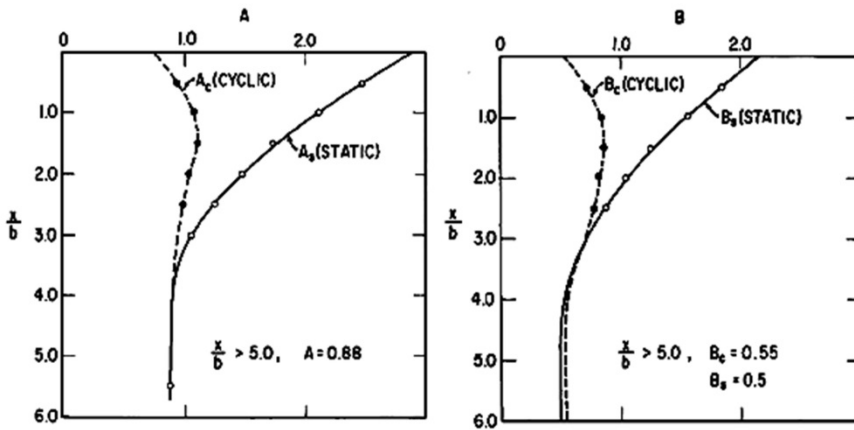
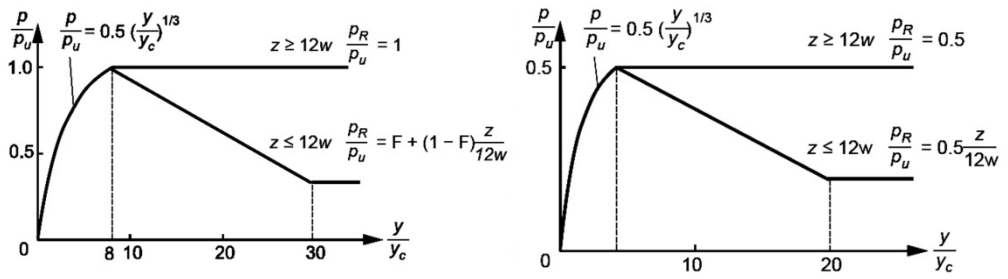


Fig. 81 Values of A and B (Reese et al., 1974)

Elastic-plastic method: p-y curves proposed by Sullivan et al. (1979) for clay

The p-y curves proposed by Sullivan et al. (1979) can be used for both soft and stiff clays, which can be divided into two segments, as illustrated in Fig. 82. The p-y curves can consider both static and cyclic loads, which can be obtained by formulae (57) to (64).



(a) Static load

(b) Cyclic load

Fig. 82 p-y curves for clay (Sullivan et al., 1979)

$$p_u = \min \left(\begin{array}{l} \left(2 + \frac{\gamma}{S_u} Z + \frac{0.833}{w} Z \right) S_u w \\ \left(3 + \frac{0.5}{w} Z \right) S_u w \\ 9 S_u w \end{array} \right) \quad (57)$$

$$y_c = A c_{50} w \quad (58)$$

For static load:

If $0 < y < 8y_c$:

$$p = \begin{cases} c_{\max} y \\ 0.5 p_u \left(\frac{y}{y_c} \right)^{1/3} \end{cases} \quad (59)$$

When $Z > 12w$,

$$\text{If } y \geq 8y_c: p = p_u \quad (60)$$

When $Z \leq 12w$,

$$\frac{p}{p_u} = \begin{cases} 1 & y = 8y_c \\ \text{Linear} & 8y_c < y < 30y_c \\ F + (1-F)Z / (12w) & y \geq 30y_c \end{cases} \quad (61)$$

For cyclic load:

If $0 < y < y_c$:

$$p = \begin{cases} c_{max} y \\ 0.5p_u \left(\frac{y}{y_c} \right)^{1/3} \end{cases} \quad (62)$$

When $Z > 12w$,

$$\text{If } y \geq y_c: p = 0.5p_u \quad (63)$$

When $Z \leq 12w$,

$$\frac{p}{p_u} = \begin{cases} 0.5 & y = y_c \\ \text{Linear} & y_c < y < 20y_c \\ 0.5Z / (12w) & y \geq 20y_c \end{cases} \quad (64)$$

where, γ is the unit weight of soil (N/m^3). S_u is the undrained shear strength (N/m^2). w is the pile width (m). Z is the depth from the ground surface (m). p_u is ultimate soil resistance per unit length of shaft (N/m^2). $c_{max} = k_h Z$. k_h and ϵ_{50} are listed in Table 20. A are 2.5 or 0.35 and F are 1 or 0.5 for different kinds of clay.

S_u (kN/m ³)	k_h (kN/m ³)	ϵ_{50}
12~25	8000	0.02
25~50	27000	0.01
50~100	80000	0.007
100~200	270000	0.005
200~400	800000	0.004

Table 20

Values of S_u , k_h and ϵ_{50} (Sullivan et al., 1979)

Elastic-plastic method: p-y curves proposed by using modified Romberg-Osgood model (1982)

Based on detailed investigations, some researcheres used the modified Romberg-Osgood model (Desai & Wu, 1976; Desai, 1976) to simulate the soil-pile interaction in IABs (Abendroth & Greimann, 2005; Greimann et al., 1987; Greimann

et al., 1984a; Greimann et al., 1986; Talbott, 2008; Wolde-Tinsae et al., 1983; Wolde-Tinsae et al., 1982; Yang et al., 1982). Formulae (65) to (68) can be used to consider both static and cyclic loads. By comparing with the other p-y curves, this relationship was suggested by Hong (2002) to simulate the lateral earth pressure-pile displacement relationship in an IAB for sand.

For static load:

$$p = \frac{k_h y}{\left[1 + \left| \frac{y}{y_u} \right|^n \right]^{1/n}} \quad (65)$$

$$y_u = \frac{p_u}{k_h} \quad (66)$$

For cyclic load, the hysteresis loops which can model the actual behavior of the pile and soil can be constructed by adopting the following two rules (Pyke, 1980). 1. The tangent modulus on each loading reversal assumes a value equal to the initial tangent modulus for the initial loading curve. 2. The shape of unloading or reloading curves is the same as that of the initial loading curve, except that the load scale is modified by a factor of c , which empirically accounts for cyclic degradation.

$$p = p_c + \frac{k_h (y - y_c)}{\left[1 + \left(\frac{1}{c} \left| \frac{y - y_c}{y_u} \right| \right)^n \right]^{1/n}} \quad (67)$$

$$c = \left| \pm 1 - \frac{p_c}{p_u} \right| \quad (68)$$

where, k_h is the initial stiffness and p_u is the ultimate soil resistance, as listed in Table 21 (Davisson, 1970; O'Neill et al., 1981; Poulos & Davis, 1980). p is the soil resistance. p_c is the soil resistance at the last reversal. n is the shape parameter, as illustrated in Fig. 83. y is the displacement. y_c is the displacement at the last reversal. y_u is the ultimate displacement.

Soil type	n	p_u (use smallest value)	k_h
Soft and stiff clay	1	$p_u = 9S_u w$ or $p_u = \left(3 + \frac{\gamma}{S_u} Z + \frac{0.5}{w} Z \right) S_u w$	$\frac{p_u}{y_c}$

Very stiff clay	2	$p_u = 9S_u w$ or $p_u = (3 + \frac{\gamma}{S_u} Z + \frac{2}{w} Z) S_u w$	$\frac{p_u}{2\gamma_c}$
Sand	3	$p_u = \gamma Z [w(k_p - k_a) + Zk_p \tan \alpha \tan \beta + Zk_o \tan \beta (\tan \phi - \tan \alpha)]$ $p_u = \gamma Z k_p^3 + 2k_p^2 k_o \tan \phi - k_a w$	$\frac{J\gamma Z}{1.35}$

Table 21

Parameters for p-y curve (Greimann et al., 1984a)

where, γ is the unit weight of soil (N/m^3). S_u is the undrained shear strength (N/m^2). w is the pile width (m). Z is the depth from the ground surface (m). J are 200 for loose sand, 600 for medium sand and 1500 for dense sand. γ_c is the displacement at one-half of the ultimate soil reaction. $2.5w\epsilon_{50}$ for soft and stiff clay and $2w\epsilon_{50}$ for very stiff clay. ϵ_{50} is the strain corresponding to one-half of the maximum principal stress difference, of which the typical values are 0.02 for soft clay, 0.01 for medium clay and 0.005 for stiff clay. Φ is the internal friction angle of soil (degree). α is $\Phi/2$ for dense or medium sand and $\Phi/3$ for loose sand (degree). $\beta=45+\Phi/2$ (degree). $k_p=\tan^2(45+\Phi/2)$. $k_a=\tan^2(45-\Phi/2)$. $k_o=1-\sin\Phi$.

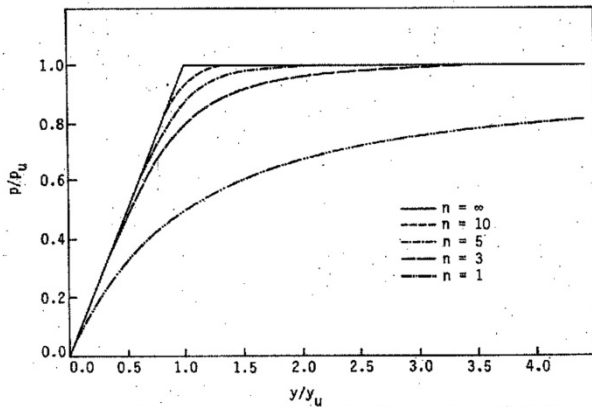


Fig. 83 Non-dimensional form of the modified Ramberg-Osgood equation (Greimann et al., 1984a)

For the purpose of design, the soil-pile interaction can be simplified as a bilinear soil resistance-displacement relationship for p-y curves, as shown in Fig. 84 (Greimann & Wolde-Tinsae, 1988; Greimann et al., 1984a). In this case, the calculation method of the ultimate soil resistance and stiffness can use the same approach as the modified Romberg-Osgood model.

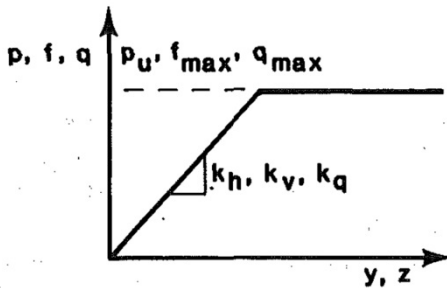


Fig. 84 Bilinear soil resistance-displacement relationships for p - y curves, t - z curves and Q - z curves (Greimann & Wolde-Tinsae, 1988)

Elastic-plastic method: p - y curves proposed by Mokwa et al. (1997)

A cubic parabola relationship of p - y curves was proposed by Mokwa et al. (1997), as shown in formulae (69) and (70). The p - y curves was used by Mokwa & Duncan (2000) to compute the lateral load resistance of piles.

$$p_u = (\gamma ZK_q + CK_c)Mw \quad (69)$$

$$p = 0.5p_u \left[\frac{y}{A\varepsilon_{50}w} \right]^{1/3} \quad (70)$$

where, w is the pile width (m). ε_{50} is the strain corresponding to one-half of the maximum principal stress difference. A is a parameter that controls the displacement magnitude (recommended as 2.5), which ranges from 0.35~2.65 (Evans & Duncan, 1982) or 0.72~2.65 (Mokwa et al., 1997). p_u is the maximum value of p at the large displacement, based on the ultimate load theory proposed by Hansen & Christensen (1961). M is an empirical modification factor of 0.85 (Helmers, 1997). The principal advancement of this theory is the development of expressions for K_q and K_c . K_q is a coefficient for the frictional component of net soil resistance under 3D conditions, and K_c is a coefficient for the cohesive component of net soil resistance under 3D conditions.

Elastic-plastic method: p - y curves proposed by American Petroleum Institute (2000)

A family of the lateral earth pressure-pile displacement relationship curves suggested by American Petroleum Institute (2000), so-called as API method, has been chosen by many researchers to simulate the soil-pile interaction in IABs (Briseghella et al., 2010; Civjan et al., 2007; Faraji et al., 2001; Kalayci et al., 2009;

Kalayci et al., 2012; Kalayci et al., 2011; Shoukry et al., 2006; Ting & Faraji, 1998; Zordan et al., 2011a, b; Zordan et al., 2011c).

The API method consists of several previous studies of p - y curves for soft clay, stiff clay and sand, which will be described in detail as follows.

p - y curves proposed by Matlock (1970) for soft clay

A well-known p - y curve calculation approach for soft clay was proposed by Matlock (1970), as shown in Fig. 85. It can consider both static and cyclic loads, based on the research on laterally loaded piles in soft clay involving extensive field tests with instrumented piles, experiments with laboratory models, and parallel developments of analytical methods and correlations. The family of p - y curves for soft clay can be obtained by formulae (71) to (78). By comparing with other kinds of p - y curves, this relationship was suggested by Hong (2002) to simulate the laterl earth pressure-pile displacement relationship in IABs for clay.

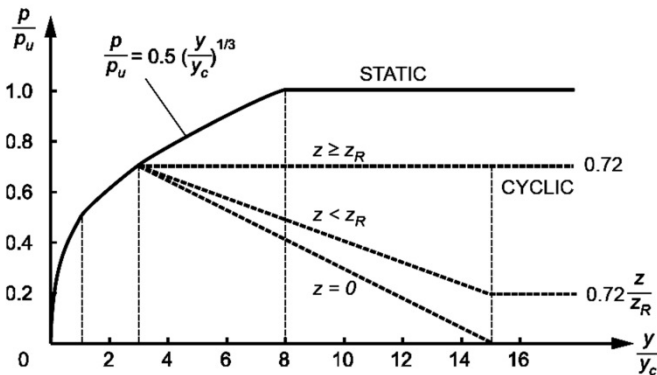


Fig. 85 p - y curves in soft clay (Matlock, 1970)

$$y_c = 2.5\epsilon_{50}w \quad (71)$$

$$Z_R = \frac{6S_u w}{\gamma w + JS_u} \quad (72)$$

If $Z \geq Z_R$:

$$p_u = 9S_u w \quad (73)$$

If $Z < Z_R$:

$$p_u = \left(3 + \frac{\gamma}{S_u} Z + \frac{J}{w} Z\right) S_u w \quad (74)$$

For static load:

$$\frac{p}{p_u} = 0.5 \left(\frac{y}{y_c} \right)^{1/3} \leq 1 \quad (75)$$

For cyclic load:

When $P \leq 0.72P_u$

$$\frac{p}{p_u} = 0.5 \left(\frac{y}{y_c} \right)^{1/3} \quad (76)$$

When $P > 0.72P_u$:

If $Z \geq Z_R$:

$$\frac{p}{p_u} = 0.72 \quad y > 3y_c \quad (77)$$

If $Z < Z_R$:

$$\frac{p}{p_u} = \begin{cases} 0.72 & y = 3y_c \\ \text{Linear} & 3y_c < y < 15y_c \\ 0.72Z / Z_R & y \geq 15y_c \end{cases} \quad (78)$$

where, γ is the unit weight of soil (N/m^3). S_u is the undrained shear strength (N/m^2). w is the pile width (m). Z is the depth from the ground surface (m). p_u is the ultimate soil resistance per unit length of shaft (N/m^2). J is approximately 0.5 for common clay and 0.25 for stiff clay. ϵ_{50} is the strain corresponding to one-half of the maximum principal stress difference, of which the typical values are 0.02 for soft clay, 0.01 for medium clay and 0.005 for stiff clay (Skempton, 1951).

The key points of p - y curves for soft clay are listed in Table 22 which can be used for design (American Petroleum Institute, 2000).

Soft clay					
Static load		Cyclic load			
		$Z \geq Z_R$		$Z < Z_R$	
p/p_u	y/y_c	p/p_u	y/y_c	p/p_u	y/y_c
0	0	0	0	0	0
0.5	1	0.5	1	0.5	1
0.72	3	0.72	3	0.72	3
1	8	0.72	∞	$0.72Z/Z_R$	15
1	∞			$0.72Z/Z_R$	∞

Table 22

Key points of p - y curves for soft clay (American Petroleum Institute, 2000)

p - y curves proposed by Reese & Welch (1975) and Reece et al. (1975) for stiff clay

For static load, the ultimate bearing capacity of the stiff clay would be higher than that of the soft clay. Due to rapid deterioration under cyclic loading, the ultimate resistance will be reduced to something considerably less and should be so considered in cyclic design. The nonlinear stress-strain relationship for stiff clay is generally more brittle than that for soft clay. In developing stress-strain curves and subsequent p-y curves for cyclic loads, good judgment should reflect the rapid deterioration of the load capacity at large deflections for stiff clay (American Petroleum Institute, 2000). Based on the p-y curves for soft clay (Matlock, 1970), the p-y curves for stiff clay above the water table was proposed by Reese & Welch (1975) by formulae (79) to (85), as shown in the following.

$$y_c = 2.5\varepsilon_{50}w \quad (79)$$

$$Z_R = \frac{6S_u w}{\gamma w + JS_u} \quad (80)$$

When $Z \leq Z_R$:

$$p_u = \left(3 + \frac{\gamma}{S_u}Z + \frac{J}{w}Z\right)S_u w \quad (81)$$

When $Z > Z_R$:

$$p_u = 9S_u w \quad (82)$$

For static load:

$$\frac{p}{p_u} = 0.5\left(\frac{y}{y_c}\right)^{1/4} \leq 1 \quad (83)$$

For cyclic load, the p- y_{cyclic} curve was defined based on the formulae of static loads

$$\frac{p}{p_u} = 0.5\left(\frac{y}{y_c}\right)^{1/4} \leq 1 \quad (84)$$

$$y_{cyclic} = y + 9.6y_c \left(\frac{p}{p_u}\right)^4 \log N \quad (85)$$

where, γ is the unit weight of soil (N/m^3). S_u is the undrained shear strength (N/m^2). w is the pile width (m). Z is the depth from the ground surface (m). p_u is the ultimate soil resistance per unit length of shaft (N/m^2). J is approximately 0.5 for common clay and 0.25 for stiff clay. ε_{50} is the strain corresponding to one-half of the maximum principal stress difference, of which the typical values are 0.005 or 0.01. N is the cycle number of load application.

The calculation approach of p-y curves below the water table subjected to static and cyclic loads were proposed by Reese et al. (1975), which is also suggested in API design guidelines for fixed offshore platforms (American Petroleum Institute, 2000),

as shown by formulae (86) to (97).

$$Z_R = \frac{9S_u w}{\gamma w + 2.83S_u} \quad (86)$$

$$y_c = \varepsilon_{50} w \quad (87)$$

If $Z \leq Z_R$:

$$\rho_u = \left(2 + \frac{\gamma}{S_u} Z + \frac{2.83}{w} Z\right) S_u w; \quad (88)$$

If $Z > Z_R$:

$$\rho_u = 11S_u w \quad (89)$$

For static load:

When $0 < y \leq Ay_c$:

$$\frac{\rho}{\rho_u} = \begin{cases} k_h Z \left(\frac{y_c}{\rho_u}\right) \left(\frac{y}{y_c}\right) \\ 0.5 \left(\frac{y}{y_c}\right)^{1/2} \end{cases} \quad (90)$$

When $Ay_c < y \leq 6Ay_c$:

$$\frac{\rho}{\rho_u} = 0.5 \left(\frac{y}{y_c}\right)^{1/2} - 0.055 \left(\frac{y - Ay_c}{Ay_c}\right)^{1.25} \quad (91)$$

When $6Ay_c < y \leq 18Ay_c$:

$$\frac{\rho}{\rho_u} = 0.5(6A)^{1/2} - 0.411 - \frac{0.0625}{y_c} (y - 6Ay_c) \quad (92)$$

When $y > 18Ay_c$:

$$\frac{\rho}{\rho_u} = 0.5(6A)^{1/2} - 0.411 - 0.75A \quad (93)$$

For cyclic load:

$$y_p = 4.1Ay_c \quad (94)$$

When $0 < y \leq 0.6y_p$:

$$\frac{\rho}{\rho_u} = \begin{cases} k_h Z \left(\frac{y_c}{\rho_u}\right) \left(\frac{y}{y_c}\right) \\ B \left[1 - \left| \frac{y - 0.45y_p}{0.45y_p} \right|^{2.5} \right] \end{cases} \quad (95)$$

When $0.6y_p < y \leq 1.8y_p$:

$$\frac{p}{p_u} = 0.936B - \frac{0.085}{y_c}(y - 0.6y_p) \quad (96)$$

When $1.8y_p < y$:

$$\frac{p}{p_u} = 0.936B - \frac{0.102}{y_c}y_p \quad (97)$$

where, γ is the unit weight of soil (N/m^3). S_u is the undrained shear strength (N/m^3). w is the pile width (m). Z is the depth from the ground surface (m). p_u is the ultimate soil resistance per unit length of shaft (N/m^2). A and B are parameters illustrated in Fig. 86. k_h and ϵ_{50} are listed in Table 23.

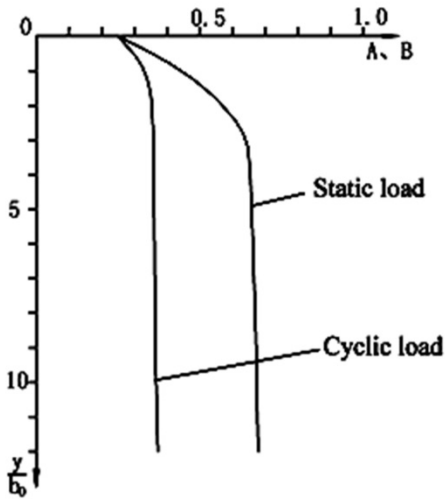


Fig. 86 Values of A and B (Reece et al., 1975)

S_u (kN/m^3)	k_h for static load (kN/m^3)	k_h for cyclic load (kN/m^3)	ϵ_{50}
50~100	135000	55000	0.007
100~200	270000	110000	0.005
200~400	540000	220000	0.004

Table 23

Values of S_u , k_h and ϵ_{50} (Reece et al., 1975)

p-y curves proposed by O'Neill & Murchison (1983) for sand

For sand, the p-y curves (illustrated in Fig. 87) can be obtained from formulae (98) to (100), which is also suggested in API design guidelines for fixed offshore platforms (American Petroleum Institute, 2000).

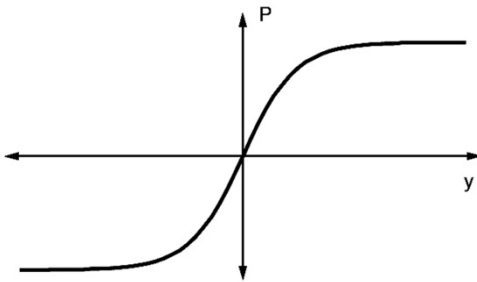


Fig. 87 p - y curves in sand (O'Neill & Murchison, 1983)

$$p_{us} = (C_1 \times Z + C_2 \times D) \times \gamma \times Z \tag{98}$$

$$p_{ud} = C_3 \times D \times \gamma \times Z \tag{99}$$

$$P = A \times p_u \times \tanh \left[\frac{k \times Z}{A \times p_u} \times y \right] \tag{100}$$

where p_{us} is the ultimate resistance at the shallow depth (kN/m). p_{ud} is the ultimate resistance at the deep depth (kN/m). γ is the effective unit weight of soil (kN/m³). Z is the depth below the earth surface (m). Φ is the internal friction angle (degree). C_1 , C_2 , C_3 are the coefficients determined by Φ , which can be obtained from Fig. 88. D is the pile diameter (m). A is the factor to account for static or cyclic loads with the value of 0.9 for cyclic loads. k is the initial modulus of the subgrade reaction (kN/m³) determined by Φ , which can be obtained from Fig. 89.

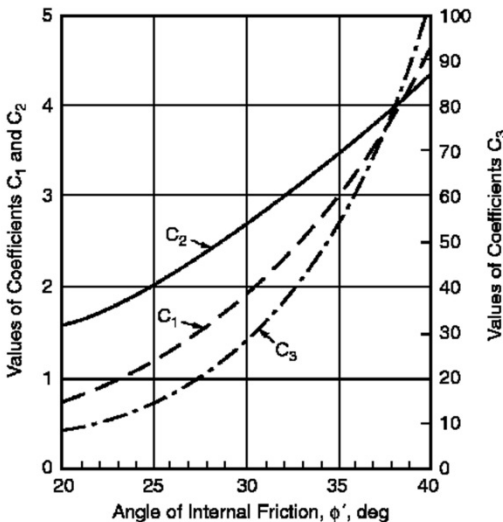


Fig. 88 Coefficients C_1 , C_2 and C_3 as function of Φ (American Petroleum Institute, 2000)

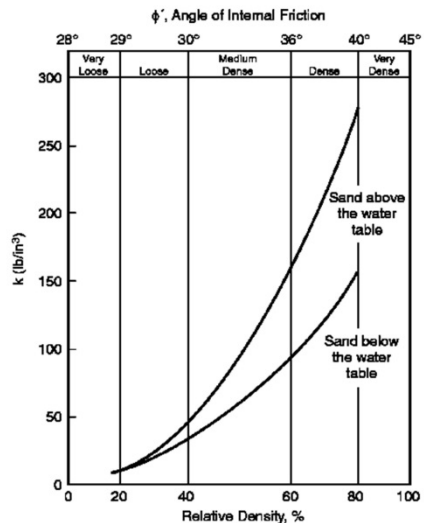


Fig. 89 Relative density, % (American Petroleum Institute, 2000)

Vertical earth pressure-pile displacement relationship

Some vertical earth pressure-pile displacement relationship curves, which can be applied to the IAB analysis, will be introduced in the following.

Relationship proposed by American Petroleum Institute (2000)

A family of skin friction-pile settlement relationship curves illustrated in Fig. 90 can be used respectively for clay and sand, if there is no more definitive criterion. The key points of t-z curves are listed in Table 24. In the t-z curves, z is the local pile deflection (mm); D is the pile diameter (mm); t is the mobilized soil-pile skin friction (kPa) and t_{max} is the maximum soil-pile skin friction (kPa), which can be calculated by formulae (101) or (103) for clay or sand.

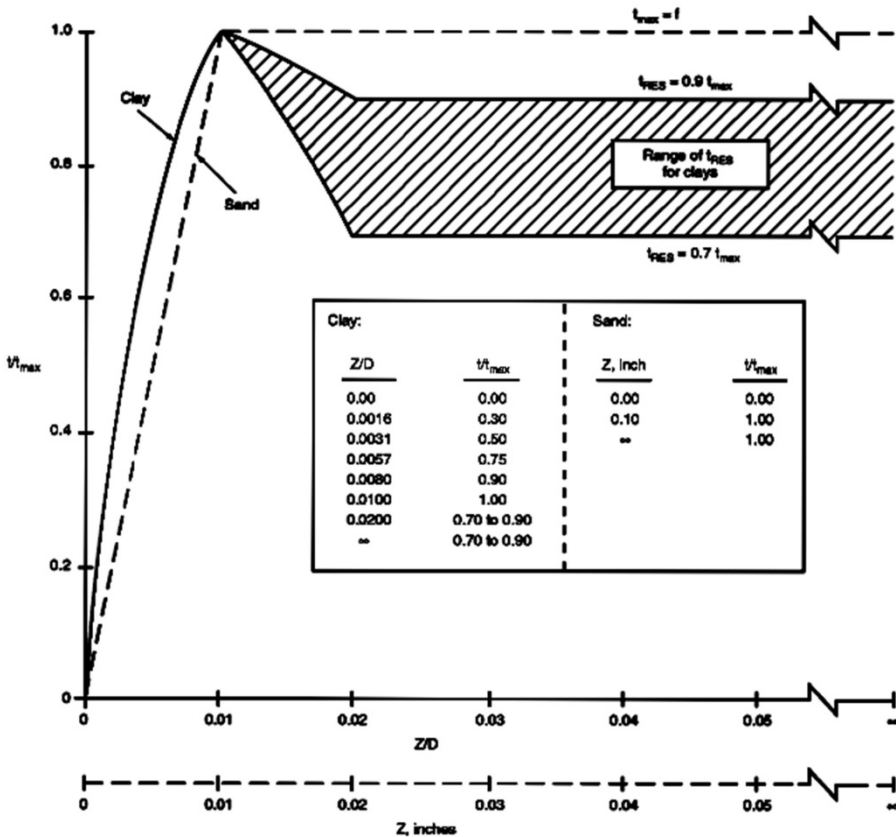


Fig. 90 t-z curves (American Petroleum Institute, 2000)

Clays		Sands	
z/D	t/t _{max}	z (inches)	t/t _{max}
0	0	0	0
0.0016	0.3	0.1	1
0.0031	0.5	∞	1
0.0057	0.75		
0.0080	0.9		
0.01	1		
0.02	0.7 to 0.9		
∞	0.7 to 0.9		

Table 24

Key points of t-z curves for clay or sand (American Petroleum Institute, 2000)

For clay:

$$t_{\max} = \alpha S_u \quad (101)$$

where, S_u is the undrained shear strength of soil (kPa) and α is a dimensionless factor, which can be calculated by formula (102).

$$\begin{aligned} \alpha &= 0.5\psi^{-0.5} & \psi &\leq 1 \\ \alpha &= 0.5\psi^{-0.25} & \psi &> 1 \end{aligned} \quad (102)$$

$$\alpha \leq 1$$

where, $\psi = S_u/p_0$, $p_0 = \gamma Z$ which is the effective overburden pressure (kPa). γ is the effective unit weight of soil and Z is the depth below the earth surface.

For sand:

$$t_{\max} = K p_0 \tan \delta \quad (103)$$

where, K is the lateral earth pressure coefficient with the assumed value of 1. p_0 is the effective overburden pressure (kPa). δ is the friction angle between soil and pile (degree).

For the bearing stress-pile settlement relationship, one Q-z curve illustrated in Fig. 91 is recommended in API design guidelines for fixed offshore platforms (American Petroleum Institute, 2000) for both clay and sand, if there is no more definitive criterion. The key points of Q-z curve are listed in Table 25. In the Q-z curve, z is the axial tip deflection (mm); D is the pile diameter (mm); Q is the mobilized end bearing capacity (KN) and Q_{\max} is the total end bearing capacity (KN), which can be calculated by formulae (104) or (105) for clay or sand.

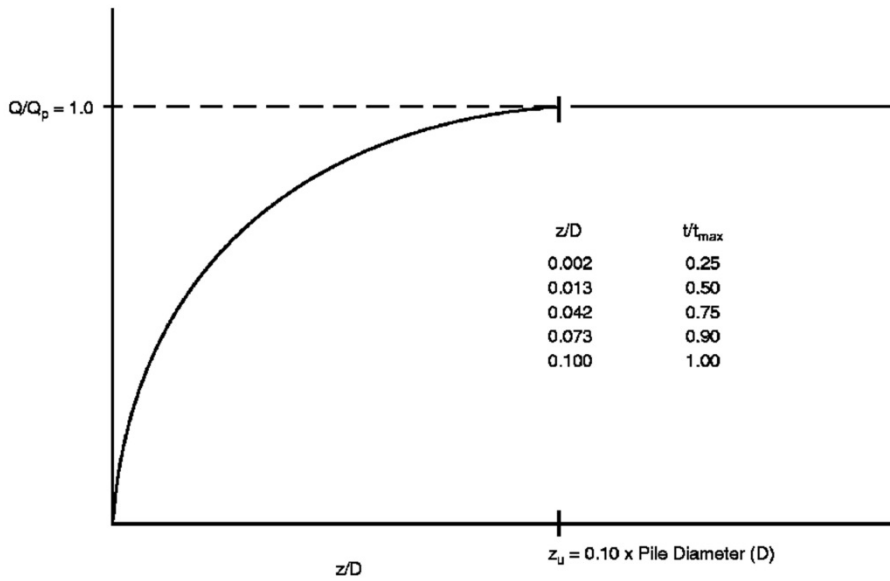


Fig. 91 Q-z curve (American Petroleum Institute, 2000)

Clays or sands	
z/D	Q/Q_{max}
0	0
0.002	0.25
0.013	0.5
0.042	0.75
0.073	0.9
0.1	1

Table 25

Key points of Q-z curves for clay or sand (American Petroleum Institute, 2000)

For clay:

$$Q_{max} = 9S_u \quad (104)$$

For sand:

$$Q_{max} = p_0 N_q \quad (105)$$

where, S_u is the undrained shear strength of soil (kPa). p_0 is the effective overburden pressure (kPa). N_q is the dimensionless bearing capacity factor.

Relationship proposed by using Ramberg-Osgood model

The Ramberg-Osgood model was suggested by Muqtadir & Morshed (1998) to predict both skin friction-pile settlement relationship and bearing stress-pile settlement relationship for sand. The modified Romberg-Osgood model (formulae (65) to (68)) can be used to simulate the vertical earth pressure-displacement relationship curves, including t-z curves and Q-z curves, with different parameters (t_u , k_v and z are used in t-z curves, and Q_u , k_Q and z are used in Q-z curves) (Abendroth & Greimann, 2005; Greimann et al., 1987; Greimann et al., 1984a; Wolde-Tinsae et al., 1983).

The parameters of t-z curves and Q-z curves are listed respectively in Table 26 and Table 27 (Matlock, 1970; O'Neill et al., 1981; Poulos & Davis, 1980; Reese et al., 1974; Sullivan et al., 1979; Vijayvergiya, 1977; Wolde-Tinsae et al., 1982).

Soil type	n	t_u (use smallest value)		k_v
		H piles	others	
clay	1	$2(d + b_f)S_u$ $2(d + 2b_f)C_A$ $2(dS_u + b_fC_A)$	$I_g S_u$ $I_g C_A$	$\frac{10t_u}{z_c}$
Sand	2	$0.02N[2(d + 2b_f)]$	$0.04NI_g$	$\frac{10t_u}{z_c}$

Table 26

Parameters for t-z curve (Greimann et al., 1984a)

where, b_f is the flange width of H piles. d is the depth of H piles. S_u is the soil undrained shear strength. C_A is the soil-structure adhesion. I_g is the gross perimeter of the pile. N is the average standard penetration blow count. z_c is the vertical displacement corresponding to the maximum force, such as 0.01m for sand and 0.006m for clay.

Soil type	n	Q_u	k_Q
clay	1	$9S_u$	$\frac{10Q_u}{z_c}$
Sand	1	$8N_{corr}$	$\frac{10Q_u}{z_c}$

Table 27

Parameters for Q-z curve (Greimann et al., 1984a)

where, S_u is the soil undrained shear strength. N_{corr} is the corrected standard penetration test blow count at the depth of the pile tip (If $N \leq 15$, $N_{corr} = N$; if $N > 15$, $N_{corr} = 15 + 0.5(N - 15)$). N is the average standard penetration blow count. z_c is the vertical displacement corresponding to the maximum force, such as 0.01m for sand and 0.006m for clay.

For the purpose of design, the bilinear soil resistance-displacement relationship curves, as shown in Fig. 84 (p.121), can be also used for t-z curves and Q-z curves with the parameters in Table 26 and Table 27 (Greimann & Wolde-Tinsae, 1988; Greimann et al., 1984a)

Relationship proposed by Greimann et al. (1986)

Formulae (106) and (107), which can be also used to simulate t-z curves and Q-z curves, were proposed by Greimann et al. (1986). The definition of parameters is the same as the modified Romberg-Osgood model described above (Table 26 and Table 27).

t-z curves:

$$\frac{t}{t_u} = 2 \sqrt{\frac{z}{z_c}} - \frac{z}{z_c} \quad (106)$$

Q-z curves:

$$\frac{Q}{Q_u} = \left(\frac{z}{z_c} \right)^{1/3} \quad (107)$$

3.1.2.3 Equivalent cantilever method

Another simulation approach, so-called equivalent cantilever method, was proposed by many researchers to design the piles of IABs (Abendroth & Greimann, 1989, 2005; Burke, 1993a; Burke, 1993b; Dicleli, 2000a, b; Greimann & Wolde-Tinsae, 1988; Greimann et al., 1987; Hambly & Nicholson, 1990; Husain & Bagnariol, 1996), which can be used to calculate the displacement, force and moment at the top of a pile. Therefore, the soil-pile system can be simplified as an equivalent cantilever column. The equivalent-cantilever length (L_e) for a pile is a function of both pile properties and soil profiles at the location of the pile, which can be calculated by formula (108). This numerical method is based on the assumption that embedded piles can be represented as a column with fixed or pinned-head conditions at the top

and with a base fixed at some distance below the ground surface, as illustrated in Fig. 92.

$$L_e = l_e + l_u \quad (108)$$

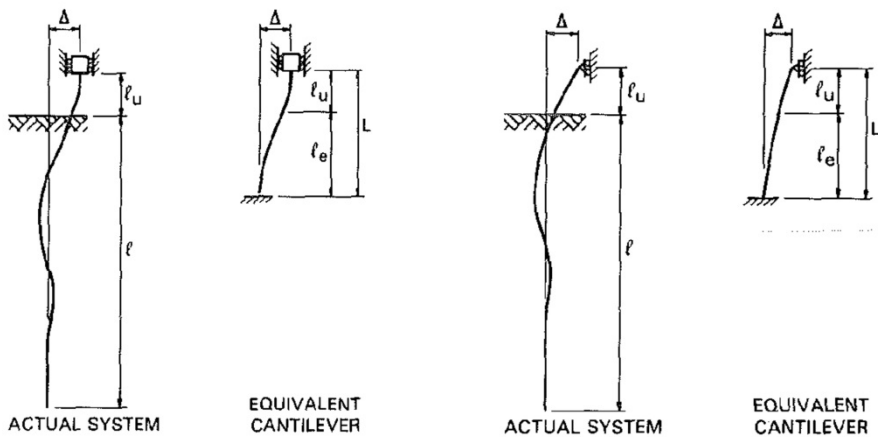
where, l_e is the equivalent embedded length and l_u is the length above the ground.

For a pile embedded in soil, a critical length (l_c) can be calculated by formulae (109) and (110). Beyond this length, the horizontal displacement at the pile head has minimal effects on horizontal displacements, shear forces and bending moments in the pile.

$$l_c = 4R \quad (109)$$

$$R = \left(\frac{EI}{k_h} \right)^{\frac{1}{4}} \quad (110)$$

where, k_h is the horizontal stiffness of the uniform soil.



(a) Fixed-Headed Condition

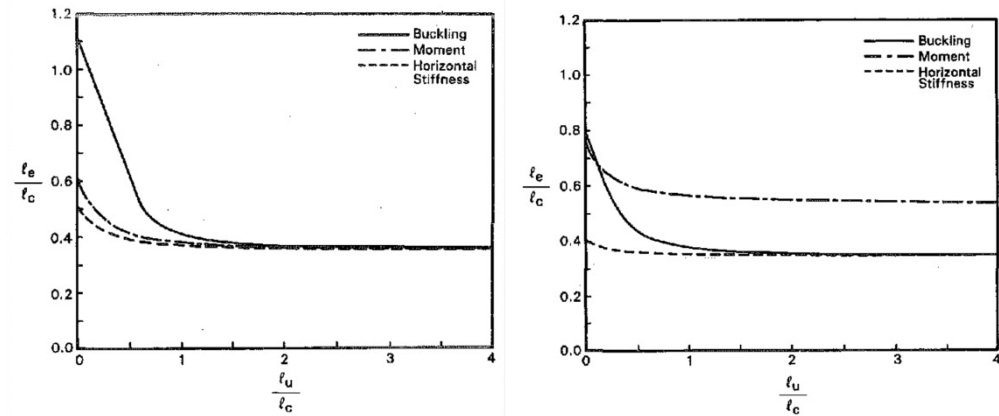
(b) Pinned-Headed Condition

Fig. 92 Cantilever idealization of pile (Abendroth & Greimann, 1989)

For each equivalency, the boundary condition at the pile head is fixed (no rotation) or pinned (no moment). The longitudinal expansion or contraction of the bridge superstructure at the integral abutment can produce the horizontal displacement at the top of the equivalent system. Three types of equivalencies can be taken into account. For example, the horizontal stiffness of the equivalent cantilever is equal to the horizontal stiffness of a pile in soil, which can be used to compute the

RETROFIT OF EXISTING BRIDGES WITH CONCEPT OF INTEGRAL ABUTMENT BRIDGE

displacements at the pile head and the maximum bending moments in the pile due to thermal movements. The maximum moment in the equivalent cantilever is equal to the maximum moment in a pile in soil, which can be chosen to calculate the forces and moments in the pile due to gravity load. The elastic-buckling load of an equivalent cantilever is equal to elastic-buckling load of a pile in soil, which can be used to consider the axial-compressive strength of the pile as a structural member. The equations for determining three equivalent embedded lengths corresponding to different equivalencies in a non-dimensional format for fixed-head and pinned-head piles embedded in a uniform soil are listed in Table 28 and illustrated in Fig. 93.



(a) Fixed-Headed Condition

(b) Pinned-Headed Condition

Fig. 93 Equivalent cantilevers for piles embedded in a uniform soil (Abendroth & Greimann, 1989)

Equivalencies	Equivalent Embedded Length
	Fixed-Head Pile
Horizontal stiffness	$\frac{l_e}{l_c} = \sqrt[3]{\frac{256\left(\frac{l_u}{l_c}\right)^4 + 256\sqrt{2}\left(\frac{l_u}{l_c}\right)^3 + 192\left(\frac{l_u}{l_c}\right)^2 + 48\sqrt{2}\left(\frac{l_u}{l_c}\right) + 12}{256\left(\frac{l_u}{l_c}\right) + 64\sqrt{2}}} - \frac{l_u}{l_c}$
Moment	$\frac{l_e}{l_c} = \sqrt[3]{\frac{128\left(\frac{l_u}{l_c}\right)^4 + 128\sqrt{2}\left(\frac{l_u}{l_c}\right)^3 + 96\left(\frac{l_u}{l_c}\right)^2 + 24\sqrt{2}\left(\frac{l_u}{l_c}\right) + 6}{128\left(\frac{l_u}{l_c}\right)^2 + 64\sqrt{2}\left(\frac{l_u}{l_c}\right) + 16}} - \frac{l_u}{l_c}$

Buckling	$\frac{l_e}{l_c} = \left(\frac{2p}{b_e l_u} - 1 \right) \frac{l_u}{l_c}$
	Pinned-Head Pile
Horizontal stiffness	$\frac{l_e}{l_c} = \sqrt[3]{\left(\frac{l_u}{l_c}\right)^3 + \frac{3\sqrt{2}}{4}\left(\frac{l_u}{l_c}\right)^2 + \frac{3}{8}\left(\frac{l_u}{l_c}\right)} - \frac{l_u}{l_c}$
Moment	$\frac{l_e}{l_c} = \sqrt{\frac{3}{16(Q_M)_{\max}} \left[\frac{32\sqrt{2}}{3}\left(\frac{l_u}{l_c}\right)^3 + 16\left(\frac{l_u}{l_c}\right)^2 + 4\sqrt{2}\left(\frac{l_u}{l_c}\right) + 1 \right]} - \frac{l_u}{l_c}$
Buckling	$\frac{l_e}{l_c} = \left(\frac{\pi}{0.7\beta_e l_u} - 1 \right) \frac{l_u}{l_c}$

Table 28

Equations for equivalent embedded length of piles

where, l is the length of the actual pile embedded in the ground. l_u is the length above the ground. l_e is the equivalent embedded length. l_c is the critical length.

For piles embedded in a non-uniform soil, which means that the soil profile is layered or does not have a constant horizontal stiffness along the soil depth, the equivalent soil stiffness (k_e) should be developed through an iterative procedure to replace the horizontal stiffness (k_h) in uniform soil and to determine the equivalent cantilevers (Greimann et al., 1987).

An example using the equivalent cantilever method on the design of an integral abutment was conducted by Barker et al. (1990). Some tests were carried out by Girton et al. (1991) to certificate that the equivalent cantilever column model is sufficiently accurate for design. This method is widely accepted by bridge engineers and proposed in some codes (Arockiasamy et al., 2004; Bonczar et al., 2005a; Bonczar et al., 2005b; Feldmann et al., 2010; Massachusetts Department of Transportation, 2007; Wagle & Watt, 2011). However, this method appears to be overly conservative, because it does not consider the effects of abutment-approach backfill interactions and the influence of the induced stresses in the superstructure (Arsoy, 2000).

3.1.3 Numerical software for soil-structure interaction

Many researchers used the spring element with the soil-structure relationship mentioned above in some general finite element programs, such as Sap2000, Midas, Lusas, SOFiSTiK, ANSYS and so on, to consider the effect of soil-structure

interaction on IABs. However, some researchers chose some special numerical programs to obtain the soil-structure interaction, as introduced in the following.

For the soil-abutment interaction, the program SAGE, which is capable of analyzing 2D plane strain soil-structure interaction problems, was used by Arsoy (2000) to study the performance of abutments in IABs due to temperature variations. In order to investigate the structural behavior of piers of integral abutment bridge, the program Zsoil, which is specialized in the modeling of the soil behavior, was used by Dreier (2008) to consider the interaction between the pier foundations and surrounding soil. Dreier et al. (2011) chose the 2D finite element program GEFDYN, which has the ability to reproduce the complex behavior of gravel backfills and to simulate the interaction between the embankment and the bridge end. For the behavior of the backfill of the embankment, the mechanical model built by program Hujoux, which uses an elastic-plastic approach with multiple plastic mechanisms and can cover all soil types, can be adopted (Aubry et al., 1982; Hujoux, 1985)

For the soil-pile interaction, the program LPILE, which is capable of analyzing the behavior of piles under lateral loads based on the finite difference method and the approximate 3D soil-pile interaction through the use of nonlinear p-y curves, has been chosen widely by many researchers (Arockiasamy et al., 2004; Arsoy, 2000; Dehne & Hassiotis, 2003; Khodair & Hassiotis, 2005). The program FB-Pier was used by Arockiasamy et al. (2004) to incorporate both the vertical soil-pile interaction (using hyperbolic tip resistance-vertical displacement curves) and the lateral soil-pile interaction (using nonlinear soil resistance-horizontal pile displacement curves). Moreover, three different methods, including the pile analysis software COM624P, beam elements with linear soil springs, the stiffness derived from COM624P and beam elements with multi-linear soil springs using p-y curves proposed by Reese (1986), were used by Fennema et al. (2005) to simulate the soil-pile interaction of a monitored three-span IAB. In this analysis, the comparison among three methods shown that the multi-linear soil springs from p-y curves is a valid approach to model soil-pile interaction in numerical models, which can eliminate many assumptions and numerous iterations that must be performed when using COM624P. Khodair & Hassiotis (2005) chose ABAQUS to study the nonlinear soil-pile interaction in an IAB subjected to an imposed displacement and rotation according to thermal load. The pile and soil are both simulated by solid element. For the soil-pile interaction, the surface-to-surface contact algorithm was chosen, defining the exterior surface of the pile as the master surface and the interior surface of the sand as the slave surface. The tangential contact between the pile and surrounding sands was defined as a friction coefficient estimated through the tangent of the friction angle between two

materials. In order to investigate the pile displacement capacity for super-long IABs, the finite element program Opensees was chosen to carry out an optimization procedure of pile design (Lan, 2012). The optimization method associates the finite element method with global optimization algorithm was used in this pile design optimization procedure.

Some finite element programs can be used to simulate both soil-abutment interaction and soil-pile interaction. For example, the 2D finite element program Plaxis was used by Kerokoski & Laaksonen (2005) and Kerokoski (2006) to investigate the soil-structure interaction of an IAB 'Haavistonjoki Bridge' based on hardening soil earth model.

3.2 IAB modeling approach

Different from the SSB, the substructure of the IAB is linked with the superstructure by hinged connections or rigid connections. It means that the bridge and the soil around the bridge foundations can resist the load together, especially the lateral force. Therefore, in order to predict the structural behaviors of IABs accurately, the modeling approach for the IAB is quite important. Based on a typical three-span IAB, as illustrated in Fig. 94, the common used modeling methods will be introduced in the following.

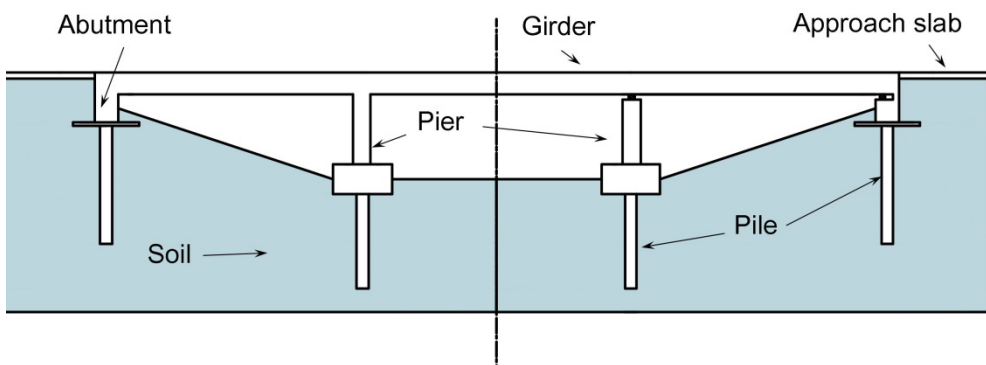


Fig. 94 Typical three-span IAB

3.2.1 Simplified model

Conventionally, an IAB can be idealized as a 2D continuous equivalent beam model as illustrated in Fig. 95, which could be statically resolved manually since moment

distribution method (Cross, 1932) had been developed. In this model, piers, abutments, piles and surrounding soil in the actual structure are replaced by simple supports. Therefore, the influence of the bridge substructure and surrounding soil are neglected. Full composite action between the slab and the girder is assumed as the beam element. Consequently, the 2D continuous equivalent beam model is used only for the bridge superstructure design (Burke, 1993a; Burke, 1993b; Hambly & Nicholson, 1990; Hayward, 1992; Husain & Bagnariol, 1996; Soltani & Kukreti, 1992).

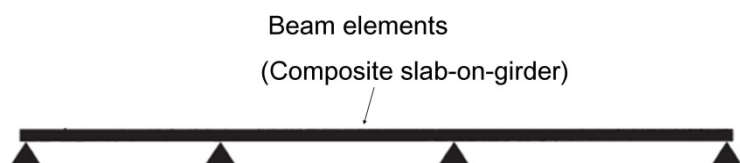


Fig. 95 Simplified structure model for deck design (Dicleli, 2000a)

A modified 2D continuous equivalent beam model was proposed by Feldmann et al. (2011), which can be used to calculate the inner force of a single-span IAB considering the influence of the bridge substructure by the linear rotational spring. The detailed calculation process of a single-span IAB using this model was also described by Feldmann et al. (2011).

In order to design the superstructure-abutment connection, a 2D continuous frame model which consider rigid connection between different components of bridge as shown in Fig. 96, was proposed (Burke, 1993a; Burke, 1993b; Hambly & Nicholson, 1990; Husain & Bagnariol, 1996). In the frame model, the piles beneath abutments are taken into account using the equivalent cantilever approach that has been introduced above. The pier is simulated as simple roller supports. Similar to the 2D continuous beam model, the superstructure in frame model is also simulated as composited slab-on-girder section. However, this model can not consider the correlation between the temperature variation and the magnitude of earth pressure. A maximum passive earth pressure with the tringular distribution is assumed conservatively for design.

The above models are easier and less time consuming when conducted manually; however, they cannot fully assess the global response of the IAB, including the effects of several loading conditions and soil-structure interactions.

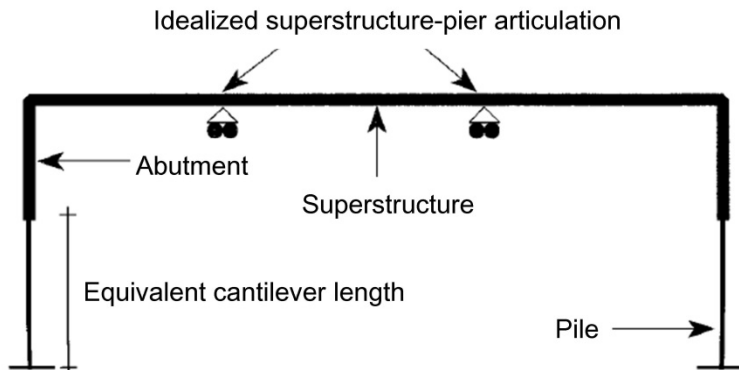


Fig. 96 Simplified structure model for superstructure-abutment connection design (Dicleli, 2000a)

3.2.2 Finite element model

Until computers began to be widely used in the design and analysis of structures, the finite element method has been the most widely practiced method, which is able to simulate the complicated structural behaviors under complicated structural loads, including permanent load, highway live load and thermal load. Consequently, the finite element model is a good approach of conducting the research on IABs. Generally, for a finite element model of the IAB, it should implement structural elements (beams and plates), an algorithm to account for the soil-structure interaction, and thermal load capabilities in the finite elements (Krier, 2009a). However, many researchers, due to many reasons, such as different finite element software, particular considerations by different researchers, different hypotheses according to various actual situations, and so on. They can be distinguished by different aspects, mainly including 2D or 3D model, with or without the consideration of soil-structure interaction, simulation of pile using equivalent cantilever approach or soil-spring approach, and so on. Some finite element models are introduced in the following, which are divided by different modeling approaches of piles.

3.2.2.1 Pile modeling by equivalent cantilever approach

The schematic diagram of the 2D finite element model with piles modeling by the equivalent cantilever approach is illustrated in Fig. 97 (Dicleli, 2000a, b; Dicleli & Erhan, 2010). In this model, some connection elements are added between different bridge components, such as superstructure-abutment, superstructure-pier, abutment-pile and pier-pile, in order to simulate different stiffness of these connections. In addition, the pier should be simulated by beam elements to replace roller simply supports in original frame modals. Moreover, the relationship between

the later earth pressure and abutment movement caused by temperature variations should be considered.

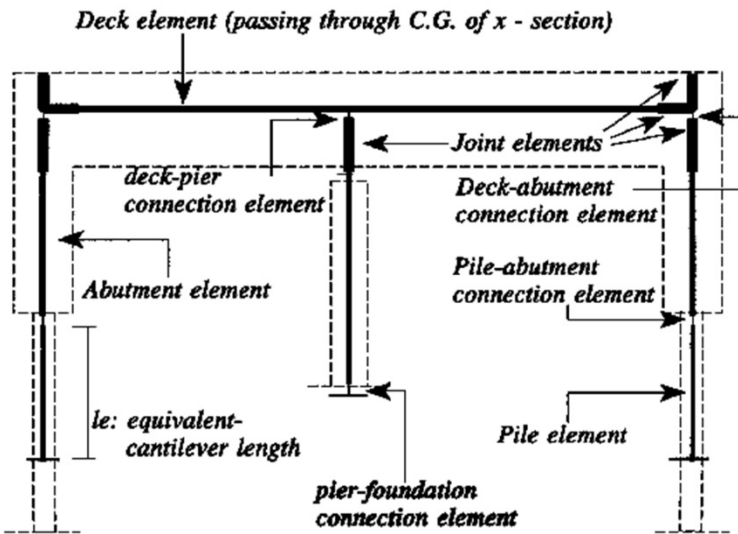


Fig. 97 2D finite element model with piles modeling by equivalent cantilever approach (Dicleli, 2000a)

In order to understand the performance of the IAB more clearly, the 3D finite element model with piles modeling by the equivalent cantilever approach was used by some researchers (Faraji, 1997; Hong, 2006), as illustrated in Fig. 98. The soil-abutment interaction in these 3D models can be simulated as linear spring elements by using the iterative equivalent linear approach (Hong, 2006) or nonlinear spring elements with the lateral earth pressure-abutment movement relationship curves (Faraji, 1997).

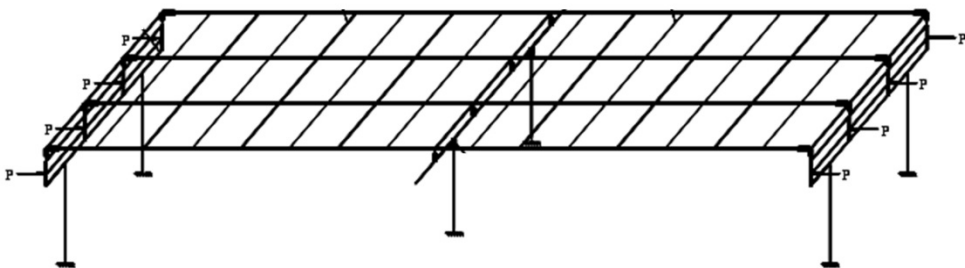


Fig. 98 3D finite element model with pile modeling by equivalent cantilever approach (Hong, 2006)

3.2.2.2 Pile modeling by soil-spring approach

Besides the equivalent cantilever approach, many researchers adopted the soil-spring approach to simulate the soil-pile interaction in the IAB. The equivalent cantilever approach and soil-spring approach are compared in Fig. 99. When modeling piles by using the equivalent cantilever approach, the pile beyond the equivalent length can be neglected and the fixed support is installed at the bottom of the equivalent length. However, when modeling piles by using the soil-spring approach, the actual pile length must be considered and the movable simple roller, which fixes only the vertical translation, should be installed at the pile bottom. The pile element should be divided into some segments. The lateral spring and vertical spring can be attached to each node along the pile length. In the case of friction piles, the movable simple roller at the bottom can be replaced by a vertical spring with a stiffness representing the bearing stress-pile settlement relationship of the pile.

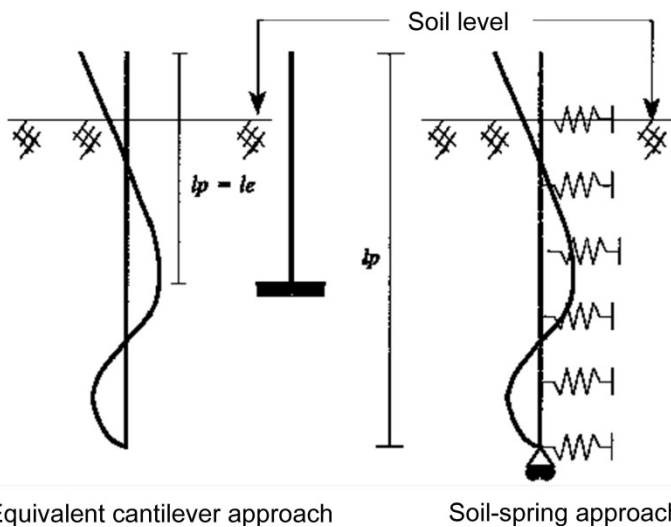


Fig. 99 Comparison of equivalent cantilever approach and soil-spring approach (Diciceli, 2000b)

Using the soil-spring approach, the soil-abutment interaction and soil-pile interaction in IABs can be simulated as a series of discrete linear or nonlinear spring elements along the abutment height and pile length. Some researchers chose 2D finite element models with the soil-spring approach to carry out the analyses of IABs (Briseghella et al., 2010; Diciceli & Erhan, 2008, 2009, 2010; Erhan & Diciceli, 2009a, b; Lan, 2012; Pugasap et al., 2009; Talbott, 2008; Zordan et al., 2011a, b; Zordan et al., 2011c)

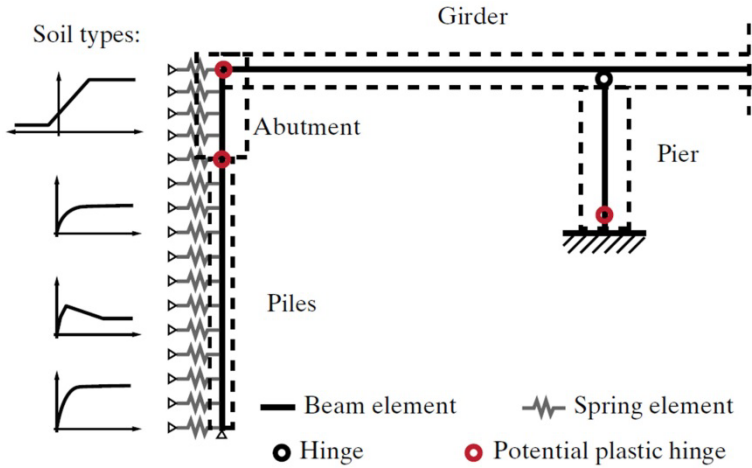


Fig. 100 2D finite element model with pile modeling by soil-spring approach (Zordan et al., 2011b)

The 3D finite element model with soil-spring approach shown in Fig. 101, has been used by many researchers, because it can provide more realistic representation of the performance of IABs (Dicleli & Erhan, 2008, 2009; Erhan & Dicleli, 2009a, b; Faraji et al., 2001; Hong, 2002; Kalayci et al., 2009; Kalayci et al., 2012; Kalayci et al., 2011; Pugasap et al., 2009; Shoukry et al., 2006). In the 3D model, the horizontal springs should be attached at each node in both orthogonal directions along the pile length to simulate the 3D lateral soil-pile interaction.

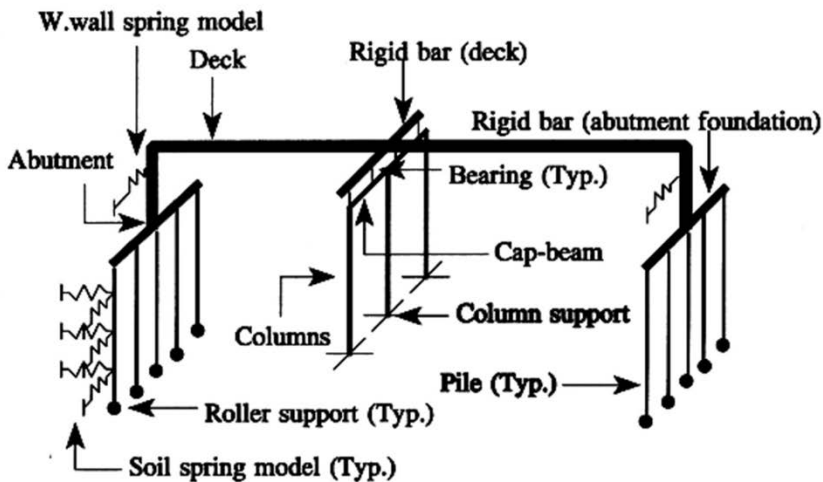


Fig. 101 3D finite element model with pile modeling by soil-spring approach (Dicleli, 2000a)

Based on the soil-spring approach, the condensed pile model was proposed by Kim (2008) which can be also used to simulate the soil-pile interaction in IABs. The

condensed pile model composed of a nonlinear lateral spring and a nonlinear rotational spring can be chosen to replace the conventional full pile model, which has a series of discrete nonlinear lateral springs along the pile length, as shown in Fig. 102. The mechanical properties of the condensed pile model can be calculated by some specialized finite element programs for pile, such as COM624P (Kim & Laman, 2010a, b).

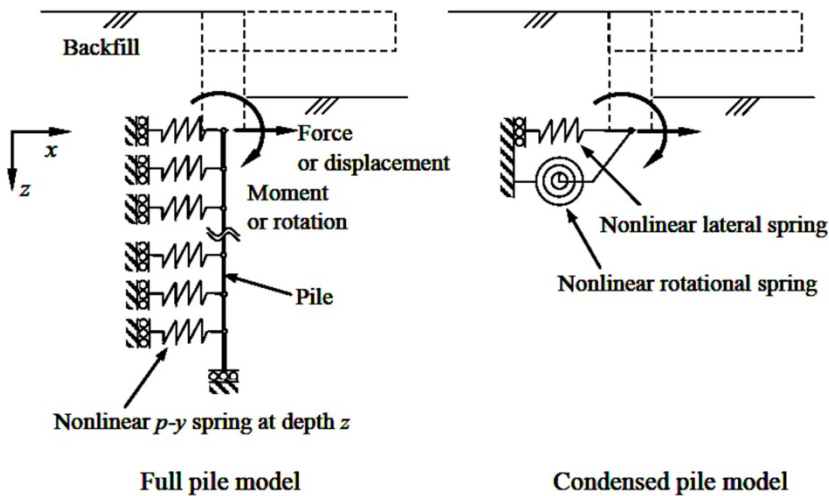


Fig. 102 Comparison of full pile model and condensed pile model (Kim, 2008)

3.3 Plastic hinge modeling

As is known to all, the bending moment of a frame element can reach the material capability when the loading is significant enough. Analyzing the plastic limit of frame elements subjected to bending an abrupt transition from elastic to ideally plastic moment is assumed. When the plastic moment is reached, a plastic hinge is formed in the element, which allows a large rotation to occur at constant plastic moment. Most finite element models choose the approach of applying plastic hinges to frame elements in order to simulate the deformation of a beam section where the plastic bending occurs (Megson, 2005). The method of plastic hinge has been widely used by many researchers to analyze the performance of structures, especially subjected to seismic load, cyclic thermal load and so on (Lan, 2012; Mazzarolo, 2012; Priestley & Seible, 1996).

3.3.1 General modeling approach

Generally, the inelastic properties of beam-column elements in finite element models can be represented using two approaches, which are the concentrated plasticity approach (Anagnostopoulos, 1981; Powell & Chen, 1986; Wen & Farhoomand, 1970) and the distributed plasticity approach (Corradi & Poggi, 1984; Hobbs & Jowharzadeh, 1978; Meek & Loganathan, 1990). Five idealized types of models that can be used to simulate the inelastic response of beam-column elements are compared in Fig. 103, which are differentiated by the way that plasticity is distributed through the member cross sections and along its length.

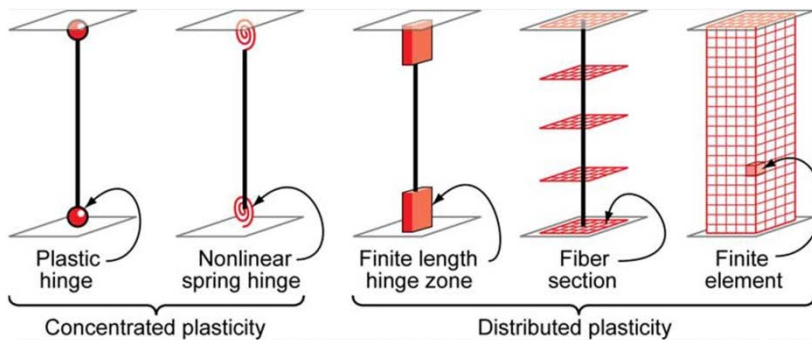


Fig. 103 Idealized models of beam-column elements (Deierlein et al., 2010)

In this section, the concentrated plasticity approach with the plastic hinge and the distributed plasticity approach with a finite length hinge zone will be introduced. Usually, the plastic hinge extends along a short length. However, the concentrated plasticity approach, which can lump the inelastic properties of the beam-column element into a plastic hinge at the end of one linear-elastic element, is sufficiently accurate and has a significant computational advantage. Moreover, it may be better suited to capturing the nonlinear degrading response of members through calibration by using member test data on phenomenological moment-rotations and hysteresis curves. However, some researchers indicated that the concentrated plasticity approach is sufficient for the limit state analysis. In order to obtain more accurate results, such as detailed variations of the stress or strain through the section and along the member, important local behaviors, and the nonlinear interaction of flexural and shear, the distributed plasticity approach can be chosen. However, it will cost more time compared to the concentrated plasticity approach (Deierlein et al., 2010; Izzuddin & Elnashai, 1993a, b). For the IAB, the concentrated plasticity approach can be used to analyze the plastic behaviors of piers; however, in order to obtain simulate the plastic performance of piles, the distributed plasticity approach can be chosen. The reason will be introduced in Chapter 5.

3.3.2 Moment-rotation curve

The moment-rotation ($M-\theta$) curve obtained by running section analysis or using codes tabulated properties, can be chosen to present the nonlinear property of the plastic hinge. A characteristic monotonic backbone curve proposed in some codes and literatures is shown in Fig. 104, including the following features (American Society of Civil Engineers, 2007; Applied Technology Council, 1996; Federal Emergency Management Agency, 1997a, b, 2000, 2005).

1. Point A corresponds to the unloaded condition,
2. Point B has resistance equal to the effective yield strength,
3. The slope from Point B to Point C shall be taken between 0~10% of the initial slope of Line AB, which can represent phenomena such as strain hardening observed for most reinforced concrete components,
4. Point C has an ordinate that represents the strength of the component, and an abscissa value equal to the deformation at which significant strength degradation begins,
5. Line CD represents the initial failure of the member, which may be associated with phenomena such as fracture of the bending reinforcement, spalling of concrete or sudden shear failure following initial yield,
6. Point D corresponds to the residual strength of the member after substantially reduced,
7. Point E corresponds to the deformation limit. If the calculated response does not exceed Point C, the backbone curve can be represented as a relation among points A, B, and C only.

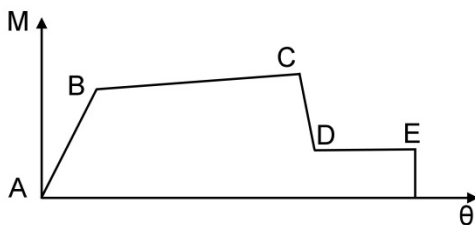


Fig. 104 General backbone relationship

The ordinate and abscissa of the five key points in the backbone curve can be justified directly through experiments or analyses. The recommended values of these parameters for the backbone curve corresponding to different materials, which can define the nonlinear moment-rotation response of the plastic hinge as a function of longitudinal and horizontal reinforcements, and axial and shear demands, can be found in some codes (American Society of Civil Engineers, 2007; Applied

Technology Council, 1996; Federal Emergency Management Agency, 1997a, b, 2000, 2005).

The product of the plastic hinge length and the moment-curvature ($M-\Phi$) curve can obtain the moment-rotation curve. The actual moment-curvature curves of sections can be determined under certain axial-moment interaction by integrating the constitutive models for fragile and ductile materials at element sections, as illustrated in Fig. 105. The idealized bilinear elastic-plastic curve proposed in some codes and programs can be used to idealize the actual moment-curvature curves (Caltrans, 2010; Computers and Structures Inc, 2011; Eurocode CEN, 2005a; MIDAS IT Co. Ltd, 2009).

The idealized bilinear elastic-perfectly plastic curve proposed in the Caltrans code (Caltrans, 2010) is shown in Fig. 105, including the following features.

1. The elastic portion of the idealized curve should pass through the point marking the first rebar yield,
2. The idealized plastic moment capacity is obtained by balancing the actual and the idealized moment-curvature curves beyond the first rebar yield point,
3. The curvature capacity at the failure limit state (Φ_u) can be defined as the concrete strain reaching crush strain or the longitudinal rebar reaching the ultimate strain.

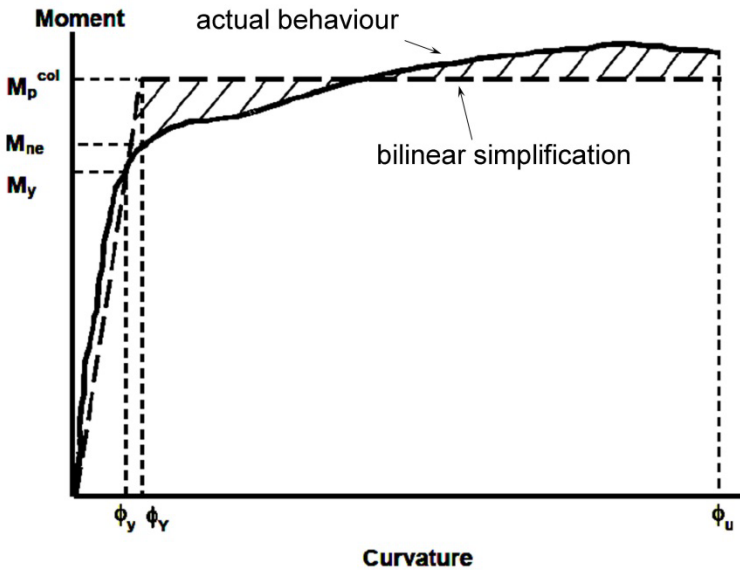


Fig. 105 Moment-curvature ($M-\Phi$) curves (Caltrans, 2010)

3.3.3 Plastic hinge length

The plastic hinge length (L_p) is another key factor for the plastic hinge, of which the definition is illustrated in Fig. 106. Theoretically, the plastic hinges occur in the sections, which have bending moments exceed nominal bending moments associated with the yielding of sections. Therefore, based on the integration of the curvature distribution, the plastic hinge length can be calculated depends on how the enhancement of strength and deformation capacity of concrete due to confinement is taken into account in the calculation of the ultimate curvature.

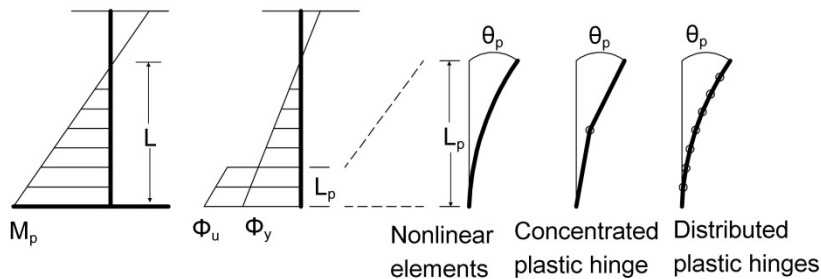


Fig. 106 Plastic hinge length

A lot of formulae proposed by many researchers theoretically or experimentally can be used to calculate the plastic hinge length (Alemdar, 2010; Biskinis & Fardis, 2009; Caltrans, 2010; Eurocode CEN, 2005a, b; Park & Paulay, 1975; Paulay & Priestley, 1992; Priestley & Seible, 1996; Scott & Fenves, 2006). Some commonly used equations are introduced in the following.

In Eurocode8 Part2 (Eurocode CEN, 2005a), the plastic hinge occurring at the top or the bottom junction of a pier with the deck or the foundation body (footing or pile cap), can be calculated by formula (111).

$$L_p = 0.1L + 0.015d_b f_{yk} \quad (111)$$

where, L is the distance from the plastic hinge section to the section of zero moment (mm). f_{yk} is the characteristic yield stress of steel (MPa). d_b is the rebar diameter (mm).

In Eurocode8 Part3 (Eurocode CEN, 2005b), two formulae (112) and (113) can be used to predict the plastic hinge length according to different calculation approaches of the ultimate curvature.

$$L_p = 0.1L_v + 0.17h + 0.24 \frac{d_b f_y}{\sqrt{f_c}} \quad (112)$$

$$L_p = \frac{L_v}{30} + 0.2h + 0.11 \frac{d_b f_y}{\sqrt{f_c}} \quad (113)$$

where, L_v is the ratio moment/shear (mm). h is the depth of cross-section (mm). f_y is the steel yield stress (MPa). f_c is the strength of concrete (MPa). d_b is the rebar diameter (mm).

In the USA codes (Caltrans, 2010; Imbsen, 2007), the plastic hinge length of columns and piles can be estimated respectively by formulae (114) and (115).

$$L_p = 0.08L + 0.022d_b f_y \geq 0.044d_b f_y \quad (114)$$

$$L_p = D^* + 0.08H_{o-max} \quad (115)$$

where, L is the member length from the point of maximum moment to the point of contraflexure (mm). f_y is the steel yield stress (MPa). d_b is the longitudinal rebar diameter (mm). D^* is the diameter for circular shafts or the least cross section dimension for oblong shafts (mm). H_{o-max} is the length of pile shaft/column from point of maximum moment to point of contraflexure above ground considering the base of plastic hinge at the point of maximum moment (mm).

The plastic hinge region length is also defined in Caltrans code (Caltrans, 2010), including 1.5 times the cross sectional dimension in the direction of bending, the region of column where the moment exceeds 75% of the maximum plastic moment and 1/4 of the member length from the point of maximum moment to the point of contraflexure.

Based on a large database including over 1000 tests of flexure controlled reinforced concrete members in uniaxial bending with or without axial force, the calculation equations (116) and (117) for plastic hinge length subjected to cyclic load or monotonic load were proposed by fitting the test results (Panagiotakos & Fardis, 2001).

$$L_{p,cy} = 0.12L_v + 0.014a_{s1} d_b f_y \quad (116)$$

$$L_{p,mon} = 1.5L_{p,cy} = 0.18L_V + 0.021a_{st}d_b f_y \quad (117)$$

3.3.4 Acceptance criteria

For informational purposes, some additional limit states, which can be specified in the plastic hinge as acceptance criteria, are defined in some codes.

Three limit states, which are Damage Limitation (DL), Significant Damage (SD), and Near Collapse (NC), have been defined in Eurocode8 Part3 (Eurocode CEN, 2005b). The yielding rotation corresponding to the yield bending moment is chosen as the capacity for the DL limit state, in which the structure is only lightly damaged, structural elements are prevented from significant yielding and retain their strength and stiffness properties. In this case, the structure does not need any repair measures. The yielding rotation for beams and columns can be evaluated by formulae (118) and (119). The first term in formulae accounts for the flexural contribution, the second term represents the contribution of shear deformation and the third term considers the anchorage slip of bars.

$$\theta_y = \phi_y \frac{L_V + a_v z}{3} + 0.00135 \left(1 + 1.5 \frac{h}{L_V} \right) + \frac{\varepsilon_y}{d - d'} \frac{d_b f_y}{6\sqrt{f_c}} \quad (118)$$

$$\theta_y = \phi_y \frac{L_V + a_v z}{3} + 0.0013 \left(1 + 1.5 \frac{h}{L_V} \right) + 0.13\phi_y \frac{d_b f_y}{\sqrt{f_c}} \quad (119)$$

where, ϕ_y is the yield curvature. $a_v z$ is the tension shift of the bending moment diagram. L_V is the ratio moment/shear. h is the depth of cross section. f_y is the steel yield stress (MPa). f_c is the concrete strength (MPa). d_b is the rebar diameter. d and d' are the depths to the tension and compression reinforcements, respectively. The detailed information of parameters and other formulae of the yielding rotation for different structural components can be found in Eurocode8 Part3 (Eurocode CEN, 2005b).

The rotation capacity corresponding to the SD limit state can be assumed as 75% of the ultimate rotation (θ_u). In this level, the structure is significantly damaged, some residual lateral strength and stiffness remain and vertical elements are capable of sustaining vertical loads. Therefore, the repair of the structure is likely to be uneconomic.

The rotation capacity corresponding to the NC limit state in Eurocode8 can be calculated by formula (120). In this level, the structure is heavily damaged, low residual lateral strength and stiffness remain, and vertical elements have only a little capacity to sustain vertical loads. The structure is near collapse. The formula (120) composed by the elastic part and plastic part can be used.

$$\theta_u = \frac{1}{\gamma_{e1}} \left(\theta_y + (\phi_u - \phi_y) L_p \left(1 - \frac{0.5L_p}{L_v} \right) \right) \quad (120)$$

where, θ_y is the yielding rotation. ϕ_y is the yield curvature. ϕ_u is the ultimate curvature. L_v is the ratio moment/shear. L_p is the plastic hinge length.

Similarly, three limit states of acceptance criteria, which are Immediate Occupancy (IO), Life Safety (LS) and Collapse Prevention (CP), are adopted in the codes in USA (American Society of Civil Engineers, 2007; Applied Technology Council, 1996; Federal Emergency Management Agency, 1997a, b, 2000, 2005). The recommended values of the deformation or deformation ratio are shown in Fig. 107. At the IO Level, the damage is relatively limited, the structure retains safe to occupy and any repairs are minor. At the LS Level, some substantial damages has occurred to the structure, and it may have lost a significant amount of its original stiffness. However, the structure remains stable and has significant reserve capacity. The hazardous nonstructural damage is controlled. At the CP Level, the structure has experienced extreme damages and remains standing, but only barely. If laterally deformed beyond this point, the structure can experience instability and collapse. The CP limit state is equivalent to the NC limit state in Eurocode8 (Mazzarolo, 2012)

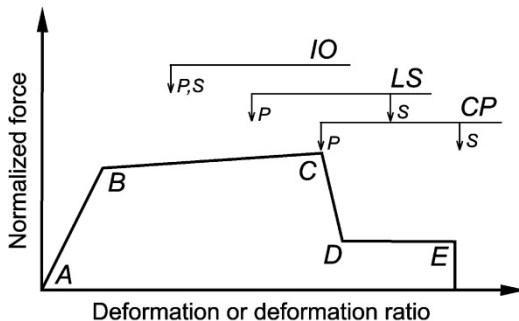


Fig. 107 Acceptance criteria in FEMA 356 (Federal Emergency Management Agency, 2000)

4. PROPOSED RETROFITTING METHODS WITH FIAB CONCEPT

As introduced in Chapter 2, the IAB concept has been applied to retrofit several existing bridges all over the world. Moreover, some specifications with respect to the conversion procedure from conventional SSBs into IABs have been proposed. In order to find the most approximate retrofitting approach, the real conditions of existing bridges should be taken into account, including total lengths, skew angles, types of bridge components (such as girders, piers, abutments and piles), temperature variations, soil conditions and so on. During retrofitting, some key issues should be paid more attention to. For example, the components of existing bridges should be reused as many as possible, in order to reduce the retrofitting cost and shorten the construction period. The new parts of bridges after retrofitting should be coordinated with the existing parts, such as the width of the new approach slab must be able to satisfy the requirements of both adjacent deck slab and pavement. In detail, the removal of concrete in some special parts of existing bridges should be careful, such as the prestressed concrete girder ends due to the congested anchorage zone areas at girder ends. New reinforcements should be effectively connected to existing ones by some techniques. Moreover, some other problems in existing bridges, such as leaking drainage systems, damaged bearings, spalling of concrete, corroded reinforcements and so on, should be resolved simultaneously.

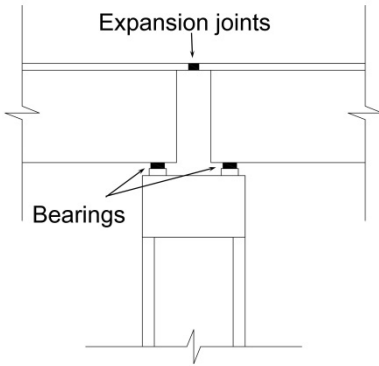
According to previous experience, the retrofitting process with the FIAB concept is easier than that with the SIAB concept. Because transforming to the SIAB needs to demolish a larger part of existing abutments and excavate more backfill in order to create the spaces for new end diaphragms that will connect directly to the backfill than converting to the FIAB. Moreover, the FIAB concept can resolve the potential durability problems of existing bearings. Therefore, this paper chooses the FIAB as the analytical object. Moreover, the influence of different superstructure-substructure connection flexibility on the performance of the FIAB has been considered as a key problem, which has been the focus of a significant research effort in the past decade. According to the detailed definition of the FIAB as listed in Table 2 (p.18), the retrofitting approaches of superstructure-pier connections and superstructure-abutment connections used in this paper are described respectively in the following.

4.1 Retrofit of superstructure-pier connection

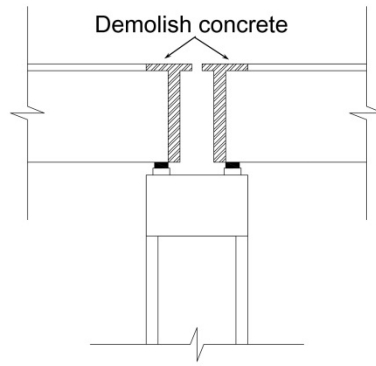
4.1.1 Hinged connection

As defined in Table 2 (p.18), FIAB1 and FIAB3 choose the hinged connection as the superstructure-pier connections. In this paper, the approach, which can make decks and girders continuous, and change existing bearings to the steel beam, was used. The negative bending moment can be resisted by the continuous superstructure. The steel beam can work as a shear connection to transfer forces between the superstructure and substructure, which has been widely used by many researches and in many guidelines (Briseghella & Zordan, 2006; Lan, 2012; Zordan & Briseghella, 2007; Zordan et al., 2011a, b). The detailed retrofitting phases of transforming existing simply supported superstructure-pier connections (Fig. 108(a)) into hinged ones used in this paper are introduced in the following.

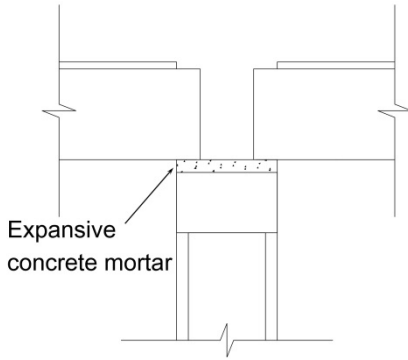
1. Remove existing expansion joints. Partially demolish the concrete of existing deck slabs and girder ends to create the spaces for new continuous superstructures. Prepare concrete surfaces to eliminate existing damages and increase their roughness by sandblasting or other techniques, such as installing shear studs or brushing epoxy adhesive with high shear strength on existing deck slabs and girders, in order to improve the connection between existing concrete and new-cast concrete (Fig. 108(b)).
2. Make existing bearings invalid and choose one material to separate the superstructure and pier caps that is good for the rotation of the force transmission device, for example, the expansive concrete mortar (Fig. 108(c)).
3. Position the reinforcements of new deck slabs and diaphragms. Extend new reinforcements in existing girders up to a certain length, in order to strengthen the resistance capacity of the additional hogging moments after retrofitting (Fig. 108(d)).
4. Drill some holes on the top surface of each pier. Install steel beams in these holes as the force transmission device (Fig. 108(e)).
5. Cast concrete to complete hinged superstructure-pier connections, including deck slabs, end diaphragms and a certain length of existing girders, as shown in Fig. 108(f). The hinged connection can be obtained by installing the steel beams between piers and the new continuous superstructure, which can transfer forces in three directions, while cannot transfer bending moments.



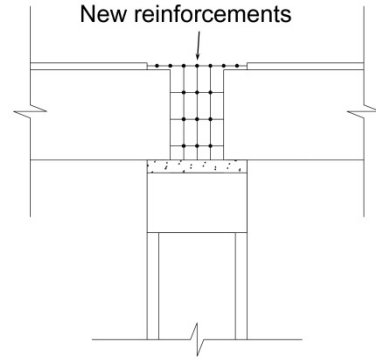
(a) Existing simply supported superstructure-pier joints



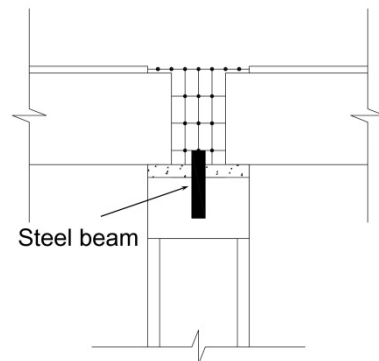
(b) Remove expansion joints and demolish concrete



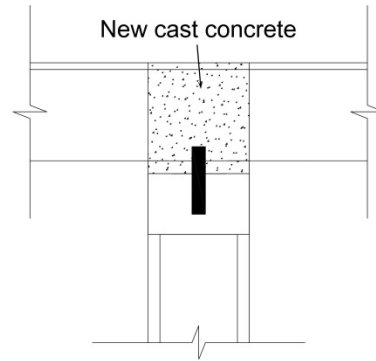
(c) Make bearings invalid



(d) Position new reinforcements



(e) Install steel beam



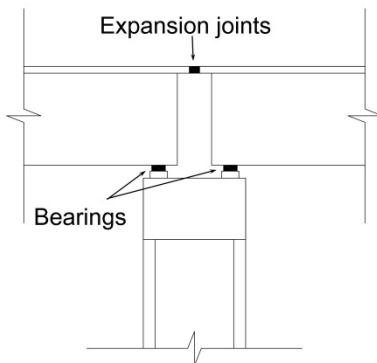
(f) Cast concrete

Fig. 108 Conversion of existing superstructure-pier connections in SSBs to hinged superstructure-pier connections in FIABs (Zordan et al., 2011a)

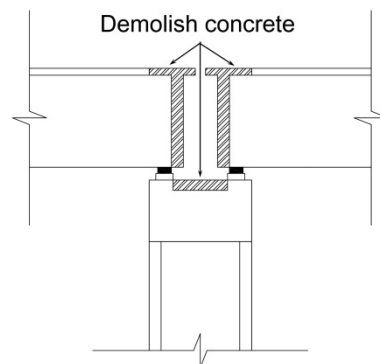
4.1.2 Rigid connection

FIAB2 and FIAB4 defined in Table 2, (p.18), choose the rigid connection as the superstructure-pier connections. The detailed retrofitting phases of transforming existing simply supported superstructure-pier connections (Fig. 109(a)) into rigid ones used in this paper are described in the following.

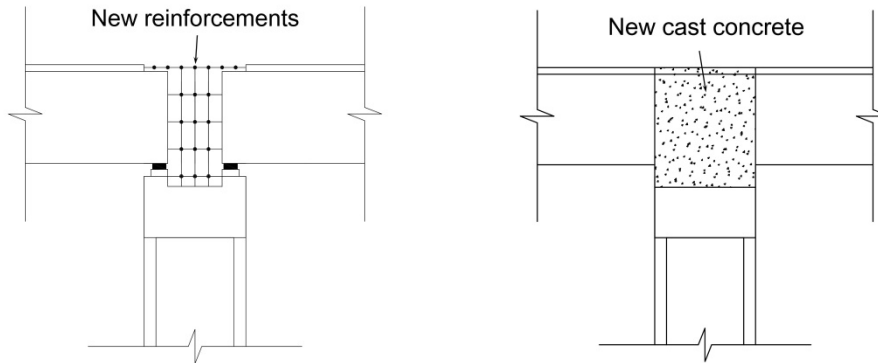
1. This step is similar to the first step of the hinged superstructure-pier connection construction. In addition, partially demolish the concrete of pier top parts (Fig. 109(b)).
2. Position the reinforcements of new deck slabs and diaphragms. Extend new reinforcements in existing girders up to a certain length, in order to strengthen the resistance capacity of the additional hogging moments after retrofitting. Moreover, effectively connect new reinforcements to the existing reinforcements in pier caps (Fig. 109(c)). The existing bearings can be removed or retain. They will become invalid after retrofitting.
3. Cast concrete to complete rigid superstructure-pier connections, including deck slabs, end diaphragms, a certain length of existing girders and top parts of piers, as illustrated in Fig. 109(d). The rigid connection can be obtained between piers and the new continuous superstructure, which can transfer all forces and bending moments.



(a) Existing simply supported superstructure-pier joints



(b) Remove expansion joints and demolish concrete



(c) Position new reinforcements

(d) Cast concrete

Fig. 109 Conversion of existing superstructure-pier connections in SSBs to rigid superstructure-pier connections in FIABs

4.2 Retrofit of superstructure-abutment connection

The retrofit of existing simply supported superstructure-abutment connections can be also divided into two aspects, including the hinged connection and the rigid connection.

4.2.1 Hinged connection

According to the detailed definitions in Table 2 (p.18), FIAB1 and FIAB2 choose hinged connections as the superstructure-abutment connections. In this paper, the approach, which can make decks and girders continuous, and change existing bearings to the steel beam, was used. The negative bending moment can be resisted by the superstructure. The steel beam can work as a shear connection to transfer forces between the superstructure and substructure, which has been widely used by many researches and in many guidelines (Briseghella & Zordan, 2006; Lan, 2012; Wolde-Tinsae et al., 1988b; Zordan & Briseghella, 2007; Zordan et al., 2011a, b). The detailed retrofitting phases of converting existing simply supported superstructure-abutment connections (Fig. 110(a)) into hinged ones used in this paper are introduced in the following.

1. Remove existing expansion joints and approach slabs if there are. Excavate some parts of existing backfill behind abutments. Demolish partially the concrete of deck slabs, girder ends, abutment wingwalls and backwalls in existing bridges. In some cases, maybe the total height of abutment wingwalls or backwalls need be dismantled. The height of abutment wingwalls or backwalls should remain as more

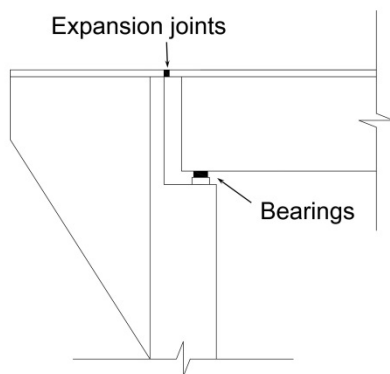
as possible in order to save retrofitting costs and construction time. Prepare the concrete surfaces to eliminate existing damages and increase the roughness using the same techniques introduced in Section 4.1.1 (Fig. 110(b)).

2. Similar to the retrofitting approach of hinged superstructure-pier connections, choose expansive concrete mortar as the material, which can make existing bearings invalid and separate the superstructure and abutments, in order to ensure the rotation of the force transmission device (Fig. 110 (c)).

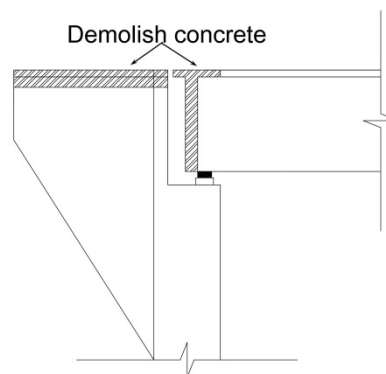
3. Position the reinforcements of new deck slabs, end diaphragms and approach slabs. Extend the reinforcements in existing girders up to a certain length, in order to strengthen the resistance capacity of the additional hogging moments after retrofitting. Install some mechanical connections, such as shear studs and mounting barriers, or sliding materials, such as the plain elastomeric bearing strip, which can be used to connect new approach slabs or deck slabs to existing abutment wingwalls or backwalls (Fig. 110(d)).

4. Insert the steel beams to the pre-drilled holes on the top surface of each abutment (Fig. 110(e)).

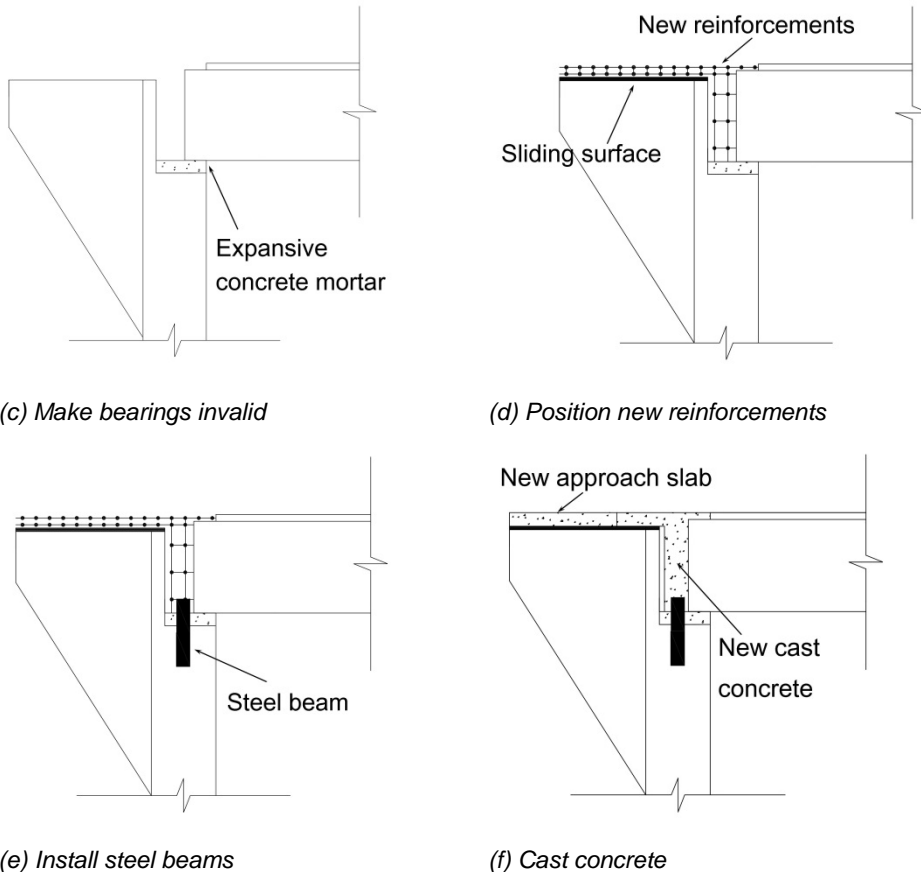
5. Cast concrete to complete hinged superstructure-abutment connections, including deck slabs, end diaphragms and a certain length of existing girders. Cast abutment wingwalls and backwalls. Restore the backfill behind abutments. Cast concrete again to construct new approach slabs (Fig. 110(f)). The lengths of deck slabs and approach slabs should be determined. The detailed configurations of new approach slabs, the connections between deck slabs and approach slabs, and the connections between approach slabs and pavements also need to be investigated. The hinged connection can be obtained by installing the steel beams between abutments and the superstructure, which can transfer the forces in three directions, while cannot transfer bending moments.



(a) Existing simply supported superstructure-abutment joints



(b) Remove expansion joints and approach slabs, and demolish concrete



(c) Make bearings invalid (d) Position new reinforcements
 (e) Install steel beams (f) Cast concrete
 Fig. 110 Conversion of existing superstructure-abutment connections in SSBs to hinged superstructure-abutment connections in FIABs (Zordan et al., 2011a)

4.2.2 Rigid connection

FIAB3 and FIAB4 defined in Table 2 (p.18), choose rigid connections as the superstructure-abutment connections. The detailed retrofitting phases of transforming existing simply supported superstructure-abutment connections (Fig. 111(a)) into rigid ones used in this paper are described in the following.

1. This step is similar to the first step of the hinged superstructure-abutment connection construction. In addition, partially demolish the concrete of retained abutment backwalls and the top parts of abutment stems (Fig. 111(b)).
2. Position the reinforcements of new deck slabs, end diaphragms and approach slabs. Extend new reinforcements in existing girders up to a certain length, in order to strengthen the resistance capacity of the additional hogging moments after retrofitting. Moreover, effectively connect new reinforcements to the existing reinforcements in retained abutment backwalls and the top parts of abutment stems.

RETROFIT OF EXISTING BRIDGES WITH CONCEPT OF INTEGRAL ABUTMENT BRIDGE

Install some mechanical connections or the sliding material, which can be used to connect new approach slabs or deck slabs and existing abutment wingwalls or backwalls (Fig. 111(d)). The existing bearings can be removed or retain. They will become invalid after retrofitting.

3. Cast concrete to complete rigid superstructure-abutment connections, including deck slabs, end diaphragms, a certain length of existing girders, abutment backwalls and top parts of abutment stems. Cast abutment wingwalls. Restore the backfill behind abutments. Cast concrete again to construct new approach slabs (Fig. 111(d)). The lengths of deck slabs and approach slabs should be determined. The detailed configurations of new approach slabs, the connections between deck slabs and approach slabs, and the connections between approach slabs and pavements need to be investigated. The rigid connection can be obtained between abutments and the superstructure, which can transfer all forces and bending moments.

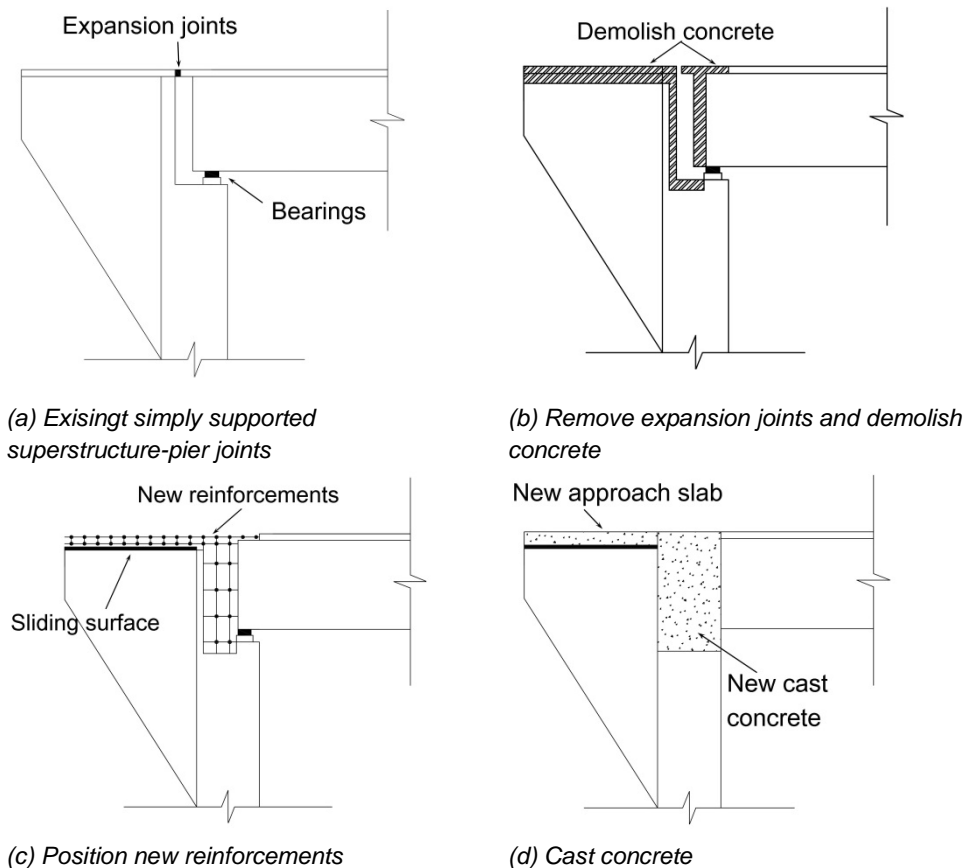


Fig. 111 Conversion of existing superstructure-abutment connections in SSBs to rigid superstructure-abutment connections in FIABs

5. CASE STUDY

In Italy, many bridges of road and railway infrastructural networks are between 50 and 150 years old (Malerba, 2010). In order to understand well the performance of existing bridges after retrofitting with the IAB concept, the case study is going to be presented on an existing typical SSB 'Viadotto Serrone' in Italy.

5.1 Viadotto Serrone

The case study presented concerns a simply supported flyover 'Viadotto Serrone' located at an important highway connecting Salerno (SA) and Potenza (PZ) in the south of Italy (Fig. 112), which has a history of more than 40 years. This flyover is composed of two separated SSBs to satisfy the requirement of traffic in two directions (SA-PZ and PZ-SA). The geometrical information and materials of the two bridges are nearly the same, except the pier height. Therefore, one SSB (SA-PZ) is chosen as the example to analyze in this paper.



Fig. 112 Viadotto Serrone

The main features of the existing bridge are listed in Table 29. The elevation layout is shown in Fig. 113. The details of superstructure cross sections are illustrated in Fig. 114. The total length of this bridge is 120.9m with three spans. The clear length of each span is 38.2m. Each span has three transverse beams, which are located respectively at the both ends and the middle. The existing superstructure is composed of three prestressed concrete girders supporting one reinforced concrete slab deck. Two types of girder cross sections are chosen, including T-girder cross

RETROFIT OF EXISTING BRIDGES WITH CONCEPT OF INTEGRAL ABUTMENT BRIDGE

section and I-girder cross section. Both girder ends with the length of 2.3m use the T-girder cross section. The remaining parts of girders use the I-girder cross section. The width of the deck cross section is 9.5m including one carriageway with the dimension of 8.5m×0.2m and two footpaths with the dimension of 0.5m×0.18m at both sides.

Total length	120.9m	
Number of spans	3	
Single span clear length	40.3m and 38.2m	
Static scheme	Simply supported	
Girder information	Number per span	3
	Height	2.7m
	Type	T-girder and I-girder
Deck information	One carriageway	8.5m×0.2m
	Two footpaths	0.5m×0.18m each
Pier height (Cap+Column+Footing)	Pier-A	1.8+13.7+2.5m
	Pier-B	1.8+19.7+2.5m
Abutment height (Backwall+Stem+Footing)	Abutment-A	3+5+2m
	Abutment-B	3+1.5+2m
Pile	Number per each abutment or pier	5
	Cross section shape	Circular
	Diameter	1.8m
	Length	30m beneath abutments 27m beneath piers

Table 29
Main features of 'Viadotto Serrone (SA-PZ)'

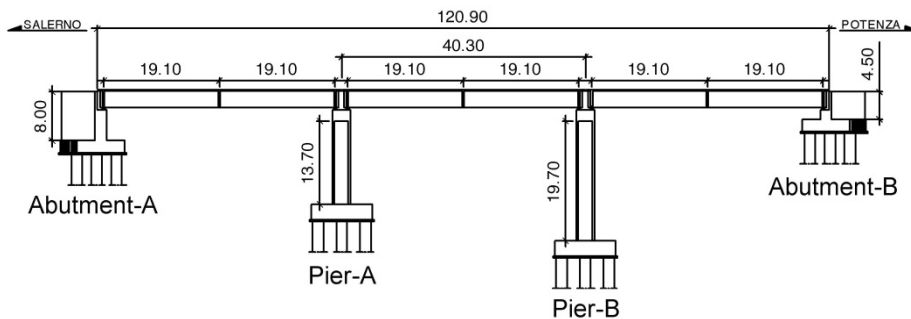
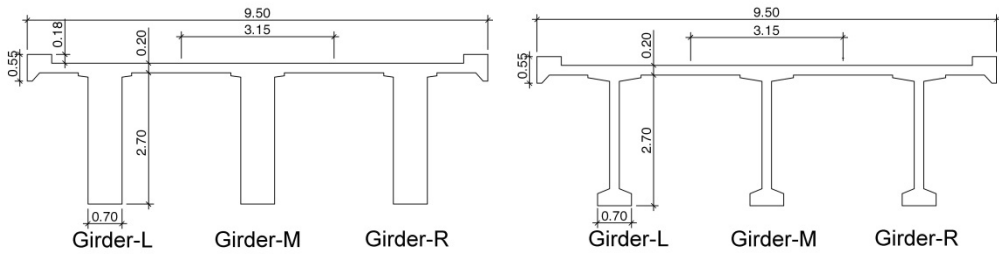


Fig. 113 Elevation layout of 'Viadotto Serrone' (Unit: m)



(a) Cross section at the end of girder (b) Cross section in the middle of girder
 Fig. 114 Typical superstructure cross sections in 'Viadotto Serrone' (Unit: m)

For the substructure, the heights of two pier columns are different, which are 13.7m in Pier-A and 19.7m in Pier-B. The box cross section shown in Fig. 115 is chosen as the cross section of the pier supporting a cap beam on the top. The pier footing with the height of 2m is arranged at the bottom of each pier column. Five piles with the length of 27m support each pier. The details of piers in both longitudinal and transverse directions are illustrated in Fig. 116. Two abutments in the existing bridge are the U-shaped gravity abutment, which is composed of one abutment backwall, one abutment stem, one abutment footing and two abutment wingwalls. The heights of two abutment stems are different, which are 5m in Abutment-A and 1.5m in Abutment-B. The details of two abutments can be found in Fig. 117. Five piles with the length of 30m support each abutment. All piles beneath piers and abutments are designed as the circular reinforced concrete pile with the diameter of 1.8m. The arrangement and number of piles are illustrated in Fig. 118.

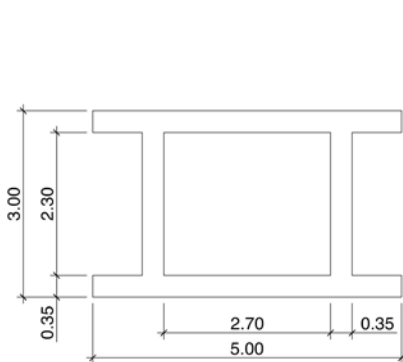
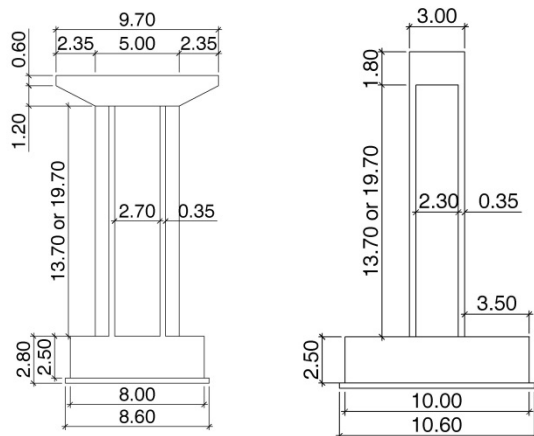
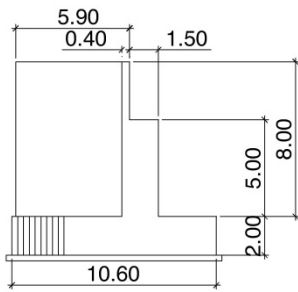


Fig. 115 Pier cross section in 'Viadotto Serrone' (Unit: m)

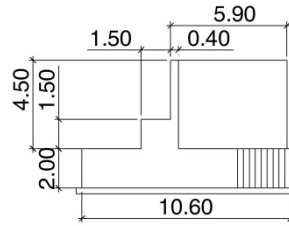


(a) Longitudinal direction (b) Transverse direction
 Fig. 116 Elevation layout of pier in 'Viadotto Serrone' (Unit: m)

RETROFIT OF EXISTING BRIDGES WITH CONCEPT OF INTEGRAL ABUTMENT BRIDGE

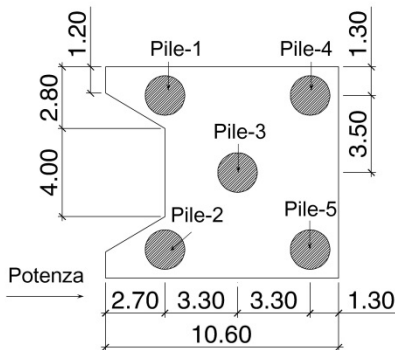


(a) Abutment-A

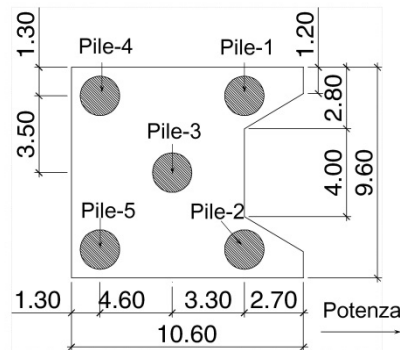


(b) Abutment-B

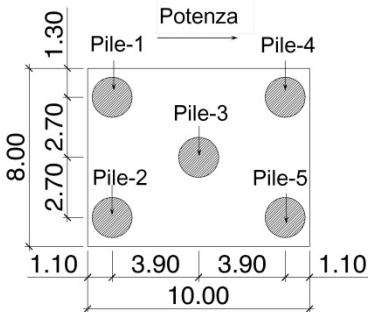
Fig. 117 Elevation layout of abutments in 'Viadotto Serrone' (Unit: m)



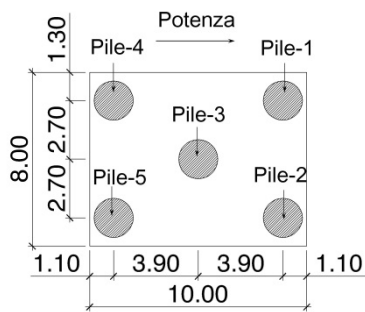
(a) Piles beneath Abutment-A



(b) Piles beneath Abutment-B



(c) Piles beneath Pier-A



(b) Piles beneath Pier-B

Fig. 118 Arrangement and number of piles in 'Viadotto Serrone' (Unit: m)

5.2 Finite element model

In this analysis, the most important in finite element modeling is to ensure that the finite element model can simulate the performance of bridges before and after retrofiting. It means that the appropriate finite element model used in this paper

should have the main features listed in the following. The typical model scheme of the bridge after retrofitting with the details concerning the main features and the information of elements is illustrated in Fig. 119.

1. 3D finite element model with frame element and plate element,
2. Nonlinear area spring elements are attached perpendicularly to backwalls, stems and wingwalls to simulate the lateral soil-abutment interaction.
3. Three series of nonlinear line spring elements are attached along the full length of piles to simulate the soil-pile interaction, including two series in lateral directions and one series in vertical direction.
4. Concentrated plastic hinges are arranged at the top and bottom of piers and distributed plastic hinge zones are applied to the top part of piles.
5. The stages of retrofitting process are considered.
6. There is no approach slab in existing bridge. Therefore, the approach slab modeling in finite element model is neglected; however, the displacement transferring from bridge ends to approach slabs will be checked.

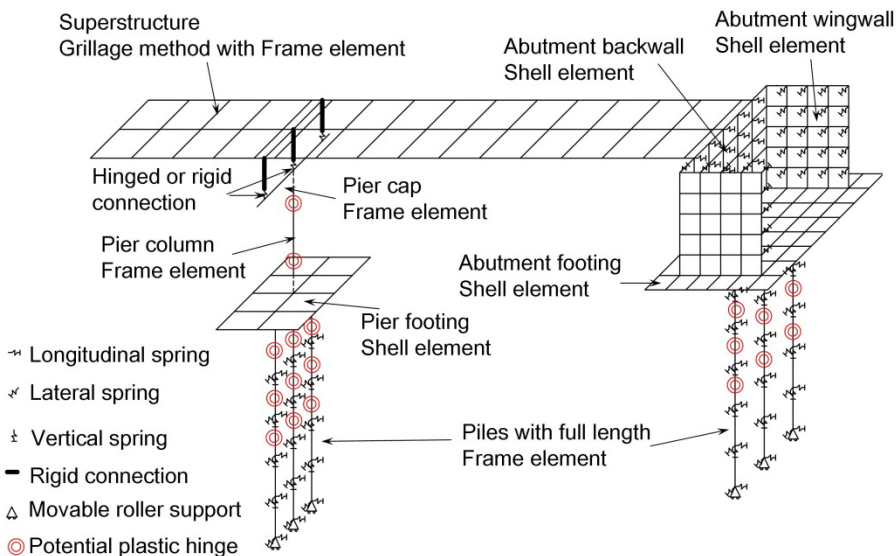


Fig. 119 Typical model scheme of bridge after retrofitting

Based on the above requirements, the 3D nonlinear structural model which can simulate the existing SSB and the different subtypes of FIABs after retrofitting can be built by the general finite element software Sap2000 (Computers and Structures Inc, 2011). In this model, the effects of different kinds of nonlinearities can be considered, including the material nonlinearity (elastic-plastic constitutive relationships and plastic hinges), the geometrical nonlinearity (P- Δ effect), the boundary condition nonlinearity (nonlinear soil-structure interactions) and the

RETROFIT OF EXISTING BRIDGES WITH CONCEPT OF INTEGRAL ABUTMENT BRIDGE

nonlinear staged construction. The 3D finite element model of the bridge after retrofitting with the number of different bridge components is illustrated in Fig. 120.

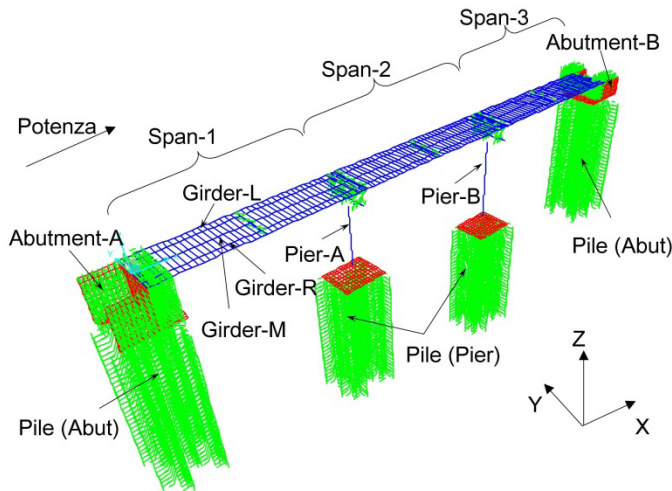


Fig. 120 3D finite element model in Sap2000

The details of the 3D model, which can be used to analyze the performance of the existing SSB and different subtypes of FIABs after retrofitting, are presented in the following. In the following analysis, in order to describe clearly, all internal forces and displacements of different bridge components are defined in Table 30. The subscripts X, Y and Z corresponds to the global coordinate axes (X, Y and Z), which denote respectively the longitudinal direction, the transverse direction and the vertical direction of the bridge with the global coordinate axes.

F_A	Axial force
F_{SX}, F_{SY}, F_{SZ}	Shear forces in longitudinal, transverse and vertical directions
T	Torsion
M_X, M_Y, M_Z	Bending moments around the axes in longitudinal, transverse and vertical directions
U_X, U_Y, U_Z	Displacement in longitudinal, transverse and vertical directions

Table 30

Definitions of the internal forces of bridge

According to previous studies (Dicleli & Erhan, 2010), the locations of the internal forces which can reach the maximum value should be considered as the critical sections. All the possible locations of critical sections for the SSB and FIAB after retrofitting should be taken into account, as illustrated in Fig. 121. The definitions of these critical sections are listed in Table 31.

The zero points of different bridge components are defined, as illustrated in Fig. 121, which will be used in following analyses. The left points of Span-1 can be set as the zero point of the superstructure. For vertical components, such as piers, abutments and piles, the top points are assumed as the zero points.

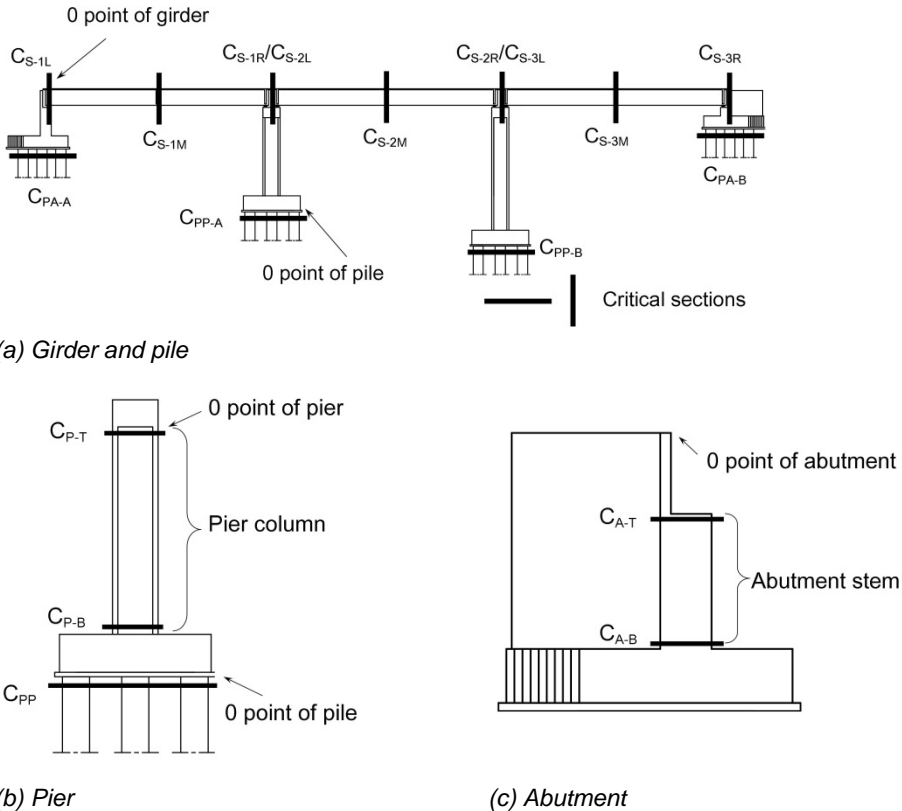


Fig. 121 Definition of zero points and the critical sections

C_S	Critical section of span	-1, -2, -3	Number of span	L, M, R	Left, middle or right points of span
C_A	Critical section of abutment stem	-A, -B	Number of abutment	T, B	Top or bottom of stem
C_P	Critical section of pier	-A, -B	Number of pier	T, B	Top or bottom of pier
C_{PA}	Critical section of pile beneath abutment	-A, -B	Number of abutment	-1, -2, -3, -4, -5	Number of pile
C_{PP}	Critical section of pile beneath pier	-A, -B	Number of pier	-1, -2, -3, -4, -5	Number of pile

Table 31
Definitions of critical sections

In this model, the internal forces and displacements of each node in the two-node frame element can be illustrated in figures to show the results. However, in order to obtain the internal forces of area elements at a certain height, the section cut function implemented in Sap2000 (Computers and Structures Inc, 2011) should be used. The section cut function can obtain the resultant force of all area elements at a certain coordinate in the vertical direction by creating a virtual plane. In this case, several virtual planes are created along the abutment stem. As mentioned above, the top points of abutments are set as the zero points in the vertical direction. Therefore, the coordinates of two abutment stem the vertical direction will start from -3 to -8 in Abutment-A and from -3 to -4.5 in Abutment-B. From the YZ plane of view, the virtual planes in both abutment stems can be set at the middle height of each row of area elements. Therefore, the corresponding coordinates are -3.5, -4.5, -5.5, -6.5 and -7.5 in Abutment-A (the horizontal lines in Fig. 122), and -3.5 and -4.25 in Abutment-B. For the displacements of area elements, the middle node at a certain coordinate in the vertical direction, for example -3, -4, -5, -6, -7 and -8 in Abutment-A (the circular points in Fig. 122) and -3, -4, -4.5 in Abutment-B, can be chosen.

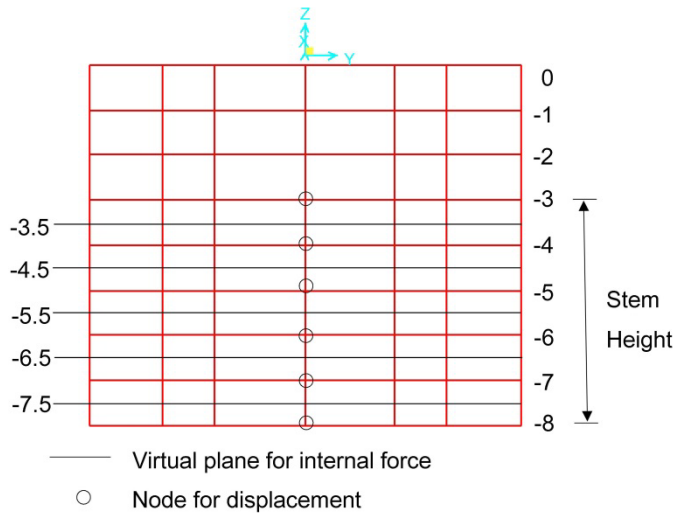


Fig. 122 Stem and backwall of Abutment-A in YZ plane of view

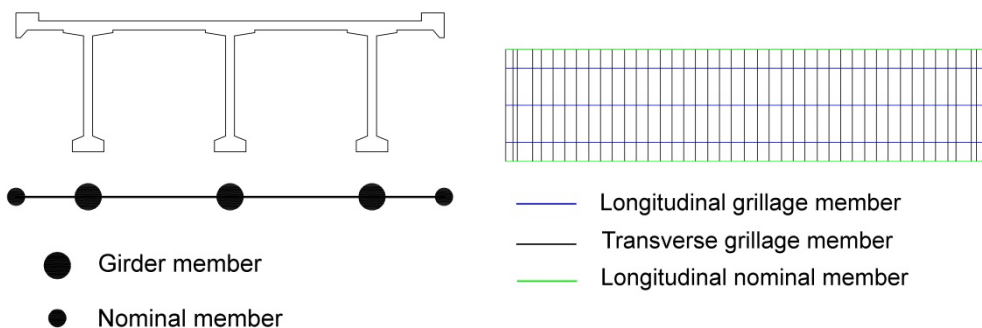
5.2.1 Modeling method and elements information

5.2.1.1 Modeling of superstructure

As introduced above, the superstructure of the existing bridge is the typical spaced

girder-and-slab deck, which is composed of three girders at 3.15m centers connected integrally across their tops by a deck slab, as illustrated in Fig. 114 (p.161). When transferring the load longitudinally to the supports, the deck slab acts in concert with the girders as their top flanges. At the same time, the greater deflections of the most heavily loaded girders bend the deck slab transversely, so that it transfers and shares out the load to neighboring girders (Hambly, 1990). Therefore, the grillage method, which can convert the bridge superstructure into a network of two-node three-dimensional frame elements, is a sufficiently accurate approach that can be chosen in this case to simulate the bridge superstructure.

The cross section and plan view of grillage mesh in this bridge are illustrated in Fig. 123. It is both convenient and physically reasonable to place longitudinal grillage members coincident with the centerlines of the prototype girders. Three rows of longitudinal grillage members in one span were modeled by 129 frame elements. The properties of the section composed of one girder and partial deck slab with the width of 3.15m were applied to the longitudinal grillage members. The transverse grillage members were placed at the interval of 1m, except the positions of transverse beams and girder cross section variations. The real behaviors of the slab deck with the width of 1m were applied to the transverse grillage members considering the weight as zero. Six frame elements were used to simulate the transverse beams in each span. Two lines of nominal members were arranged longitudinally at the both edges of the cross section, in order to connect the extended transverse grillage members. Comparing with those used elsewhere in the grillage network, very small section properties were assigned to these nominal members. In this model, a small cross section was applied to the nominal members to obtain the small section properties. Moreover, the weight of the longitudinal nominal members should be also set as zero (O'Brien & Keogh, 1999).



(a) Cross section

(b) Plan view of one span

Fig. 123 Grillage mesh of the superstructure in 'Viadotto Serrone'

5.2.1.2 Modeling of substructure

In the ordinary analysis of the SSB, the substructure modeling can be neglected and simplified as the simply supported boundary condition. However, due to the particularity of this case, the substructure in the existing SSB must be simulated. It is assumed to reuse the existing substructure in FIABs after retrofitting.

Six two-node three-dimensional frame elements were used to model the cap beam of each pier. The two-node three-dimensional frame element with the length of 2m was also chosen to simulate the pier column. All piles in this bridge were modeled by the two-node three-dimensional frame elements with the length of 1m. The backwalls, stems, wingwalls and footings of abutments, and the footings of piers were simulated by four-node shell elements. The cap-column and column-footing connections were modeled as the rigid connection through the body constraint implemented in Sap2000 (Computers and Structures Inc, 2011), which can fully link all 6 degrees of freedom of several joints, as shown in Fig. 124. The top node of each pile was connected to the corresponding node on the footing of pier or abutment by the link element with the rigid property, as shown in Fig. 125.

5.2.1.3 Modeling of connection between superstructure and substructure

In this analysis, the existing bearings were idealized as the two-node three-dimensional frame element by using the Frame-Releases function implemented in Sap2000 (Computers and Structures Inc, 2011), which can release some specified degrees of freedom at both ends of the selected frame element. Due to the limited information and the long history of the existing bridge that is more than 40 years, it is difficult to determine the accurate mechanical behaviors of existing rubber bearings. Therefore, the typical simply supported connection for the three-span SSB was chosen in the model, as illustrated in Fig. 126. In order to simulate the real position and arrangement of bearings, the rigid link elements were chosen to connect the top nodes of bearings to the corresponding nodes of the superstructure, and link the bottom nodes of bearings to the corresponding nodes of pier caps or abutment stems. The modeling of bearings on the pier cap is shown in Fig. 124.

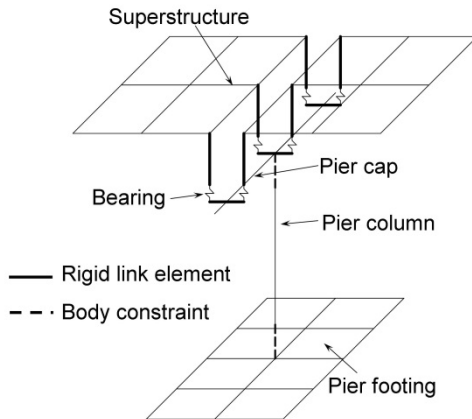


Fig. 124 Modeling of connection between superstructure and pier

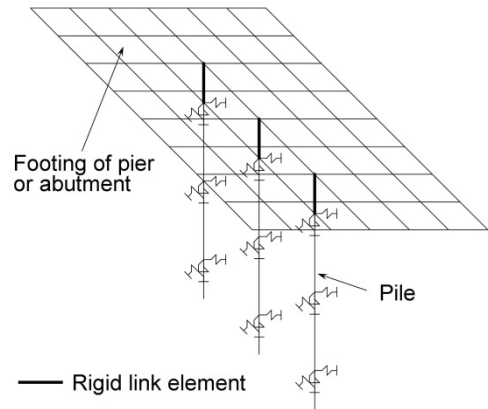


Fig. 125 Modeling of connection between piles and footing of abutment or pier

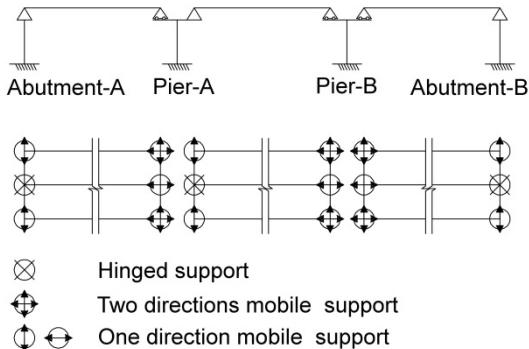


Fig. 126 Typical three-span simply supported connection

Using the proposed retrofitting approach described in Chapter 4, existing bearings should be replaced by steel beams for hinged connections. Moreover, in order to achieve the rigid connection, existing bearings should be removed and the superstructure and the substructure should be cast integrally. The typical hinged and rigid connections in different types of three-span FIABs are illustrated in Fig. 127. When simulating the hinged connection, the steel beams were modeled by two-node three-dimensional frame elements and the Frame-Releases function implemented in Sap2000 (Computers and Structures Inc, 2011). The rigid connection was simulated by the two-node three-dimensional frame element. The modeling of hinged or rigid connections on the pier cap is demonstrated in Fig. 128.

Different to the SSB, the adjacent superstructure ends over piers should be connected rigidly by the frame element to simulate the new constructed diaphragms in the IAB after retrofitting, as illustrated in Fig. 128. In addition, the rigid connection

RETROFIT OF EXISTING BRIDGES WITH CONCEPT OF INTEGRAL ABUTMENT BRIDGE

between the superstructure and abutment backwalls should be also added when analyzing the FIAB3 and FIAB4.

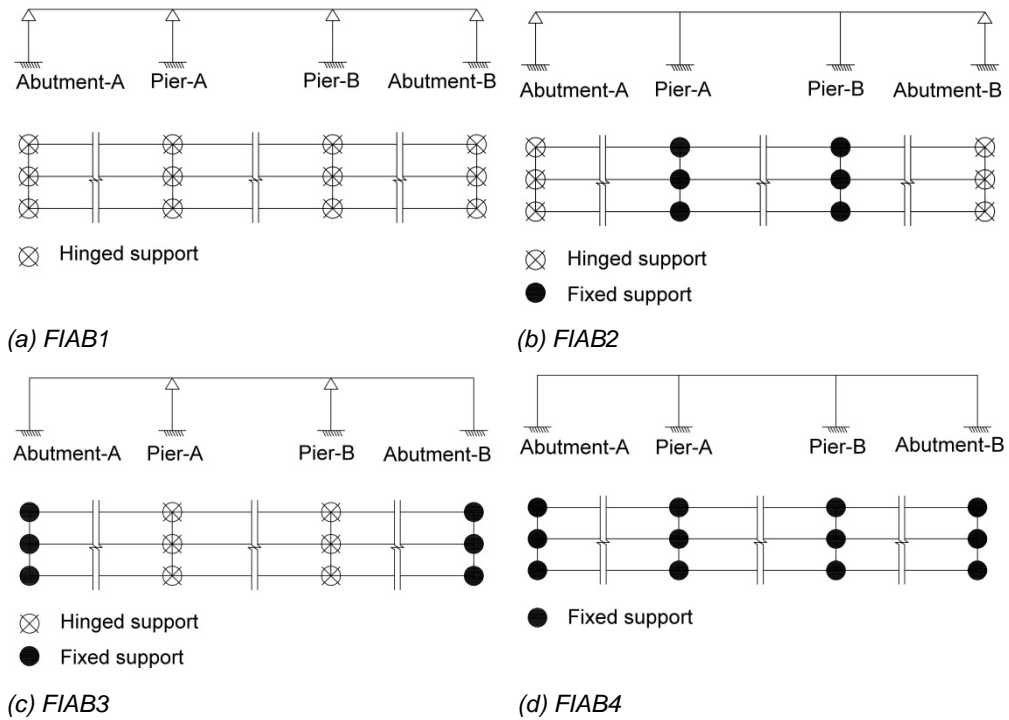


Fig. 127 Typical three-span fully integral connections

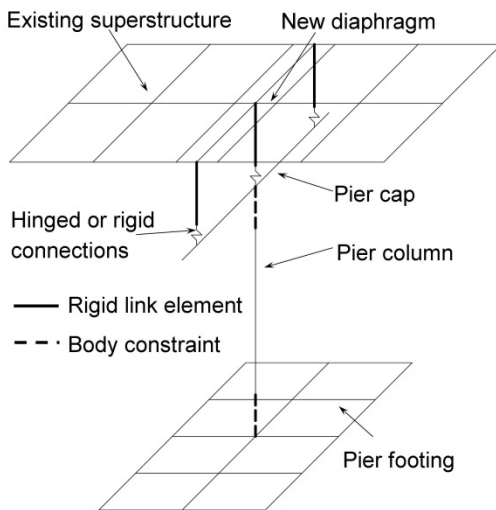


Fig. 128 Modeling of fully integral connections on pier cap

5.2.2 Material

From the investigation report of this bridge, the strength of concrete and rebar could be found as $R > 400 \text{ kg/cm}^2$ and $\sigma_s = 4400 \text{ kg/cm}^2$, respectively, which can be considered as C35/45 and B450C according to the Italian code NTC 2008 (Ministero delle Infrastrutture, 2008). The mechanical properties of the prestressing tendon in this bridge is $R_{ak} > 165 \text{ kg/mm}^2$ and $R_{ak(0.2)} > 145 \text{ kg/mm}^2$. The detailed material properties are listed in Table 32.

Mechanical properties	Concrete C35/45	Rebar B450C	Tendon
E (MPa)	27800	2×10^5	1.96×10^5
f_{ck} or f_y/f_u (MPa)	35	450/540	1450/1650
f_{cd} or f_{yd}/f_{ud} (MPa)	19.8	391/470	1260/1435
γ_c or γ_s	1.5	1.15	1.15
μ	0.2	0.3	0
M (kg)	2548.5	7850	7850
α_T ($10^{-6}/^\circ\text{C}$)	10	12	12

Table 32

Material properties in 'Viadotto Serrone'

The design strengths of different materials were used in this analysis. The formula (121) can be used to calculate the design compression strength of concrete. The design yield and ultimate stress of rebar and the prestressing tendon can be obtained by formula (122).

$$f_{cd} = \alpha_{cc} f_{ck} / \gamma_c \quad (121)$$

$$f_d = f_k / \gamma_s \quad (122)$$

where, α_{cc} is the coefficient taking account of long-term effects on the compressive strength and of unfavorable effects resulting from the way the load is applied, which is 0.85 in the literature (Ministero delle Infrastrutture, 2008).

The nonlinear constitutive relationships of different materials were considered in this case, which will be used to define the plastic hinge. The Park steel stress-strain relationship curve illustrated in Fig. 129, which can be obtained by formulae (123) to (125), was chosen for rebar (Park, 1992).

$$f = \begin{matrix} E\varepsilon & \varepsilon \leq \varepsilon_y \\ f_y & \varepsilon_y < \varepsilon \leq \varepsilon_{sh} \\ f_y \left(\frac{m(\varepsilon - \varepsilon_{sh}) + 2}{60(\varepsilon - \varepsilon_{sh}) + 2} + \frac{(\varepsilon - \varepsilon_{sh})(60 - m)}{2(30r + 1)^2} \right) & \varepsilon_{sh} < \varepsilon \leq \varepsilon_{su} \end{matrix} \quad (123)$$

$$m = \frac{(f_u / f_y)(30r + 1)^2 - 60r - 1}{15r^2} \quad (124)$$

$$r = \varepsilon_{su} - \varepsilon_{sh} \quad (125)$$

where, f_y and f_u are listed in Table 32. ε_{sh} and ε_{su} can use Caltrans default strain (Caltrans, 2010), which are dependent on the rebar diameter (d_s), as listed in Table 33.

ε_{su}	$d_s \leq 0.034\text{m}$	$\varepsilon_{su} = 0.09$
	$d_s > 0.034\text{m}$	$\varepsilon_{su} = 0.06$
ε_{sh}	$d_s \leq 0.026\text{m}$	$\varepsilon_{sh} = 0.015$
	$0.026\text{m} < d_s \leq 0.03\text{m}$	$\varepsilon_{sh} = 0.0125$
	$0.03\text{m} < d_s \leq 0.038\text{m}$	$\varepsilon_{sh} = 0.0115$
	$0.038\text{m} < d_s \leq 0.05\text{m}$	$\varepsilon_{sh} = 0.0075$
	$d_s > 0.05\text{m}$	$\varepsilon_{sh} = 0.005$

Table 33
Caltrans default value of ε_{sh} and ε_{su} (Caltrans, 2010)

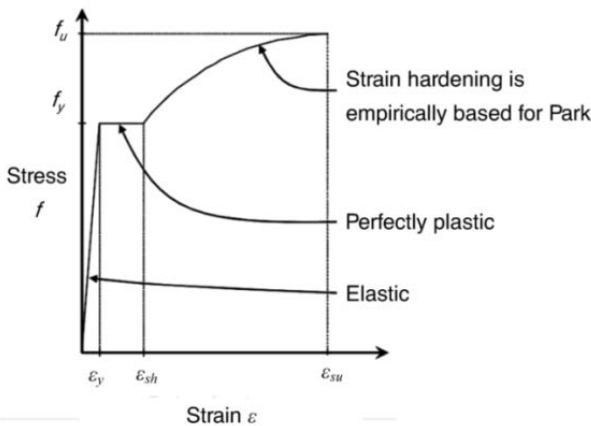


Fig. 129 Park stress-strain relationship curve for rebar

For the prestressing tendon, the idealized elastic-plastic stress-strain relationship

curve was chosen, as illustrated in Fig. 130. In this relationship, the yield stress (f_y) and the ultimate stress (f_u) of tendon are listed in Table 32. The tendon yield strain (ϵ_y) can be calculated by f_y/E and the ultimate strain (ϵ_u) can be set as 0.03.

For concrete, many formulae can be used to describe the unconfined and confined constitutive relationship of normal concrete with discreteness. The most frequently used Mander concrete stress-strain relationship curve was chosen in this analysis (Mander & Priestley, 1988), which includes three relationship curves corresponding to unconfined concrete, confined concrete with circular cross section and confined concrete with rectangular cross section, respectively.

The Mander unconfined concrete stress-strain relationship curve illustrated in Fig. 131, is composed of the curved portion and the linear portion, which can be calculated by formulae (126) and (127).

$$f = \begin{cases} \frac{f_c (\epsilon / \epsilon_c) r}{r - 1 + (\epsilon / \epsilon_c)^r} & \epsilon \leq 2\epsilon_c \\ \left(\frac{2f_c r}{r - 1 + 2^r} \right) \left(\frac{\epsilon_u - \epsilon}{\epsilon_u - 2\epsilon_c} \right) & 2\epsilon_c < \epsilon \leq \epsilon_u \end{cases} \quad (126)$$

$$r = \frac{E}{E - (f_c / \epsilon_c)} \quad (127)$$

The Mander confined concrete stress-strain relationship curves for circular section (Fig. 131) and for rectangular section can be calculated by formulae (128) to (132).

$$f = \begin{cases} \frac{f_{cc} (\epsilon / \epsilon_c) r}{r - 1 + (\epsilon / \epsilon_c)^r} \end{cases} \quad (128)$$

$$r = \frac{E}{E - (f_{cc} / \epsilon_{cc})} \quad (129)$$

$$f_{cc} = f_c \left(2.254 \sqrt{1 + \frac{7.94 f'_L}{f_c}} - 2 \frac{f'_L}{f_c} - 1.254 \right) \quad (130)$$

$$\epsilon_{cc} = \left[5 \left(\frac{f_{cc}}{f_c} - 1 \right) + 1 \right] \epsilon_c \quad (131)$$

$$\varepsilon_{cu} = 0.004 + 1.4\varepsilon_{su}\rho_s \frac{f_y}{f_{cc}} \quad (132)$$

where, f_c is the compressive strength of unconfined concrete, as listed in Table 32. ε_c is the yield strain corresponding to f_c (2.25×10^{-3} for C35/45 (Eurocode CEN, 2004a)). ε_u is the ultimate strain of unconfined concrete with the value of 6×10^{-3} . f_{cc} is the compressive strength of confined concrete, which can be calculated by formula (130) for circular section or obtained from a chart for rectangular section (Mander & Priestley, 1988). ε_{cc} is the concrete strain corresponding to f_{cc} , which can be obtained by formula (131). ε_{cu} is the ultimate strain of confined concrete, which can be influenced by the stress (f_y) and ultimate strain (ε_{su}) of rebar and volumetric ratio (ρ_s) of transverse reinforcing steel and calculated by formula (132). E is the modulus of elasticity, which can be calculated by equations $E=4700(f_c)^{0.5}$ for unconfined concrete and $E=5000(f_c)^{0.5}$ for unconfined concrete. The calculation methods of all other parameters can be found in the literature (Mander & Priestley, 1988).

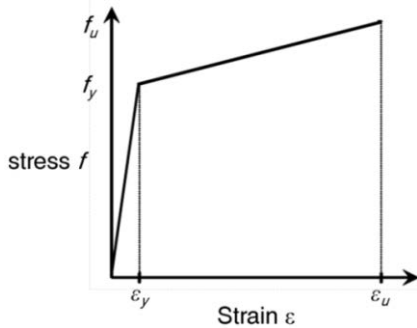


Fig. 130 Elastic-plastic stress-strain relationship curve of prestressing tendon

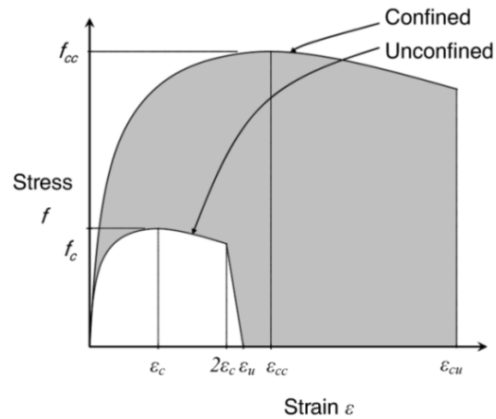


Fig. 131 Mander concrete stress-strain relationship curve

5.2.3 Modeling of soil-structure interaction

In order to carry out the research on the IAB, the detailed geotechnical investigation should be performed on site to obtain the real mechanical properties of the backfill behind abutments and the soil around piles. However, in many retrofitting projects, the detailed geotechnical investigation information is limited due to several reasons. In this case, the recommended values in some codes or literatures can be chosen to calculate the soil-structure interaction for the existing bridge before and after retrofitting, as listed in Table 34. Two typical kinds of soil were taken into account, including clay and sand. Each one has three classes, which are soft, medium and

stiff for clay; and loose, medium and dense for sand. For some properties with the values in a certain range, the intermediate values were chosen in this analysis.

Soil type	Clay			Sand			Reference
	Soft	Medium	Stiff	Loose	Medium	Dense	
Unit weight γ (N/m^3)	15710	17281	18852	17281	18852	20423	(Greimann et al., 1984a)
Soil-structure friction angle δ (Degree)				20	25	30	(American Petroleum Institute, 2000)
Dimensionless bearing capacity N_q				12	20	40	(American Petroleum Institute, 2000)
Internal friction angle Φ (Degree)	19~24	19~29	27~31	29~33	31~37	35~42	(Robertson & Powell, 1997)
Undrained shear strength S_u (N/m^2)	12000~ 25000	25000~ 50000	50000~ 100000				(Coduto, 2001)
Cohesion c (N/m^2)	11970~ 23940	23940~ 47880	47880~ 95760				(Barker et al., 1991)

Table 34

Recommended soil information from literatures

Besides the mechanical properties of soil, the height of the backfill behind abutments and the soil around piles in 'Viadotto Serrone' is another important factor, which is illustrated in Fig. 132. The backfill behind abutments is as high as the abutment tops with the horizontal ground surface and no soil is in front of the abutments. As introduced above, the abutment used in the existing bridge is the U-shaped abutment. Therefore, the backwall and stem in two abutments are subjected to lateral earth pressure at one side and all abutment wingwalls are subjected to lateral earth pressure at both sides. The full length of piles beneath the footings of abutments and piers are embedded in soil.

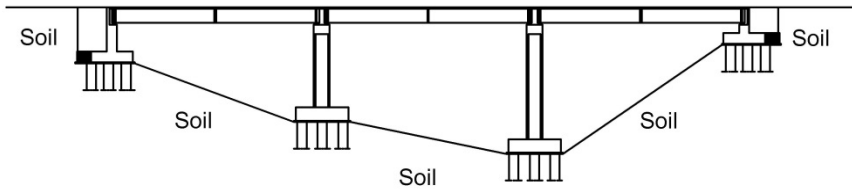
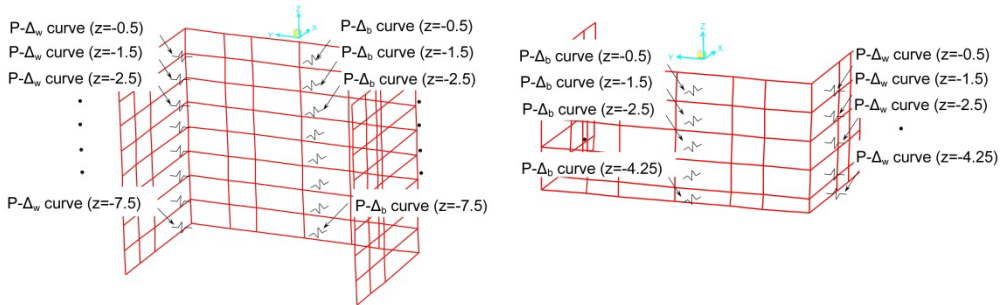


Fig. 132 Soil height in 'Viadotto Serrone'

5.2.3.1 Modeling of soil-abutment interaction

In this case, the backwalls, stems and wingwalls of two abutments were all modeled by four-node shell elements. Therefore, the soil-abutment interaction can be simulated by a series of discrete area springs with nonlinear lateral earth pressure-abutment movement relationship curves (P- Δ curve) corresponding to different depth from the abutment top, as shown in Fig. 133(a) and (b). In this paper, the Δ_b denotes the movement of abutment backwalls and stems, while, the Δ_w denotes the movement of abutment wingwalls.



(a) Abutment-A

(b) Abutment-B

Fig. 133 Arrangement of area springs

As introduced in Section 3.1.1, many approaches can be used to consider the soil-abutment interaction in finite element model. By summing up, it could be found that the approach proposed by Clough & Duncan (1991) and adopted in 'Manuals for the Design of Bridge Foundations' (NCHRP method) (Barker et al., 1991) has been widely accepted by many researchers to analyze the IAB. Therefore, it was chosen in this analysis with the assumption that the at-rest earth pressure coefficient (K_o) varying linearly to active pressure coefficient (K_a) or passive earth pressure coefficient (K_p). The typical lateral earth pressure coefficient-abutment movement relationship curves for clay and sand are shown in Fig. 134. It is noteworthy when there is no abutment movement, at-rest earth pressure (P_o) exists. This

phenomenon was simulated in the model by assigning a very large initial slope to the lateral earth pressure coefficient-abutment movement relationship curve, which allows earth pressure to reach the at-rest level immediately when the movement is very small ($\Delta=0.0001H$), where H is the abutment height (Dicleli & Albhaisi, 2003, 2004b). Based on the relationship in Fig. 134, the lateral earth pressure-abutment movement relationship curves corresponding to different depths from the abutment top can be calculated, as illustrated in Fig. 135, by the Bell's relation (formulae (11) and (12) (p.83)) that is suitable for both cohesive and cohesionless soil (Bell, 1915). These nonlinear properties were assigned to area springs. Besides the nonlinear relationship, the effective stiffness that can be used in linear load cases should be also assigned to the nonlinear area springs in Sap2000 (Computers and Structures Inc, 2011). The secant slope of the lateral earth pressure-abutment movement relationship curve between $\Delta=0$ and $\Delta=0.001H$, where H is the abutment height, was used to obtain the effective stiffness in this analysis (Dicleli & Erhan, 2008, 2009, 2010; Erhan & Dicleli, 2009a, b).

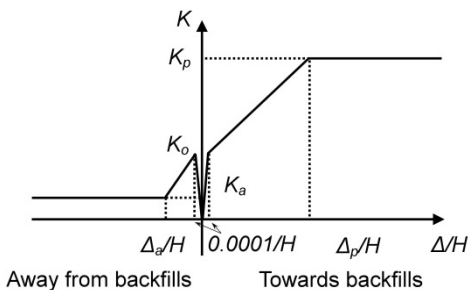


Fig. 134 Typical lateral earth pressure coefficient-abutment movement relationship

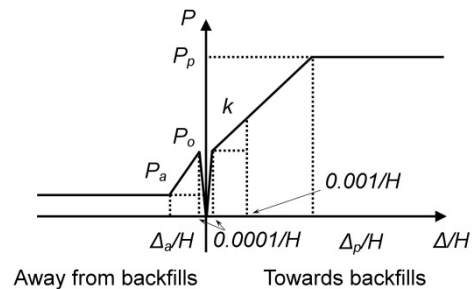


Fig. 135 Typical lateral earth pressure-abutment movement relationship

In order to introduce the soil-abutment interaction used in this model in detail, the P - Δ_b curves for medium sand and medium clay corresponding to the depth of 0.5m are chosen as examples, as illustrated respectively in Fig. 136(a) and (b). Both active and passive earth pressures are taken into account. These curves were calculated by using the recommended values listed in Table 34. For cohesionless soil (medium sand in Fig. 136(a)), at-rest earth pressure (P_o) changes linearly to active pressure (P_a) or passive earth pressure (P_p). However, for cohesive soil (medium clay in Fig. 136(b)), due to the influence of soil cohesion, the earth pressure will have a significant increment with the value of $2c(K)^{0.5}$, when the abutment starts moving towards backfill. Similarly, the earth pressure will have a significant decrement with the value of $2c(K)^{0.5}$, when the abutment starts moving away from backfill. From the formula (11) (p.83), it could be found that if the backfill

is cohesive, the soil down to a depth of $2c/(\gamma(K)^{0.5})$ is theoretically in a tension zone. In this analysis, the lateral earth pressure in the tension zone was set as zero. The effective stiffness of the $P-\Delta_b$ curves for both soil types are illustrated as the hollow square lines in Fig. 136.

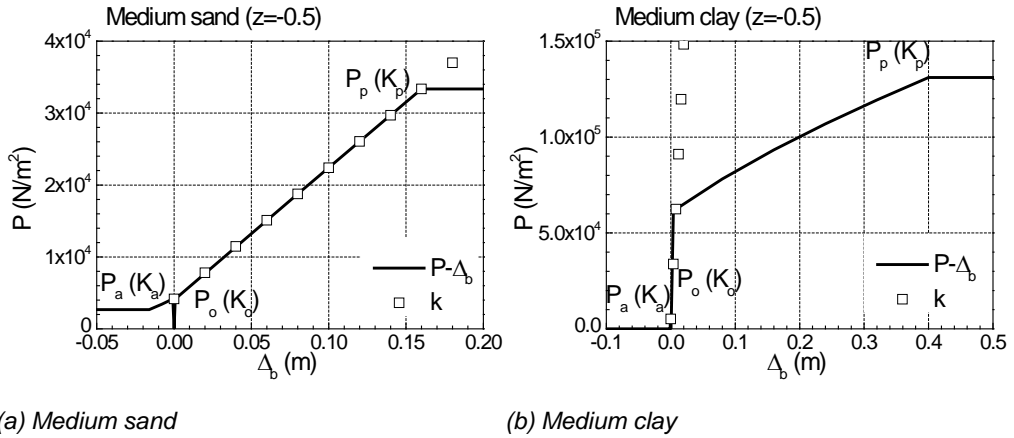


Fig. 136 $P-\Delta_b$ curves of area springs for abutment backwalls and stems

The $P-\Delta_w$ curves for medium sand or medium clay corresponding to the depth of 0.5m are chosen as examples, as illustrated respectively in Fig. 137(a) and (b). In this case, wingwalls are subjected to lateral earth pressure at both sides. Therefore, the combined $P-\Delta_w$ curves (the solid line in Fig. 137) assigned to nonlinear area springs, were obtained by superposing of two original $P-\Delta_w$ curves in both sides (the dashed line in Fig. 137). The effective stiffness of the combined $P-\Delta_w$ curves for both soil types are illustrated as the hollow square lines in Fig. 137.

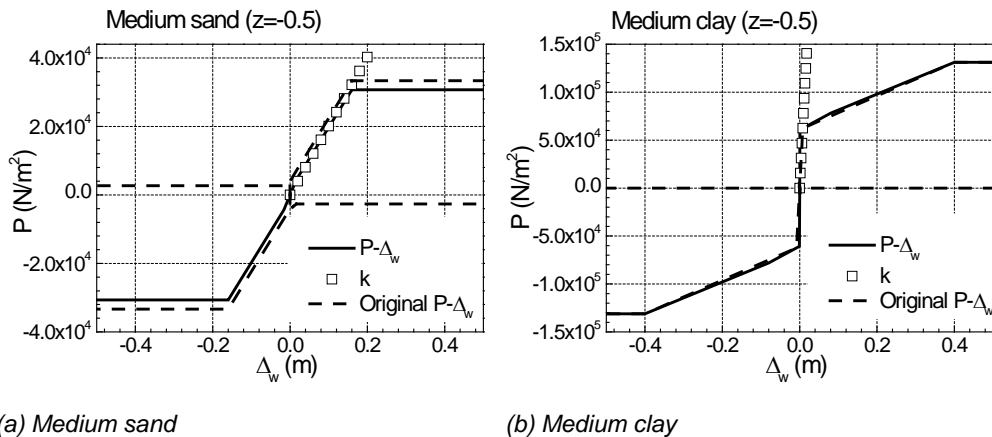
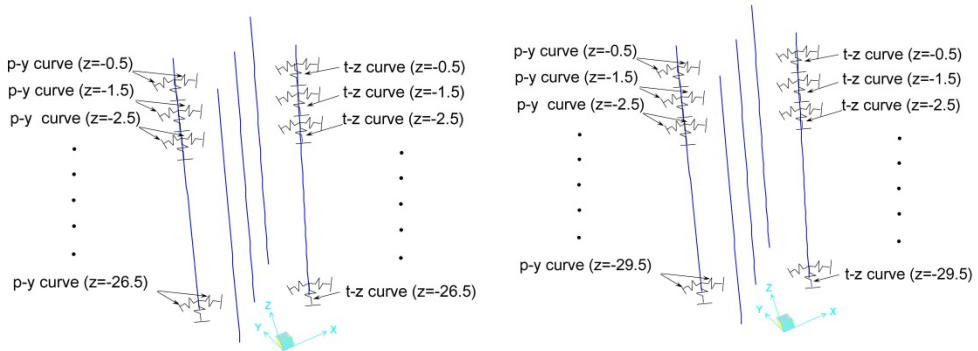


Fig. 137 $P-\Delta_w$ curves of area springs for abutment wingwalls

5.2.3.2 Modeling of soil-pile interaction

In this case, the piles beneath the footings of abutments and piers were modeled by the two-node three-dimensional frame element. Therefore, in order to simulate the soil-pile interaction, three series of line springs with nonlinear properties were attached along the pile length, as illustrated in Fig. 138(a) and (b). For spring properties, two series of horizontal line springs in orthogonal directions chose the lateral earth pressure-pile displacement relationship curve, and one series of vertical line springs used the vertical skin friction-pile settlement relationship curve.



(a) Piles beneath pier footings

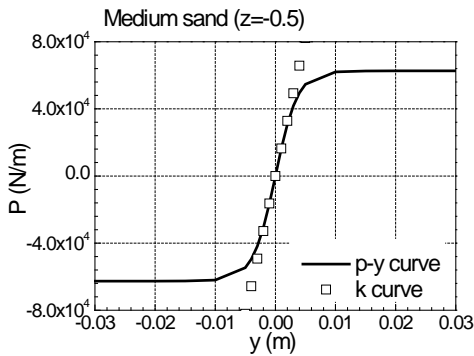
(b) Piles beneath abutment footings

Fig. 138 Arrangement of line springs for piles

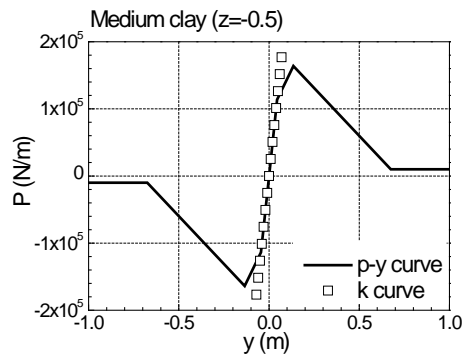
As introduced in Section 3.1.2, many methods can be used to consider the soil-pile interaction in finite element model. Among them, the method proposed in American Petroleum Institute (API method) (American Petroleum Institute, 2000) could be considered as the most commonly used method for IAB analysis. Therefore, it was adopted in this analysis, including the lateral earth pressure-pile displacement relationship curve (p-y curve) and the vertical skin friction-pile settlement relationship curve (t-z curve).

In order to explain the soil-pile interaction in detail, the p-y curve and t-z curve for medium sand or medium clay corresponding to the depth of 0.5m are chosen as examples, which are illustrated respectively as the solid lines in Fig. 139 and Fig. 140. These curves were calculated by using the recommended values listed in Table 34. Similar to the area springs, the effective stiffness, which will be used in linear load cases, must be assigned to the nonlinear line springs in Sap2000 (Computers and Structures Inc, 2011), which is illustrated as the hollow square lines in Fig. 139 and Fig. 140. Using the approach proposed by Haliburton (1971), the initial modulus

between $y=0$ and $y=0.001$ was defined as the effective stiffness of the p-y curve for sand, while, the secant modulus connecting $P=0$ and $P=0.5P_u$ was chosen as the effective stiffness of the p-y curve for clay. The same approach could be used to obtain the effective stiffness of the t-z curves for both sand and clay.

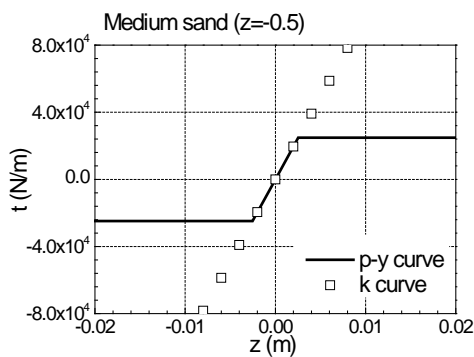


(a) Medium sand

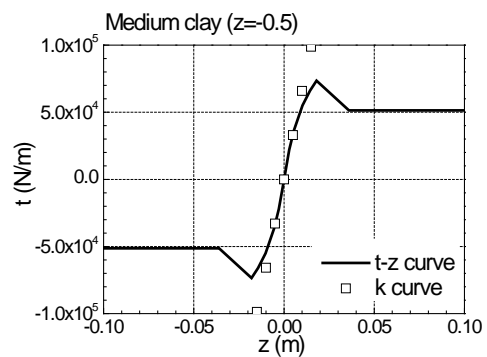


(b) Medium clay

Fig. 139 p-y curves of line springs for piles



(a) Medium sand



(b) Medium clay

Fig. 140 t-z curves of line springs for piles

If the design of existing bridges is reasonable, the foundation systems of existing bridges should have sufficient bearing capacity to avoid the bridge settlement subjected to vertical load cases, including the dead load, the superimposed dead load, the highway live load, and so on. Consequently, the moveable simple roller supports were arranged at pile bottoms

5.2.4 Modeling of plastic hinge

In this model, many bridge components, such as girders, piers and piles, were simulated by the frame element. Therefore, in order to evaluate accurately the

nonlinear material responses of the bridge before and after retrofiting, plastic hinges should be applied to the critical sections in the bridge. Some tentative plastic hinge properties have been provided in references; however, it could retrieve generally conservative values that lead to underestimating real section ductility. In this case, the plastic hinge properties should be obtained by using a better approach that is composed of the moment-curvature curve and the plastic hinge length, which are computed for each member accounting for specific geometry and rebar (Mazzarolo, 2012). Several different types of plastic hinges can be used through finite element program Sap2000 (Computers and Structures Inc, 2011), including axial P, shear V2, shear V3, torsion T, moment M2 and moment M3 and interacting P-M2-M3 plastic hinges, in which the number indicates the local coordinate axes of the element.

In program Sap2000, the plastic hinge property can be defined through the moment-curvature relationship or the moment-rotation relationship (Computers and Structures Inc, 2011). In this model, the plastic hinge properties were simulated by the idealized bilinear elastic-perfectly plastic moment-curvature relationship curve. However, the relationship curves should be modified into a specific format for Sap2000, because the elastic behavior of the frame element occurs over member length, and then deformation beyond the elastic limit occurs entirely within plastic hinges, which are modeled in discrete locations (Computers and Structures Inc, 2011). Consequently, only the inelastic part of the curves should be considered when defining the plastic hinge properties in Sap2000, as illustrated in Fig. 141. The inelastic part of the curves can be achieved by modifying the complete curves. Firstly, the elastic part should be removed. Then, the plastic moment (M_p) keeps constant when the curvature value changes from the yield point to the ultimate one. Finally, the residual strength, which can define the failure branch in this relationship, is taken as 20% of the plastic moment, and the deformation limit can be set as 1.5 times of the ultimate curvature, as suggested in some codes (American Society of Civil Engineers, 2007; Applied Technology Council, 1996; Federal Emergency Management Agency, 1997a, b, 2000, 2005).

For acceptance criteria, three limit states proposed in Eurocode8 Part3 (Eurocode CEN, 2005b) were chosen in this analysis, which are Damage Limitation (DL), Significant Damage (SD), and Near Collapse (NC), respectively. The curvature value corresponding to the limit states of Damage Limitation (DL), Significant Damage (SD) and Near Collapse (NC) could be set as the yield point, 3/4 of the ultimate point and the ultimate point, respectively. As mentioned above, only the inelastic part of the moment-curvature relationship should be considered when defining the plastic hinge properties in Sap2000. Therefore, the curvature value corresponding to the limit

states of Damage Limitation (DL), Significant Damage (SD), and Near Collapse (NC) were set respectively as 0, $(0.75\Phi_u - \Phi_y)$ and $(\Phi_u - \Phi_y)$, as illustrated in Fig. 141.

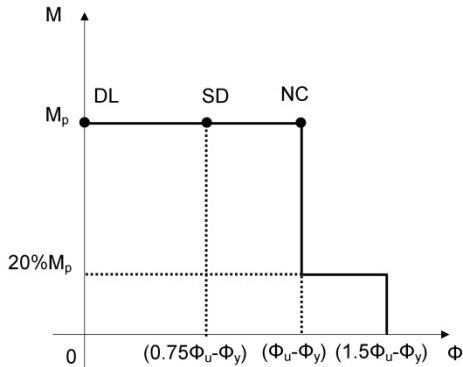


Fig. 141 Typical plastic hinge's moment-curvature curve in Sap2000

5.2.3.1 Pier plastic hinge

In this model, the interacting P-M2-M3 plastic hinge defined through the moment-curvature relationship curve, the interaction surface and the plastic hinge length were assigned to the top and bottom of piers. For the P-M2-M3 plastic hinge, the moment-rotation curve can be used to describe the post-yield behavior of a beam-column element subjected to combined axial and biaxial-bending conditions, and the 3D interaction surface can indicate the envelope of yield points. The plastic rotational capacity of the plastic hinge is directly proportional to the column curvature capacity through the plastic hinge length. Moreover, the moment-curvature curve of the pier depends on the axial load. The detailed information of the interacting P-M2-M3 plastic hinges in piers will be introduced in the following.

In order to obtain the moment-curvature relationship curve of the pier, the detailed geometric information of the cross section and the corresponding rebar information should be determined firstly. In this bridge, the geometric information of the cross section and the rebar arrangements of two piers are the same, as illustrated in Fig. 142. Two programs Sap2000 and XTRACT (Computers and Structures Inc, 2011; TRC/Imbsen Software Systems, 2007), were chosen to build models (Fig. 143). Setting the axial force as zero, two actual moment-curvature relationship curves can be obtained (solid lines in Fig. 144). It could be found that the curves obtained through both programs are generally in good agreement. Therefore, in the following analysis, the program Sap2000 can be chosen to calculate the actual moment-curvature relationship curves. According to the stipulations in Caltrans code (Caltrans, 2010), the actual moment-curvature relationship curves can be

transformed into the idealized bilinear elastic-perfectly plastic curve (dashed line in Fig. 144). The curvature capacity at the failure limit state (ϕ_u) can be defined as the concrete strain reaching unconfined crush strain or the longitudinal rebar reaching the ultimate strain.

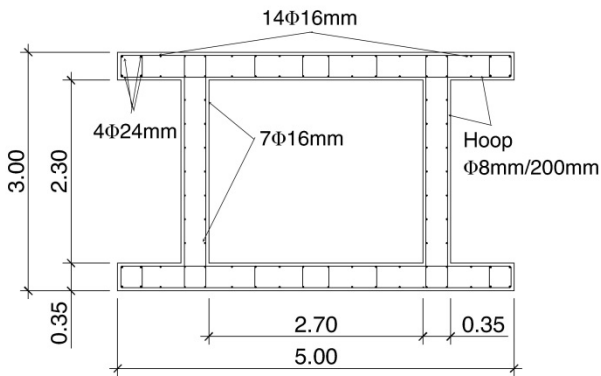
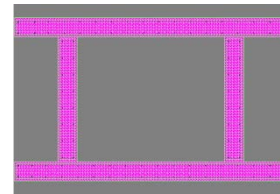
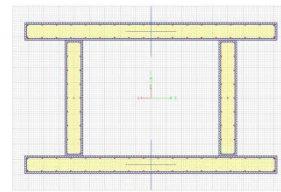


Fig. 142 Cross section and rebar information of pier



(a) XTRACT



(b) Sap2000

Fig. 143 Cross section analysis models of pier

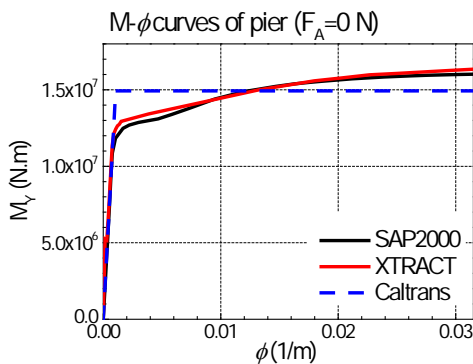
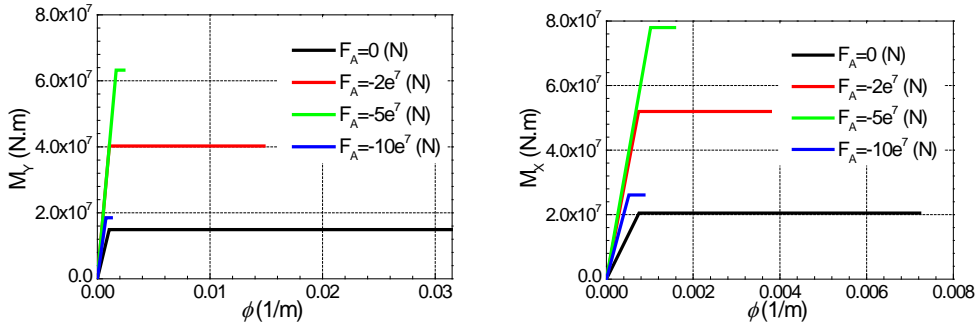


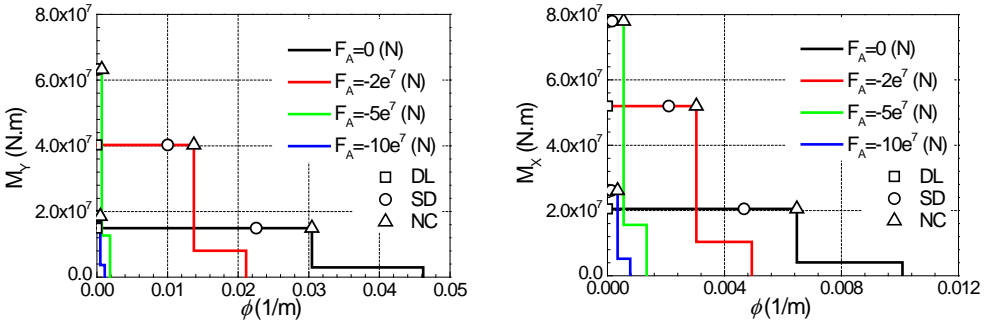
Fig. 144 Actual and idealized moment-curvature relationship curves of pier

The curvature capacity of the P-M2-M3 plastic hinge will change according to different axial load levels. In order to simulate accurately the P-M2-M3 plastic hinge properties, a series of moment-curvature relationship curves at different axial load levels should be calculated. The idealized moment-curvature relationship curves of the pier at different axial load levels and the corresponding moment-curvature relationship curves used in Sap2000 with the symbols of acceptance criteria are illustrated in Fig. 145(a) and (b).

RETROFIT OF EXISTING BRIDGES WITH CONCEPT OF INTEGRAL ABUTMENT BRIDGE



(a) Idealized moment-curvature relationship curves



(b) Moment-curvature curves relationships and acceptance criteria used in Sap2000

Fig. 145 Moment-curvature curves of pier at different axial load levels

The P-M2-M3 interaction surface is another key factor for the definition of the pier plastic hinge, which can be obtained by program Sap2000, as illustrated in Fig. 146. The P, M2 and M3 in the local coordinate axes corresponds to the F_A , M_y and M_x of pier in the global coordinate axes.

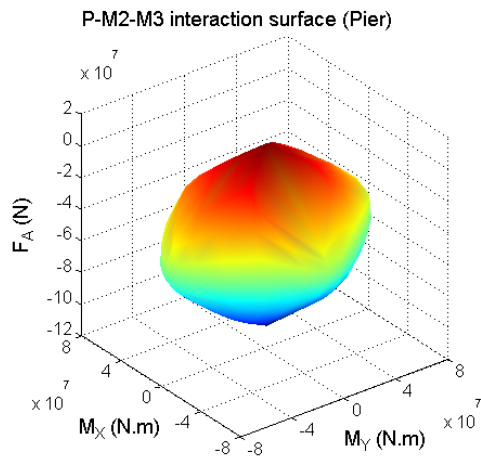


Fig. 146 P-M2-M3 interaction surface of pier

In this case, the plastic hinge length of pier can be calculated by equation (111) (p.147) proposed in Eurocode8 Part2 (Eurocode CEN, 2005a). The calculation procedure of the pier plastic hinge length is described in the following (Washington State Department of Transportation, 2012). The detailed information of the plastic hinge lengths of two piers in this model are listed in Table 35.

1. Obtain the axial forces at the top and bottom of the pier (P_{top} and P_{bottom}) subjected to the combination of dead load and superimposed dead load.
2. Run the section analysis to get the corresponding idealized moment-curvature relationship curves of pier corresponding to the axial load obtained in the first step. Determine the plastic moments (M_{p-top} and $M_{p-bottom}$) in these idealized moment-curvature relationship curves.
3. Calculate the length from the top or bottom points to the inflection point (L_{top} and L_{bottom}) through the pier length (L), M_{p-top} and $M_{p-bottom}$.
4. Calculate the plastic hinge length at the top and bottom of the pier (L_{p-top} and $L_{p-bottom}$) by equation (111) (p.147).
5. Convert the absolute plastic hinge length into the relative one along the frame elements, which can be used in Sap2000.

Mechanical properties	Pier-A	Pier-B
P_{top} (N)	-7×10^6	-7×10^6
M_{p-top} (N.m)	24×10^6	24×10^6
P_{bottom} (N)	-8.7×10^6	-9.5×10^6
$M_{p-bottom}$ (N.m)	26×10^6	27×10^6
L (m)	13.7	19.7
L_{top} (m)	6.56	9.26
L_{bottom} (m)	7.14	10.44
L_{p-top} (m)	0.76	1.03
$L_{p-bottom}$ (m)	0.82	1.15

Table 35

Detailed information of plastic hinge lengths of two piers

5.2.3.2 Pile plastic hinge

It is noteworthy that a capacity design approach can be used to prevent the damage to piles in a new bridge. However, this case is the retrofitting project based on existing bridges. Therefore, the pile plastic hinge should be considered in this case, in order to check if the existing cross section of piles could satisfy the requirement of bridge after retrofitting. The concentrated plasticity approach was adopted to derive analytical models to determine the ductility of piles in several selected limit states

(Chai, 2002; Song et al., 2005). However, the concentrated hinge model cannot be applied when the location of the maximum moment in a pile varies with the development of soil plasticity around the pile. Instead, the distributed hinge model is more appropriate as it uses plastic hinges within a possible zone of plasticity in the pile to trace the development of the plastic zone. Accordingly, with lateral loads increase the plasticity can spread, rather than being concentrated at a single point (Chiou et al., 2008; Chiou et al., 2009). In this case, the distributed plasticity approach was chosen to simulate the plastic hinge of the pile. According to the definition in Sap2000, the distributed plasticity approach can be modeled by a series of plastic hinges in order to capture plasticity distributed along member length. For example, ten plastic hinges could be inserted at relative locations within the element of 0.05, 0.15, 0.25,..., 0.95, each with deformation properties based on an assumed hinge length of one-tenth the element length (Computers and Structures Inc, 2011).

The cross section geometric information and the rebar information of piles beneath the footings of piers and abutments are the same, as illustrated in Fig. 147. Two programs Sap2000 and XTRACT (Computers and Structures Inc, 2011; TRC/Imbsen Software Systems, 2007), were chosen to build models (Fig. 148). Considering the axial force as zero, the actual moment-curvature curves (solid line) and the idealized bilinear elastic-perfectly plastic curve (dashed line) obtained by using Caltrans code (Caltrans, 2010) are compared in Fig. 149. Using the Mander confined concrete stress-strain curve introduced in Section 5.2.2, it could be found that the influence of the confinement produced by circular hoop rebar on the core concrete is significant. Therefore, the curvature capacity at the failure limit state (Φ_u) can be defined as the concrete strain reaching confined crush strain or the longitudinal rebar reaching the ultimate strain.

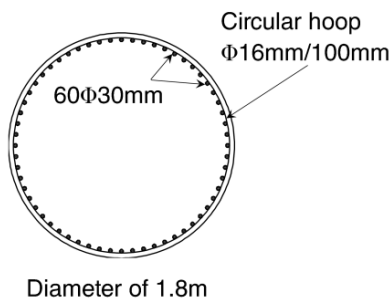


Fig. 147 Cross section and rebar information of pile

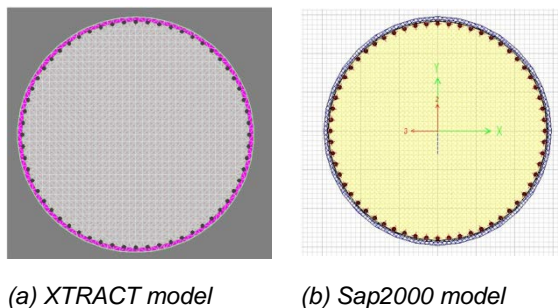


Fig. 148 Cross section analysis models of pile

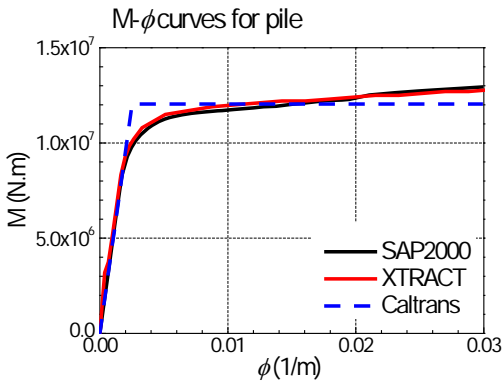
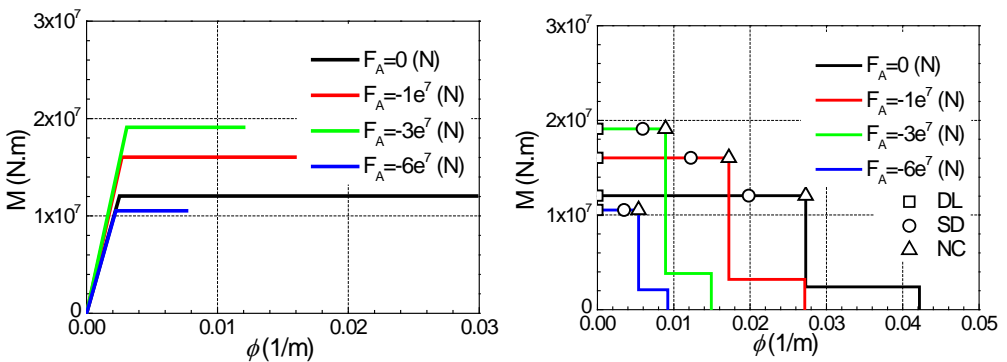


Fig. 149 Actual and idealized moment-curvature relationship curves of pile

As mentioned above, the curvature capacity of P-M2-M3 plastic hinge will change according to different axial load levels. A series of idealized moment-curvature relationship curves of the pile at different axial load levels and the corresponding moment-curvature relationship curves used in Sap2000 with the symbols of acceptance criteria are illustrated in Fig. 150(a) and (b).



(a) Idealized moment-curvature relationship curves (b) Moment-curvature relationship curves and acceptance criteria used in Sap2000

Fig. 150 Moment-curvature curves relationship of pile at different axial load levels

The P-M2-M3 interaction surface is another key factor for the definition of pile plastic hinge, which can be obtained by program Sap2000, as illustrated in Fig. 151. In this case, the P, M2 and M3 in the local coordinate axes corresponds to the F_A , M_Y and M_X of pile in the global coordinate axes.

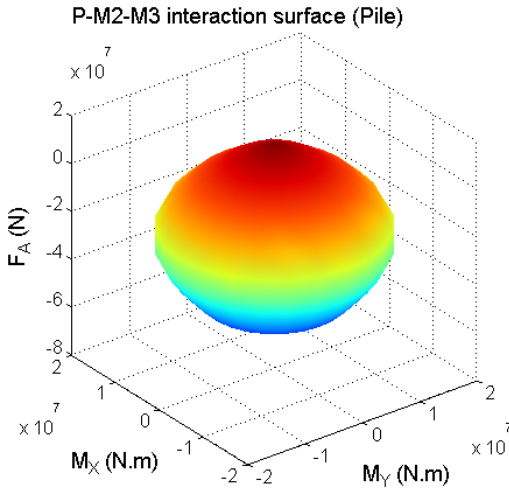


Fig. 151 P-M2-M3 interaction surface of pile

It is well known that, the proper arrangement of distributed plastic hinges for a pile is important to identify the location of the plastic zone developed in the pile. Although the density of distributed hinges should be as dense as possible, a reasonable interval is necessary for the sake of computational cost. The distributed plastic hinges along the pile can be arranged according to the guideline proposed by Chiou et al. (2009), which includes two steps, including estimating the possible range of the plastic zone developed in a pile, and choosing a reasonable distribution of plastic hinges so that the development of the plastic zone can be properly traced. In order to decide the range of plastic zone for a pile-soil system, two possible locations that a plastic zone may develop should be taken into account in this case. The plastic zone of a pile may occur at a certain depth below the ground surface or at the pile head under a restrained-head condition (fixed-head condition) (Chiou et al., 2008). When the possible range of plastic zone (L_p) is determined, the plastic hinge length of distributed hinges (l_p) can be chosen to be a fraction of this range ($L_p/10$) to grasp the gradual spreading of the plastic zone (Chiou et al., 2008; Chiou et al., 2009).

The plastic zone length of pile, which occurs at a certain depth below the ground surface, can be estimated according to the beam theory. It is assumed the moment distribution of the pile is continuous and differentiable along the pile, and the location of maximum moment is the location without shear force. The free body in the plastic zone with the lateral earth pressure (p) and the end moments at the upper and lower edges of the free body are the yield moment (M_y) and the ultimate moment (M_u), respectively, as illustrated in Fig. 152(a). The yield moment (M_y) and the ultimate moment (M_u) can be obtained through cross section analysis. The plastic zone

length (L_p) can be estimated by the equilibrium of moments about the top point by formula (133). From formula (133), it could be found that L_p can get the minimum value when the lateral earth pressure (p) is set to be the ultimate values of p-y curves corresponding to different depths (p_{ult}). Therefore, the formula (133) can be modified to equation (134), which divides the uniform lateral earth pressure into several layers with different lateral earth pressure, as illustrated in Fig. 152(b). Consequently, the plastic zone length (L_p) can be calculated by formula (135). The plastic zone length (L_p) of pile that occurs at a certain depth below the ground surface used in this case could be obtained, which are 8m and 15m for sand and clay, respectively. Moreover, the corresponding plastic hinge length of distributed hinges (l_p) could be chosen as 0.5m and 1m for sand and clay.

$$L_p \geq \sqrt{2(M_u - M_y) / p} \quad (133)$$

$$M_u - M_y - \sum_{i=1}^n p_i L_i (L_i / 2 + \sum_{i=1}^n L_{i-1}) = 0 \quad (134)$$

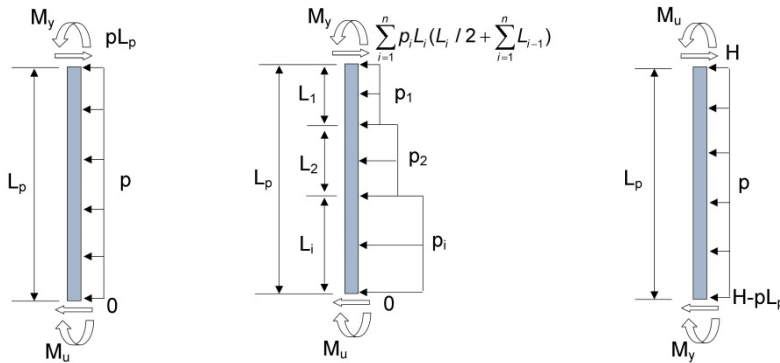
$$L_p = \sum_{i=1}^n L_i \quad (135)$$

The plastic zone length of pile, which occurs at the pile head under a restrained-head condition, can be calculated by the equilibrium of moments about the bottom point by formulae (136) and (137). For a fixed-head pile subjected to a uniform lateral earth pressure (p), as illustrated in Fig. 153, the ultimate moment (M_u) and shear force (H) occur at the pile head, the lower end of the plastic zone is subjected to the yield moment (M_y) and shear force ($H - pL_p$). Through the similar approach, the formulae for uniform lateral earth pressure can be modified into the equations suitable for variable lateral earth pressure. The plastic zone length (L_p) of pile that occurs at the pile head under a restrained-head condition used in this model could be obtained, which are 2m and 3m for sand and clay, respectively. The corresponding plastic hinge length of distributed hinges (l_p) could be chosen as 0.2m and 0.25m for sand and clay.

$$M_u - M_y - HL_p + pL_p^2 / 2 = 0 \quad (136)$$

$$H = 2M_u \sqrt[4]{E_s / (4EI)} \quad (137)$$

where, E_s is the subgrade reaction modulus and EI is the flexural rigidity of pile.



(a) Uniform lateral earth pressure (b) Variable lateral earth pressures

Fig. 152 Plastic zone of pile occurs at a certain depth below the ground surface

Fig. 153 Plastic zone of a pile occurs at the pile head under a restrained-head condition

5.2.5 Modeling of retrofitting process

As introduced above, the finite element model has been used by many researchers to design and analyze the IAB; however, most of them only consider the effect of the loads at the final stage assuming a completed structure (Dicleli, 2000a, b). It is obvious that the retrofit of an existing SSB with the IAB concept is carried out in stages. Therefore, each stage must be analyzed to ensure that the structure has adequate capacity to sustain the applied loads particular to the stage under consideration. Two stages could be considered in this analysis. The typical loads applied at each stage are listed in Table 36. In the first stage, the existing bridge does not have any changes. Therefore, the SSB is subjected to dead load, prestressed load and superimposed dead load. In the second stage, the highway live load, the thermal load and the seismic load could be applied to the SSB without retrofitting or the IAB after retrofitting.

Stage number	Stage name	Loads applied in the stage
1	SSB before retrofitting	Dead load
		Prestressed load
		Superimposed dead load
2	SSB without retrofitting or IAB after retrofitting	Highway live load
		Thermal load
		Seismic load

Table 36
Summary of stage loading

As introduced above, the biggest difference between the SSB and the IAB is the connection method between the superstructure and the substructure. Therefore, the retrofitting with the IAB concept is mainly concerned about the transformation process of these elements from simply supported bearings to hinged or rigid connections. In order to simulate the retrofitting process, the construction stage approach implemented in Sap2000 (Computers and Structures Inc, 2011) was chosen. The details of the retrofitting procedure simulation can be found in the flow chart (Fig. 154).

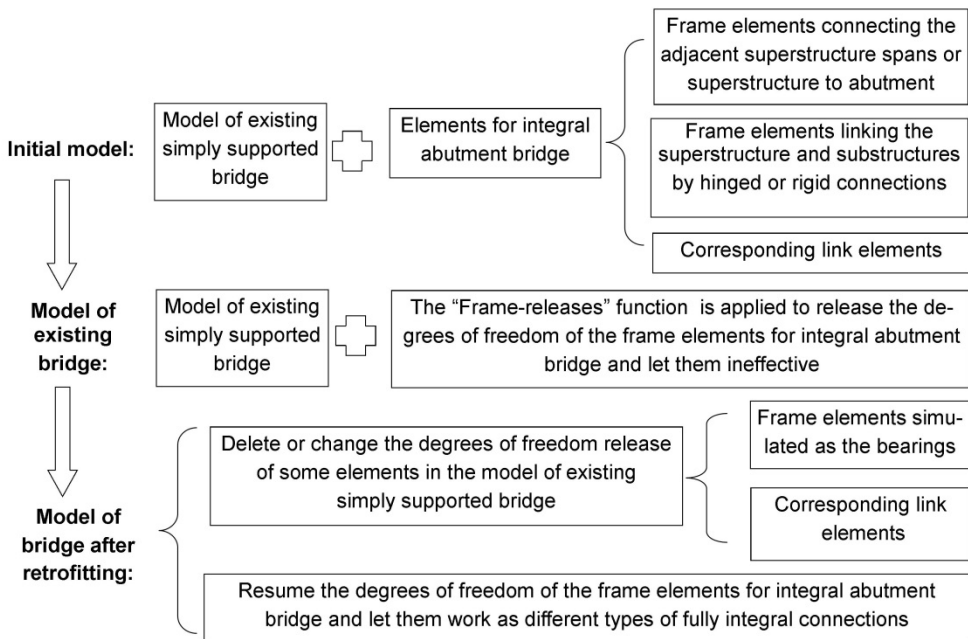
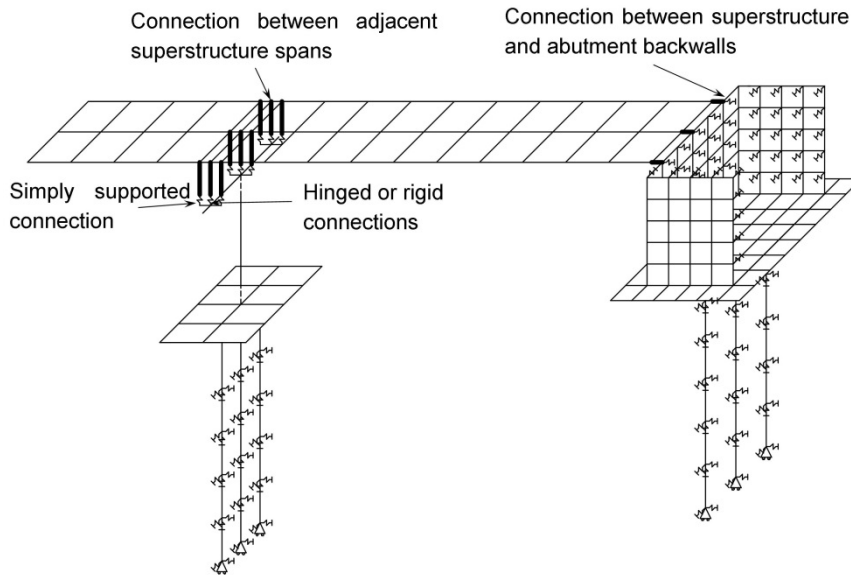


Fig. 154 Flow chart of retrofitting process

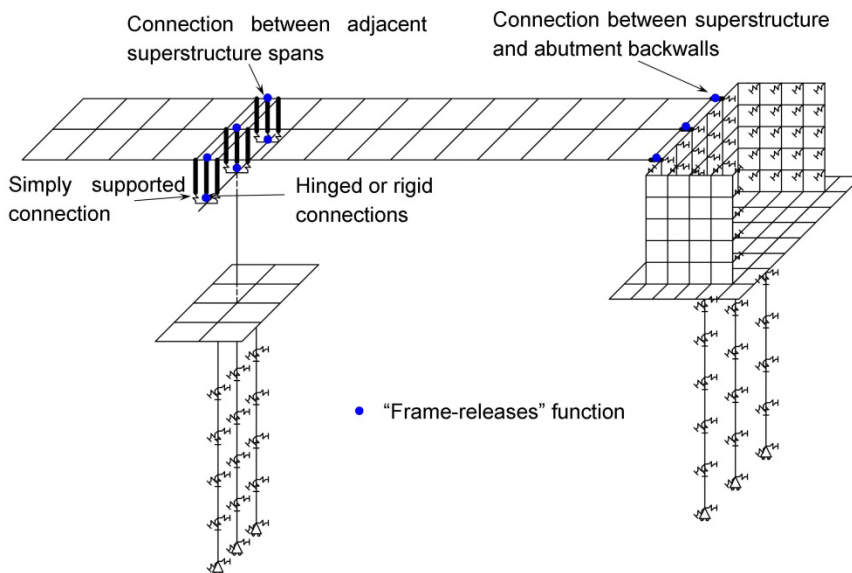
In the first stage, the initial model is built. It includes not only all the components in the existing SSB, but also the elements in the IAB after retrofitting, such as the frame elements which will be used to simulate the diaphragm and the hinged or rigid connection (Fig. 155(a)). Based on the initial model, the model of existing SSB can be obtained by applying the Frame-releases function to release specified degrees of freedom of the frame elements, which are built in the first step for the IAB. Then, it could be found that the frame elements for the IAB are still in the model; however, they are ineffective. With this model, the influence of the loads belonging to stage one (Table 36) on existing SSB can be analyzed (Fig. 155(b)). In order to transform the model from existing SSB to the IAB after retrofitting, two steps should be considered. In the first step, some of the frame elements modeled as the simply

RETROFIT OF EXISTING BRIDGES WITH CONCEPT OF INTEGRAL ABUTMENT BRIDGE

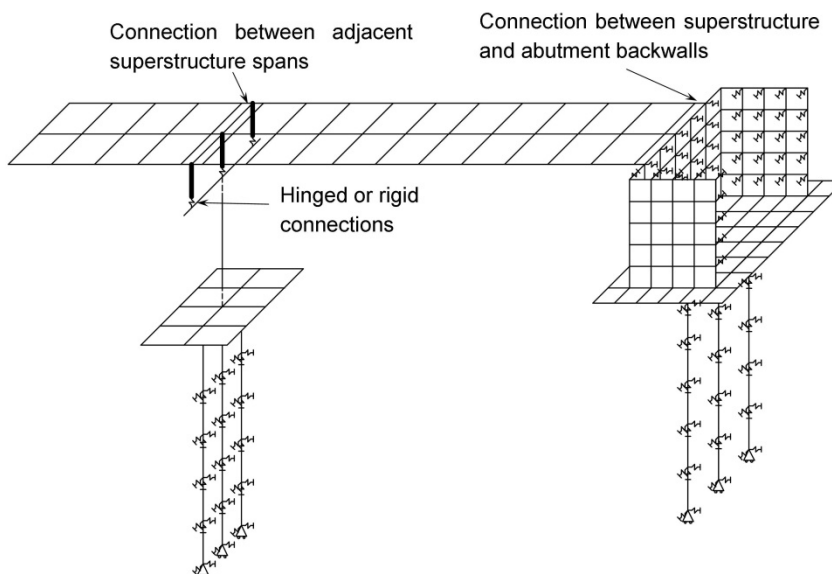
supported bearings should be deleted. Others can use the function of Change releases in the construction stage approach implemented in Sap2000 (Computers and Structures Inc, 2011) to change from the simply supported connection to hinged or rigid connections. In the second step, the frame elements for the IAB, which have been made ineffective in last stage, should be resumed. Finally, the model of the IAB after retrofitting can be obtained (Fig. 155(c)).



(a) Initial model



(b) Model of existing SSB



(c) Model of IAB after rehabilitation
 Fig. 155 Modeling of retrofitting process

5.3 Load case

The existing bridge ‘Viadotto Serrone’ was designed and constructed in 1972 by using the original codes listed in Table 37. However, the retrofitting procedure may be conducted in next few years through the updated code listed in Table 37.

Original codes:
1. “Aggiornamento delle norme tecniche per la progettazione, la esecuzione e il collaudo dei ponti stradali” published at: 4 May 1990 is chosen for permanent load, traffic load and loads combinations (DM 1990) (Ministero dei lavori pubblici, 1990).
2. “Norme tecniche relative ai criteri generali per la verifica di sicurezza delle costruzioni e dei carichi e sovraccarichi” published at: 16 January 1996 is chosen for thermal load (DM 1996) (Ministero dei lavori pubblici, 1996).
3. “Norme tecniche per le costruzioni in zone sismiche” published at: 16 January 1996 is chosen for earthquake load (DM 1996) (Ministero dei lavori pubblici di concerto & Ministro dell'interno, 1996).
Updated code:
“Nuove norme tecniche per le costruzioni” published at: 14 January 2008 is chosen for permanent load, traffic load, temperature load, earthquake load and loads combinations (NTC 2008) (Ministero delle Infrastrutture, 2008).

Table 37

Original and updated Italian codes

5.3.1 Permanent load

The definitions of permanent load in DM 1990 and NTC 2008 are the same, as listed in Table 38. The arrangement of the superimposed dead load including the weight of asphalt ($0.15 \times 20 \times 10^3 \text{ N/m}^2$), footpaths ($0.18 \times 25 \times 10^3 \text{ N/m}^2$) and barriers (750 N/m), is illustrated in Fig. 156.

Self-weight of structures g_1	Superimposed dead load (pavement, footpaths, barriers and so on) g_2	Other permanent load (soil forces, hydraulic loads and so on) g_3
---------------------------------	--	---

Table 38
Permanent load

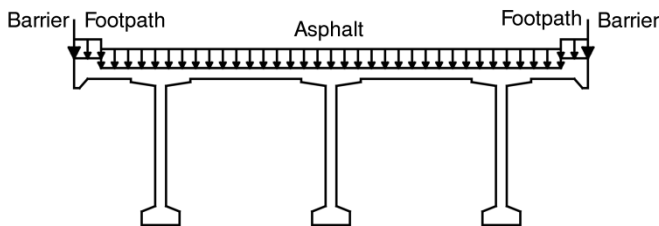


Fig. 156 Arrangement of superimposed dead load

5.3.2 Deformation

The deformations are composed of shrinkage, creep, prestressed loads, and thermal loads in both DM 1990 and NTC 2008.

The time-dependent effects, such as shrinkage and creep, are generally relevant in the first 3 years after the construction of the bridge which could last for approximately 30 years and thereafter dissipate (Pugasap et al., 2009). Consequently, the time-dependent effects can be neglected in this analysis, because the existing bridge has already used more than 40 years.

The prestressed load can be obtained through initial prestress minus relaxation loss. The relaxation loss can be calculated by equation (138) (Ministero delle Infrastrutture, 2008). In this analysis, the relaxation loss is 25%. Therefore, the prestressed stress applied to the transverse and longitudinal tendons in this model can be set as 904 MPa.

For Class 1: wire or strand-ordinary relaxation

$$\Delta\sigma_{pr} / \sigma_{pi} = 5.39\rho_{1000} e^{6.7\mu} (t / 1000)^{0.75(1-\mu)} 10^{-5} \quad (138)$$

where, the initial prestress (σ_{pi}) is 123kg/mm² (1206MPa) obtained from the investigation report of the existing bridge. ρ_{1000} is the relaxation loss at 1000 hours after tensioning and at a mean temperature of 20°C, which can be chosen as 8(%), according to Class 1 tendon. $\mu = \sigma_{pi} / f_y$, f_y is the characteristic value of the tensile strength of the prestressing steel. t is the time after tensioning (in hours), which is 350400 in this case, because the existing bridge has been in service for 40 years (1972~2012).

For the thermal load, the uniform bridge temperature components are considered in both codes with the value of $\pm 15^\circ\text{C}$ for the concrete bridge.

5.3.3 Highway live load

For the highway live load, the traffic load and crowd load are taken into account, which are different in DM 1990 and NTC 2008.

In DM 1990, the importance of this bridge belongs to Category 1. The traffic load line with the width of 3.5m is composed of the concentrated load (q_{1a}) and the distributed line load (q_{1b}). In the load line No.1, q_{1a} with the total value of 60t and the loading area length of 15m is divided by three axes with the space of 1.5m and, and q_{1b} with the value of 3t/m is applied to the middle line of the traffic load line except the area of q_{1a} . The scheme is illustrated in Fig. 157. For the traffic load line No.2, the dimension and arrangement of loads are the same as load line No.1, but the values are equal to 50% of q_{1a} and q_{1b} , respectively. For the other traffic load line, the load values can be set as 35% of q_{1a} and q_{1b} , respectively. There is no distributed load applied on remaining area. The q_{1e} with the value of 0.4t/m is chosen as the crowd load, which is applied to the middle line of two footpaths.

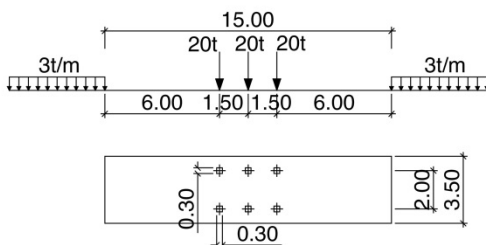


Fig. 157 Scheme of q_{1a} and q_{1b} in DM 1990

The cross section width of the carriageway in this case is 8.5m. Therefore, two traffic load lines could be arranged with the total width of $3.5 \times 2 = 7\text{m}$, and the width of remaining area is 1.5m. The crowd load (q_{1e}) can be applied to both footpaths. The superstructure cross section in 'Viadotto Serrone' is symmetrical around the global coordinate axis Z. Therefore, the typical asymmetrical arrangement of traffic load lines and crowd load lines in the transverse direction is illustrated in Fig. 158, which can be used to consider the most unfavorable loading state for Girder-L. The Girder-M and Girder-R can be designed as the same as Girder-L. In the longitudinal direction, the concentrate loads (q_{1a}) can move along the whole length of bridge and the distributed line load (q_{1b}) can be arranged along the whole length of bridge except the area of q_{1a} . The arrangement of traffic loads in the longitudinal direction is illustrated in Fig. 159.

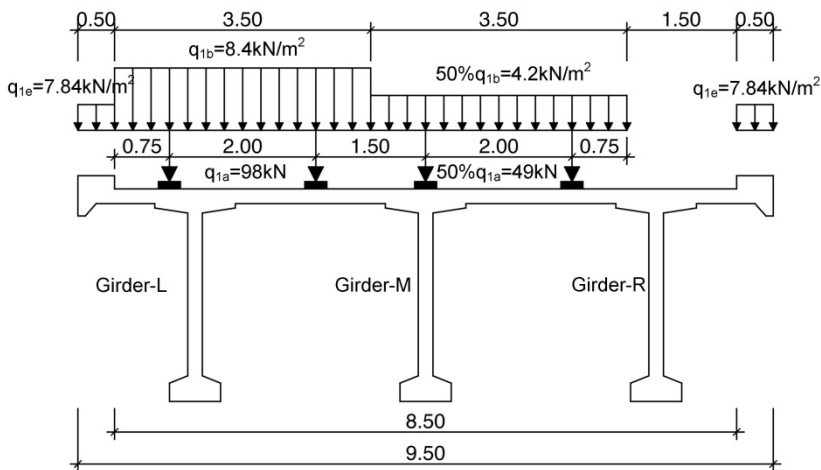


Fig. 158 Arrangement of highway live load in DM 1990 in transverse direction

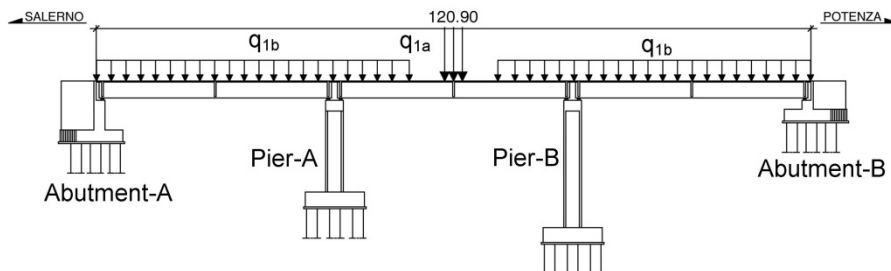


Fig. 159 Arrangement of highway live load in DM 1990 in longitudinal direction

In NTC 2008, the traffic load group 1 which includes the most characteristic load model 1 (Schema di carico 1) (Fig. 160) and the crowd load with the uniformly

distributed load 2.5kN/m^2 were chosen to simulate the highway live load in this analysis. The width of load line is 3m . Each load line is composed of a concentrated load (Q_{ik}) and a distributed pressure (q_{ik}). The values of Q_{ik} and q_{ik} are 300kN and 9kN/m^2 , 200kN and 2.5kN/m^2 , and 100kN and 2.5kN/m^2 for the load line No.1, No.2 and No.3, respectively. The remaining area only has the distributed pressure of 2.5kN/m^2 .

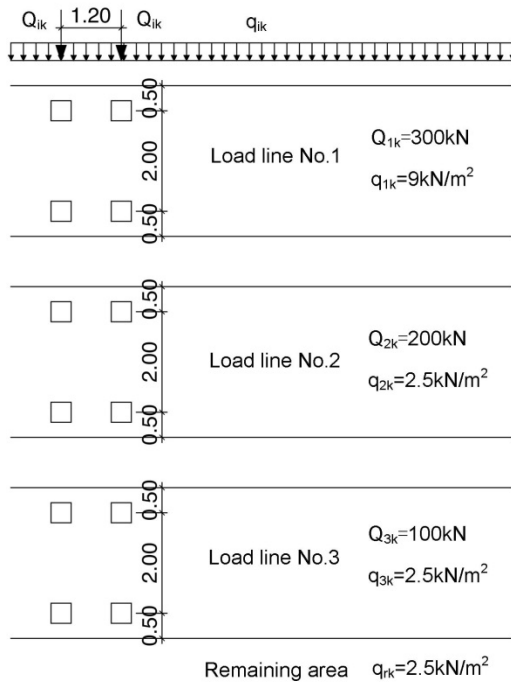


Fig. 160 Scheme of load model 1 in NTC 2008

According to NTC 2008, two load lines could be arranged with the width of $3 \times 2 = 6\text{m}$. The width of remaining area is 2.5m . The crowd load could be applied to both footpaths with each 0.5m wide. Similar to the DM 1990, the typical asymmetrical arrangement of traffic load lines and crowd load lines in the transverse direction is illustrated in Fig. 161, which can be also used to consider the most unfavorable loading state for Girder-L. In the longitudinal direction, the concentrate loads can move along the whole superstructure length and the distributed loads (q_{ik}) could be applied to the whole superstructure length. The arrangement of traffic loads in longitudinal direction is shown in Fig. 162.

RETROFIT OF EXISTING BRIDGES WITH CONCEPT OF INTEGRAL ABUTMENT BRIDGE

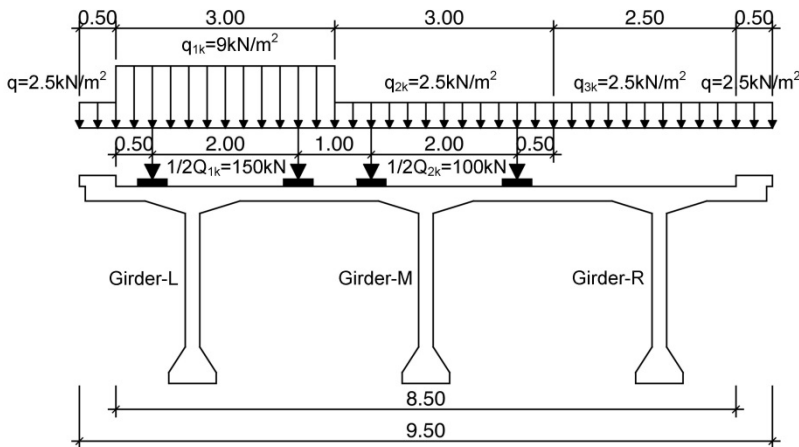


Fig. 161 Arrangement of highway live load in NTC 2008 in transverse direction

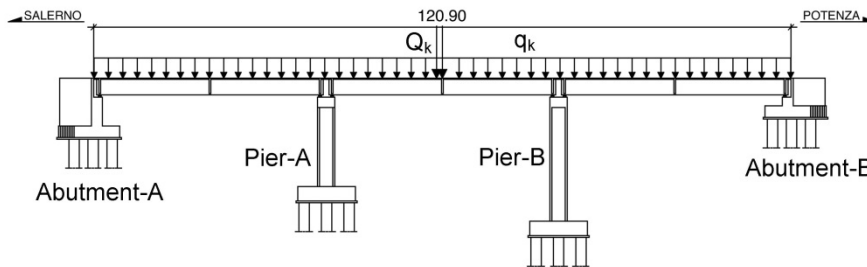


Fig. 162 Arrangement of highway live load in NTC 2008 in longitudinal direction

5.3.4 Seismic load

In DM 1996, there is no specialized specification for the bridge. A general dynamic analysis is proposed, and it is considered in linear elastic range. The response spectrum in terms of acceleration can be obtained by equation (139), as illustrated in Fig. 163.

$$a/g = C \cdot I \cdot R \quad (139)$$

where, a is the spectral acceleration. g is the acceleration of gravity. C is the coefficient of seismic intensity $C=(S-2)/100$. S is the degree of seismic activity ($S \geq 2$) whose value can be obtained from Fig. 164 ($S=12$ for Area category I, $S=9$ for Area category II, $S=6$ for Area category III, N.C. means the area without classification). 'Viadotto Serrone' is located between Salerno and Potenza, which belongs to the area category II. I is the coefficient of seismic protection, and it is set as 1.4, 1.2 and 1.0 for structures whose earthquake resistance is of primary

importance, structures that present a particular risk to their characteristics of use and structures do not respectively belong to the categories above. R is the coefficient of relative response to the direction, and it can be calculated by $R=0.862/T^{2/3}$ for $T>0.8s$ and $R=1.0$ for $T\leq 0.8s$. T is the period of the vibration mode.

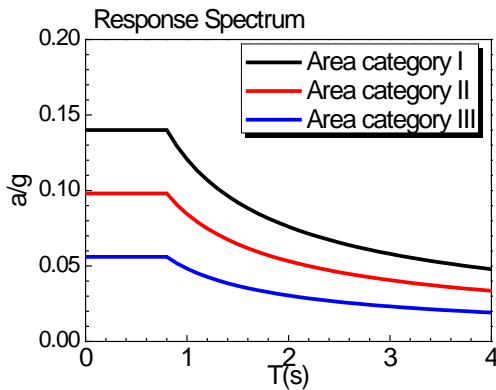


Fig. 163 Response Spectrum in DM 1996

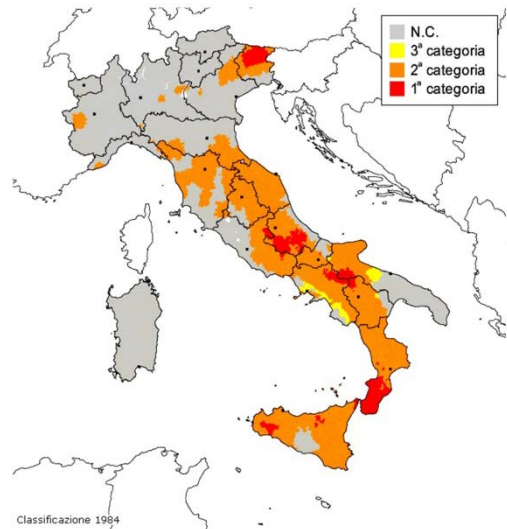


Fig. 164 Area category classification of Italy in 1984

In NTC 2008, the response spectrum method, time history method and pushover method can be used. In order to compare with DM 1996, the detailed information of the response spectrum method is introduced in the following.

In order to obtain the response spectrum, the longitude and latitude of 'Viadotto Serrone' can be got from Google map (Long: 15.37; Lat: 40.6), as shown in Fig. 165.



Fig. 165 Longitude and latitude of 'Viadotto Serrone'

The horizontal and vertical response spectra are illustrated respectively in Fig. 166. The limit state SLV with the behavior factor $q=1$ could be chosen in this analysis, because after retrofitting the existing SSB will be converted into the IAB which is more rigid and can move together with the ground (Ministero delle Infrastrutture, 2008). According to the investigation report, the average shear wave velocity ($v_{s,30}$) is 578 m/s corresponding to the ground type B. The topographic category is T1, and the corresponding coefficient $S_T=1$ could be chosen. The horizontal response spectrum can be obtained by formula (140). The vertical response spectrum can be obtained by formulae (142) and (143).

For horizontal response spectrum:

$$\begin{aligned}
 0 \leq T < T_B \quad S_e(T) &= a_g \cdot S \cdot \eta \cdot F_0 \cdot \left[\frac{T}{T_B} + \frac{1}{\eta \cdot F_0} \left(1 - \frac{T}{T_B} \right) \right] \\
 T_B \leq T < T_C \quad S_e(T) &= a_g \cdot S \cdot \eta \cdot F_0 \\
 T_C \leq T < T_D \quad S_e(T) &= a_g \cdot S \cdot \eta \cdot F_0 \cdot \left(\frac{T_C}{T} \right) \\
 T_D \leq T \quad S_e(T) &= a_g \cdot S \cdot \eta \cdot F_0 \cdot \left(\frac{T_C \cdot T_D}{T^2} \right)
 \end{aligned} \tag{140}$$

$$\eta = \sqrt{10 / (5 + \xi)} \geq 0.55 \tag{141}$$

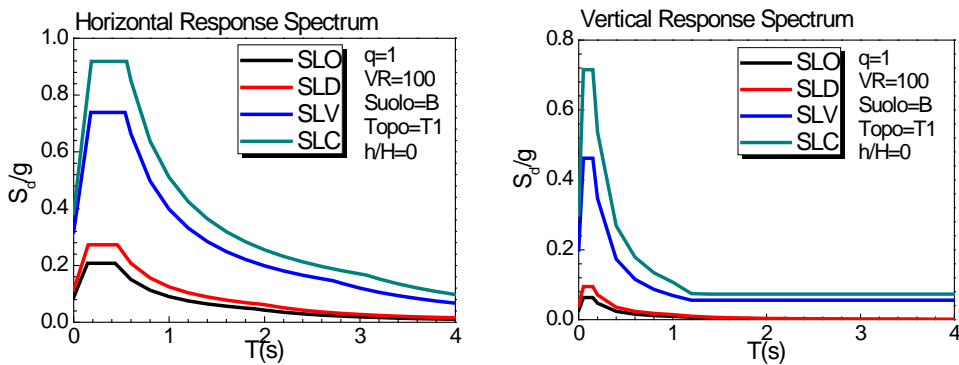
For vertical response spectrum:

$$\begin{aligned}
 0 \leq T < T_B \quad S_{ve}(T) &= a_g \cdot S \cdot \eta \cdot F_v \cdot \left[\frac{T}{T_B} + \frac{1}{\eta \cdot F_v} \left(1 - \frac{T}{T_B} \right) \right] \\
 T_B \leq T < T_C \quad S_{ve}(T) &= a_g \cdot S \cdot \eta \cdot F_v \\
 T_C \leq T < T_D \quad S_{ve}(T) &= a_g \cdot S \cdot \eta \cdot F_v \cdot \left(\frac{T_C}{T} \right) \\
 T_D \leq T \quad S_{ve}(T) &= a_g \cdot S \cdot \eta \cdot F_v \cdot \left(\frac{T_C \cdot T_D}{T^2} \right)
 \end{aligned} \tag{142}$$

$$F_v = 1.35 \cdot F_0 \cdot (a_g / g)^{0.5} \tag{143}$$

where, a_g is the peak horizontal ground acceleration. $S=S_S S_T$. S_S is the stratigraphic amplification coefficient and S_T is the topographic amplification coefficient. η is the damping correction coefficient that can be calculated by formula (141). ξ is the value of viscous damping, if $\xi=5\%$, $\eta=1$. F_0 is the maximum value of the spectrum amplification factor in the horizontal acceleration. $T_C=C_C T_C^*$ is the

corresponding initial period of the constant spectral velocity branch, T_C^* is the initial period of the constant spectral velocity branch and C_C is the coefficient depending on the category below ground. $T_B=T_C/3$ is the corresponding initial period of the constant spectral acceleration branch. $T_D=4a_g/g+1.6$ is the corresponding initial period of the constant spectral displacement branch. F_V can be calculated by formula (143).



(a) Horizontal response spectrum

(b) Vertical response spectrum

Fig. 166 Response spectrum of 'Viadotto Serrone' in NTC 2008

5.3.5 Loads combination

Based on DM 1990, the load cases and corresponding load combination factors listed in Table 39 can be used to investigate the ultimate limit state of the bridge. The major steps are described in the following. Each load case should be applied to bridge firstly. Then, the influence of each load case should be amplified by the corresponding load combination factor, as listed in Table 39. It finds that each load case has two load combination factors. The selection of the load combination factor is based on whether the load case is favorable or not. Both of them could be considered in order to obtain the envelope value. Finally, the influence of all load cases can be added together to conduct the ultimate limit state design of the bridge.

Action group	Self-weight g_1	Superimposed dead load g_2	Prestressed load e_1	Thermal load e_3	Highway live load q_1
U II	1.5 (1.0)	1.5 (1.0)	1.2 (0.85)	1.2 (0.0)	1.5 (0.0)

Table 39

Load cases and load combination factors in DM 1990

For the seismic analysis, no loads combination has been prescribed in DM 1990 and DM 1996

In NTC 2008, the ultimate limit state of bridge can be obtained through the same procedure of DM 1990, which can be summarized as the formula (144). The load combination factors of different load cases corresponding to the ultimate limit state are listed in Table 40.

$$\gamma_{G1}G_1 + \gamma_{G2}G_2 + \gamma_p P + \gamma_{Q1}Q_{k1} + \gamma_{Q2}\psi_{02}Q_{k2} + \dots \quad (144)$$

	Self-weight G ₁	Superimposed dead load G ₂	Prestressed load P	Thermal load ε ₃	Highway live load Q
Y	1.35 (1.0)	1.5 (0.0)	1.0 (1.0)	1.2 (0.0)	1.35 (0.0)
ψ	--	--	--	0.6	concentrated load 0.75; distributed load 0.4

Table 40
Load cases and load combination factors in NTC 2008

For the seismic analysis, the loads combination corresponding to the limit state SLV can be obtained by formula (145) in NTC 2008.

$$E(SLV) + G_1 + G_2 + P + \sum_{i \geq 1} \psi_{2i} Q_{ki} \quad (145)$$

where, E is the seismic action and Q is the thermal action with the coefficient ψ_2 of 0.5.

5.3.6 Comparison between original and updated codes

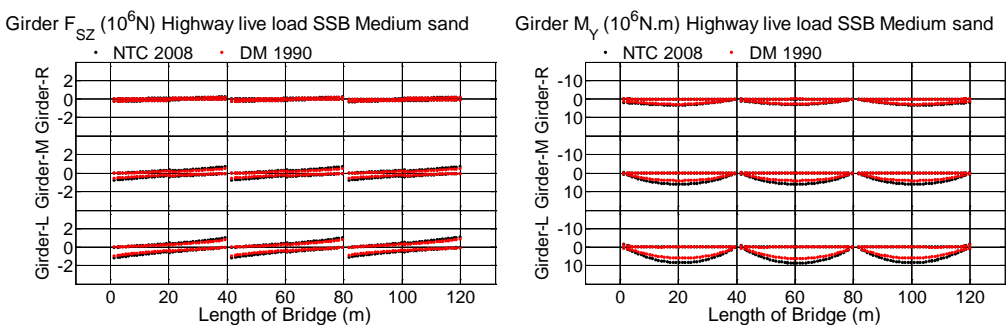
In this section, the performance of existing SSB was investigated respectively by both original and updated codes, including the static analysis and the seismic analysis (Xue et al., 2012), in order to select the appropriate design code for the further research. The medium sand is chosen as the soil condition to simulate the soil-structure interaction in all finite element models. Due to space limitations in this paper, only the performance of girders is chosen as the example to illustrate in the following figures.

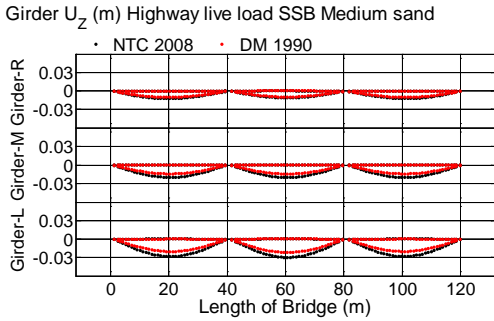
5.3.6.1 Static analysis

All single load cases (listed in Table 39 and Table 40) and the loads combination (Section 5.3.5) should be taken into account to conduct the static analysis. Among these single load cases, only the highway live load needs to be analyzed due to its different provisions in two codes. The definitions of the other four load cases, including the dead load, the superimposed dead load, the prestressed load and the thermal load, are the same in two codes.

In order to obtain the most unfavorable influence of highway live load, the moving load function implemented in Sap2000 (Computers and Structures Inc, 2011) should be used. The moving load can be defined as the combinations of paths and vehicles. The paths can represent where the highway live load acts on the superstructure by importing the relative distances between the central lines of load lines and the corresponding frame elements of girders. In this case, the arrangements of the traffic load lines and crowd load lines in the transverse direction are illustrated respectively in Fig. 158 and Fig. 161 corresponding to DM 1990 and NTC 2008 (Section 5.3.3). Moreover, the load on each path can be simulated by defining vehicles, which can consider the combination of the concentrated load and the distributed line load, as illustrated in Fig. 157 and Fig. 160 corresponding to DM 1990 and NTC 2008 (Section 5.3.3). By using the function of vehicles, the concentrated load can move automatically along the paths in longitudinal direction and the distributed line load can be applied to the unfavorable part of the influence line.

The F_{SZ} , M_Y and U_Z of girders under highway live load in NTC 2008 and DM 1990 are compared in Fig. 167. The black points and red points represent respectively the values obtained through NTC 2008 and DM 1990, which will be used in all figures in this section.

(a) F_{SZ} of girders(b) M_Y of girders



(c) U_z of girders

Fig. 167 Influence of different codes on the performance of girders under highway live load

As introduced above, the typical arrangement of traffic load lines and crowd load lines in the transverse direction can consider the most unfavorable loading state for Girder-L. Therefore, the Girder-L could be chosen as the critical component. The ultimate M_y , U_z and F_{sz} at the critical sections of Girder-L are listed in Table 41. In order to show clearly the differences between original and updated codes, the discrepancies calculated by formula (146) are also listed in Table 41. The results indicate that the performance of girders in SSB under highway live load in NTC 2008 is larger than that in DM 1990.

$$D_V = \frac{|V_{newcode}| - |V_{oldcode}|}{|V_{newcode}|} \tag{146}$$

Girder-L	DM 1990	NTC 2008	Discrepancy
F_{sz} (N) C_{S-2R}	8.5e5	1.1e6	21%
positive M_y (N.m) C_{S-2M}	6.0e6	8.5e6	30%
deflection U_z (m) C_{S-2M}	-0.021	-0.030	28%

Table 41

Influence of different codes on the ultimate M_y , U_z and F_{sz} of Girder-L under highway live load and the corresponding discrepancies

Besides the influence of single load case, the effects of the static loads combinations in two codes on the performance of the SSB were also compared. The static loads combination corresponding to the ultimate limit state, as listed in Table 39 and Table 40 (Section 5.3.5), were chosen. The F_{sz} , M_y and U_z of girders under static loads combination in NTC 2008 and DM 1990 are compared in Fig. 168.

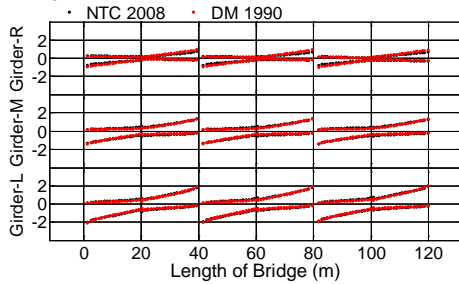
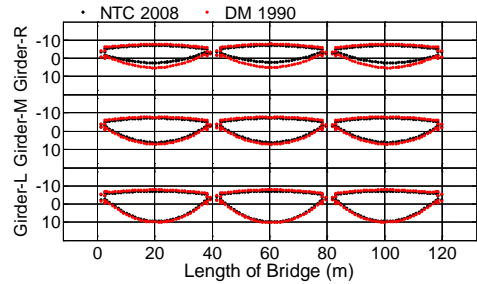
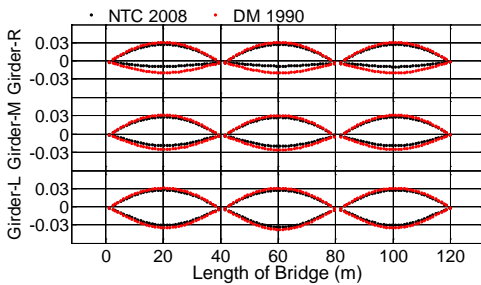
Girder F_{SZ} (10^6 N) Combination load SSB Medium sand(a) F_{SZ} of girdersGirder M_Y (10^6 N.m) Combination load SSB Medium sand(b) M_Y of girdersGirder U_Z (m) Combination load SSB Medium sand(c) U_Z of girders

Fig. 168 Influence of different codes on the performance of girders under static loads combination

The Girder-L could be chosen as the critical component. The ultimate F_{SZ} , M_Y , U_Z at the critical sections of Girder-L and the corresponding discrepancies calculated by formula (146) are listed in Table 42. The results observe that the performance of girders in SSB under static loads combination in NTC 2008 is slightly smaller than that in DM 1990.

Girder-L	DM 1990	NTC 2008	Discrepancy
F_{SZ} (N) C_{S-2R}	1.9e6	1.9e6	-3%
positive M_Y (N.m) C_{S-2M}	1.0e7	9.7e6	-4%
negative M_Y (N.m) C_{S-2M}	-8.1e6	-7.2e6	-11%
camber U_Z (m) C_{S-2M}	0.031	0.028	-12%
deflection U_Z (m) C_{S-2M}	-0.037	-0.033	-11%

Table 42

Influence of different codes on the ultimate M_Y , U_Z and F_{SZ} of Girder-L under static loads combination and the corresponding discrepancies

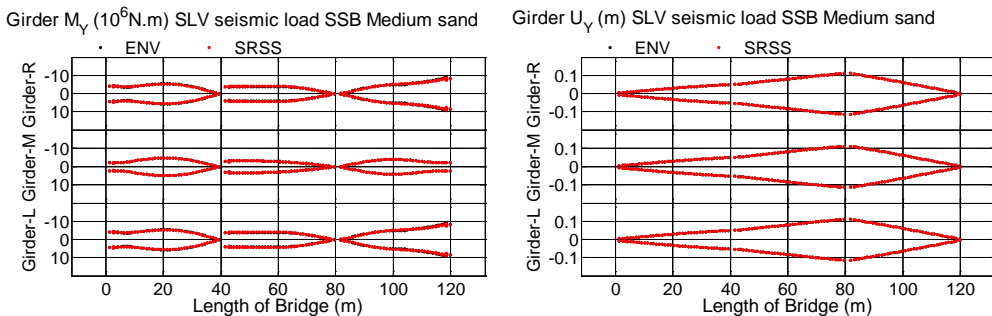
5.3.6.2 Seismic analysis

In order to investigate the differences between the performance of simply supported bridge under the seismic load in NTC 2008 and DM 1996, the response spectrum analysis was carried out. According to DM 1996, the response spectrum belonging to the area category I (the black line in Fig. 163) was chosen; however, based on NTC 2008, the horizontal response spectrum corresponding to the limit state SLV (the blue line in Fig. 166(a)) was selected (Section 5.3.4). It is well known that the response spectrum analysis is a linear analysis case. Therefore, the nonlinear soil-structure interaction relationship curves defined in area springs and line springs are all neglected, and they are replaced by the effective stiffness (k) of the soil-structure interaction relationship curves (Section 5.2.3).

The response spectrum analysis should be conducted in both longitudinal and transverse directions. In order to obtain the composite action of two directions, two combination approaches can be used, which are the Envelope combination method (formula (147)) and the SRSS combination method (formula (148)) (Eurocode CEN, 2005a; Ministero delle Infrastrutture, 2008). These two combination approaches were compared firstly. The M_Y and U_Y of girders illustrated in Fig. 169 indicates that the composite actions of two directions obtained through two combination methods (ENV and SRSS) are nearly the same. Consequently, only the SRSS combination will be considered in this paper.

$$ENV = Envelope(E_x + 0.3E_y; 0.3E_x + E_y) \tag{147}$$

$$SRSS = \sqrt{E_x^2 + E_y^2} \tag{148}$$



(a) M_Y of girders

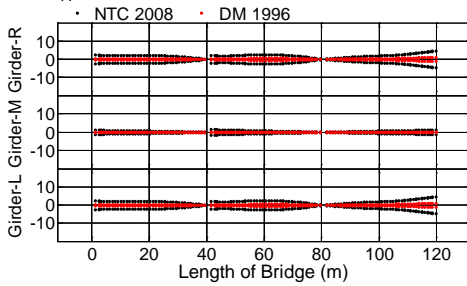
(b) U_Y of girders

Fig. 169 Influence of different combination approaches on the performance of girders under response spectrum in NTC 2008

The internal forces of girders under response spectrum in NTC 2008 and DM 1996

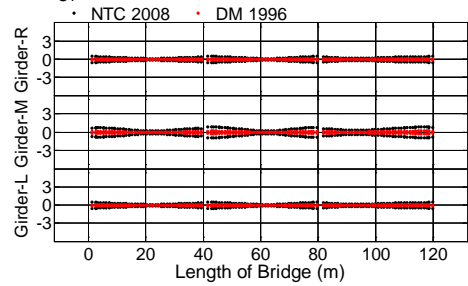
are compared in Fig. 170.

Girder F_A (10^6N) ESRSS load SSB Medium sand



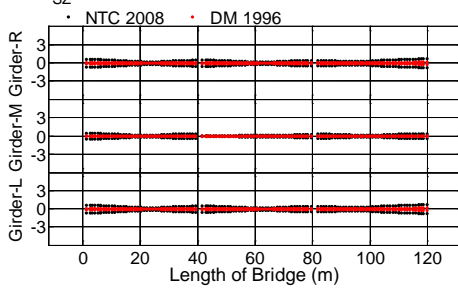
(a) F_A of girders

Girder F_{SY} (10^6N) ESRSS load SSB Medium sand



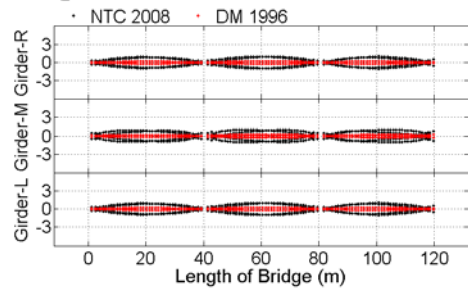
(b) F_{SZ} of girders

Girder F_{SZ} (10^6N) ESRSS load SSB Medium sand



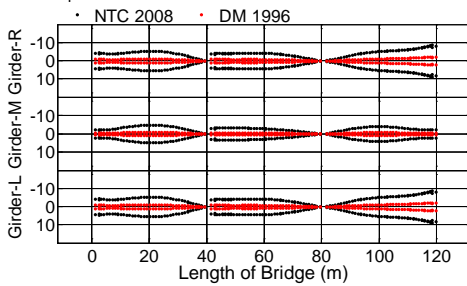
(c) F_{SY} of girders

Girder M_Z (10^6N.m) ESRSS load SSB Medium sand



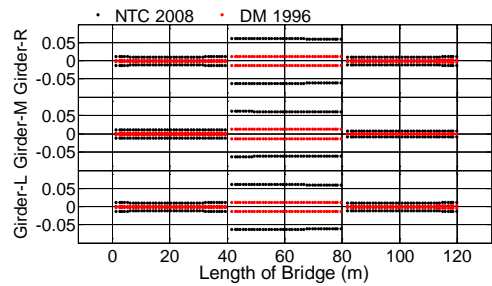
(d) M_Z of girders

Girder M_Y (10^6N.m) ESRSS load SSB Medium sand



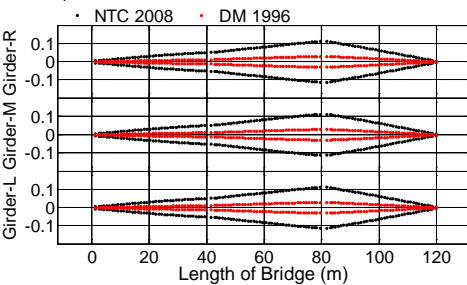
(e) M_Y of girders

Girder U_X (m) ESRSS load SSB Medium sand



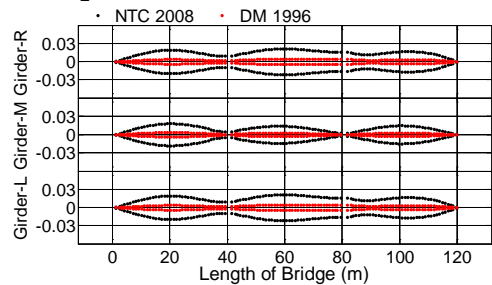
(f) U_X of girders

Girder U_Y (m) ESRSS load SSB Medium sand



(g) U_Y of girders

Girder U_Z (m) ESRSS load SSB Medium sand



(h) U_Z of girders

Fig. 170 Influence of different codes on the performance of girders under response spectrum

The Girder-L could be chosen as the critical component, of which the ultimate internal forces at the critical sections and the corresponding discrepancies calculated by formula (146) are listed in Table 43. The results indicate that the performance of girders under response spectrum in NTC 2008 is significantly larger than that in DM 1996.

Girder-L	DM 1996	NTC 2008	Discrepancy
Tension F_A (N) C_{S-3R}	1.2e6	4.6e6	74%
positive F_{SZ} (N) C_{S-3R}	1.7e5	7.2e5	76%
positive F_{SY} (N) C_{S-3R}	1.3e5	5.4e5	76%
positive M_Z (N.m) C_{S-3R}	2.4e5	9.9e5	76%
positive M_Y (N.m) C_{S-3R}	2.1e6	8.2e6	74%
positive U_X (m) C_{S-2M}	0.013	0.061	79%
positive U_Y (m) C_{S-2R}	0.029	0.112	74%
camber U_Z (m) C_{S-2R}	0.005	0.021	78%

Table 43

Influence of different codes on the ultimate internal forces of Girder-L under response spectrum and the corresponding discrepancies

There is no seismic loads combination defined in DM 1990 and DM 1996. Therefore, the comparison between the performance of the SSB under seismic loads combination in two codes will not be considered in this analysis.

5.3.6.3 Summary

According to the comparisons conducted above, the results are summarized in Table 44.

Load cases			The influence on the performance of bridge
Static	Single load case	Permanent load	Same
		Deformation	Same
		Highway live load	NTC 2008 (20%~30%)
	Static loads combination		DM 1990 (0~10%)
Seismic	Response spectrum		NTC 2008 (70%~80%)

Table 44

Summary of the comparison results between the original and updated codes

It could be found that the SSB performance under static loads combination in NTC 2008 is slightly smaller than that in DM 1990 and the gap less than 10%; however, the SSB performance under highway live load and response spectrum in NTC 2008 is larger than that in the original codes, which are 20–30% and 70–80%, respectively. Consequently, the NTC 2008 could be chosen as the design code in this paper.

5.4 Model verification

With advances in numerical modeling, it is generally expected that the finite element model can reliably simulate both the static and dynamic structural behaviors of the real structure. However, the validity of the finite element model should be checked firstly.

5.4.1 Finite element model verification

In order to verify the finite element model of the existing SSB simulated through Sap2000, another finite element model of 'Viadotto Serrone' was built by the general finite element program MIDAS CIVIL 2009 (MIDAS IT Co. Ltd, 2009), as illustrated in Fig. 171. In this model, the existing abutments and piles were replaced by the fixed boundary conditions. The superstructure, piers and the superstructure-substructure interactions could be simulated by using the same approaches as the finite element model in Sap2000.

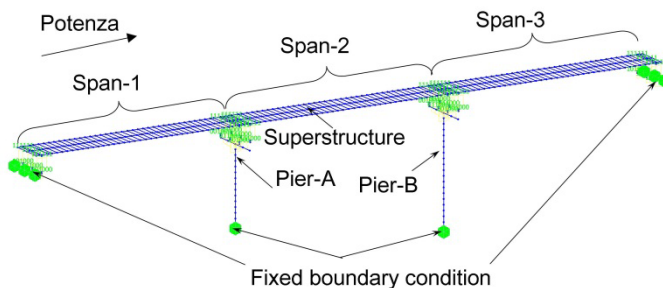


Fig. 171 3D finite element model of 'Viadotto Serrone' in MIDAS CIVIL 2009

Based on two finite element models, the modal analysis was carried out. The sum of modal participating mass ratios for all six degrees of freedom can exceed 90%. The first five frequencies and the corresponding mode shapes obtained from two finite element models are compared in Table 45. The frequency discrepancy D_F calculated by formula (149) are also listed in Table 45.

RETROFIT OF EXISTING BRIDGES WITH CONCEPT OF INTEGRAL ABUTMENT BRIDGE

$$D_F = \frac{f_{SAP2000} - f_{Midas}}{f_{SAP2000}} \quad (149)$$

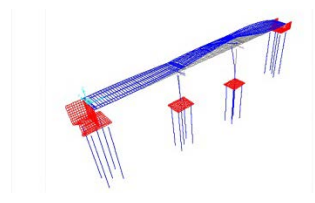

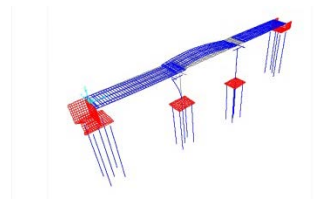
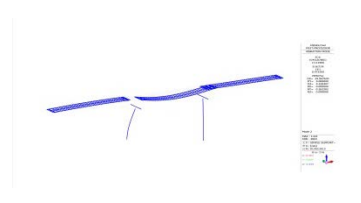
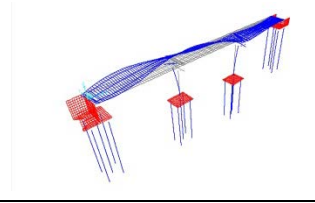
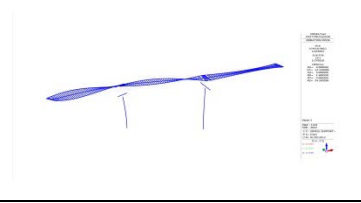
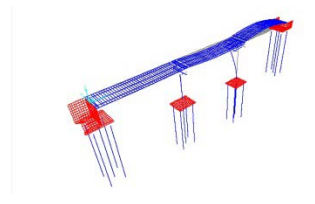
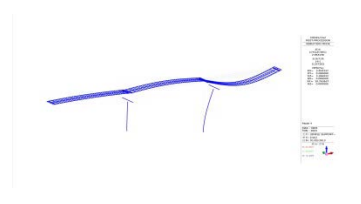
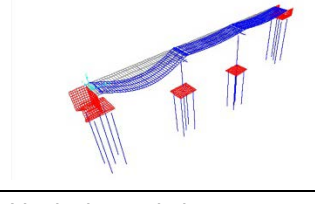
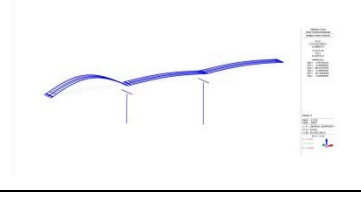
No	Frequency		Mode shape	
	Sap2000	Midas	Sap2000	Midas
1	1.79	1.79		
	D _F =0%		Lateral translation and Torison	
2	2.08	2.11		
	D _F =-1.4%		Longitudinal translation and Vertical translation	
3	2.60	2.63		
	D _F =-1.1%		Lateral translation and Torison	
4	2.88	2.96		
	D _F =-2.7%		Longitudinal translation and Vertical translation	
5	3.06	3.06		
	D _F =0%		Vertical translation	

Table 45
Comparison between the frequencies and mode shapes of two models

The Modal Assurance Criterion (MAC) approach which is probably the most useful tool to correlate two sets of mode shape vectors obtained experimentally or theoretically, was also chosen in this analysis to check the validity of the finite element model (Allemang, 2003; Pastor et al., 2012). It has been used for numerous years as a statistical indicator, which is most sensitive to large differences and relatively insensitive to small differences in the mode shapes. In this case, the first ten mode shapes obtained from two finite element models are compared by formula (150), which can be defined as a scalar constant relating the degree of consistency (linearity) between one modal and another reference modal vector. The MAC approach can produce a coefficient ranging from zero (representing no consistent correspondence) to one (representing a consistent correspondence). In general, values that are larger than 0.9 indicate consistent correspondence whereas small values indicate poor resemblance of two shapes (Pastor et al., 2012). The 3-D presentation of the MAC values illustrated in Fig. 172 shows that the MAC values of the first ten mode shapes obtained from two finite element models are all larger than 0.9, which means that the finite element model of the existing SSB could be used in the following analysis.

$$MAC(\varphi_{A,i}, \varphi_{B,j}) = \frac{(\varphi_{A,i}^T \varphi_{B,j})^2}{(\varphi_{A,i}^T \varphi_{A,i})(\varphi_{B,j}^T \varphi_{B,j})} \quad (150)$$

where, $\varphi_{A,i}$ is the i -th mode of data set A and $\varphi_{B,j}$ is the j -th mode of data set B.

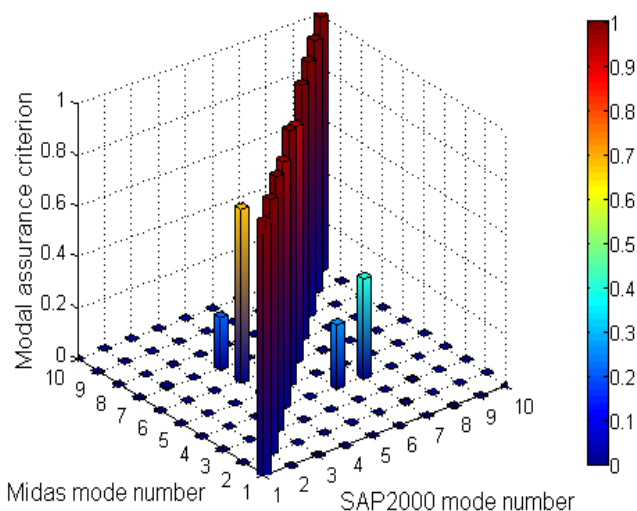


Fig. 172 3-D presentation of MAC values

5.4.2 Retrofitting process modeling verification

As described above, the finite element model should be able to simulate two different static schemes in two stages, which are the SSB subjected to dead load, prestressed load and superimposed dead load, and the IAB after retrofitting under highway live load, thermal load and seismic load. All these load cases could be applied one by one in the following sequence, as shown in Fig. 173, by using the nonlinear analysis type and the nonlinear staged construction analysis type implemented in Sap2000 (Computers and Structures Inc, 2011).

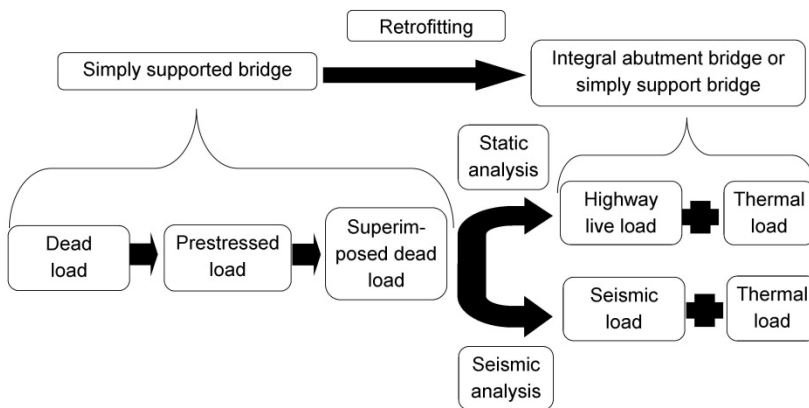


Fig. 173 Sequences of different load cases

In order to verify of the transformation simulation, the analysis considering the static load case in NTC 2008 was conducted on five different types of finite element models, including the SSB without retrofitting, and FIAB1, FIAB2, FIAB3 and FIAB4 after retrofitting defined in Table 2 (p.18). In this analysis, the combination influence of the dead load, prestressed load and superimposed load in the first stage, which should be applied one by one to the SSB before retrofitting, could be named as the permanent load. The thermal load and the highway live load in the second stage were considered in this verification. The thermal load could be set as -15°C. The highway live load composed of the concentrated traffic load, distributed traffic pressure and the crowd load, was applied to the fixed positions as illustrated in Fig. 161 and Fig. 162 (p.198), without the consideration of moving load for the purpose of simplification. The medium sand listed in Table 34 (p.165) could be chosen to simulate the soil-structure interaction.

The U_z and M_y of girders and the U_x and M_y of piers obtained from five different finite element models subjected to permanent load, highway live load and thermal

load are compared respectively in Fig. 174 and Fig. 175. It could be observed that the M_Y and U_Z of girders and M_Y and U_X of piers obtained from different finite element models subjected to permanent loads are nearly the same, which means that the static schemes of all finite element models are simply supported when they are subjected to permanent loads. However, the influence of highway live load on the M_Y and U_Z of girders and the thermal load on the M_Y and U_X of piers in different bridge types after retrofitting are different. It represents that all finite element models could be transformed into different bridge types after retrofitting by using the construction stage method implemented in Sap2000, when they are subjected to highway live load and thermal load. In conclusion, the finite element model built through Sap2000 could consider the retrofitting process by using the approach defined in Section 5.2.5 and can be used in further analyses.

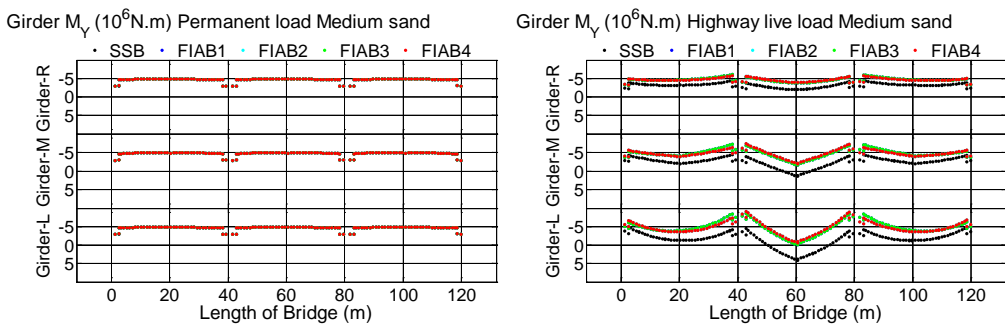
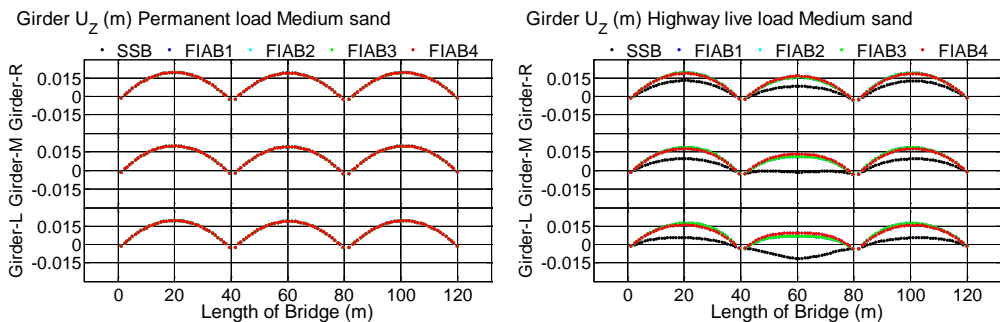
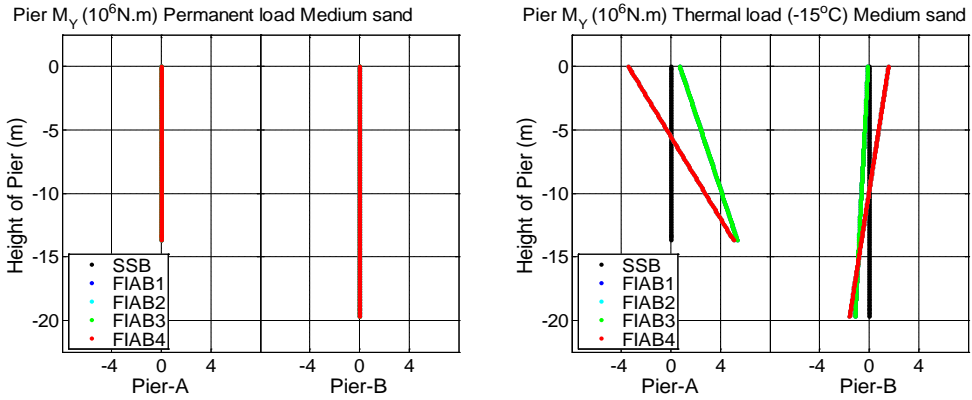
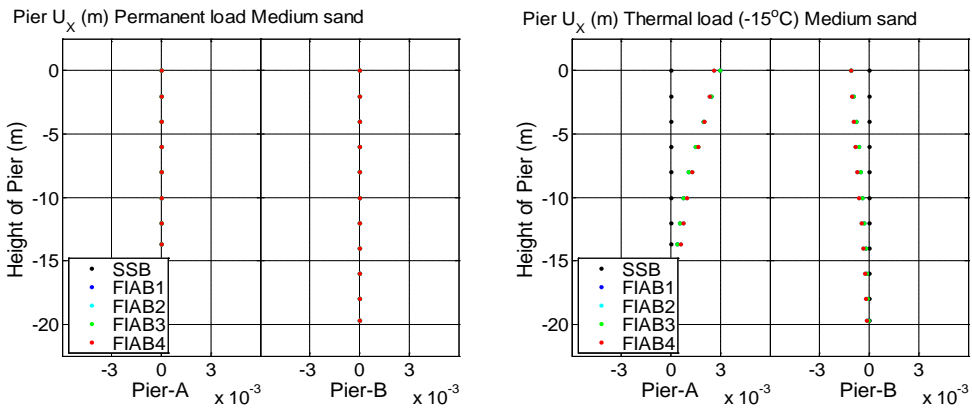
(a) M_Y of girders(b) U_Z of girders

Fig. 174 Influence of different bridge types on the performance of girders

RETROFIT OF EXISTING BRIDGES WITH CONCEPT OF INTEGRAL ABUTMENT BRIDGE



(a) M_Y of piers



(b) U_x of piers

Fig. 175 Influence of different bridge types on the performance of piers

5.4.3 Necessity of soil-structure interaction simulation in IAB

In this section, the necessity of simulating the real soil-structure interaction on site in the finite element models of bridges after retrofitting is discussed. Two groups of finite element models using different approaches to simulate the boundary conditions were built, as illustrated in Fig. 176. One group used nonlinear spring elements to simulate the soil-structure interaction. The medium sand listed in Table 34 (p.165) could be chosen as the real soil condition in this analysis. In the other group, the lateral movements of abutments and piles were fixed to simulate the rigid soil-structure connection, which is usually adopted in the analysis of the SSB. The NTC 2008 was considered as the design code in this section.

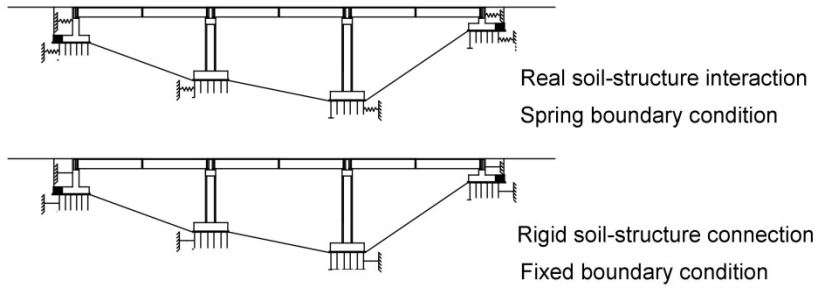
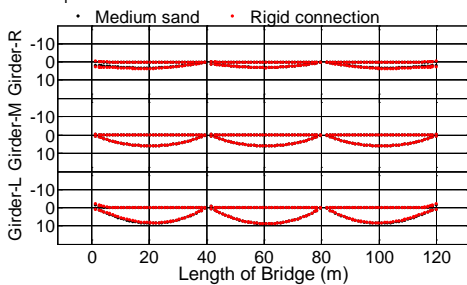


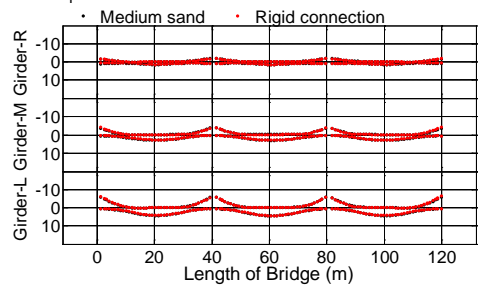
Fig. 176 Different simulation methods of soil-structure interaction

Taking girders or piers as the research objects, the differences between two boundary condition simulation methods are discussed in the following. The performance of girders under highway live load in three different bridge types, including the SSB and the FIAB4, is illustrated in Fig. 177. It finds that considering the real soil-structure interaction, the performance of girders under highway live load is similar to that using the rigid connection. Therefore, the simulation of the real soil-structure interaction can be replaced by the rigid boundary condition for all bridge types when considering the highway live load.

Girder M_y ($10^6\text{N}\cdot\text{m}$) Highway live load SSB

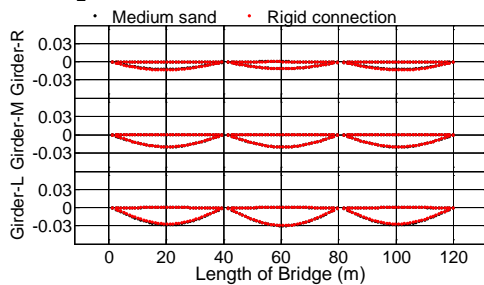


Girder M_y ($10^6\text{N}\cdot\text{m}$) Highway live load FIAB4

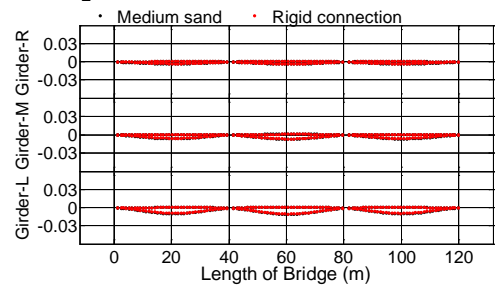


(a) M_y of girders

Girder U_z (m) Highway live load SSB



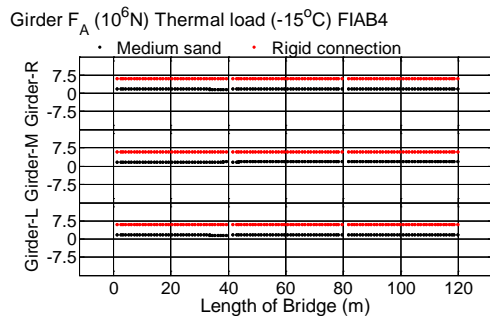
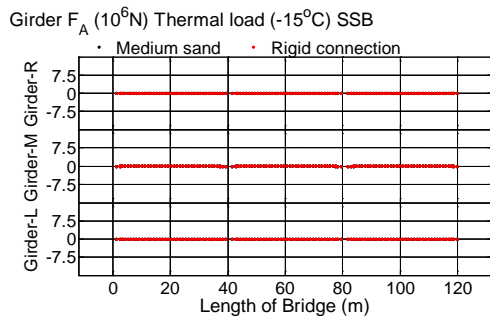
Girder U_z (m) Highway live load FIAB4



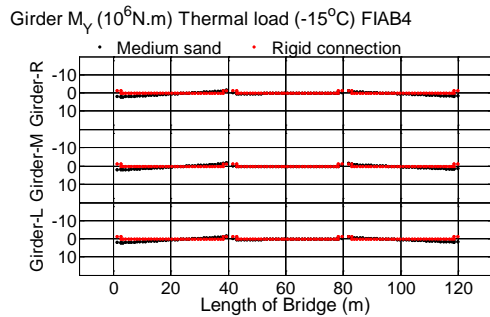
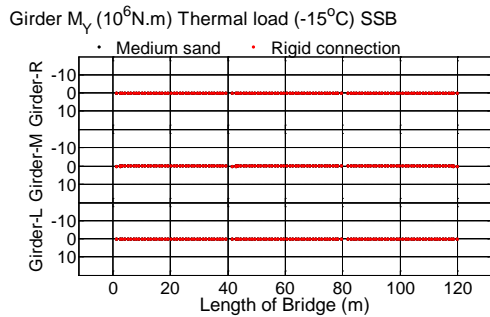
(b) U_z of girders

Fig. 177 Influence of different boundary condition simulation methods on the performance of girders under highway live load

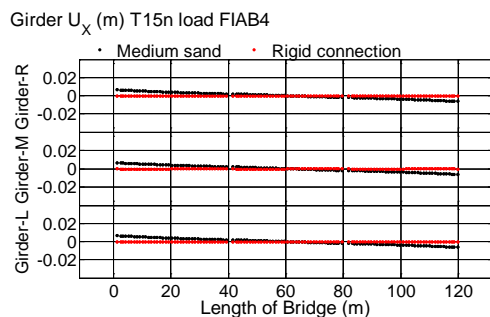
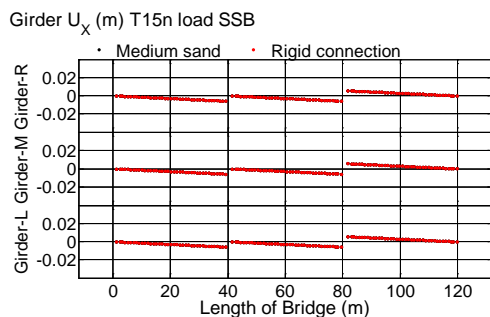
Considering the thermal load as -15°C , the performance of girders in SSB and FIAB4, and the performance of piers in FIAB1 and FIAB4 are illustrated respectively in Fig. 178 and Fig. 179. It could be found that under thermal load, the performance of girders and piers in SSB considering the real soil-structure interaction is the same as that using the rigid connection; however, the performance of girders and piers in FIAB4 considering the real soil-structure interaction is different to that using the rigid connection.



(a) F_A of girders

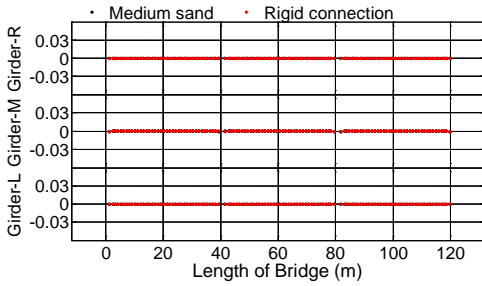


(b) M_Y of girders

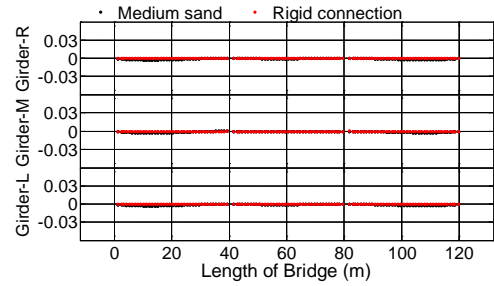


(c) U_X of girders

Girder U_z (m) T15n load SSB



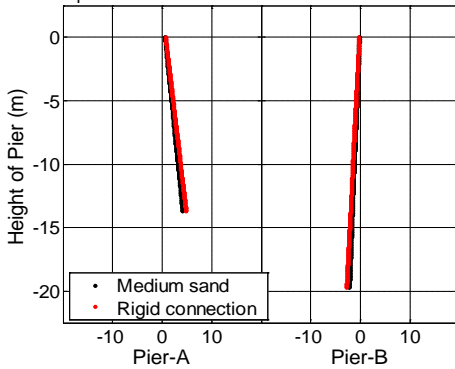
Girder U_z (m) T15n load FIAB4



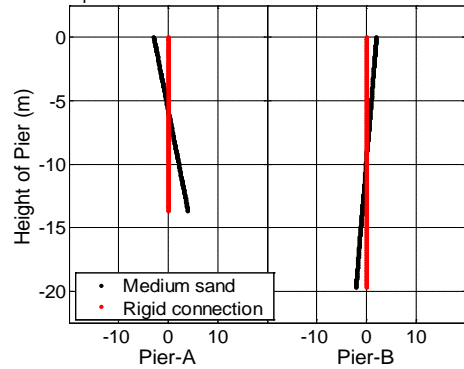
(d) U_z of girders

Fig. 178 Influence of different boundary condition simulation methods on the performance of girders under thermal load (-15°C)

Pier M_y ($10^6\text{N}\cdot\text{m}$) T15n load FIAB1

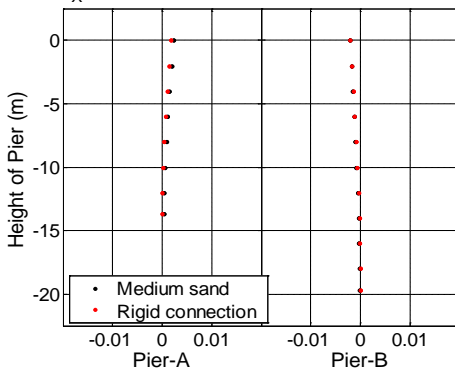


Pier M_y ($10^6\text{N}\cdot\text{m}$) T15n load FIAB4

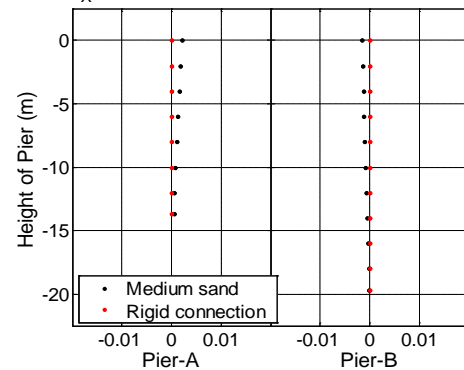


(a) M_y of piers

Pier U_x (m) T15n load FIAB1



Pier U_x (m) T15n load FIAB4



(b) U_x of piers

Fig. 179 Influence of different boundary condition simulation methods on the performance of piers under thermal load (-15°C)

In order to show the differences clearly, the Girder-L and Pier-A were chosen as the critical components. The ultimate internal forces at the critical sections of Girder-L

and Pier-A in FIAB1 and FIAB4 under thermal load (-15°C) corresponding to two boundary condition simulation methods are listed in Table 46. The discrepancies between two boundary condition simulation methods can be calculated by formula (151). It could be observed that, for FIAB1, the variation trends of the internal forces of girders or piers using the rigid connection are the same as those considering the real soil-structure interaction; but the values are different. However, for FIAB4, the variation trends of the internal forces of girders or piers using the rigid connection are completely different to those the real soil-structure interaction. It proves that, in order to obtain the real performance of IABs after retrofitting, the real soil-structure interaction on site should be simulated in the finite element model.

$$D_v = \frac{|V_{realsoil}| - |V_{rigidconnection}|}{|V_{realsoil}|} \quad (151)$$

Girder-L in FIAB1	Rigid connection	Medium sand	Discrepancy
F _A (N) C _{S-2M}	3.6e6	2.0e6	-82%
M _Y (N.m) C _{S-1L}	6.5e6	3.6e6	-78%
U _X (m) C _{S-1L}	0.005	0.007	24%
U _Z (m) C _{S-1M}	-0.013	-0.007	-80%
Girder-L in FIAB4	Rigid connection	Medium sand	Discrepancy
F _A (N) C _{S-2M}	6.0e6	1.9e6	-212%
M _Y (N.m) C _{S-1L}	6.6e4	2.1e6	97%
U _X (m) C _{S-1L}	0.000	0.007	100%
U _Z (m) C _{S-1M}	0.000	-0.003	92%
Pier-A in FIAB1	Rigid connection	Medium sand	Discrepancy
M _Y (N.m) C _{P-AB}	4.8e6	4.1e6	-16%
U _X (m) C _{P-AT}	0.002	0.002	19%
Pier-A in FIAB4	Rigid connection	Medium sand	Discrepancy
M _Y (N.m) C _{P-AB}	4.0e2	4.0e6	100%
U _X (m) C _{P-AT}	0.000	0.002	100%

Table 46

Influence of different boundary condition simulation methods on the ultimate internal forces of Girder-L and Pier-A under thermal load (-15°C) and the corresponding discrepancies

If abutments or piles are chosen as the analysis objects, the real soil-structure interaction must be simulated, because the performance of abutments and piles considering the real soil-structure interaction must be larger than that using the fixed boundary condition.

6. STATIC SENSITIVE ANALYSIS

Based on the finite element model of ‘Viadotto Serrone’ verified in Chapter 5, a large number of sensitive analyses considering the static load cases were carried out in this chapter. The most important factors and their influence could be find out and adopted as the guideline of retrofitting existing SSBs with the IAB concept.

6.1 Different bridge types

According to the introduction in Chapter 4, using the FIAB concept can make the construction of retrofitting process easier and resolve the more potential durability problems than using the SIAB concept can achieve. Therefore, the performance of four subtypes of FIABs after retrofitting (FIAB1, FIAB2, FIAB3 and FIAB4), as shown in Table 47, would be analyzed in this analysis.

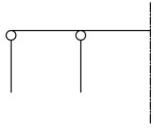
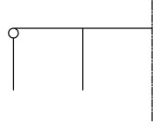
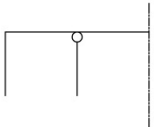
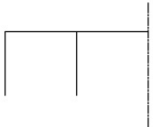
Superstructure-substructure connection		Superstructure-Pier connection			
		Hinged connection		Rigid connection	
Superstructure-Abutment connection	Hinged connection	FIAB1		FIAB2	
	Rigid connection	FIAB3		FIAB4	

Table 47
Detailed definitions and abbreviations of FIAB subtypes

The performance of the SSB without retrofitting can be chosen as a sample for comparison to indicate the advantages and disadvantages of different retrofitting approaches. If the performance of bridge components in FIABs is larger than that in SSB, the corresponding bridge components should be paid attention to. Because, if the cross sections of these bridge components keep the same without any changes

after retrofitting, the internal forces caused by external loads may exceed their internal resistance capacities and bring additional risks. The NTC 2008 was chosen as the design code and the medium sand was considered as the soil on site.

6.1.1 Load case

According to previous studies on IABs, the horizontal load case, including temperature variations, creep and shrinkage, and long-term prestress shortening can cause the expansion and contraction cycles of bridge superstructures and lead to the cyclic lateral movements of piles and abutments, and the change of soil pressure (Arsoy, 2000; Arsoy et al., 2002; Duncan & Arsoy, 2003; Flener, 2004; Hassiotis & Xiong, 2007; Springman et al., 1996). The components of IABs should be designed to resist and/or absorb this horizontal movement (American Association of State Highway and Transportation Officials, 2007). Most of the existing bridges, which need to be retrofitted in Italy, have been built more than 30 years. Therefore, the influence of creep, shrinkage and long-term prestress shortening should be quite small. The thermal load should be considered as the most important horizontal load case.

In this analysis, the uniform bridge temperature components (ΔT_{exp} and ΔT_{con}) defined by formulae (152) and (153), can be applied to the finite element models to simulate the expansion and contraction cycles of bridge superstructures, respectively. According to the updated Italian code NTC 2008 (Ministero delle Infrastrutture, 2008) introduced in Section 5.3.2, ΔT_{exp} and ΔT_{con} can be set as $\pm 15^\circ\text{C}$. Moreover, in order to expand the research scope, the $\pm 40^\circ\text{C}$ considered in some European Countries (Feldmann et al., 2010; Pétursson et al., 2011) were also taken into account as the extreme thermal load case. In USA, Europe and China, the temperature variations along the superstructure depth are considered in the codes. In this case, the temperature variations were not considered for the purpose of simplification.

$$\Delta T_{exp} = T_{max} - T_0 \quad (152)$$

$$\Delta T_{con} = T_0 - T_{min} \quad (153)$$

where, T_{max} and T_{min} are maximum and minimum uniform bridge temperature components, respectively. T_0 is initial temperature when structural element is restrained.

For the vertical load case, the dead load, prestressed load and superimposed dead load are all applied to bridges in the first stage, which is the SSB. Therefore, only the highway live load in the second stage will be considered as the vertical load case in this analysis by using moving load function implemented in Sap2000 (Computers and Structures Inc, 2011)

6.1.2 Girder

6.1.2.1 Thermal load

The performance of girders in different bridge types subjected to thermal load (-40°C) is compared in Fig. 180. It could be found that the F_A , M_Y and U_Z of girders in FIABs are significantly larger than those in SSB. For the U_X of girders, the ultimate values in FIABs appear at the both ends near abutments, which is different to the positions of the ultimate U_X of girders appeared in SSB. Each span can expand or contract individually due to bearings in SSB. Therefore, the ultimate U_X of girders in SSB occur at the ends of spans, which do not have hinged supports.

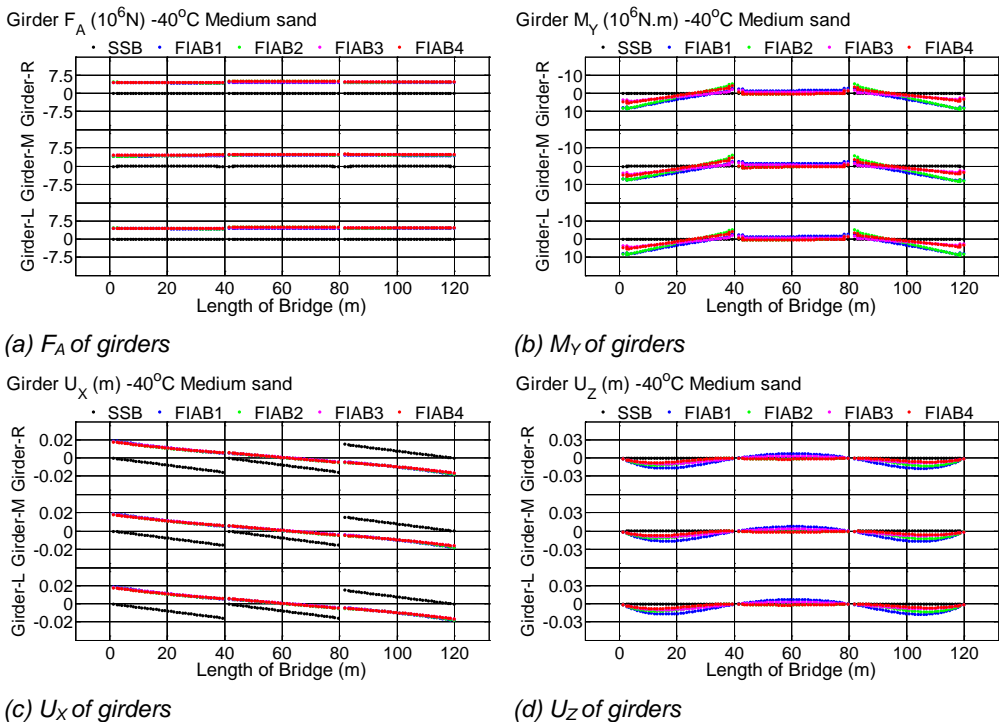


Fig. 180 Influence of different bridge types on the F_A , M_Y , U_X and U_Z of girders under thermal load (-40°C)

RETROFIT OF EXISTING BRIDGES WITH CONCEPT OF INTEGRAL ABUTMENT BRIDGE

The superstructure in 'Viadotto Serrone' is symmetric around the global coordinate axis X. Therefore, under thermal load, the performance of three girders (Girder-L, Girder-M and Girder-R) should be the same. In order to show the difference clearly, the Girder-L was selected as the critical component. Some critical sections of Girder-L corresponding to different internal forces were chosen.

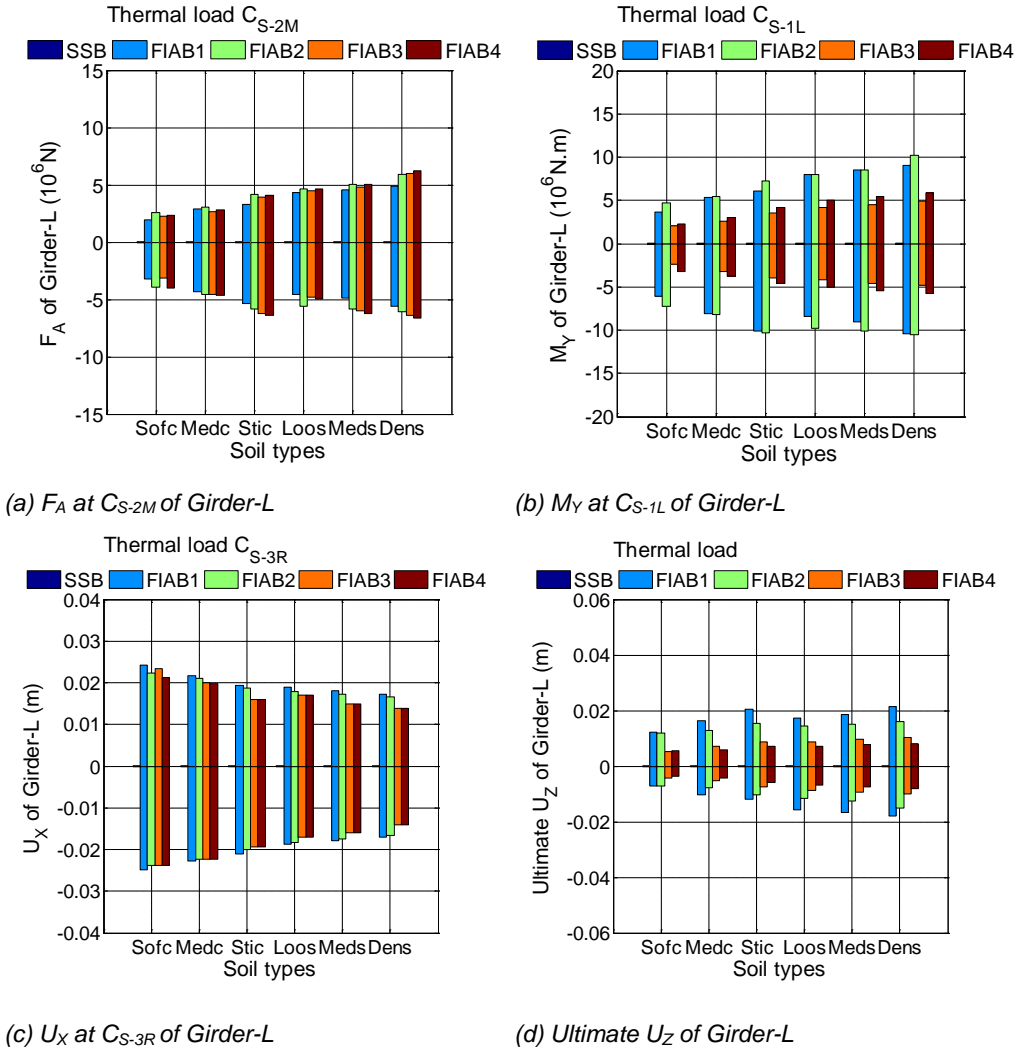


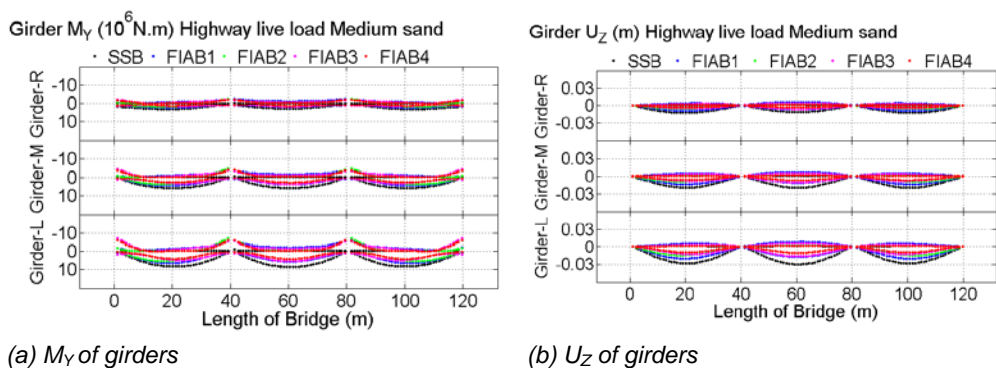
Fig. 181 Influence of different bridge types on the ultimate F_A , M_Y , U_X and U_Z of Girder-L under thermal load ($\pm 40^\circ\text{C}$)

From Fig. 180(a), it could be found that, the F_A along the length of girders in different bridge types are nearly the same. Therefore, the mid-span point of span2 (C_{S-2M}) could be selected as the critical section. From Fig. 180(b) and (c), it could be observed that, the ultimate positive and negative M_Y and U_X of girders due to positive

and negative thermal loads appear at the girder-ends near two abutments (C_{S-1L} and C_{S-3R}). The F_A , M_Y and U_X at the corresponding critical sections of Girder-L in different bridge types under thermal load ($\pm 40^\circ\text{C}$) are illustrated in Fig. 181(a), (b) and (c). For the U_Z of girders, the locations of the ultimate values in different bridge types are different. Therefore, the maximum vertical deflection and invert arch of Girder-L in different bridge types due to positive and negative thermal loads are compared in Fig. 181(d). The results indicate that the F_A and U_X at the critical sections of girders in different subtypes of FIABs are similar, as illustrated in Fig. 181(a) and (c). The ultimate M_Y and U_Z of girders in FIAB1 and FIAB2 are significantly larger than those in FIAB3 and FIAB4, as shown in Fig. 181(b) and (d).

6.1.2.2 Highway live load

The performance of girders in different bridge types under highway live load is compared in Fig. 182. It indicates that the F_{SZ} of girders in different bridge types are similar. However, the M_Y and U_Z of girders in different bridge types are different.



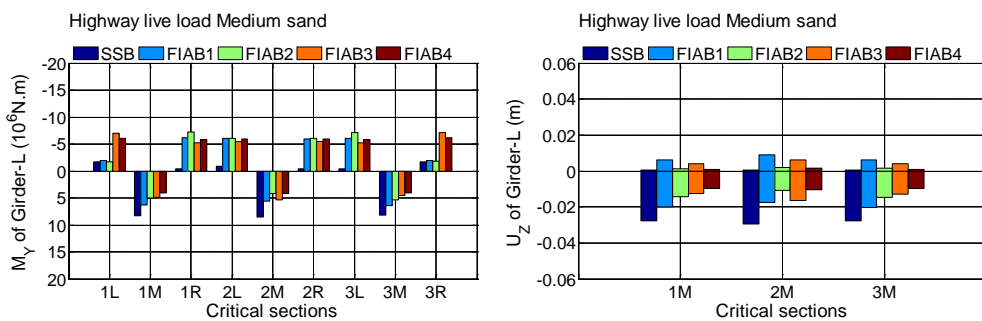
(a) M_Y of girders

(b) U_Z of girders

Fig. 182 Influence of different bridge types on the M_Y and U_Z of girders under highway live load

The Girder-L was chosen as the critical component. In order to investigate clearly the differences among the performance of girders in different bridge types under highway live load, some corresponding critical sections of Girder-L could be selected. For example, nine critical sections of Girder-L were chosen to analyze the M_Y of girders, including the positive M_Y at the mid-span points and the negative M_Y at the two girder ends of each span. For the vertical deflection of girder (U_Z), the mid-span points of each span should be considered as the critical sections. The M_Y and U_Z at the critical sections of Girder-L in different bridge types are compared in Fig. 183, which indicates that the M_Y and U_Z at the critical sections of Girder-L in different bridge types are different.

For the M_Y of girders under highway live load, the retrofit with the FIAB concept could reduce the positive M_Y at the mid-span points of each span. However, these retrofitting approaches increase the unfavorable negative M_Y at the both girder ends of each span. Considering the critical sections near abutments (C_{S-1L} and C_{S-3R}), the M_Y of girders in FIAB3 and FIAB4 after retrofitting are larger than those in FIAB1 and FIAB2. Moreover, considering the critical sections near piers (C_{S-1R} , C_{S-2L} , C_{S-2R} and C_{S-3L}), all the retrofitting methods increase the M_Y of girders subjected to highway live load a lot. The U_Z at the mid-span points of each span in SSB under highway live load could be reduced through retrofitting.



(a) M_Y of girders

(b) U_Z of girders

Fig. 183 Influence of different bridge types on the ultimate M_Y and U_Z of Girder-L under highway live load

6.1.2.3 Loads combination

From the investigation above, it could be found that no matter which external load case is considered, the M_Y and U_Z of girders in five bridge types are different. Therefore, two types of loads combinations listed in Table 48 were taken into account.

Loads combination	Load cases
Combination1	Highway live load + Thermal load ($\pm 15^\circ\text{C}$)
Combination2	Highway live load + Thermal load ($\pm 40^\circ\text{C}$)

Table 48

Loads combination of highway live load and thermal load

The influence of different bridge types on the M_Y of girders under two loads combinations are illustrated in Fig. 184. Comparing the M_Y of girders in FIABs with those in SSB, it could be found that the negative M_Y of girders in FIABs are larger.

The positive M_Y in some parts of girders in FIABs are larger than those in SSB. For example, the positive M_Y of girders at the left part of Span-1 and right part of Span-3 in FIAB1 and FIAB2 are larger than those in SSB. Furthermore, the positive M_Y at the parts of girders near both abutments in FIAB3 and FIAB4 could also exceed those in SSB. It could be observed that the adverse influence of retrofitting process on the M_Y of girders is mainly due to the thermal load. Therefore, with the thermal load changing from $\pm 15^\circ\text{C}$ to $\pm 40^\circ\text{C}$, the differences between the M_Y of girders in FIABs and those in SSB become larger. Moreover, the lengths of regions, in which the positive M_Y of girders in FIABs are larger than those in SSB, become longer.

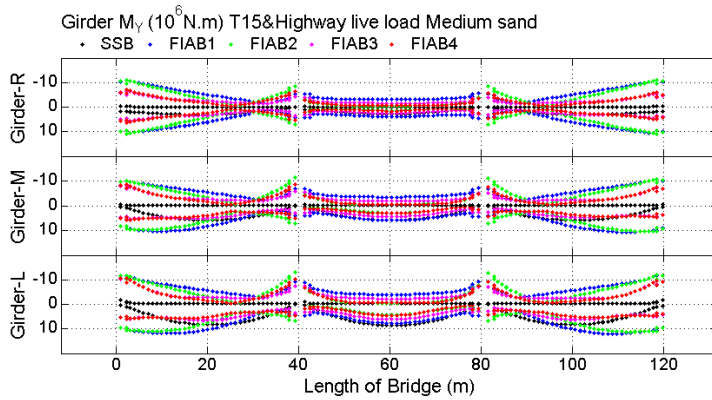
In order to find the appropriate retrofitting approach which can bring minimum adverse effect, the M_Y of girders in different subtypes of FIABs are sorted from maximum to minimum. It could be found that, under Combination1, the positive and negative M_Y of girders along Span-1 and Span-3 in FIAB3 and FIAB4 are less than those in FIAB1 and FIAB2, except the negative M_Y of girders near two abutments. The positive and negative M_Y of girders along Span-2 in FIAB2, FIAB3 and FIAB4 are less than those in FIAB1. Considering Combination2, the positive and negative M_Y of girders along Span-1 and Span-3 in FIAB3 and FIAB4 are less than those in FIAB1 and FIAB2. Moreover, the differences among the M_Y of girders in different subtypes of FIABs under Combination2 is larger than those under Combination1.

The U_z of girders in different bridge types under two loads combinations are illustrated in Fig. 184(c) and (d). It could be observed that the invert arches of whole girders and the vertical deflections in some parts of girders in FIABs are larger than those in SSB. For example, the vertical deflections of girders in Span-1 and Span-3 in FIAB1, and in the left part of Span-1 and right part of Span-3 in FIAB2 could exceed those in SSB. As introduced above, the U_z of girders in SSB caused by the highway live load could be reduced through retrofitting. Therefore, the unfavorable influence of retrofitting methods on the U_z of girders is mainly due to the thermal load. With the thermal load changing from $\pm 15^\circ\text{C}$ to $\pm 40^\circ\text{C}$, the differences between the U_z of girders in FIABs and those in the become larger. Moreover, the lengths of regions, in which the vertical deflections of girders in FIABs are larger than those in SSB, become longer.

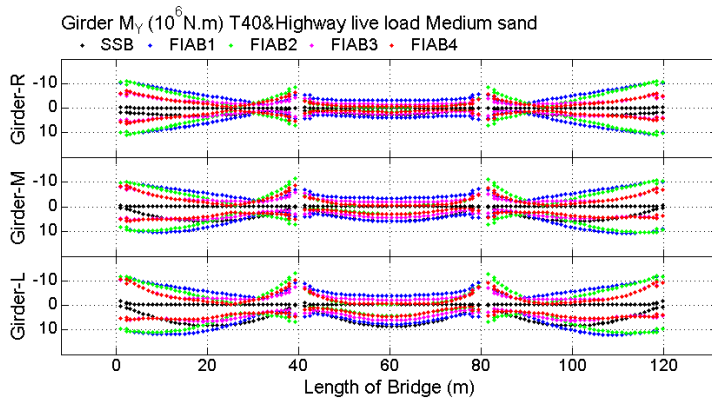
The U_z of girders in different subtypes of FIABs are sorted from maximum to minimum. It could be found that, considering two loads combinations, the vertical deflections and invert arches of girders along Span-1 and Span-3 could be sorted from maximum to minimum as FIAB1>FIAB2>FIAB3>FIAB4. However, the vertical deflections and invert arches of girders along Span-2 could be sorted from maximum

RETROFIT OF EXISTING BRIDGES WITH CONCEPT OF INTEGRAL ABUTMENT BRIDGE

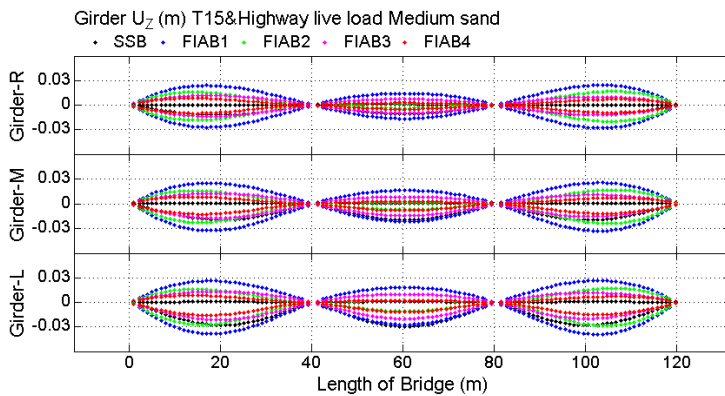
to minimum, as $FIAB1 > FIAB3 > FIAB2/FIAB4$.



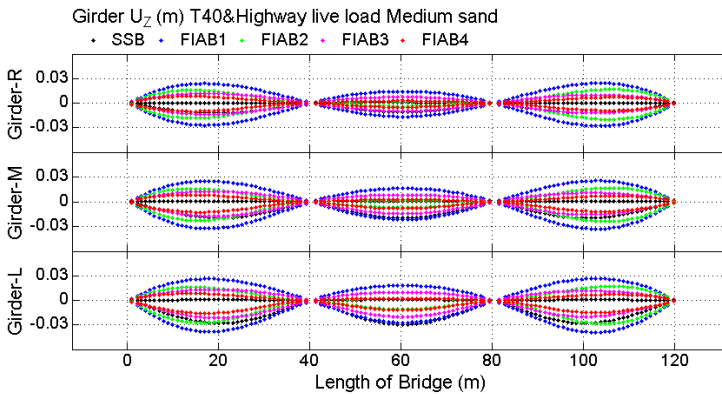
(a) M_Y of girders under Combination 1



(b) M_Y of girders under Combination 2



(c) U_Z of girders under Combination 1



(d) U_z of girders under Combination2

Fig. 184 Influence of different bridge types on the M_y and U_z of girders under the combination of highway live load and thermal load

6.1.3 Pier

6.1.3.1 Thermal load

The performance of piers in different bridge types under thermal load (-40°C) are illustrated in Fig. 185. It could be found that the F_{sx} , M_y and U_x of piers in FIABs are significantly larger than those in SSB. In order to investigate the differences among the performance of piers in different subtypes of FIABs, some critical sections were chosen. From Fig. 185(a), it could be observed that the F_{sx} of piers under thermal load is the same along the pier column. Therefore, the top points of two piers (C_{P-T}) could be chosen as the critical sections. The Fig. 185(b) indicates that the ultimate M_y of piers in FIAB1 and FIAB3 appear at the bottom points of two piers (C_{P-B}) because the links between the superstructure and piers are hinged connections. However, the ultimate M_y of piers in FIAB2 and FIAB4, which have rigid superstructure-pier connections, occur at the top points or the bottom points of two piers (C_{P-T} or C_{P-B}). Consequently, in order to analyze the differences among the M_y of piers in different subtypes of FIABs, the top points and bottom points of two piers (C_{P-T} or C_{P-B}) could be selected as the critical sections. From Fig. 185(c), it could be found that the ultimate U_x of piers under thermal load appear at the top points of two piers (C_{P-T}).

RETROFIT OF EXISTING BRIDGES WITH CONCEPT OF INTEGRAL ABUTMENT BRIDGE

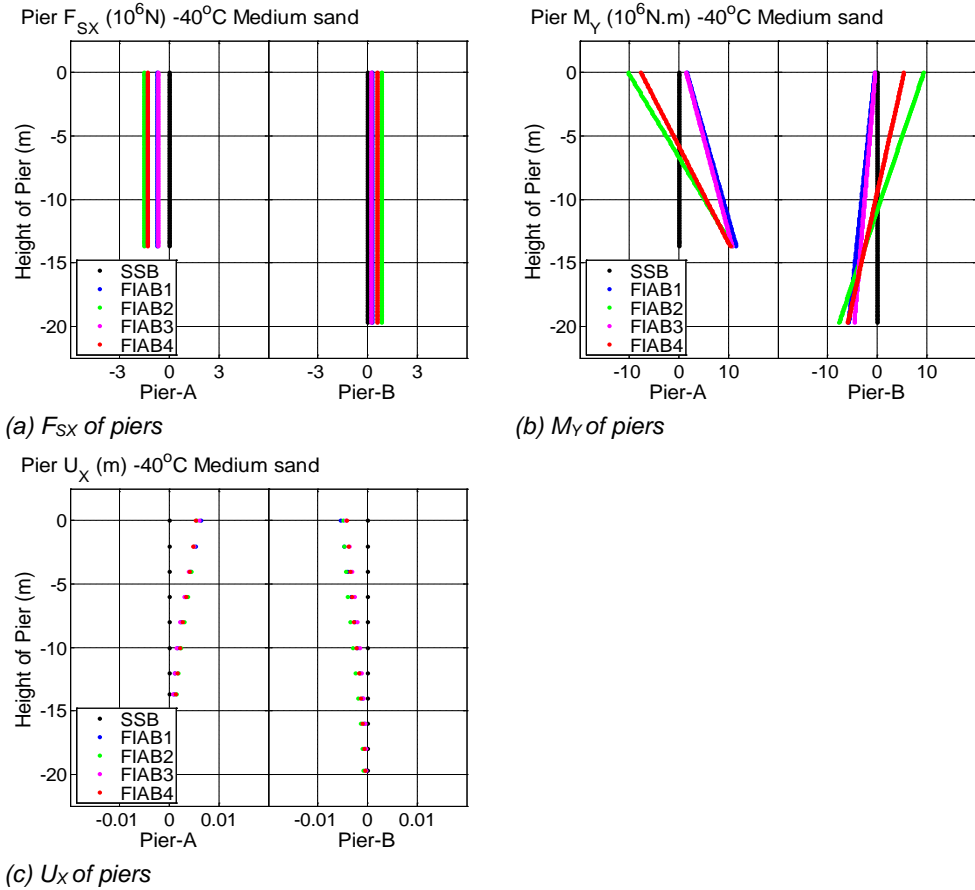
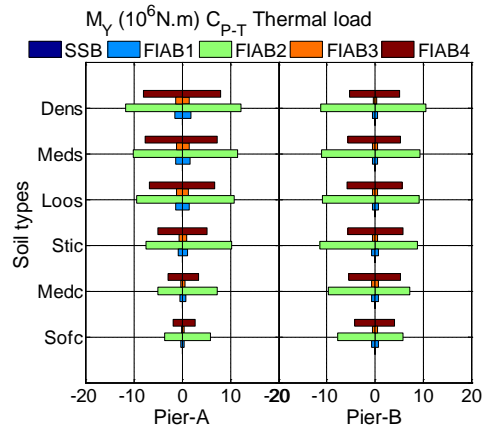
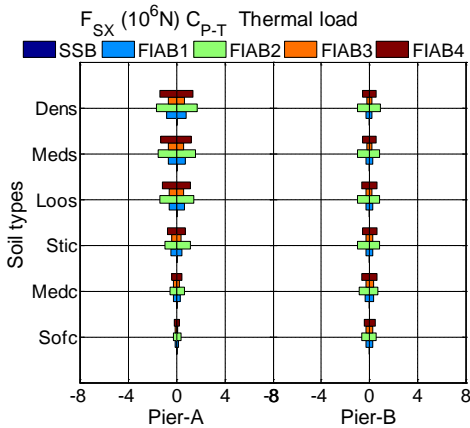


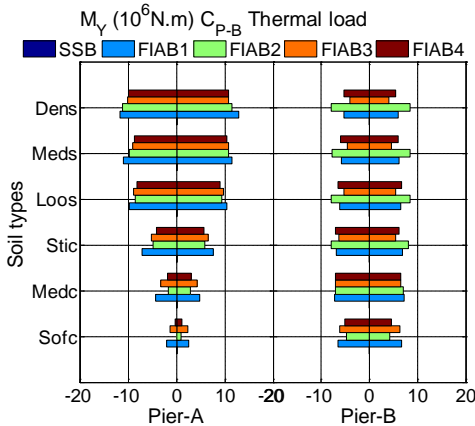
Fig. 185 Influence of different bridge types on the F_{SX} , M_Y and U_X of piers under thermal load ($-40^{\circ}C$)

The F_{SX} , M_Y and U_X at the critical sections of piers in different bridge types subjected to thermal load ($\pm 40^{\circ}C$) are compared in Fig. 186. It could be observed that, the differences among the U_X of piers in different subtypes of FIABs are small, as illustrated in Fig. 186(d). However, the F_{SX} and M_Y of piers in four subtypes of FIABs are different. When considering the thermal load, the ultimate F_{SX} and M_Y at C_{P-T} of piers in FIAB2 and FIAB4 are larger than those in FIAB1 and FIAB3. Moreover, for the M_Y at C_{P-B} of piers, the differences among different retrofitting approaches is not quite large, as shown in Fig. 186(c).

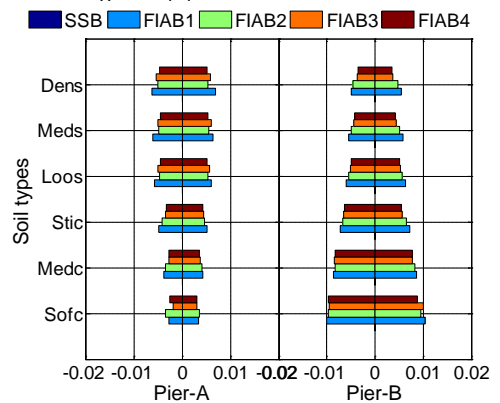


(a) F_{SX} at C_{P-T} of piers

(b) M_Y at C_{P-T} of piers



(c) M_Y at C_{P-B} of piers



(d) U_X at C_{P-T} of piers

Fig. 186 Influence of different bridge types on the ultimate F_{SX} , M_Y and U_X of piers under thermal load ($\pm 40^\circ C$)

6.1.3.2 Highway live load

In order to analyze the influence of different bridge types on the performance of piers subjected to highway live load, the M_Y of piers are illustrated in Fig. 187. It could be found that the M_Y along the pier columns in FIABs are different to those in SSB.

The top and bottom points of two piers, which can obtain the ultimate M_Y of piers in different bridge types, could be selected as the critical sections. The M_Y at the critical sections of piers in different bridge types under highway live load are compared in Fig. 188. It could be observed that the retrofitting solutions of FIAB2 and FIAB4 can amplify the M_Y at the top points of piers under highway live load, comparing with those in SSB. However, the M_Y at the critical sections of piers in FIAB1 and FIAB3

are less or equal to those in SSB.

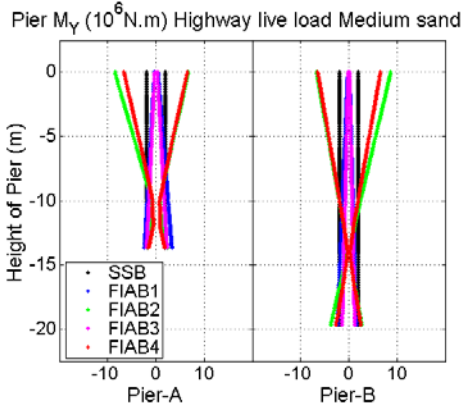


Fig. 187 Influence of different bridge types on the M_Y of piers under highway live load

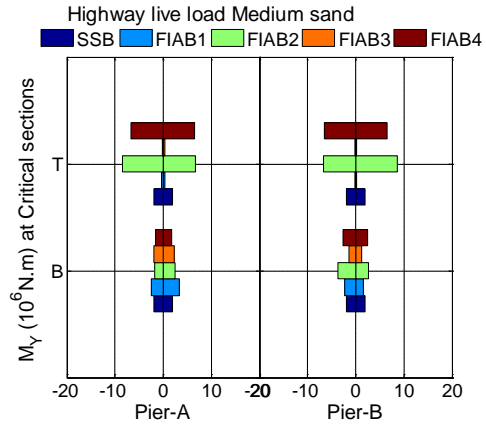
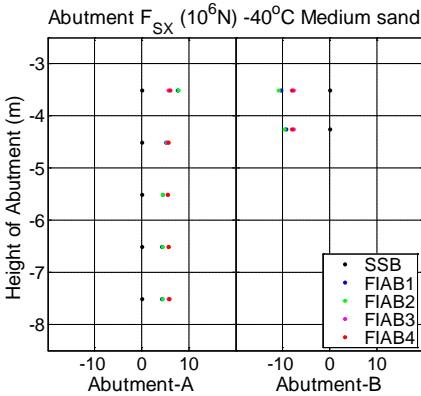


Fig. 188 Influence of different bridge types on the ultimate M_Y of piers under highway live load

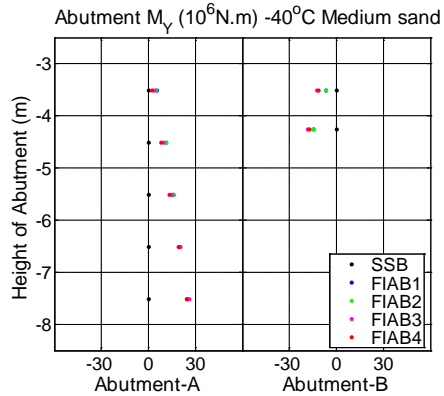
6.1.4 Abutment stem

6.1.4.1 Thermal load

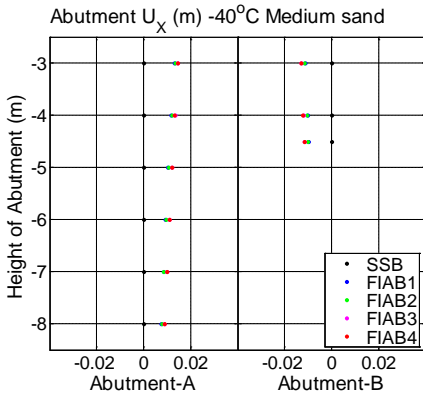
The performance of abutment stems in different bridge types subjected to thermal load (-40°C) are illustrated in Fig. 189. It could be found that the F_{SX} , M_Y and U_X of abutment stems in FIAB are significantly larger than those in SSB. From Fig. 189(a) and (c), it could be observed that, the ultimate F_{SX} and U_X of abutment stems in FIABs under thermal load could be found at the top points (C_{A-T}). However, the ultimate M_Y of abutment stems occur at the bottom points (C_{A-B}).



(a) F_{SX} of Abutment stems



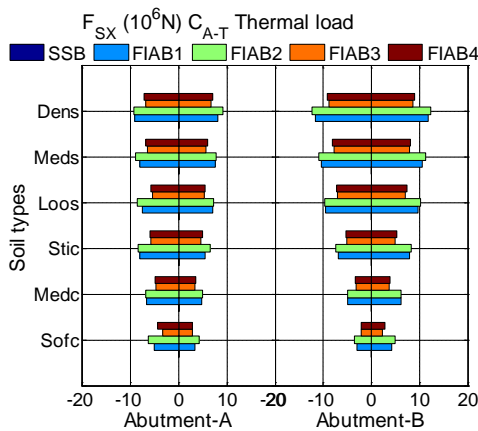
(b) M_Y of Abutment stems



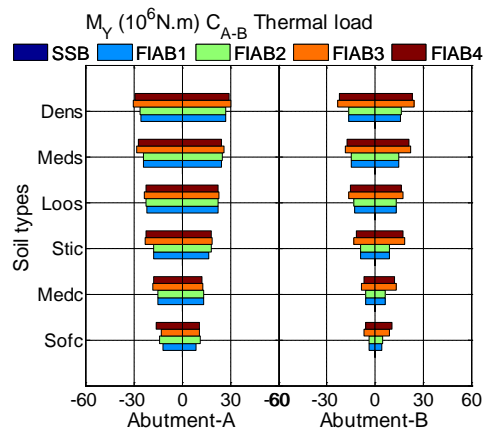
(c) U_x of Abutment stems

Fig. 189 Influence of different bridge types on the F_{SX} , M_Y and U_x of abutment stems under thermal load (-40°C)

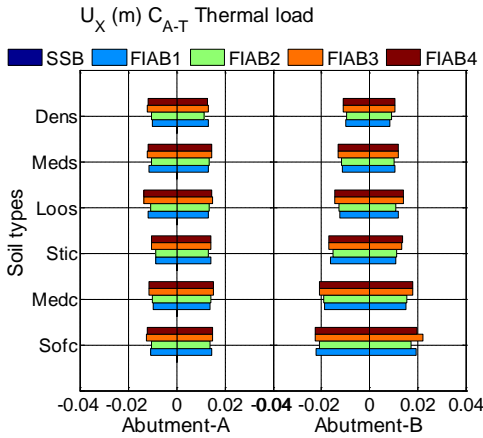
The F_{SX} , M_Y and U_x at the critical sections of abutment stems in different subtypes of FIABs subjected to thermal load ($\pm 40^\circ\text{C}$) are illustrated in Fig. 190. The comparisons indicate that the F_{SX} at C_{A-T} of abutment stems in FIAB3 and FIAB4 subjected to thermal load are slightly smaller than those in FIAB1 and FIAB2. On the contrary, the M_Y at C_{A-B} of abutment stems in FIAB3 and FIAB4 are slightly larger than those in FIAB1 and FIAB2. The U_x of abutment stems in different subtypes of FIABs are similar.



(a) F_{SX} at C_{A-T} of Abutment stems



(b) M_Y at C_{A-B} of Abutment stems



(c) U_x at C_{A-T} of Abutment stems

Fig. 190 Influence of different bridge types on the ultimate F_{sx} , M_y and U_x of abutment stems under thermal load ($\pm 40^\circ C$)

6.1.4.2 Highway live load

In order to analyze the influence of different bridge types on the performance of abutment stems under highway live load, the M_y of abutment stems are illustrated in Fig. 191. It could be found that the M_y of abutment stems in FIABs are larger than or equal to those in SSB. The M_y at the top points of abutment stems (C_{A-T}) in different bridge types under highway live load are compared in Fig. 192. It could be observed that the M_y at the top points of abutment stems in FIAB3 and FIAB4 under highway live load are larger than those in FIAB1 and FIAB2.

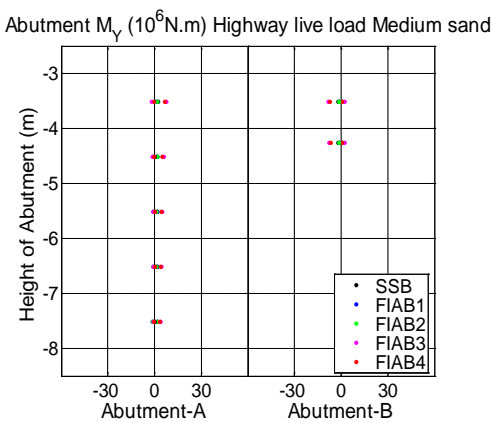


Fig. 191 Influence of different bridge types on the M_y of abutment stems under highway live load

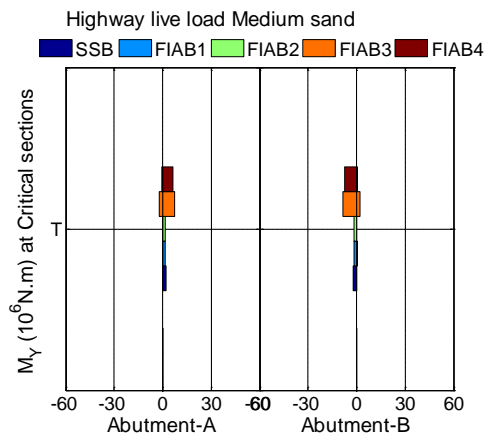
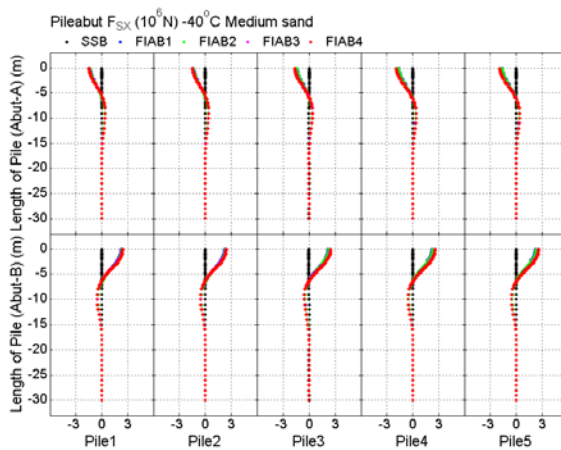
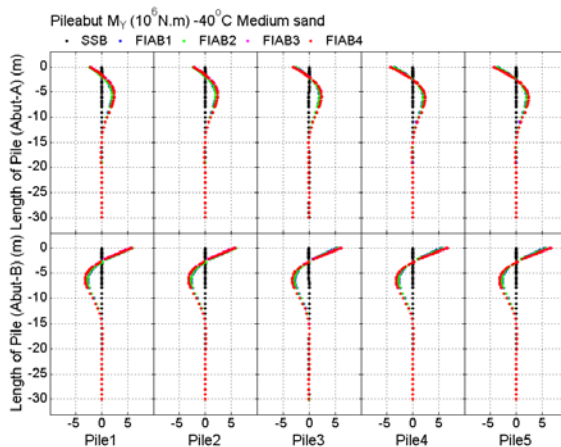


Fig. 192 Influence of different bridge types on the ultimate M_y of abutment stems under highway live load

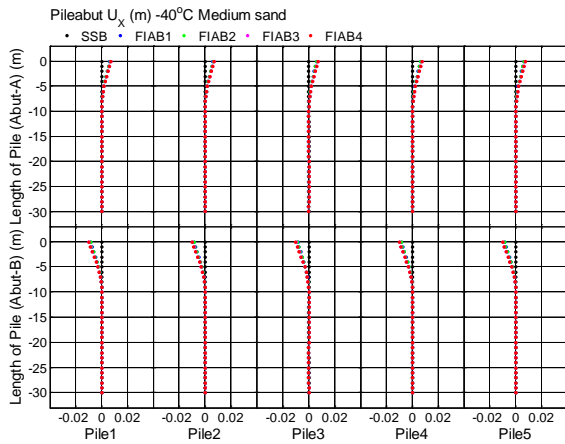
6.1.5 Pile

6.1.5.1 Thermal load

Under thermal load (-40°C), the performance of piles beneath abutments and piers in different bridge types are illustrated respectively in Fig. 193 and Fig. 194. It could be observed that the F_{Sx} , M_y and U_x of piles in FIABs are larger than those in SSB. By comparing Fig. 193 and Fig. 194, it could be found that the performance of piles beneath abutments subjected to thermal load is significantly larger than those of piles beneath piers. In 'Viadotto Serrone', the cross sections and the material properties of all piles are the same. Therefore, only the performance of piles beneath abutments under thermal load will be taken into account in this chapter.

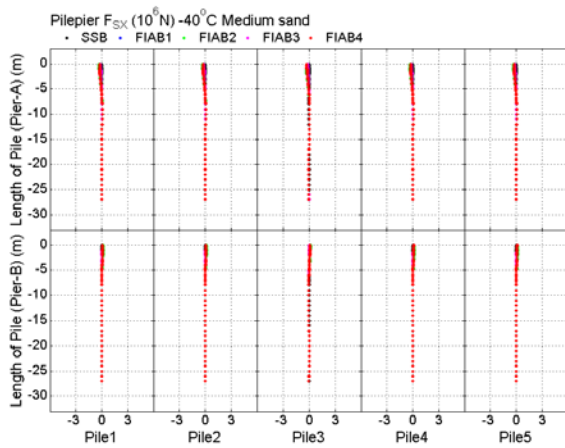
(a) F_{Sx} of piles(b) M_y of piles

RETROFIT OF EXISTING BRIDGES WITH CONCEPT OF INTEGRAL ABUTMENT BRIDGE

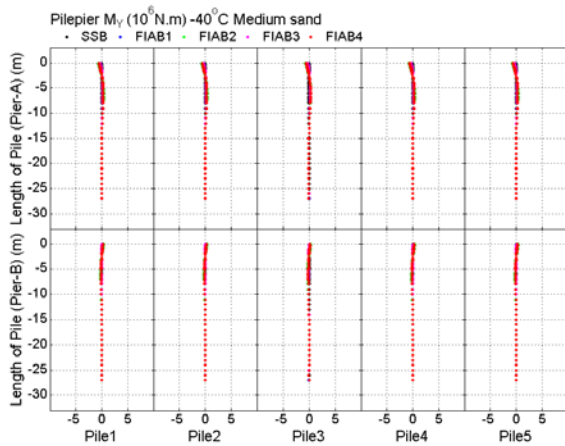


(c) U_x of piles

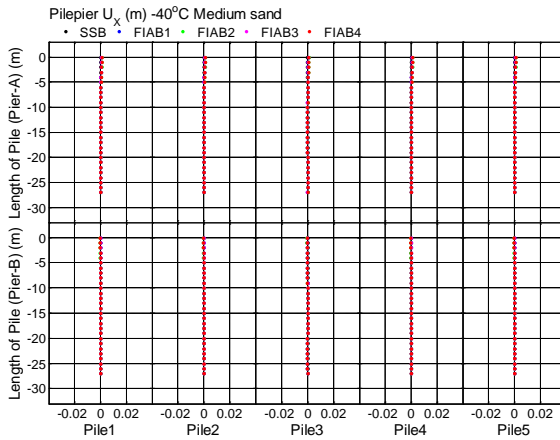
Fig. 193 Influence of different bridge types on the performance of piles beneath abutments under thermal load (-40°C)



(a) F_{sx} of piles



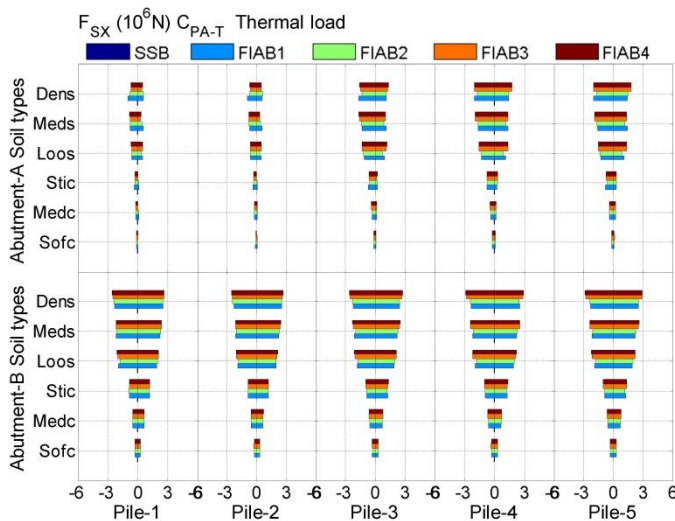
(b) M_y of piles



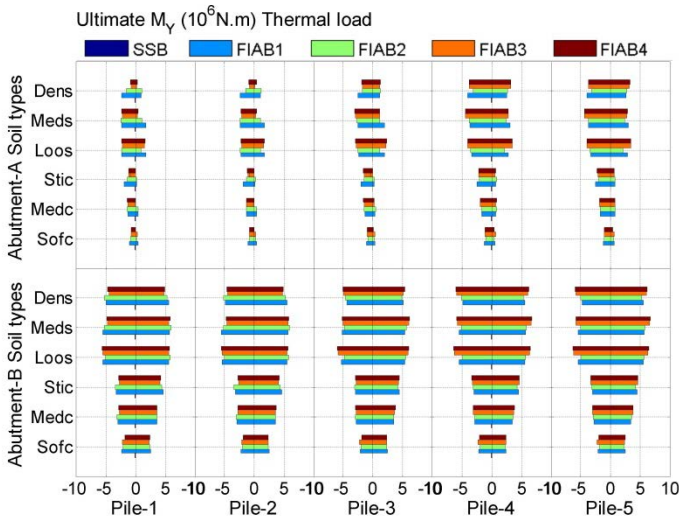
(c) U_x of piles

Fig. 194 Influence of different bridge types on the performance of piles beneath piers under thermal load (-40°C)

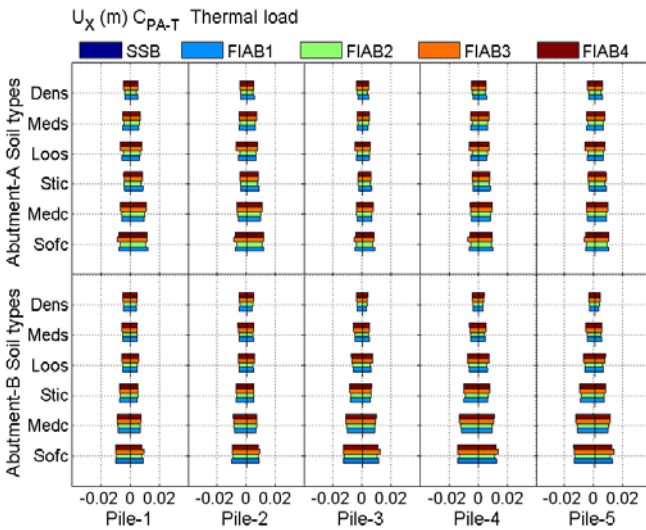
From Fig. 193(a) and (c), it could be found that, the ultimate F_{SX} and U_x of piles in different subtypes of FIABs under thermal load occur at the top points (C_{PA-T}). The position of the ultimate M_y of piles is not fixed, which could occur at two possible locations, including the top points and the points at a certain depth (about -5m when the soil is medium sand). The F_{SX} , M_y and U_x at the critical sections of piles in different subtypes of FIABs subjected to thermal load ($\pm 40^{\circ}\text{C}$) are compared in Fig. 195, which indicates that the differences among the performance of piles beneath abutments in four subtypes of FIABs subjected to the thermal load are quite small.



(a) F_{SX} at C_{PA-T} of piles



(b) Ultimate M_y of piles

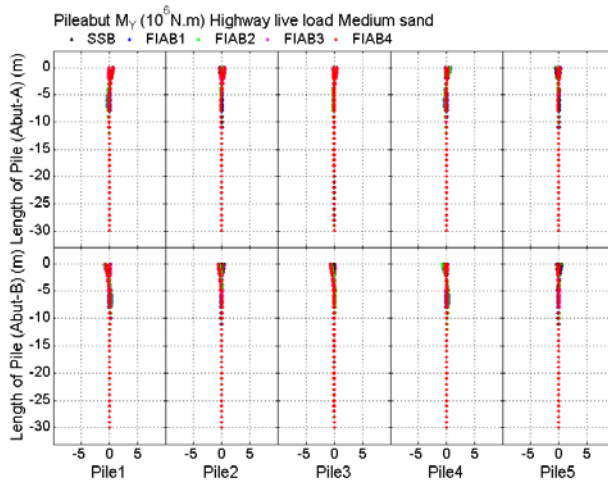
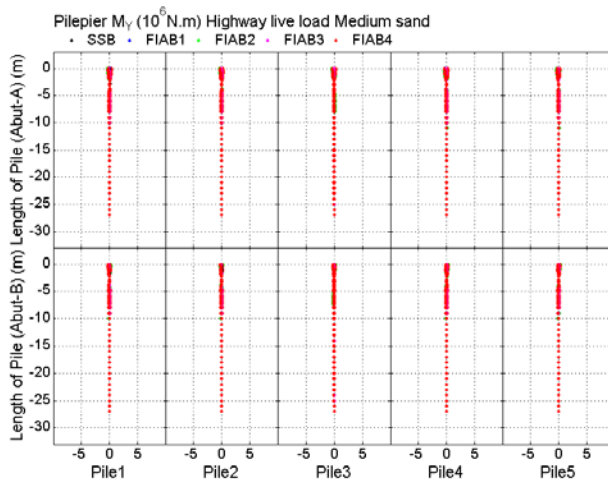


(c) U_x at C_{PA-T} of piles

Fig. 195 Influence of different bridge types on the ultimate F_{sx} , M_y and U_x of piles beneath abutments under thermal load ($\pm 40^\circ\text{C}$)

6.1.5.2 Highway live load

In order to analyze the influence of different bridge types on the performance of piles under highway live load, the M_y of piles beneath abutments and piers are illustrated respectively in Fig. 196(a) and (b). It could be found that under highway live load, the M_y of piles in all bridge types are quite small.

(a) M_y of piles beneath abutments(b) M_y of piles beneath piersFig. 196 Influence of different bridge types on the M_y of piles under highway live load

6.1.6 Summary

It is well known that, the difficulties of the retrofit on different bridge components depend on many factors. Therefore, the recommended retrofiting solution corresponding to different bridge components are proposed, which could help engineers to choose the most suitable one for different cases. In order to provide the guideline of choosing the suitable retrofiting approach, the adverse influence of different bridge types on the performance of different bridge components are sorted from maximum to minimum and listed in Table 49. If the retrofit of the girders in existing SSBs are difficult, FIAB3 or FIAB4 could be considered as the suitable retrofiting solutions. FIAB1 or FIAB3 could bring minimum unfavorable influence on

RETROFIT OF EXISTING BRIDGES WITH CONCEPT OF INTEGRAL ABUTMENT BRIDGE

piers. If the shear resistance of existing abutment stems is not enough, FIAB3 or FIAB4 could be chosen. Moreover, if the bending resistance of existing abutment stems is not enough, FIAB1 or FIAB2 could be suggested.

Component	Internal force	Different FIABs
Girder	F_A	FIAB1≈FIAB2≈FIAB3≈FIAB4
	M_Y at span1 or span3	FIAB1≈FIAB2>>FIAB3≈FIAB4
	M_Y at span2	FIAB1>>FIAB3>FIAB2≈FIAB4
	U_X	FIAB1≈FIAB2≈FIAB3≈FIAB4
	U_Z at span1 or span3	FIAB1>>FIAB2>FIAB3>FIAB4
	U_Z at span2	FIAB1>>FIAB3>FIAB2≈FIAB4
Pier	F_{SX} at C_{P-T}	FIAB2>FIAB4>>FIAB1≈FIAB3
	M_Y at C_{P-T}	FIAB2>FIAB4>>FIAB1≈FIAB3
	M_Y at C_{P-B}	FIAB1≈FIAB2≈FIAB3≈FIAB4
	U_X at C_{P-T}	FIAB1≈FIAB2≈FIAB3≈FIAB4
Abutment stem	F_{SX} at C_{A-T}	FIAB1≈FIAB2>>FIAB3≈FIAB4
	M_Y at C_{A-B}	FIAB3≈FIAB4>>FIAB1≈FIAB2
	U_X at C_{A-T}	FIAB1≈FIAB2≈FIAB3≈FIAB4
Pile	F_{SX} at C_{AP-T}	FIAB1≈FIAB2≈FIAB3≈FIAB4
	M_Y at C_{AP-T}	FIAB1≈FIAB2≈FIAB3≈FIAB4
	U_X at C_{AP-T}	FIAB1≈FIAB2≈FIAB3≈FIAB4

Table 49

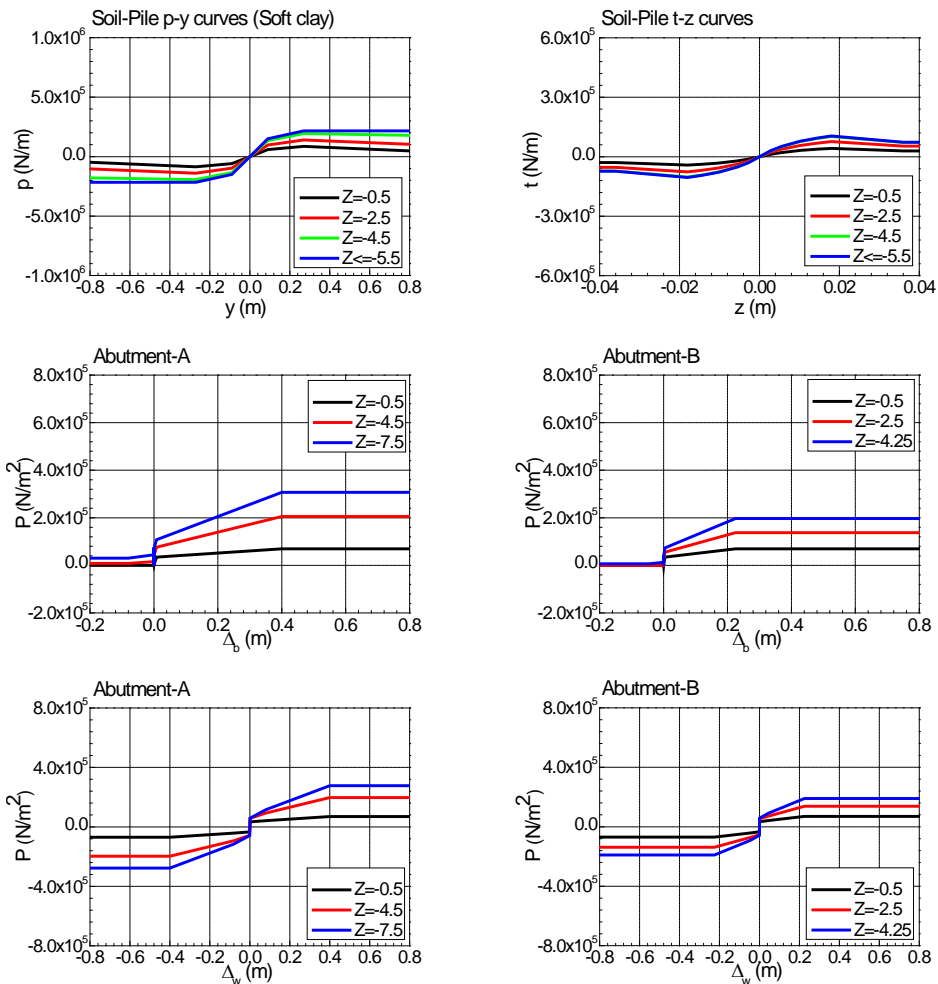
Adverse influence of different subtypes of FIABs on the performance of different bridge components (the symbol “≈”, “>” and “>>” denote respectively the differences between two FIABs can be neglected, is enough to pay attention to and is quite significant.).

6.2 Different soil conditions

According to the study in Section 5.4.3, it could be found that the soil-structure interaction of the IAB should be simulated by using the soil properties on site. For the backfill behind abutments, the natural soil must be excavated before the abutment construction and filled back with a certain type of soil chosen by engineers. However, the soil around piles is usually the original one on site. In this parametric analysis, the properties of the backfill behind abutments and the soil around piles were assumed the same. All soil types listed in Table 34 (p.165) were taken into account. Moreover, the soil distribution defined in Fig. 132 (p.166) was chosen. The NTC 2008 was chosen as the design code.

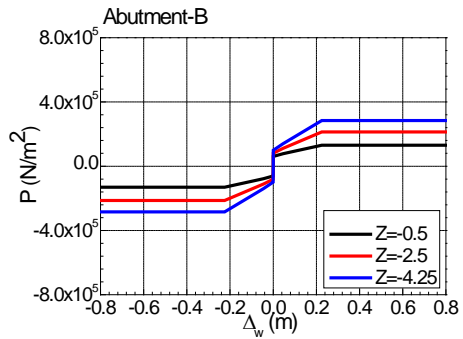
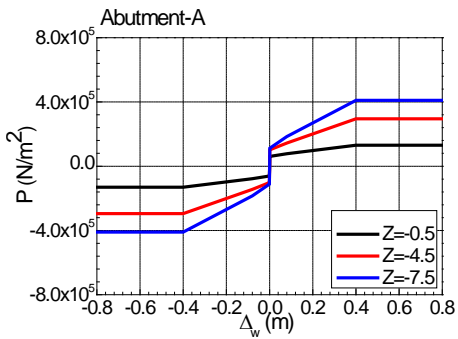
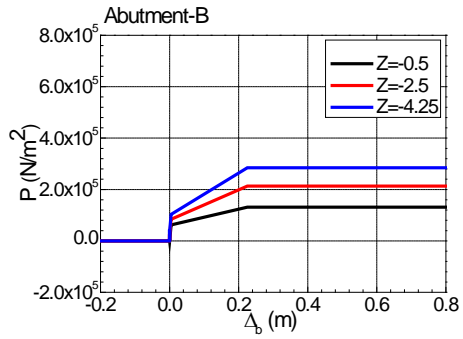
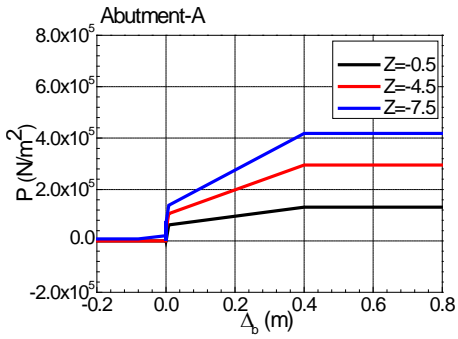
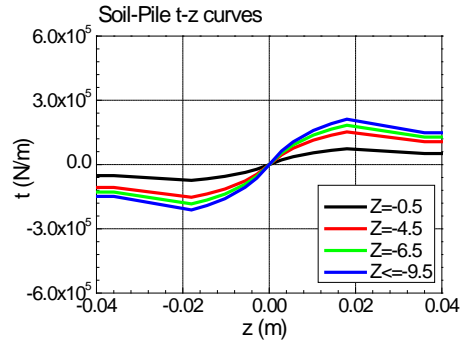
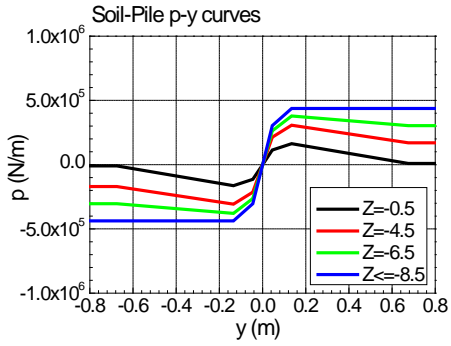
6.2.1 Soil-structure interaction

The soil-structure interaction of six types of soil corresponding to different depth, should be obtained firstly by using the soil properties listed in Table 34 (p.165), as illustrated in Fig. 197. As introduced in Section 5.2.3, the soil-abutment interaction can be represented by the lateral earth pressure-abutment movement relationship curve ($P-\Delta_b$ curve) and the lateral earth pressure-abutment wingwall movement relationship curve ($P-\Delta_w$ curve). The soil-pile interaction can be represented by the lateral earth pressure-pile displacement relationship curve ($p-y$ curve) and the vertical skin friction-pile settlement relationship curve ($t-z$ curve). These curves were used as the nonlinear properties of line springs and area springs in finite element models.

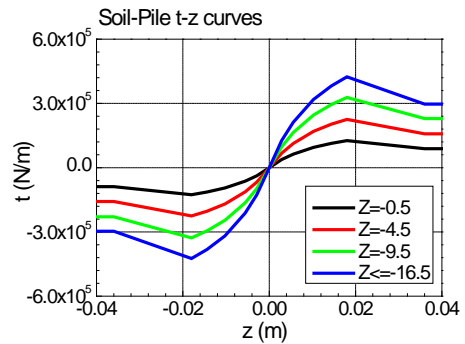
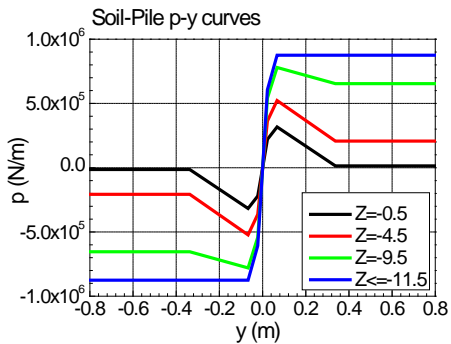


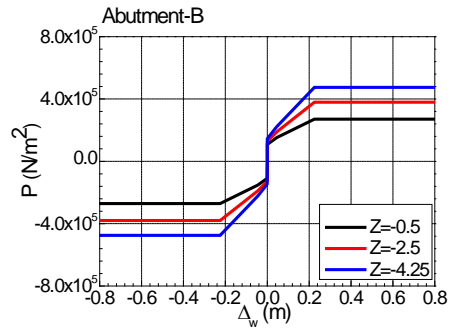
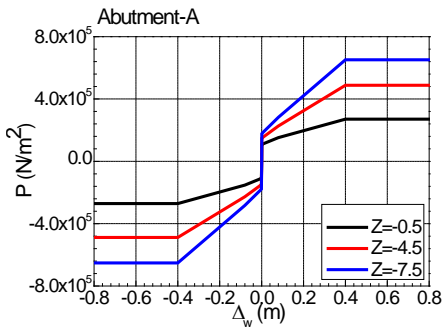
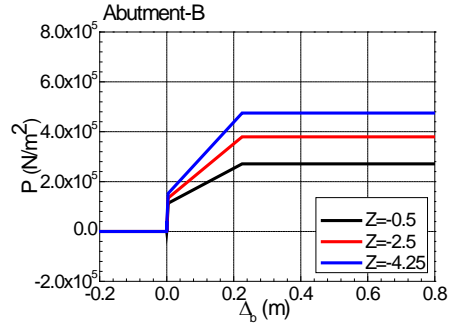
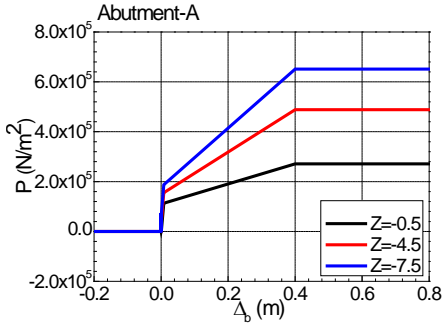
(a) Soft clay

RETROFIT OF EXISTING BRIDGES WITH CONCEPT OF INTEGRAL ABUTMENT BRIDGE

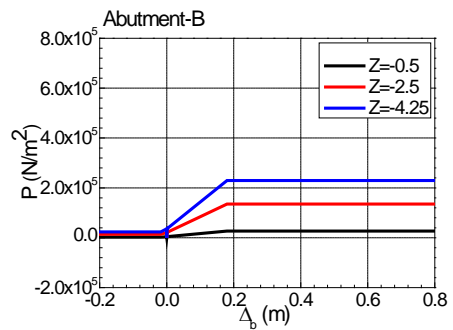
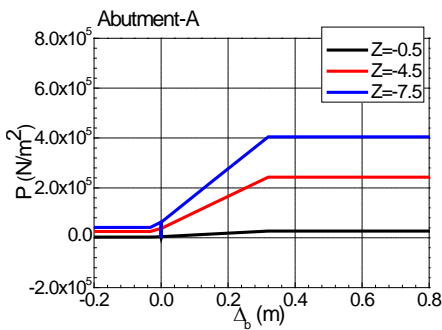
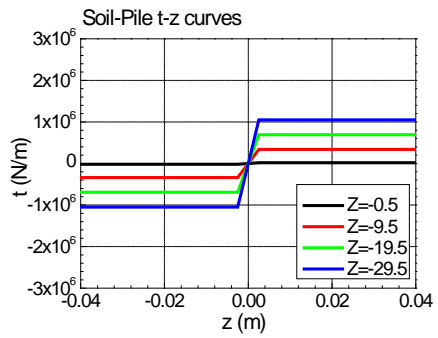
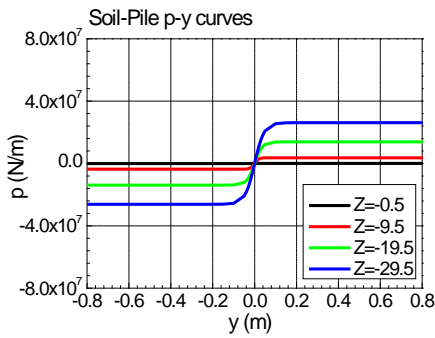


(b) Medium clay

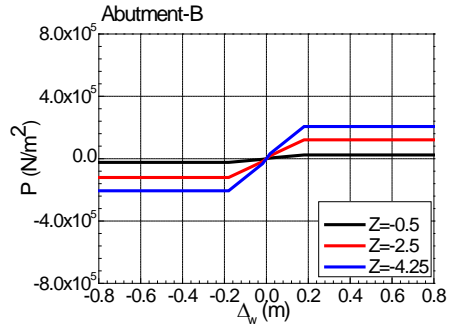
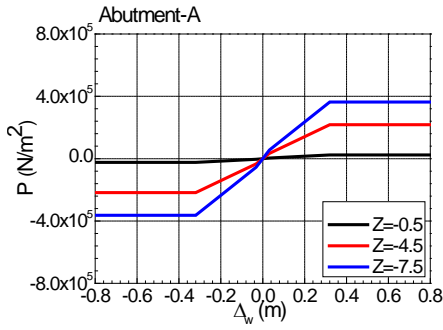




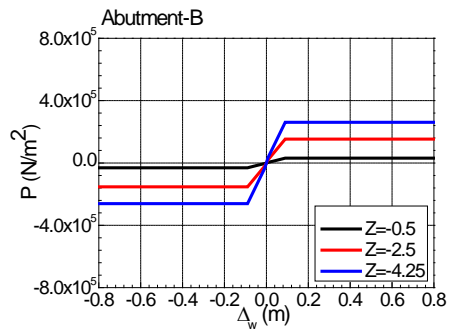
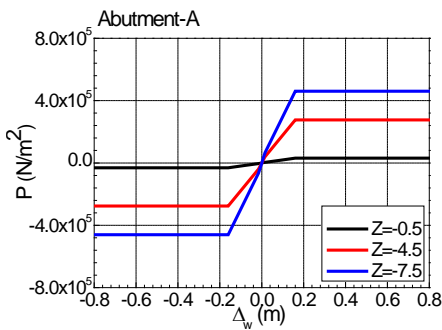
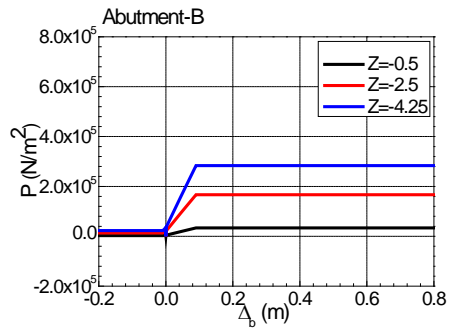
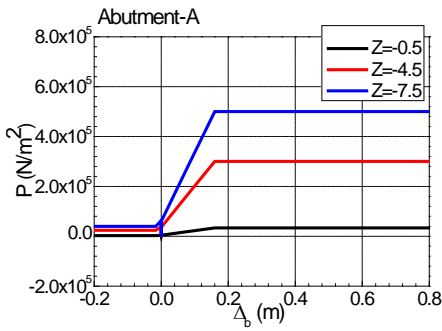
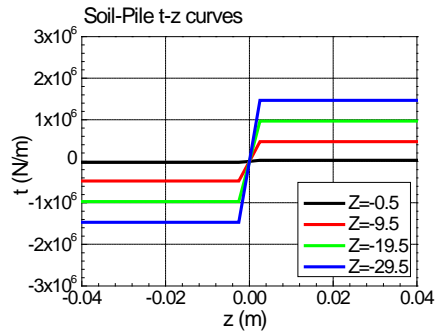
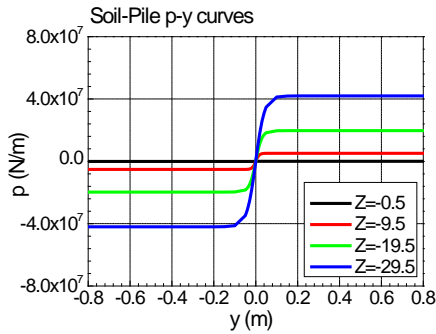
(c) Stiff clay



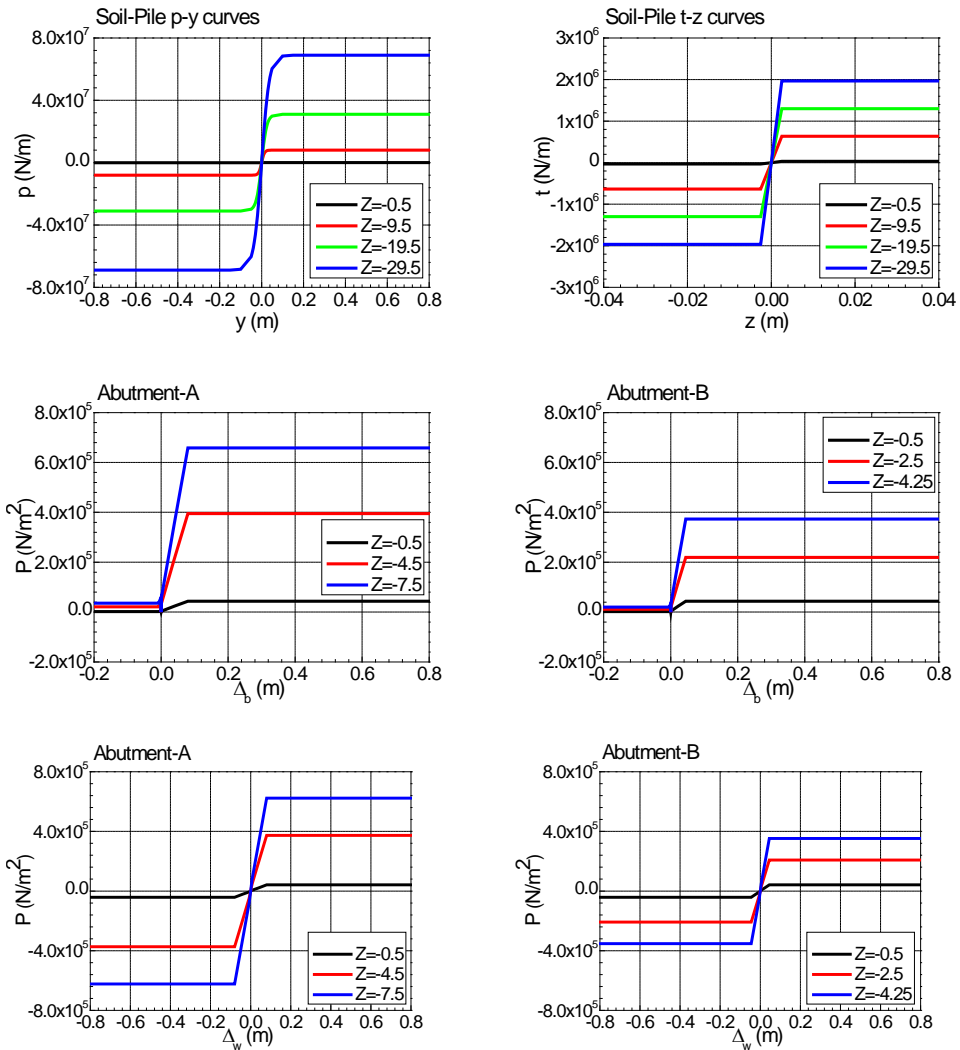
RETROFIT OF EXISTING BRIDGES WITH CONCEPT OF INTEGRAL ABUTMENT BRIDGE



(d) Loose sand



(e) Medium sand



(f) Dense sand

Fig. 197 Soil-structure interaction for six types of soil corresponding to different depth

The ultimate soil-structure interactions of six types of soil are compared in Fig. 198, including p-y curves, t-z curves, P- Δ_b curves and P- Δ_w curves. By comparison, it could be observed that, the ultimate soil pressures in the sand-pile displacement relationship curves are significantly larger than those in the clay-pile displacement relationship curves. Moreover, with the soil properties changing denser, the higher of the ultimate soil pressure could be achieved. By comparing different lateral earth pressure-abutment movement relationship curves corresponding to different soil conditions, it could be found that, with the soil properties becoming denser, the higher of the ultimate soil pressure could be reached. However, the relationship between the ultimate soil pressures in the sand-abutment-B movement relationship

curves and those in the clay-abutment movement relationship curves is not obvious.

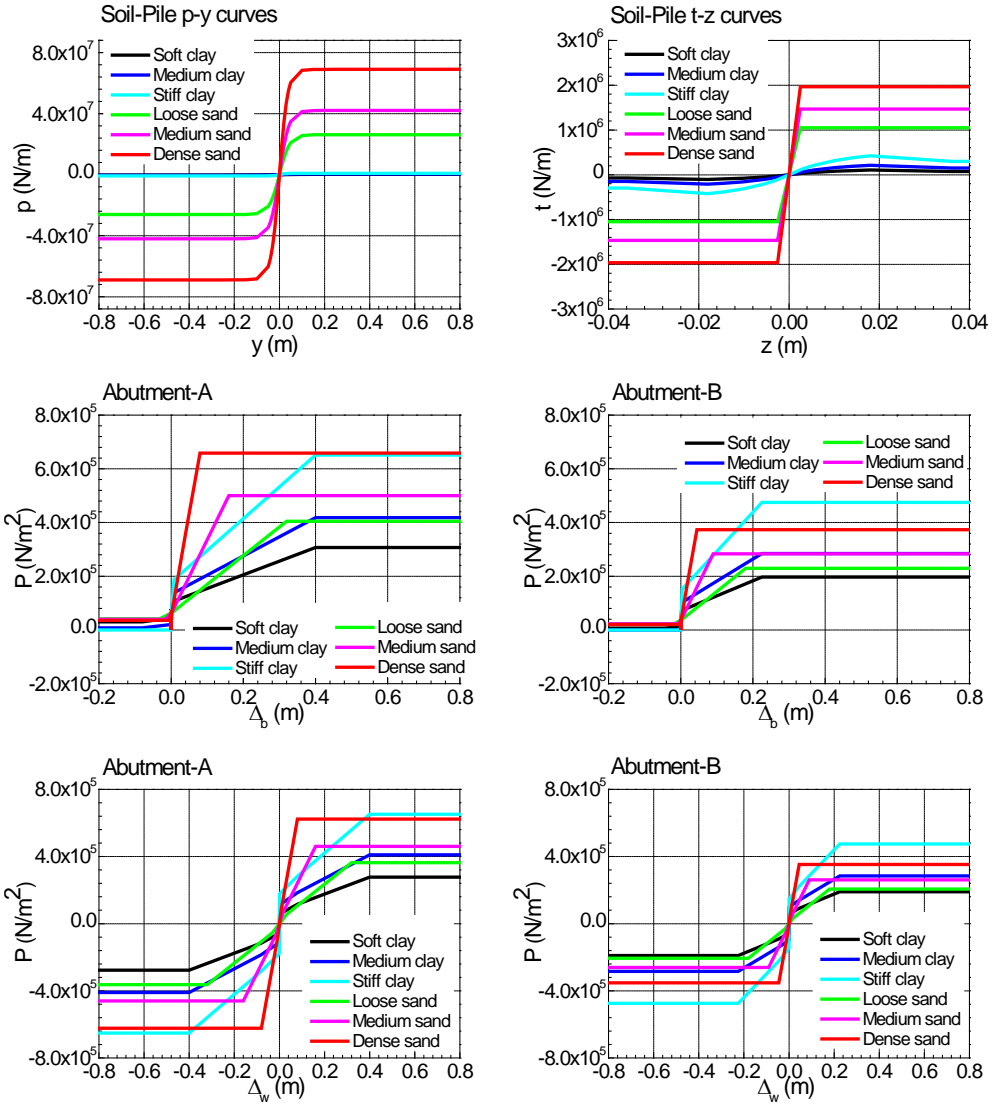
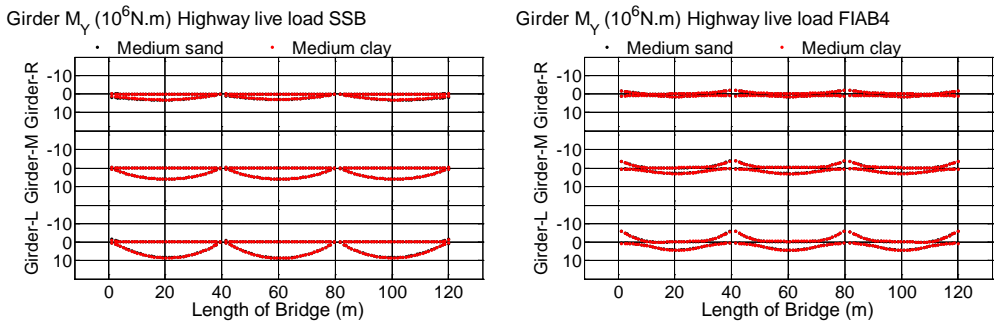


Fig. 198 Ultimate soil-structure interaction for six types of soil

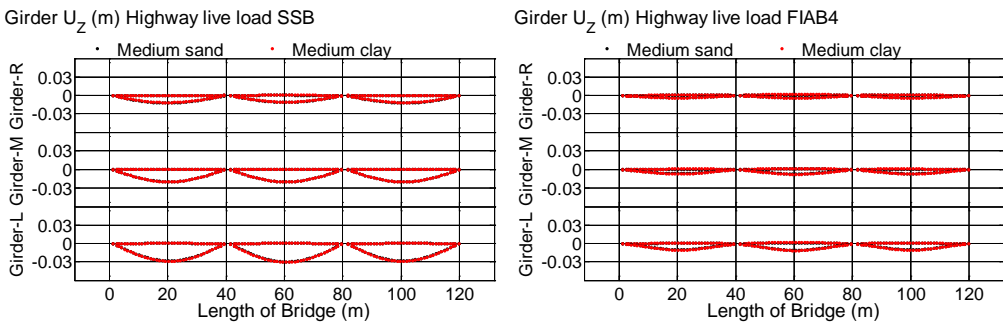
6.2.2 Vertical load case

In order to analyze the influence of different soil conditions on the performance of bridges subjected to vertical load, the highway live load simulated by moving load function implemented in Sap2000 (Computers and Structures Inc, 2011) was chosen. Due to the space limitation, only the influence of medium sand and medium clay, on the M_y and U_z of girders in SSB and FIAB4 under highway live load are illustrated in

Fig. 199. It could be found that the influence of different soil conditions is negligible. Consequently, the effects of different soil conditions can be neglected when considering vertical load cases.



(a) M_y of girders



(b) U_z of girders

Fig. 199 Influence of different soil conditions on the M_y and U_z of girders in SSB and FIAB4 under highway live load

6.2.3 Horizontal load case

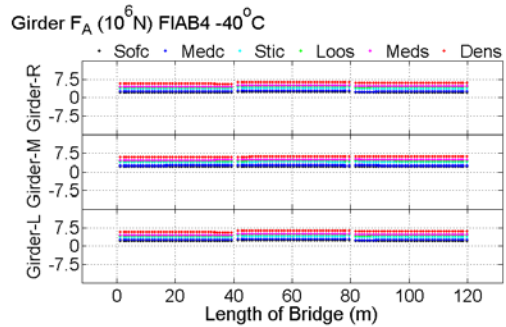
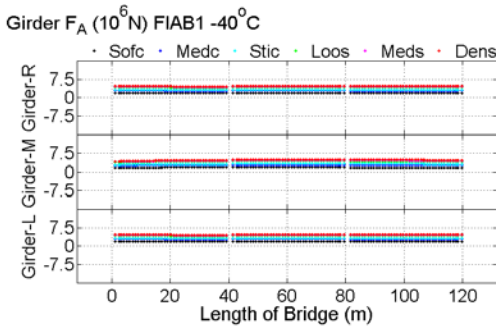
As discussed above, the thermal load is the most important horizontal load case, which must be taken into account. According to previous researches, it could be found that, there is no influence of different soil conditions on the performance of the SSB under thermal load. Therefore, only the performance of different bridge components in FIAB1 and FIAB4 under thermal load (-40°C) are illustrated in this section.

6.2.3.1 Girder

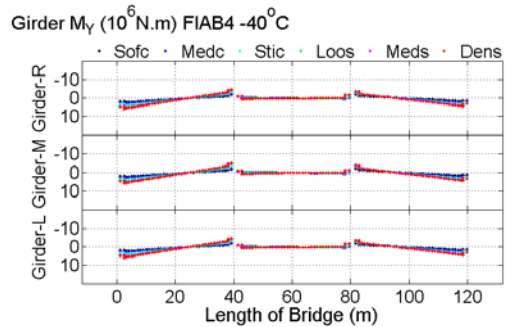
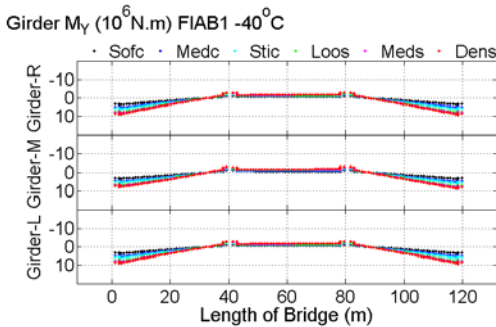
The influence of different soil conditions on the performance of girders in FIAB1 and

RETROFIT OF EXISTING BRIDGES WITH CONCEPT OF INTEGRAL ABUTMENT BRIDGE

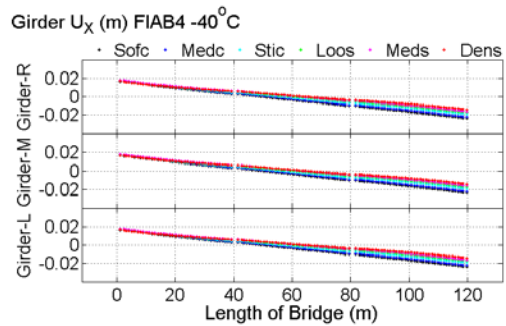
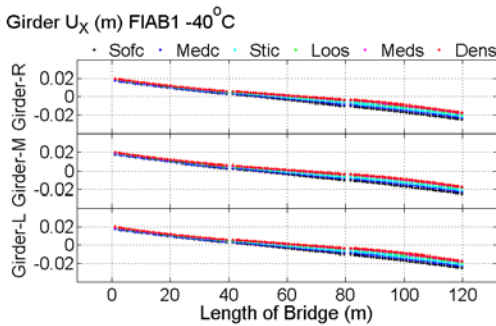
FIAB4 under thermal load (-40°C) are compared in Fig. 200. From the elevation view, the main girders of 'Viadotto Serrone' can be divided by the global coordinate axis Y at the mid-span point of span2 into the left and right parts. When considering the thermal load, the performance of girders at the left part is not the same as that at the right part due to some reasons. One reason is the different heights of two abutment stems, which can produce different soil-abutment interactions, as shown in Fig. 197. The other reason is the different heights of two piers in this case, as illustrated in Fig. 113 (p.160).



(a) F_A of girders



(b) M_Y of girders



(c) U_X of girders

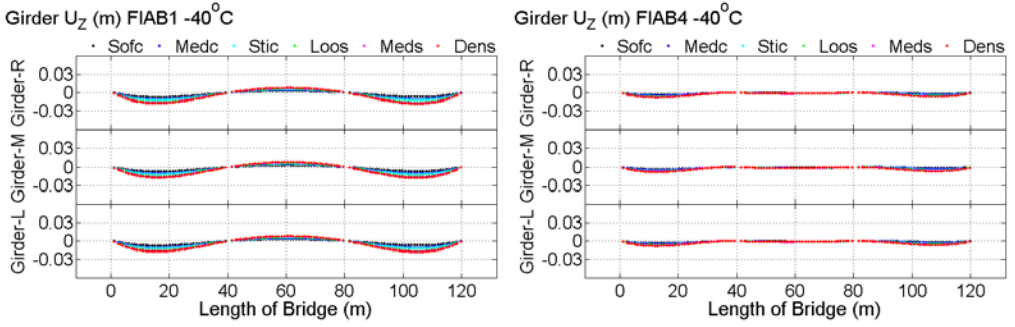
(d) U_z of girders

Fig. 200 Influence of different soil conditions on the performance of girders under thermal load (-40°C)

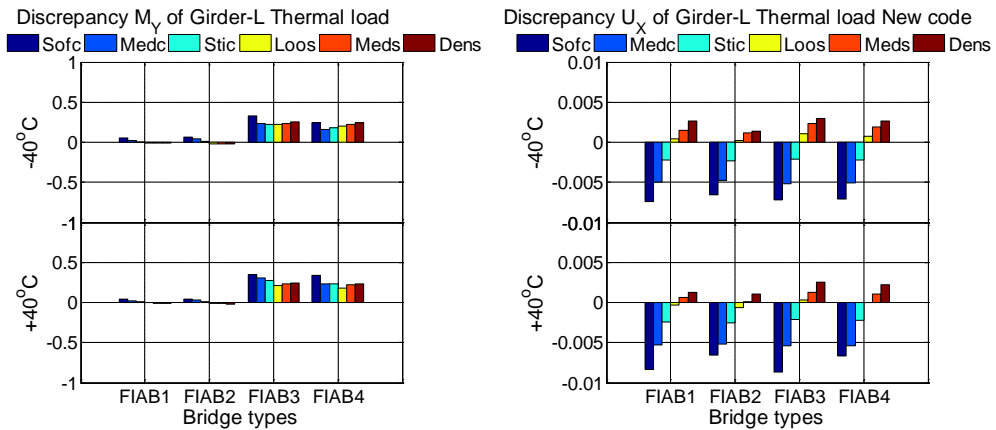
The Girder-L was chosen as the critical component. For the F_A of girders, the mid-span point of Span-2 (C_{S-2M}) was chosen as the critical section. From Fig. 200(b) and (c), it could be observed that the M_Y and U_X of girders near two abutments (C_{S-1L} and C_{S-3R}) reach the ultimate value. For the U_Z of girders, the maximum vertical deflection and invert arch of Girder-L in different bridge types due to positive and negative thermal load were selected.

In order to find out the locations of the ultimate M_Y and U_X of girders corresponding to different soil conditions, the discrepancies which can be calculated by formula (154) are illustrated in Fig. 201. The positive value means that the M_Y and U_X of girders near the abutment with higher height is larger than those near the abutment with lower height, and vice versa. From Fig. 201(a), it could be found that the M_Y of girders near the higher abutment in FIAB3 and FIAB4 are equal to or larger than those near the lower abutment. The Fig. 201(b) indicates that, when the soil condition is sand, the ultimate U_X of girders occur at the critical section near the higher abutment; however, the differences between the ultimate U_X of girders at two critical sections are less than 0.003m, which can be neglected. When the soil condition is clay, the ultimate U_X of girders appear at the critical section near the lower abutment. Consequently, the M_Y at C_{S-1L} and the U_X at C_{S-3R} could be chosen in the following analysis.

$$\text{For forces: } D_V = \left(\left| V_{C_{S-1L}} \right| - \left| V_{C_{S-3R}} \right| \right) / \left| V_{C_{S-1L}} \right| \quad (154)$$

$$\text{For displacements: } D_V = \left| V_{C_{S-1L}} \right| - \left| V_{C_{S-3R}} \right|$$

RETROFIT OF EXISTING BRIDGES WITH CONCEPT OF INTEGRAL ABUTMENT BRIDGE



(a) M_Y of Girder-L

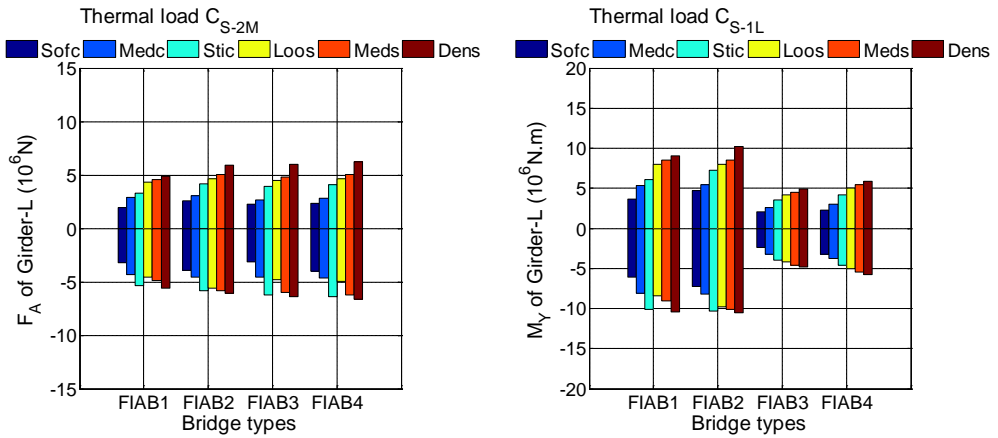
(b) U_X of Girder-L

Fig. 201 Influence of different soil conditions on the differences between the M_Y and U_X at two critical sections of Girder-L under thermal load ($\pm 40^\circ\text{C}$)

Considering different soil conditions, the ultimate F_A , M_Y , U_X and U_Z of Girder-L under thermal load ($\pm 40^\circ\text{C}$) are compared in Fig. 202. It could be found that under thermal load, the F_A , M_Y and U_Z of girders increase with the soil properties changing from soft to dense for both soil types. The ultimate value can be obtained when the soil condition is dense sand. When the thermal load is negative, the positive F_A , M_Y and negative U_Z of girders with the soil condition of clay are smaller than those with the soil condition of sand. It is because that, the active lateral soil pressure behind abutments is quite small corresponding to the passive lateral soil pressure. Therefore, the earth pressure-pile displacement relationship can play an important role in the horizontal resistance force of soil. Moreover, the ultimate soil pressure in the lateral earth pressure-pile displacement relationship would increase, when the soil properties changing from soft clay to dense sand, as illustrated in Fig. 198 (p.244). However, when considering the positive thermal load, the F_A , M_Y and U_Z of girders with the soil condition of stiff clay should be paid attention to, which may be larger than those with the soil condition of loose sand or medium sand. The cause of this phenomenon is that, the passive lateral soil pressure behind abutments is quite large subjected to positive thermal load. Furthermore, the relationship between the ultimate soil pressures in the sand-abutment movement relationship curves and those in the clay-abutment movement relationship curves is not obvious, as illustrated in Fig. 198 (p.244).

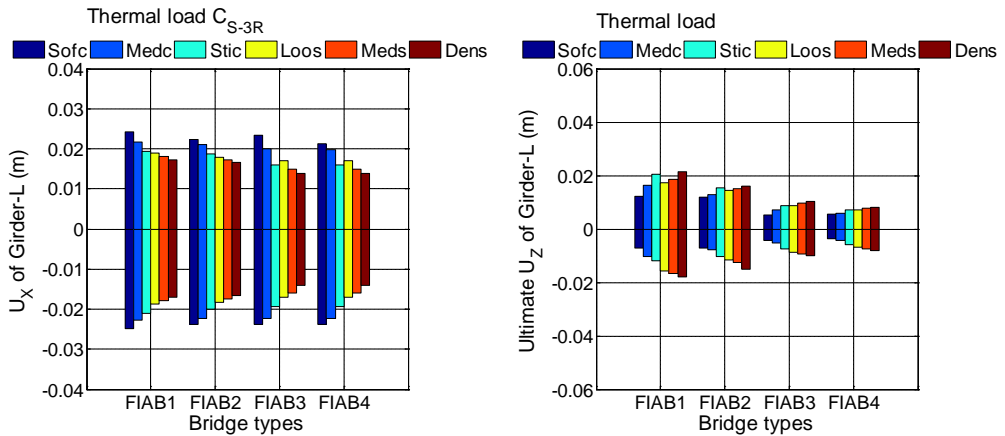
The maximum U_X of girders under thermal load appear at C_{S-3R} of Girder-L considering the soil type as soft clay. Moreover, it could be observed that, the U_X at C_{S-3R} of Girder-L decrease with the soil conditions changing from soft clay to dense

sand.



(a) F_A of Girder-L

(b) M_Y of Girder-L



(c) U_X of Girder-L

(d) U_Z of Girder-L

Fig. 202 Influence of different soil conditions on the ultimate F_A , M_Y , U_X and U_Z of Girder-L under thermal load ($\pm 40^\circ C$)

The total expansion and contraction of Girder-L corresponding to positive and negative thermal variations can be calculated by formula (155), as illustrated in Fig. 203. The larger of the U_X can be achieved with the softer of the soil condition on site. It could be also found that the influence of the negative thermal load on the lateral movement of girders is always larger than the effect of the positive thermal load, which is also indicated in previous studies (Lan, 2012). It is due to the fact that the passive lateral earth pressure behind abutments is significantly larger the active lateral earth pressure, corresponding to the same movement, as illustrated in Fig. 135 (p.167).

$$U_{X-SUM} = U_X(C_{S-1L}) - U_X(C_{S-3R}) \tag{155}$$

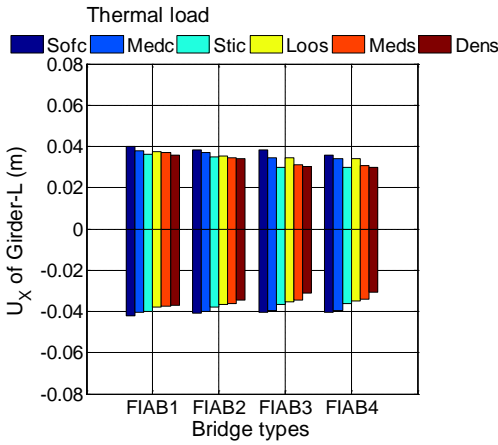
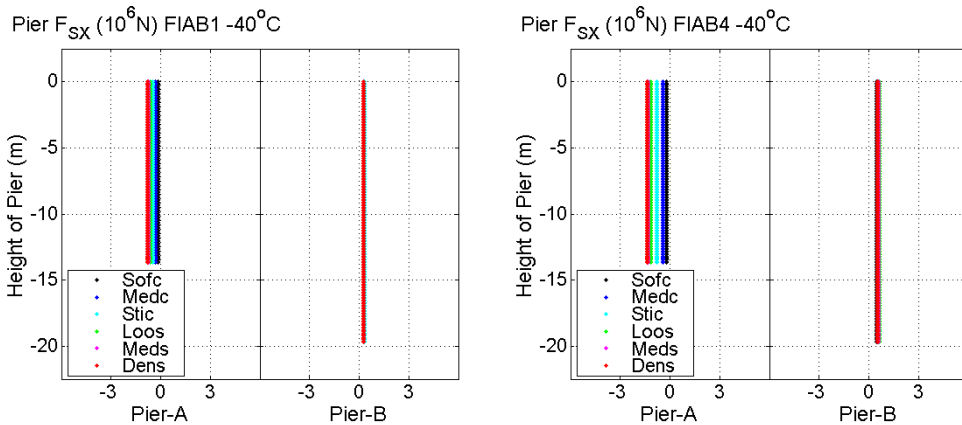


Fig. 203 Influence of different soil conditions on the expansion and contraction of Girder-L under thermal load ($\pm 40^{\circ}C$)

6.2.3.2 Pier

The influence of different soil conditions on the performance of piers in FIAB1 and FIAB4 under thermal load ($-40^{\circ}C$) are compared in Fig. 204. From Fig. 204, it could be observed that the influence of different soil conditions on the U_x of Pier-B is larger than those of Pier-A. However, the effects of different soil conditions on the F_{sx} and M_y of Pier-B are smaller than those of Pier-A. It is because the height of Pier-B is higher than that of Pier-A.



(a) F_{sx} of piers

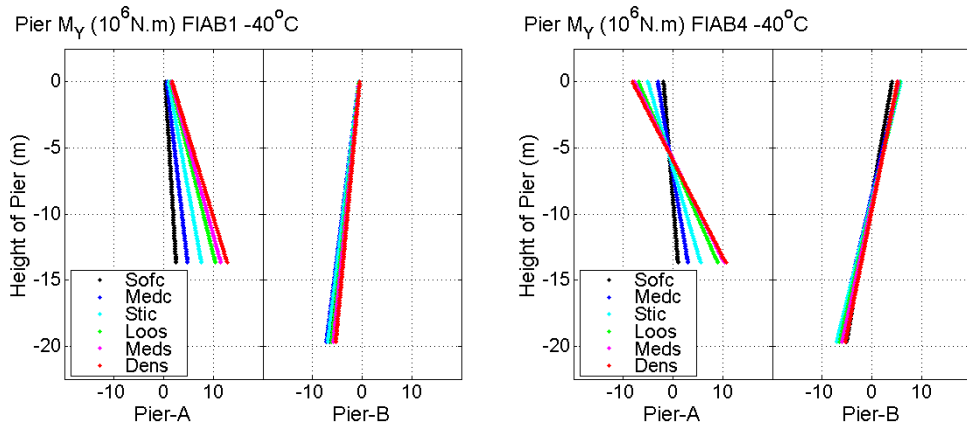
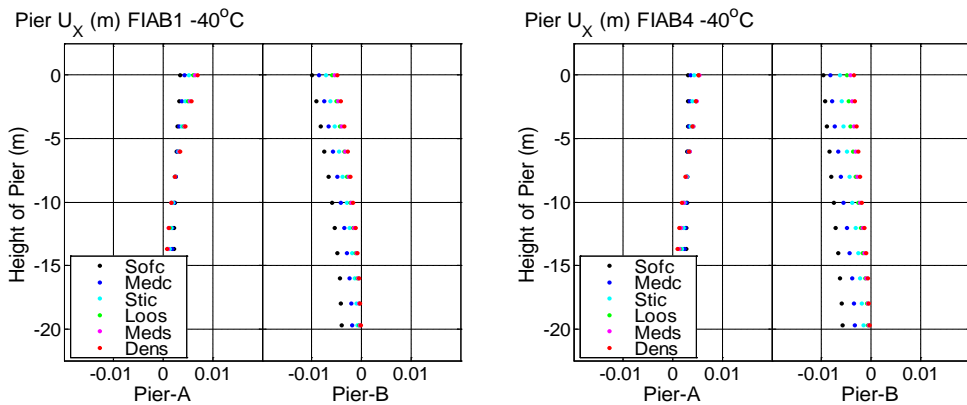
(b) M_Y of piers(c) U_X of piers

Fig. 204 Influence of different soil conditions on the performance of piers under thermal load (-40°C)

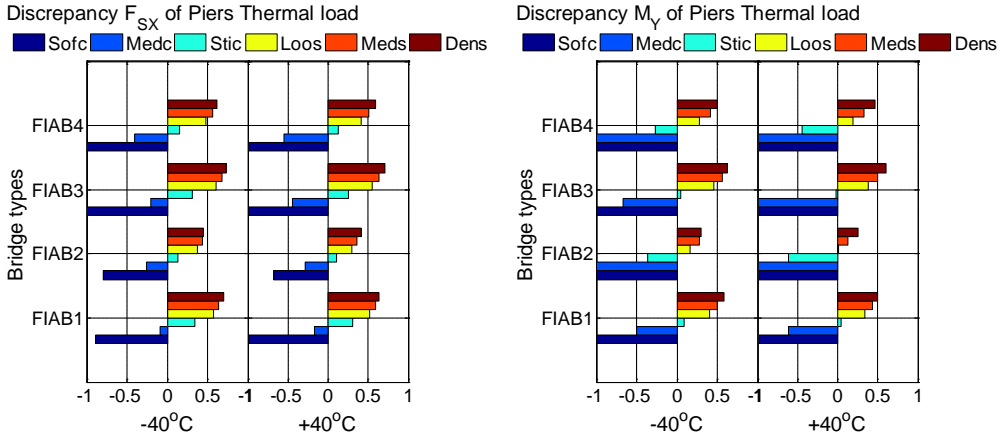
In order to find out the differences between the effects of different soil conditions on the performance of Pier-A and Pier-B subjected to thermal load, the M_Y at the bottom points (C_{P-B}), and the F_{SX} and U_X at the top points (C_{P-T}) of two piers are compared. The discrepancies, which can be calculated by formula (156), are illustrated in Fig. 205. The positive value represents that the ultimate F_{SX} , M_Y and U_X at the critical sections of the shorter pier (Pier-A) is larger than those of the longer one (Pier-B), and vice versa. From Fig. 205(a), it could be found, when the soil condition is sand and stiff clay, the ultimate F_{SX} occur at the top of Pier-A; however, when the soil condition is soft clay and medium clay, the ultimate values appear at the top of Pier-B. When the soil condition is sand, the ultimate M_Y occur at the bottom of Pier-A; however, when the soil condition is clay, the ultimate values appear at the bottom of Pier-B. For the U_X at C_{P-T} of piers, the ultimate values in Pier-A are larger than those in Pier-B when the soil condition is sand; however, the differences are quite small

RETROFIT OF EXISTING BRIDGES WITH CONCEPT OF INTEGRAL ABUTMENT BRIDGE

(less than 0.003m), which can be neglected. Therefore, the ultimate U_x at C_{P-T} of Pier-B could be chosen to carry out the further research.

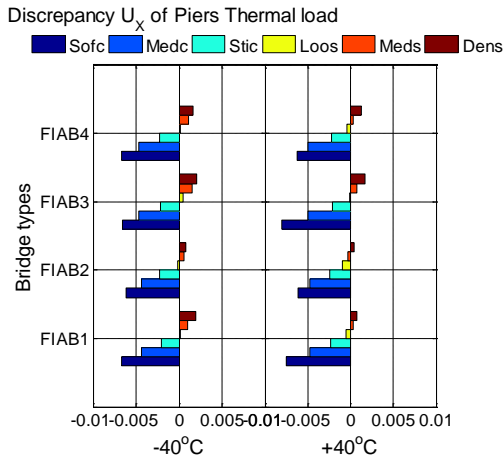
For forces: $D_V = (|V_{Pier-A}| - |V_{Pier-B}|) / |V_{Pier-A}|$ (156)

For displacements: $D_V = |V_{Pier-A}| - |V_{Pier-B}|$



(a) F_{SX} of piers

(b) M_Y of piers

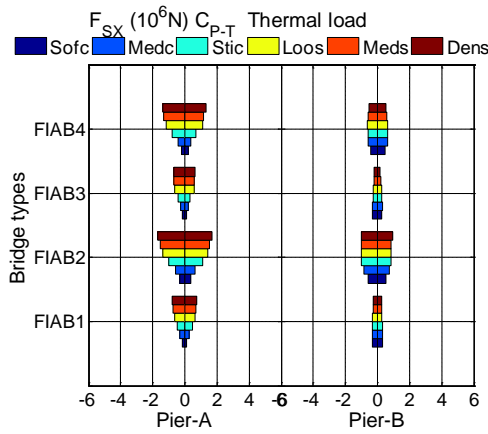


(c) U_x of piers

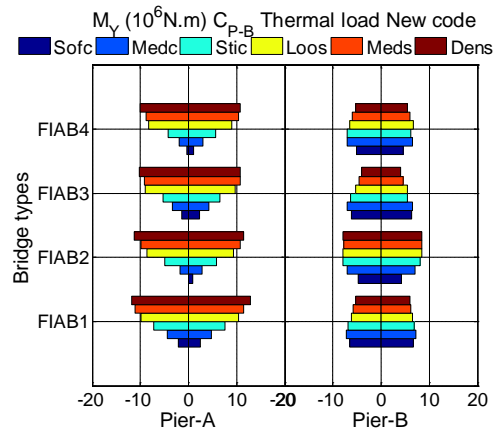
Fig. 205 Influence of different soil conditions on the differences between the F_{SX} , M_Y and U_x at the critical sections of two piers under thermal load ($\pm 40^\circ\text{C}$)

The ultimate F_{SX} , M_Y and U_x of piers under thermal load considering different soil conditions are illustrated in Fig. 206. It could be found that the ultimate F_{SX} and M_Y of piers occur in Pier-A, when considering the soil condition as dense sand. However,

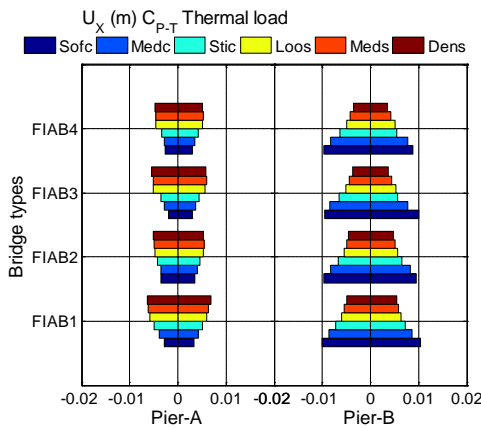
the maximum U_x of piers appear at the top point of Pier-B with the soil condition of soft clay.



(a) F_{Sx} of piers



(b) M_Y of piers



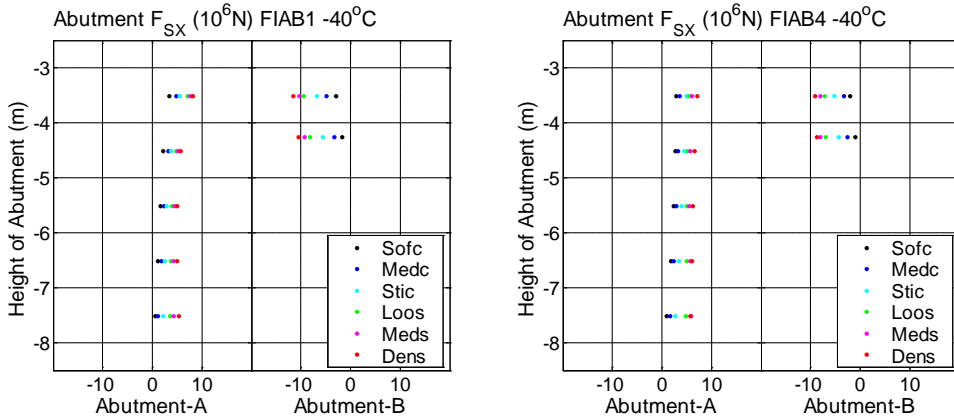
(c) U_x of piers

Fig. 206 Influence of different soil conditions on the ultimate F_{Sx} , M_Y and U_x of two piers under thermal load ($\pm 40^\circ\text{C}$)

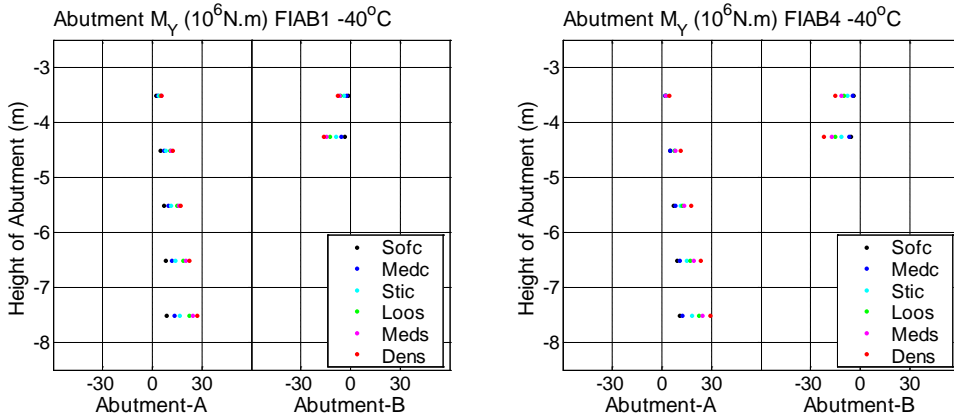
6.2.3.3 Abutment stem

The influence of different soil conditions on the performance of abutment stems in FIAB1 and FIAB4 under thermal load (-40°C) are compared in Fig. 207.

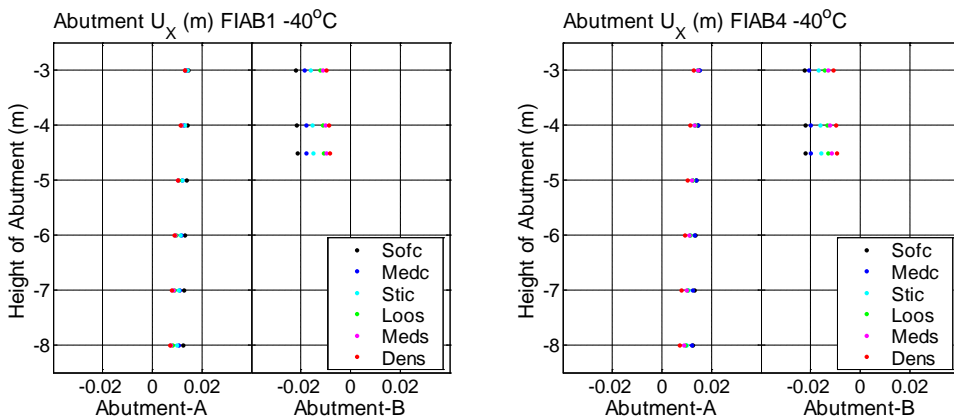
RETROFIT OF EXISTING BRIDGES WITH CONCEPT OF INTEGRAL ABUTMENT BRIDGE



(a) F_{SX} of Abutment stems



(b) M_Y of Abutment stems



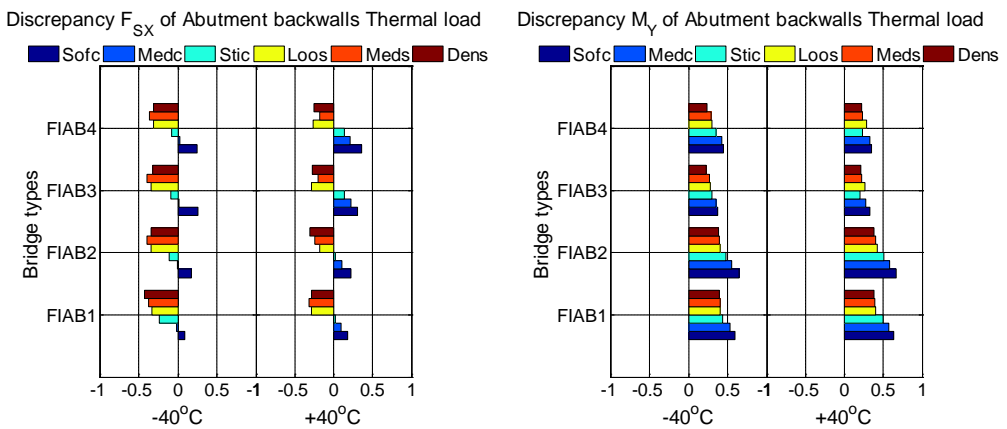
(c) U_X of Abutment stems

Fig. 207 Influence of different soil conditions on the performance of abutment stems under thermal load (-40°C)

In order to find out the differences between the effects of different soil conditions on the performance of Abutment-A and Abutment-B subjected to thermal load, the F_{SX} and U_X at the top points (C_{A-T}) and the M_Y at the bottom points (C_{A-B}) of abutment stems can be selected as the critical sections. The discrepancies, which can be calculated by formula (157), are illustrated in Fig. 208. The positive value represents the ultimate F_{SX} , M_Y and U_X at the critical sections of the abutment with higher stem (Abutment-A) is larger than those of the abutment with lower stem (Abutment-B), and vice versa. From Fig. 208, it could be observed that, when the soil condition is soft clay and medium clay, the ultimate F_{SX} occur at the stem top in Abutment-A; however, when the soil condition is sand, the ultimate values appear at the stem top in Abutment-B. Considering all soil conditions, the M_Y at the stem bottom in Abutment-A is larger than those in Abutment-B. For the U_X of abutment stems, when the soil condition is sand, the ultimate values occur at the stem top in Abutment-A; however, the differences between two abutment stems are less than 0.003m, which can be neglected. Therefore, when the soil condition is clay, the ultimate values appear at the stem top in Abutment-B.

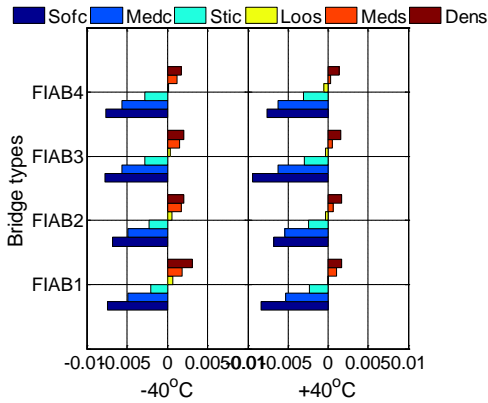
$$\text{For forces: } D_V = (|V_{Abutment-A}| - |V_{Abutment-B}|) / |V_{Abutment-A}| \quad (157)$$

$$\text{For displacements: } D_V = |V_{Abutment-A}| - |V_{Abutment-B}|$$

(a) F_{SX} of Abutment stems(b) M_Y of Abutment stems

RETROFIT OF EXISTING BRIDGES WITH CONCEPT OF INTEGRAL ABUTMENT BRIDGE

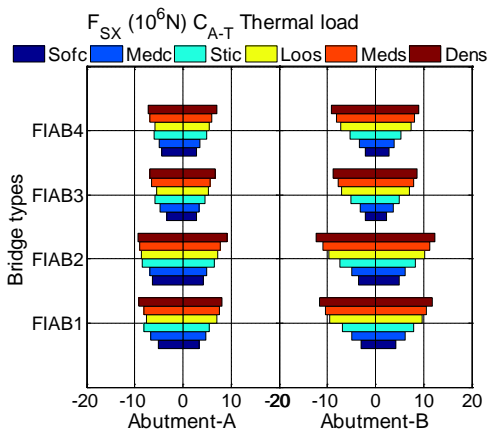
Discrepancy U_x of Abutment backwalls Thermal load



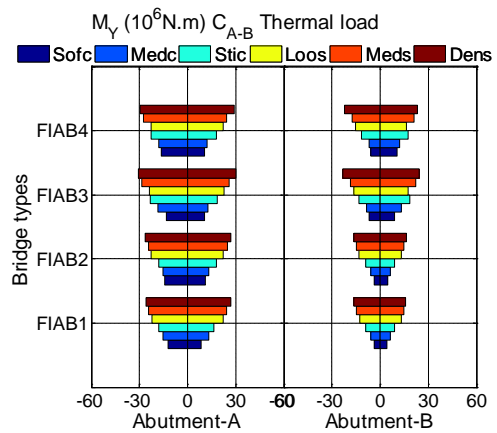
(c) U_x of Abutment stems

Fig. 208 Influence of different soil conditions on the differences between the F_{SX} , M_Y and U_x at the critical sections of two abutment stems under thermal load ($\pm 40^\circ\text{C}$)

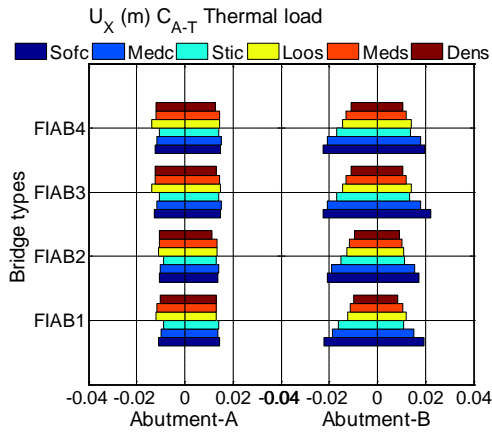
The ultimate F_{SX} , M_Y and U_x of abutment stems considering different soil conditions are illustrated in Fig. 209. It could be observed that the ultimate F_{SX} occur at the stem top in Abutment-B and the ultimate M_Y appear at the stem bottom in Abutment-A when considering the soil condition as dense. Moreover, the maximum U_x appear at the stem top in Abutment-B with the soil condition of soft clay.



(a) F_{SX} of Abutment stems



(b) M_Y of Abutment stems

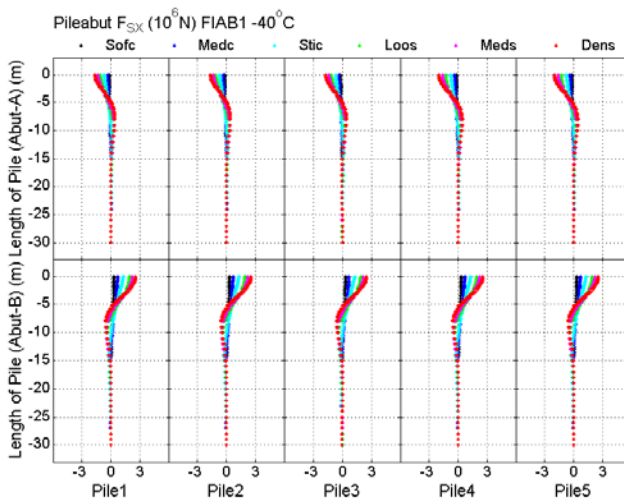


(c) U_x of Abutment stems

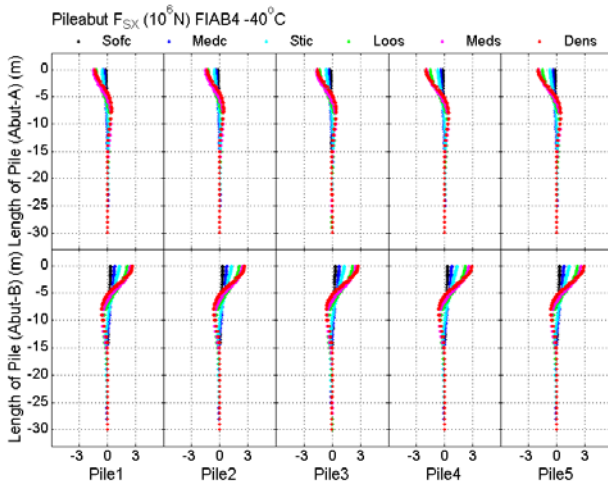
Fig. 209 Influence of different soil conditions on the ultimate F_{SX} , M_Y and U_x of abutment stems under thermal load ($\pm 40^\circ\text{C}$)

6.2.3.4 Pile

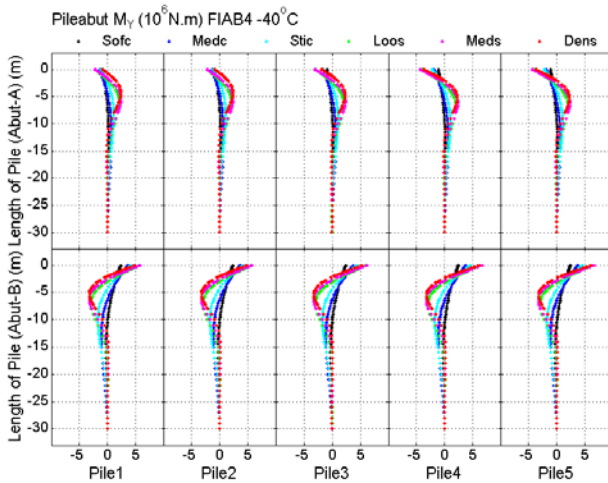
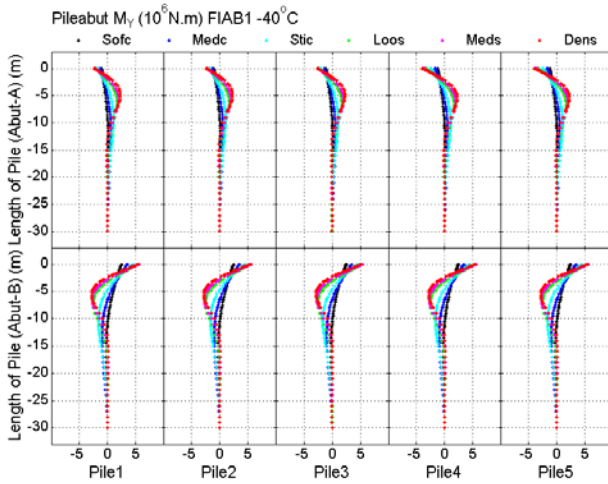
The comparison in Section 6.1.5 indicates that, subjected to thermal load, the performance of piles beneath abutments is significantly larger than that of piles beneath piers. Therefore, only the performance of piles beneath abutments will be taken into account in the following analysis. The influence of different soil conditions on the performance of piles beneath abutments in FIAB1 and FIAB4 under thermal load (-40°C) are compared in Fig. 210.



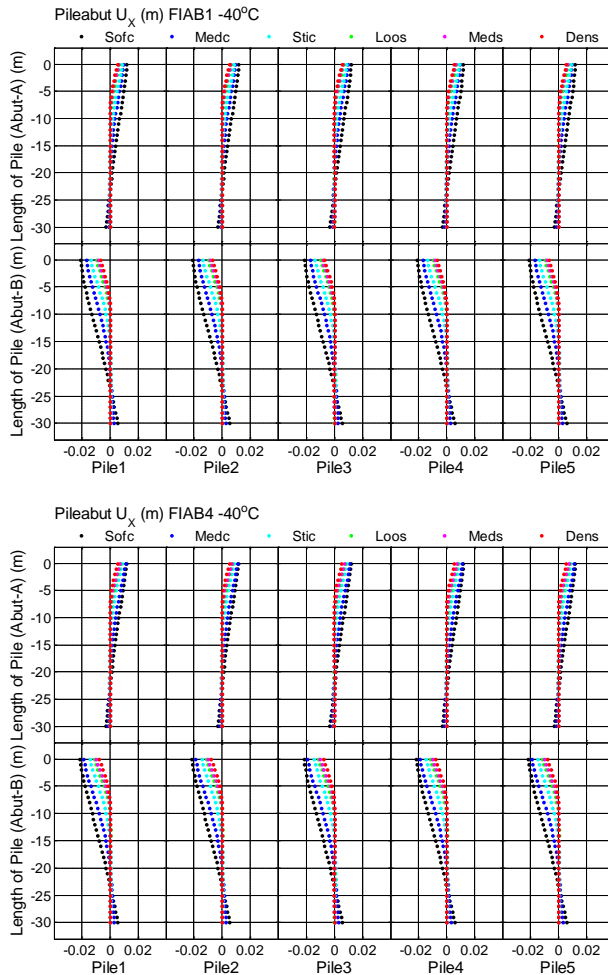
RETROFIT OF EXISTING BRIDGES WITH CONCEPT OF INTEGRAL ABUTMENT BRIDGE



(a) F_{SX} of piles beneath abutments



(b) M_Y of piles beneath abutments



(c) U_x of piles beneath abutments

Fig. 210 Influence of different soil conditions on the performance of piles beneath abutments under thermal load (-40°C)

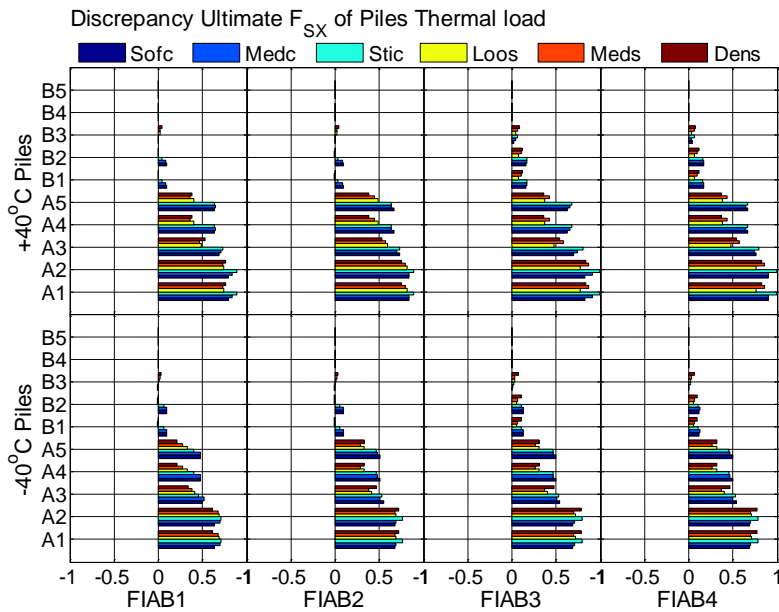
From Fig. 210, it could be found that, no matter which soil condition is considered, the ultimate F_{SX} and U_x of piles in FIAB1 and FIAB2 under thermal load will appear at the top points (C_{PA-T}). For the M_Y of piles under thermal load, when the soil condition is sand, the maximum values could occur at the top points and the points at the depth of about -5m. However, when the soil condition is clay, the ultimate values could appear at the top points and the points at the depth of approximate -10m. These points are within the length of distribution plastic zone described in Section 5.2.4. In order to conduct the analysis, only the maximum M_Y of piles were taken into account.

As introduced in Section 5.1, ten piles are arranged beneath the two abutments. The

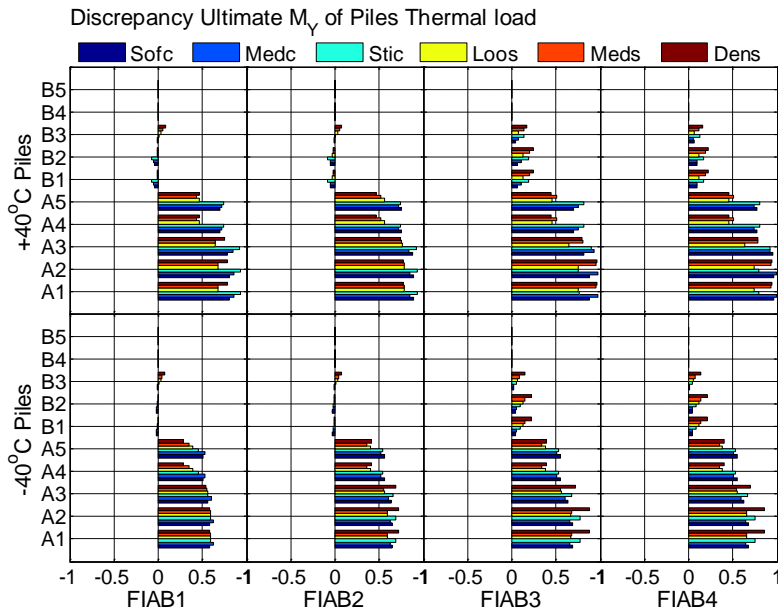
numbers of them are illustrated in Fig. 118 (p.162). In order to carry out the further research, the performance at the corresponding critical sections of ten piles is compared firstly to find out the most critical pile. The discrepancies among ten piles could be calculated by formula (158), as illustrated in Fig. 211. In the formula (158), the $V_{Pileabut-n}$ denotes the other nine piles except the Pile-5 beneath Abutment-B. The positive discrepancy means that the ultimate F_{SX} , M_Y and U_X at the critical sections of the Pile-5 beneath Abutment-B is larger than those of the other piles beneath abutments. From Fig. 211, it could be observed that, for all soil conditions, the ultimate F_{SX} and M_Y of piles occur at the top of Pile-4 or Pile-5 beneath Abutment-B. For the U_X of piles, when the soil condition is dense sand, the ultimate values of Pile-4 or Pile-5 beneath Abutment-B can be slightly smaller than those of the other piles beneath abutments; however, the differences are less than 0.003m, which can be neglected. Considering the other soil conditions, the ultimate values occur at the top of Pile-4 or Pile-5 beneath Abutment-B.

For forces:
$$D_V = (|V_{Pileabut-B5}| - |V_{Pileabut-n}|) / |V_{Pileabut-B5}| \tag{158}$$

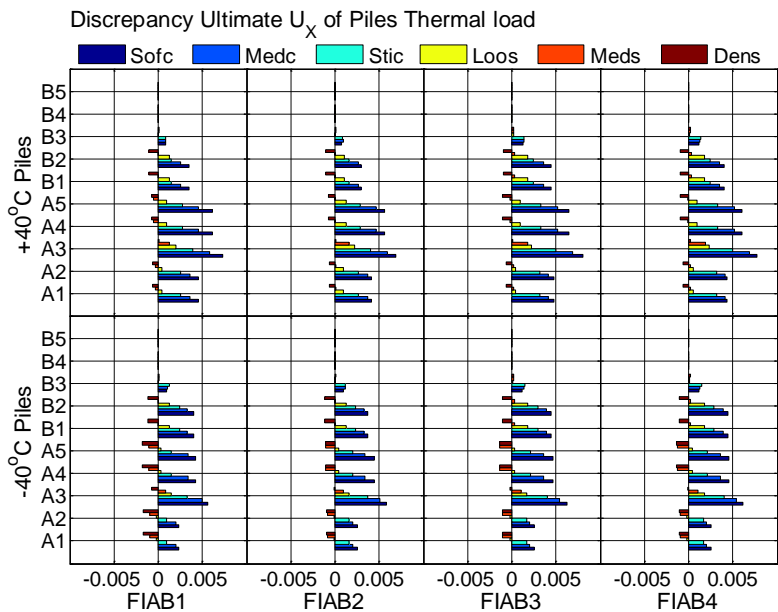
For displacements:
$$D_V = |V_{Pileabut-B5}| - |V_{Pileabut-n}|$$



(a) F_{SX} of piles



(b) M_y of piles

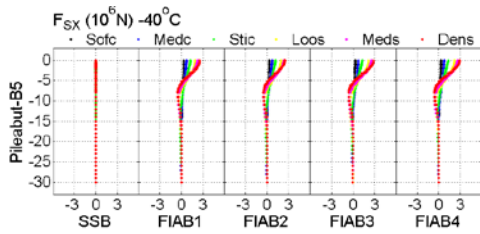


(c) U_x of piles

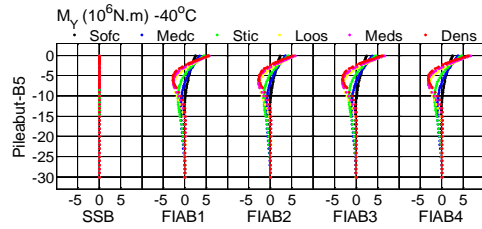
Fig. 211 Influence of different soil conditions on the difference among the F_{sx} , M_y and U_x at the critical sections of piles under thermal load ($\pm 40^\circ\text{C}$)

From the comparison above, the Pile-5 beneath Abutment-B could be chosen as the most critical pile. The influence of different soil conditions on its performance under thermal load (-40°C) is illustrated in Fig. 212.

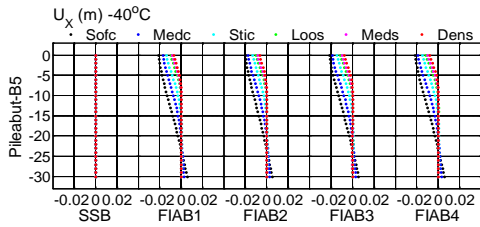
RETROFIT OF EXISTING BRIDGES WITH CONCEPT OF INTEGRAL ABUTMENT BRIDGE



(a) F_{SX} of Pile-5 beneath Abutment-B



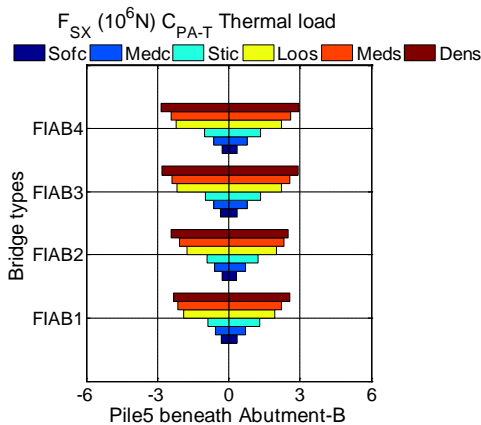
(b) M_Y of Pile-5 beneath Abutment-B



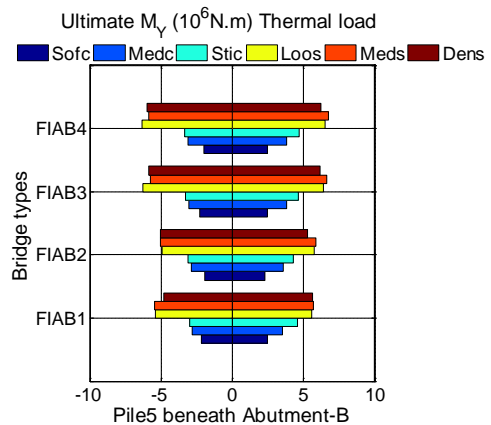
(c) U_X of Pile-5 beneath Abutment-B

Fig. 212 Influence of different soil conditions on the performance of Pile-5 beneath Abutment-B under thermal load (-40°C)

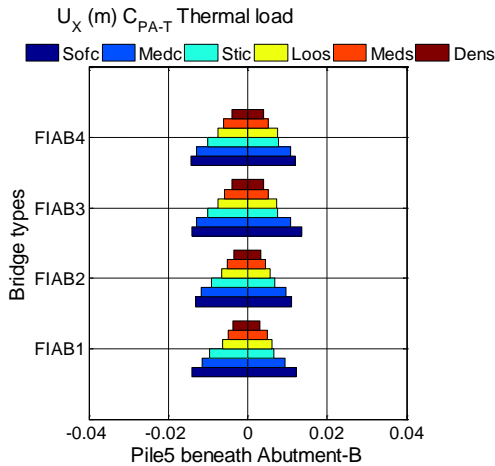
The ultimate F_{SX} , M_Y and U_X of Pile-5 beneath Abutment-B considering different soil conditions are illustrated in Fig. 213. It could be found that, with the soil condition changing from soft to dense, the ultimate F_{SX} and M_Y of Pile-5 beneath Abutment-B increase; however, the maximum U_X will decrease.



(a) F_{SX} of Pile-5 beneath Abutment-B



(b) M_Y of Pile-5 beneath Abutment-B



(c) U_x of Pile-5 beneath Abutment-B

Fig. 213 Influence of different soil conditions on the ultimate F_{sx} , M_y and U_x of Pile-5 beneath Abutment-B under thermal load ($\pm 40^\circ\text{C}$)

6.2.4 Summary

The influence of different soil conditions on the performance of different bridges under highway live load is nearly the same. However, when considering the thermal load, the effect of different soil conditions is significant.

Due to the special arrangement of the substructure heights in 'Viadotto Serrone', the performance of the corresponding bridge components located at the left part and right part of bridge is different, which are divided by the global coordinate axis Y at the mid-span point of span2. Comparing the performance of these corresponding bridge components under thermal load, such as C_{S-1L} and C_{S-3R} of girders; Pier-A and Pier-B; Abutment-A and Abutment-B; and ten piles beneath two abutments, the one with larger internal forces could be considered as the most dangerous component or critical section, which needs to be paid more attention to, as summarized in Table 50.

The comparison among different soil conditions shows that in general under thermal load, with the soil condition changing from soft to dense, the forces and bending moments of different bridge components and vertical deflections of girders increase; however, the horizontal displacements of different bridge components decrease.

RETROFIT OF EXISTING BRIDGES WITH CONCEPT OF INTEGRAL ABUTMENT BRIDGE

Component	Internal force	Most dangerous component or critical section
Girder	M_Y	C_{S-1L} near Abutment-A
	U_X	C_{S-3R} near Abutment-B
Pier	F_{SX}	Pier-A (sand and stiff clay) Pier-B (soft clay and medium clay)
	M_Y	Pier-A (sand) Pier-B (clay)
	U_X	Pier-B
Abutment stem	F_{SX}	Abutment-A (soft clay and medium clay) Abutment-B (sand and stiff clay)
	M_Y	Abutment-A
	U_X	Abutment-B
Pile	F_{SX}	Pile4 and Pile5 beneath Abutment-B
	M_Y	Pile4 and Pile5 beneath Abutment-B
	U_X	Pile4 and Pile5 beneath Abutment-B

Table 50

Most dangerous component or critical section under thermal load

6.3 Different substructure heights

As investigated above, it could be found that the asymmetric substructure heights in ‘Viadotto Serrone’ make noticeable effects on the performance of different bridge components under horizontal load, for example the thermal load in this case.

6.3.1 Research cases definition

In this section, the heights of piers and abutments (including the backwall and stem) are chosen as the parameters. Based on two pier heights in real case (13.7m and 19.7m), another two assumed values (7.7m and 25.7m) were chosen. These four heights could form an arithmetic sequence and cover the range of pier heights in normal cases. For the abutment heights, two values in real case (4.5m and 8m) were taken into account, which could also cover the range of abutment heights in normal cases. Based on these assumptions, fifteen cases, including fourteen idealized cases and one real case, could be used to investigate the influence of substructure heights, as listed in Table 51. In order to investigate the effects of different pier heights on the performance of girders under thermal load, the heights of two abutments should be equal (4.5m or 8m), and the pier heights change from 7.7m to

25.7m. The effects of different abutment heights on the performance of bridges under thermal load could be studied by fixing the heights of two piers as equal (7.7m, 13.7m, 19.7m or 25.7m), and changing the abutment heights from 4.5m to 8m.

	Column	1	2	3	4	5
Row	Case	$H_{PA} = H_{PB} = 7.7$	$H_{PA} = H_{PB} = 13.7$	$H_{PA} = H_{PB} = 19.7$	$H_{PA} = H_{PB} = 25.7$	$H_{PA} = 13.7$ $H_{PB} = 19.7$
1	$H_{AA} = H_{AB} = 4.5$	a4.5p7.7	a4.5p13.7	a4.5p19.7	a4.5p25.7	a4.5pReal
2	$H_{AA} = H_{AB} = 8$	a8p7.7	a8p13.7	a8p19.7	a8p25.7	a8pReal
3	$H_{AA} = 8$ $H_{AB} = 4.5$	aRealp7.7	aRealp13.7	aRealp19.7	aRealp25.7	Real case

Table 51

Definitions of different types of piers and abutments (H_{PA} means the height of Pier-A; H_{PB} means the height of Pier-B; H_{AA} means the height of Abutment-A; H_{AB} means the height of Abutment-B; Real means that the heights of piers and abutments are the same as those in 'Viadotto Serrone')

By analyzing the cases with the symmetric substructure heights, it could be found that the performance of the bridge components located at the left part and right part of the bridge is equal under thermal load. The validity of the finite element model is checked again.

6.3.2 Girder

6.3.2.1 Influence of pier heights

The influence of different pier heights on the performance of Girder-L in FIABs under thermal load ($\pm 40^\circ\text{C}$) is illustrated in Fig. 214. Due to the space limitation, the cases with the soil condition of medium sand and the abutment height of 4.5m are chosen to analyze in the following. From Fig. 214, it could be found that the influence of different pier heights on the performance of Girder-L in FIABs under thermal load is negligible, which can be neglected.

RETROFIT OF EXISTING BRIDGES WITH CONCEPT OF INTEGRAL ABUTMENT BRIDGE

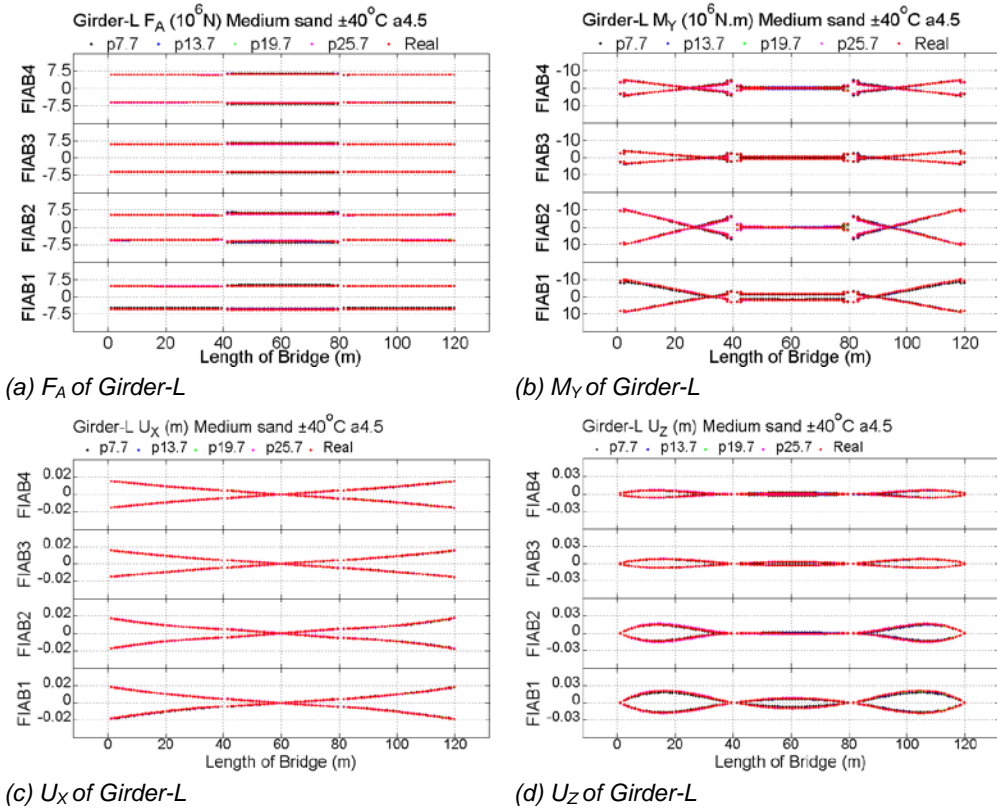


Fig. 214 Influence of different pier heights on the performance of Girder-L in FIABs under thermal load ($\pm 40^\circ\text{C}$)

6.3.2.2 Influence of abutment heights

The influence of different abutment heights on the performance of Girder-L in FIABs under thermal load ($\pm 40^\circ\text{C}$) is illustrated in Fig. 215. Due to the space limitation, the cases with the soil condition of medium sand and the pier height of 7.7m are chosen to analyze in the following. By comparing two cases ‘a4.5p7.7’ and ‘a8p7.7’, it could be found that under thermal load, different abutment heights have noticeable effects on the performance of Girder-L in FIABs.

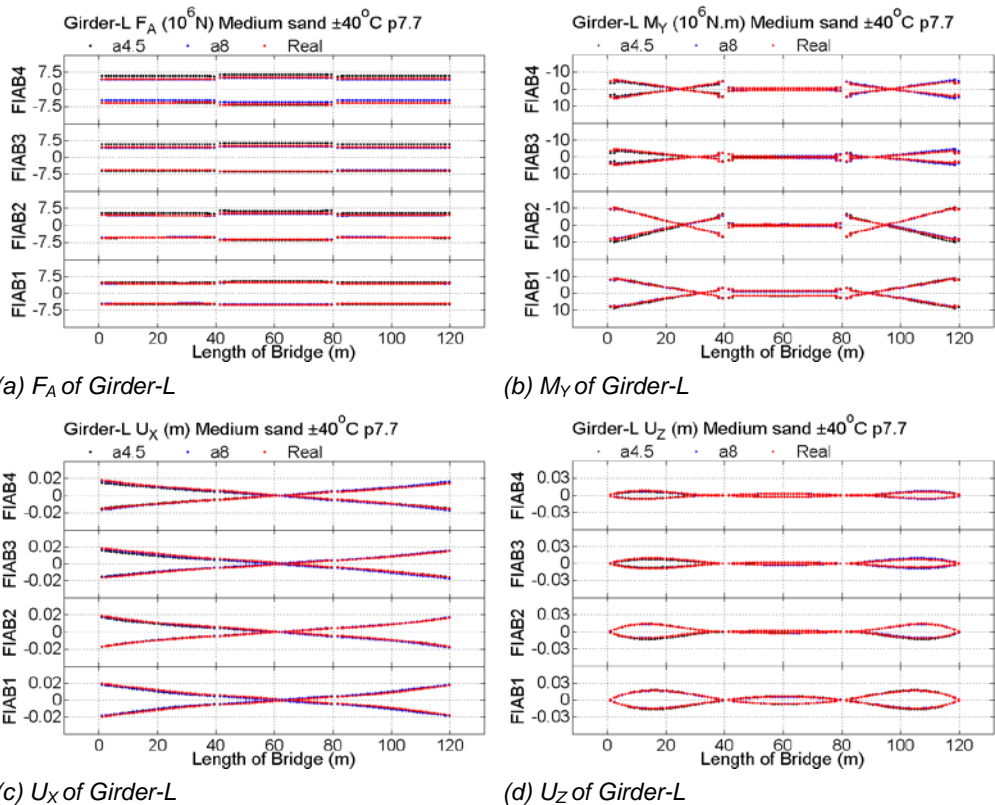


Fig. 215 Influence of different abutment heights on the performance of Girder-L in FIABs under thermal load ($\pm 40^\circ\text{C}$)

6.3.2.3 Different soil conditions and bridge types

As investigated above, it could be found that the influence of different pier heights on the performance of girders in FIABs under thermal load is negligible. Therefore, the heights of two piers are set as 7.7m in the following analysis due to the space limitation. Considering all soil conditions, the influence of different abutment heights on the performance of Girder-L in FIAB1 and FIAB4 under thermal load ($\pm 40^\circ\text{C}$) is illustrated in Fig. 216. It could be observed that, the locations of the critical sections corresponding to the ultimate internal forces of Girder-L in FIABs do not change due to soil variations. For example, the F_A along girder length are nearly the constant, the ultimate M_Y and U_X occur at the points near two abutments, and the maximum U_Z appear in Span-1 or Span-3.

RETROFIT OF EXISTING BRIDGES WITH CONCEPT OF INTEGRAL ABUTMENT BRIDGE

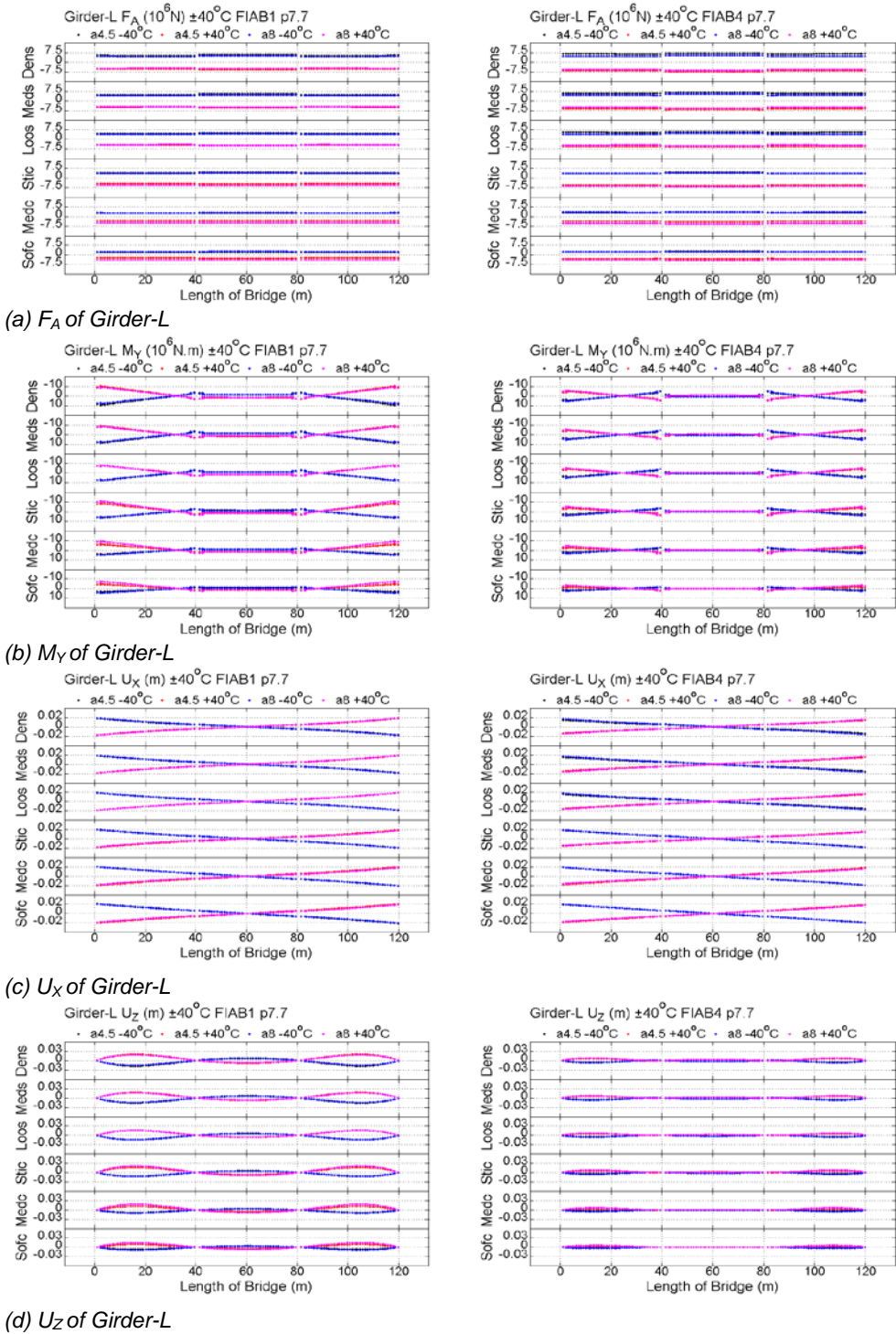


Fig. 216 Influence of different abutment heights on the performance of Girder-L in FIAB1 and FIAB4 under thermal load ($\pm 40^\circ\text{C}$) considering all soil conditions

In order to show the influence of different abutment heights and soil conditions clearly, the ultimate F_A , M_Y , U_X and U_Z of Girder-L in FIABs are compared in Fig. 217. In general, when the soil condition and the bridge type are fixed, the influence of different abutment heights on the ultimate internal forces of Girder-L in FIABs is not large. When the soil is clay, with the abutment heights increase, the ultimate F_A , M_Y and U_Z of Girder-L in all subtypes of FIABs increase, while, the ultimate U_X of Girder-L in all subtypes of FIABs decrease. When the soil is sand, with the abutment heights increase, the ultimate M_Y and U_Z of Girder-L in FIAB3 and FIAB4 and U_X of Girder-L in all subtypes of FIABs increase, while, the ultimate F_A of Girder-L in all subtypes of FIABs and the M_Y and U_Z of Girder-L in FIAB1 and FIAB2 decrease.

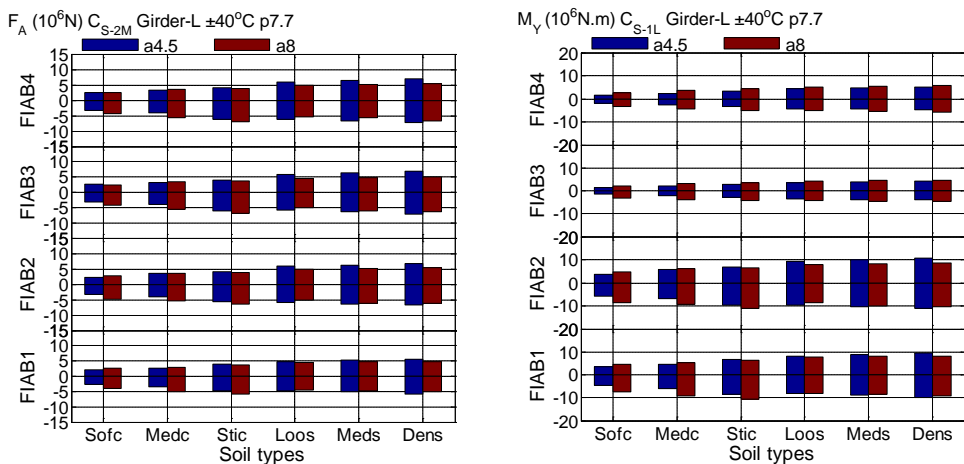
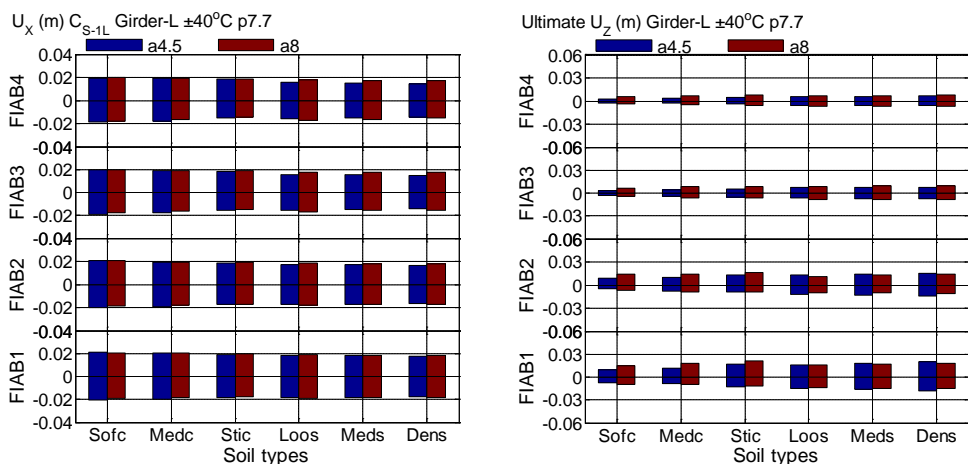
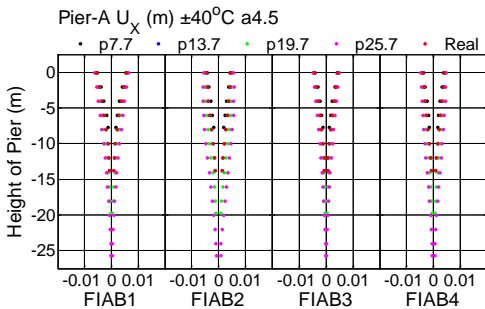
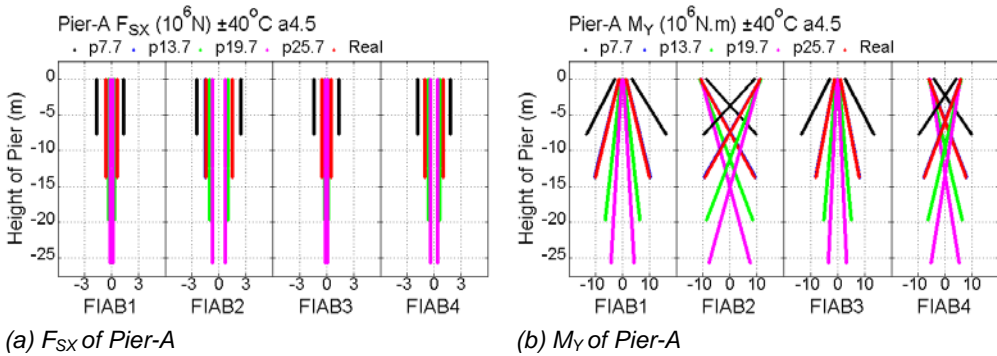
(a) F_A of Girder-L(b) M_Y of Girder-L(c) U_X of Girder-L(d) U_Z of Girder-L

Fig. 217 Influence of different abutment heights on the ultimate internal forces of Girder-L in FIABs under thermal load ($\pm 40^\circ\text{C}$) considering all soil conditions

6.3.3 Pier

6.3.3.1 Influence of pier heights

The influence of different pier heights on the performance of Pier-A in FIABs under thermal load ($\pm 40^\circ\text{C}$) is illustrated in Fig. 218. Due to the space limitation, the cases with the soil condition of medium sand and the abutment height of 4.5m are chosen to analyze in the following. It could be found that the effects of different pier heights on the performance of piers in FIABs are significant. Considering the cases that have equal pier heights, such as ‘a4.5p7.7’, ‘a4.5p13.7’, ‘a4.5p19.7’ and ‘a4.5p25.7’, with the pier heights increase, the F_{SX} of piers decrease; however, the U_x of piers increase. The M_Y of piers could be divided into two conditions corresponding to two superstructure-pier connection methods. For FIAB1 and FIAB3 that have hinged superstructure-pier connections, the M_Y of piers decrease with the pier heights increase. For FIAB2 and FIAB4 that have rigid superstructure-pier connections, with the pier heights increase, the ultimate M_Y at the bottom points of piers decrease, while, the ultimate M_Y at the top points of piers increase.



(c) U_x of Pier-A

Fig. 218 Influence of different pier heights on the performance of Pier-A in FIABs under thermal load ($\pm 40^\circ\text{C}$)

The case 'a4.5pReal' that has different heights of two piers was chosen to compare with the cases that have equal heights of two piers, such as 'a4.5p7.7', 'a4.5p13.7', 'a4.5p19.7' and 'a4.5p25.7', as illustrated in Fig. 219. It could be found that, the performance of Pier-A with the height of 13.7m in the case 'a4.5pReal' is the same as the performance of piers in the case 'a4.5p13.7', and the performance of Pier-B with the height of 19.7m can be predicted by using the behaviors of piers in the case 'a4.5p19.7'.

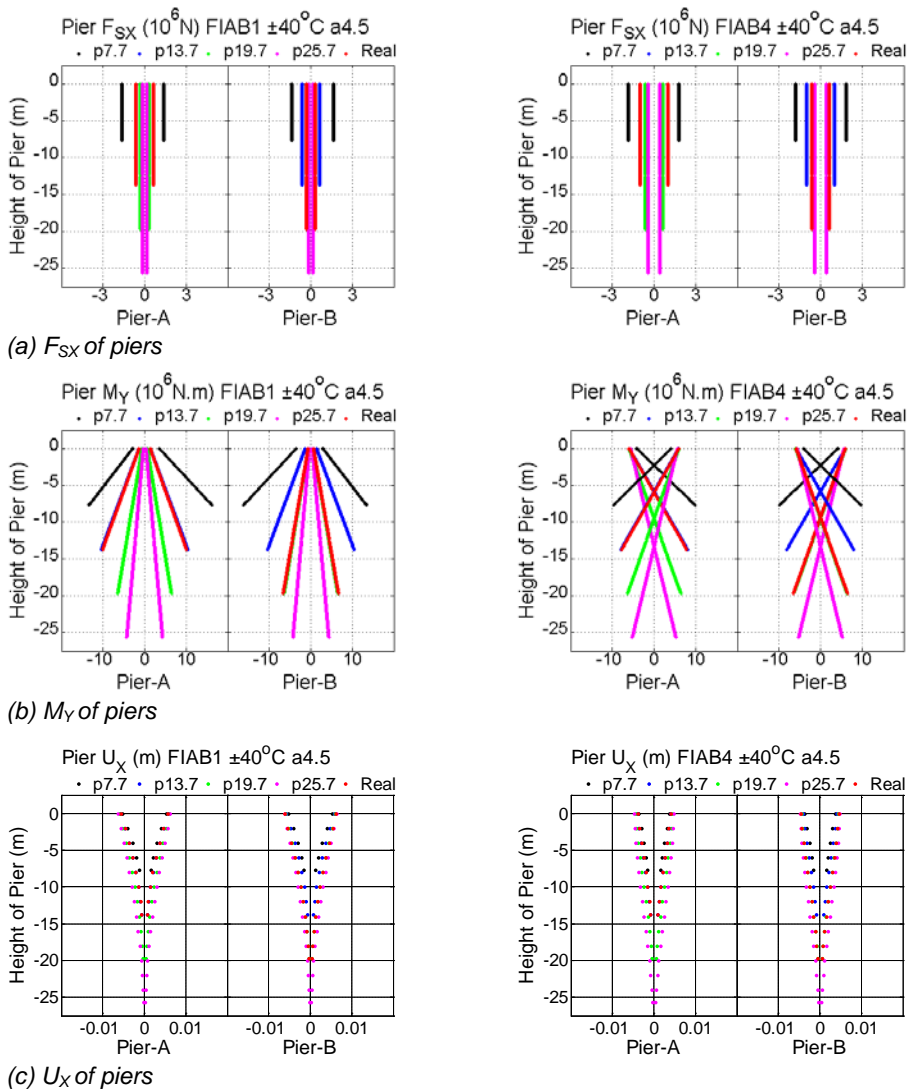
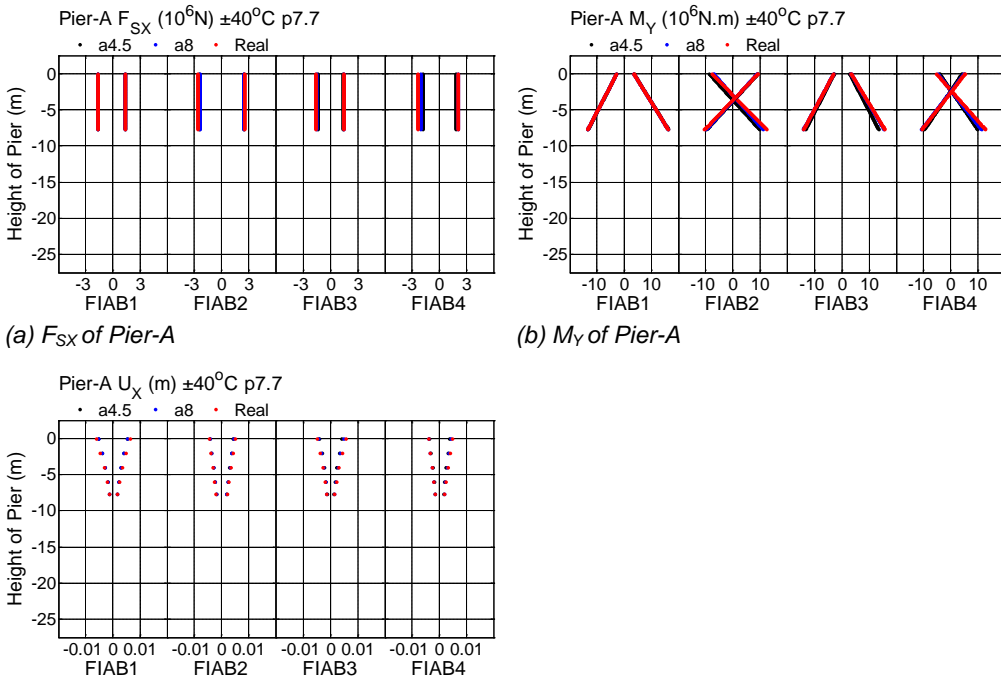


Fig. 219 Influence of different pier heights on the performance of piers in FIAB1 and FIAB4 under thermal load ($\pm 40^\circ\text{C}$)

6.3.3.2 Influence of abutment heights

The influence of different abutment heights on the performance of Pier-A in FIABs under thermal load ($\pm 40^{\circ}\text{C}$) is illustrated in Fig. 220. Due to the space limitation, the cases with the soil condition of medium sand and the pier height of 7.7m are chosen to analyze in the following. By comparing the two cases ‘a4.5p7.7’ and ‘a8p7.7’, it could be observed that under thermal load, different abutment heights have noticeable effects on the performance of Pier-A.

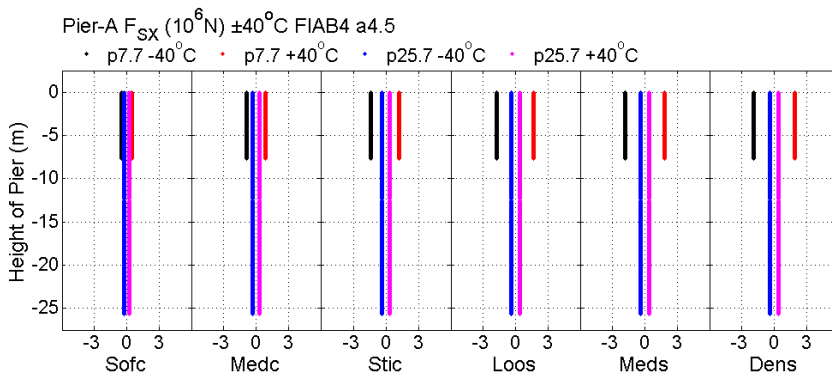
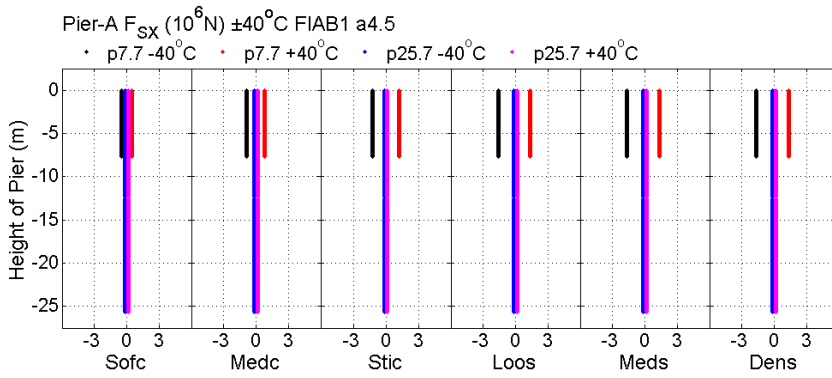


(a) F_{SX} of Pier-A
 (b) M_Y of Pier-A
 (c) U_X of Pier-A
 Fig. 220 Influence of different abutment heights on the performance of Pier-A in FIABs under thermal load ($\pm 40^{\circ}\text{C}$)

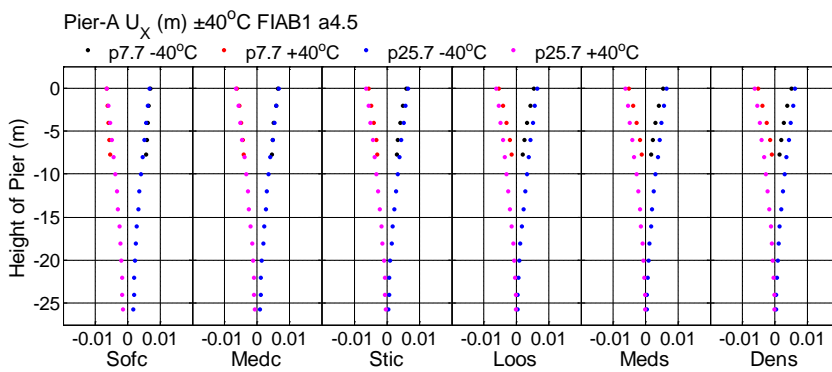
6.3.2.3 Different soil conditions and bridge types

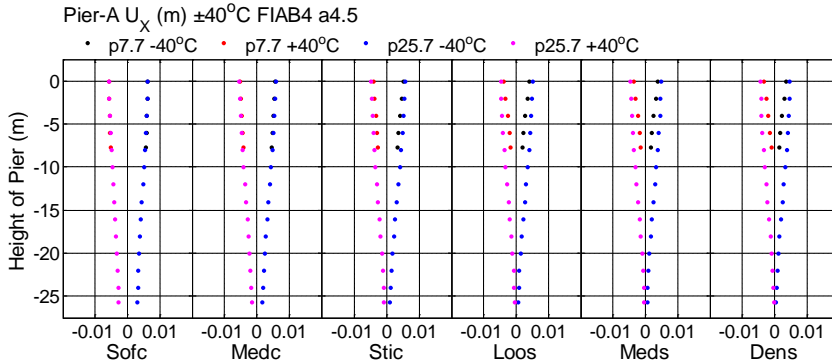
As investigated above, it could be found that under thermal load, the influence of different abutment heights on the performance of Pier-A in FIABs is smaller than the effects of different pier heights. Therefore, the heights of two abutments are set as 4.5m in this analysis due to the space limitation. The influence of different pier heights on the F_{SX} and U_X of Pier-A in FIAB1 and FIAB4 under thermal load ($\pm 40^{\circ}\text{C}$) considering all soil conditions are illustrated in Fig. 221. It could be observed that, the locations of the critical sections corresponding to the ultimate F_{SX} and U_X of

Pier-A do not change due to soil variations. For example, the F_{sx} along the height of pier column is constant and the ultimate U_x always occur at the top points of piers.



(a) F_{sx} of Pier-A

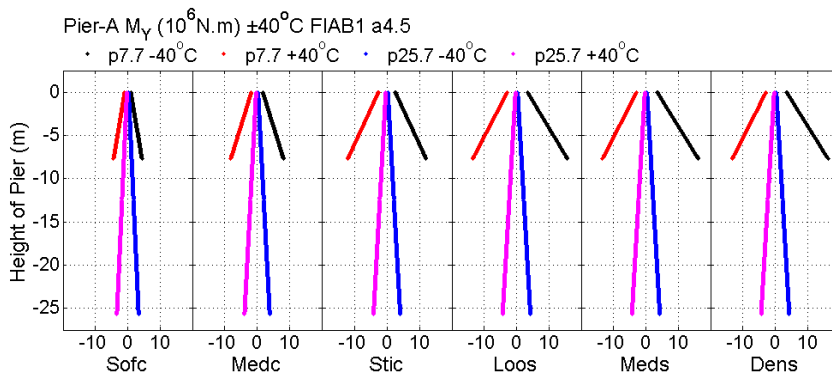




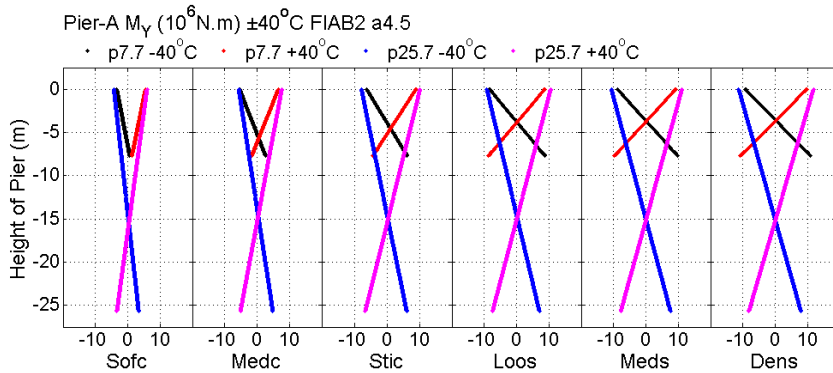
(b) U_x of Pier-A

Fig. 221 Influence of different pier heights on the F_{sx} and U_x of Pier-A in FIAB1 and FIAB4 under thermal load ($\pm 40^\circ\text{C}$) considering all soil conditions

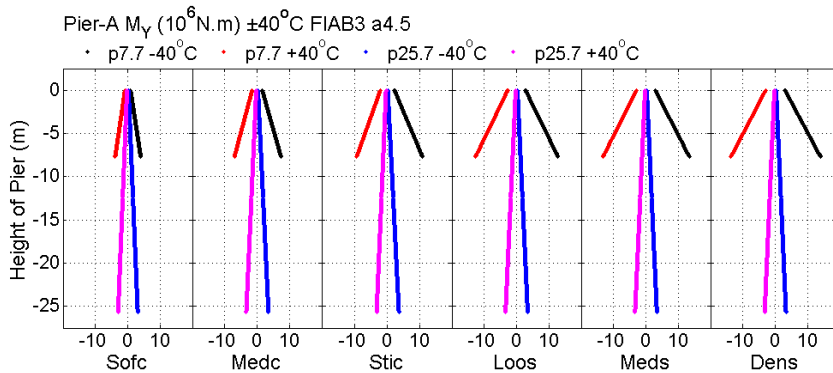
The influence of different pier heights on the M_y of Pier-A in four subtypes of FIABs under thermal load ($\pm 40^\circ\text{C}$) considering all soil conditions are illustrated in Fig. 222. For FIAB1 and FIAB3 that have hinged superstructure-pier connections, the ultimate M_y of piers occur at the bottom points of piers in all soil conditions. For FIAB2 and FIAB4 that have rigid superstructure-pier connections, when the pier heights are 7.7m, the locations corresponding to the ultimate M_y of piers appear at top points or bottom points corresponding to different soil conditions. However, the differences among the locations corresponding to the ultimate M_y of piers in different soil conditions would decrease with the pier heights increase. Consequently, both M_y at the top and bottom points of piers should be considered in the following analysis.



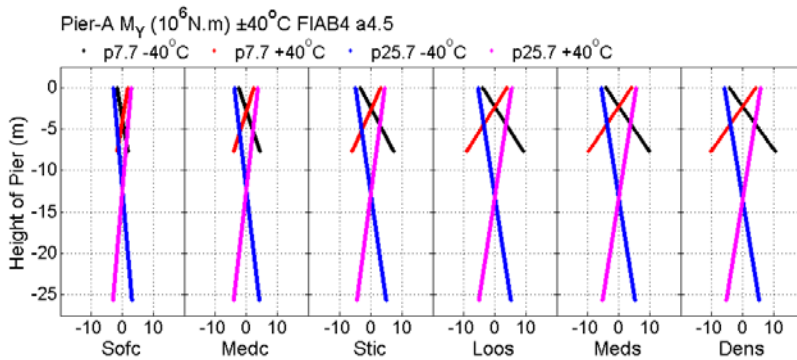
(a) FIAB1



(b) FIAB2



(c) FIAB3



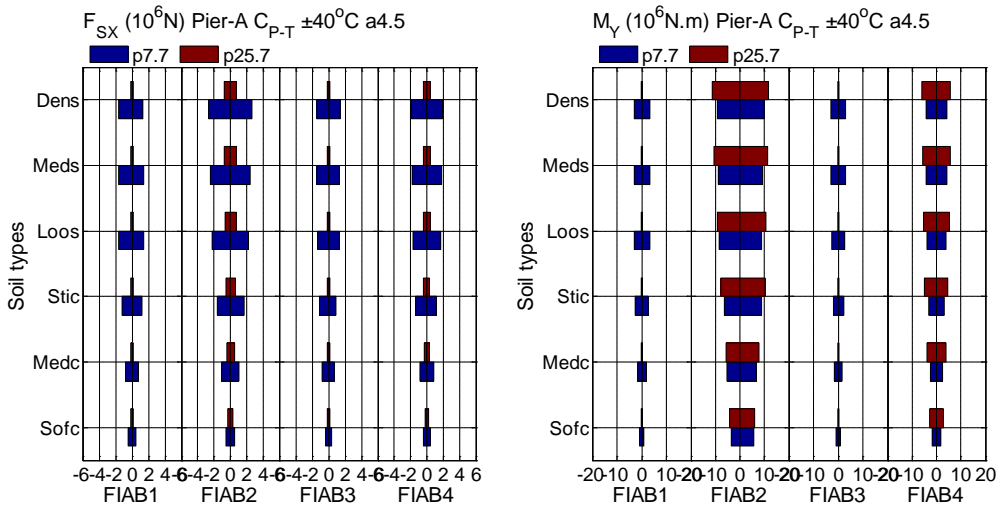
(d) FIAB4

Fig. 222 Influence of different pier heights on the M_Y of Pier-A in FIABs under thermal load ($\pm 40^\circ\text{C}$) considering all soil conditions

In order to show the influence of different pier heights and soil conditions clearly, the ultimate internal forces of Pier-A, including the F_{SX} , M_Y and U_X at the top point (C_{P-T}), and the M_Y at the bottom point (C_{P-B}), are compared in Fig. 223. It could be observed that no matter which soil conditions is considered, with the pier heights increase, the

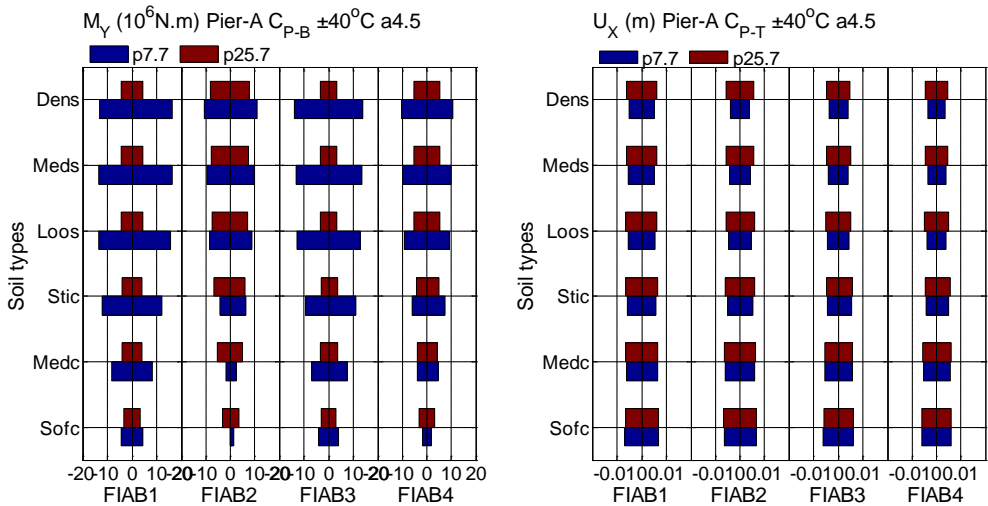
RETROFIT OF EXISTING BRIDGES WITH CONCEPT OF INTEGRAL ABUTMENT BRIDGE

ultimate F_{SX} of Pier-A in all FIABs and the ultimate M_Y of Pier-A in FIAB1 and FIAB3 decrease, while, the ultimate U_X of Pier-A in all FIABs and the M_Y at the top points of Pier-A in FIAB2 and FIAB4 increase. When the soil is sand, with the pier heights increase, the ultimate M_Y at the bottom points of Pier-A in FIAB2 and FIAB4 decrease. When the soil is clay, with the pier heights increase, the ultimate M_Y at the bottom points of Pier-A in FIAB2 and FIAB4 increase.



(a) F_{SX} of Pier-A

(b) M_Y of Pier-A top



(c) M_Y of Pier-A bottom

(d) U_X of Pier-A

Fig. 223 Influence of different pier heights on the ultimate internal forces of Pier-A in FIABs under thermal load ($\pm 40^\circ C$) considering six soil conditions

6.3.4 Abutment stem

6.3.4.1 Influence of pier heights

The influence of different pier heights on the performance of Abutment-A stem in FIABs under thermal load ($\pm 40^\circ\text{C}$) is illustrated in Fig. 224. Due to the space limitation, the cases with the soil condition of medium sand and the abutment height of 4.5m are chosen to analyze in the following. From Fig. 224, it could be observed that the influence of different pier heights on the performance of abutment stems under thermal load is negligible.

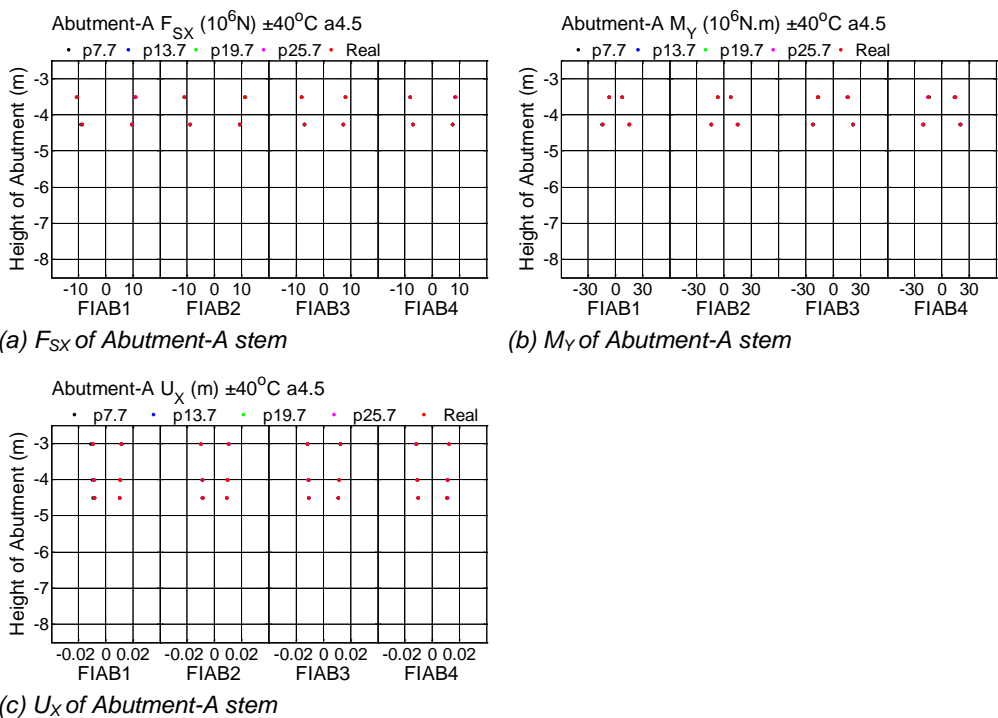
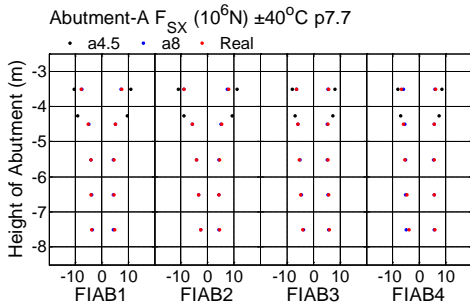


Fig. 224 Influence of different pier heights on the performance of Abutment-A stem in FIABs under thermal load ($\pm 40^\circ\text{C}$)

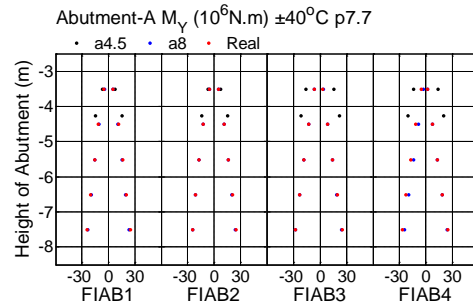
6.3.4.2 Influence of abutment heights

The influence of different abutment heights on the performance of Abutment-A stem in FIABs under thermal load ($\pm 40^\circ\text{C}$) is illustrated in Fig. 225. Due to the space limitation, the cases with the soil condition of medium sand and the pier height of 7.7m are chosen to analyze in the following. By comparing two cases 'a4.5p7.7' and 'a8p7.7', it could be found that under thermal load, the effect of different abutment

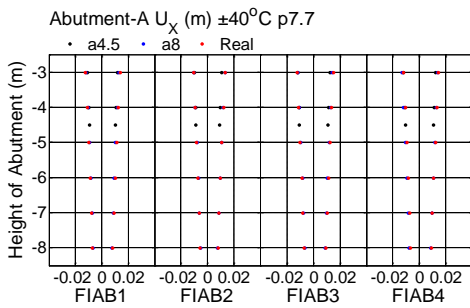
heights on the performance of abutment stems is significant. With the abutment heights increase, the F_{SX} and M_Y of abutment stems decrease; however, the U_X of abutment stems and the maximum M_Y at the bottom of abutment stems increase.



(a) F_{SX} of Abutment-A stem



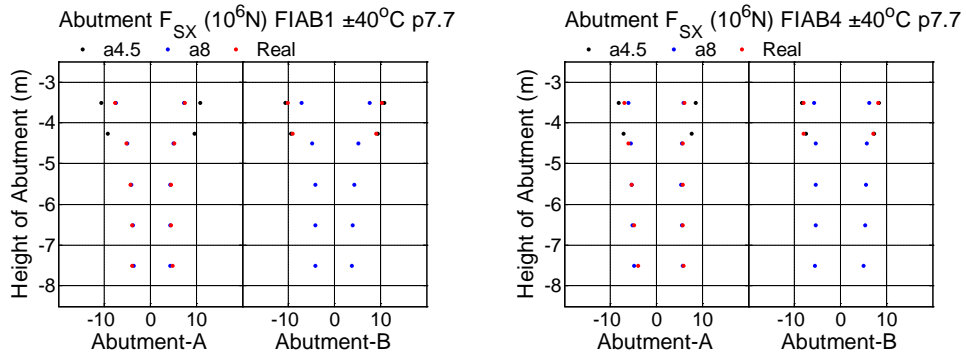
(b) M_Y of Abutment-A stem



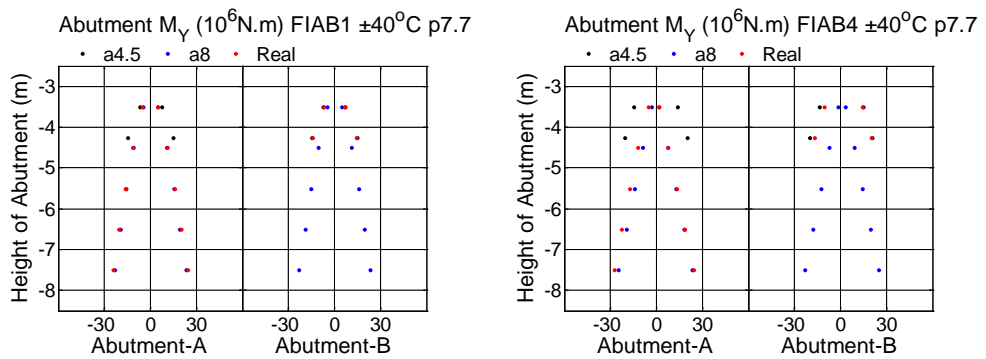
(c) U_X of Abutment-A stem

Fig. 225 Influence of different abutment heights on the performance of Abutment-A stem in FIABs under thermal load ($\pm 40^\circ\text{C}$)

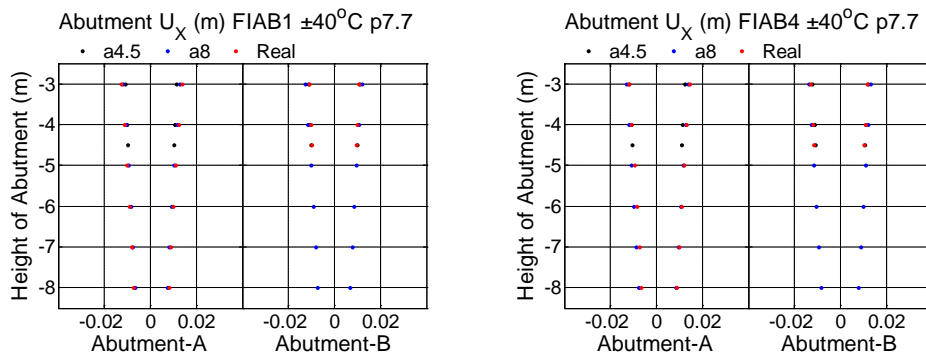
The case 'aRealp7.7' that has different heights of two abutments was chosen to compare with the cases that have equal abutment heights, such as 'a4.5p7.7' and 'a8p7.7', as illustrated in Fig. 226. It could be found that, the performance of Abutment-A stem in the case 'aRealp7.7' is similar to the performance of abutment stems in the case 'a8p7.7', and the performance of Abutment-B could be predicted by using the behaviors of abutment stems in the case 'a4.5p7.7'.



(a) F_{SX} of abutment stems



(b) M_Y of abutment stems



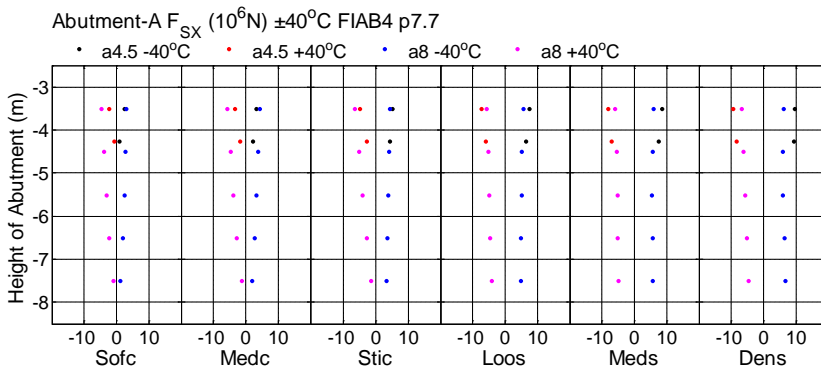
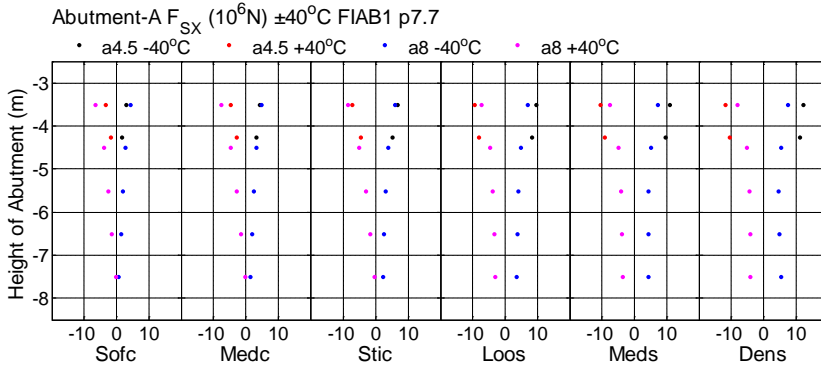
(c) U_X of abutment stems

Fig. 226 Influence of different abutment heights on the performance of abutment stems in FIAB1 and FIAB4 under thermal load ($\pm 40^\circ\text{C}$)

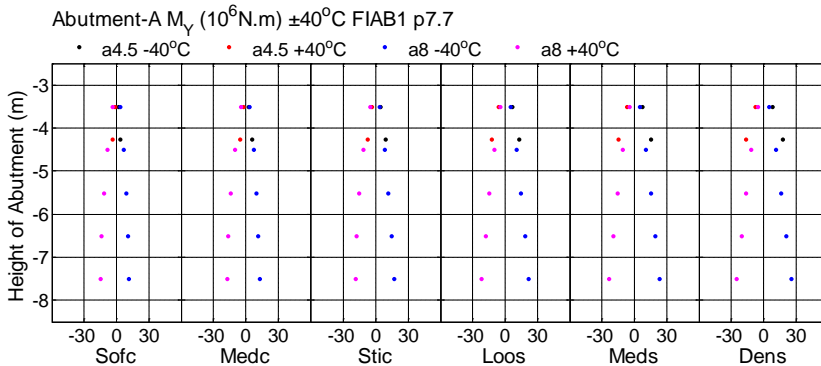
6.3.4.3 Different soil conditions and bridge types

From the investigation mentioned above, it could be found that under thermal load, the influence of different pier heights on the performance of abutment stems in FIABs is negligible. Therefore, the heights of two piers are set as 7.7m in this analysis due to the space limitation. The influence of different abutment heights on

the F_{SX} , M_Y and U_X of Abutment-A stem in FIAB1 and FIAB4 under thermal load ($\pm 40^\circ\text{C}$) considering all soil conditions are illustrated in Fig. 227. It could be observed that, the locations of the critical sections corresponding to the ultimate internal forces of Abutment-A stem in FIABs do not change due to soil variations. For example, the ultimate F_{SX} and U_X always occur at the top points of abutment stems and the maximum M_Y appear at the bottom points of abutment stems.



(a) F_{SX} of Abutment-A stem



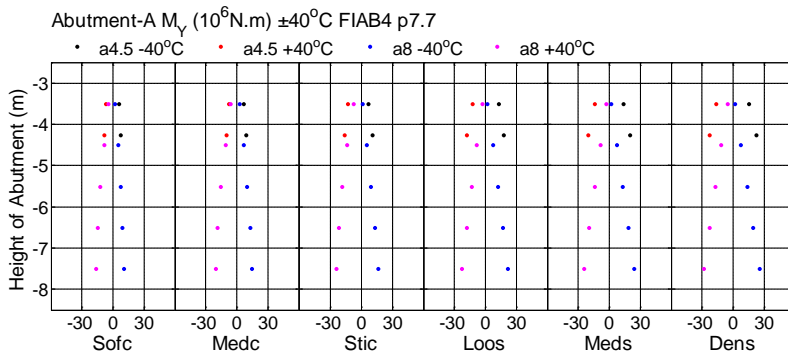
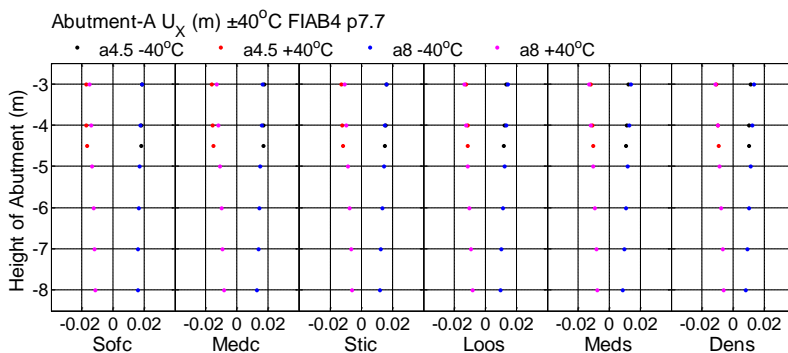
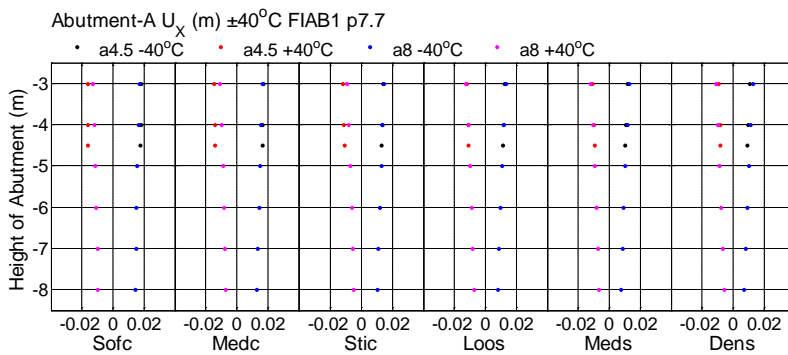
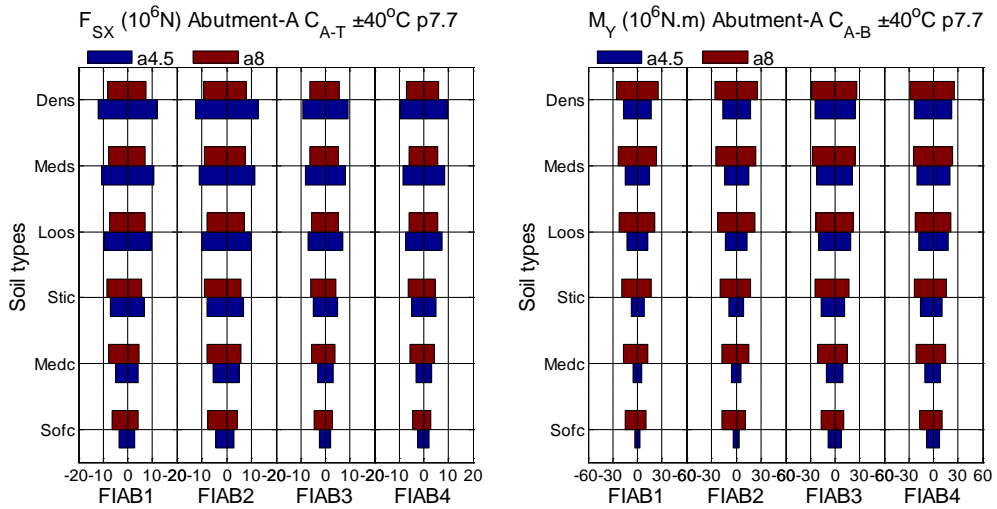
(b) M_Y of Abutment-A stem(c) U_X of Abutment-A stem

Fig. 227 Influence of different abutment heights on the performance of Abutment-A stem in FIAB1 and FIAB4 under thermal load ($\pm 40^\circ\text{C}$) considering all soil conditions

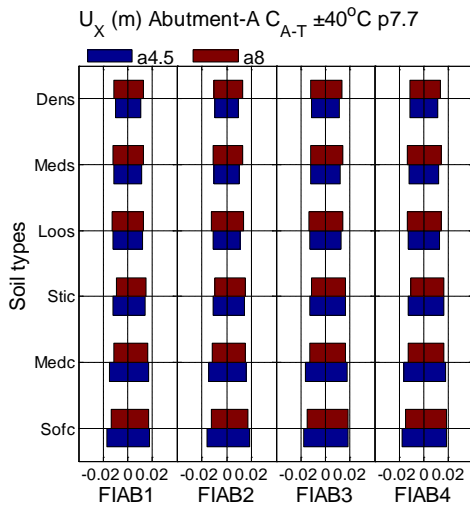
The ultimate internal forces at the corresponding critical sections of Abutment-A stem, including the F_{SX} and U_X at the top point (C_{A-T}), and the M_Y at the bottom point (C_{A-B}), are compared in Fig. 228 to show the influence of different abutment heights and soil conditions. It could be found that, for all FIABs, with the abutment heights increase, the ultimate M_Y of Abutment-A stem in all soil types, the ultimate F_{SX} of Abutment-A stem in clay and the ultimate U_X of Abutment-A stem in sand increase. On the contrary, for all FIABs, with the abutment heights increase, the ultimate F_{SX} of

Abutment-A stem in sand and the ultimate U_x of Abutment-A stem in clay increase.



(a) F_{SX} of Abutment-A stem

(b) M_Y of Abutment-A stem



(c) U_x of Abutment-A stem

Fig. 228 Influence of different abutment heights on the ultimate internal forces of Abutment-A stem in FIABs under thermal load ($\pm 40^\circ\text{C}$) considering all soil conditions

6.3.5 Pile

Considering the thermal load, only the performance of piles beneath abutments is taken into account in following research, because it is significantly larger than the performance of piles beneath piers under thermal load.

6.3.5.1 Influence of pier heights

The influence of different pier heights on the performance of Pile-5 beneath Abutment-A in FIABs under thermal load ($\pm 40^\circ\text{C}$) is illustrated in Fig. 229. Due to the space limitation, the cases with the soil condition of medium sand and the abutment height of 4.5m are chosen to analyze in the following. It could be found that the influence of different pier heights on the performance of piles beneath abutments under thermal load is negligible.

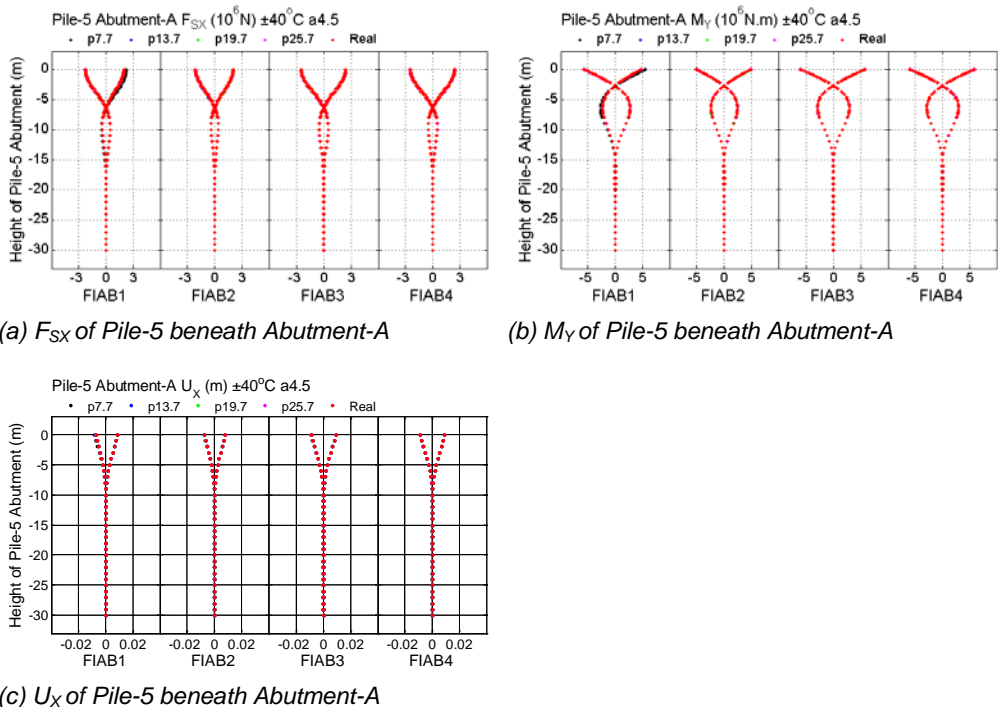
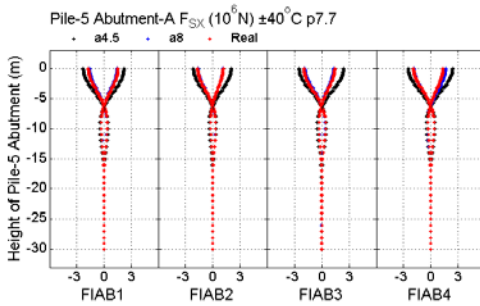


Fig. 229 Influence of different pier heights on the performance of Pile-5 beneath Abutment-A in FIABs under thermal load ($\pm 40^\circ\text{C}$)

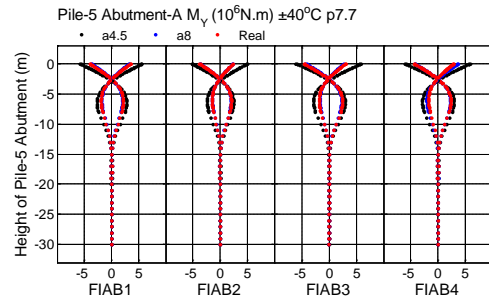
6.3.5.2 Influence of abutment heights

The influence of different abutment heights on the performance of Pile-5 beneath Abutment-A in FIABs under thermal load ($\pm 40^\circ\text{C}$) is demonstrated in Fig. 230. Due to the space limitation, the cases with the soil condition of medium sand and the pier height of 7.7m are chosen to analyze in the following. By comparing two cases 'a4.5p7.7' and 'a8p7.7', it could be found that under thermal load, the effect of different abutment heights on the performance of piles beneath abutments is significant. The F_{SX} , M_Y and U_X of piles beneath abutments would decrease with the

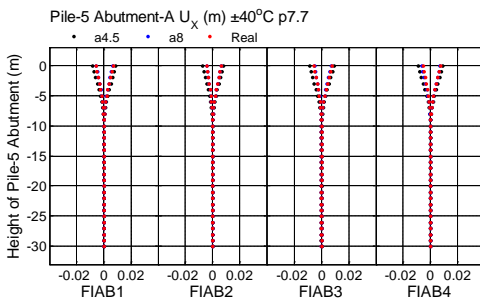
abutment heights increase.



(a) F_{SX} of Pile-5 beneath Abutment-A



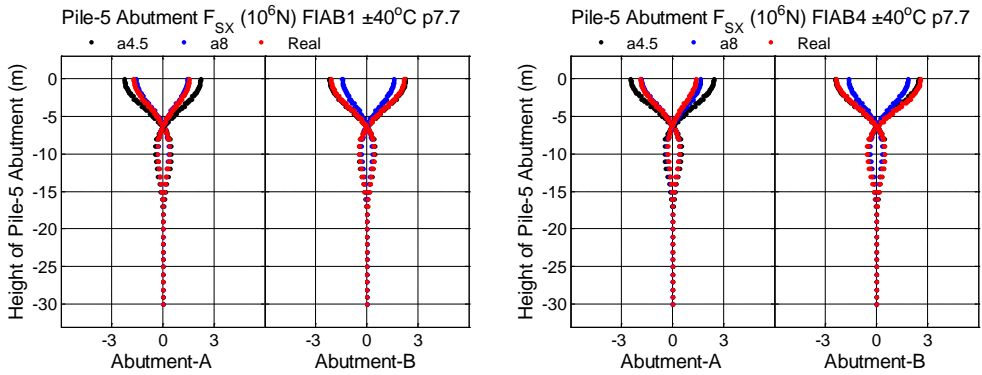
(b) M_Y of Pile-5 beneath Abutment-A



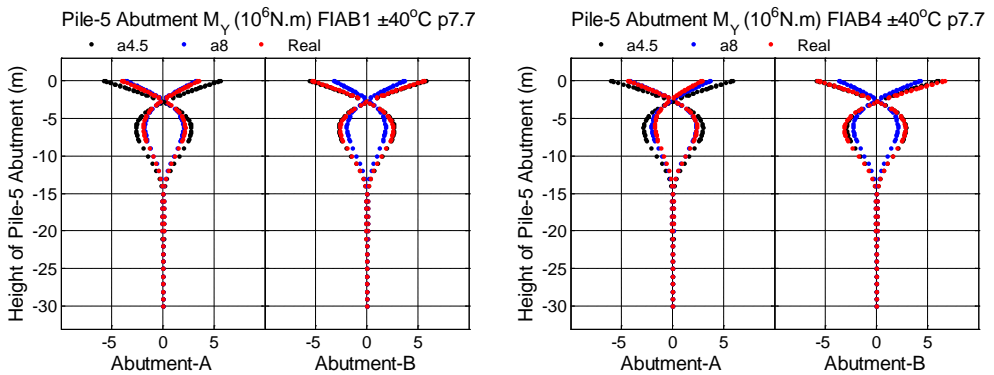
(c) U_X of Pile-5 beneath Abutment-A

Fig. 230 Influence of different abutment heights on the performance of Pile-5 beneath Abutment-A in FIABs under thermal load ($\pm 40^\circ\text{C}$)

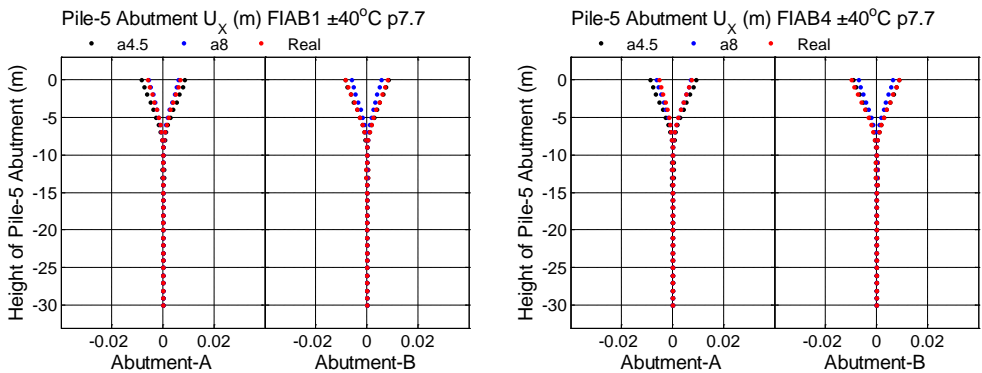
The case 'aRealp7.7' that has different abutment heights was chosen to compare with the cases that have equal abutment heights, such as 'a4.5p7.7' and 'a8p7.7', as illustrated in Fig. 231. It could be observed, the performance of Pile-5 beneath Abutment-A is similar to the performance of Pile-5 beneath abutments in the case 'a8p7.7', and the performance of Pile-5 beneath Abutment-B could be predicted by using the behaviors of Pile-5 beneath abutments in the case 'a4.5p7.7'.



(a) F_{SX} of Pile-5 beneath Abutment-A



(b) M_Y of Pile-5 beneath Abutment-A



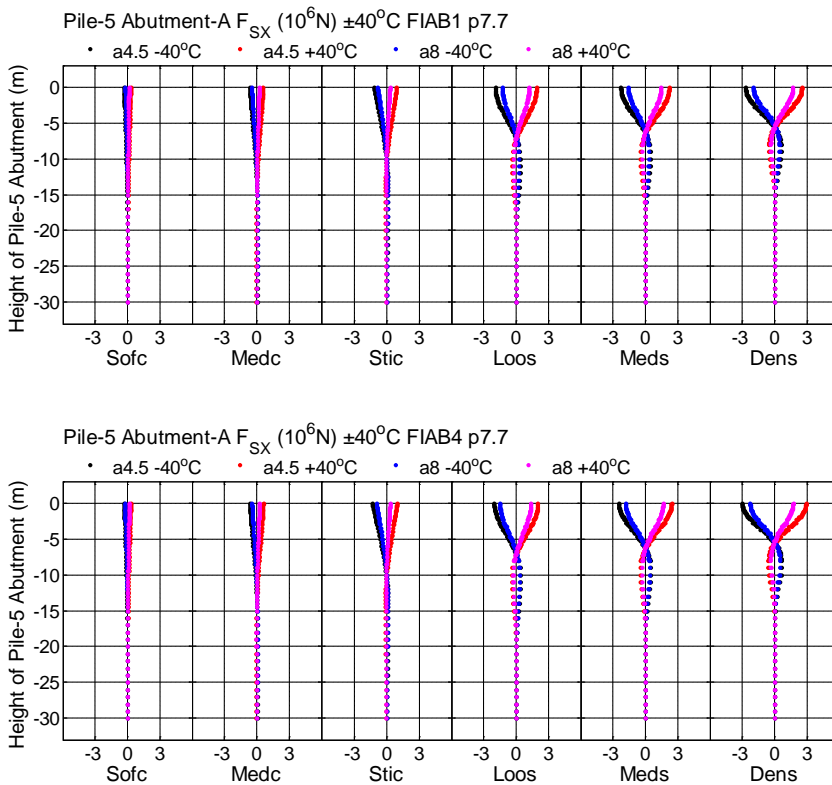
(c) U_X of Pile-5 beneath Abutment-A

Fig. 231 Influence of different abutment heights on the performance of Pile-5 beneath Abutment-A in FIAB1 and FIAB4 under thermal load ($\pm 40^\circ\text{C}$)

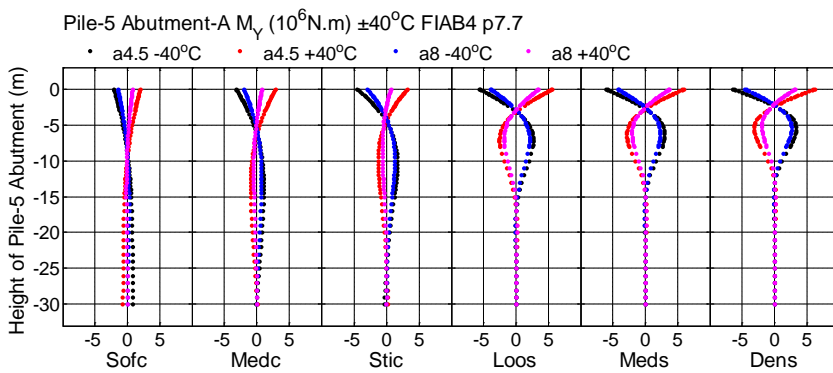
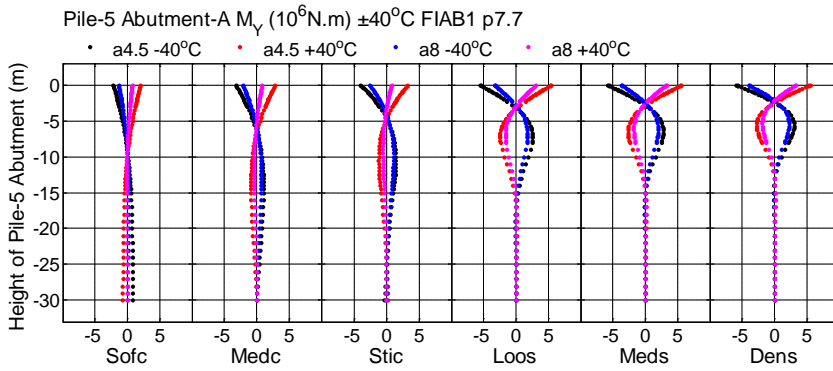
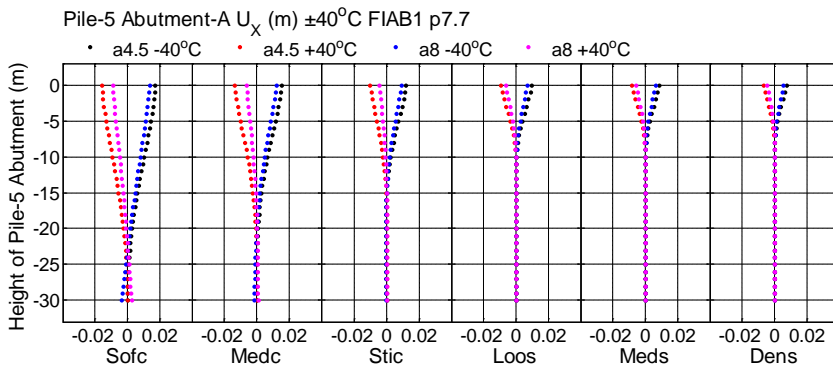
6.3.5.3 Different soil conditions and bridge types

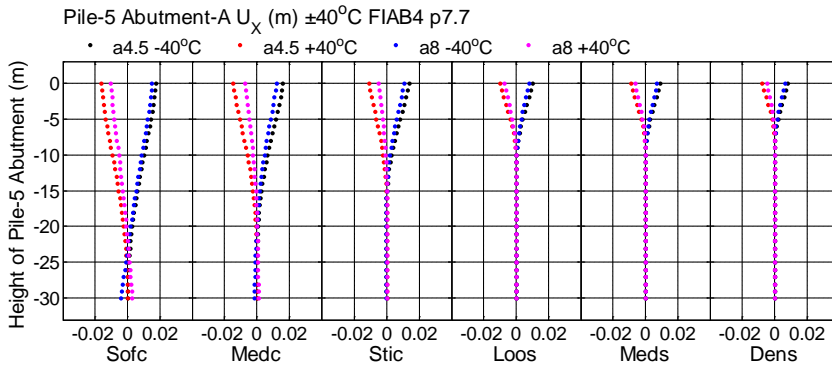
As investigated above, it could be found that under thermal load, the influence of

different pier heights on the performance of piles beneath abutments is negligible. Therefore, the heights of two piers are set as 7.7m in this analysis due to the space limitation. The influence of different abutment heights on the F_{SX} , M_Y and U_X of Pile-5 beneath Abutment-A in FIAB1 and FIAB4 under thermal load ($\pm 40^\circ\text{C}$) considering all soil conditions are illustrated in Fig. 232. It could be observed that, the locations of the critical sections corresponding to the ultimate F_{SX} and U_X of Pile-5 beneath Abutment-A in all FIABs do not change due to soil variations, which occur at the top points of piles. However, the maximum M_Y of piles may appear at two locations, which are the top points or the points at a certain depth of about -5m for sand, and the top points or the points at a certain depth of approximate -10m for clay. For the purpose of simplification, only the M_Y at the top points of piles in FIABs are considered in the following analysis.



(a) F_{SX} of Pile-5 beneath Abutment-A

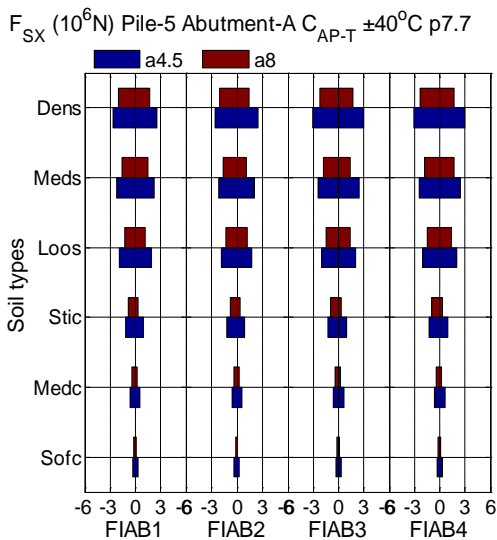
(b) M_Y of Pile-5 beneath Abutment-A



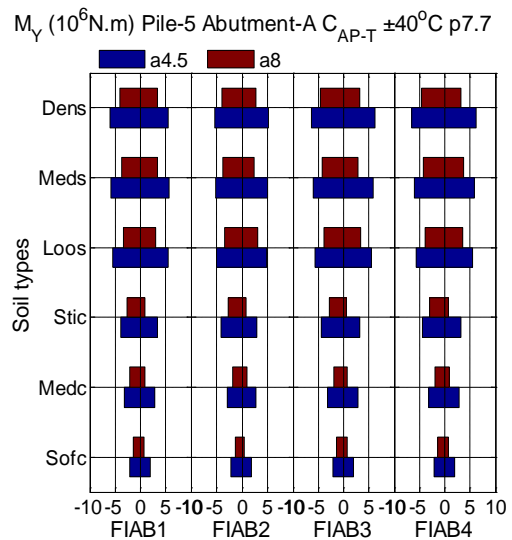
(c) U_x of Pile-5 beneath Abutment-A

Fig. 232 Influence of different abutment heights on the performance of Pile-5 beneath Abutment-A in FIAB1 and FIAB4 under thermal load ($\pm 40^\circ\text{C}$) considering all soil conditions

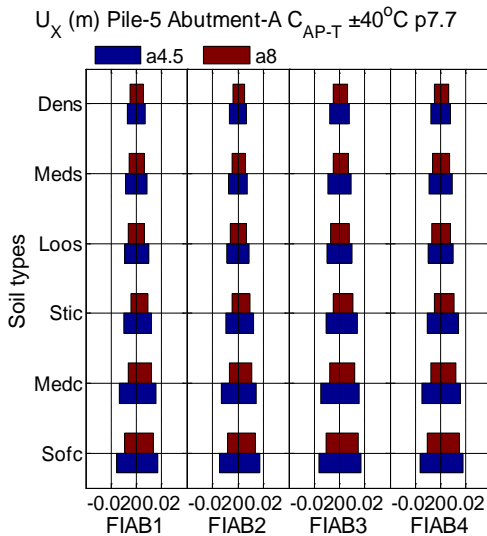
In order to show the influence of different abutment heights and soil conditions clearly, the ultimate F_{SX} , M_Y and U_X at the top point (C_{AP-T}) of Pile-5 beneath Abutment-A are compared in Fig. 233. It could be found that, no matter which soil conditions are considered, the ultimate F_{SX} , M_Y and U_X of Pile-5 beneath Abutment-A in all FIABs decrease with the abutment heights increase.



(a) F_{SX} of Abutment-A backwall



(b) M_Y of Abutment-A backwall



(c) U_x of Abutment-A backwall

Fig. 233 Influence of different abutment heights on the ultimate internal forces of Pile-5 beneath Abutment-A in FIABs under thermal load ($\pm 40^\circ\text{C}$) considering all soil conditions

6.3.6 Summary

The influence of different substructure heights on the performance of different subtypes of FIABs under thermal load is analyzed. It could be found that the influence of different abutment heights on the performance of girders, abutment stems and piles beneath abutments is noticeable or remarkable; however, different pier heights can only affect the performance of piers. When the substructure heights are symmetric around the global coordinate axis Y at the mid-span point of Span-2, the performance of the corresponding bridge components located at the left part and right part of bridge should be equal under thermal load. If the heights of two piers are different, only the performance of piers can be different. However, if the heights of two abutments are different, the performance of girders, abutment stems and piles beneath abutments could be different. Moreover, the influence of different substructure heights on the performance of different subtypes of FIABs considering different soil conditions, are summarized in Table 52. This results could not only help engineers to choose the most suitable retrofitting process for different cases, but also provide the guideline which could be used in the design of new IABs.

The differences between the effects of different abutment heights on the performance of bridges in clay and that in sand is mainly due to the lateral soil-structure interaction behind two abutments and around piles. From the lateral

RETROFIT OF EXISTING BRIDGES WITH CONCEPT OF INTEGRAL ABUTMENT BRIDGE

earth pressure-pile displacement relationship (p-y curve) and the lateral earth pressure-abutment movement relationship (P- Δ_b curve) (Section 6.2.1), it could be found that, considering the soil condition as sand, the horizontal resistance force produced by p-y curves on the piles is more than ten times larger than that produced by P- Δ_b curves behind two abutments. However, when the soil condition is clay, the horizontal resistance force produced by p-y curves on the piles is smaller than that produced by P- Δ_b curves behind two abutments. Therefore, with the abutment heights increase, the U_x of girders and abutment stems increase when the soil condition is sand, while, the U_x of girders and abutment stems decrease when the soil condition is clay. In general, the performance of different bridge components in the case with different substructure heights can be predicted by the corresponding idealized cases with equal substructure heights. Moreover, when the soil condition is soft clay, the special arrangement of substructure heights should be paid more attention to. The lateral resistance force produced by the soil is small. Therefore, the unfavorable influence of asymmetric substructure heights could be amplified.

Component	Internal force	Bridge types	With the increase of pier height		With the increase of abutment height	
			Clay	Sand	Clay	Sand
Girder	F_A	FIAB1	-	-	Increase	Decrease
		FIAB2	-	-	Increase	Decrease
		FIAB3	-	-	Increase	Decrease
		FIAB4	-	-	Increase	Decrease
	M_y	FIAB1	-	-	Increase	Decrease
		FIAB2	-	-	Increase	Decrease
		FIAB3	-	-	Increase	Increase
		FIAB4	-	-	Increase	Increase
	U_x	FIAB1	-	-	Decrease	Increase
		FIAB2	-	-	Decrease	Increase
		FIAB3	-	-	Decrease	Increase
		FIAB4	-	-	Decrease	Increase
	U_z	FIAB1	-	-	Increase	Decrease
		FIAB2	-	-	Increase	Decrease
		FIAB3	-	-	Increase	Increase
		FIAB4	-	-	Increase	Increase
Pier	F_{sx}	FIAB1	Decrease	Decrease	-	-
		FIAB2	Decrease	Decrease	-	-
		FIAB3	Decrease	Decrease	-	-

	M_Y at top	FIAB4	Decrease	Decrease	-	-
		FIAB1	-	-	-	-
		FIAB2	Increase	Increase	-	-
		FIAB3	-	-	-	-
	M_Y at bottom	FIAB4	Increase	Increase	-	-
		FIAB1	Decrease	Decrease	-	-
		FIAB2	Increase	Decrease	-	-
		FIAB3	Decrease	Decrease	-	-
	U_x	FIAB4	Increase	Decrease	-	-
		FIAB1	Increase	Increase	-	-
		FIAB2	Increase	Increase	-	-
		FIAB3	Increase	Increase	-	-
	Abutment stem	F_{sx}	FIAB4	-	-	Increase
FIAB1			-	-	Increase	Decrease
FIAB2			-	-	Increase	Decrease
FIAB3			-	-	Increase	Decrease
M_Y		FIAB4	-	-	Increase	Increase
		FIAB1	-	-	Increase	Increase
		FIAB2	-	-	Increase	Increase
		FIAB3	-	-	Increase	Increase
U_x		FIAB4	-	-	Decrease	Increase
		FIAB1	-	-	Decrease	Increase
		FIAB2	-	-	Decrease	Increase
		FIAB3	-	-	Decrease	Increase
Pile beneath abutment		F_{sx}	FIAB4	-	-	Decrease
	FIAB1		-	-	Decrease	Decrease
	FIAB2		-	-	Decrease	Decrease
	FIAB3		-	-	Decrease	Decrease
	M_Y	FIAB4	-	-	Decrease	Decrease
		FIAB1	-	-	Decrease	Decrease
		FIAB2	-	-	Decrease	Decrease
		FIAB3	-	-	Decrease	Decrease
	U_x	FIAB4	-	-	Decrease	Decrease
		FIAB1	-	-	Decrease	Decrease
		FIAB2	-	-	Decrease	Decrease
		FIAB3	-	-	Decrease	Decrease

Table 52

RETROFIT OF EXISTING BRIDGES WITH CONCEPT OF INTEGRAL ABUTMENT BRIDGE

Influence of different substructure heights on the performance of different bridge components in FIABs under thermal load

7. STATIC PERFORMANCE CHECK AFTER RETROFITTING

From the results of static sensitive analyses, it could be found that the performance of girders, piers, abutment stems and piles in FIABs after retrofitting could be larger than those in the existing SSB. Therefore, it is necessary to carry out some investigations to verify if the existing cross sections have the enough capacities to bear the forces, bending moments and displacements produced by the new bridge types after retrofitting and to point out the critical components, which need to be repaired or modified.

7.1 Force-Moment interaction diagram analysis

In this analysis, the influence of loads combinations in the updated code NTC 2008, (Table 40 (p.202)), on the performance of four subtypes of FIABs after retrofitting (FIAB1, FIAB2, FIAB3 and FIAB4 as introduced in Table 47 (p.219)), was analyzed. Two types of uniform bridge temperature components were chosen as the thermal load, which are $\pm 15^{\circ}\text{C}$ corresponding to the Italian codes (Ministero delle Infrastrutture, 2008) and $\pm 40^{\circ}\text{C}$ considered in some European Countries (Feldmann et al., 2010; Pétursson et al., 2011). The axial force (F_A) and bending moment (M) of different bridge components were chosen to compare with their force-moment resistance domains (F_A - M domain). If the F_A - M interaction diagrams of existing sections exceed the F_A - M domains, the corresponding sections should be paid more attention to and the suitable detailed retrofitting solution should be carried out during the retrofit of the whole bridge.

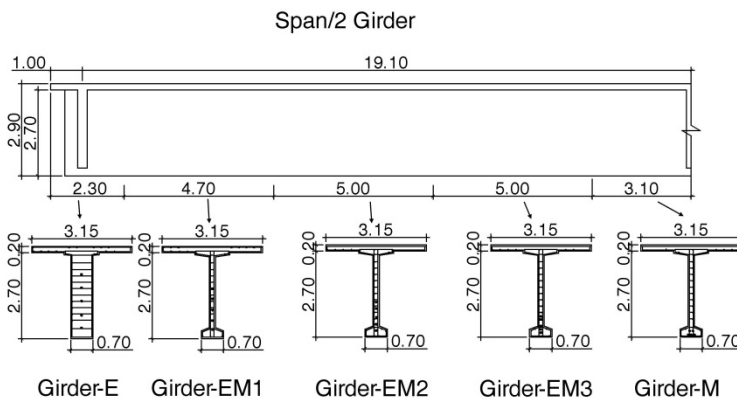
7.1.1 F_A - M domain

In order to obtain the F_A - M domain of a certain cross section, the constitutive relationships of different materials, the detailed dimensions of cross sections and the information of rebar arrangements should be known. The constitutive relationships of steel rebar, the prestressing tendon and concrete have been described in Chapter 5.2.2. The detailed dimensions of cross sections and the information of rebar arrangements corresponding to the pier and pile have been illustrated in Fig. 142

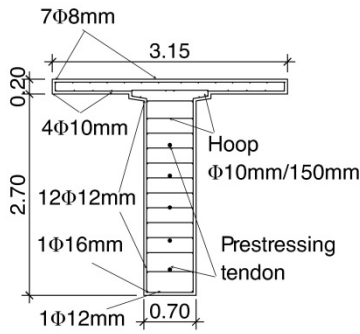
(p.183) and Fig. 147 (p.186), respectively. The detailed dimensions of section and the information of rebar arrangements of the girder and the abutment stem will be introduced in the following.

Several programs can be used to obtain the F_A - M domain of a certain cross section, such as VcaSlu (Prof. Piero Gelfi, 2011), XTRACT (TRC/Imbsen Software Systems, 2007), Sap2000 (Computers and Structures Inc, 2011) and so on. Based on information from Fig. 142 (p.183) for pier and Fig. 147 (p.186) for pile, the F_A - M_Y domain of pier cross section obtained by XTRACT and Sap2000, and the F_A - M_Y domain of pile cross section obtained by VcaSlu and Sap2000, could be obtained, as illustrated respectively in Fig. 236(b) and (d). It indicates that the F_A - M domain obtained by three programs are nearly the same. Therefore, the Sap2000 could be chosen as the program to carry out the further research.

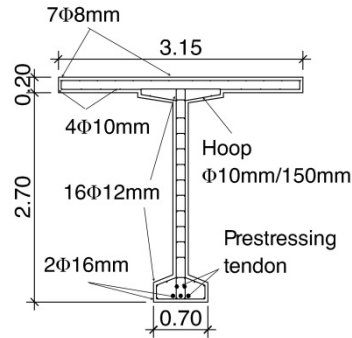
According to the variations of the cross section dimensions and the prestressing tendon arrangements in the superstructure, the girders in one span could be divided into nine segments from the elevation view, as shown in Fig. 234(a). Girder-E denotes the segment that is near the end of each girder, Girder-M represents the segment that is in the middle of each girder, and Girder-EM1, Girder-EM2 and Girder-EM3 are the segments between Girder-E and Girder-M. Due to the space limitation, the detailed dimensions of cross sections and the information of rebar arrangements for Girder-E and Girder-M are chosen as examples to illustrate respectively in Fig. 234(b) and (c). The cross sections of Girder-M, Girder-EM1, Girder-EM2 and Girder-EM3 are I-girder cross section and the cross section of Girder-E is T-girder cross section. When calculating the F_A - M_Y domain, the prestressing tendons are considered as normal steel rebar. The F_A - M_Y domains corresponding to different segments of girders are shown in Fig. 236(a).



(a) Elevation of half-span girder



(b) Cross section of Girder-E



(c) Cross section of Girder-M

Fig. 234 Elevation of half-span girder and cross section of Girder-E and Girder-M

The detailed dimensions of the cross section and the information of rebar arrangements for the stems in two abutments are the same, which is illustrated in Fig. 235. The cross section of the abutment stem is rectangular shape. The F_A - M_Y domain of abutment stem cross section is illustrated in Fig. 236(d).

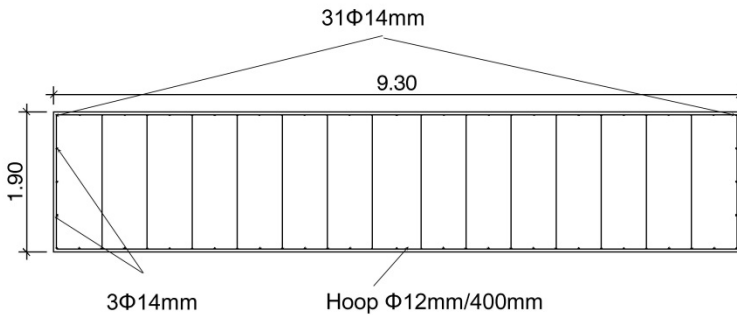
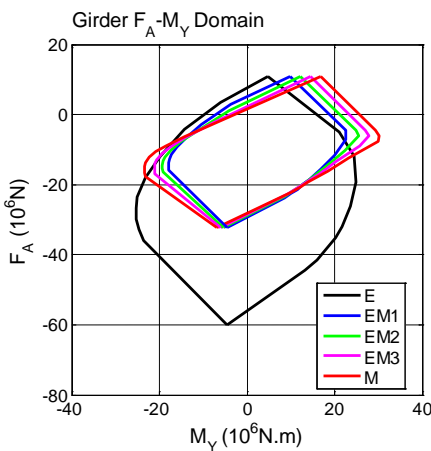
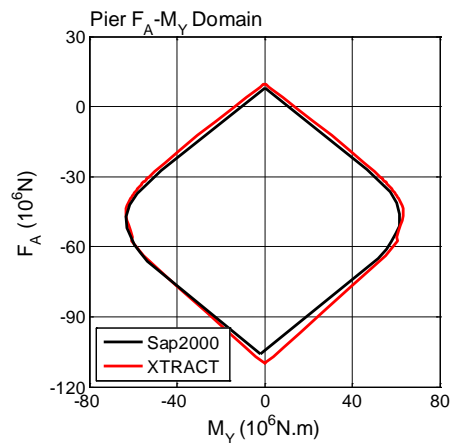


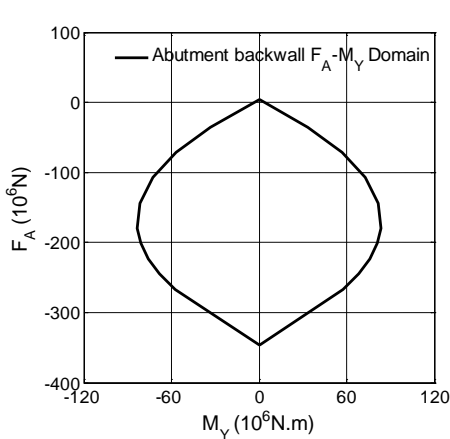
Fig. 235 Cross section of abutment stem



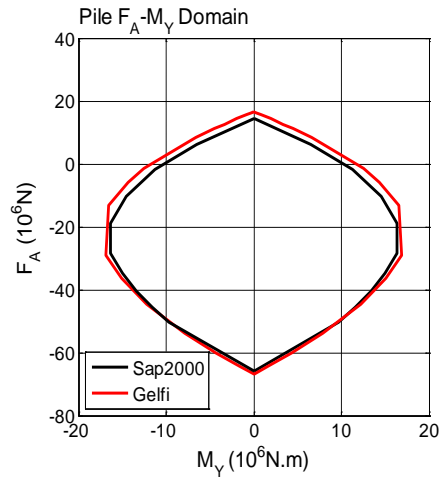
(a) F_A - M_Y domain of girder



(b) F_A - M_Y domain of pier



(c) F_A - M_Y domain of abutment stem
Fig. 236 F_A - M_Y domain



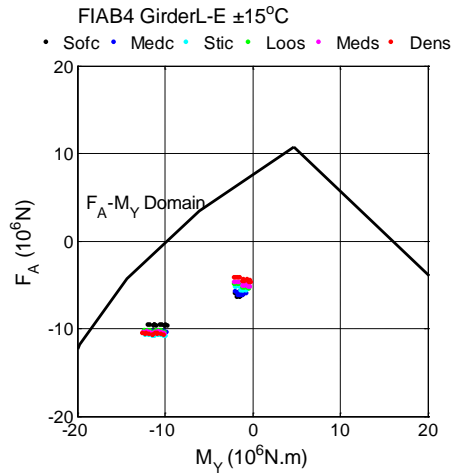
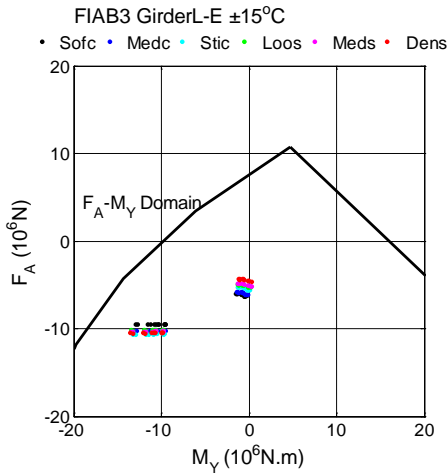
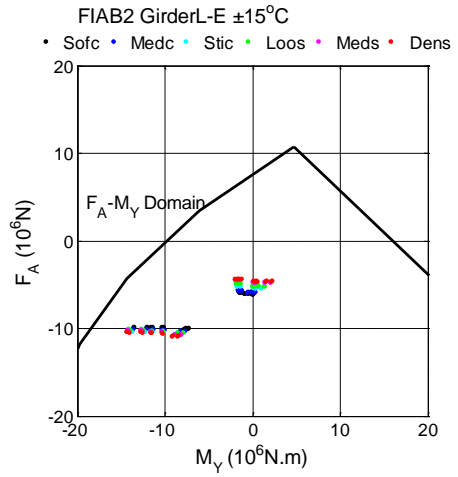
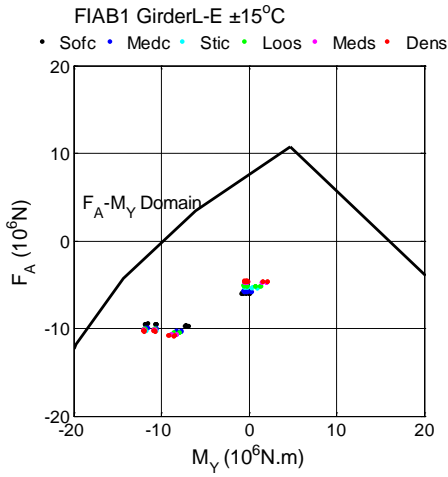
(d) F_A - M_Y domain of pile

7.1.2 F_A - M interaction diagram check

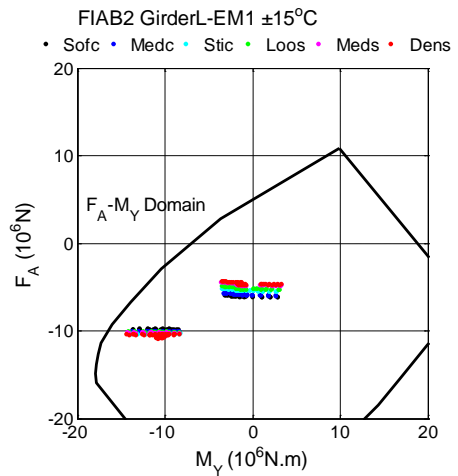
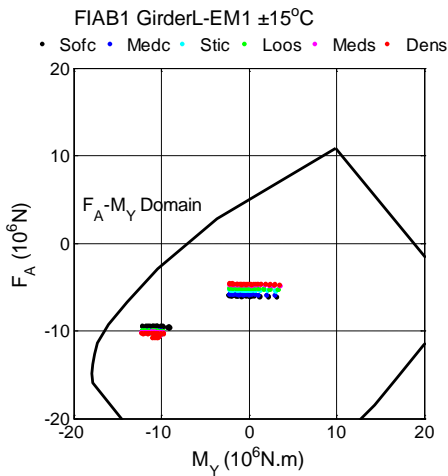
For different bridge components, the F_A - M_Y interaction diagrams of cross sections under loads combinations should be compared with the corresponding F_A - M_Y domains. The loads combinations defined in Table 40 (p.202) considering two kinds of thermal loads ($\pm 15^\circ\text{C}$ and $\pm 40^\circ\text{C}$), six types of soil with the properties listed in Table 34 (p.165) and five bridge types, including the existing SSB and four subtypes of FIABs, could be taken into account in this verification. It could be found that all the F_A - M_Y interaction diagrams of different bridge components in SSB are within the limits of the corresponding F_A - M_Y domains. Due to the space limitation, the figures of the SSB will not be illustrated in this section.

7.1.2.1 Girder

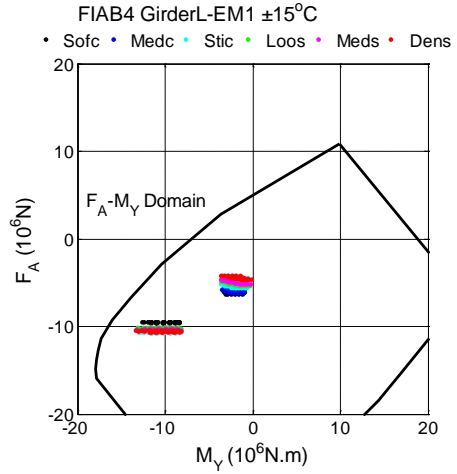
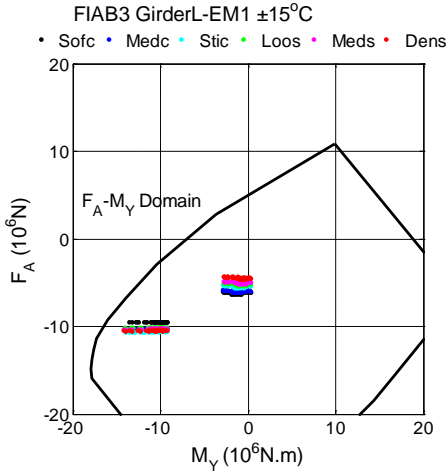
The F_A - M_Y interaction diagrams of Girder-L and the corresponding F_A - M_Y domains of different girder segments are compared in Fig. 237 and Fig. 238. It could be found that, if the existing bridge is located in the countries, which consider the thermal load as $\pm 15^\circ\text{C}$, the existing cross sections of girders can be reused after retrofitting, because no F_A - M_Y interaction diagrams of Girder-L in FIABs could exceed the limits of the corresponding F_A - M_Y domains. However, if the retrofitting work will be conducted in the countries, which have severe temperature variations ($\pm 40^\circ\text{C}$) and the soil conditions are sand and stiff clay, Girder-EM1 in FIAB1 and FIAB2 should be paid attention to. Some retrofitting works should be conducted on the Girder-EM1 to increase the resistance capacity of the negative M_Y .



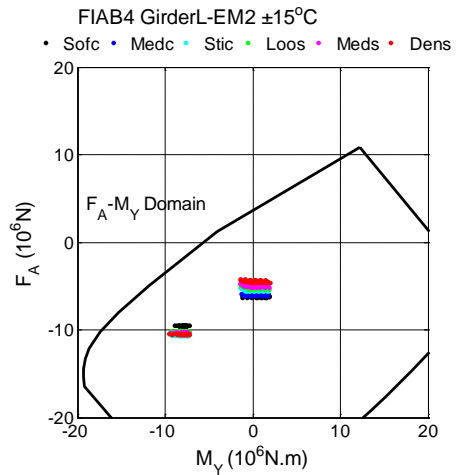
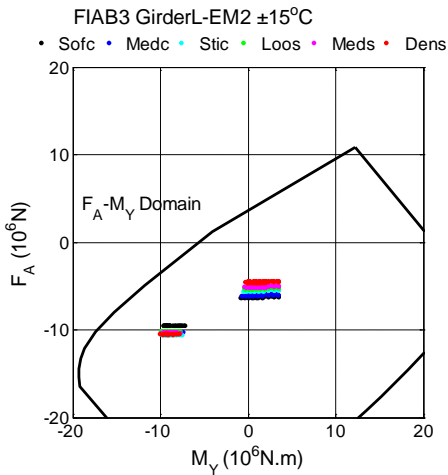
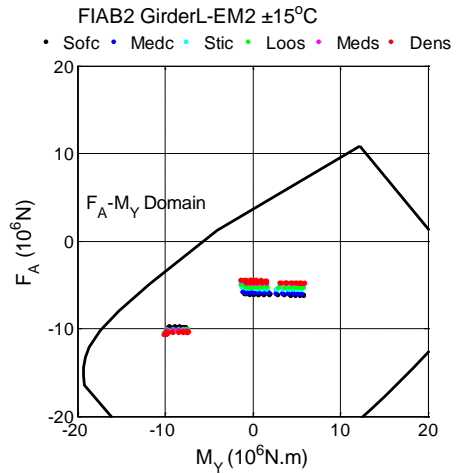
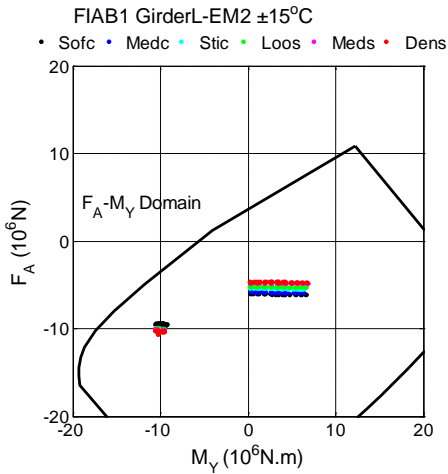
(a) Girder-E



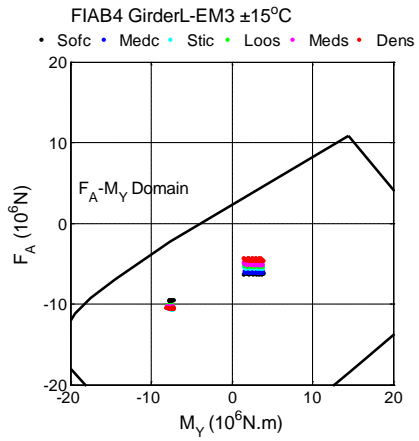
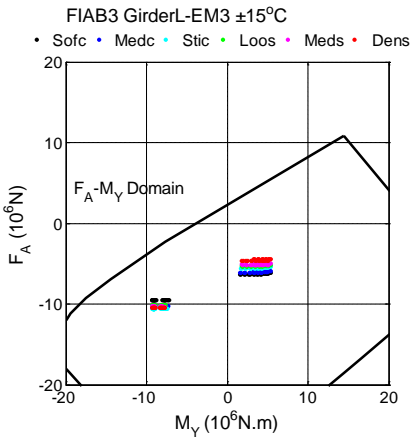
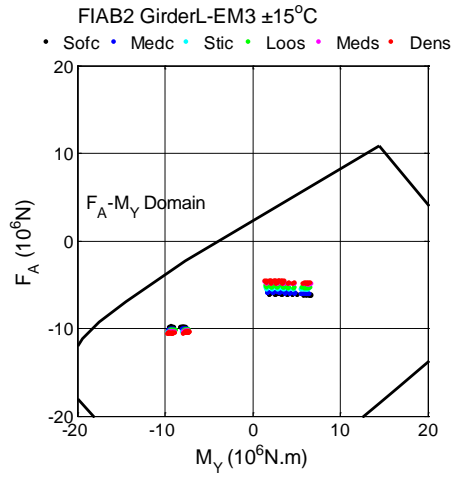
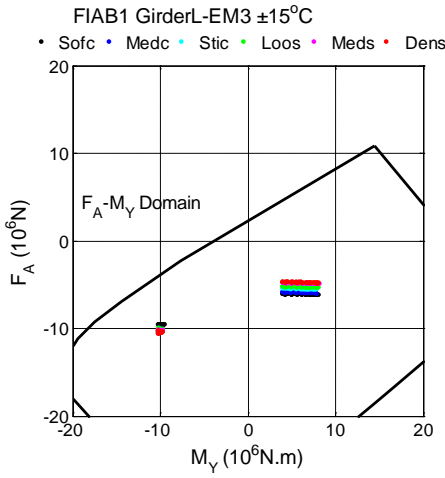
RETROFIT OF EXISTING BRIDGES WITH CONCEPT OF INTEGRAL ABUTMENT BRIDGE



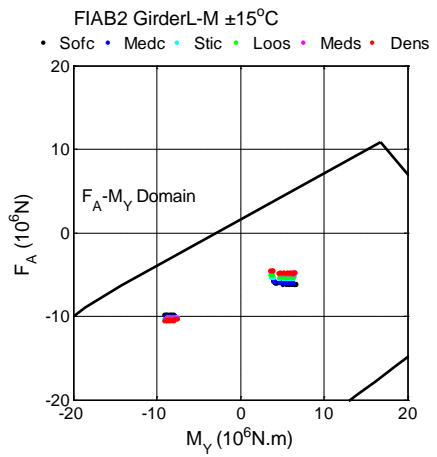
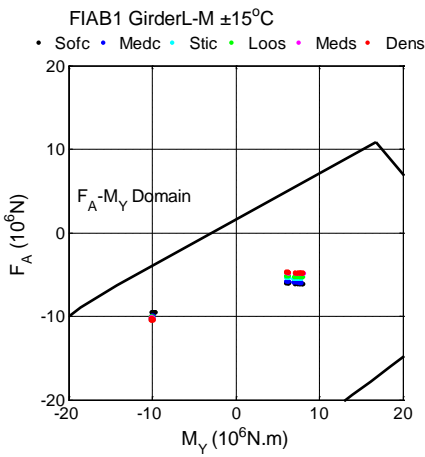
(b) Girder-EM1



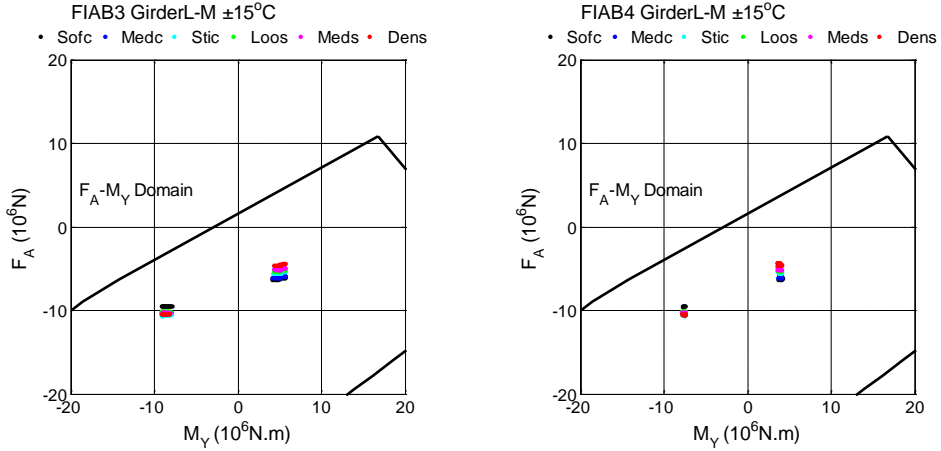
(c) Girder-EM2



(d) Girder-EM3

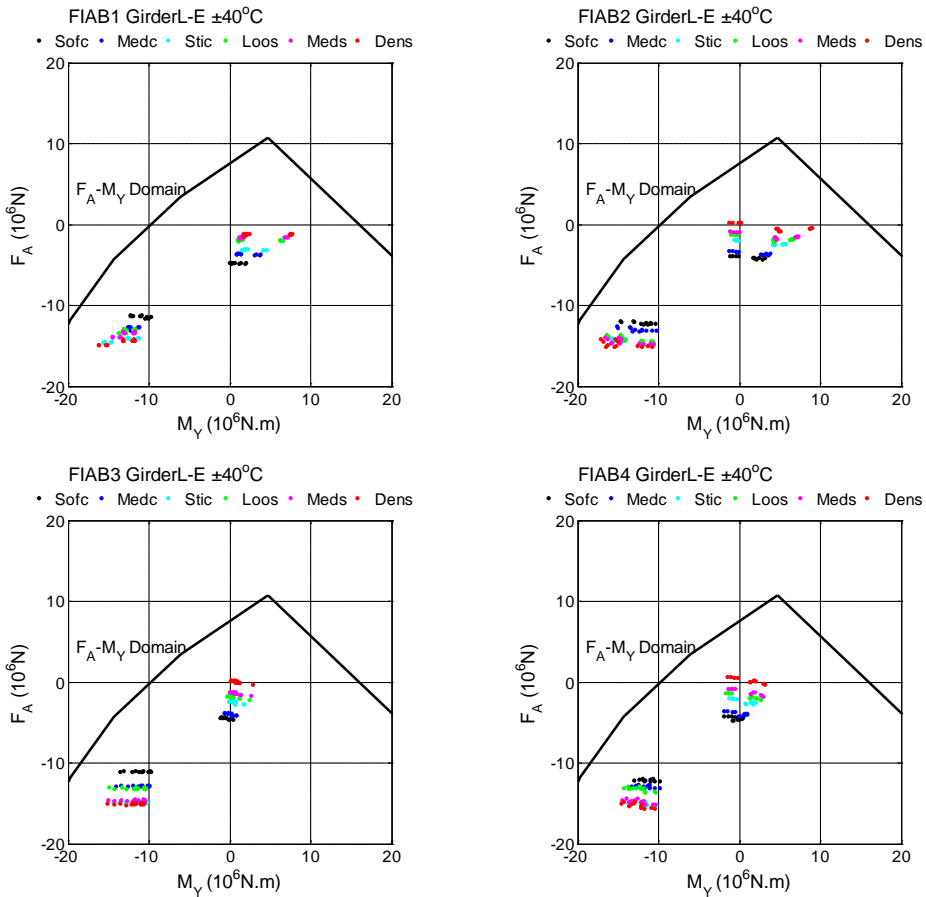


RETROFIT OF EXISTING BRIDGES WITH CONCEPT OF INTEGRAL ABUTMENT BRIDGE

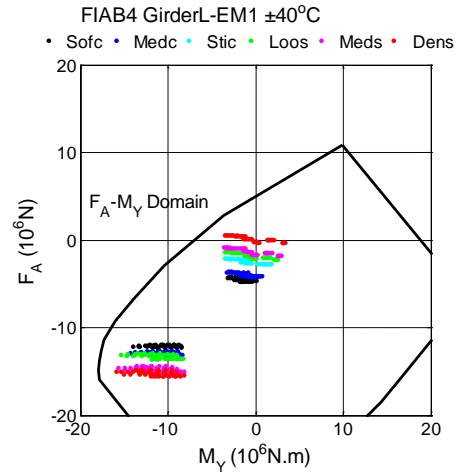
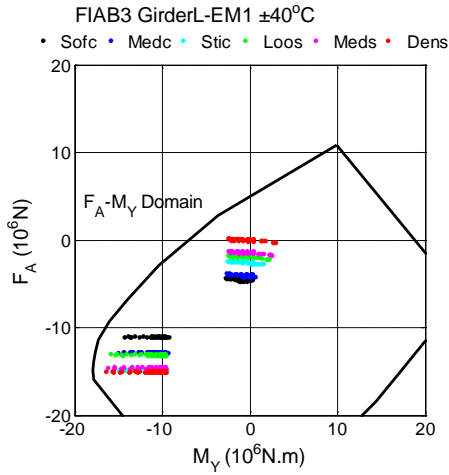
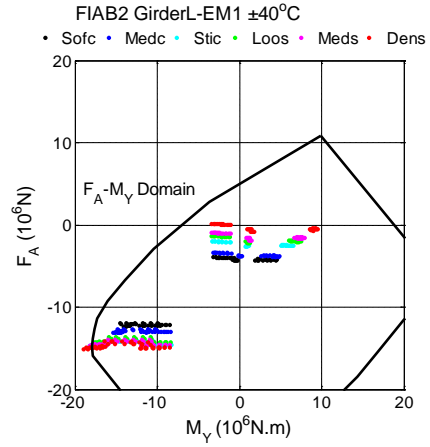
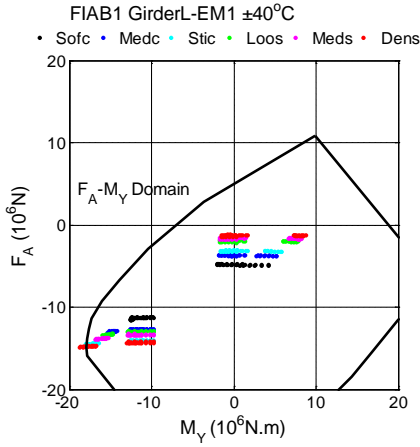


(e) Girder-M

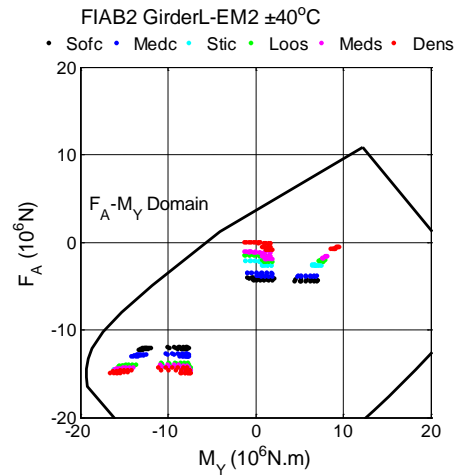
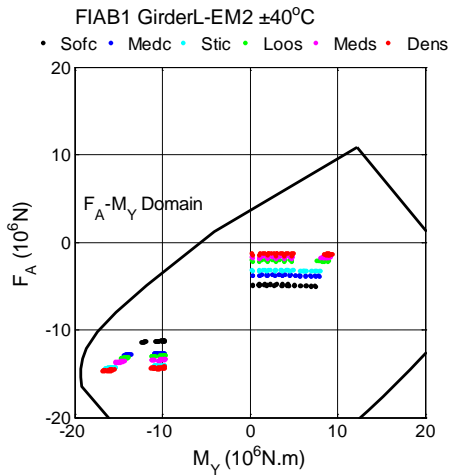
Fig. 237 Comparison between F_A - M_Y interaction diagrams of Girder-L under loads combination ($\pm 15^{\circ}\text{C}$) and the corresponding F_A - M_Y domains



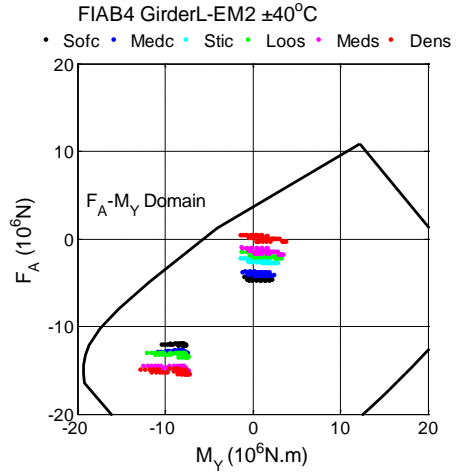
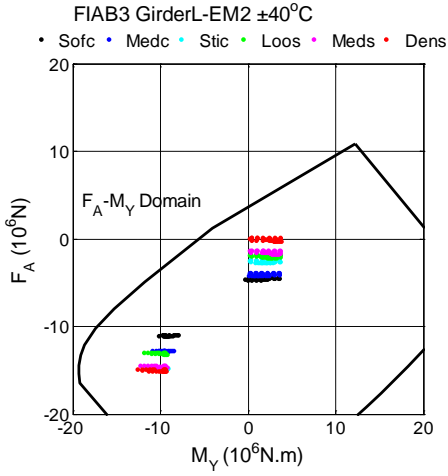
(a) Girder-E



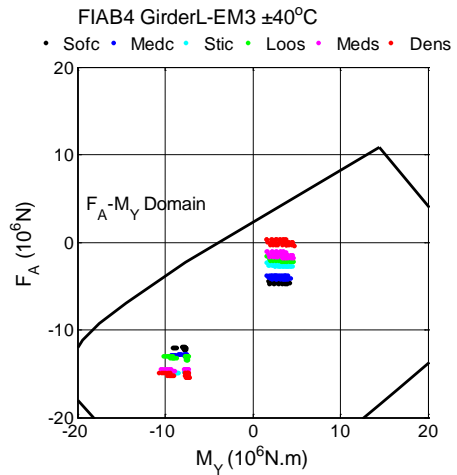
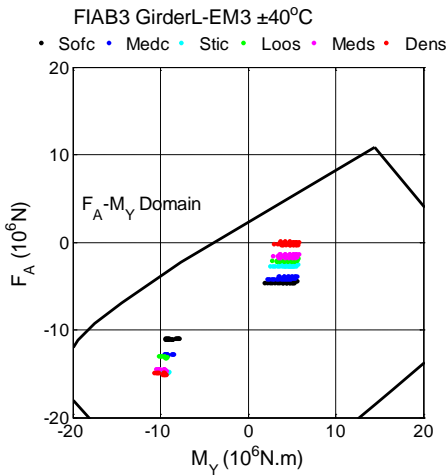
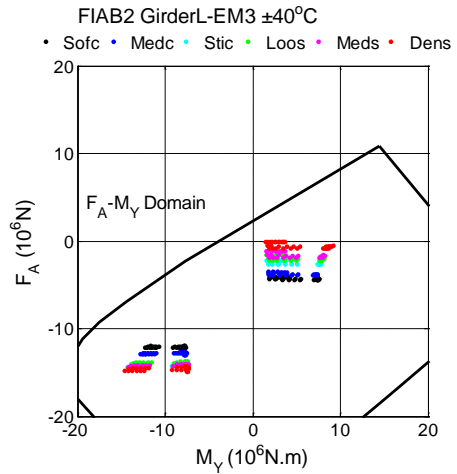
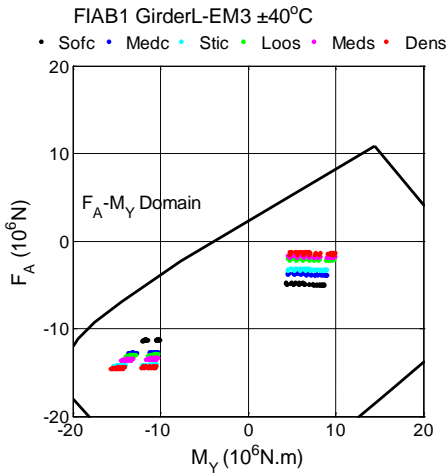
(b) Girder-EM1



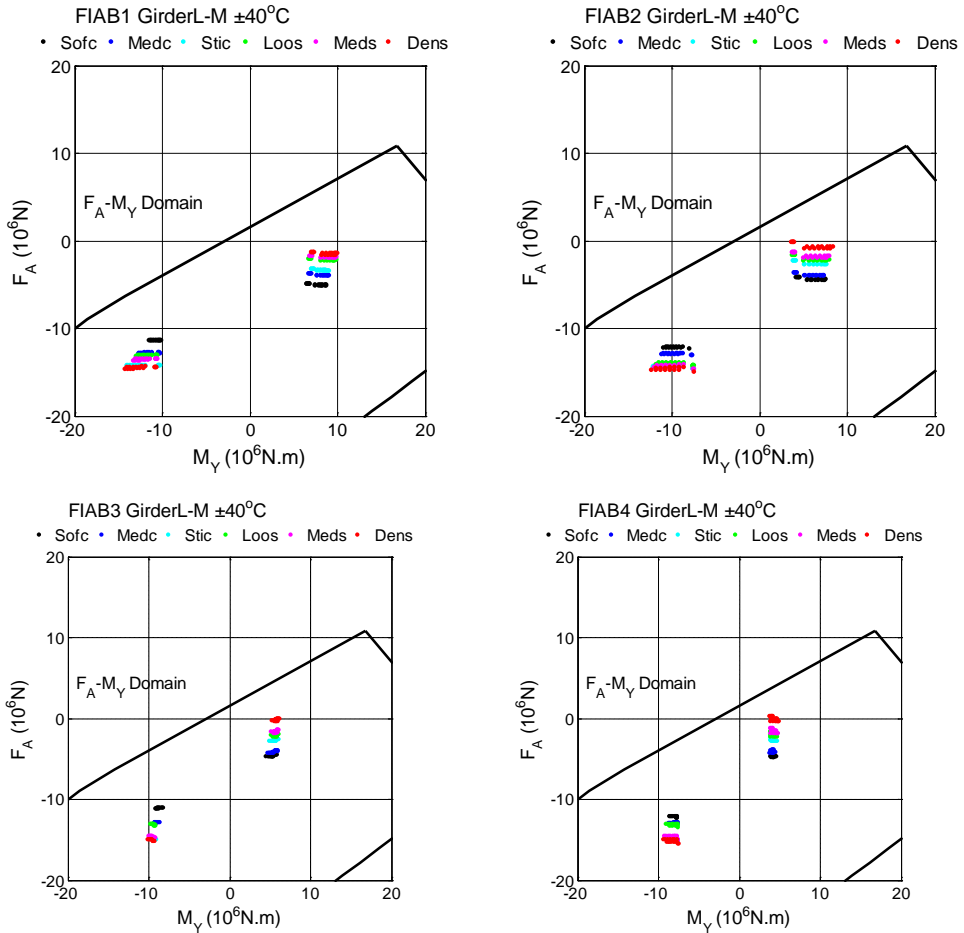
RETROFIT OF EXISTING BRIDGES WITH CONCEPT OF INTEGRAL ABUTMENT BRIDGE



(c) Girder-EM2



(d) Girder-EM3



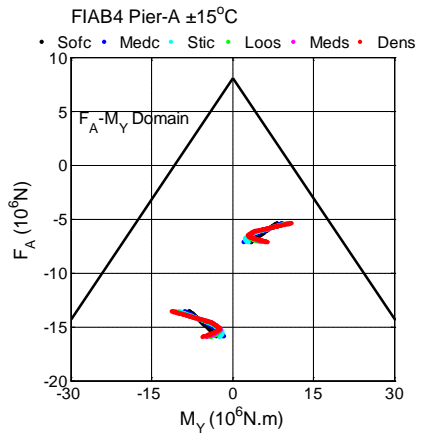
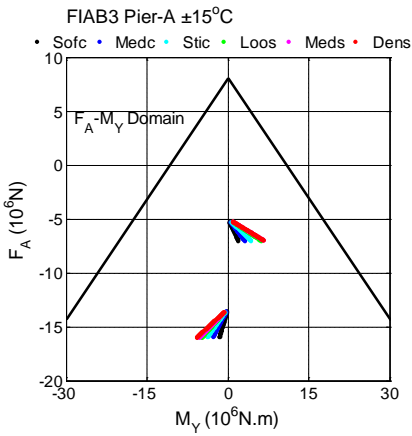
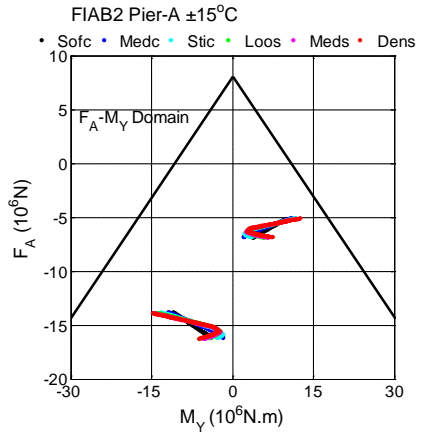
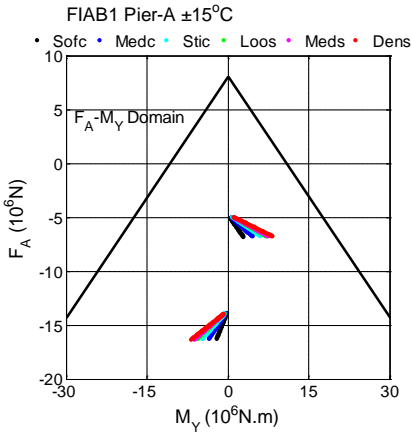
(e) Girder-M

Fig. 238 Comparison between F_A - M_Y interaction diagrams of Girder-L under loads combination ($\pm 40^\circ\text{C}$) and the corresponding F_A - M_Y domains

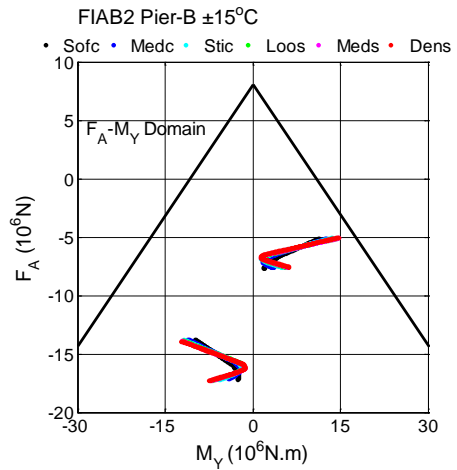
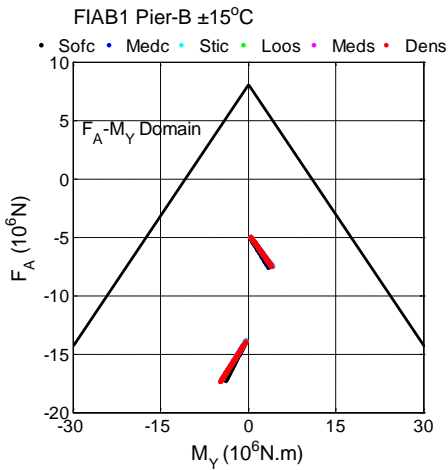
7.1.2.2 Pier

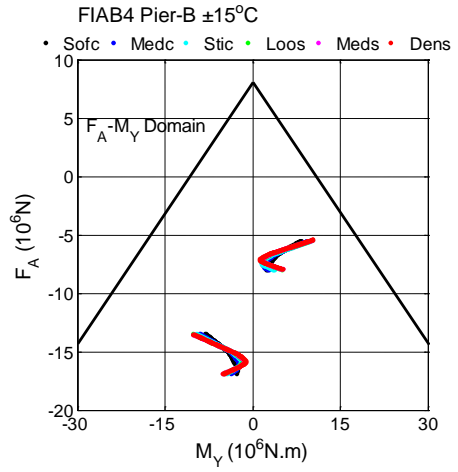
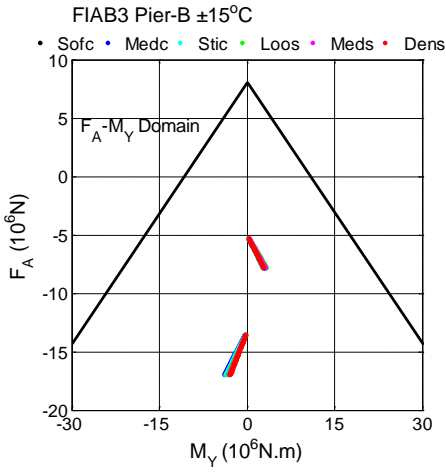
The F_A - M_Y interaction diagrams of piers and the corresponding F_A - M_Y domain of the pier are compared in Fig. 239 and Fig. 240. It could be observed that, if the existing bridge is located in the countries, which consider the thermal load as $\pm 15^\circ\text{C}$, no retrofitting work needs to be done on existing piers after retrofitting, because all the F_A - M_Y interaction diagrams of piers in integral abutment bridges are within the limit of the corresponding F_A - M_Y domain of the pier. However, if the existing bridge was constructed in the countries, which have severe temperature variations ($\pm 40^\circ\text{C}$) and the soil condition is sand and stiff clay, the retrofitting work should be conducted on the upper part of two piers in FIAB2.

RETROFIT OF EXISTING BRIDGES WITH CONCEPT OF INTEGRAL ABUTMENT BRIDGE



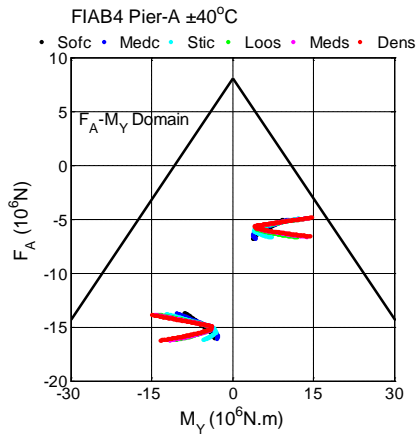
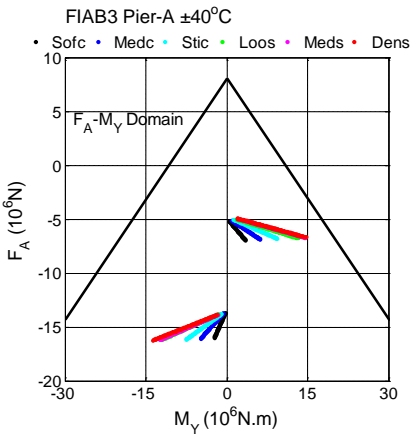
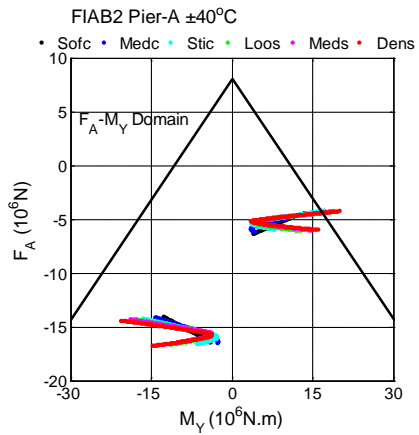
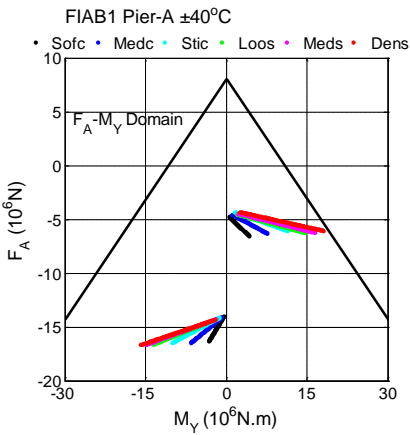
(a) Pier-A





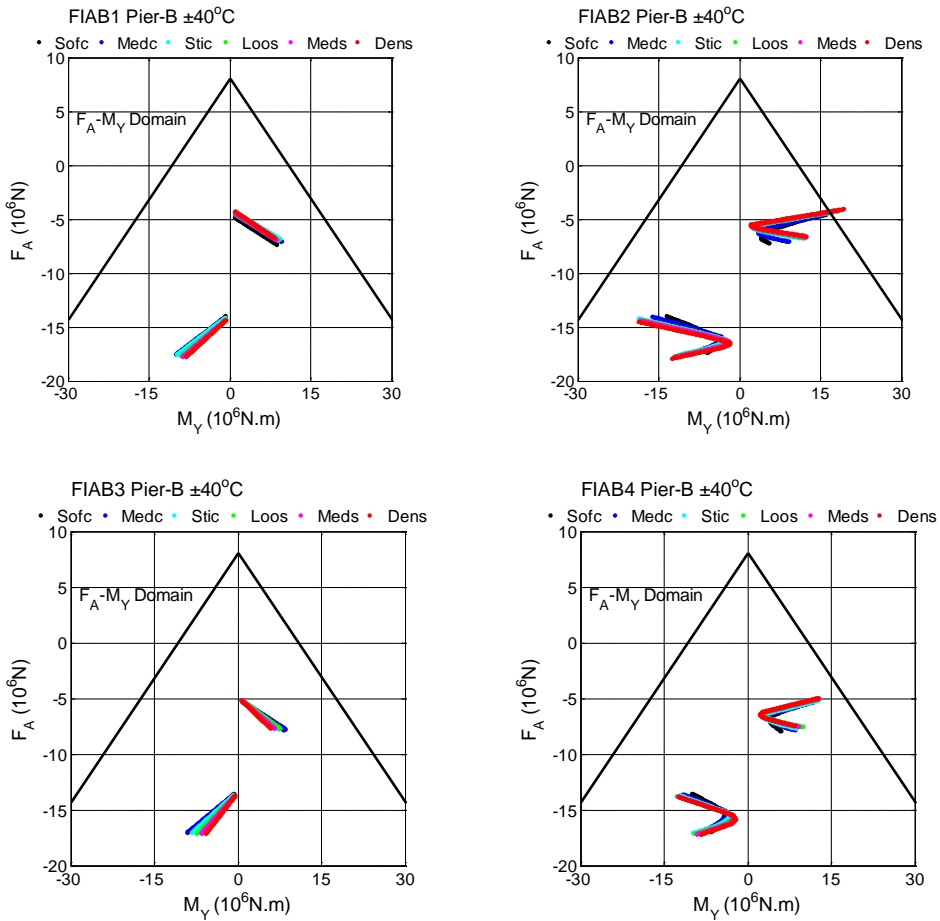
(b) Pier-B

Fig. 239 Comparison between F_A - M_Y interaction diagrams of piers under loads combination ($\pm 15^\circ\text{C}$) and the corresponding F_A - M_Y domain



(a) Pier-A

RETROFIT OF EXISTING BRIDGES WITH CONCEPT OF INTEGRAL ABUTMENT BRIDGE

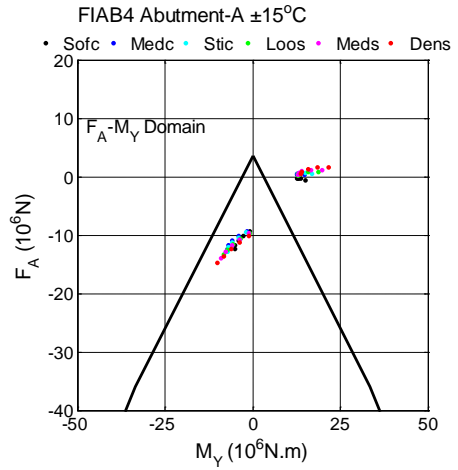
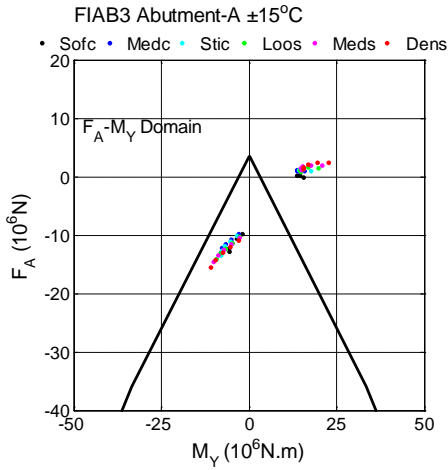
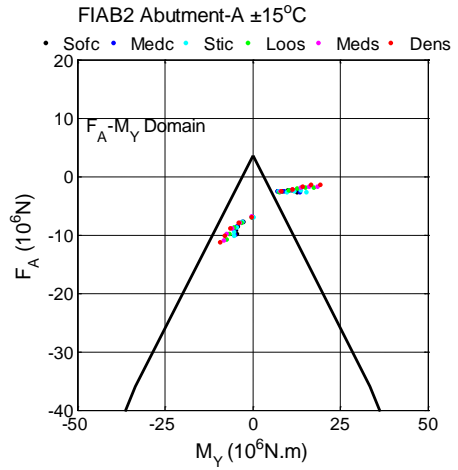
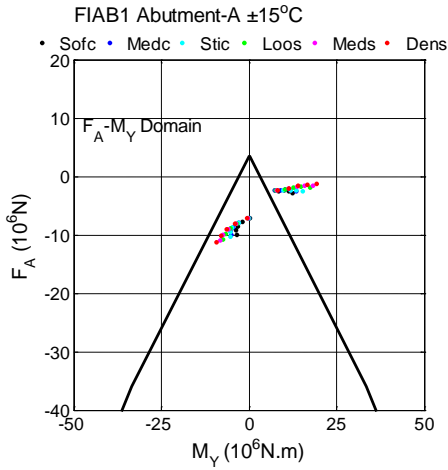


(b) Pier-B

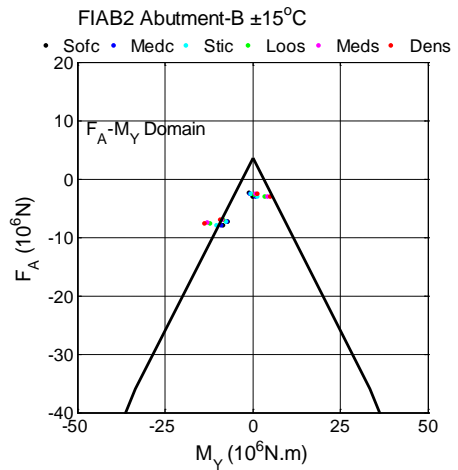
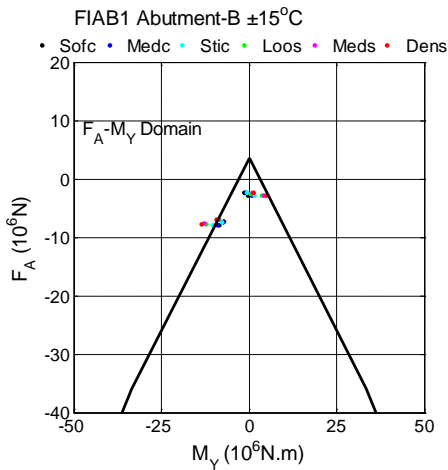
Fig. 240 Comparison between F_A - M_Y interaction diagrams of piers under loads combination ($\pm 40^\circ\text{C}$) and the corresponding F_A - M_Y domain

7.1.2.3 Abutment stem

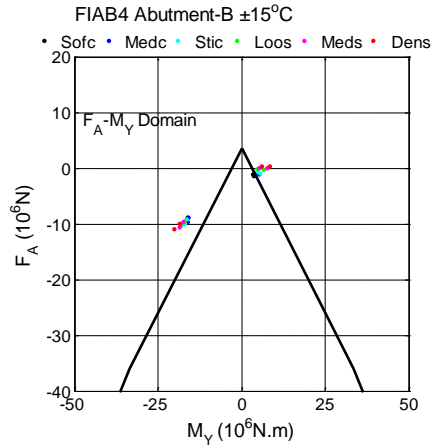
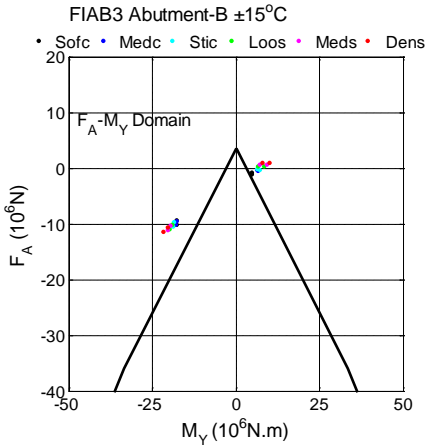
For abutment stems, the F_A - M_Y interaction diagrams and the corresponding F_A - M_Y domain are compared in Fig. 241 and Fig. 242. It could be found that, nearly all the F_A - M_Y interaction diagrams of abutment stems in FIABs could exceed the limits of the corresponding F_A - M_Y domain of the abutment stem. Therefore, the existing abutment stem cannot be reused without any changes after retrofitting in all countries. If the retrofitting project will be carried out in the countries with slight temperature variations, the retrofit of the abutment stem will be less than that in the countries with violent temperature variations. Moreover, converting into FIAB1 or FIAB2, the retrofit of the abutment stem will be less than that in FIAB3 or FIAB4. The denser the soil is, the more retrofitting works should be conducted.



(a) Abutment-A

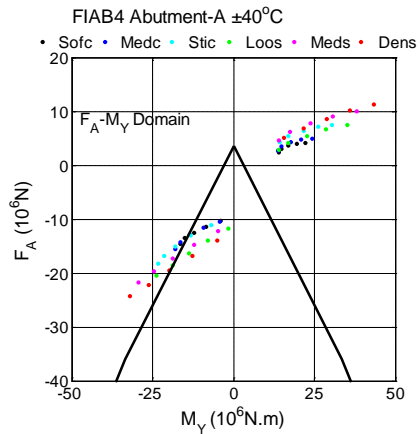
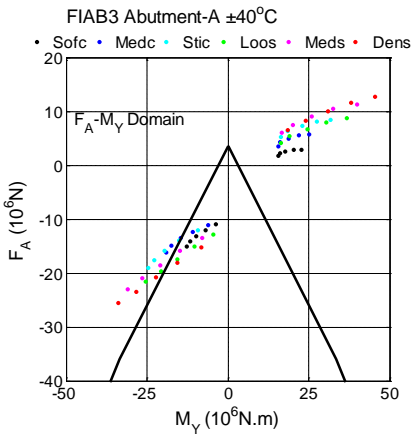
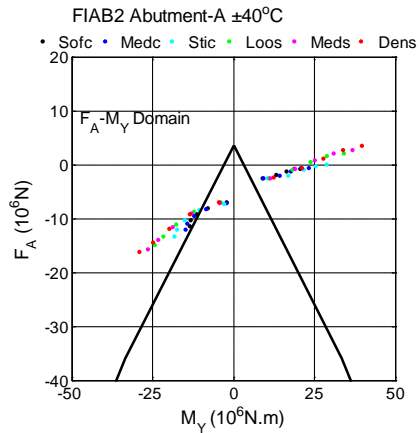
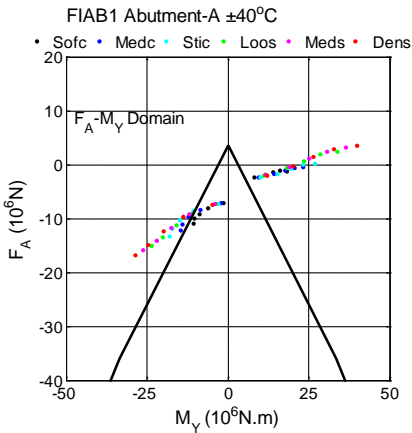


RETROFIT OF EXISTING BRIDGES WITH CONCEPT OF INTEGRAL ABUTMENT BRIDGE

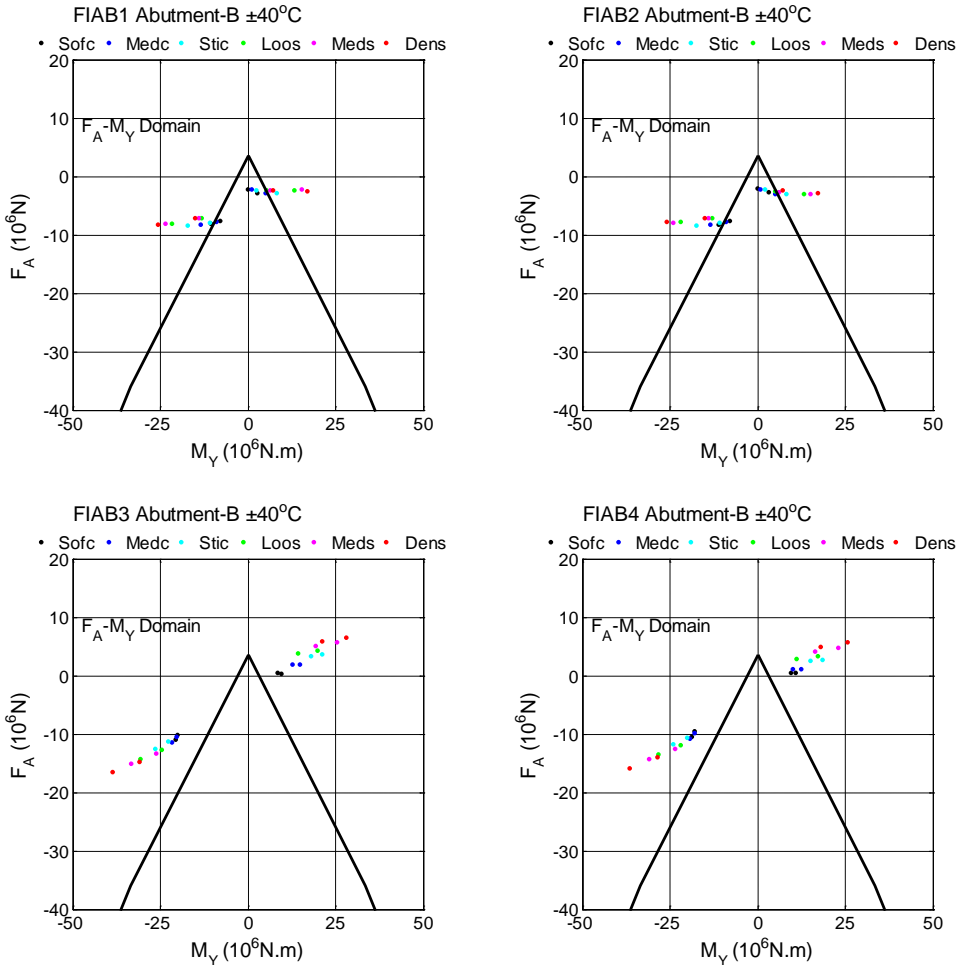


(b) Abutment-B

Fig. 241 Comparison between F_A - M_Y interaction diagram of abutment stems under loads combination ($\pm 15^\circ\text{C}$) and the corresponding F_A - M_Y domain



(a) Abutment-A



(b) Abutment-B

Fig. 242 Comparison between F_A - M_Y interaction diagram of abutment stems under loads combination ($\pm 40^\circ\text{C}$) and the corresponding F_A - M_Y domain

7.1.2.4 Pile

As found above, the M_Y of pile beneath piers under both vertical and horizontal load cases are quite small. Considering the thermal load as $\pm 40^\circ\text{C}$, the F_A - M_Y interaction diagrams of Pile-5 beneath Pier-B in four subtypes of FIABs and the corresponding F_A - M_Y domain of the pile are chosen as examples to compared in Fig. 243. It could be observed that, no matter which soil condition is considered, all the F_A - M_Y interaction diagrams of piles beneath piers in FIABs are within the limit of the corresponding F_A - M_Y domain of pile considering the thermal load as $\pm 40^\circ\text{C}$. Therefore, the piles beneath piers can remain constant after retrofitting in all countries.

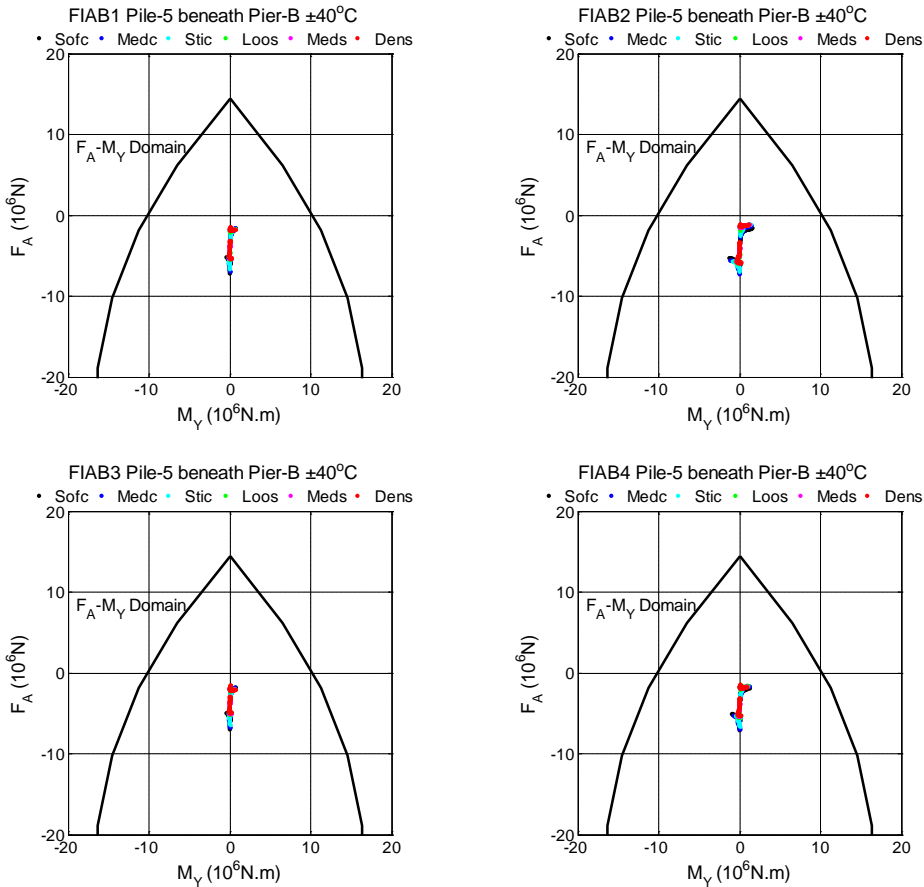
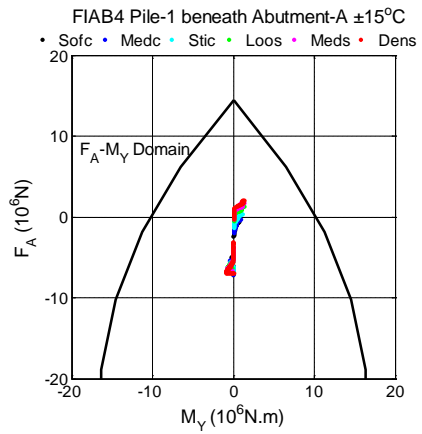
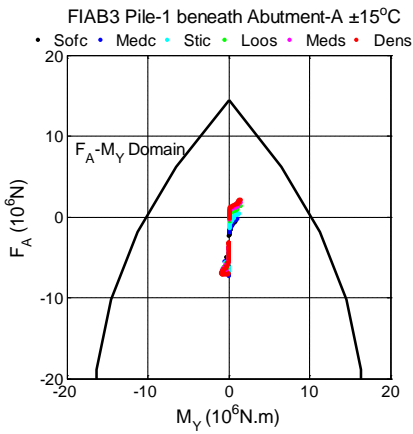
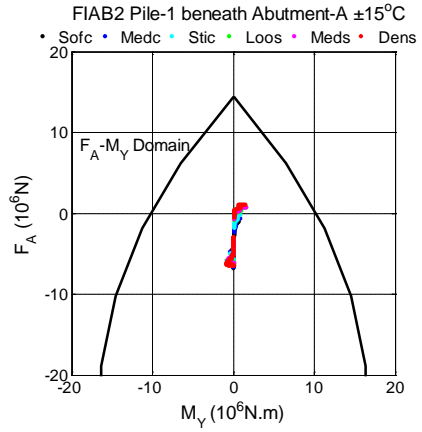
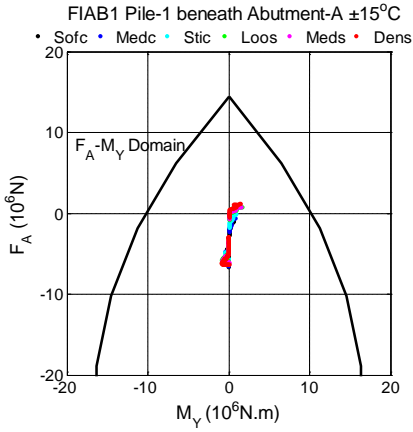
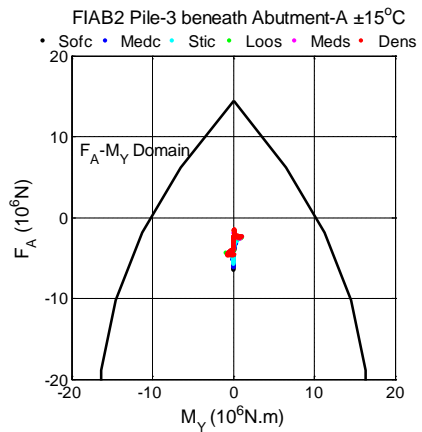
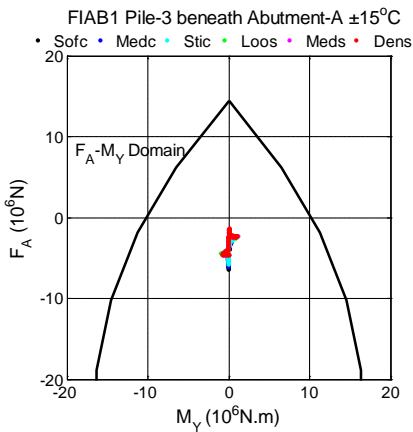


Fig. 243 Comparison between F_A - M_Y interaction diagram of Pile-5 beneath Pier-B under loads combination ($\pm 40^\circ\text{C}$) and the corresponding F_A - M_Y domain

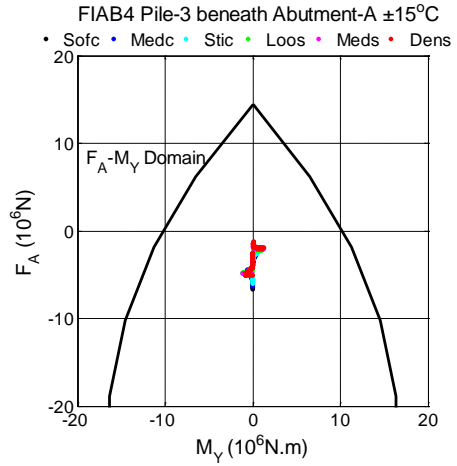
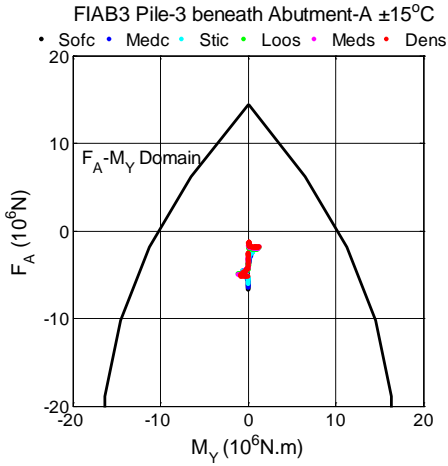
The F_A - M_Y interaction diagrams of piles beneath abutments and the corresponding F_A - M_Y domain of the pile are compared in Fig. 244 and Fig. 245. Due to the space limitation, only the Pile-1, Pile-3 and Pile-5 beneath two abutments are considered. It could be found that, if the existing bridge is located in the countries, which consider the thermal load as $\pm 15^\circ\text{C}$, no retrofitting work needs to be done on existing piles beneath abutments after retrofitting. It is because that all the F_A - M_Y interaction diagrams of piles beneath abutments in FIABs are within the limit of the corresponding F_A - M_Y domain of the pile. However, if the existing bridge was constructed in the countries, which have severe temperature variations ($\pm 40^\circ\text{C}$) and when the soil condition is sand, the top parts of Pile-1, Pile-2, Pile-4 and Pile-5 beneath Abutment-B in FIAB3 and FIAB4 should be paid attention to. For the piles beneath Abutment-A in all subtypes of FIABs, the existing piles can be reused after retrofitting no matter which soil condition is considered.



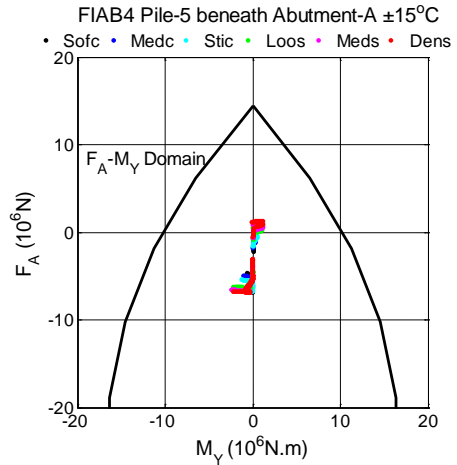
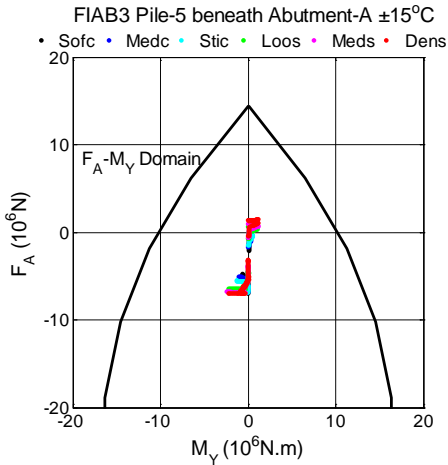
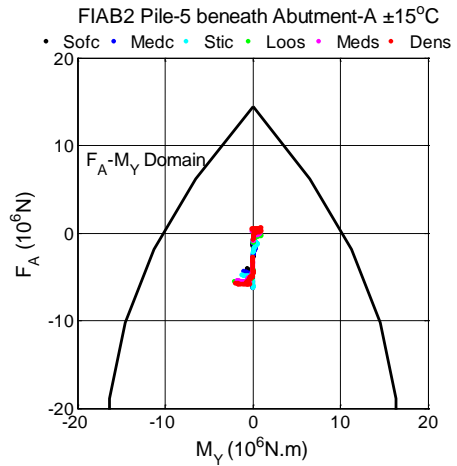
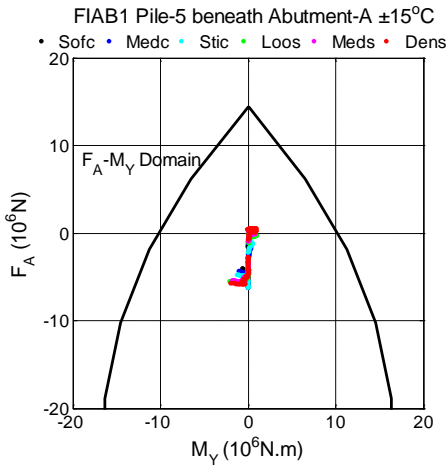
(a) Pile-1 beneath Abutment-A



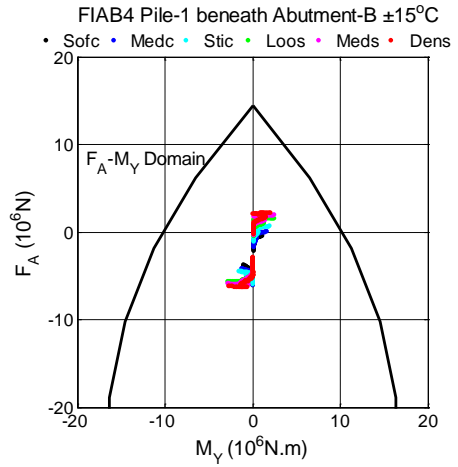
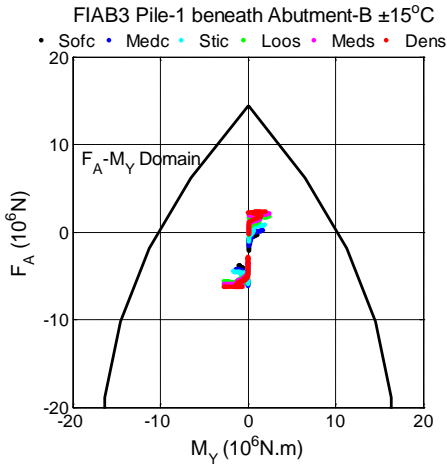
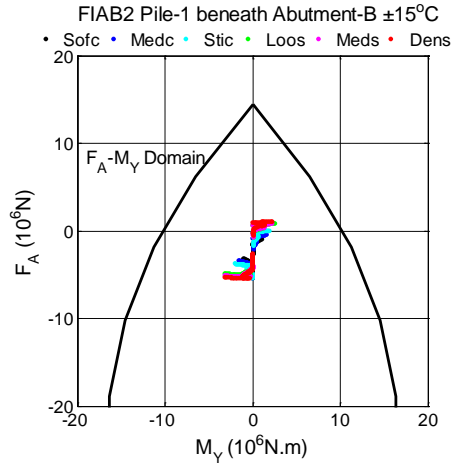
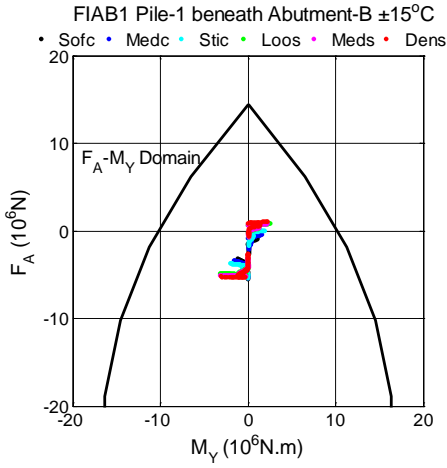
RETROFIT OF EXISTING BRIDGES WITH CONCEPT OF INTEGRAL ABUTMENT BRIDGE



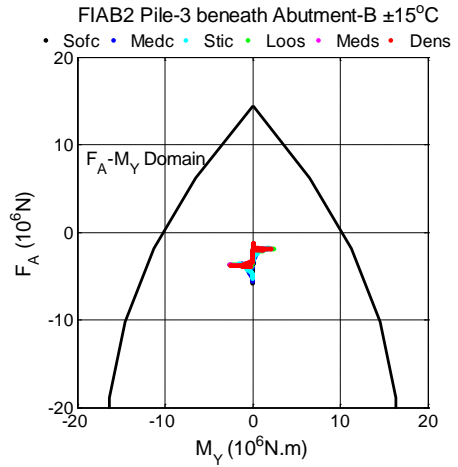
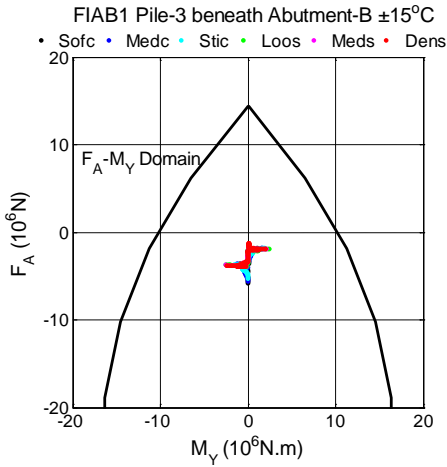
(b) Pile-3 beneath Abutment-A



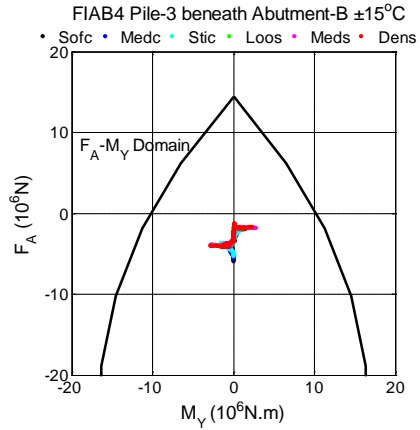
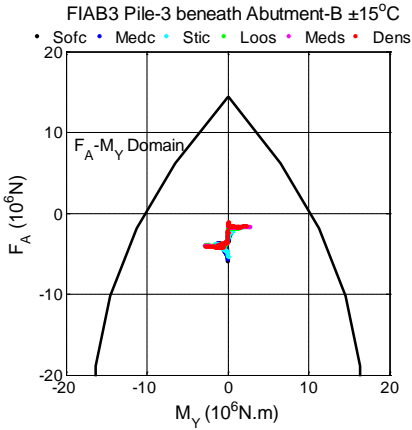
(c) Pile-5 beneath Abutment-A



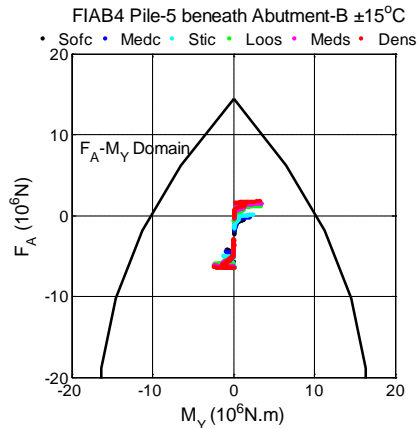
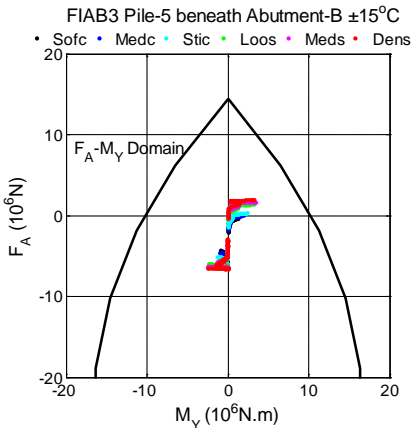
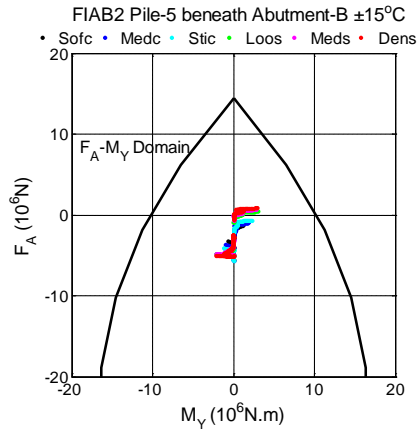
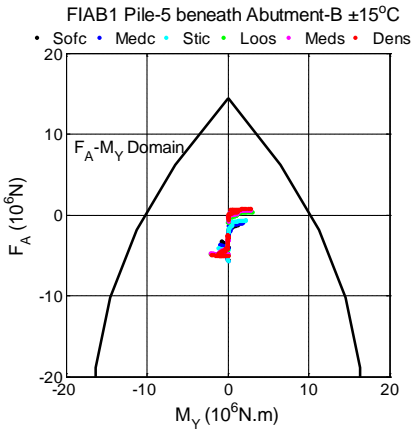
(d) Pile-1 beneath Abutment-B



RETROFIT OF EXISTING BRIDGES WITH CONCEPT OF INTEGRAL ABUTMENT BRIDGE

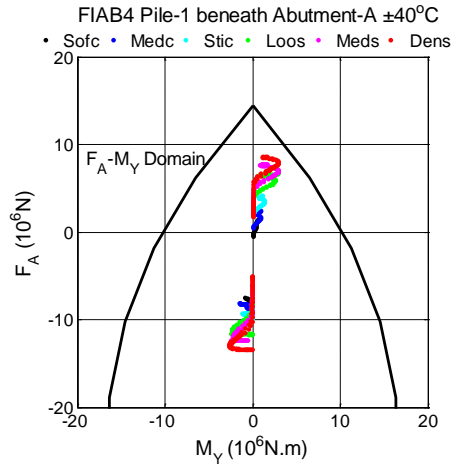
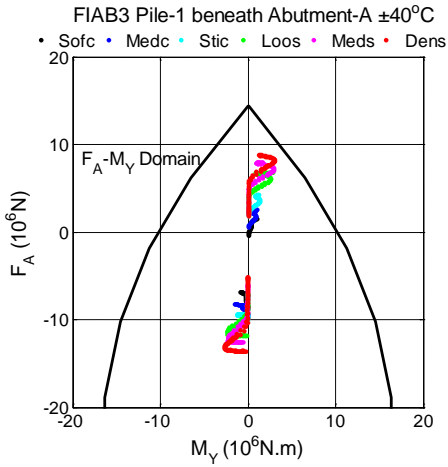
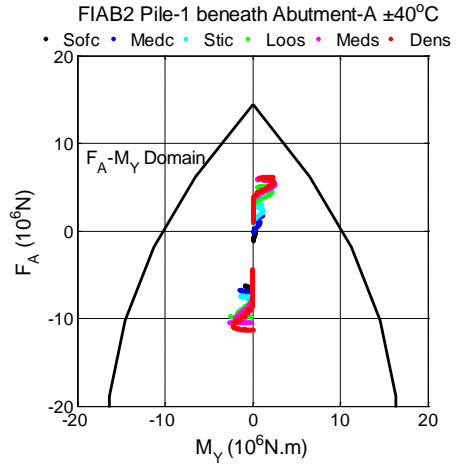
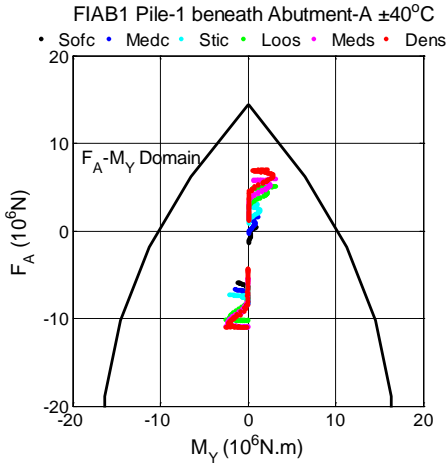


(e) Pile-3 beneath Abutment-B

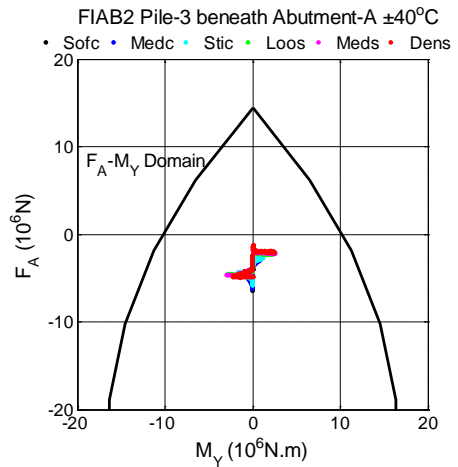
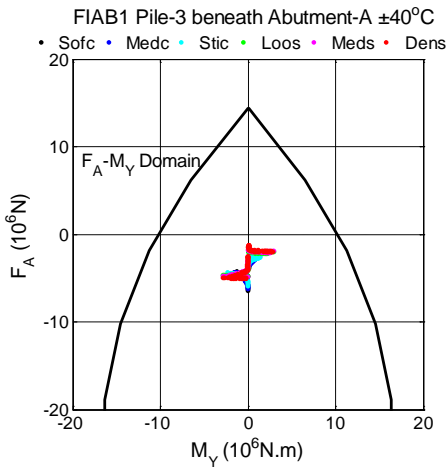


(f) Pile-5 beneath Abutment-B

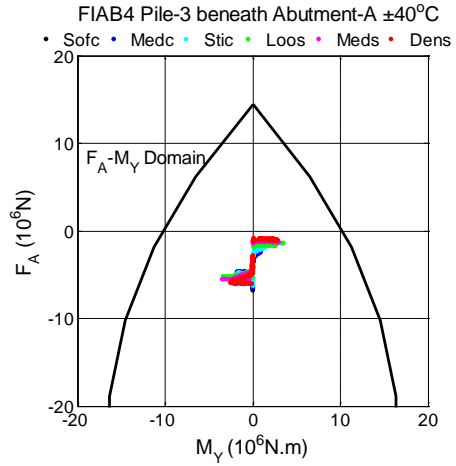
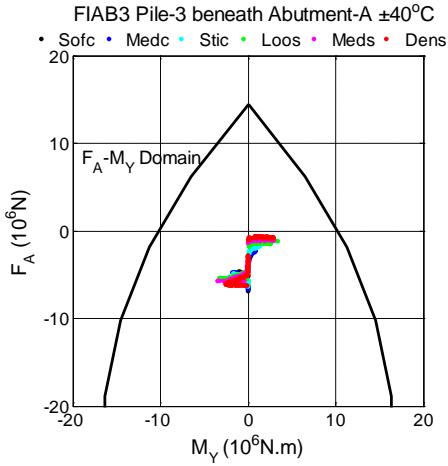
Fig. 244 Comparison between F_A - M_Y interaction diagram of piles beneath abutments under loads combination ($\pm 15^\circ\text{C}$) and the corresponding F_A - M_Y domain



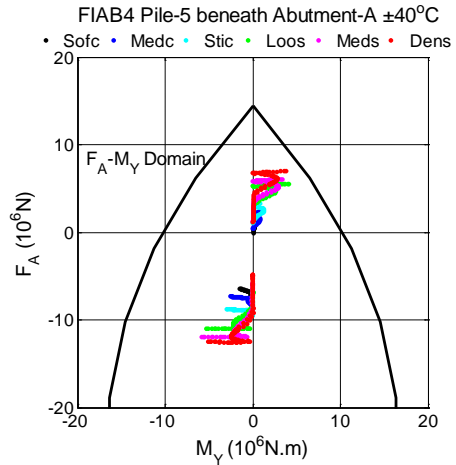
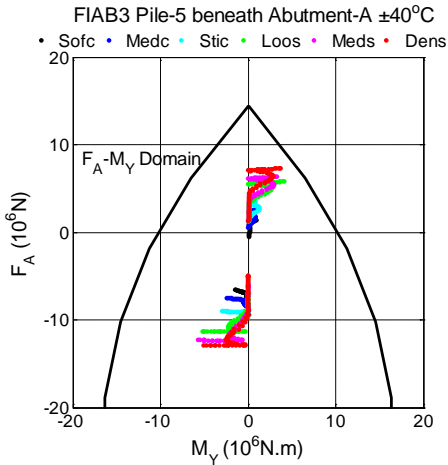
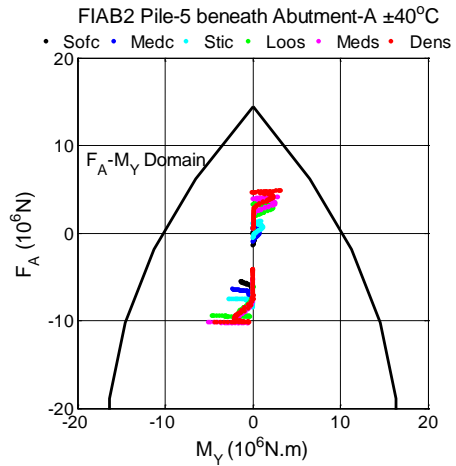
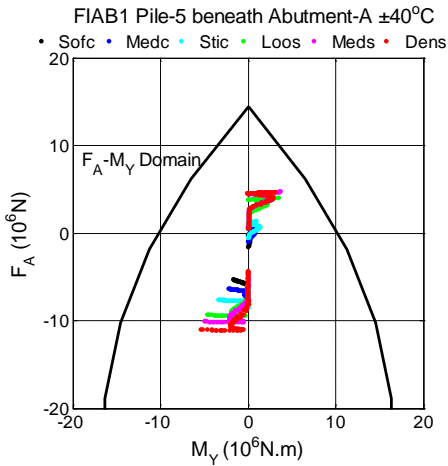
(a) Pile-1 beneath Abutment-A



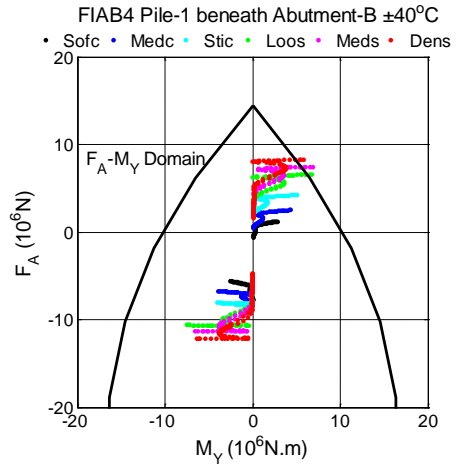
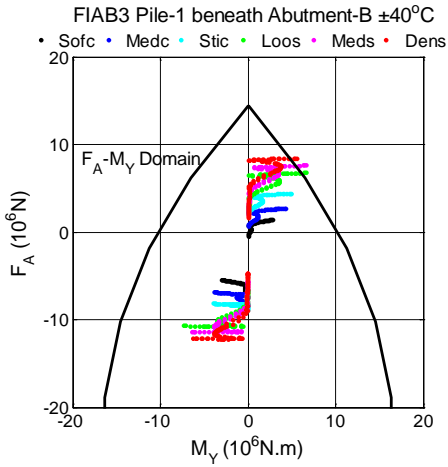
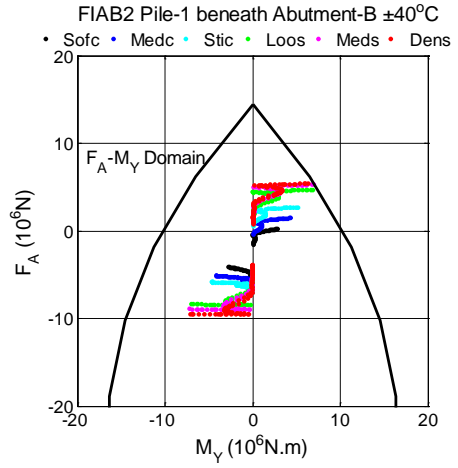
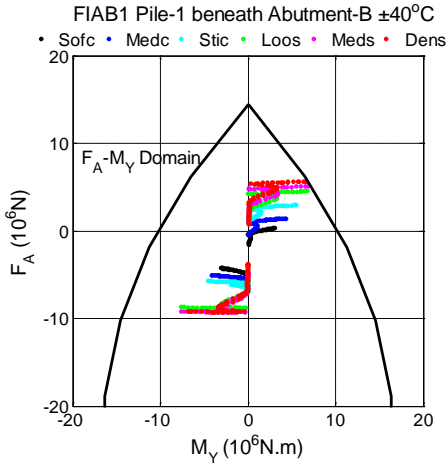
RETROFIT OF EXISTING BRIDGES WITH CONCEPT OF INTEGRAL ABUTMENT BRIDGE



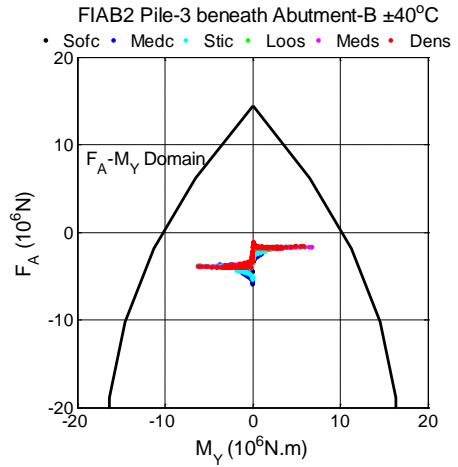
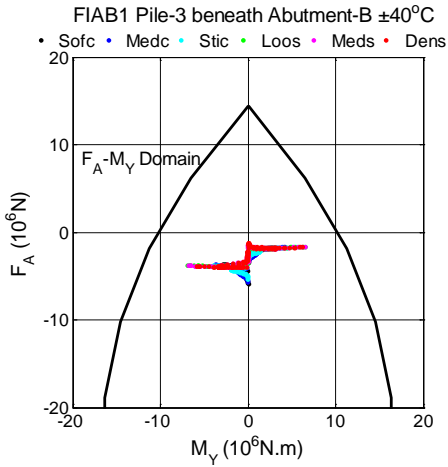
(b) Pile-3 beneath Abutment-A



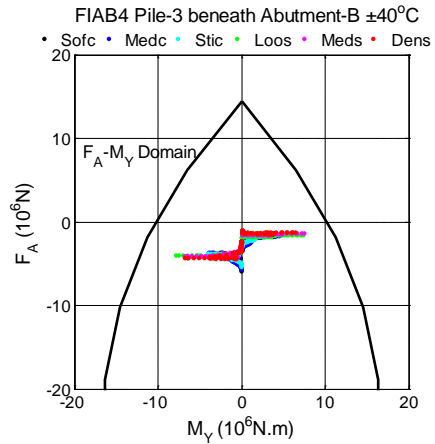
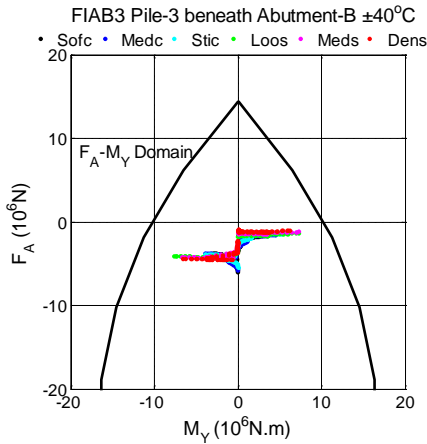
(c) Pile-5 beneath Abutment-A



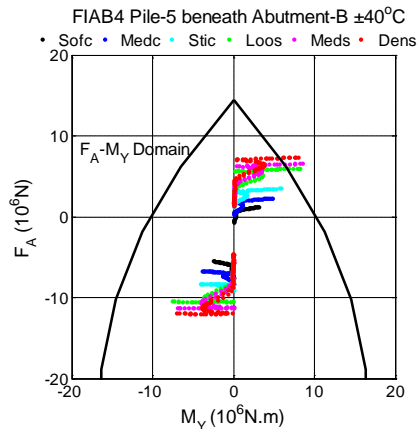
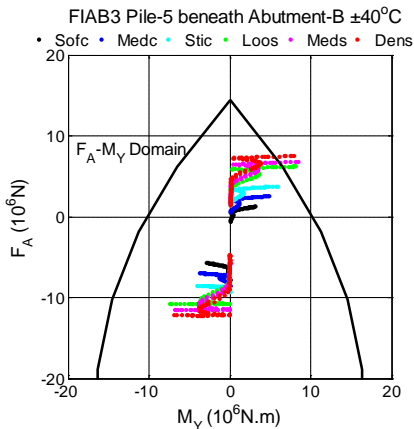
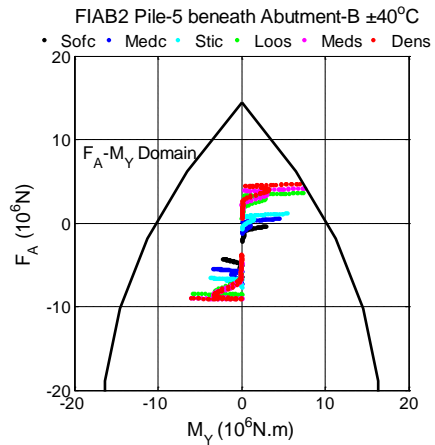
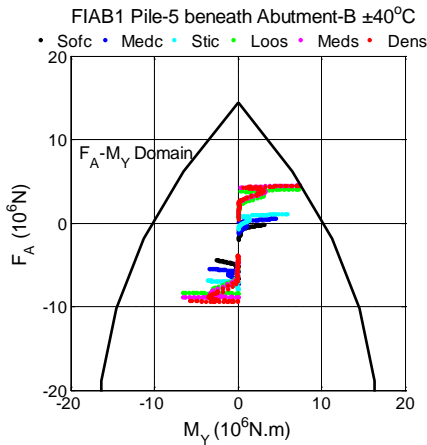
(d) Pile-1 beneath Abutment-B



RETROFIT OF EXISTING BRIDGES WITH CONCEPT OF INTEGRAL ABUTMENT BRIDGE



(e) Pile-3 beneath Abutment-B



(f) Pile-5 beneath Abutment-B

Fig. 245 Comparison between F_A - M_Y interaction diagram of piles beneath abutments under loads combination ($\pm 40^\circ\text{C}$) and the corresponding F_A - M_Y domain

7.1.2.5 Summary

According to the F_A - M_Y interaction diagram check conducted above, the bridge components, which need to be retrofitted after converting into different subtypes of FIABs, are summarized in Table 53. It could be observed that, if the existing bridge is located in the countries, which consider the thermal load as $\pm 15^\circ\text{C}$, only the abutment stems need be retrofitted during transformation. However, if the existing bridge was constructed in the countries, which have severe temperature variations ($\pm 40^\circ\text{C}$), not only the abutment stems, but also some other bridge components need to be retrofitted. It is well known that, the difficulties of the retrofitting work on different bridge components depend on many factors. Therefore, based on the Table 53, the suitable retrofitting solution could be chosen by engineers for different cases. Consequently, in order to retrofit existing SSBs with the IAB concept, the most critical factor is to improve the M_Y resistance capacity of the abutment stem. It is because that, the M_Y resistance capacity of the abutment stem can be designed as a quite small value in the SSB, thanks to the expansion joints and bearings. Moreover, converting into FIAB1 or FIAB2, the retrofit of the abutment stem will be less than that in FIAB3 or FIAB4..

Bridge type	Soil type	Girder	Pier	Abutment stem	Pile beneath pier	Pile beneath abutment	
FIAB1	Soft clay	Satisfied	Satisfied	Two abutments (± 15 and $\pm 40^\circ\text{C}$) not satisfied	Satisfied	Satisfied	
	Medium clay	Satisfied	Satisfied		Satisfied	Satisfied	
	Stiff clay	Girder-EM1 ($\pm 40^\circ\text{C}$) not satisfied	Satisfied		Satisfied	Satisfied	Satisfied
	Loose sand		Satisfied		Satisfied	Satisfied	Satisfied
	Medium sand		Satisfied		Satisfied	Satisfied	Satisfied
	Dense sand		Satisfied		Satisfied	Satisfied	Satisfied
FIAB2	Soft clay	Satisfied	Satisfied	Two abutments (± 15 and $\pm 40^\circ\text{C}$) not	Satisfied	Satisfied	
	Medium clay	Satisfied	Satisfied		Satisfied	Satisfied	

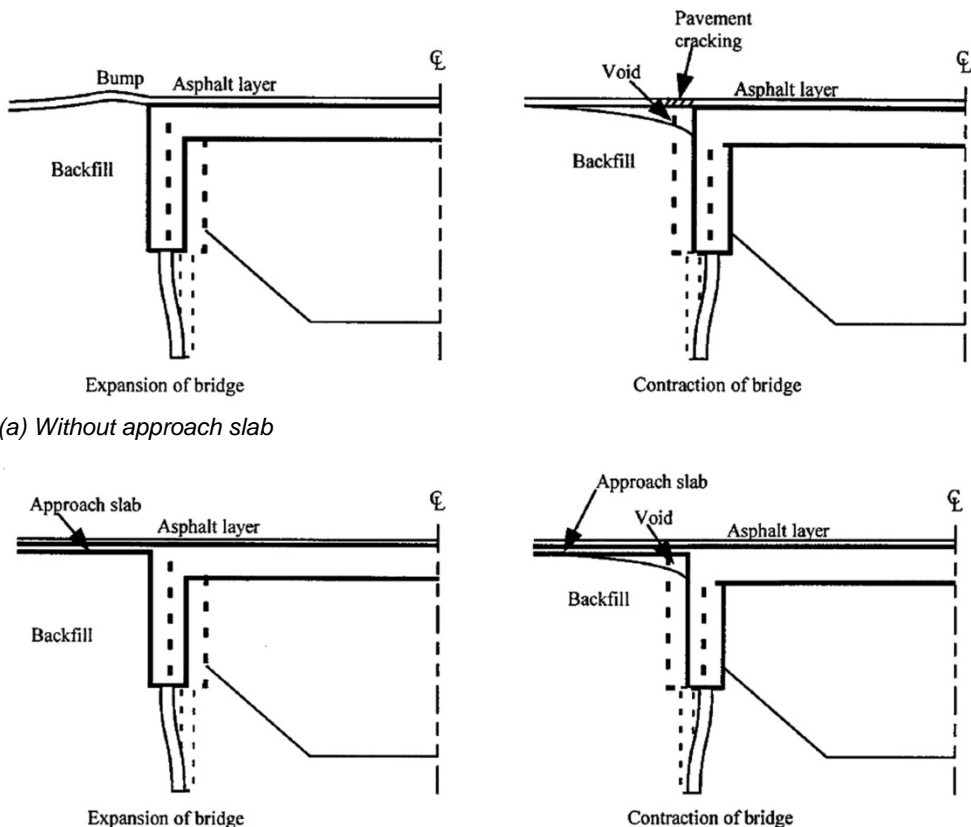
RETROFIT OF EXISTING BRIDGES WITH CONCEPT OF INTEGRAL ABUTMENT BRIDGE

	Stiff clay	Girder-EM1 ($\pm 40^{\circ}\text{C}$) not satisfied	Upper part of two piers ($\pm 40^{\circ}\text{C}$) not satisfied	satisfied	Satisfied	Satisfied
	Loose sand				Satisfied	Satisfied
	Medium sand				Satisfied	Satisfied
	Dense sand				Satisfied	Satisfied
FIAB3	Soft clay	Satisfied	Satisfied	Two abutments (± 15 and $\pm 40^{\circ}\text{C}$) not satisfied	Satisfied	Satisfied
	Medium clay	Satisfied	Satisfied		Satisfied	Satisfied
	Stiff clay	Satisfied	Satisfied		Satisfied	Satisfied
	Loose sand	Satisfied	Satisfied		Satisfied	Top parts of Pile-1, 2, 4, 5 beneath Abutment-B ($\pm 40^{\circ}\text{C}$) not satisfied
	Medium sand	Satisfied	Satisfied		Satisfied	
	Dense sand	Satisfied	Satisfied		Satisfied	
FIAB4	Soft clay	Satisfied	Satisfied	Two abutments (± 15 and $\pm 40^{\circ}\text{C}$) not satisfied	Satisfied	Satisfied
	Medium clay	Satisfied	Satisfied		Satisfied	Satisfied
	Stiff clay	Satisfied	Satisfied		Satisfied	Satisfied
	Loose sand	Satisfied	Satisfied		Satisfied	Top parts of Pile-1, 2, 4, 5 beneath Abutment-B ($\pm 40^{\circ}\text{C}$) not satisfied
	Medium sand	Satisfied	Satisfied		Satisfied	
	Dense sand	Satisfied	Satisfied		Satisfied	

Table 53
Critical bridge components after retrofitting

7.2 Consideration of approach slab

The IAB offers various advantages over the SSB equipped with expansion joints and bearings, which require regular inspection and maintenance. However, due to their jointless construction, the horizontal displacement (U_x) caused by the imposed deformation, such as creep, shrinkage and temperature variations, will transfer directly from both bridge ends to the adjacent road pavements, which may cause 'Bump' or 'Void' problems, as illustrated in Fig. 246(a). In order to resolve these problems, the approach slab (or called link slab, transition slab, or drag plate) was proposed by many researchers, as shown in Fig. 246(b), which can work together with backfill, approach fill, and foundation soil to form the approach system of an IAB.



(a) Without approach slab

(b) With approach slab

Fig. 246 Problems caused by horizontal displacement in integral abutment bridge (Arsoy et al., 1999)

The approach slab has many advantages. For example, the joints can be eliminated or the location of joints can be moved away from the abutment stem. A transition from the approach to the bridge can be provided if embankment settlement occurs. A greater load distribution at bridge ends can be obtained, which can reduce the

damage to abutments, especially from overweight vehicles. The void can be spanned. A ramp can be provided for the differential settlement between abutments and embankments. A better seal could be achieved against water percolation and erosion of the backfill material (Arockiasamy et al., 2004; Arsoy et al., 1999; Briaud, 1997). When properly design both bridge and approach slab, these bridges can usually withstand without visible distress the pressure generated by both pavements and bridges (Arsoy et al., 1999; Burke, 2009; Puppala et al., 2009). According to the survey in USA (Maruri & Petro, 2005), most states require to construct the approach slab as part of the IAB. While in Europe, the approach slab was not required for the IAB. However, most countries indicated that approach slabs are desirable (White et al., 2010).

Although the approach slab has been considered as a suitable solution, there is still no standard in the detailing of approach slabs, including the connection to the abutment stem and the interface between the approach slab and approach fill (Feldmann et al., 2010; Maruri & Petro, 2005). Moreover, the design of approach slab is a complex interdisciplinary problem dealing with both geotechnical and structural aspects and only open-minded interdisciplinary teamwork is believed to have a chance to resolve it correctly (Feldmann et al., 2010). Due to the difficulties of design, the approach slab is not currently favored by most of the highway authorities (Iles, 2006). Moreover, the inappropriate design of the approach slab may make it as the most critical problem (Dreier, 2008). As investigated in USA (Maruri & Petro, 2005), the approach slab settlement, cracking and bump at the interface between the approach slab and approach fill are the major problems in the approach slab. Furthermore, based on the problems experienced by different states in USA with reference to IABs, the majority of states, 46% and 28%, declared to have problems related to the behavior of the approach slab, as shown in Fig. 247. Besides new IABs, the problem of the approach slab can be also found in the retrofitting project with the IAB concept, such as the 'Isola della Scala Bridge', which was opened to traffic in 2007 and no mentionable damage has been noticed until now, except for some uniformly distributed cracks in approach slabs (Zordan et al., 2011b). Consequently, the special attention must be paid to the selection of an appropriate approach slab. A large number of researches have been carried out and some typical configurations of approach slabs have been suggested by many researchers based on experience, experimental tests, numerical simulations, and simple calculation methods (Abendroth & Greimann, 2005; Arsoy et al., 1999; Burke, 2009; Connal, 2004; Dreier, 2010a; Dreier, 2010b; Dreier et al., 2011; Feldmann et al., 2010; Flener, 2004; Greimann et al., 1987; Greimann et al., 2008; Greimann et al., 1984b; Kerokoski, 2006; Maruri & Petro, 2005; Puppala et al., 2009; White et al.,

2005; White et al., 2010; Yang et al., 1982)

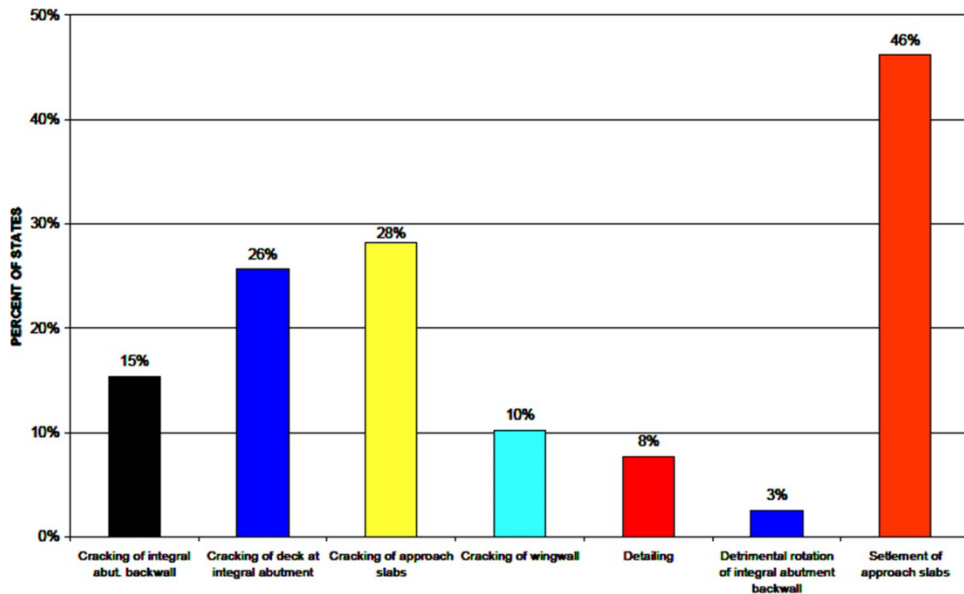


Fig. 247 Problems experienced with IABs (Maruri & Petro, 2005)

The consideration of the approach slab adopted in Switzerland (Dreier, 2010a; Dreier, 2010b; Dreier et al., 2011) is used in this retrofitting project. The mechanical behaviors of the approach slab can be investigated focusing on the pavement settlement at the end of the approach slab and on the cracking of the pavement between the bridge end and the approach slab. As introduced above, the design of the approach slab is a combination task between both geotechnical and structural aspects. Consequently, the soil-structure interaction between the approach slab and the embankment should be considered. Based on the finite element model, which can simulate the complex behaviors of backfill and the interaction between the embankment and the structural elements of the bridge end, the geometric dimension of the approach slab can be investigated, including the length (l_{TS}), slope (α_{TS}), thickness (h_{TS}) and buried depth ($e_{TS,0}$) of the approach slab, as shown in Fig. 248. From previous analyses, it could be observed that the imposed horizontal displacement will cause a local settlement of the pavement at the end of the approach slab, due to the active plastic mechanical development in the embankment, as shown in Fig. 248. This settlement at the end of the approach slab, which can reduce the planarity of the road pavement and degrade the comfort of the road users, can be chosen as the key problem for the serviceability limit state. The slope variation criterion (χ) stipulated in Swiss code can be adopted to quantify the planarity of the road pavement, which can be efficiently evaluated by formula (159),

RETROFIT OF EXISTING BRIDGES WITH CONCEPT OF INTEGRAL ABUTMENT BRIDGE

as displayed in Fig. 249. According to the Swiss code, χ_{adm} is equal to 28‰ for normal roads and 20‰ for highways.

$$\chi(x) = \frac{w(x) - w(x - 1m)}{1m} - \frac{w(x + 1m) - w(x)}{1m} \leq \chi_{adm}(x) \quad (159)$$

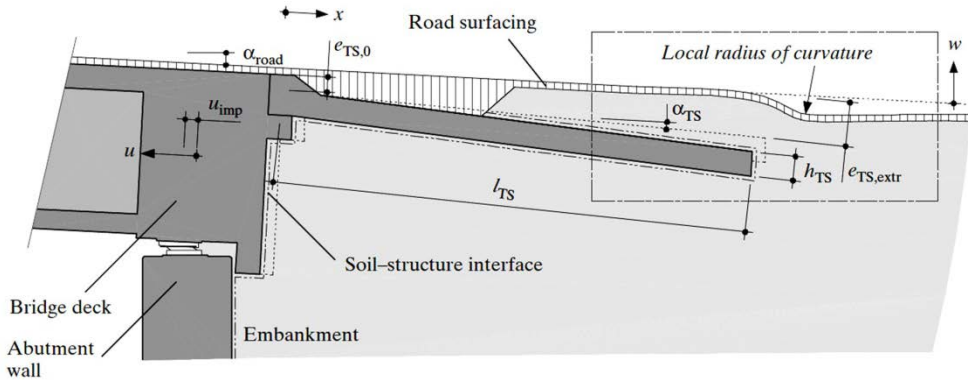


Fig. 248 Geometry and materials of approach slab (Dreier et al., 2011)

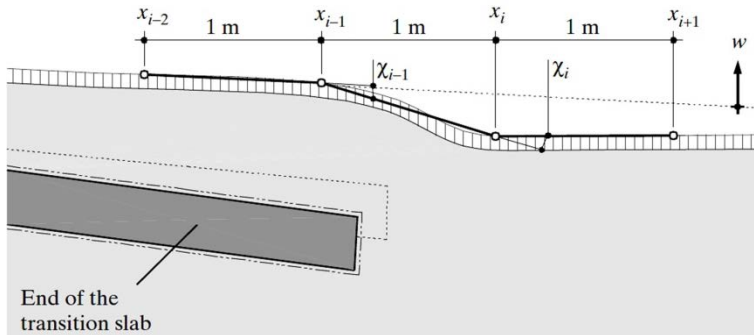


Fig. 249 Definition of the slope variation criterion according to Swiss codes (Dreier et al., 2011)

Through a series of numerical analyses, it could be found that if the geometric information of the approach slab uses the recommended value in Swiss code, the admissible imposed displacement ($u_{imp.adm}$) corresponding to the $\chi_{adm}=20‰$ for highways can reach 43mm, as shown in Fig. 250. It could be also observed that the ultimate value of $u_{imp.adm}$ is controlled by the case “hole”, which will appear when IABs contract subjected to negative thermal load and abutments moves forward from backfill. When retrofitting existing bridges with the IAB concept, the imposed horizontal displacement caused by creep and shrinkage can be neglected that is an advantage comparing with the new constructed IAB.

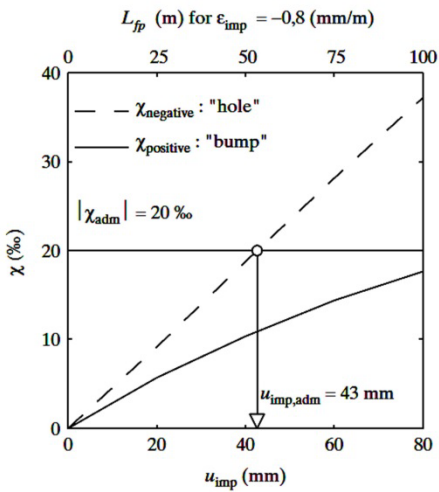


Fig. 250 Determination of the admissible imposed displacement for $\chi_{adm}=20\text{‰}$ according to Swiss codes (Dreier et al., 2011)

For the detailed connection between the approach slab and bridge end, one improved connection detail proposed by Dreier can be considered as a suitable solution adopted in this case, as illustrated in Fig. 251 (Dreier, 2010a; Dreier, 2010b; Dreier et al., 2011). It is designed based on the currently recommended connection in Switzerland for IABs; however, with easier construction. It is a concrete hinge reinforced against shear failure by the diagonal connection reinforcement and can lead to a distribution of the rotation of the approach slab over the entire length of the concrete hinge (l_{ch}). The experimental test and numerical analysis of this improved connection were conducted, which indicated that the resulting cracks have only small openings that cannot propagate to the road surfacing (Dreier, 2010a).

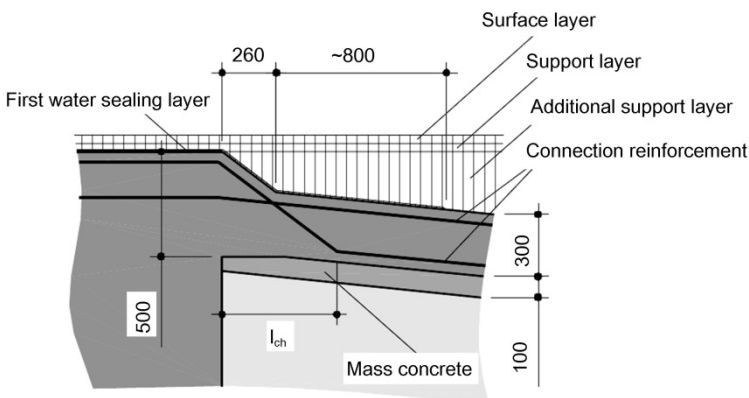
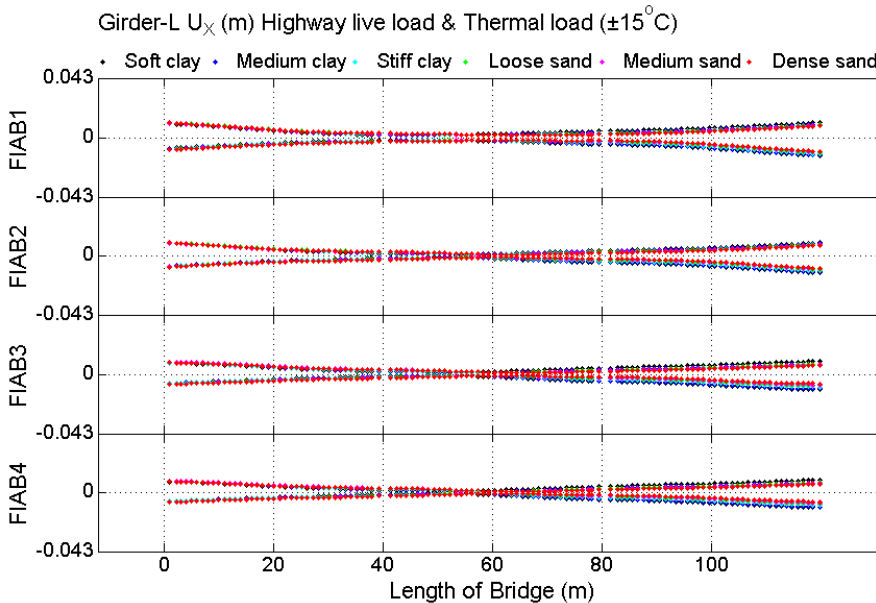
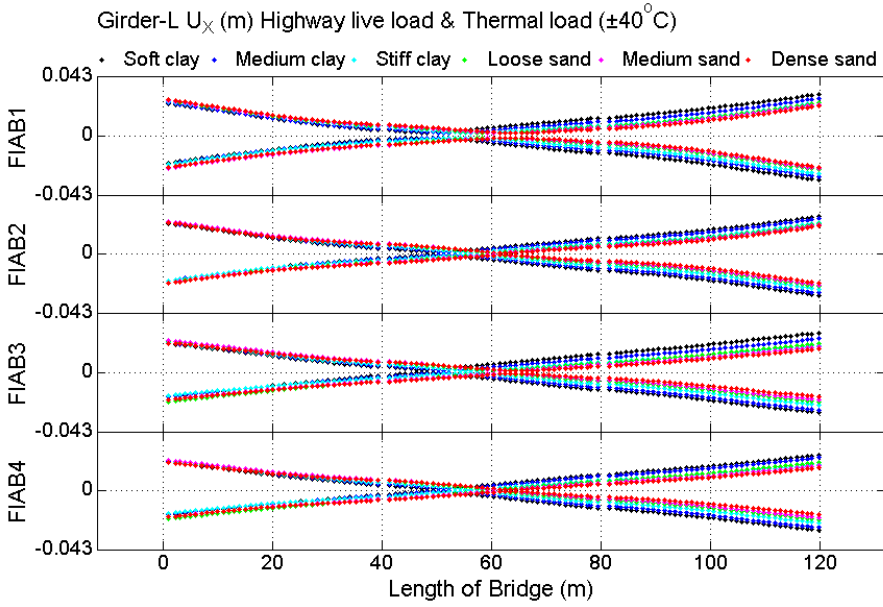


Fig. 251 Improved connection detail between approach slab and abutment (Dreier et al., 2011)

In this case, the admissible imposed displacement ($u_{imp.adm}$) can be chosen as the limit value of the horizontal displacement at bridge ends after retrofitting. As mentioned in Section 5.2.1, there is no approach slab in the existing SSB, because the horizontal displacement can be released through expansion joints. However, the approach slab should be considered in FIABs after retrofitting. According to previous studies, it could be found that the approach slab can be easily built with no major interference to the existing structures (Zordan & Briseghella, 2007). Therefore, the modeling of the approach slab in the finite element model is neglected; however, the horizontal displacements transferring from bridge ends to approach slabs could be considered as the critical factor to select the suitable approach slab. The approach slab will be constructed during retrofitting procedure. Therefore, only the horizontal displacement (U_x) under highway live load and thermal load should be taken into account, as illustrated in Fig. 252. It could be observed that, no matter which soil condition is considered, the U_x at bridge ends corresponding to the ultimate limit state in four subtypes of FIABs are less than 43mm. Consequently, the problem of the connections between bridge ends and road pavements in ‘Viadotto Serrone’ after retrofitting could be resolved by using the recommended geometric dimension of approach slab in Swiss code and the improved connection detail (as illustrated in Fig. 251). It can avoid special considerations to ensure the approach slab will be durable and performs satisfactorily at the serviceability limit state.



(a) Under highway live load and thermal load ($\pm 15^{\circ}\text{C}$)



(b) Under highway live load and thermal load ($\pm 40^\circ\text{C}$)

Fig. 252 U_x of Girder-L in FIABs under highway live load and thermal load

8. SEISMIC SENSITIVE ANALYSIS

Besides the static analysis, the seismic behaviors of IABs after retrofitting should be also investigated, which is another important decisive factor in the extension of this retrofitting technique. Some studies on the seismic responses of IABs have been carried out. With respect to the seismic performance, the benefits of IABs over SSBs include increased redundancies, larger damping due to the soil-structure interaction, smaller displacements and elimination of the loss of girder support that is the most common damage in SSBs in seismic events (Itani & Pekcan, 2011; Masrilayanti & Weekes, 2012; Wasserman & Walker, 1996).

8.1 Literature review

Some researchers found that the seismic responses of the IAB are mainly dominated by the soil-structure interaction, including the soil-abutment interaction and the soil-pile interaction.

A parametric study was conducted to find the difference between the bridge analyzed with and without the consideration of the soil-structure interaction. It could be observed that, when considering the soil-structure interaction, the calculated forces and moments at piers are greater by 25~60% and the displacements by 25~75%, depending on soil properties, than those without the consideration of soil-structure interaction. The abutments attract a large portion of seismic forces, particularly in the longitudinal direction (Karantzakis & Spyrakos, 2000). In order to verify the structural improvements achieved, the vibration tests were conducted on a bridge before and after retrofitting. The measure results indicated that the retrofitting process increases the first vibration mode of the bridge from 5 Hz to 8.8 Hz. Therefore, it could be found that the conversion from SSBs to FIABs is effective in flexural strengthening of the deck (Jayaraman & Merz, 2001). The influence of different soil-structure interactions on the mode shapes and seismic responses of a single-span post-tensioned IAB were studied (Spyrakos & Loannidis, 2003). Seven types of soil-abutment interactions were considered in a sensitive modal analysis, including six types with different backfill spring stiffness and one type with the fixed

boundary condition. The comparison indicated that the vibration frequencies change about 20% in extreme cases, and the different backfill spring stiffness does not have a significantly effect on the seismic responses of the bridge. However, the existence of backfill has a significant effect on the dynamic characteristics and seismic responses of the bridge. Dehne & Hassiotis (2003) conducted a seismic analysis on an IAB and concluded that the IAB system with the dense compacted soil behind abutments and loose sand around piles can achieve the best performance characteristics under longitudinal and transverse earthquake excitation. The influence of the backfill resistance on the IAB was analyzed by using three types of design response spectra, including the current AASHTO, Expected Event (EE) and Maximum Considered Event (MCE) design spectra. It could be observed that considering the backfill resistance, bridges up to 305m in length experience no damage by using both current AASHTO and Expected Event (EE) design spectra. For the Maximum Considered Event (MCE) design spectrum, bridges less than 213m in length experience no damage and bridges between 213m and 305m in length experience acceptable damages (Talbot, 2008). The modal analysis and the nonlinear time history analysis were carried out by Farahani (2010) to find the influence of different soil properties on the seismic behaviors of the IAB. It could be found that compacting the sand backfill behind abutments can increase the dominant longitudinal frequency of the bridge considerably more than increasing the clay stiffness around piles. Compacting the backfill in IABs is recommended, which can improve the seismic performance of the IAB. Based on analytical investigations and available experimental researches, it could be found that the soil-structure interaction can reduce the seismic demand on the piers and their footings. However, it can bring a larger demand on the piles due to large cyclic deformations. The modal analysis was performed to investigate the effect of the soil-abutment interaction and soil-pile interaction on the global system behaviors. It could be observed that the most significant change in bridge dynamic properties is due to the soil-pile interaction. The pushover analysis was also conducted, which indicated that in the longitudinal direction, about 72% of the seismic force could be resisted by the passive resistance of the soil-abutment interaction. Moreover, in the transverse direction, about 40% of the transverse seismic force can be resisted by the soil-pile interaction for each abutment (Itani & Pekcan, 2011; Pekcan et al., 2010). The effects of different stiffness of the soil-structure interaction on the seismic behaviors of the IAB, including the backfill response, deck and bearing displacements, and the performance of piers, steel H piles beneath abutments and piles beneath piers, were investigated through modal analysis and nonlinear time history analysis. It concluded that the stiffness of the soil-structure interaction have significant effects on the seismic performance of the IAB, particularly under large-intensity

earthquakes. Moreover, IABs built on soft soil are expected to exhibit a better seismic performance if all piles are end bearing (Dicleli & Erhan, 2011). Therefore, six types of soil listed in Table 34 (p.165) should be considered as a key parameter in the following analysis.

The stiffness of the nonlinear springs, which represents the connection between the steel girder and the abutment, was chosen as an analytical parameter by Itani & Pekcan (2011), including the rigid connection and the flexible connection. The modal analysis and the pushover analysis were performed to investigate the effects of different girder-abutment connection flexibilities on the global system behavior under seismic load. It indicated that the addition of the girder-abutment connection flexibility in the model can not only increase the vibration periods but also change the mode shapes. In order to find the influence of different abutment participation on the vibration properties of IABs, the vibration properties of a two-span concrete IAB obtained from its motions recorded during actual earthquake events were analyzed. It could be found that the abutment flexibility is an important element in the earthquake design of IABs (Goel, 1997). In this paper, four subtypes of FIABs as defined in Table 47 (p.219), which have different superstructure-substructure connection flexibilities, could be chosen as research objects in this chapter.

The modal analysis and the response spectrum analysis could be conducted on 'Viadotto Serrone' to find out the most important factors and their influence, which could be used to guide the design of the retrofitting process.

8.2 Finite element model

In order to carry out the analysis, the suitable finite element model should be chosen firstly. Based on the comparison between the analytical result and measured bridge response data, the 3D model was suggested because it is adequate in capturing the bridge seismic response, such as the reduction in vibrating periods and coupling of mode shapes in three major directions (i.e., longitudinal, transverse and vertical.) (Dehne & Hassiotis, 2003; Dicleli & Erhan, 2011; Shamsabadi & Yan, 2010).

From previous studies, it could be found that the simulation of the soil-structure interaction is a key point in the finite element model. In current state-of-the-art of modeling the effect of soil behind abutments, some experts chose the simple simulation approach, in which the participating mass of the soil behind abutments is not considered and only the spring element with linear or nonlinear soil stiffness is

RETROFIT OF EXISTING BRIDGES WITH CONCEPT OF INTEGRAL ABUTMENT BRIDGE

taken into account (Biondini et al., 2010; Caltrans, 2010; Itani & Pekcan, 2011; Karantzikis & Spyrakos, 2000; Talbott, 2008). It is because that, the effective embankment soil is very difficult to determine without the complete information on embankment size and soil properties. Moreover, without shake table experiments with the reasonable scale to determine the effective participating soil mass, the computational models will have limited capabilities and may produce results that vary by more than several folds (Itani & Pekcan, 2011). However, some researchers proposed that the soil in embankment should be simulated, because from the strong-motion earthquake data and analytical studies, not the near-field but the far-field embankment response has a significant effect on the displacement demands of the IAB (Carvajal, 2011), as illustrated in Fig. 253.

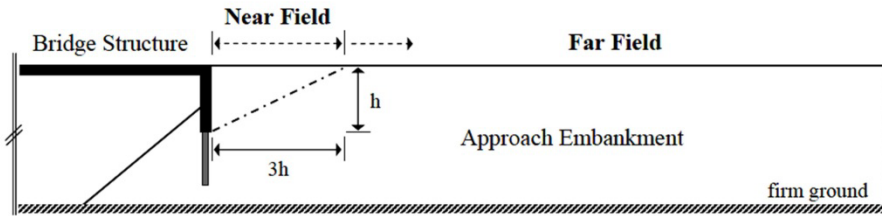
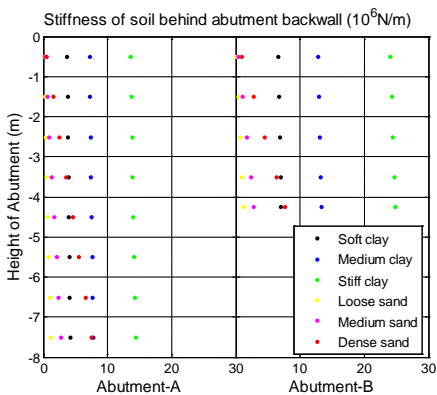
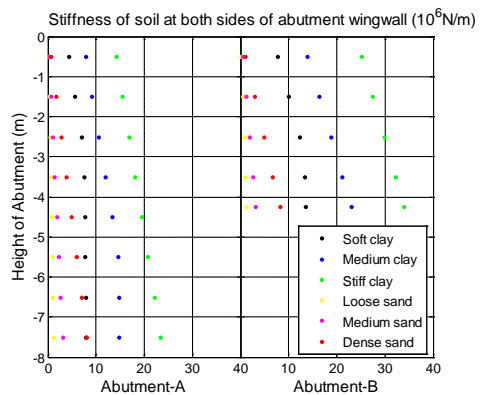


Fig. 253 Near and far field of an approach embankment (Carvajal, 2011)

In this analysis, the far-field embankment response is taken into account. The stiffness (k) of the soil-structure interactions corresponding to six soil conditions can be obtained by using the method introduced in Chapter 5.2.3. The stiffness changes with the increase of depth. The stiffness of p - y curve, t - z curve, P - Δ_b curve and P - Δ_w curve are illustrated in Fig. 254.



(a) Stiffness of P - Δ_b curve



(b) Stiffness of P - Δ_w curve

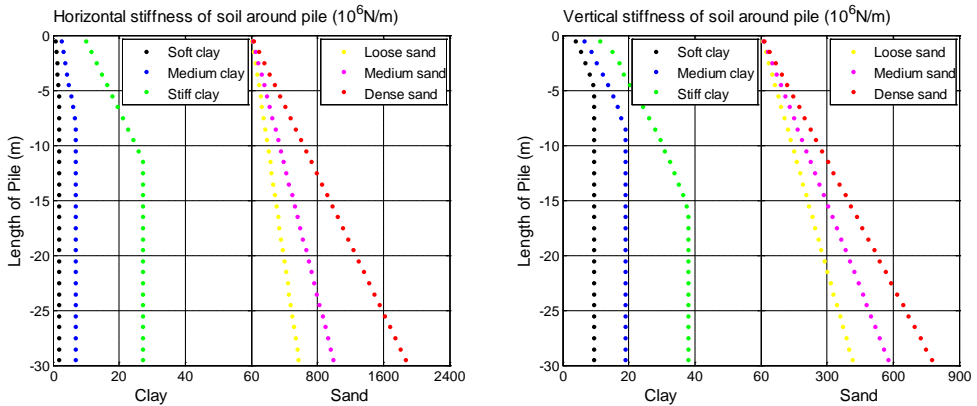
(c) Stiffness of p - y curve(d) Stiffness of t - z curve

Fig. 254 Stiffness of soil-structure interaction

The damping coefficient is another important coefficient, which should be paid attention to. Some experts used the damping coefficient of 5% in the model (Dehne & Hassiotis, 2003; Farahani, 2010). However, some researchers found that the damping coefficient of integral abutment bridge with the soil would increase during a seismic event. The beneficial effect of the increased damping can lead to a more economical retrofit (Goel, 1997; Itani & Pekcan, 2011). However, from the safety point of view, the damping is assumed as 0.05 in this analysis.

The plastic hinges should be assigned to critical points when analyzing the seismic performance of the bridge (Biondini et al., 2010; Dicleli & Erhan, 2011; Itani & Pekcan, 2011). In this case, the concentrated plastic hinge assigned at the top and bottom of pier columns, and the distributed plastic hinge zone arranged along the upper part of piles have been defined in Chapter 5.2.4.

Consequently, the 3D finite element model proposed in Chapter 5.2 could be chosen as the analytical tool in this section.

8.3 Modal analysis

In bridge engineering, the modal analysis can use the overall mass and stiffness of a structure to find the various periods, at which it will naturally resonate. These vibration periods are quite important to note in earthquake engineering, as it is imperative that the natural frequency of the bridge does not match the frequency of expected earthquakes in the region, in which the bridge is to be constructed. In this

section, the modal analyses were performed to investigate the effects of different bridge types and different soil-structure interactions on the global system behavior. For this purpose, thirty different cases considering five bridge types, including the existing SSB and four subtypes of FIABs after retrofitting, as defined in Table 47 (p.219), and six soil-structure interactions with the soil properties listed in Table 34 (p.165), were analyzed. As explained before, the stiffness illustrated in Fig. 254 can be used for the linear soil-abutment and soil-pile springs.

8.3.1 Mode shape and vibration period

Due to the space limitation, only the main transverse translation mode shape, the main longitudinal translation mode shape and the corresponding vibration periods (T_H , which is corresponding to the main transverse translation mode shape and the T_L , which is corresponding to the main longitudinal translation mode shape) are summarized in Table 54. It could be found that, no matter which soil condition is chosen, the mode shape of mode 1 in all bridge types is the coupled transverse translation and superstructure rotation. For the main longitudinal translation model shape, the soil property variations could only change the vibration period in SSB, FIAB2 and FIAB4; however, the mode shape keeps the same, which are mode 2 in SSB and mode 3 in FIAB2 and FIAB4. When considering FIAB1 and FIAB3, the soil property variations could change not only the vibration period but also the mode shape. For example, when considering the soil conditions as sand and stiff clay, the main longitudinal translation model shape in FIAB1 would appear at mode 4; however, when considering the soil conditions as medium clay and soft clay, the main longitudinal translation model shape in FIAB1 would appear at mode3.

Bridge type	SSI	Mode	T_H	Mode	T_L
SSB	Dense sand	1	0.695	2	0.554
	Medium sand	1	0.713	2	0.565
	Loose sand	1	0.734	2	0.578
	Stiff clay	1	0.786	2	0.630
	Medium clay	1	0.888	2	0.739
	Soft clay	1	1.114	2	1.007
FIAB1	Dense sand	1	0.622	4	0.287
	Medium sand	1	0.637	4	0.299
	Loose sand	1	0.654	4	0.316
	Stiff clay	1	0.698	4	0.295
	Medium clay	1	0.783	3	0.377
	Soft clay	1	0.968	3	0.565

FIAB2	Dense sand	1	0.618	3	0.249
	Medium sand	1	0.634	3	0.267
	Loose sand	1	0.651	3	0.293
	Stiff clay	1	0.695	3	0.278
	Medium clay	1	0.780	3	0.377
	Soft clay	1	0.966	3	0.553
FIAB3	Dense sand	1	0.600	4	0.246
	Medium sand	1	0.620	4	0.275
	Loose sand	1	0.641	3	0.307
	Stiff clay	1	0.685	4	0.251
	Medium clay	1	0.776	3	0.366
	Soft clay	1	0.964	3	0.559
FIAB4	Dense sand	1	0.596	3	0.228
	Medium sand	1	0.616	3	0.258
	Loose sand	1	0.638	3	0.288
	Stiff clay	1	0.681	3	0.251
	Medium clay	1	0.774	3	0.361
	Soft clay	1	0.962	3	0.539

Table 54

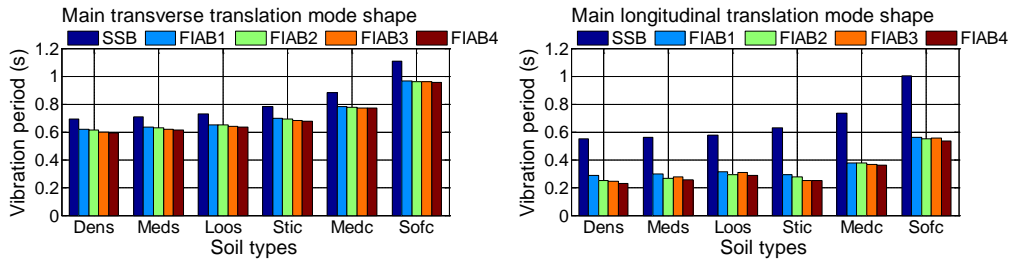
Summarization of the main transverse translation and longitudinal translation mode shapes and vibration periods

8.3.2 Different bridge types

The effects of different bridge types on the vibration periods, including T_H and T_L , are illustrated in Fig. 255(a) and (b), respectively. It could be observed that if the existing SSB is transformed into FIABs after retrofitting, the corresponding T_H would decrease to about 85% and T_L could be obviously reduced to less than 50%, which is similar to the vibration test results on an IAB before and after retrofitting obtained by Jayaraman & Merz (2001).

By comparing different subtypes of FIABs, it could be observed that the T_H corresponding to FIAB1 and FIAB2 are nearly the same, which are a little larger than those corresponding to FIAB3 and FIAB4. Therefore, the influence of different superstructure-abutment connection flexibilities on the T_H is larger than the influence of different superstructure-pier connection flexibilities. However, the effects of different superstructure-substructure connection flexibilities on the T_H would decrease with the soil condition changes softer. Furthermore, different subtypes of FIABs could have noticeable effects on the T_L . The T_L in FIAB1 and FIAB4 could be

considered as the maximum and minimum values, respectively.



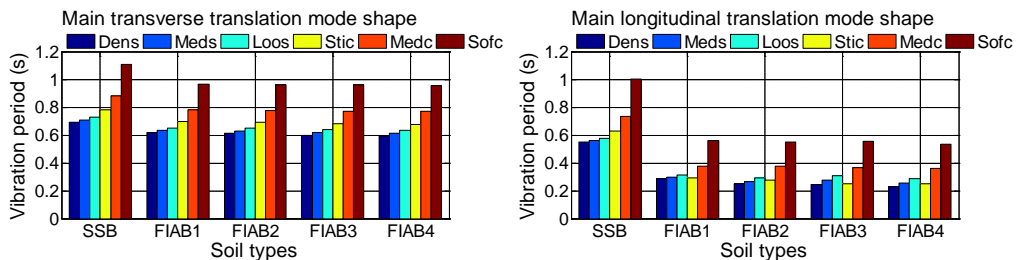
(a) T_H

(b) T_L

Fig. 255 Influence of different bridge types on main vibration periods

8.3.3 Different soil conditions

The effects of different soil conditions on the vibration periods (T_H and T_L) are illustrated in Fig. 256(a) and (b), respectively. It could be found that for all bridge types, when the soil properties changing from dense sand to loose sand or from stiff clay to soft clay, the T_H and T_L increase. Moreover, the increments of T_H and T_L among three types of clay are significantly larger than those among three types of sand. When the soil condition is sand, the T_H could be smaller than those considering the soil condition as clay. However, when the soil condition is stiff clay, the T_L in four subtypes of FIABs could be smaller than those considering the soil condition as medium sand and loose sand, which should be paid attention to.



(a) T_H

(b) T_L

Fig. 256 Influence of different soil properties on main vibration periods

8.3.4 Different substructure heights

As described above, the substructure heights in ‘Viadotto Serrone’ are asymmetric. In order to expand the research scope, the modal analysis is also applied to the idealized cases with symmetric substructure heights, including the ‘a4.5p7.7’,

'a4.5p25.7', 'a8p7.7' and 'a8p25.7' listed in Table 51 (p.265). The influence of different substructure heights on the T_H and T_L are illustrated in Fig. 257. It could be found that the influence of different pier heights on the T_H in all bridge types and T_L in SSB are significantly larger than the effect of different abutment heights. Moreover, the influence of different abutment heights on the different substructure heights on the T_L in four subtypes of FIABs is quite small.

From Fig. 257, it could be observed that when the pier height is 7.7m, the T_H of FIABs after retrofitting are similar to or slightly smaller than the T_H of the SSB before retrofitting; however, the effects of the retrofitting process transforming the SSB into FIABs on the T_L are large. When the pier height is 25.7m, the T_H and T_L of FIABs after retrofitting are significantly smaller than the T_H and T_L of the SSB before retrofitting. The T_L of FIABs could be reduced to 25~30% of the T_L in the SSB. It is because that, in the SSB with high pier heights, the mode 1 could change from the transverse translation mode shape to the longitudinal translation mode shape; however, in FIABs, the mode 1 is transverse translation mode shape and the main longitudinal translation mode shape appears at mode 4.

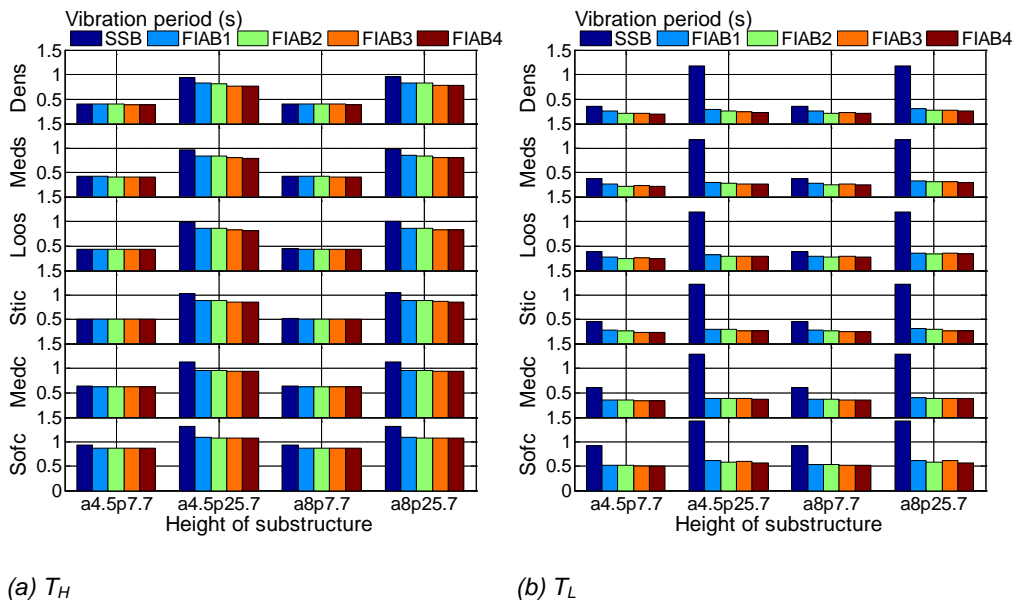


Fig. 257 Influence of different substructure heights on vibration periods

8.4 Response spectrum analysis

8.4.1 Response spectrum

In order to investigate the performance of the SSB and FIABs under seismic load, the response spectrum analysis was carried out by using the horizontal response spectrum corresponding to the limit state SLV. It is well known that the response spectrum analysis is a linear analysis case. Therefore, the nonlinear soil-structure interaction relationship curves defined in springs should be replaced by the stiffness illustrated in Fig. 254. Based on the comparison between two combination methods (Envelope and SRSS) in Chapter 5.3.6, the SRSS combination is considered in the following analysis. The soil type is chosen as the parameter in this study. Therefore, according to the updated Italian code NTC 2008 (Ministero delle Infrastrutture, 2008), three types of horizontal response spectra corresponding to the soil types B, C and D are considered, as illustrated in Fig. 258. The relationship between the soil types and different types of horizontal response spectra are listed in Table 55. The detailed calculation approach of the response spectrum can be found in Chapter 5.3.4.

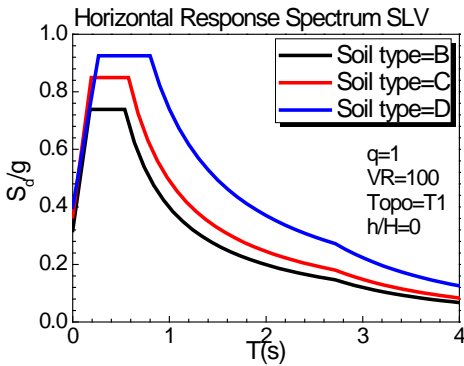


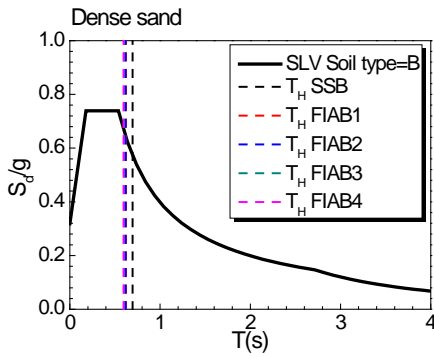
Fig. 258 Horizontal response spectra corresponding to soil types B, C and D

Soil condition	Dense sand	Medium sand	Loose sand	Stiff clay	Medium clay	Soft clay
Soil type in response spectrum	B	C	D	C	D	D

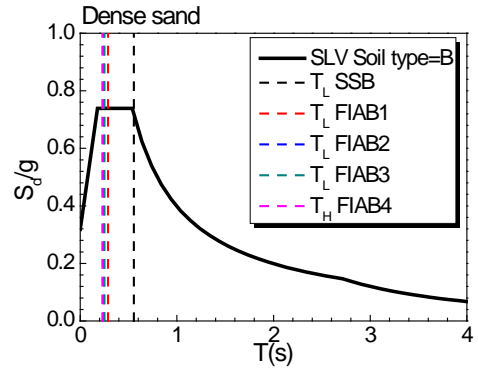
Table 55 Relationship between the soil condition and the different soil types in response spectrum

The T_H and T_L of different bridge types considering different soil conditions are compared with the corresponding horizontal response spectra (SLV), as illustrated in Fig. 259. It could be observed that after retrofitting with the IAB concept, the vibration periods of the main transverse translation mode shape and the longitudinal

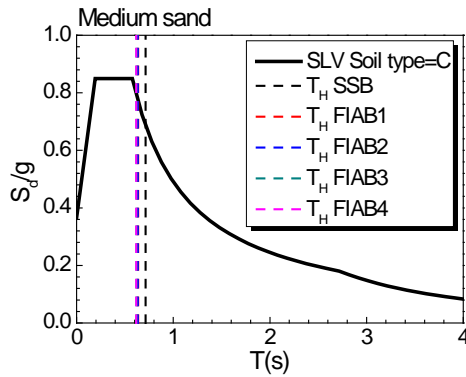
translation mode shape would decrease. As a result, the corresponding acceleration in the response spectra will keep the same or increase.



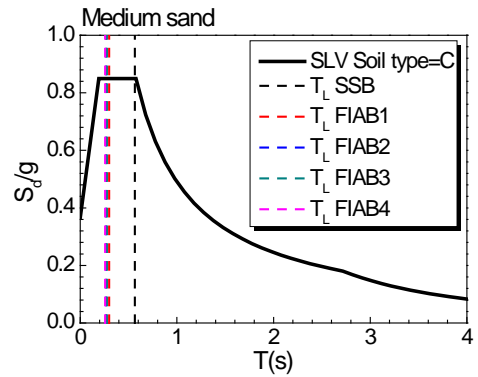
(a) Dense sand T_H



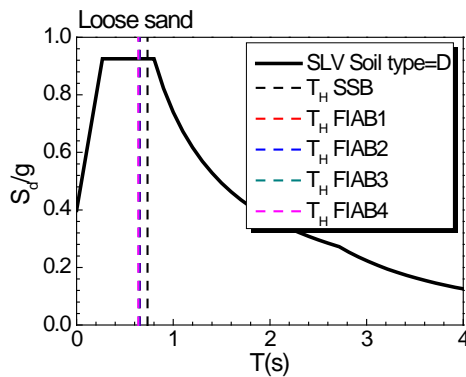
(b) Dense sand T_L



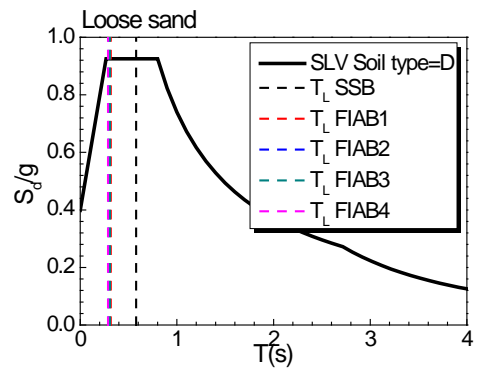
(c) Medium sand T_H



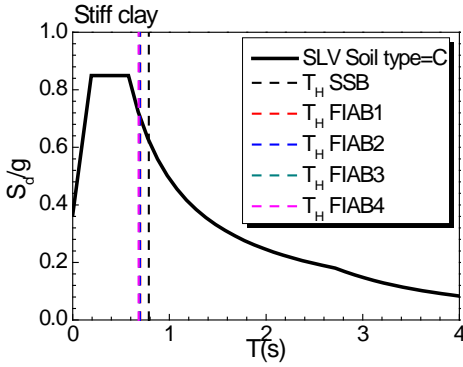
(d) Medium sand T_L



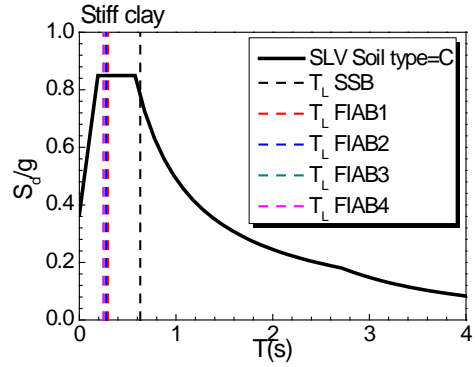
(e) Loose sand T_H



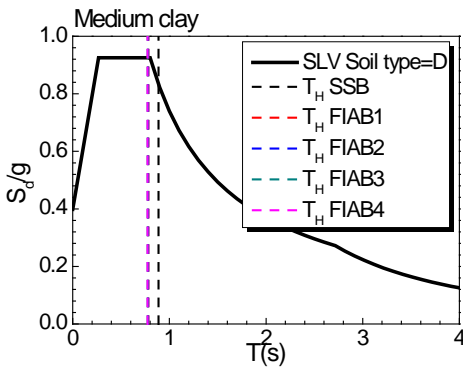
(f) Loose sand T_L



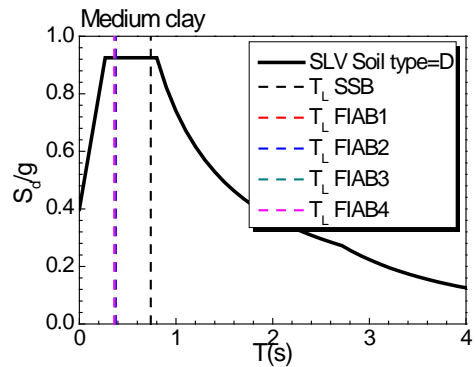
(g) Stiff clay T_H



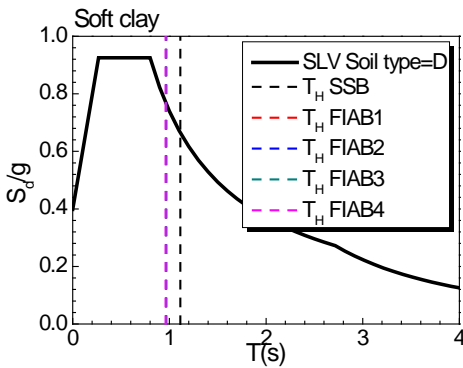
(h) Stiff clay T_L



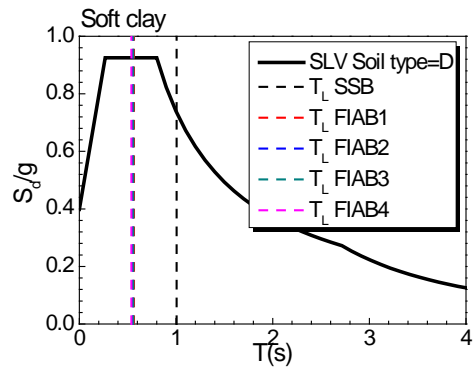
(i) Medium clay T_H



(j) Medium clay T_L



(k) Soft clay T_H



(l) Soft clay T_L

Fig. 259 T_H and T_L of different bridge types considering different soil types and the corresponding horizontal response spectra (SLV)

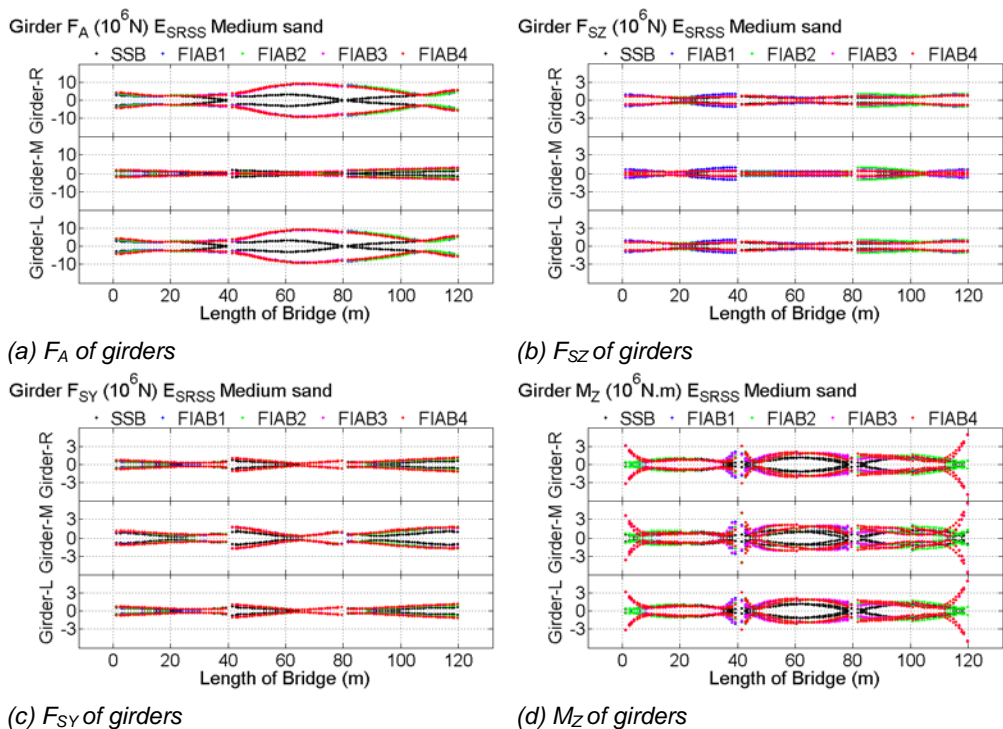
8.4.2 Different bridge types

In this analysis, the seismic performance of the existing SSB and four subtypes of

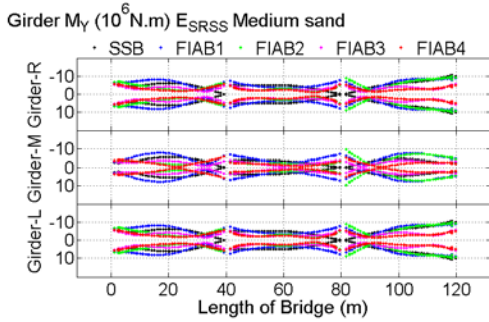
FIABs (FIAB1, FIAB2, FIAB3 and FIAB4) after retrofitting was analyzed. The performance of the SSB can be chosen as a sample for comparison to indicate the advantages and disadvantages of different retrofitting approaches. If the performance of different bridge components in FIABs is larger than that in the SSB, the corresponding bridge components should be checked after retrofitting. The SRSS combination of horizontal response spectra corresponding to the limit state SLV in two directions is considered in following studies.

8.4.2.1 Girder

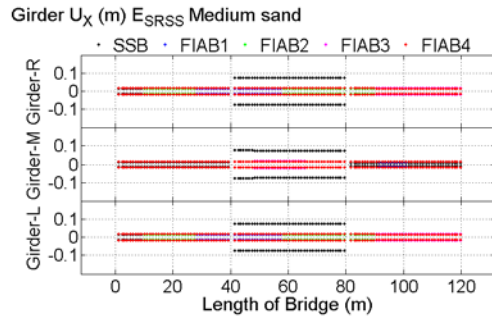
The performance of girders in all bridge types considering the soil as medium sand is compared in Fig. 260. It could be found that the distributions of F_A , M_Z , M_Y and U_Y of girders in FIABs are different to those in SSB. For example, the ultimate U_Y of girders in FIABs appear at the middle point of Span-2, which is totally different to the positions of the extreme U_Y of girders appeared in the SSB, which occur at the right end of Span-2.



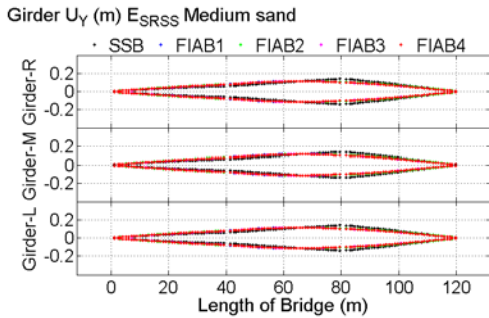
RETROFIT OF EXISTING BRIDGES WITH CONCEPT OF INTEGRAL ABUTMENT BRIDGE



(e) M_Y of girders



(f) U_X of girders



(g) U_Y of girders

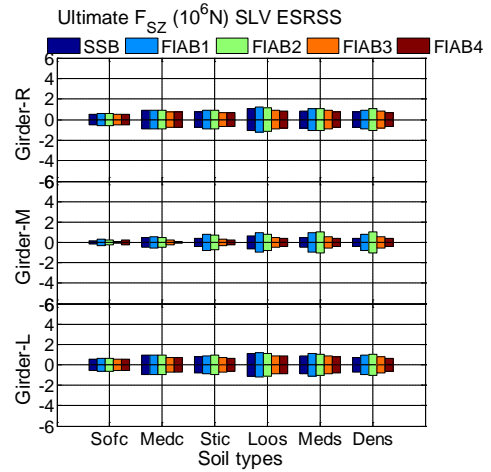
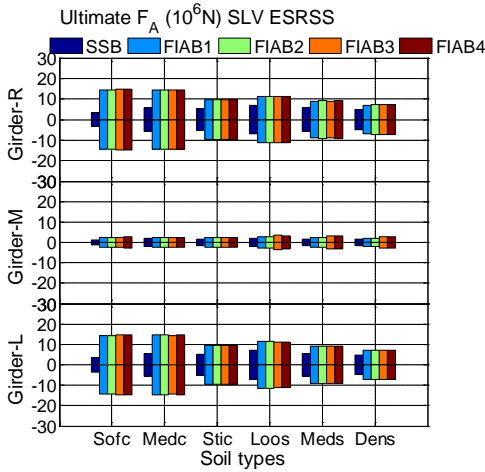
Fig. 260 Influence of different bridge types on the performance of girders under seismic load (SLV ESRSS)

In order to show the differences clearly, the ultimate value of the internal force of girders in different bridge types could be selected as the research target, as illustrated in Fig. 261. The performance of the edge-girder (Girder-L and Girder-R) is different to that of the mid-girder (Girder-M). From Fig. 261(a), (b) and (e), it could be found that the ultimate F_A , F_{SZ} and M_Y of Girder-L and Girder-R under response spectrum are larger than those of Girder-M. On the contrary, the ultimate F_{SY} and M_Z of Girder-L and Girder-R under response spectrum are smaller than those of Girder-M, as illustrated in Fig. 261(c) and (d). Therefore, in the following analysis, the ultimate values of three girders should be considered.

By comparing the seismic performance of girders in SSB with that in FIABs, it could be found that the ultimate F_A , F_{SY} and M_Z of girders in SSB are significantly smaller than those in FIABs; however, the ultimate M_Y , U_X and U_Y of girders in SSB are larger than those in FIABs.

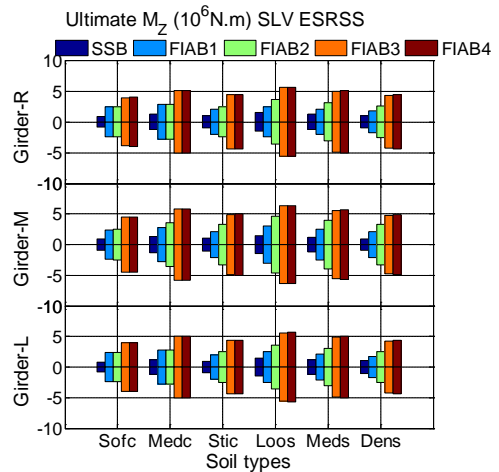
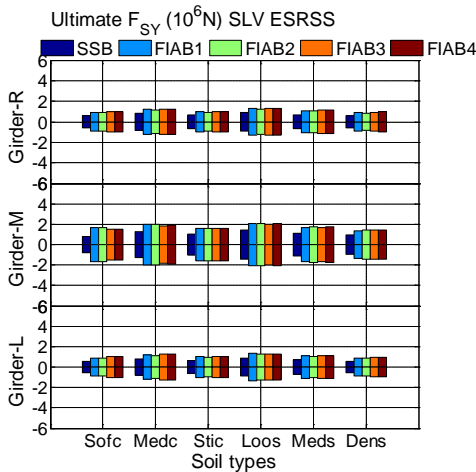
By comparing the seismic performance of girders in different subtypes of FIABs, it could be observed that the ultimate F_A , F_{SY} , U_X and U_Y of girders in different subtypes of FIABs are similar. The ultimate F_{SZ} and M_Y of girders in FIAB3 and

FIAB4 under response spectrum are smaller than those in FIAB1 and FIAB2. Conversely, the ultimate M_z of girders in FIAB3 and FIAB4 under response spectrum are obviously larger than those in FIAB1 and FIAB2.



(a) F_A of girders

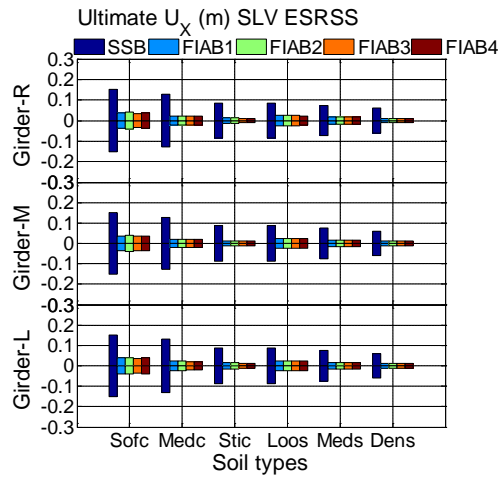
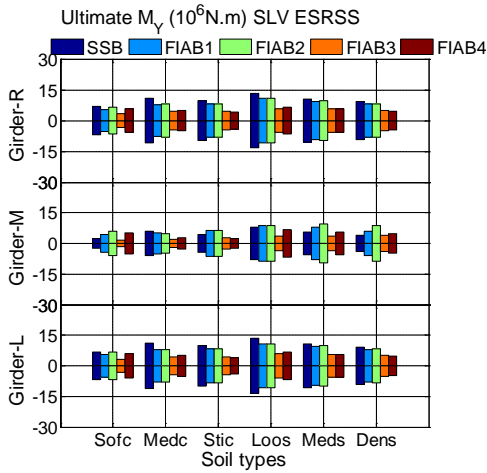
(b) F_{SZ} of girders



(c) F_{SY} of girders

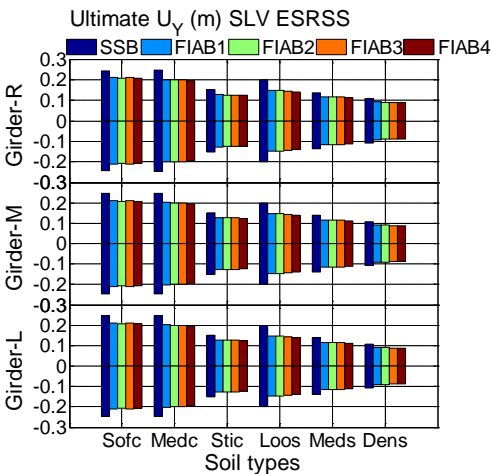
(d) M_z of girders

RETROFIT OF EXISTING BRIDGES WITH CONCEPT OF INTEGRAL ABUTMENT BRIDGE



(e) M_y of girders

(f) U_x of girders

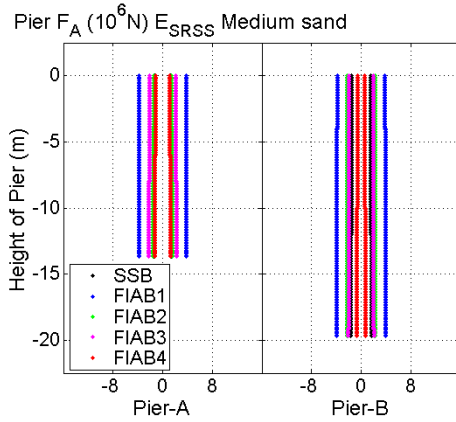


(g) U_y of girders

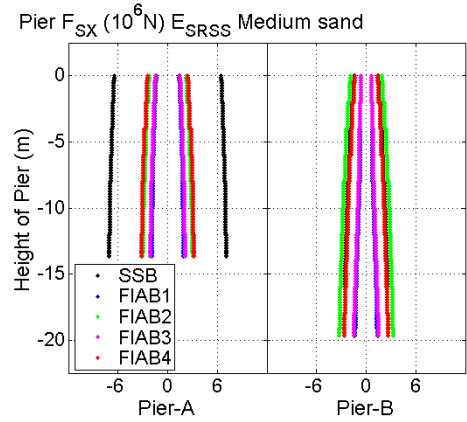
Fig. 261 Influence of different bridge types on the ultimate internal forces of girders under seismic load (SLV ESRSS)

8.4.2.2 Pier

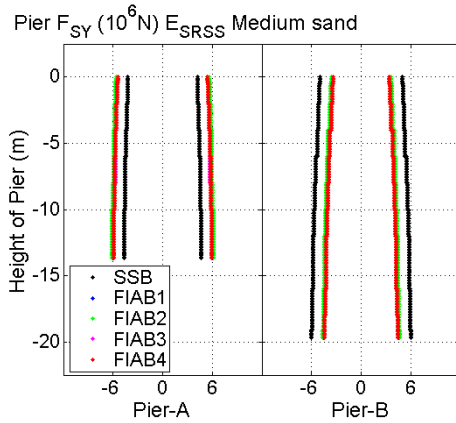
The performance of piers in different bridge types considering the soil as medium sand are shown in Fig. 262. It could be found that the internal force distributions of piers in FIABs are similar to those in SSB, except the M_y of piers in FIAB3 and FIAB4.



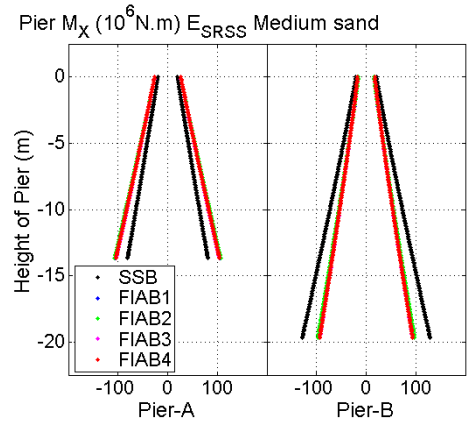
(a) F_A of piers



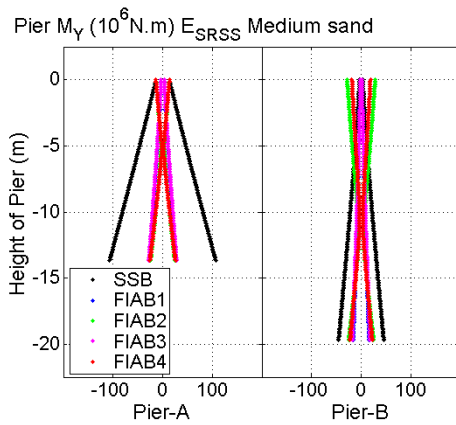
(b) F_{SX} of piers



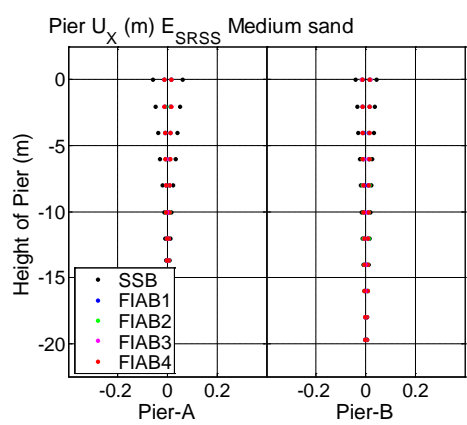
(c) F_{SY} of piers



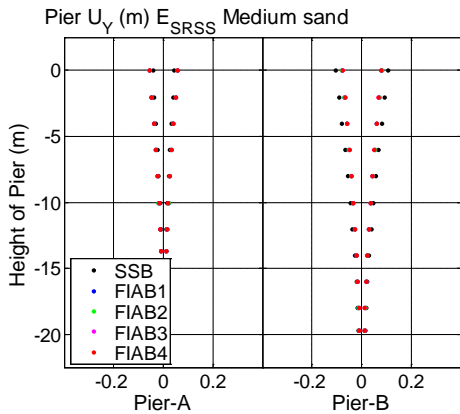
(d) M_X of piers



(e) M_Y of piers



(f) U_X of piers

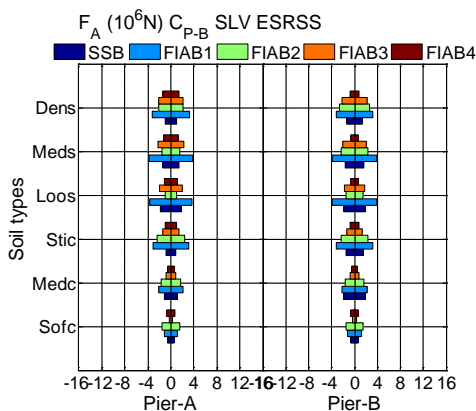


(g) U_Y of piers

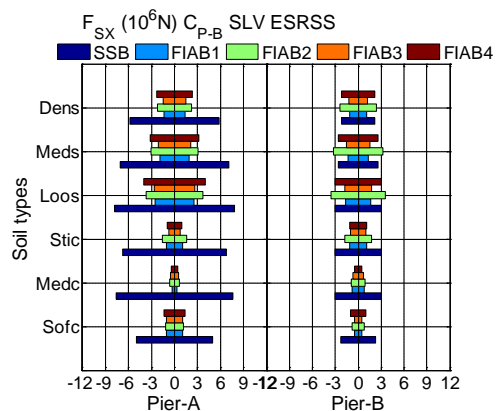
Fig. 262 Influence of different bridge types on the performance of piers under seismic load (SLV ESRSS)

In order to show the differences clearly, the ultimate value of the internal force of piers in different bridge types could be chosen as the research target, as compared in Fig. 263, in which the abbreviation ' C_{P-B} ' denotes the critical sections at the bottom of two piers. Due to the asymmetric substructure heights introduced above, the performance of two piers may be different. The larger value of two piers will be chosen to carry out the following analysis.

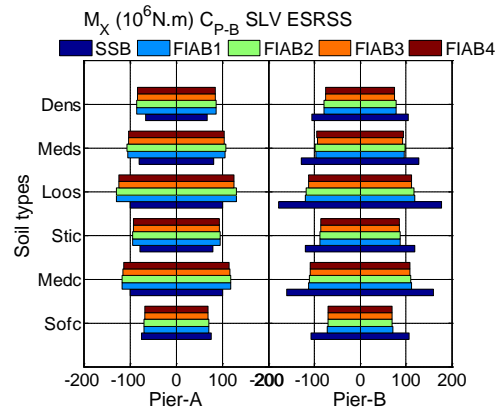
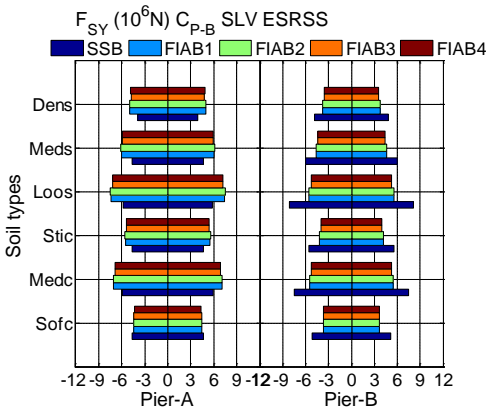
By comparing the seismic performance of piers in SSB with that in FIABs, it could be found the ultimate values of all internal forces of piers in SSB are larger than those in FIABs, except the F_A of piers. Furthermore, the ultimate F_A of piers in FIAB1 is the maximum among different subtypes of FIABs.



(a) F_A of piers

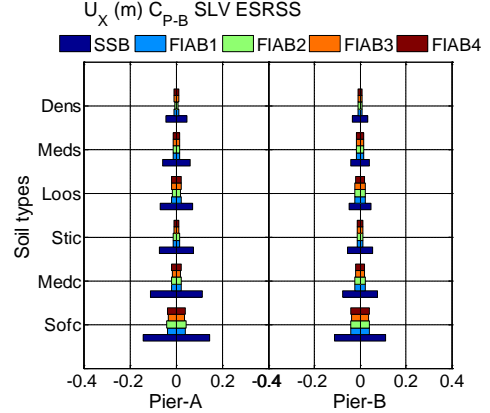
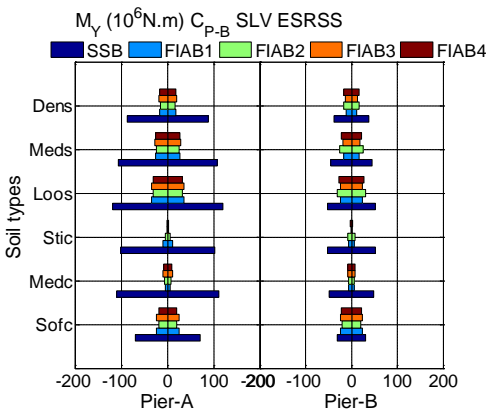


(b) F_{SX} of piers



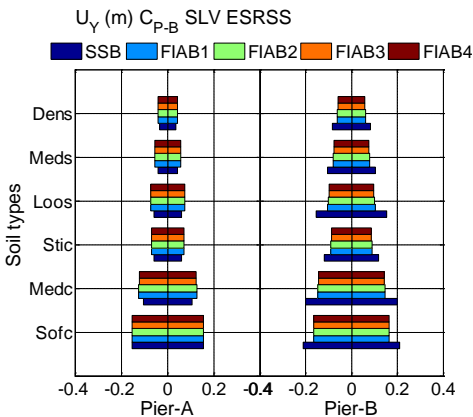
(c) F_{SY} of piers

(d) M_X of piers



(e) M_Y of piers

(f) U_X of piers

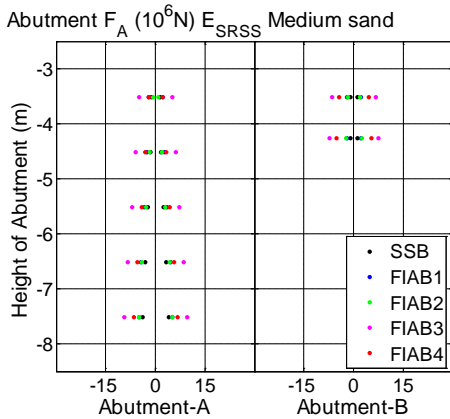


(g) U_Y of piers

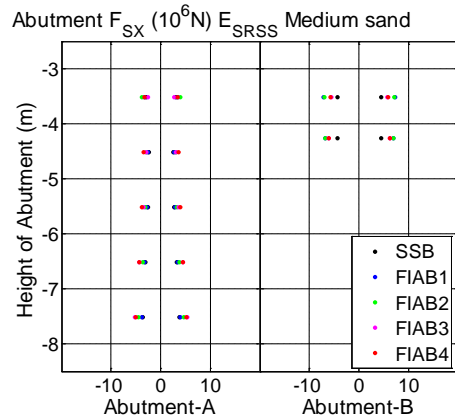
Fig. 263 Influence of different bridge types on the ultimate internal forces of piers under seismic load (SLV ESRSS)

8.4.2.3 Abutment stem

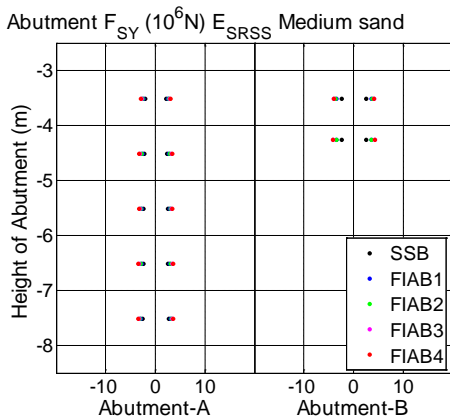
The performance of abutment stems in different bridge types considering the soil as medium sand are illustrated in Fig. 264. It could be found that the internal force distributions of abutment stems in FIABs are similar to those in SSB.



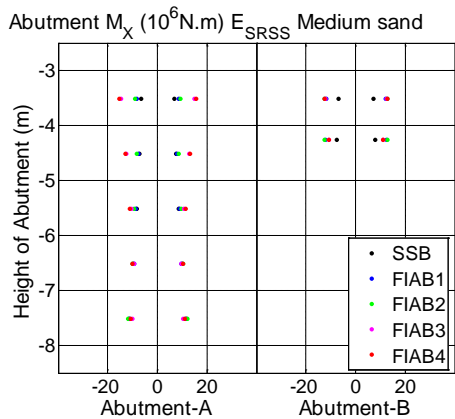
(a) F_A of abutment stems



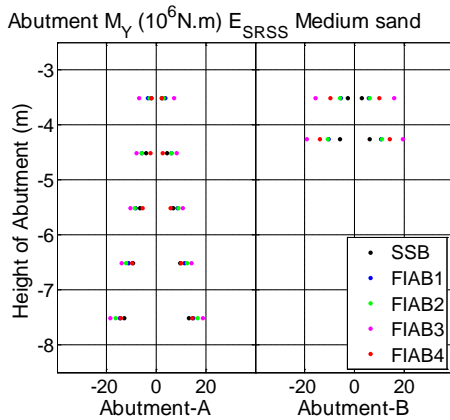
(b) F_{SX} of abutment stems



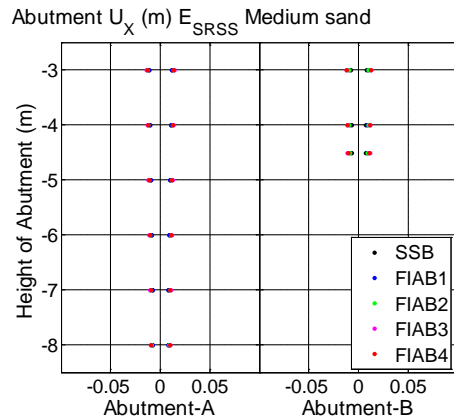
(c) F_{SY} of abutment stems



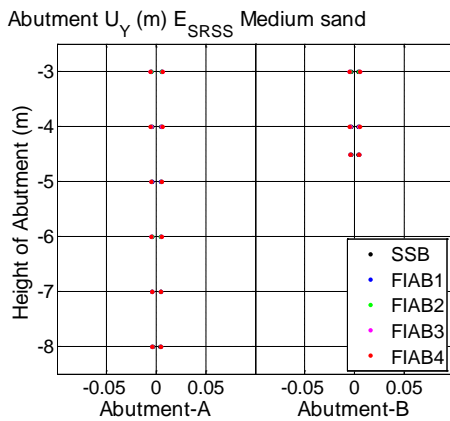
(d) M_X of abutment stems



(e) M_Y of abutment stems



(f) U_X of abutment stems



(g) U_Y of abutment stems

Fig. 264 Influence of different bridge types on the performance of abutment stems under seismic load (SLV ESRSS)

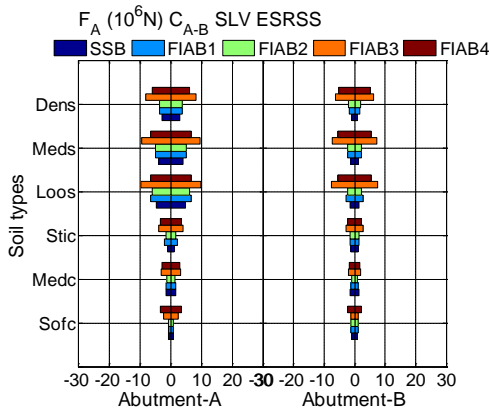
In order to show the differences clearly, the ultimate value of the internal force of abutment stems in different bridge types could be chosen as the research target, as compared in Fig. 265, in which the abbreviations ‘ C_{A-T} ’ and ‘ C_{A-B} ’ represent the critical sections at the top and bottom of two abutment stems. Similarly, the larger value of two abutment stems will be chosen to carry out the following comparisons.

By comparing the seismic performance of abutment stems in SSB with that in FIABs, it could be found the ultimate values of all internal forces of abutment stems in SSB are equal to or smaller than those in FIABs.

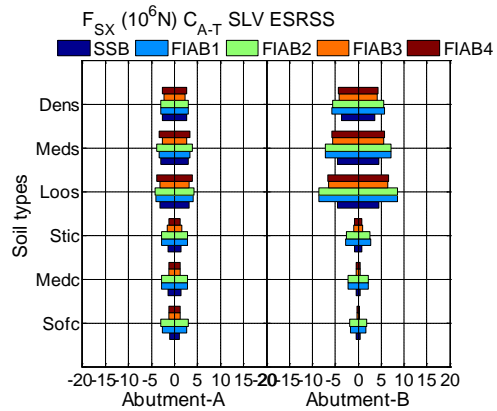
By comparing the seismic performance of abutment stems in different subtypes of FIABs, it could be observed that the ultimate F_{SY} , U_X and U_Y of abutment stems in

RETROFIT OF EXISTING BRIDGES WITH CONCEPT OF INTEGRAL ABUTMENT BRIDGE

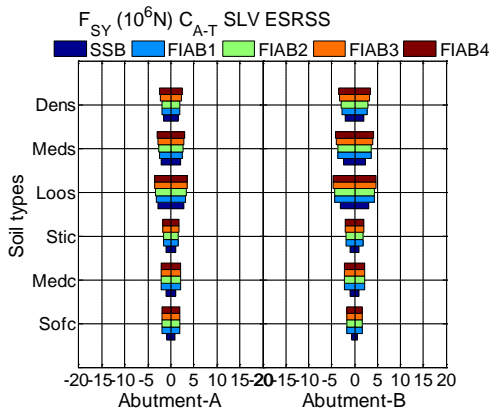
different subtypes of FIABs are nearly the same. The ultimate F_{SX} of abutment stems in FIAB3 and FIAB4 under response spectrum are smaller than those in FIAB1 and FIAB2. The ultimate F_A and M_Y of abutment stems in FIAB3 could be the maximum among different FIABs under seismic load. When the soil condition is sand, the ultimate M_X of abutment stems in FIAB3 and FIAB4 under response spectrum is larger than that in FIAB1 and FIAB2; however, when the soil condition is clay, the regulation is opposite.



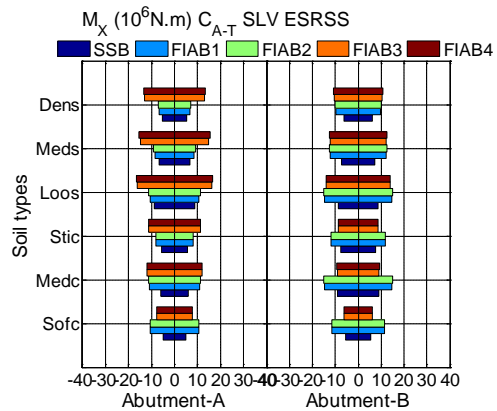
(a) F_A of abutment stems



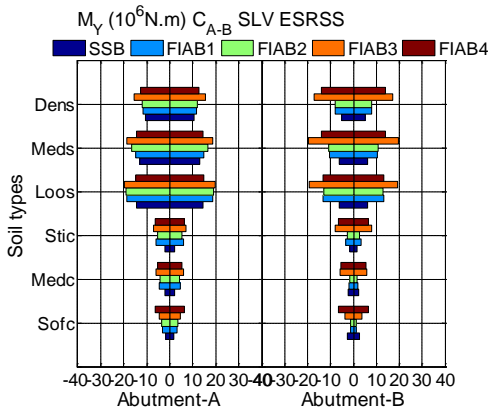
(b) F_{SX} of abutment stems



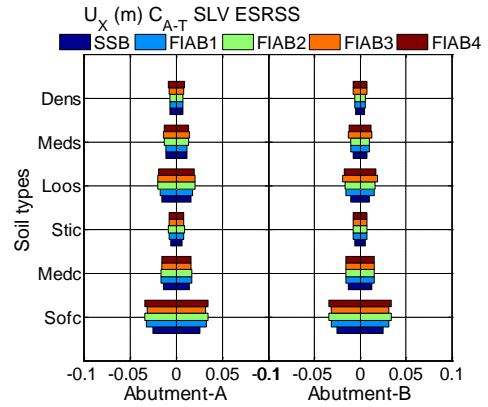
(c) F_{SY} of abutment stems



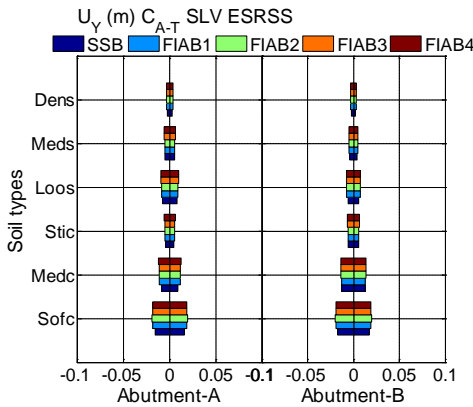
(d) M_X of abutment stems



(e) M_Y of abutment stems



(f) U_X of abutment stems



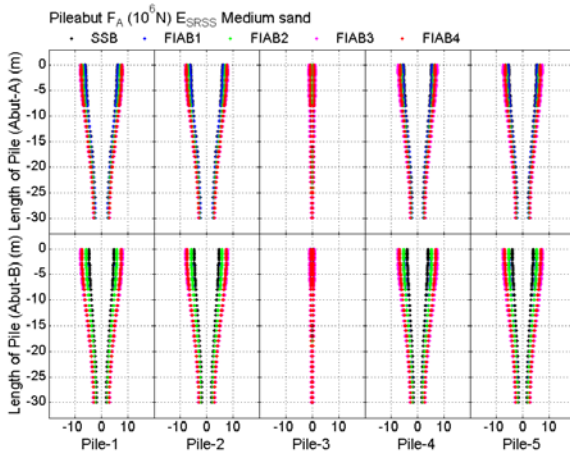
(g) U_Y of abutment stems

Fig. 265 Influence of different bridge types on the ultimate internal forces of abutment stems under seismic load (SLV ESRSS)

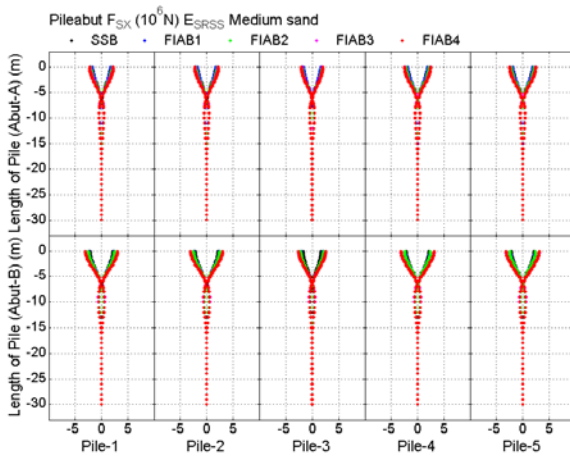
8.4.2.4 Pile beneath abutments

The performance of piles beneath abutments in different bridge types considering the soil as medium sand are illustrated in Fig. 266. It could be found that the internal force distributions of piles beneath abutments in FIABs are similar to those in SSB.

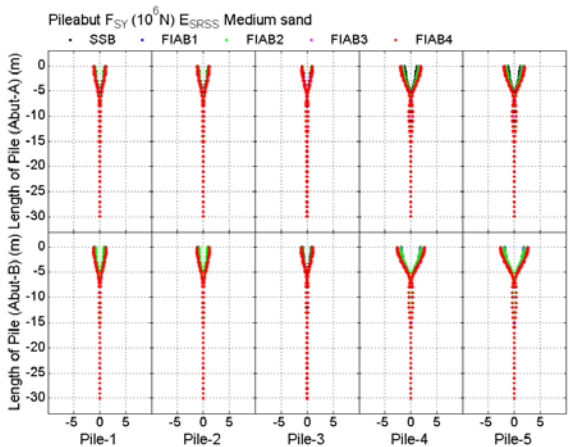
RETROFIT OF EXISTING BRIDGES WITH CONCEPT OF INTEGRAL ABUTMENT BRIDGE



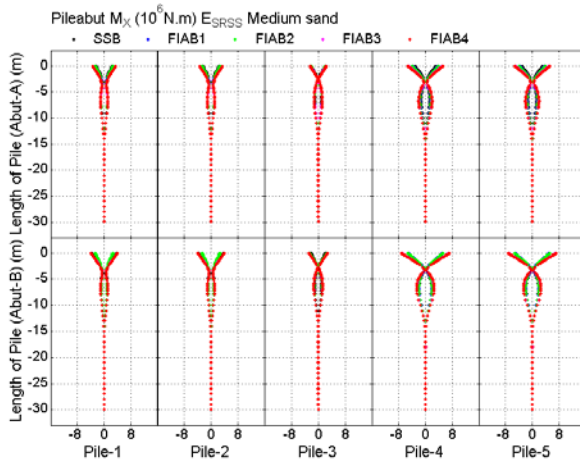
(a) F_A of piles beneath abutments



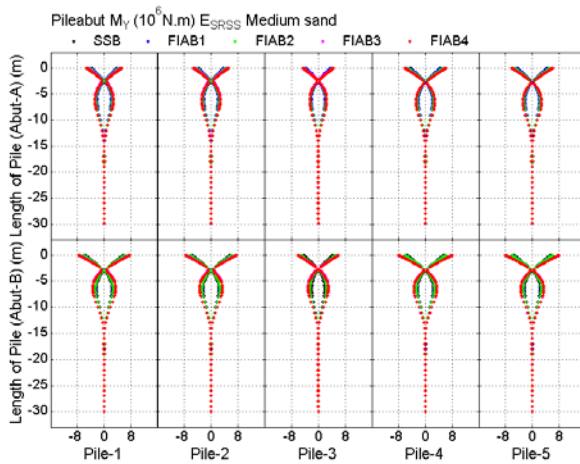
(b) F_{SX} of piles beneath abutments



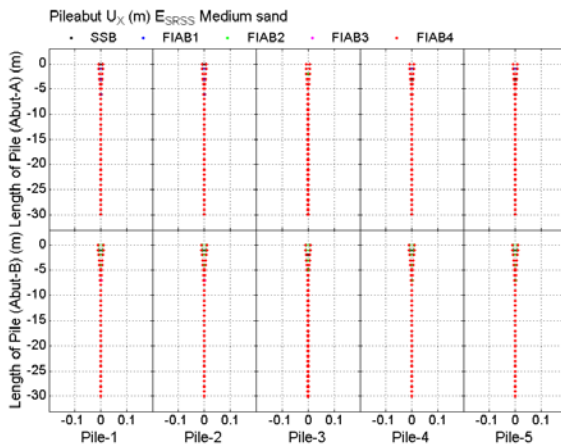
(c) F_{SY} of piles beneath abutments



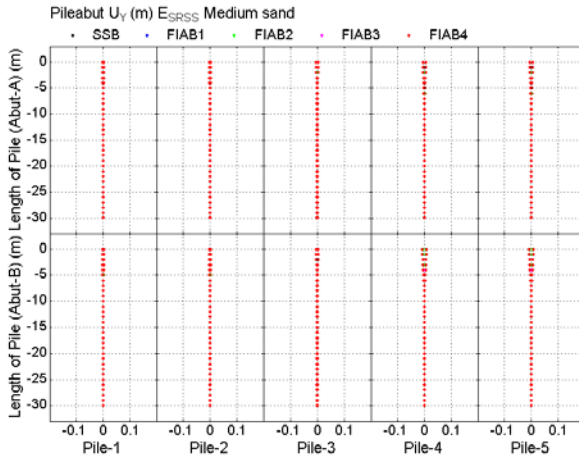
(d) M_x of piles beneath abutments



(e) M_y of piles beneath abutments



(f) U_x of piles beneath abutments



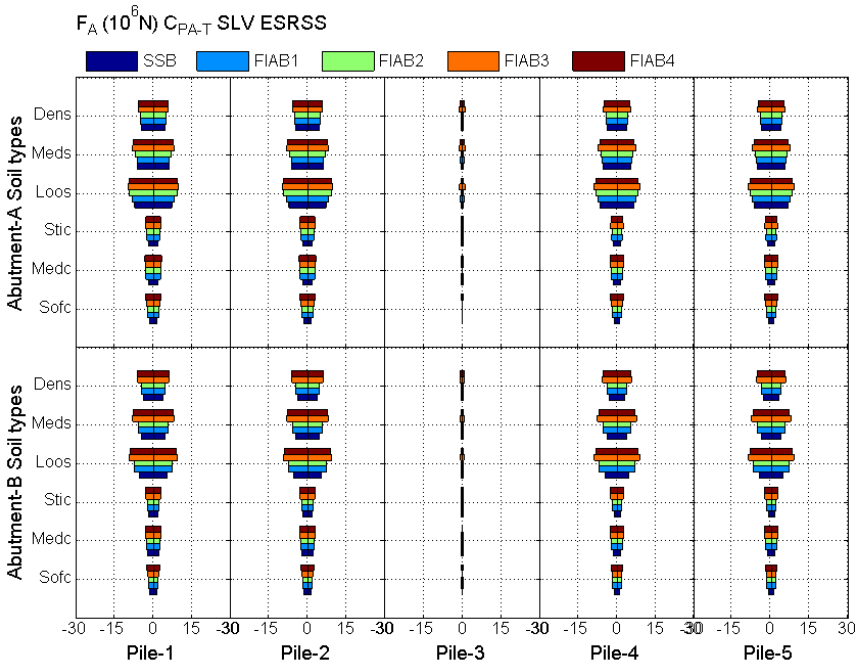
(g) U_Y of piles beneath abutments

Fig. 266 Influence of different bridge types on the performance of piles beneath abutments under seismic load (SLV ESRSS)

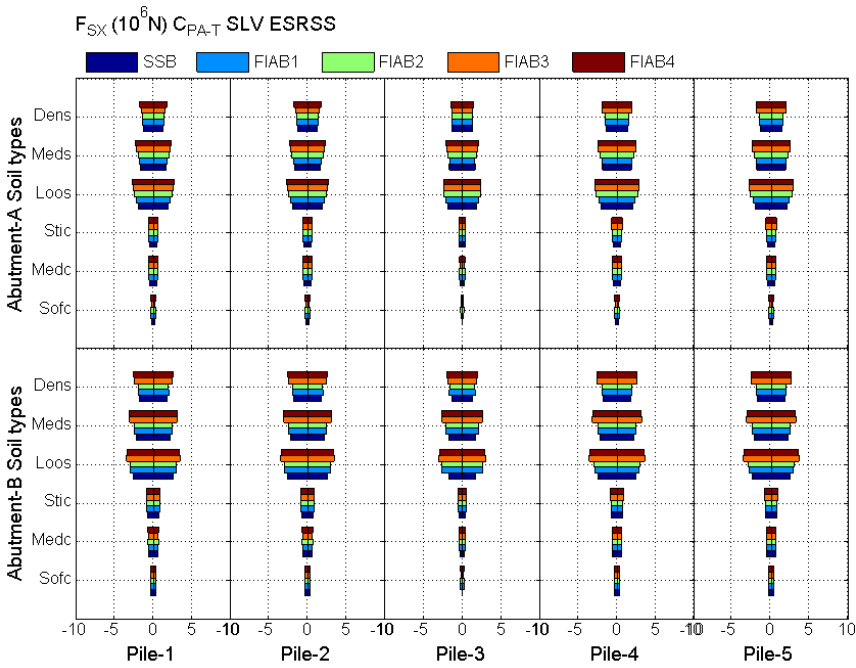
In order to show the differences clearly, the ultimate value of the internal force of piles beneath abutments in different bridge types could be selected as the research target, as compared in Fig. 267, in which the abbreviation 'C_{PA-T}' denotes the critical sections at the top of piles beneath abutments.

By comparing the seismic performance of piles beneath abutments in SSB with that in FIABs, it could be found the ultimate value of all internal force of piles beneath abutments in SSB are equal to or smaller than those in FIABs.

By comparing the seismic performance of piles beneath abutments in different subtypes of FIABs, it could be observed all ultimate forces and bending moments in FIAB3 and FIAB4 under response spectrum are larger than those in FIAB1 and FIAB2; however the ultimate displacements (U_x and U_y) in different subtypes of FIABs are nearly the same.

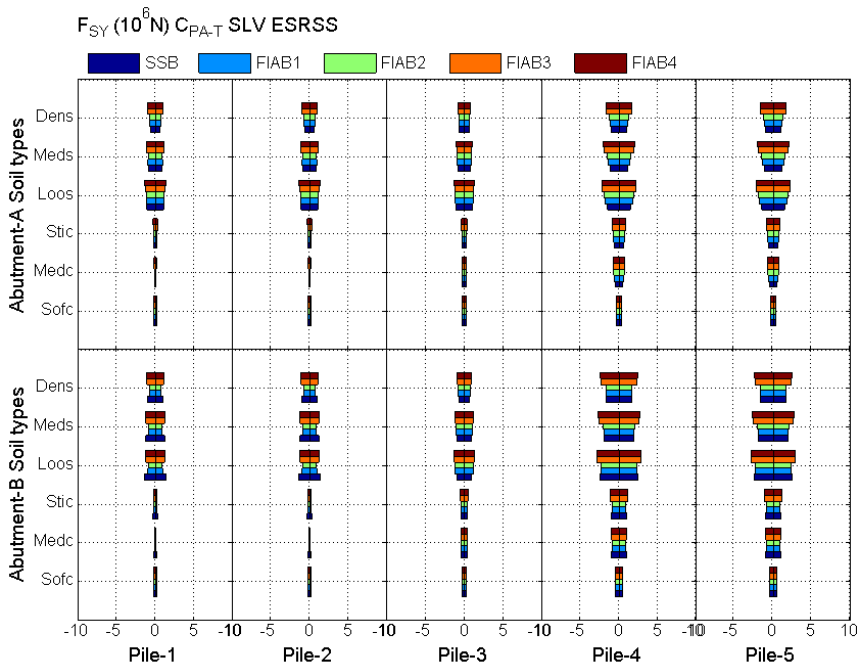


(a) F_A of piles beneath abutments

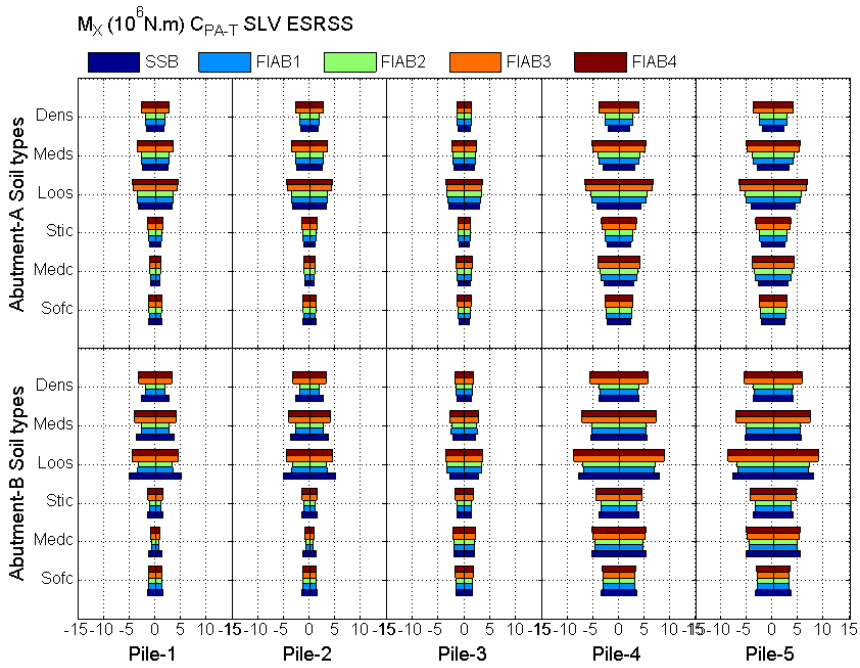


(b) F_{SX} of piles beneath abutments

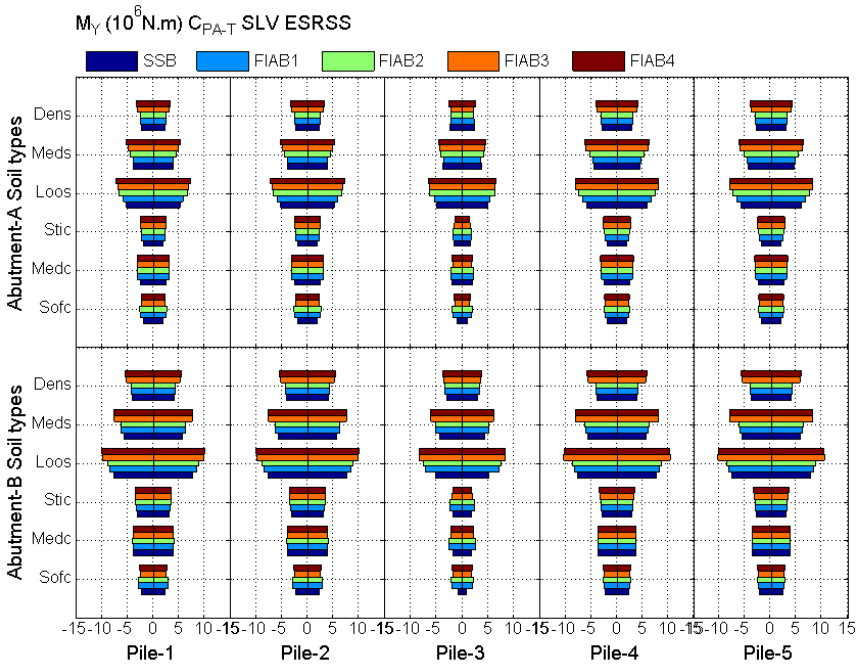
RETROFIT OF EXISTING BRIDGES WITH CONCEPT OF INTEGRAL ABUTMENT BRIDGE



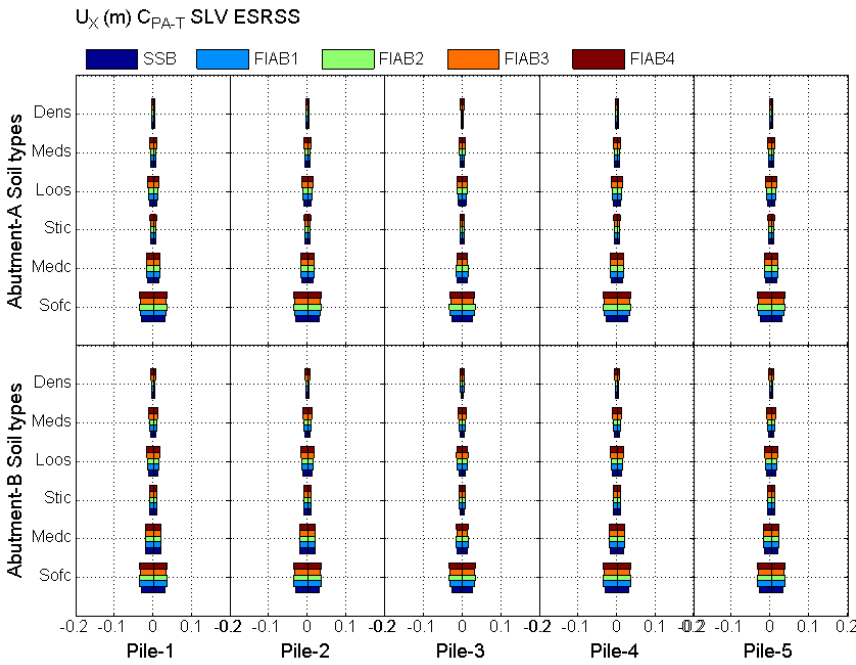
(c) F_{SY} of piles beneath abutments



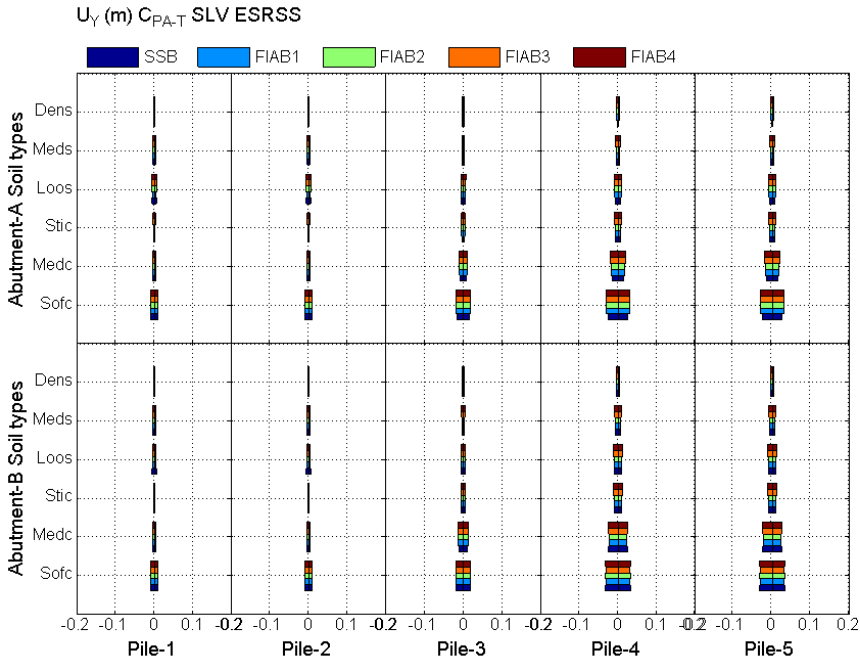
(d) M_X of piles beneath abutments



(e) M_y of piles beneath abutments



(f) U_x of piles beneath abutments

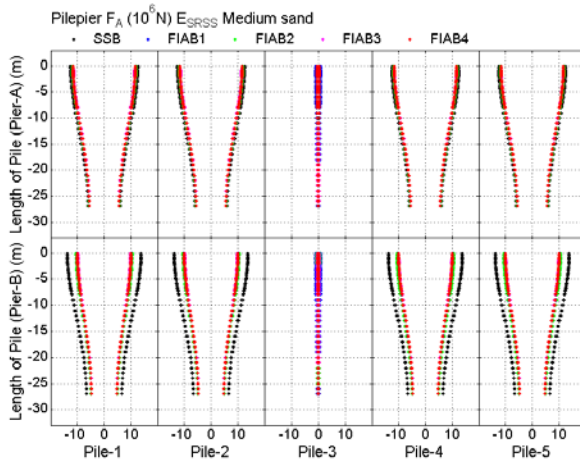


(g) U_Y of piles beneath abutments

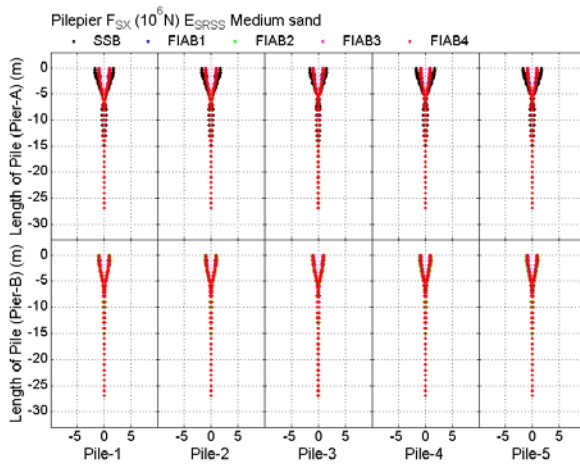
Fig. 267 Influence of different bridge types on the ultimate internal forces of piles beneath abutments under seismic load (SLV ESRSS)

8.4.2.5 Pile beneath piers

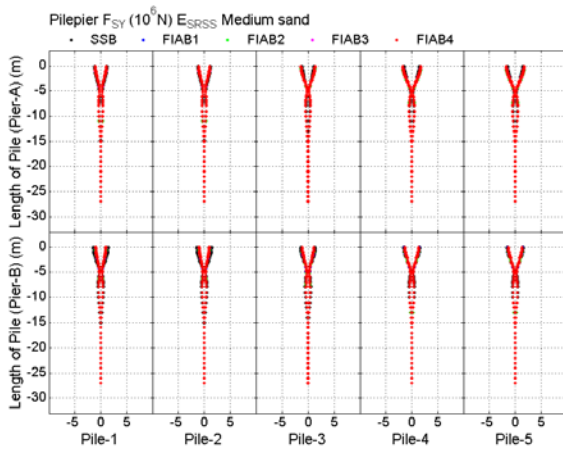
Different to the static load case, the mechanical properties of piles beneath piers under seismic load is quite large, which cannot be neglected. The performance of piles beneath piers in different bridge types considering the soil as medium sand are illustrated in Fig. 268. It could be also observed that the internal force distributions of piles beneath piers in FIABs are similar to those in SSB.



(a) F_A of piles beneath piers

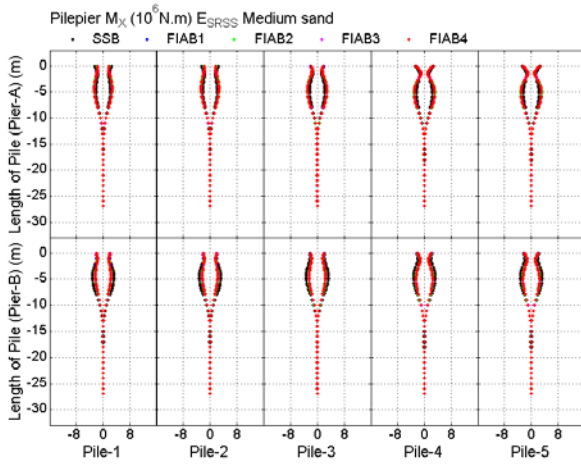


(b) F_{SX} of piles beneath piers

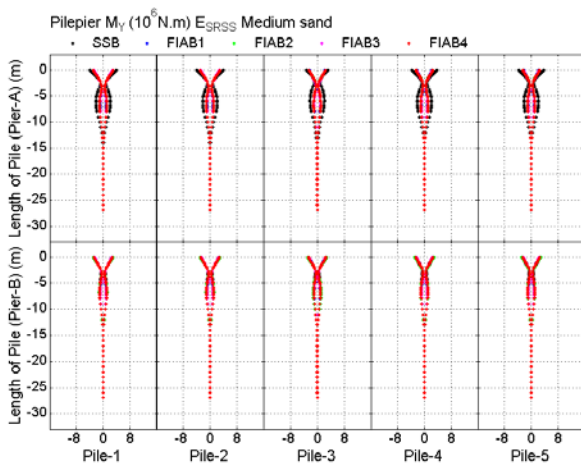


(c) F_{SY} of piles beneath piers

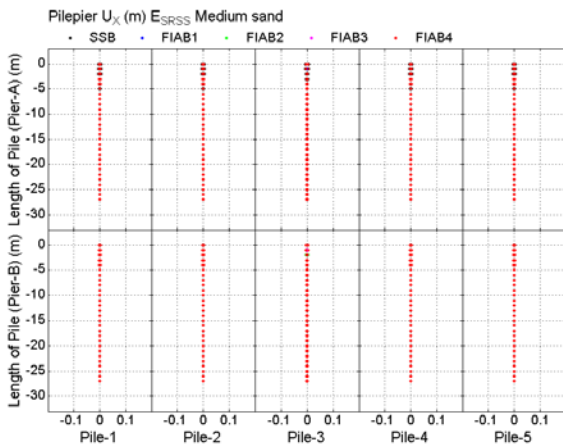
RETROFIT OF EXISTING BRIDGES WITH CONCEPT OF INTEGRAL ABUTMENT BRIDGE



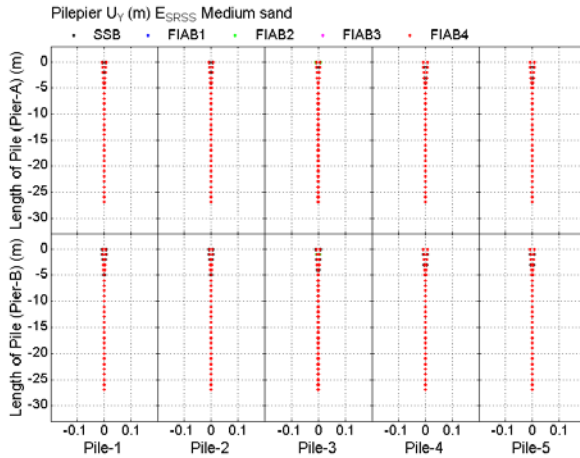
(d) M_x of piles beneath piers



(e) M_y of piles beneath piers



(f) U_x of piles beneath piers



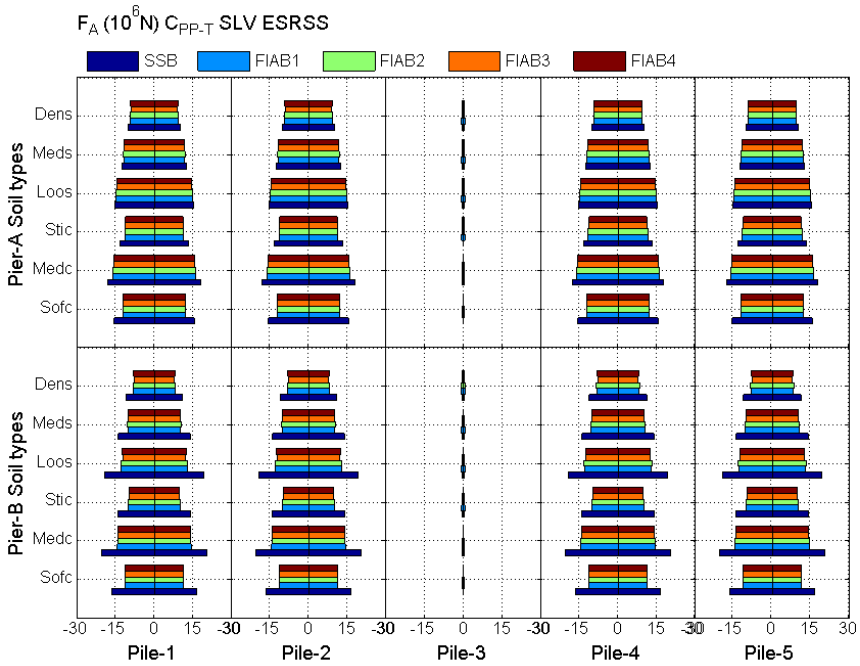
(g) U_Y of piles beneath piers

Fig. 268 Influence of different bridge types on the performance of piles beneath piers under seismic load (SLV ESRSS)

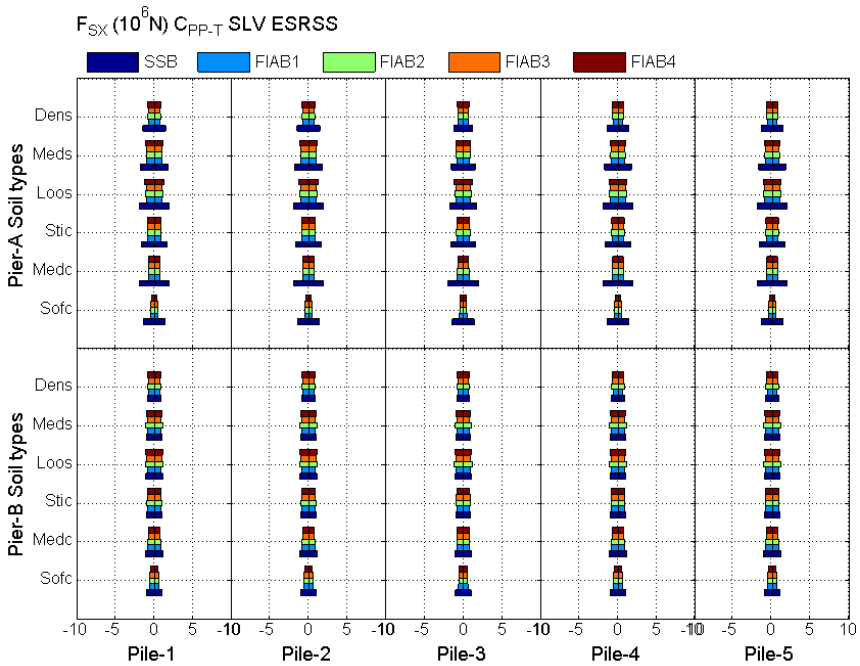
In order to show the differences clearly, the ultimate value of the internal force of piles beneath piers in different bridge types could be selected as the research target, as compared in Fig. 269, in which the abbreviation 'C_{PP-T}' denotes the critical sections at the top of piles beneath piers.

By comparing the seismic performance of piles beneath piers in SSB with that in FIABs, it could be found the ultimate values of all internal forces of piles beneath piers in SSB are equal to or larger than those in FIABs. Moreover, all internal forces of piles beneath piers in different subtypes of FIABs under response spectrum are nearly the same.

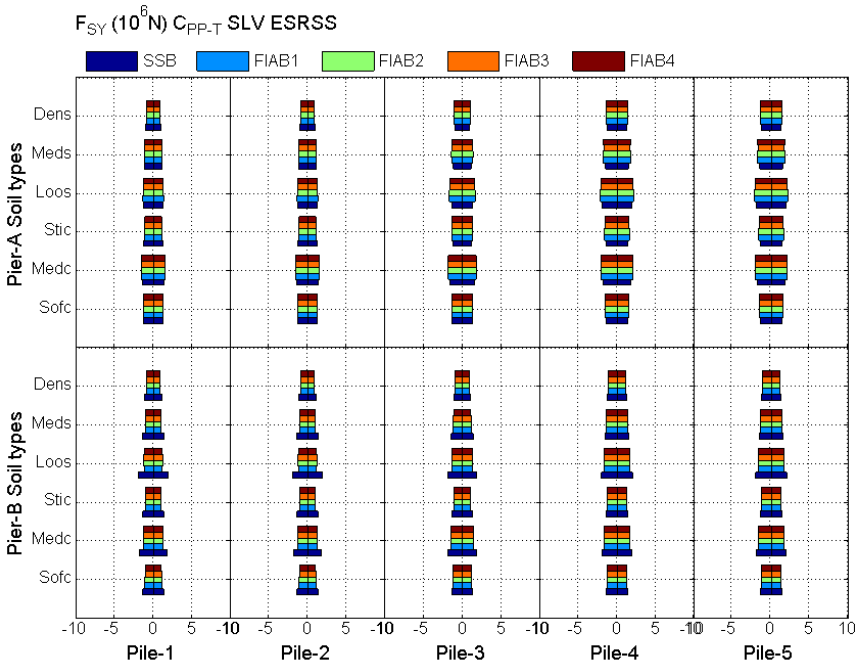
RETROFIT OF EXISTING BRIDGES WITH CONCEPT OF INTEGRAL ABUTMENT BRIDGE



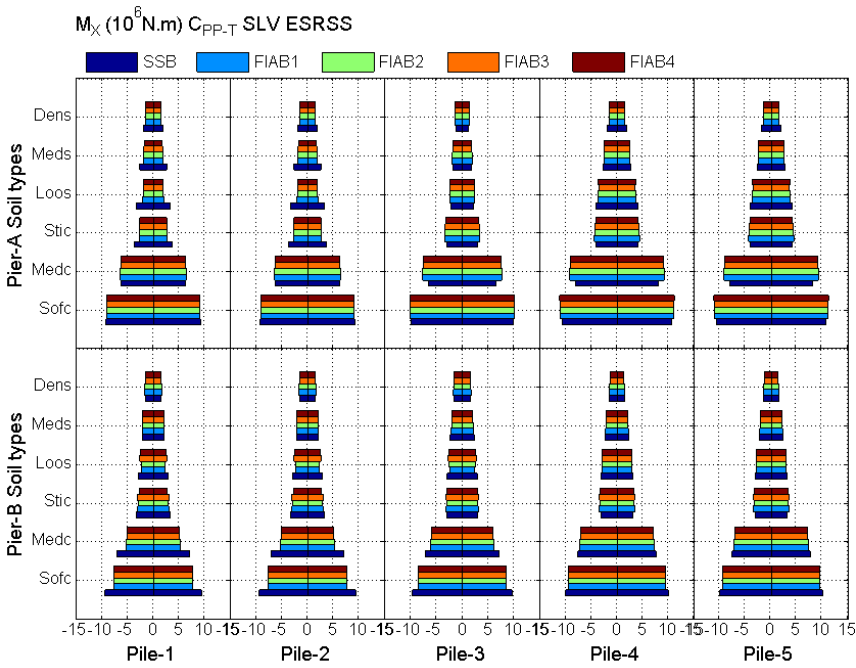
(a) F_A of piles beneath piers



(b) F_{SX} of piles beneath piers

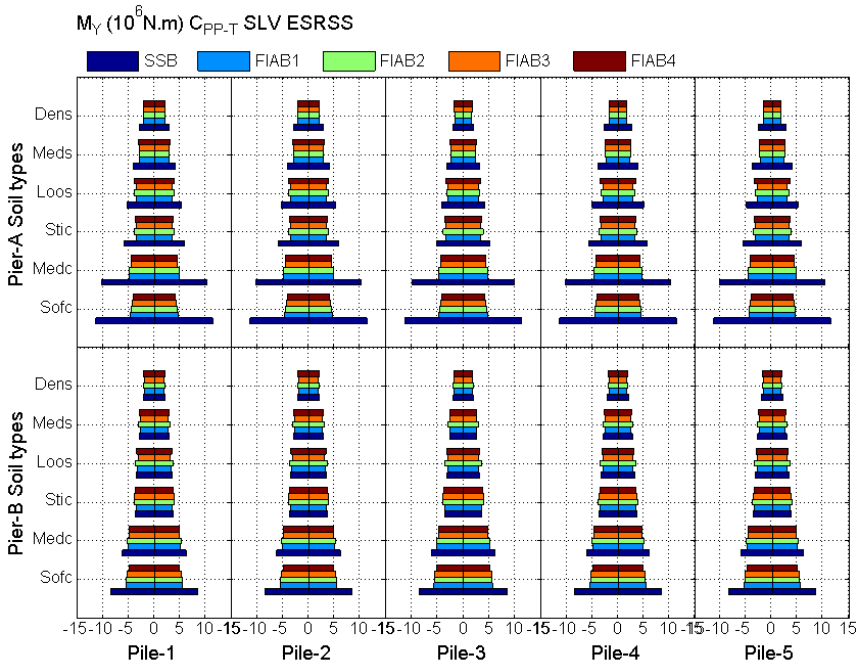


(c) F_{SY} of piles beneath piers

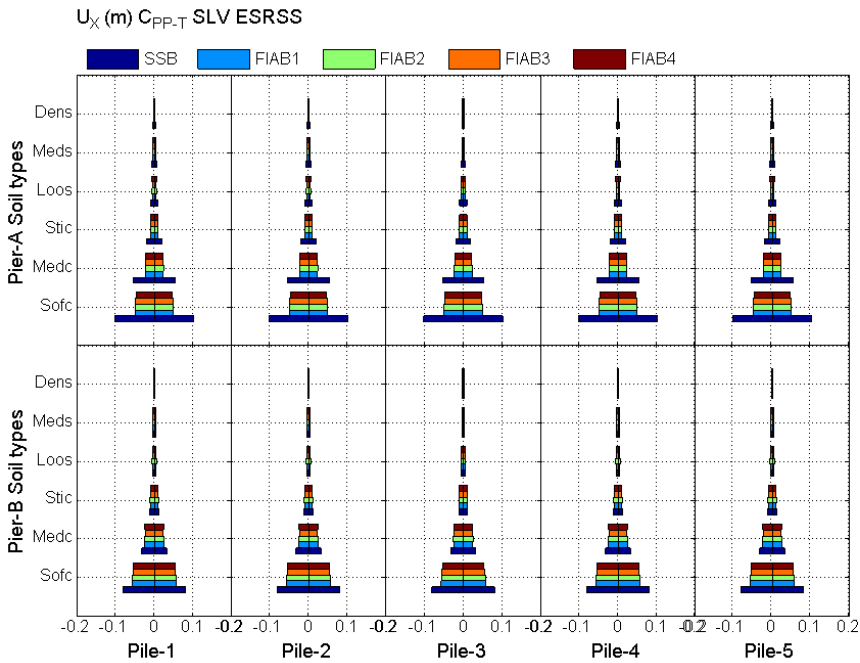


(d) M_x of piles beneath piers

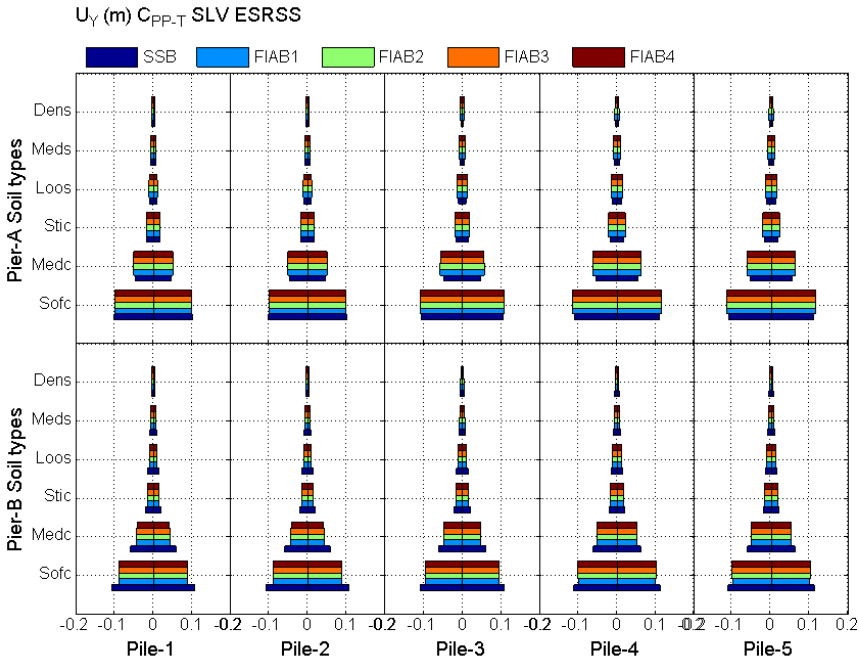
RETROFIT OF EXISTING BRIDGES WITH CONCEPT OF INTEGRAL ABUTMENT BRIDGE



(e) M_Y of piles beneath piers



(f) U_X of piles beneath piers



(g) U_v of piles beneath piers

Fig. 269 Influence of different bridge types on the ultimate internal forces of piles beneath piers under seismic load (SLV ESRSS)

8.4.2.6 Summary

The results of the seismic sensitive analysis considering different bridge types have been described above. It could be found that some internal forces of different bridge components in SSB are larger than those in FIABs under seismic load, as listed in Table 56. It means that, if the existing bridge was designed according to the appropriate seismic load, the resistance capacities of existing sections should be enough to bear the internal forces in any new bridge types after retrofitting, then, these existing sections can be reused after retrofitting without any checks. On the contrary, if the internal forces of different bridge components in SSB are smaller than those in FIABs under seismic load, these internal forces should be improved to satisfy the requirements of the new bridge types. In this case, the investigation on the differences among different subtypes of FIABs (compared in Table 56) is quite useful, which could help engineers to choose the most suitable retrofitting method for different cases. In conclusion, it could be found that FIAB1 or FIAB2 could be considered as the most suitable retrofitting solutions of the existing SSB from the seismic point of view.

RETROFIT OF EXISTING BRIDGES WITH CONCEPT OF INTEGRAL ABUTMENT BRIDGE

Components	Internal forces	Different bridge types	
Girder	F_A	SSB<FIAB	FIAB1≈FIAB2≈FIAB3≈FIAB4
	F_{SZ}	SSB<FIAB	FIAB1≈FIAB2>FIAB3≈FIAB4
	F_{SY}	SSB<FIAB	FIAB1≈FIAB2≈FIAB3≈FIAB4
	M_Z	SSB<FIAB	FIAB3≈FIAB4>>FIAB1≈FIAB2
	M_Y	SSB>FIAB	-
	U_X	SSB>FIAB	-
	U_Y	SSB>FIAB	-
Pier	F_A	SSB<FIAB	FIAB1>FIAB2≈FIAB3>FIAB4
	F_{SX}	SSB>FIAB	-
	F_{SY}	SSB>FIAB	-
	M_X	SSB>FIAB	-
	M_Y	SSB>FIAB	-
	U_X	SSB>FIAB	-
	U_Y	SSB>FIAB	-
Abutment stem	F_A	SSB<FIAB	FIAB3>FIAB4>>FIAB1≈FIAB2
	F_{SX}	SSB<FIAB	FIAB1≈FIAB2>FIAB3≈FIAB4
	F_{SY}	SSB<FIAB	FIAB1≈FIAB2≈FIAB3≈FIAB4
	M_X	SSB<FIAB	Sand:FIAB3≈FIAB4>FIAB1≈FIAB2 Clay:FIAB1≈FIAB2>FIAB3≈FIAB4
	M_Y	SSB<FIAB	FIAB3>FIAB4>FIAB1≈FIAB2
	U_X	SSB<FIAB	FIAB1≈FIAB2≈FIAB3≈FIAB4
	U_Y	SSB<FIAB	FIAB1≈FIAB2≈FIAB3≈FIAB4
Pile beneath abutment	F_A	SSB<FIAB	FIAB3≈FIAB4>FIAB1≈FIAB2
	F_{SX}	SSB<FIAB	FIAB3≈FIAB4>FIAB1≈FIAB2
	F_{SY}	SSB<FIAB	FIAB3≈FIAB4>FIAB1≈FIAB2
	M_X	SSB<FIAB	FIAB3≈FIAB4>FIAB1≈FIAB2
	M_Y	SSB<FIAB	FIAB3≈FIAB4>FIAB1≈FIAB2
	U_X	SSB<FIAB	FIAB1≈FIAB2≈FIAB3≈FIAB4
	U_Y	SSB<FIAB	FIAB1≈FIAB2≈FIAB3≈FIAB4
Pile beneath pier	F_A	SSB>FIAB	-
	F_{SX}	SSB>FIAB	-
	F_{SY}	SSB>FIAB	-
	M_X	SSB>FIAB	-
	M_Y	SSB>FIAB	-
	U_X	SSB>FIAB	-
	U_Y	SSB>FIAB	-

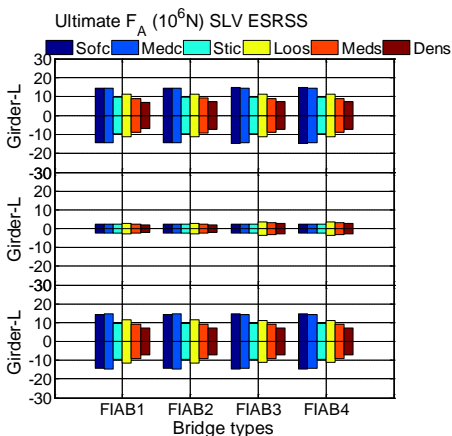
Table 56

Adverse influence of different bridge types on the performance of different bridge components under seismic load (the symbol “≈”, “>” and “>>” denote that the difference between two integral abutment bridge types can be neglected; is enough to pay attention to; and is quite significant, respectively).

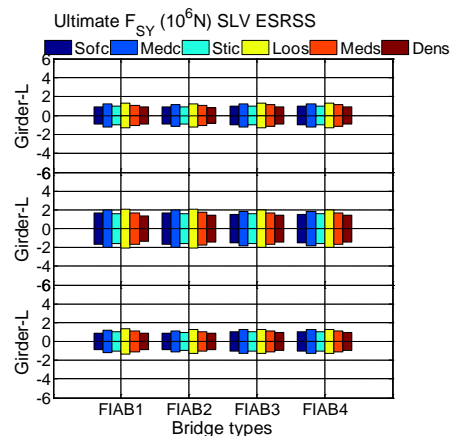
8.4.3 Different soil conditions

In this analysis, six types of soil with the properties listed in Table 34 (p.165) could be chosen as the parameter. The SRSS combination of horizontal response spectra corresponding to the limit state SLV in two directions is considered in following studies.

Based on the results of the seismic sensitive analysis considering different bridge types, it could be found that some internal forces of different bridge components in SSB are smaller than those in FIABs under seismic load, as listed in Table 56, which should be paid more attention to. Therefore, the ultimate internal force of these critical bridge components in FIABs could be chosen as the research object in this section, as illustrated in Fig. 270 to Fig. 273.

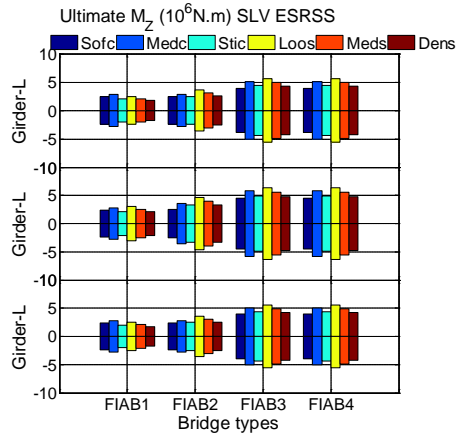
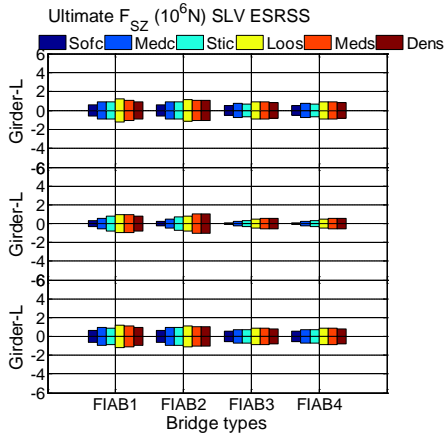


(a) F_A of girders



(b) F_{Sz} of girders

RETROFIT OF EXISTING BRIDGES WITH CONCEPT OF INTEGRAL ABUTMENT BRIDGE



(c) F_{Sy} of girders

(d) M_z of girders

Fig. 270 Influence of different soil conditions on the ultimate internal forces of girders under seismic load (SLV ESRSS)

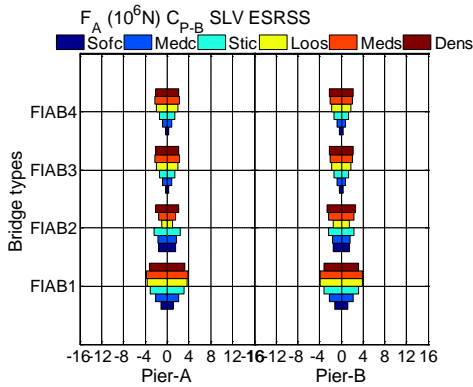
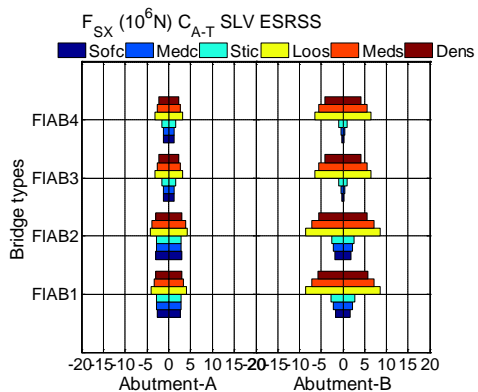
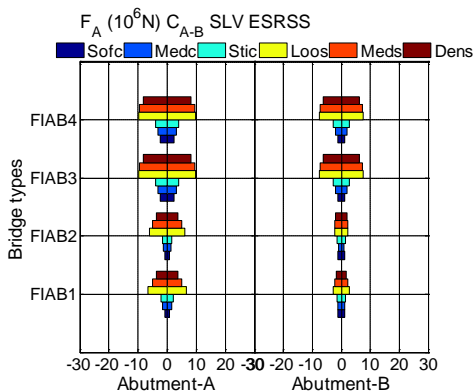
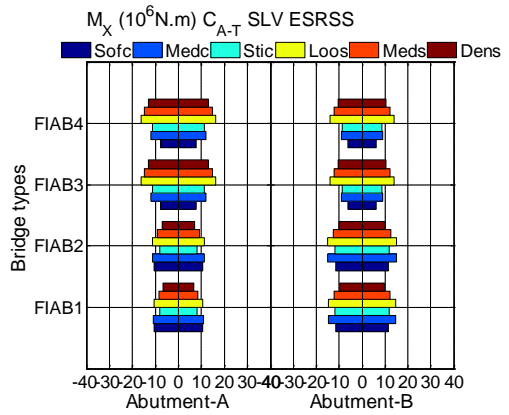
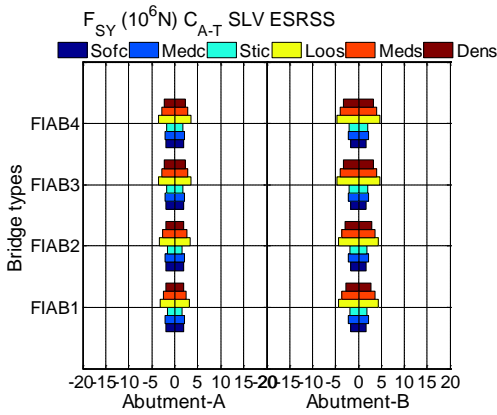


Fig. 271 Influence of different soil conditions on the ultimate F_A of piers under seismic load (SLV ESRSS)



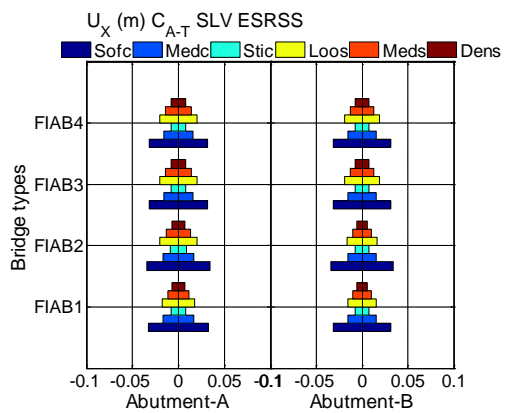
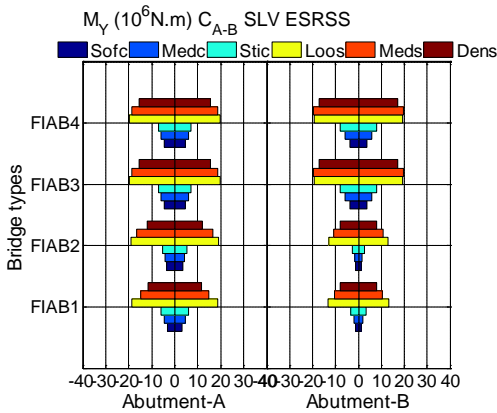
(a) F_A of abutment stems

(b) F_{Sx} of abutment stems



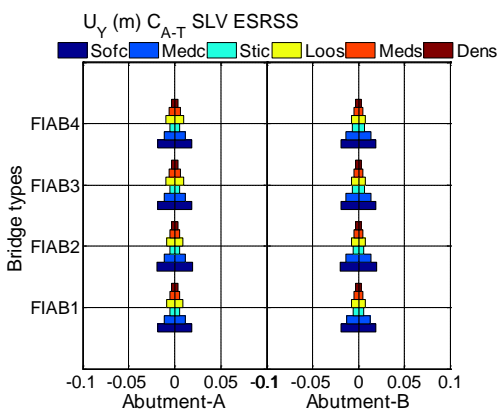
(c) F_{SY} of abutment stems

(d) M_X of abutment stems



(e) M_Y of abutment stems

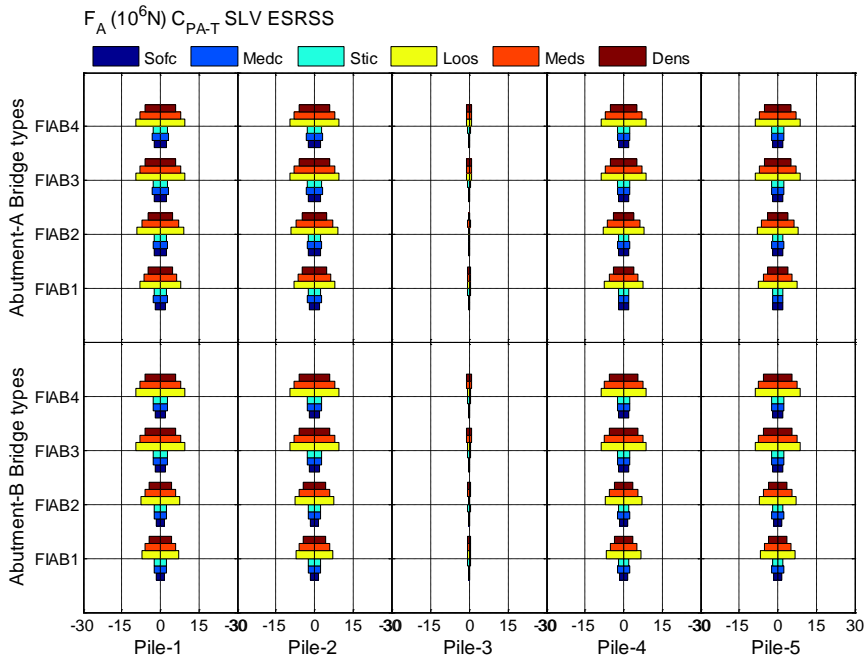
(f) U_X of abutment stems



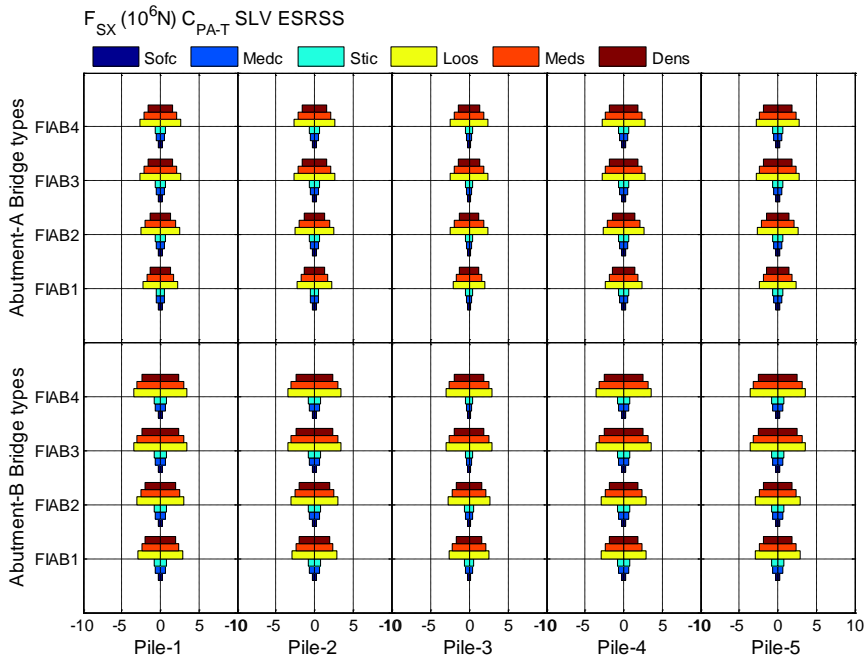
(g) U_Y of abutment stems

Fig. 272 Influence of different soil conditions on the ultimate internal forces of abutment stems under seismic load (SLV ESRSS)

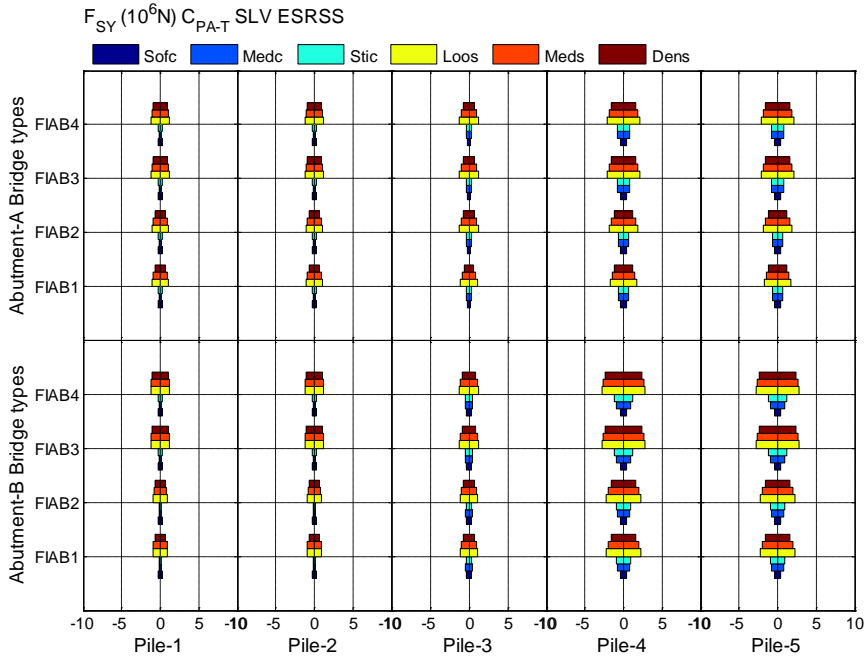
RETROFIT OF EXISTING BRIDGES WITH CONCEPT OF INTEGRAL ABUTMENT BRIDGE



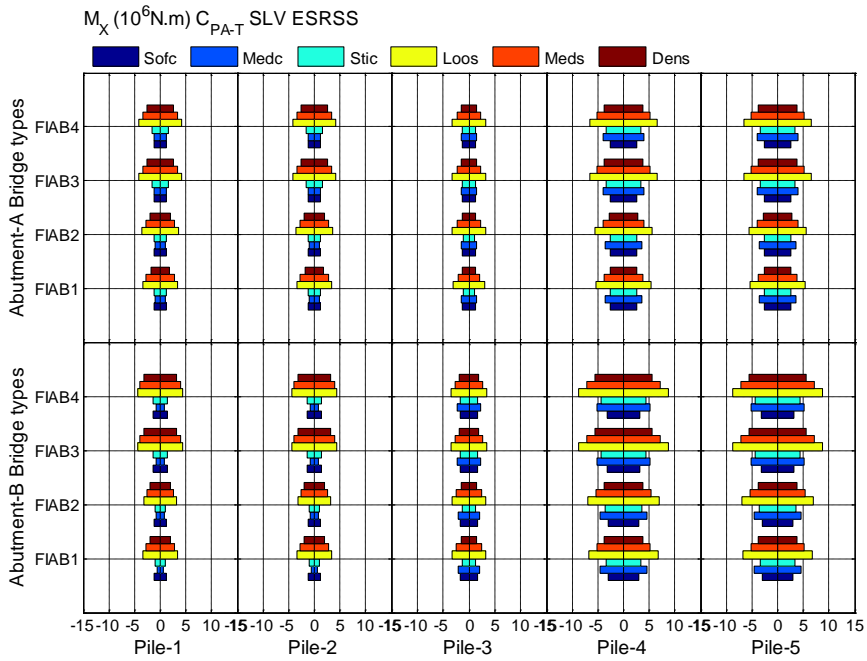
(a) F_A of piles beneath abutments



(b) F_{SX} of piles beneath abutments

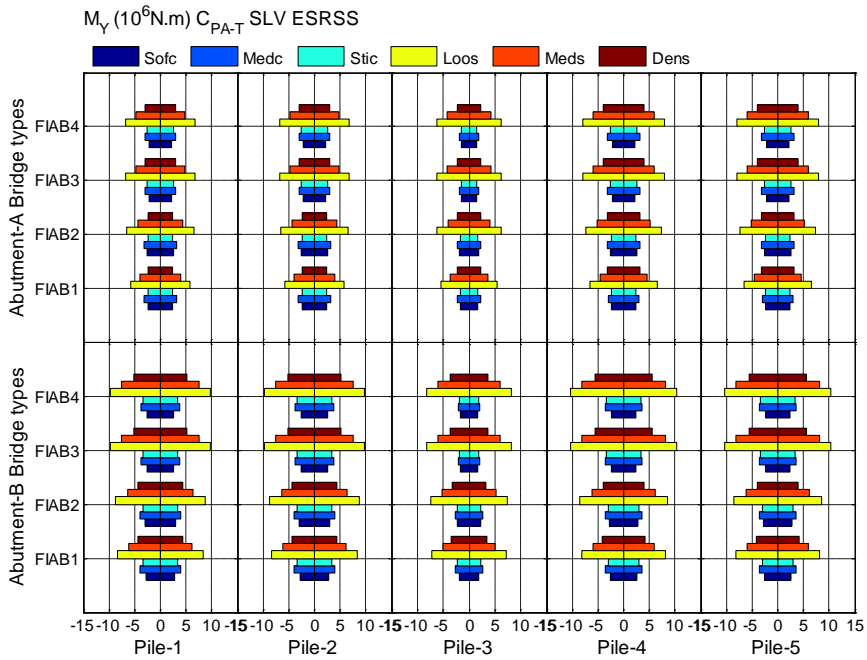


(c) F_{SY} of piles beneath abutments

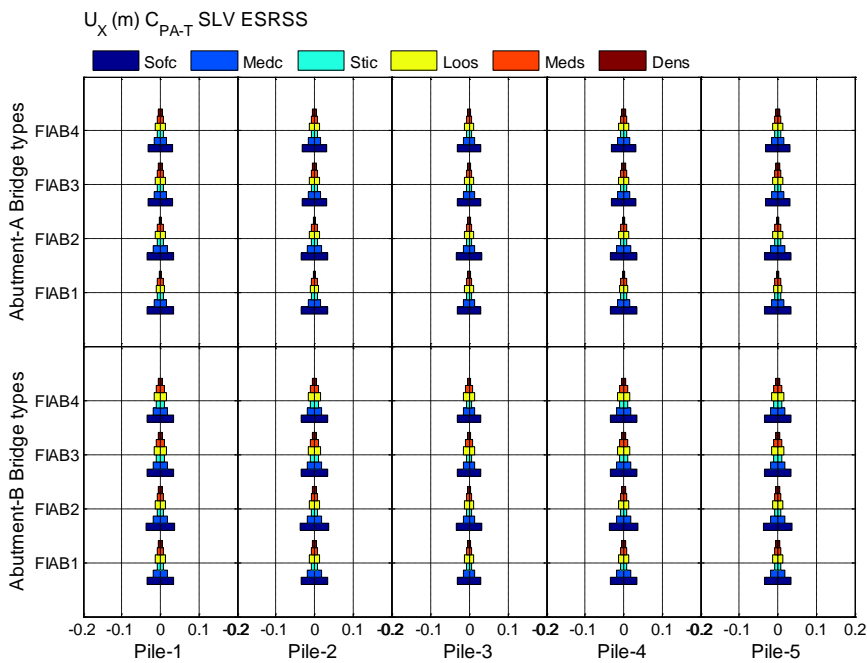


(d) M_X of piles beneath abutments

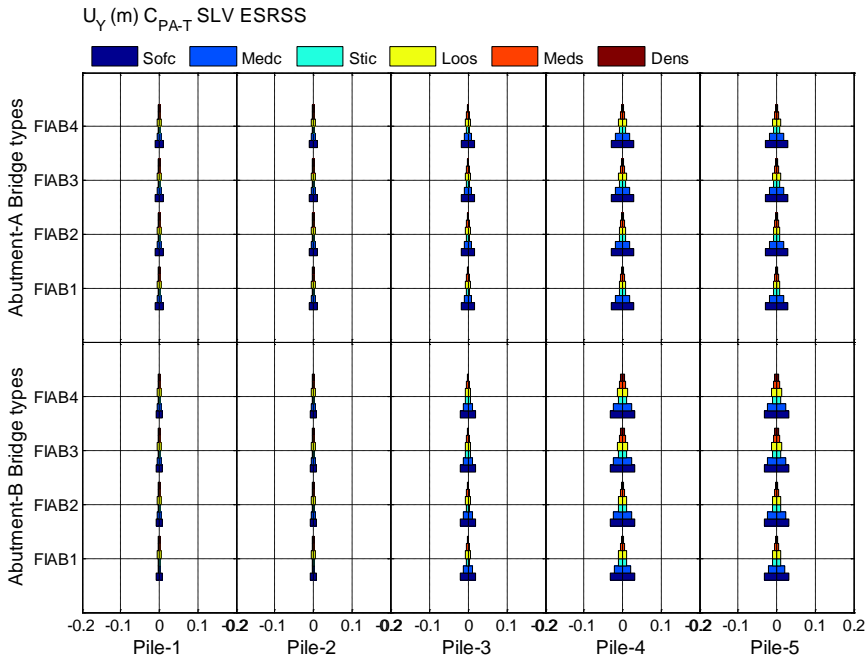
RETROFIT OF EXISTING BRIDGES WITH CONCEPT OF INTEGRAL ABUTMENT BRIDGE



(e) M_Y of piles beneath abutments



(f) U_X of piles beneath abutments



(g) U_y of piles beneath abutments

Fig. 273 Influence of different soil conditions on the ultimate internal forces of piles beneath abutments under seismic load (SLV ESRSS)

The influence of different soil conditions on the performance of different bridge components in FIABs are taken into account, as listed in Table 57. In conclusion, the loose sand can be considered as the most unfavorable soil condition, which could produce the maximum forces and bending moments of different bridge components in FIABs under response spectrum. Moreover, the displacements of FIABs under seismic load should be restricted, such as 0.06m (Karantzikis & Spyarakos, 2000) or 0.043m due to the durability limitation of the approach slab proposed in Swiss code (Dreier et al., 2011). In this case, the soft clay should be paid attention to. The stiff clay, medium sand and dense sand can be considered as the suitable soil conditions if the displacement of bridge after retrofitting is limited.

Component	Internal force	Different soil conditions
Girder	F_A	Sofc≈Medc>>Loos>Stic≈Meds>Dens
	F_{SZ}	Medc≈Loos>Sofc≈Stic≈Meds>Dens
	F_{SY}	Loos>Medc≈Stic≈Meds≈Dens>Sofc
	M_Z	Loos>Medc≈Meds>Stic≈Dens>Sofc
Pier	F_A	Dens≈Meds>Loos>Stic>Medc>Sofc
Abutment	F_A	Loos>Meds>Dens>Stic>Medc>Sofc

RETROFIT OF EXISTING BRIDGES WITH CONCEPT OF INTEGRAL ABUTMENT BRIDGE

stem	F_{SX}	Loos>Meds>Dens>Stic≈Medc≈Sofc
	F_{SY}	Loos>Meds>Dens>Stic≈Medc≈Sofc
	M_X	FIAB1&2: Medc≈Loos>Stic≈Meds≈Sofc>Dens FIAB3&4: Loos>Meds>Dens>Stic≈Medc>Sofc
	M_Y	Loos>Meds>Dens>Stic>Medc>Sofc
	U_X	Sofc>Medc≈Loos>Meds>Stic≈Dens
	U_Y	Sofc>Medc≈Loos>Meds>Stic≈Dens
Pile beneath abutment	F_A	Loos>Meds>Dens>Stic>Medc>Sofc
	F_{SX}	Loos>Meds>Dens>Stic≈Medc≈Sofc
	F_{SY}	Loos>Meds>Dens>Stic≈Medc≈Sofc
	M_X	Loos>Meds>Dens≈Medc>Stic≈Sofc
	M_Y	Loos>Meds>Dens>Medc>Stic≈Sofc
	U_X	Sofc>Medc≈Loos>Meds>Stic≈Dens
	U_Y	Sofc>Medc>Stic≈Loos≈Meds>Dens

Table 57

Adverse influence of different soil conditions on the performance of different bridge components under seismic load (the symbol “≈”, “>” and “>>” denote that the difference between two integral abutment bridge types can be neglected; is enough to pay attention to; and is quite significant, respectively).

CONCLUSIONS

The research investigates the performance of existing SSBs retrofitted with the IAB concept, in order to eliminate expansion joints and bearings and resolve the durability problems fundamentally. The literature survey on the practical applications of this approach in worldwide was carried out firstly, including retrofitting motivations, detailed processes and structural performance after retrofitting. Besides, another literature review on the critical issues of analysis on the IAB, such as soil-structure interactions, modelling approaches and plastic hinge simulations, was conducted in order to find out the most suitable method in modelling. Based on the retrofitting techniques proposed by engineers in worldwide, the detailed techniques of the retrofitting approach with the FIAB concept used in this paper were proposed. Four different subtypes of FIABs could be obtained through different retrofitting techniques on the superstructure-pier connection and the superstructure-abutment connection, including the hinged connection and the rigid connection. A simply supported prestressed concrete bridge 'Viadotto Serrone' was chosen as case study. The finite element model, which can consider soil-structure interactions, non-linear behaviors and retrofitting processes, was built. The comparison between the original and updated Italian codes was carried out. Another investigation was conducted to prove the necessity of considering soil-structure interactions in the IAB. Based on the appropriate finite element model, a large number of static sensitive analyses were carried out, considering different thermal actions, different bridge types, different soil conditions and different substructure heights. Then, the verification was conducted in order to check if the existing sections could be reused after retrofitting without any improvements and to point out the critical components, which need to be repaired or modified. Moreover, a preliminary research on the seismic performance of the bridge after retrofitting with the IAB concept was carried out through modal analysis and response spectrum analysis.

Main findings

Based on the literature reviews and parametric analyses, the main findings achieved section by section are drawn as following:

Chapter 1

RETROFIT OF EXISTING BRIDGES WITH CONCEPT OF INTEGRAL ABUTMENT BRIDGE

- Many SSBs have still been used all over the world. Nowadays, the majority of them are affected by some durability problems, such as damaged expansion joints and bearings, and so on.
- Many researchers try to propose some retrofitting methods to resolve the durability problems of expansion joints and bearings fundamentally by eliminating expansion joints and bearings.
- Arise in United States, the IAB have been widely applied in worldwide. They perform well with better structural performance, fewer maintenance problems and more economical construction than conventional bridges.
- Two subtypes of SIABs and four subtypes of FIABs are defined based on different flexibilities of superstructure-substructure connections, including the hinged connection and the rigid connection.

Chapter 2

- The IAB concept has been used in some retrofitting projects all over the world, including North America, Europe and Asia. However, the number is not so large.
- The construction of the girder-pier connections or the girder-abutment connections is of most importance. Some retrofitting techniques proposed by different engineers are introduced. The performance of IABs after retrofitting is summarized.

Chapter 3

- Many theoretical and empirical lateral earth pressure-abutment movement relationships can be used to simulate the soil-abutment interaction in the IAB. By comparison, the relationship proposed in the 'Manuals for the Design of Bridge Foundations' (so-called as NCHRP method) can be considered as the most commonly used in the design and analysis of IABs.
- For the pile embedded in soil, many theoretical and empirical earth pressure-pile displacement relationships can be used to simulate the soil-pile interaction. By comparison, the design method recommended by

the American Petroleum Institute (so-called as API method), concluding the studies on p - y curves, can be considered as most widely approach used in sophisticated nonlinear soil modelling in IABs.

- Different from the SSB, both superstructure and substructure of the bridge, and even the surrounding soil should be considered when modeling the IAB. Based on a typical three-span IAB, the common used modeling approaches are summarized, including the simplified model and the refined finite element model. The 3D finite element model with the soil-spring method is adopted in this analysis, which can provide more realistic representation of the performance of IABs
- Similar to the SSB, the concentrated plastic hinge should be assigned to the top and bottom of pier columns. Moreover, the distributed plastic hinge zone along the upper part of piles should be considered in the IAB. The definition of the distributed plastic hinge zone responds to different soil types.

Chapter 4

- Based on the summary of the retrofitting techniques used in worldwide, the detailed techniques of the retrofitting approach with the FIAB concept used in this paper are proposed. Using the FIAB concept can resolve the potential durability problems of existing bearings and make the construction of retrofitting process easier than using the SIAB concept can achieve. Using this retrofitting method, the retrofitting cost can be reduced and the retrofitting period can be shortened, because most part of existing bridges can be reused.
- Four different subtypes of FIABs can be obtained through different retrofitting techniques on the superstructure-pier connection and the superstructure-abutment connection, including the hinged connection and the rigid connection.

Chapter 5

- The 3D finite element model with frame elements and plate elements, which can simulate soil-structure interaction by nonlinear area and line spring elements, calculate the performance of the bridge before and after

retrofitting and consider the nonlinear behaviors of bridge by assigning plastic hinges, is built by Sap2000. Another finite element program Midas can verify the validity of this finite element model.

- The original and updated Italian design codes are compared through static analysis and seismic analysis. The definitions of the dead load, superimposed dead load, prestressing load and thermal load in both codes are the same; however, the definitions of the highway live load and the static loads combination in both codes are different. The comparison results indicate that the performance of the SSB under static loads combination in NTC 2008 is slightly smaller than that in DM 1990, which is less than 10%; however, the performance of the SSB under highway live load in NTC 2008 is larger than that in DM 1990, which is 20~30%.
- For the seismic load, the response spectrum stipulated in DM 1996 is completely different to that in NTC 2008. The results of seismic analysis indicate that the performance of the SSB under response spectrum in NTC 2008 is significantly larger than that in DM 1996, which is 70~80%.
- The retrofitting procedure simulation is very important in the analysis of the IAB, because the dead load, prestressed load and superimposed dead load are applied to the simply supported static scheme, and the highway live load, thermal load and seismic load are applied to the IAB after retrofitting. The retrofitting procedure can be simulated by using the nonlinear staged construction analysis type implemented in Sap2000.
- The differences between considering the soil-structure interaction as the soil property on site or as the rigid connection are analyzed. For the SSB, the difference is quite small; however, in order to obtain the actual performance of the IAB, the simulation of the soil-structure interaction by using the soil property on site must be carried out.

Chapter 6

- Based on the appropriate finite element model, a static sensitive analysis considering different bridge types, including the SSB and four subtypes of FIABs, was carried out. When considering the thermal load, the performance of four subtypes of FIABs is larger than that in SSB. When

considering the highway live load, the retrofitting with the IAB concept can reduce the positive bending moments and the vertical deflections of girders at the mid-span points of each span; however, it can increase the negative values at the both girder-end points of each span, which are unfavorable. The retrofitting approaches of FIAB2 and FIAB4 can amplify the bending moments at the top points of piers, comparing with those in SSB. However, the bending moments in FIAB1 and FIAB3 are less than or equal to those in SSB. The bending moments of abutment stems in four subtypes of FIABs are larger than or equal to those in SSB.

- By comparing different subtypes of FIABs, it could be observed that FIAB3 or FIAB4 can be considered as the suitable retrofitting solutions if the retrofit of girders in existing bridges are difficult. FIAB1 and FIAB3 can be considered as the best retrofitting solutions, which can bring minimum unfavorable influence on the piers. If the shear resistance of existing abutment stems is not enough, FIAB3 or FIAB4 can be considered as the suitable retrofitting solutions. Moreover, if the bending resistance of existing abutment stems is not enough, FIAB1 or FIAB2 can be considered as the suitable retrofitting solutions.
- In this case, the geometric dimensions and material properties of piles beneath the abutments and piers are the same. Under thermal load, the analysis of piles beneath piers can be neglected, because its performance is nearly one tenth of the performance of piles beneath abutments.
- Another parametric analysis, which investigates the influence of different soil conditions, is conducted. It could be observed that the effects of different soil conditions on the performance of bridges under highway live load are nearly the same. However, the effects of different soil conditions on the performance of bridges under thermal load are significant. In general, under thermal load, with the soil condition changing from soft to dense, the forces and bending moments of different bridge components and the vertical deflections of girders increase; however, the horizontal displacements decrease.
- The influence of different substructure heights on the performance of different subtypes of FIABs under thermal load is analyzed, because of the asymmetric substructure heights in case study. It could be found that the

performance of different bridge components in the case with different substructure heights can be predicted by the corresponding idealized cases with equal substructure heights. Moreover, when the soil condition is soft clay, the special arrangement of substructure heights should be paid more attention to. It is because the lateral resistance force produced by the soil is small and the influence of asymmetric substructure heights is amplified.

- When the substructure heights are symmetric, the performance of the corresponding bridge components located at the left part and right part of the bridge should be equal under thermal load. If the heights of two piers are different, the performance of piers is different. Moreover, if the heights of two abutments are different, the performance of girders, abutment stems and piles beneath abutments is different.

Chapter 7

- Using the F_A -M domain of existing cross sections, the static performance check of different bridge components after retrofitting can be conducted. It could be observed that, if the existing bridge is located in the countries, which consider the thermal load as $\pm 15^\circ\text{C}$, only the abutment stems need to be retrofitted during transformation. However, if the existing bridge is located in the countries, which have severe temperature variations as $\pm 40^\circ\text{C}$, not only the abutment stems, but also some other bridge components need the retrofitting work. For example, the Girder-EM1 in FIAB1 and FIAB2 and the upper part of piers in FIAB2 when the soil condition is sand or stiff clay, and the top parts of piles (Pile-1, Pile-2, Pile-4 and Pile-5) beneath Abutment-B in FIAB3 and FIAB4 when the soil condition is sand should be paid attention to. Engineers can use these results to choose the suitable retrofitting solution for different cases.
- The most critical factor of the retrofitting technique with the IAB concept is to improve the bending moment resistance capacity of abutment stems. It is because that, the bending moment resistance capacity is always designed as a quite small value in the SSB, due to the expansion joints and bearings.
- Generally, there is no approach slab in existing SSB, because the horizontal displacement can be released through expansion joints. The modeling of the approach slab in the finite element model can be neglected; however, the

horizontal displacement transferring from bridge ends to approach slabs should be considered as a critical factor. The approach slab can be constructed during the transforming process. Therefore, only the horizontal displacement under highway live load and thermal load should be taken into account.

- In this case, no matter which soil condition is considered, the horizontal displacements at bridge ends corresponding to the ultimate limit state in four subtypes of FIABs are less than 43mm. It means that the problem of the connections between bridge ends and road pavements can be resolved by using the approach slab with the recommended geometric dimension in Swiss code and the improved connection detail, which can avoid special considerations to ensure the approach slab will be durable and performs satisfactorily at the serviceability limit state.

Chapter 8

- From the results of the modal analysis, it could be observed that the retrofitting with the FIAB concept can reduce the vibration period corresponding to the main transverse translation model shape (T_H) to about 85% and the vibration period corresponding to the main longitudinal translation model shape (T_L) to less than 50%.
- Comparing different subtypes of FIABs, it could be observed that the T_H in FIAB1 and FIAB2 are nearly the same, which are a little larger than those in FIAB3 and FIAB4. Furthermore, different subtypes of FIABs have noticeable effects on the T_L . In generally, it could be found that the T_L in FIAB1 and FIAB4 could be considered respectively as the maximum and minimum values.
- The effects of different soil conditions on the vibration periods are summarized. By comparison, it could be found that in all bridge types, when the soil properties changing from dense sand to loose sand or from stiff clay to soft clay, the vibration periods increase. Moreover, the vibration period increment among three types of clay is significantly larger than that among three types of sand. When the soil condition is sand, the T_H are smaller than those considering the soil condition as clay. However, when the soil condition is stiff clay, the T_L in four subtypes of FIABs are smaller than those

considering the soil condition as medium sand and loose sand.

- The influence of different substructure heights on the vibration period is investigated. It could be found that the influence of pier height variations on the T_H in all bridge types and the T_L in SSB is significantly larger than the effects of abutment height variations. Moreover, the influence of substructure heights on the T_L in four subtypes of FIABs is quite small.
- When the pier height is 7.7m, the T_H in FIABs are similar to or slightly smaller than those in SSB; however, the influence of the retrofitting process on the T_L is large. When the pier height is 25.7m, the T_H and T_L in FIABs are significantly smaller than those in SSB. Especially, the T_L in FIABs can be reduced to 25~30% of the T_L in SSB. Moreover, when the pier height is 25.7m, the mode 1 in SSB can change from transverse translation mode shape to longitudinal translation mode shape; however, in FIABs, the mode 1 is the main transverse translation mode shape and the mode 4 is the main longitudinal translation mode shape.
- Through response spectrum analysis, it could be found some internal forces of different bridge components in the SSB are smaller than those in FIABs, which should be paid more attention to. In this case, the investigation on the differences among different types of FIABs is quite useful. In conclusion, it could be found that FIAB1 or FIAB2 can be considered as the more suitable retrofitting solutions than FIAB3 and FIAB4 from the seismic point of view.
- Some internal forces of different bridge components in the SSB are larger than those in FIABs under seismic load, such as the M_Y , U_X and U_Y of girder, all internal forces of pier except the F_A and all internal forces of pile beneath piers. It means that, if the existing bridge was designed according to the appropriate seismic load, the resistance capacities of existing sections should be enough to bear the internal forces in any new bridge types after retrofitting, then, these existing sections can be reused after retrofitting without any improvements.
- Different to the static analysis results, the mechanical properties of piles beneath piers under seismic load is quite large, which cannot be neglected.
- The influence of different soil conditions on the seismic performance of

different subtypes of FIABs is studied. The results indicate that the loose sand can be considered as the most unfavorable soil condition, which can produce the maximum forces and bending moments of different bridge components in FIABs under response spectrum. Moreover, when the displacement of FIABs under seismic load is restricted, the soft clay should be paid attention to. The stiff clay, medium sand and dense sand can be considered as the suitable soil conditions when the displacement of bridges after retrofitting is limited.

Conclusions

Based on the findings achieved section by section, the main conclusions are listed as following:

- Due to the advantages in terms of life-cycle costs, durability, enhanced structural response and ease of maintenance, the IAB's concept can be fruitfully applied in the retrofitting process of existing simply supported bridge.
- From the knowledge and experience of the Author and from the Case Study, it is proved that the introduction of updated Code causes an increase in the forces acting on the bridge superstructure and foundations in both static and seismic points of view.
- The decreased degrees of freedom in the transformed Integral Bridges after retrofitting usually implies a more favorable distribution of internal forces with a consequent overall increase of the safety factor both for vertical and seismic loads.
- The simulation of the soil-structure interaction using the real soil property on site is quite important to achieve the real performance of integral abutment bridge. When the soil conditions are those characteristic of sand and stiff clay, the static performance of bridge after retrofitting should be checked, being this a potentially challenging situation for this type of retrofitting. Moreover, when the soil condition is loose sand, great attention should be paid to the critical case of seismic loads.
- The performance of the approach slab with reference to the ultimate

RETROFIT OF EXISTING BRIDGES WITH CONCEPT OF INTEGRAL ABUTMENT BRIDGE

displacement of the bridge has proved to be a critical and challenging issue in the long-term behavior of any Integral Bridges and cause of flaws in the expected enhanced overall structural response.

Recommendations for future investigations

The present study preliminarily introduces the static and dynamic performance of existing bridges retrofitted with the FIAB concept through parametric analyses. In order to properly retrofit existing bridges, there are still many factors and uncertainties in structural and non-structural considerations for analysis and design.

A more comprehensive investigation on the soil properties and the corresponding soil-structure interactions should be developed. The experimental investigation on the static and dynamic soil-structure interactions should be established.

The seismic behaviors of the FIAB after retrofitting could be investigated deeply, through pushover analysis and nonlinear time history analysis.

Further investigations through a detailed finite element analysis of the girder-pier connection or the girder-abutment connection, should be conducted to consider accurately the connection flexibility. The detailed configuration between the superstructure and the substructure, such as different embedment lengths and girder widths, should be developed.

Research is also recommended to evaluate the static and dynamic performance of existing bridges retrofitted with the SIAB concept.

REFERENCES

Abendroth, R.E. and Greimann, L.F., (1989), *Abutment pile design for jointless bridges*, Journal of Structural Engineering, 115, 11, 2914-2929

Abendroth, R.E. and Greimann, L.F. (2005). *Field testing of integral abutments*. 2901 South Loop Drive, Suite 3100, Ames, IA 50010-8634, Center for Transportation Research and Education, Iowa State University

Akiyama, H., (2008), *Fundamentally Structural Characteristics of Integral Bridges*, Doctor, Kanazawa University

Aktan, H., Attanayake, U. and Ulku, E. (2008). *Combining Link Slab, Deck Sliding over Backwall, and Revising Bearings*. Kalamazoo, MI, Western Michigan University

Alampalli, S. and Yannotti, A.P., (1998), *In-service performance of integral bridges and jointless decks*, Transportation Research Record: Journal of the Transportation Research Board, 1624, 1-7

Alberta Ministry of Transportation, (2012), *Alberta transportation bridge structures design criteria v. 7.0 Appendix A: integral abutment design guidelines*, Alberta, Canada, Alberta Government,

Alemdar, Z.F., (2010), *Plastic hinging behavior of reinforced concrete bridge columns*, Doctor, University of Kansas

Allemang, R.J., (2003), *The modal assurance criterion—twenty years of use and abuse*, Sound and Vibration, 37, 8, 14-23

American Association of State Highway and Transportation Officials, A., (2007), *AASHTO LRFD Bridge Design Specifications (SI Units 4th Edition)* American Association of State Highway and Transportation Officials, 444 North Capitol Street, N.W., Suite 249. Washington, D.C. 20001

American Petroleum Institute, (2000), *Recommended Practice for Planning, Designing and Constructing Fixed Offshore Platforms—Working Stress Design*, API RECOMMENDED PRACTICE 2A-WSD (RP 2A-WSD) TWENTY-FIRST EDITION, 1220 L Street, Northwest Washington, D.C. 20005-4070, American Petroleum Institute,

American Society of Civil Engineers, (2007), *Seismic rehabilitation of existing buildings*, ASCE/SEI standard 41-06, Reston, Virginia, USA, American Society of Civil Engineers,

Anagnostopoulos, S.A., (1981), *Inelastic Beams for Seismic Analyses of Structures*,

RETROFIT OF EXISTING BRIDGES WITH CONCEPT OF INTEGRAL ABUTMENT BRIDGE

Journal of the Structural Division, 107, 7, 1297-1311

Applied Technology Council, (1996), *ATC-40, Seismic evaluation and retrofit of concrete buildings*, Redwood City, California, ATC 40

Arockiasamy, M., Butrieng, N. and Sivakumar, M., (2004), *State-of-the-art of integral abutment bridges: design and practice*, Journal of Bridge Engineering, 9, 5, 497-506

Arsoy, S., (2000), *Experimental and analytical investigations of piles and abutments of integral bridges*, Doctor, Virginia Polytechnic Institute and State University

Arsoy, S., (2004), *Mobilization of passive earth pressures behind abutments of jointless bridges*, Transportation Research Record: Journal of the Transportation Research Board, 1868, 199-204

Arsoy, S., Barker, R.M. and Duncan, J.M. (1999). *The behavior of integral abutment bridges*, Virginia. Dept. of Transportation, Virginia Transportation Research Council, Virginia Polytechnic Institute, State University. Charles E. Via Dept. of Environmental Engineering

Arsoy, S., Barker, R.M. and Duncan, J.M. (2002). *Experimental and analytical investigations of piles and abutments of integral bridges*. Charlottesville, Virginia, Department of Civil and Environmental Engineering, Virginia Polytechnic Institute and State University

Ashour, M. and Norris, G., (2000), *Modeling lateral soil-pile response based on soil-pile interaction*, Journal of geotechnical and geoenvironmental engineering, 126, 5, 420-428

Aubry, D., Hujeux, J.C., Lassoudiere, F. and Meimon, Y., (1982), *A double memory model with multiple mechanisms for cyclic soil behaviour*, Proceedings of the Int. Symp. Num. Mod. Geomech, Zürich, Switzerland, 3-13

Baguelin, F., Jezequel, J.F. and Shields, D.H., (1978), *The pressuremeter and foundation engineering*. Trans. Tech. Publications, Aedermannsdorf

Bakare, T. Tajudeen Bakare, P.E.'s Projects. from <http://www.linkedin.com/pub/tajudeen-bakare-p-e/a/873/314>

Bakeer, R.M., Mattei, N.J., Almalik, B.K., Carr, S.P. and Homes, D. (2005). *Evaluation of DOTD Semi-Integral Bridge and Abutment System*, Louisiana Department of Transportation and Development, Louisiana Transportation Research Center

Barker, J.M., Duncan, J.M., Rojiani, K.B., Ooi, P.S.K., Tan, C.K. and Kim, S.G. (1991). *Manuals for the Design of Bridge Foundations: Shallow Foundations, Driven Piles, Retaining Walls and Abutments, Drilled Shafts, Estimating Tolerable Movements, and Load Factor Design Specifications and Commentary*. Barker, R. M., Duncan, J., Rojiani, K., Ooi, P., Tan, C. and Kim, S. Washington D.C., Transportation

Research Board

Barker, R.M., Duncan, J.M., Kim, S.G. and Rojiani, K.B. (1990). *Application of LRFD to design of an integral abutment*. Third International Conference on Short and Medium Span Bridges. Toronto, Canada

Bell, A.L., (1915), *The lateral pressure and resistance of clay and the supporting power of clay foundations*, Ice Virtual Library, 233-272

Biondini, F., Camnasio, E. and Palermo, A. (2010). *Lifetime seismic performance of concrete bridges*. Bridge Maintenance, Safety, Management and Life-Cycle Optimization. Frangopol, D. M., Sause, R. and Kusko, C. S. Philadelphia, Pennsylvania, USA, International Association for Bridge Maintenance and Safety

Biskinis, D. and Fardis, M.N., (2009), *Deformations of concrete members at yielding and ultimate under monotonic or cyclic loading (including repaired and retrofitted members)*,

Bonczar, C., Breña, S.F., Civjan, S., DeJong, J., Crellin, B. and Crovo, D. (2005a). *Field Data and FEM Modeling of the Orange-Wendell Bridge*. Proceedings of the 2005 FHWA Conference: Integral abutment and jointless bridges. Baltimore Maryland, United States, Constructed Facilities Center, College of Engineering and Mineral Resources, West Virginia University

Bonczar, C., Brena, S.F., Civjan, S.A., DeJong, J. and Crovo, D. (2005b). *Integral Abutment Pile Behavior and Design - Field Data and FEM Studies*. Proceedings of the 2005 FHWA Conference: Integral abutment and jointless bridges. Baltimore, Maryland, Constructed Facilities Center, College of Engineering and Mineral Resources, West Virginia University: 174-184

Braun, A., Seidl, G. and Weizenegger, M. (2006a). *Frame structures in bridge construction Design, analysis and economic considerations*. International Workshop on the Bridges with Integral Abutments. Collin, P., Veljkovic, M. and Pétursson, H. Luleå, Sweden, Luleå University of Technology: 25-35

Braun, A., Seidl, G. and Weizenegger, M., (2006b), *Rahmentragwerke im Brückenbau. Konstruktion, Berechnung und volkswirtschaftliche Betrachtung*, Beton - und Stahlbetonbau, 101, 3, 187-197

Brettmann, T. and Duncan, J.M., (1996), *Computer application of CLM lateral load analysis to piles and drilled shafts*, Journal of geotechnical engineering, 122, 6, 496-498

Briaud, J.L., (1997), *Sallop: simple approach for lateral loads on piles*, Journal of geotechnical and geoenvironmental engineering, 123, 10, 958-964

Briaud, J.L., Smith, T.D. and Tucker, L.M. (1985). *A pressuremeter method for laterally loaded piles*. 11th International conference on Soil Mechanics and Foundation Engineering. Rotterdam, The Netherlands: 1353-1356

RETROFIT OF EXISTING BRIDGES WITH CONCEPT OF INTEGRAL ABUTMENT BRIDGE

Briseghella, B., Lan, C. and Zordan, T. (2010). *Optimized Design for Soil-Pile Interaction and Abutment Size of Integral Abutment Bridges*. 34th International Symposium on Bridge and Structural Engineering. Venice, Italy, International Association for Bridge and Structural Engineering

Briseghella, B., Siviero, E. and Zordan, T., (2004), *A Composite Integral Bridge in Trento, Italy: Design and Analysis*, IABSE Symposium 'Metropolitan Habitats and Infrastructure', Shanghai, China, International Association for Bridge and Structural Engineering, 297-302

Briseghella, B. and Zordan, T., (2004), *Adjustable Deck Solutions for "Veneto Strade" Flyovers*, IABSE Symposium 'Metropolitan Habitats and Infrastructure', Shanghai, China, International Association for Bridge and Structural Engineering, 307-312

Briseghella, B. and Zordan, T., (2006), *Integral abutment bridge concept applied to the rehabilitation of a simply supported prestressed conventional concrete superstructure*, Structural Concrete, Thomas Telford and fib, Salisbury, UK., 8, 1, 25-33

Briseghella, B., Zordan, T., Lan, C. and Xue, J. (2012). *Superlong Integral Abutment Bridge*. 20th China national bridge conference. Wuhan, China,(in Chinese).

Broms, B.B., (1964), *Lateral resistance of piles in cohesionless soils*, Journal of the soil mechanics and foundation division, 90, SM2, 27-63

Broms, B.B., (1965), *Design of laterally loaded piles*, Journal of the soil mechanics and foundation division,

Broms, B.B. and Ingelson, I., (1971), *Earth pressure against the abutments of a rigid frame bridge*, Geotechnique, 21, 1, 15-28

Bros, B., (1972), *The Influence of Model Retaining Wall Displacement on Active and Passive Earth Pressures in Sand*, Fifth Eur Conf On Soil Proc/Sp/, 241-249

Burdette, E.G., Howard, S.C., Ingram, E.E., Deatherage, J.H. and Goodpasture, D.W., (2005), *Behavior of Pile Supported Integral Abutments*, Integral Abutment and Jointless Bridges (IAJB 2005),

Burke, M.P., (1990), *Integral bridges*, Transportation research record, 1275, 53-61

Burke, M.P., (1993a), *Design of integral concrete bridges*, Concrete International, 15, 6, 37-42

Burke, M.P. (1993b). *Integral bridges: attributes and limitations*. Transportation research record 1393. 500 Fifth Street, NW. Washington, DC 20001 USA, Transportation Research Board: 1-8

Burke, M.P., (2009), *Integral and Semi-Integral Bridges*. Wiley-Blackwell, Oxford, UK

- Caicedo, J.M., Wieger, G., Ziehl, P. and Rizos, D. (2011). *Simplifying bridge expansion joint design and maintenance*. Columbia, South Carolina, Department of Civil and Environmental Engineering, University of South Carolina
- Caltrans, (2010), *Seismic Design Criteria*, 1120 N Street, Sacramento, California, California Department of Transportation, V1.6
- Canadian Geotechnical Society, (1978), *Canadian foundation engineering manual Part4 Excavations and Retaining Structures*. Canadian Geotechnical Society. Foundations Committee
- Canadian Geotechnical Society, (2006), *Canadian Foundation Engineering Manual 4th Edition*,
- Caquot, A. and Kerisel, J., (1948), *Tables for the calculation of passive pressure, active pressure and bearing capacity of foundations*. Gautier-Villars, Paris
- Card, G.B. and Carder, D.R. (1993). *A literature review of the geotechnical aspects of the design of integral bridge abutments*. TRL PROJECT REPORT. Crowthorne, England, Transport Research Laboratory
- Carvajal, J.C., (2011), *Seismic Embankment-Abutment-Structure Interaction of the Integral Abutment Bridges*, PhD, The University of British Columbia
- Chai, Y.H., (2002), *Flexural Strength and Ductility of Extended Pile-Shafts - I: Analytical Model*, Journal of Structural Engineering, 128, 5, 586-594
- Chang, B.K.F., (2003), *Simplified procedure for analysis of laterally loaded single piles and pile groups*, Master, University of Hawaii at Manoa
- Chen, Y., (1997), *Important Considerations, Guidelines, and Practical Details of Integral Bridges*, Journal of Engineering Technology, 14, 16-19
- Chiou, J.S., Yang, H.H. and Chen, C.H. (2008). *Plastic hinge setting for nonlinear pushover analysis of pile foundations*. The 14th World Conference on Earthquake Engineering. Beijing, China
- Chiou, J.S., Yang, H.H. and Chen, C.H., (2009), *Use of plastic hinge model in nonlinear pushover analysis of a pile*, Journal of geotechnical and geoenvironmental engineering, 135, 9, 1341-1346
- Civjan, S.A., Bonczar, C., Brena, S.F., DeJong, J. and Crovo, D., (2007), *Integral abutment bridge behavior: Parametric analysis of a Massachusetts bridge*, Journal of Bridge Engineering, 12, 1, 64-71
- Clough, G.W. and Duncan, J.M. (1991). *Earth pressures*. Foundation engineering handbook, 2nd edition. Fang, H. Y. New York, NY, Van Nostrand Reinhold
- Coduto, D.P., (2001), *Foundation Design: Principles and Practices*. Prentice Hall,

New Jersey

Cole, R.T. and Rollins, K.M., (2006), *Passive earth pressure mobilization during cyclic loading*, Journal of geotechnical and geoenvironmental engineering, 132, 9, 1154-1164

Collin, P., Veljkovic, M. and Pétursson, H. (2006). *International Workshop on the Bridges with Integral Abutments*. Luleå, Sweden, Luleå University of Technology

Computers and Structures Inc (2011). *CSI Analysis Reference Manual For SAP2000*. Berkeley, California, USA

Connal, J., (2004), *Integral Abutment Bridges—Australian and US Practice*, Austroads 5th Bridge Conference, Hobart, Australia, Seminar on Design & Construction of Integral Bridges. Kuala Lumpur,

Corradi, L. and Poggi, C., (1984), *A refined finite element model for the analysis of elastic-plastic frames*, International journal for numerical methods in engineering, 20, 12, 2155-2174

Coulomb, C.A., (1776), *Essai sur une application des règles de maximis & minimis à quelques problèmes de statique, relatifs à l'architecture*. De l'Imprimerie Royale

Coyle, H.M. and Reese, L.C., (1966), *Load transfer for axially loaded piles in clay*, Journal of Soil Mechanics & Foundations Division, 92, SM2, Proc Paper 4702, 1-26

Coyle, H.M. and Sulaiman, I.H., (1967), *Skin friction for steel piles in sand*, Journal of Soil Mechanics & Foundations Division, 92, SM6, 261-278

Cross, H., (1932), *Analysis of continuous frames by distributing fixed-end moments*, American Society of Civil Engineers Transactions, 96, 1, 1-10

Culmann, K., (1866), *Die Graphische Statik*. Verlag von Meyer & Zeller, Zurich

Danish Geotechnical Institute, (1978), *Code of Practice for Foundation Engineering*, Danish Geotechnical Institute, Bulletin No.32

Davisson, M.T. (1970). *Lateral load capacity of piles*, Highway Research Record

Davisson, M.T. and Gill, H.L., (1963), *Laterally loaded piles in a layered soil system*, Journal of the Soil Mechanics and Foundations Division, 89, 3, 63-94

Dehne, Y. and Hassiotis, H. (2003). *Seismic Analysis of Integral Abutment Bridge-Scotch Road I-95 Project*. 16th ASCE Engineering Mechanics Conference. University of Washington, Seattle

Deierlein, G.G., Reinhorn, A.M. and Willford, M.R., (2010), *Nonlinear structural analysis for seismic design*, NEHRP Seismic Design Technical Brief No, 4,

- Department of Transport, (2003), *The Design of Integral Bridges BA 42/96*, Design Manual for Roads and Bridges London, UK, Department of Transport,
- Desai, C. and Wu, T.H. (1976). *A general function for stress-strain curves*. 2nd International conference for Numerical Methods in Geomechanics. Blacksburg, ASCE: 306-318
- Desai, C.S. (1976). *Numerical methods in geomechanics*. New York, NY, American Society of Civil Engineers, ASCE
- Desai, C.S. and Christian, J.T., (1977), *Numerical Methods in Geotechnical Engineering*. McGraw-Hill Book Co., New York, N.Y.
- Dickson, B., Franco, J.M., GangaRao, H.V.S., Justice, J., Plymale, R.E., Thippeswamy, H. and Triandafilou, L.N. (1996). *Workshop on integral abutment bridges executive summary and minutes*. Pittsburgh, Pennsylvania
- Dicleli, M., (2000a), *A rational design approach for prestressed-concrete-girder integral bridges*, Engineering Structures, 22, 3, 230-245
- Dicleli, M., (2000b), *Simplified model for computer-aided analysis of integral bridges*, Journal of Bridge Engineering, 5, 3, 240-248
- Dicleli, M., (2005), *Integral abutment-backfill behavior on sand soil—Pushover analysis approach*, Journal of Bridge Engineering, 10, 3, 354-364
- Dicleli, M. and Albhaisi, S.M., (2003), *Maximum length of integral bridges supported on steel H-piles driven in sand*, Engineering Structures, 25, 12, 1491-1504
- Dicleli, M. and Albhaisi, S.M., (2004a), *Effect of cyclic thermal loading on the performance of steel H-piles in integral bridges with stub-abutments*, Journal of Constructional Steel Research, 60, 2, 161-182
- Dicleli, M. and Albhaisi, S.M., (2004b), *Estimation of length limits for integral bridges built on clay*, Journal of Bridge Engineering, 9, 6, 572-581
- Dicleli, M. and Albhaisi, S.M., (2004c), *Performance of abutment-backfill system under thermal variations in integral bridges built on clay*, Engineering Structures, 26, 7, 949-962
- Dicleli, M. and Albhaisi, S.M., (2005), *Analytical formulation of maximum length limits of integral bridges on cohesive soils*, Canadian Journal of Civil Engineering, 32, 4, 726-738
- Dicleli, M. and Erhan, S., (2008), *Effect of soil and substructure properties on live-load distribution in integral abutment bridges*, Journal of Bridge Engineering, 13, 5, 527-539
- Dicleli, M. and Erhan, S., (2009), *Live load distribution formulas for single-span*

RETROFIT OF EXISTING BRIDGES WITH CONCEPT OF INTEGRAL ABUTMENT BRIDGE

prestressed concrete integral abutment bridge girders, Journal of Bridge Engineering, 14, 6, 472-486

Dicleli, M. and Erhan, S., (2010), *Effect of soil–bridge interaction on the magnitude of internal forces in integral abutment bridge components due to live load effects*, Engineering Structures, 32, 1, 129-145

Dicleli, M. and Erhan, S., (2011), *Effect of Foundation Soil Stiffness on the Seismic Performance of Integral Bridges*, Structural Engineering International, 21, 2, 162-168

Dreier, D. (2008). *Influence of soil-structure interaction on structural behaviour of integral bridge piers*. 7th fib PhD Symposium. Stuttgart, Germany: 11-20

Dreier, D., (2010a), *Interaction Sol-Structure dans le Domaine des Ponts Intégraux*, PhD, École Polytechnique Fédérale de Lausanne,(in French).

Dreier, D., (2010b), *Modified Geometry of Transition Slabs for Integral Bridges*, Proceedings of the 1st EPFL Doctoral Conference in Mechanics, Advances in Modern Aspects of Mechanics, Lausanne, Switzerland, 107-110

Dreier, D., Burdet, O. and Muttoni, A., (2011), *Transition Slabs of Integral Abutment Bridges*, Structural Engineering International, 21, 2, 144-150

Duncan, J.M. and Arsoy, S., (2003), *Effect of bridge-soil interaction on behavior of piles supporting integral bridges*, Transportation Research Record, 1849, 91-97

Duncan, J.M., Evans Jr, L.T. and Ooi, P.S.K., (1994), *Lateral load analysis of single piles and drilled shafts*, Journal of geotechnical engineering, 120, 5, 1018-1033

Duncan, J.M. and Mokwa, R.L., (2001), *Passive earth pressures: theories and tests*, Journal of geotechnical and geoenvironmental engineering, 127, 3, 248-257

England, G.L., Bush, D.I. and Tsang, N.C.M., (2000), *Integral bridges: a fundamental approach to the time-temperature loading problem*. Thomas Telford

Erhan, S. and Dicleli, M., (2009a), *Investigation of the Applicability of AASHTO LRFD Live Load Distribution Equations for Integral Bridge Substructures*, Advances in Structural Engineering, 12, 4, 559-578

Erhan, S. and Dicleli, M., (2009b), *Live load distribution equations for integral bridge substructures*, Engineering Structures, 31, 5, 1250-1264

Eurocode CEN, (2004a), *Eurocode 2: Design of concrete structures—Part 1-1: General rules and rules for buildings*, EN 1992-1-1,

Eurocode CEN, (2004b), *Eurocode 7: Geotechnical design—Part 1: General rules*, rue de Stassart, 36 B-1050 Brussels, EUROPEAN COMMITTEE FOR STANDARDIZATION; COMITÉ EUROPÉEN DE NORMALISATION; EUROPÄISCHES KOMITEE FÜR NORMUNG, EN 1997-1

Eurocode CEN, (2005a), *Eurocode 8: Design of structures for earthquake resistance—Part 2: Bridges*, rue de Stassart, 36 B-1050 Brussels, EUROPEAN COMMITTEE FOR STANDARDIZATION; COMITÉ EUROPÉEN DE NORMALISATION; EUROPÄISCHES KOMITEE FÜR NORMUNG, EN 1998-2

Eurocode CEN, (2005b), *Eurocode 8: Design of structures for earthquake resistance—Part 3: Assessment and retrofitting of buildings*, rue de Stassart, 36 B-1050 Brussels, EUROPEAN COMMITTEE FOR STANDARDIZATION; COMITÉ EUROPÉEN DE NORMALISATION; EUROPÄISCHES KOMITEE FÜR NORMUNG, EN 1998-2

Evans, L.T. and Duncan, J.M. (1982). *Simplified analysis of laterally loaded piles*, University of California, Department of Civil Engineering

Fédération internationale du béton, (2004), *Precast Concrete Bridges: State-of-art Report*. FIB-Féd. Int. du Béton

Fan, L.C., (1997), *Bridge seismic (in chinese)*. Tongji Press, Shanghai, China

Fang, H.Y., (1991), *Foundation engineering handbook*. Springer

Fang, H.Y., Chen, T.J. and Wu, B.F., (1994), *Passive earth pressures with various wall movements*, Journal of geotechnical engineering, 120, 8, 1307-1323

Farahani, R.V., (2010), *Seismic analysis of integral abutment bridges considering soil structure interaction*, Master, University of Tennessee, Knoxville

Faraji, S. (1997). *Behavior of Integral Abutment Bridges in Massachusetts*, University of Massachusetts Transportation Research Center

Faraji, S., Ting, J.M., Crovo, D.S. and Ernst, H., (2001), *Nonlinear analysis of integral bridges: finite-element model*, Journal of geotechnical and geoenvironmental engineering, 127, 5, 454-461

Federal Emergency Management Agency, (1997a), *FEMA273, NEHRP guidelines for the seismic rehabilitation of buildings*, Washington, D.C., Federal Emergency Management Agency, FEMA 273

Federal Emergency Management Agency, (1997b), *FEMA274, NEHRP commentary on the guidelines for the seismic rehabilitation of buildings*, Washington, D.C., Federal Emergency Management Agency, FEMA 274

Federal Emergency Management Agency, (2000), *FEMA356, NEHRP guidelines for the seismic rehabilitation of buildings*, Washington DC, Federal Emergency Management Agency,

Federal Emergency Management Agency, (2005), *FEMA440, Improvement of nonlinear static seismic analysis procedures*, Washington, D.C., Federal Emergency Management Agency,

RETROFIT OF EXISTING BRIDGES WITH CONCEPT OF INTEGRAL ABUTMENT BRIDGE

Feldmann, M., Naumes, J., Pak, D., Veljkovic, M., Nilsson, M., Eriksen, J., Collin, P., Kerokoski, O., Petursson, H., Verstraete, M., Vroomen, C., Haller, M., Hechler, O. and Popa, N. (2010). *Economic and Durable Design of Composite Bridges with Integral Abutments*. Luxembourg: Publications Office of the European Union, European Commission, Publications Office of the European Union: Luxembourg. ISBN

Feldmann, M., Pak, D., Hechler, O. and MARTIN, P.-O., (2011), *A Methodology for Modelling the Integral Abutment Behaviour of Non-Symmetrically Loaded Bridges*, *Structural Engineering International*, 21, 3, 311-319

Fennema, J.L., Laman, J.A. and Linzell, D.G., (2005), *Predicted and measured response of an integral abutment bridge*, *Journal of Bridge Engineering*, 10, 6, 666-677

Finnish National Road Administration, (2000), *Steel pipe piles*, Helsinki, Finnish National Road Administration.,

Flener, E.B., (2004), *Soil-Structure Interaction for Integral Bridges and Culverts*, Doctor, Royal Institute of Technology

Fomento, M.d., (2000), *Guía para la concepción de puentes integrales en carreteras*, Madrid, Spain, Ministerio de Fomento. Centro de Publicaciones,(in Spanish).

Forschungsgesellschaft für Straßen- und Verkehrswesen (1994). *Merkblatt über den Einfluß der Hinterfüllung auf Bauwerke*. Köln

Franco, J.M., (1999), *Design and Field Testing of Jointless Bridges*, MSc, West Virginia University

Freyermuth, C.L., (1969), *Design of continuous highway bridges with precast, prestressed concrete girders*, *Journal of the Prestressed Concrete Institute*, 14, 2,

Fu, C.C. (2001). *Proposed Design of Existing Simple Span Steel Girders made Continuous*. College Park, MD 20742, The Bridge Engineering Software and Technology (BEST) Center Department of Civil and Environmental Engineering University of Maryland

Fu, C.C. and Kudsı, T. (2000). *Survey and Design of Simple Span Precast Concrete Girders Made Continuous*, The Bridge Engineering Software and Technology (BEST) Center, Department of Civil and Environmental Engineering, University of Maryland

Fujiwara, M., Kazuhiro, N. and Yomamoto, S. (1992). *Elimination of expansion joints in highway bridges*. Proceedings of the 8th U.S.-Japan Bridge Engineering Workshop

Geier, R., (2010), *Development of Integral Bridge Design in Austria*, IABSE Symposium Report, Venice, Italy, International Association for Bridge and Structural Engineering, 54-61

- Geier, R., (2011), *Design and Construction of the Perschling Bridge, Austria*, Structural Engineering International, 21, 2, 195-201
- Gherardi, M., (2010), *Ponti integrali*,
- Girton, D.D., Hawkinson, T.R. and Greimann, L.F., (1991), *Validation of design recommendations for integral-abutment piles*, Journal of Structural Engineering, 117, 7, 2117-2134
- Goel, R.K., (1997), *Earthquake characteristics of bridges with integral abutments*, Journal of Structural Engineering, 123, 11, 1435-1443
- Greimann, L. and Wolde-Tinsae, A.M., (1988), *Design model for piles in jointless bridges*, Journal of Structural Engineering, 114, 6, 1354-1371
- Greimann, L.F., Abendroth, R.E., Johnson, D.E. and Ebner, P.B. (1987). *Pile Design and Tests for Integral Abutment Bridges*. Ames, Department of Civil Engineering, Engineering Research Institute, Iowa State University
- Greimann, L.F., Phares, B.M., Faris, A. and Bigelow, J. (2008). *Integral Bridge Abutment-to-Approach Slab Connection*
- Greimann, L.F., Yang, P., Edmunds, S.K. and Wolde-Tinsae, A.M. (1984a). *Design of Piles for Integral Abutment Bridges*, College of Engineering Iowa State University
- Greimann, L.F., Yang, P. and Wolde-Tinsae, A.M., (1986), *Nonlinear analysis of integral abutment bridges*, Journal of Structural Engineering, 112, 10, 2263-2280
- Greimann, L.F., Yang, P.S., Edmunds, S.K. and Wolde-Tinsae, A.M. (1984b). *Design of Piles for Integral Abutment Bridges*, College of Engineering Iowa State University
- Hällmark, R., (2006), *Low-cycle fatigue of steel piles in integral abutment bridges*, Master, Luleå University of Technology
- Haliburton, T.A., (1971), *Soil-structure interaction: Numerical analysis of beams and beam-columns*. Oklahoma State University, School of Civil Engineering
- Hambly, E.C., (1990), *Bridge deck behaviour*. Taylor & Francis
- Hambly, E.C., (1997), *Integral Bridges*, Proceedings of the Institute Civil Engineers - Transport, 123, 1, 30-38
- Hambly, E.C. and Burland, J.B. (1979). *Bridge foundations and substructures*. London, Department of the Environment Building Research Establishment
- Hambly, E.C. and Nicholson, B., (1990), *Prestressed beam integral bridges*, Structural Engineer, 68, 23, 474-481
- Hansen, J.B. (1966). *Resistance of a rectangular anchor slab*. Copenhagen, Danish

Geotechnical Institute: 12-13

Hansen, J.B. and Christensen, N.H. (1961). *The Ultimate Resistance of Rigid Piles Against Transversal Forces*. Copenhagen, Danish Geotechnical Institute

Hassiotis, S. and Xiong, K. (2007). *Deformation of Cohesionless Fill Due to Cyclic Loading*. Hoboken, N.J., Department of Civil, Environmental and Ocean Engineering, Stevens Institute of Technology

Hayward, A., (1992), *Continuous and jointless steel bridges*, Bridge design for durability. Expansion joints and continuity., Crowthorne, UK,

Helmers, M.J., (1997), *Use of ultimate load theories for design of drilled shaft sound wall foundations*, Master, Virginia Polytechnic Institute and State University

Highways Agency, (2001), *Design manual for roads and bridges BA 57/01 Design for durability*, London, Her Majesty's Stationery Office (HMSO),

Highways Agency (2003). *BA 42/96: The Design of Integral Bridges*. Design Manual for Roads and Bridges. London, UK, The Stationary Office Ltd. Volume 1, Section 3, Part 12

Ho, E. and Lukashenko, J., (2011), *Link Slab Deck Joints*, 2011 conference and exhibition of the transportation association of Canada. , Edmonton, Alberta, MMM Group,

Hobbs, R.E. and Jowharzadeh, A.M., (1978), *An incremental analysis of beam-columns and frames including finite deformations and bilinear elasticity*, Computers & structures, 9, 3, 323-330

Hong, j., (2002), *Research on the Influence of Soil-Pile Interaction on Loaded Behaviour of Integral Abutment Bridges*, Master, Fuzhou University,(in Chinese).

Hong, j., (2006), *Research on Simplified Calculating Model and Loaded Behavior of Integral Abutment Bridges*, Doctor, Fuzhou University,(in Chinese).

Hong, J. and Peng, D., (2004), *Design of Shangban Integral Abutment Bridge - Engineering Application of Jointless Bridge*, Fujian Architecture & Construction, 90, 5, 50-52,(in Chinese).

Horvath, J.S. (2005). *Integral-Abutment Bridges: Geotechnical Problems and Solutions Using Geosynthetics and Ground Improvement*. Proceedings of the 2005 FHWA Conference: Integral abutment and jointless bridges. Baltimore Maryland, United States, Constructed Facilities Center, College of Engineering and Mineral Resources, West Virginia University: 281-291

Hujeux, J.C., (1985), *Une loi de comportement pour le chargement cyclique des sols*, Génie parasismique, 287-302

- Husain, I. (2004). *Retrofitting of Existing Bridges with Joints to Semi-Integral Bridges*. Ontario, Canada, Structures Office, Ontario Ministry of Transportation
- Husain, I. and Bagnariol, D. (1996). *Integral abutment bridges*. Ontario, Canada, Structures Office, Ontario Ministry of Transportation
- Husain, I. and Bagnariol, D. (1999). *Semi-Integral Abutment Bridges*. Suite 910, 505 Consumers Road, Toronto, Ontario M2J 4V8
- Husain, I. and Bagnariol, D. (2000). *Performance of Integral Abutment Bridges*. Suite 910, 505 Consumers Road, Toronto, Ontario M2J 4V8: 20
- Husain, I. and Farago, B. (1993). *Integral abutment bridges*. Ontario, Canada, Structures Office, Ontario Ministry of Transportation
- Husain, I., Huh, B., Low, J. and McCormick, M., (2005), *Moose Creek Bridge—Case Study of a Prefabricated Integral Abutment Bridge in Canada*, Integral Abutment and Jointless Bridges (IAJB 2005),
- Iles, D.C. (2006). *Integral Bridges in the UK*. International Workshop on the Bridges with Integral Abutments. Luleå, Sweden, Luleå University of Technology
- Imbsen, R.A., (2007), *AASHTO guide specifications for LRFD seismic bridge design*. American Association of State Highway and Transportation Officials
- Itani, A.M. and Pekcan, G. (2011). *Seismic Performance of Steel Plate Girder Bridges with Integral Abutments*. Reno, Nevada, Department of Civil and Environmental Engineering University of Nevada
- Iwasaki, N., Tenma, S. and Kurita, A., (2011), *Portal Frame Bridges in Japan: State of the Art Report*, Structural Engineering International, 21, 3, 290-296
- Izzuddin, B.A. and Elnashai, A.S., (1993a), *Adaptive space frame analysis. Part I: a plastic hinge approach*, Proceedings of the Institution of Civil Engineers: Structures and Buildings, 99, 3, 303-316
- Izzuddin, B.A. and Elnashai, A.S., (1993b), *Adaptive space frame analysis. Part II: a distributed plasticity approach*, Proceedings of the Institution of Civil Engineers: Structures and Buildings, 99, 3, 317-326
- Jaky, J., (1948), *Pressure in soils*, 103-107
- Jayakumar, S., Bergmann, M., Ashraf, S. and Norrish, C. (2005). *Case Study: A Jointless Structure to Replace the Belt Parkway Bridge Over Ocean Parkway*. Proceedings of the 2005 FHWA Conference: Integral abutment and jointless bridges. Baltimore Maryland, United States, Constructed Facilities Center, College of Engineering and Mineral Resources, West Virginia University
- Jayaraman, R. and Merz, P.B. (2001). *Integral bridge concept applied to*

RETROFIT OF EXISTING BRIDGES WITH CONCEPT OF INTEGRAL ABUTMENT BRIDGE

rehabilitation an existing bridge and construct a dual-use bridge. 26th Conference on Our World In Concrete & Structures. Singapore

Jin, X., Shao, X., Peng, W. and Yan, B., (2005), *A New Category of Semi-Integral Abutment in China*, Structural Engineering International, 15, 3, 186-188

Jin, X., Shao, X., Yan, B. and Peng, W. (2004). *New Technologies in China's First Jointless Integral-abutment Bridge*. IABSE Symposium, Shanghai 2004: Metropolitan Habitats and Infrastructure. Shanghai, China

Kaar, P.H., Kriz, L.B. and Hognestad, E., (1960), *Precast-prestressed concrete bridges 1: Pilot tests of continuous girders.* , Journal of the PCA Research and Development Laboratories, 2, 2, 21-37

Kalayci, E., Breña, S.F. and Civjan, S.A., (2009), *Curved Integral Abutment Bridges—Thermal Response Predictions through Finite Element Analysis*, Structures Congress 2009, Austin, Texas, United States, ASCE, 1-10

Kalayci, E., Civjan, S.A. and Breña, S.F., (2012), *Parametric study on the thermal response of curved integral abutment bridges*, Engineering Structures, 43, 129-138

Kalayci, E., Civjan, S.A., Breña, S.F. and Allen, C.A., (2011), *Load Testing and Modeling of Two Integral Abutment Bridges in Vermont, US*, Structural Engineering International, 21, 2, 181-188

Karantzikis, M. and Spyrakos, C.C., (2000), *Seismic analysis of bridges including soil–abutment interaction*, Proceedings of the 12th World Congress on Earthquake Engineering. Paper,

Kaufmann, W. and Alvarez, M., (2011), *Swiss Federal Roads Office Guidelines for Integral Bridges*, Structural Engineering International, 21, 2, 189-194

Kerokoski, O., (2006), *Soil-Structure Interaction of Long Jointless Bridges with Integral Abutments*, Doctor, Tampere University of Technology

Kerokoski, O. and Laaksonen, A. (2005). *Soil-structure interaction of jointless bridges*. Proceedings of the 2005 FHWA Conference: Integral abutment and jointless bridges. Baltimore, Maryland, Constructed Facilities Center, College of Engineering and Mineral Resources, West Virginia University

Khodair, Y.A. and Hassiotis, S., (2005), *Analysis of soil–pile interaction in integral abutment*, Computers and Geotechnics, 32, 3, 201-209

Kim, W.S., (2008), *Load and resistance factor design for integral abutment bridges*, Doctor, The Pennsylvania State University

Kim, W.S. and Laman, J.A., (2010a), *Integral abutment bridge response under thermal loading*, Engineering Structures, 32, 6, 1495-1508

- Kim, W.S. and Laman, J.A., (2010b), *Numerical analysis method for long-term behavior of integral abutment bridges*, Engineering Structures, 32, 8, 2247-2257
- Kovac, B., (2010), *Structural response of circular concrete filled tube piers in integral bridges*, Master, UNIVERSITAT POLITÈCNICA DE CATALUNYA
- Kraft, L.M., Kagawa, T. and Ray, R.P., (1981), *Theoretical t-z curves*, Journal of the Geotechnical engineering division, 107, 11, 1543-1561
- Krier, D., (2009a), *Modeling of Integral Abutment Bridges Considering Soil-Structure Interaction Effects*, Ph.D., The University of Oklahoma
- Krier, D., (2009b), *Modeling of integral abutment bridges considering soil-structure interaction effects*, PhD, University of Oklahoma
- Krizek, J., (2009), *Integral Bridges*, Doctor, Czech Technical University in Prague.,(in Czech).
- Krizek, J., (2011), *Soil-Structure Interaction of Integral Bridges*, Structural Engineering International, 21, 2, 169-174
- Kubo, K. (1965). *Experimental Study of the Behaviour of Laterally Loaded Piles*. Proc. 6th Int. Conf. S.M. & F.E., PORT AND HARBOUR RESEARCH INST TOKYO (JAPAN). 2: 275-279
- Kumar, J. and Subba Rao, K.S., (1997), *Passive pressure coefficients, critical failure surface and its kinematic admissibility*, Geotechnique, 47, 1, 185-192
- Kunin, J. and Alampalli, S. (1999). *Integral Abutment Bridges: Current Practice in the United States and Canada, Special Report 132*. New York, Transportation Research and Development Bureau, New York State Department of Transportation,
- Kunin, J. and Alampalli, S., (2000), *Integral abutment bridges: current practice in United States and Canada*, Journal of performance of constructed facilities, 14, 3, 104-111
- Lam, C., Lai, D., Au, J., Lim, L., Young, W. and Tharmabala, B., (2008), *Development of Concrete Link Slabs to Eliminate Bridge Expansion Joints Over Piers*, 2008 Annual Conference of the Transportation Association of Canada, Toronto, Ontario,
- Lan, C., (2012), *On the Performance of Super-Long Integral Abutment Bridges: Parametric Analyses and Design Optimization*, Doctor, University of Trento
- Lawver, A., French, C. and Shield, C.K., (2000), *Field performance of integral abutment bridge*, Transportation Research Record: Journal of the Transportation Research Board, 1740, 108-117
- Leathers, R.C. (1980). *Bridge Deck Joint Rehabilitation (Retrofit)*. Technical Advisory

RETROFIT OF EXISTING BRIDGES WITH CONCEPT OF INTEGRAL ABUTMENT BRIDGE

T1540.16. Washington, D.C., Federal Highway Administration

Lehane, B.M., (2011), *Lateral Soil Stiffness Adjacent to Deep Integral Bridge Abutments*, *Géotechnique*, 61, 7, 593-603

Lehane, B.M., Keogh, D.L. and O'Brien, E.J., (1999), *Simplified elastic model for restraining effects of backfill soil on integral bridges*, *Computers & structures*, 73, 1, 303-313

Li, Y., Cheng, C. and Bao, W., (1997), *Expansion joint in highway and bridge*. China Communication Press, Beijing, China,(in Chinese).

Lin, T.Y., (2004), *Investigation of Factors Causing the Damage of Bridge Expansion Joint*, Master, Chaoyang University of Technology,(in Chinese).

Liu, D., Magliola, R.A. and Dunker, K.F. (2005). *Integral Abutment Bridges - Iowa and Colorado Experience*. Proceedings of the 2005 FHWA Conference: Integral abutment and jointless bridges. Baltimore Maryland, United States, Constructed Facilities Center, College of Engineering and Mineral Resources, West Virginia University

Loveall, C.L., (1985), *Jointless bridge decks*, *Civil Engineering*, ASCE, 55, 11, 64-67

Müller-Breslau, H., (1906), *Erddruck auf Stützmauern*. A. Kröner

Ma, J. and Jin, X., (2002), *Design Philosophy of Guandong Qingyuan Sijiu Bridge - the First Integral Bridge without Expansion in China*, *Central South Highway Engineering*, 27, 2, 32-34,(in Chinese).

Maberry, S., Camp, J.D. and Bowser, J., (2005), *New Mexico's Practice and Experience in Using Continuous Spans for Jointless Bridges*, Proceedings of the 2005 FHWA Conference: Integral abutment and jointless bridges, Baltimore Maryland, United States, Constructed Facilities Center, College of Engineering and Mineral Resources, West Virginia University, 125-135

Madhav, M.R., Kameswara, R. and Madhavan, K., (1971), *Laterally loaded pile in elasto-plastic soil*, *Soil and foundation*, 11, 2, 1-15

Malerba, P.G. (2010). *Managing old bridges*. Bridge Maintenance, Safety, Management and Life-Cycle Optimization. Frangopol, D. M., Sause, R. and Kusko, C. S. Philadelphia, Pennsylvania, USA, International Association for Bridge Maintenance and Safety

Malerba, P.G. and Comaita, G., (2011), *Twin Runway Integral Bridges at Milano Malpensa Airport, Italy*, *Structural Engineering International*, 21, 2, 206-209

Malerba, P.G. and Comaita, G. (2012). *Two integral bridges connecting the runways of the Milano Malpensa Airport*. Bridge Maintenance, Safety, Management, Resilience and Sustainability. Biondini, F. and Frangopol, D. M. Stresa, Lake

- Maggiore, Italy, International Association for Bridge Maintenance and Safety
- Mander, J. and Priestley, M.J.N., (1988), *Theoretical stress - strain model for confined concrete*, Journal of Structural Engineering, 114, 8, 1804-1826
- Martin, G.R. and Yan, L., (1995), *Modeling passive earth pressure for bridge abutments*, Earthquake-Induced Movements and Seismic Remediation of Existing Foundations and Abutments, New York, ASCE, 1-16
- Maruri, R.F. and Petro, S.H. (2005). *Integral Abutments and Jointless Bridges (IAJB) 2004 Survey Summary*. Proceedings of the 2005 FHWA Conference: Integral abutment and jointless bridges. Baltimore Maryland, United States, Constructed Facilities Center, College of Engineering and Mineral Resources, West Virginia University: 12-29
- Marx, S. and Seidl, G., (2011), *Integral Railway Bridges in Germany*, Structural Engineering International, 21, 3, 332-340
- Masrilayanti, M. and Weekes, L. (2012). *Integral Bridge: A Review on Its Behaviour under Earthquake Loads*. Bridge Maintenance, Safety, Management, Resilience and Sustainability. Biondini, F. and Frangopol, D. M. Stresa, Lake Maggiore, Italy, International Association for Bridge Maintenance and Safety
- Massachusetts Department of Transportation, (2007), *Bridge Manual*, Boston, MA, USA, Highway Division, Massachusetts Department of Transportation,
- Matlock, H. (1970). *Correlations for Design of Laterally Loaded Piles in Soft Clay*. Second Annual Offshore Technology Conference. Houston, Texas
- Mayne, P.W. and Kulhawy, F.H., (1982), *Ko-OCR Relationships in Soil*, Journal of the Geotechnical engineering division, 108, 6, 851-872
- Mayniel, K. (1808). *Traité Expérimental, Analytique et Pratique de la Poussée des Terres*, Paris
- Mazzarolo, E., (2012), *Analysis and Development of an Innovative Prefabricated Beam-to-Column Joint*, University of Trento
- McClelland, B. and Focht, J.A., (1958), *Soil modulus for laterally loaded piles*, Transactions, ASCE, 123, 1049-1063
- Meek, J.L. and Loganathan, S., (1990), *Geometric and material non-linear behaviour of beam-columns*, Computers & structures, 34, 1, 87-100
- Megson, T.H.G., (2005), *Structural and stress analysis*. Butterworth-Heinemann
- MIDAS IT Co. Ltd (2009). *Civil 2009 Online Manual*
- Miller, R.A., Castrodale, R., Mirmiran, A. and Hastak, M. (2004). *Connection of*

RETROFIT OF EXISTING BRIDGES WITH CONCEPT OF INTEGRAL ABUTMENT BRIDGE

simple-span precast concrete girders for continuity. Miller, R. A., Castrodale, R., Mirmiran, A. and Hastak, M. Washington D.C., Transportation Research Board

Ministero dei lavori pubblici, (1990), *Aggiornamento delle norme tecniche per la progettazione, la esecuzione e il collaudo dei ponti stradali,*

Ministero dei lavori pubblici, (1996), *Norme tecniche relative ai criteri generali per la verifica di sicurezza delle costruzioni e dei carichi e sovraccarichi,*

Ministero dei lavori pubblici di concerto and Ministro dell'interno, (1996), *Norme tecniche per le costruzioni in zone sismiche.,*

Ministero delle Infrastrutture, (2008), *Nuove Norme Tecniche per le Costruzioni DM Infrastrutture 14/01/2008 (NTC 2008),* Rome,

Mistry, V.C. (2005). *Integral Abutment and Jointless Bridges.* Proceedings of the 2005 FHWA Conference: Integral abutment and jointless bridges. Baltimore Maryland, United States, Constructed Facilities Center, College of Engineering and Mineral Resources, West Virginia University

Mokwa, R.L. and Duncan, J.M. (2000). *Investigation of the resistance of pile caps and integral abutments to lateral loading.* Blacksburg, Virginia, Virginia Polytechnic and State University

Mokwa, R.L., Duncan, J.M. and Helmers, M.J. (1997). *Deflections and bending moments in drilled shaft sound wall foundations under working load conditions.* Blacksburg, VA 24061 USA, Virginia Polytechnic Institute and State University

Morrison Jr, E.E. and Ebeling, R.M., (1995), *Limit equilibrium computation of dynamic passive earth pressure,* Canadian Geotechnical Journal, 32, 3, 481-487

Muqtadir, A. and Morshed, J., (1998), *Prediction of load-deformation behavior and load carrying capacity of piles in sand,*

Mwindo, M.J., (1992), *Strain dependent soil modulus of horizontal subgrade reaction,* Master, University of Missouri--Rolla

Nakamura, S.-i., Momiyama, Y., Hosaka, T. and Homma, K., (2002), *New technologies of steel/concrete composite bridges,* Journal of Constructional Steel Research, 58, 1, 99-130

Narain, J., Saran, S. and Nandakumaran, P., (1969), *Model study of passive pressure in sand,* Journal of Soil Mechanics and Foundations Division, 95, 4, 969-984

Newhouse, C.D., (2005), *Design and Behavior of Precast, Prestressed Girders Made Continuous—An Analytical and Experimental Study,* Doctor, Virginia Polytechnic Institute and State University

- Nilsson, M., (2008), *Evaluation of in-situ measurements of composite bridge with integral abutments*, Luleå University of Technology
- Nilsson, M., Eriksen, J. and Veljkovic, M., (2008), *Towards a Better Understanding of Behaviour of Bridges with Integral Abutments*, ASCE, 717-727
- O'Brien, E.J. and Keogh, D.L., (1999), *Bridge deck analysis*. Taylor & Francis
- O'Neill, M.W., Hawkins, R.A. and Mahar, L.J. (1981). *Field study of pile group action*, Federal Highway Administration
- O'Neill, M.W. and Murchison, J.M. (1983). *An Evaluation of p-y Relationships in Sands*. Houston, Texas, USA, University of Houston
- Oesterle, R.G., Glikin, J.D. and Larson, S.C. (1989). *Design of precast prestressed bridge girders made continuous*. National Cooperative Highway Research Program Report 322. Washington, D.C., National Research Council
- Ohio Department of Transportation. ODOT On-line Bridge Maintenance Manual: Preventive Maintenance/Repair Guidelines for Bridges and Culverts. from <http://www.dot.state.oh.us/Divisions/Engineering/Structures/bridge%20operations%20and%20maintenance/PreventiveMaintenanceManual/Pages/default.aspx>
- Olson, S.M., Long, J.H., Hansen, J.R., Renekis, D. and LaFave, J.M. (2009). *Modification of IDOT Integral Abutment Design Limitations and Details*. Urbana, University of Illinois at Urbana-Champaign. 51
- Ovesen, N.K. (1964). *Anchor Slabs: Calculation Methods and Model Tests*. Copenhagen, Danish Geotechnical Institute: 5-39
- Pétursson, H. and Collin, P. (2006). *Innovative solutions for integral abutments*. International Workshop on the Bridges with Integral Abutments. Luleå, Sweden, Luleå University of Technology
- Pétursson, H., Collin, P., Veljkovic, M. and Andersson, J., (2011), *Monitoring of a Swedish Integral Abutment Bridge*, Structural Engineering International, 21, 2, 175-180
- Panagiotakos, T.B. and Fardis, M.N., (2001), *Deformations of reinforced concrete members at yielding and ultimate*, ACI Structural Journal, 98, 2, 135-148
- Paraschos, A. and Amde, A.M. (2011). *A survey on the status of use, problems, and costs associated with Integral Abutment Bridges*
- Park, R., (1992), *Capacity Design of Ductile RC Building Structures for Earthquake Resistance*, The Structural Engineer, 70, 16, 279-288
- Park, R. and Paulay, T., (1975), *Reinforced concrete structures*. Wiley (John) & Sons

RETROFIT OF EXISTING BRIDGES WITH CONCEPT OF INTEGRAL ABUTMENT BRIDGE

Parker, F. and Reese, L.C. (1970). *Experimental and analytical studies of behavior of single piles in sand under lateral and axial loading*

Pastor, M., Binda, M. and Harčarik, T., (2012), *Modal Assurance Criterion*, Procedia Engineering, 48, 543-548

Patel, N. and Lai, D. (2001). *Development of Flexible Link Slab for Elimination of Existing Expansion Joints on Steel Girder Bridges*. Ontario, Canada, Structures Office, Ontario Ministry of Transportation

Paulay, T. and Priestley, M.J.N., (1992), *Seismic Design of Reinforced Concrete and Masonry Buildings*. John Wiley & Sons, Inc., New York, USA

Pekcan, G., Itani, A. and Monzon, E., (2010), *Seismic Design Recommendations for Steel Girder Bridges with Integral Abutments*, Transportation Research Board 89th Annual Meeting,

Perkun, J. and Micheal, K. (2005). *Design and Construction of Dual 630-foot, Jointless, Three-span Continuous Multi-girder Bridges in St. Albans, West Virginia, United States, Carrying U.S. Route 60 over the Coal River*. Proceedings of the 2005 FHWA Conference: Integral abutment and jointless bridges. Baltimore Maryland, United States, Constructed Facilities Center, College of Engineering and Mineral Resources, West Virginia University

Poulos, H.G. and Davis, E.H., (1980), *Pile foundation analysis and design*. RE Krieger

Powell, G.H. and Chen, P.F.S., (1986), *3D beam-column element with generalized plastic hinges*, Journal of engineering mechanics, 112, 7, 627-641

Prakash, S. and Kumar, S., (1996), *Nonlinear lateral pile deflection prediction in sands*, Journal of geotechnical engineering, 122, 2, 130-138

Prakash, S. and Sharma, H.D., (1990), *Pile foundations in engineering practice*. Wiley-Interscience

Precast/Prestressed Concrete Institute (PCI), (2001), *The State of the Art of Precast/Prestressed Integral Bridges*. Precast/Prestressed Concrete Institute, Chicago, IL, USA

Priestley, M.J.N. and Seible, F., (1996), *Seismic design and retrofit of bridges*. Wiley-Interscience

Prof. Piero Gelfi (2011). *VcaSlu*. Versione 7.7

Pugasap, K., Kim, W. and Laman, J.A., (2009), *Long-Term Response Prediction of Integral Abutment Bridges*, Journal of Bridge Engineering, 14, 2, 129-139

Puppala, A.J., Saride, S., Archeewa, E., Hoyos, L.R. and Nazarian, S. (2009).

Recommendations for Design, Construction, and Maintenance of Bridge Approach Slabs. Texas, USA, The University of Texas at Arlington, University of Texas at El Paso

Purvis, R. (2003). *Bridge deck joint performance: A synthesis of highway practice*. Washington, D.C., Transportation Research Board. 319

Pyke, R.M., (1980), *Nonlinear soil models for irregular cyclic loadings*, Journal of geotechnical and geoenvironmental engineering, 106, 6, 715-726

Qian, J.L., (2002), *Application of Simple Support Beam Continuous Deck Joints on Bridges on Beiyan Highway*, China Municipal Engineering, 98, 21-23,(in Chinese).

Ramberger, G., (2002), *Structural bearings and expansion joints for bridges*. IABSE-AIPC-IVBH, Zurich, Switzerland

Randolph, M.F. and Wroth, C.P., (1978), *Analysis of deformation of vertically loaded piles*, Journal of the Geotechnical engineering division, 104, 12, 1465-1488

Rankine, W.J.M., (1857), *On the stability of loose earth*, Philosophical Transactions of the Royal Society of London, 9-27

Reece, L.C., Cox, W. and Koop, F., (1975), *Field testing and analysis of laterally loaded piles in stiff clay*, 7th Offshore Technology Conference, Houston, USA, 671-690

Reese, L.C. (1986). *Behavior of piles and pile groups under lateral load*. Washington, D.C., Federal Highway Administration, United States Department of Transportation,

Reese, L.C., Cox, W.R. and Koop, F.D., (1974), *Analysis of Laterally Loaded Piles in Sand*, Sixth Annual Offshore Technology Conference, Houston, Texas,

Reese, L.C. and Welch, R.C., (1975), *Lateral Loading of Deep Foundations in Stiff Clay*, Journal of the Geotechnical Engineering Division, 101, 7, 633-649

Road Management Technology Center, (1995), *即設桥梁のノージョイント工法設計施工引き(案)*. 道路保全技術センター, Tokyo, Japan,(in Japanese).

Robertson, P.K. and Powell, J.J.M., (1997), *Cone penetration testing in geotechnical practice*. Taylor & Francis Group

Rodriguez, J., Martinez, F. and Marti, J., (2011), *Integral Bridge for High-Speed Railway*, Structural Engineering International, 21, 3, 297-303

Rollins, K.M. and Sparks, A., (2002), *Lateral resistance of full-scale pile cap with gravel backfill*, Journal of geotechnical and geoenvironmental engineering, 128, 9, 711-723

Rowe, P.W. and Peaker, K., (1965), *Passive earth pressure measurements*,

Géotechnique, 15, 1, 57-78

Rui-Wamba, J., García-Acón, C. and Estrada, I., (2011), *A Spanish Perspective on Integral High-Speed Railway Viaducts*, Structural Engineering International, 21, 3, 341-345

Russo, G., Bergamo, O. and Damiani, L., (2009), *Retrofitting a Short Span Bridge with a Semi-Integral Abutment Bridge: The Treviso Bridge*, Structural Engineering International, 19, 2, 137-141

Schiefer, S., Fuchs, M., Brandt, B., Maggauer, G. and Egerer, A., (2006), *Besonderheiten beim Entwurf semi - integraler Spannbetonbrücken: Eine Alternative im Brückenbau mit zunehmender Bedeutung - aufgezeigt am Beispiel der Fahrbachthalbrücke im Zuge der BAB A3 bei Aschaffenburg*, Beton - und Stahlbetonbau, 101, 10, 790-802,(in Germany).

Scott, M.H. and Fenves, G.L., (2006), *Plastic Hinge Integration Methods for Force-Based Beam-Column Elements*, Journal of Structural Engineering, 132, 2, 244-252

Seed, H.B. and Reese, L.C., (1957), *The action of soft clay along friction piles*, American Society of Civil Engineers Transactions, 122, 731-756

Shah, B.R., (2007), *3D finite element analysis of integral abutment bridges subjected to thermal loading*, Master, Kansas State University

Shamsabadi, A. (2011). *Trenching and Shoring Manual*. Burkle, K. J., Offices of Structure Construction, Department of Transportation, California

Shamsabadi, A., Ashour, M. and Norris, G., (2005), *Bridge abutment nonlinear force-displacement-capacity prediction for seismic design*, Journal of geotechnical and geoenvironmental engineering, 131, 2, 151-161

Shamsabadi, A., Rollins, K.M. and Kapuskar, M., (2007), *Nonlinear Soil-Abutment-Bridge Structure Interaction for Seismic Performance-Based Design*, Journal of geotechnical and geoenvironmental engineering, 133, 6, 707-720

Shamsabadi, A. and Yan, L., (2010), *Dynamic analysis of skewed bridges subjected to near-field ground motions considering nonlinear soil-abutment-foundation-structure interaction*,

Shanghai Municipal Engineering Administration Bureau and College of Traffic and Transportation Engineering of Tongji University (2011). *Shanghai Bridges Technical Analysis Report*. Shanghai, China,(in Chinese).

Shoukry, S.N., William, G.W., Riad, M.Y. and McBride, K.C. (2006). *Field monitoring and 3D FE modeling of an integral abutment bridge in West Virginia*. TRB 2006 Annual Meeting

- Skempton, A.W. (1951). *The bearing capacity of clays*. Building Research Congress. London: 180-189
- Smith, T.D., (1983), *Pressuremeter design method for single piles subjected to static lateral load*, Texas A & M University
- Soltani, A.A. and Kukreti, A.R., (1992), *Performance evaluation of integral abutment bridges*, Transportation research record, 1371, 17-25
- Song, S.T., Chai, Y.H. and Hale, T.H., (2005), *Analytical model for ductility assessment of fixed-head concrete piles*, Journal of Structural Engineering, 131, 7, 1051-1059
- Soubra, A.H., (2000), *Static and seismic passive earth pressure coefficients on rigid retaining structures*, Canadian Geotechnical Journal, 37, 2, 463-478
- Springman, S.M., Norrish, A.R.M. and Ng, C.W.W. (1996). *Cyclic loading of sand behind integral bridge abutments*, Transport Research Laboratory. TRL REPORT 146
- Spyrakos, C. and Loannidis, G., (2003), *Seismic behavior of a post-tensioned integral bridge including soil-structure interaction (SSI)*, Soil Dynamics and Earthquake Engineering, 23, 1, 53-63
- Steel Construction Institute, (2010a), *Composite highway bridge design*, Ascot, Berkshire, UK, Steel Construction Institute,
- Steel Construction Institute, (2010b), *Composite highway bridge design: Worked Examples*, Ascot, Berkshire, UK, Steel Construction Institute,
- Stephenson, J. (2009). *Modern methods for bridge rehabilitation: Guiding principles & A case study*. OGRA/ROMA Conference. Totonto, Canada
- Sullivan, W.R., Reese, L.C. and Fenske, C.W., (1979), *Unified Method for Analysis of laterally loaded piles in clay*, Numerical Methods in Offshore Piling, London, 22, 23,
- Swedish National Road Administration, (2002), *Vägverkets allmänna tekniska beskrivning för nybyggande och förbättring av broar*, Vägverket, Swedish National Road Administration, ATB - Bro 2002
- Tabatabai, H., Oesterle, R.G. and Lawson, T.J. (2005). *Jointless Bridges, Experimental Research and Field Studies*. Volume I
- Takano, H. (1994). *Study on jointless bridge construction in Japan*. Continuous and Integral Bridges: Proceedings of the Henderson Colloquium 'Towards Joint-Free Bridges'. Cambridge, London, Spon Pr
- Talbott, A.M., (2008), *Earthquake Resistance of Integral Abutment Bridges*, Ph.D.,

RETROFIT OF EXISTING BRIDGES WITH CONCEPT OF INTEGRAL ABUTMENT BRIDGE

Purdue University

Tandon, M. (2005). *Recent integral bridges*. International workshop on innovative bridge deck technologies. Winnipeg, Canada

Tandon, M., (2006), *Integral bridges: The final frontier*, 4th International Conference on Current and Future Trends in Bridge Design, Construction and Maintenance, Kuala Lumpur , Malaysia, Thomas Telford Services Ltd, 113-118

Tang, Q., Ma, J., Jin, X. and Shao, X. (2007). *First refurbished jointless bridge in China*. Conference of Highway Maintenance Technology. Guangdong, China, China Communication Press,(in Chinese).

Terzaghi, K., (1943), *Theoretical Soil Mechanics*, New York: John Wiley & Sons,

Terzaghi, K., (1955), *Evaluation of coefficients of subgrade reaction*, *Geotechnique*, 5, 4, 297-326

Terzaghi, K., Peck, R.B. and Mesri, G., (1996), *Soil mechanics in engineering practice*. John Wiley & Sons

Thanoon, W.A., Abdulrazeg, A.A., Noorzaei, J., Jaafar, M.S. and Kohnehpooshi, O., (2011), *Soil Structure Interaction for Integral Abutment Bridge Using Spring Analogy Approach*, IOP Conf. Series: Materials Science and Engineering, IOP Publishing, 012035

The Fort Miller Co., I. Bridge Products Project Gallery: NYS Rt. 20 over Skaneateles Lake, Skaneateles, NY.

Thompson, T.A., (1999), *Passive Earth Pressures behind Integral Bridge Abutments*, Ph.D., University of Massachusetts

Thompson, T.A. and Lutenecker, A.J. (1998). *Passive earth pressures in integral bridge abutments*. Amherst, Massachusetts, University of Massachusetts, Transportation Center. Report No. UMTC-97-16

Ting, J.M. and Faraji, S. (1998). *Streamlined analysis and design of integral abutment bridges*. Lowell, Massachusetts, Department of Civil and Environmental Engineering, University of Massachusetts. 13

Trustochowicz, G., (2005), *Optimized design of integral abutments for a three span composite bridge*, Master, Luleå University of Technology

Torricelli, L.F., Marchiondelli, A., Pefano, R. and Stucchi, R. (2012). *Integral bridge design solutions for Italian highway overpasses*. Bridge Maintenance, Safety, Management, Resilience and Sustainability. Biondini, F. and Frangopol, D. M. Stresa, Lake Maggiore, Italy, International Association for Bridge Maintenance and Safety

- TRC/Imbsen Software Systems (2007). *XTRACT v3.0.8 User Manual*. Rancho Cordova, California
- Tschebotarioff, G.P. and Johnson, E.G. (1953). *The effects of restraining boundaries on the passive resistance of sand*. Princeton, N.J., Dept. of Civil Engineering, Princeton University
- Tsiatas, G. and Boardman, W.G. (2002). *Expansion Joint Elimination for Steel Highway Bridges*. Kingston, Rhode Island, USA, University of Rhode Island, Department of Civil Engineering
- US Navy, (1986), *Design manual 7.2 Foundations and earth structures*, 200 Stovall Street Alexandria Virginia, Naval Facilities Engineering Command, Dept. of the Navy,
- Vesic, A.B., (1961), *Beams on elastic subgrade and the Winkler's hypothesis*, Proc. 5th Int. Conf. on Soil Mechanics and Foundation Engineering, Paris, 845-850
- Vijayvergiya, V.N., (1977), *Load-movement characteristics of piles*, 269-284
- Wagle, G.N. and Watt, D., (2011), *Design of Integral Bridges on M50, Ireland*, Structural Engineering International, 21, 2, 202-205
- Wallbank, E.J., (1989), *The Performance of Concrete in Bridges. A survey of 200 Highway Bridges*. Her Majesty's Stationery Office (HMSO), London, UK
- Wang, S., (2000), *Simplified Analysis for Laterally Loaded Piles in Cohesionless Soils*, Master, University of Hawaii
- Washington State Department of Transportation, (2012), *Bridge Design Manual LRFD*, Washington D.C., Washington State Department of Transportation (WSDOT), M23-50
- Wasserman, E.P., (1987), *Jointless bridge decks*, Engineering Journal, 55, 11, 93-100
- Wasserman, E.P., (2001), *Design of integral abutments for jointless bridges*, Structure Magazine, 24-33
- Wasserman, E.P., (2007), *Integral Abutment Design (Practices in the United States)*, 1st U.S. - Italy Seismic Bridge Workshop, Pavia, Italy,
- Wasserman, E.P. and Walker, J.H. (1996). *Integral abutments for steel bridges*, Tennessee Department of Transportation
- Weizenegger, M., (2003), *Hybrid Frame Bridge, River Saale, Merseburg, Germany*, Structural Engineering International, 13, 3, 179-181
- Wen, R.K. and Farhoomand, F., (1970), *Dynamic analysis of inelastic space frames*,

RETROFIT OF EXISTING BRIDGES WITH CONCEPT OF INTEGRAL ABUTMENT BRIDGE

Journal of the Engineering Mechanics Division, 96, 5, 667-686

West Virginia Department of Transportation Division of Highways, E.D., (2004), *West Virginia Division of Highways Bridge Design Manual*, Charleston, West Virginia, West Virginia Department of Transportation,

Wetmore, J. and Peterson, B. (2005). *Case Study–Jointless Bridge Beltrami County State Aid Highway 33 Over Mississippi River in Ten Lake Township, Minnesota*. Proceedings of the 2005 FHWA Conference: Integral abutment and jointless bridges. Baltimore Maryland, United States, Constructed Facilities Center, College of Engineering and Mineral Resources, West Virginia University

White, D., Sritharan, S., Suleiman, M., Mekkawy, M. and Chetlur, S. (2005). *Identification of the best practices for design, construction, and repair of bridge approaches*

White, H.I. (2007). *Integral Abutment Bridges: Comparison of Current Practice between European Countries and the United States of America*. 50 Wolf Road, Albany NY 12232, Transportation Research and Development Bureau, New York State Department of Transportation

White, H.I., Pétursson, H. and Collin, P., (2010), *Integral Abutment Bridges: The European Way*, Practice Periodical on Structural Design and Construction, 15, 3, 201-208

Winkler, E., (1868), *Die Lehre von der Elastizität und Festigkeit mit besonderer Rücksicht auf ihre Anwendung in der Technik: für polytechnische Schulen, Bauakademien, Ingenieure, Maschinenbauer, Architekten, etc.* Dominicius

Wolde-Tinsae, A.M., Greimann, L. and Yang, P., (1988a), *End Bearing Piles in Jointless Bridges*, Journal of Structural Engineering, 114, 8, 1870-1884

Wolde-Tinsae, A.M., Greimann, L.F. and Johnson, B. (1983). *Performance of integral bridge abutments*. IABSE PERIODICA 1, IABSE

Wolde-Tinsae, A.M., Greimann, L.F. and Yang, P. (1982). *Nonlinear Pile Behavior in Integral Abutment Bridges*, Dept. of Civil Engineering, Engineering Research Institute, Iowa State University

Wolde-Tinsae, A.M. and Klinger, J.E. (1987). *Integral abutment bridge design and construction*. Baltimore, Maryland, USA, Maryland State Highway Administration

Wolde-Tinsae, A.M., Klinger, J.E. and White, E.J., (1988b), *Performance of Jointless Bridges*, Journal of Performance of Constructed Facilities, 2, 2, 111-125

Xue, J., Briseghella, B., Chen, B., Zordan, T., Siviero, E., Oddone, S. and Mattia, F. (2012). *Retrofitting of simply supported bridges using integral abutment bridge concept*. Twin conference of 5th New Dimensions in Bridges, Flyovers, Overpasses & Elevated Structures and 13th International Conference on INSPECTION,

APPRAISAL, REPAIRS AND MAINTENANCE OF STRUCTURES. Wuyishan, China

Yang, P., Wolde-Tinsae, A.M. and Greimann, L.F. (1982). *Nonlinear Finite Element Study of Piles in Integral Abutment Bridges - Part 2*. Ames, Department of Civil Engineering, Engineering Research Institute, Iowa State University

Yannotti, A.P., Alampalli, S. and White, H.I., (2005), *New York State Department of Transportation's Experience with Integral Abutment Bridges*, Integral Abutment and Jointless Bridges (IAJB 2005), Baltimore, Maryland, 41-49

Zhang, J.M., Shamoto, Y. and Tokimatsu, K., (1998), *Evaluation of earth pressure under any lateral deformation*, Soils and foundations, 38, 1, 15-33

Zhang, L. and Ning, X., (1998), *Design of jointless continuous beam bridge with small side spans*, Central South Highway Engineering, 23, 2, 18-20,(in Chinese).

Zhang, X., (2002), *Research on the structural behaviours and applications of semi-integral abutment bridge* Master, Dalian University of Technology,(in Chinese).

Zhu, D.Y. and Qian, Q., (2000), *Determination of passive earth pressure coefficients by the method of triangular slices*, Canadian Geotechnical Journal, 37, 2, 485-491

Zordan, T. and Briseghella, B., (2007), *Attainment of an integral abutment bridge through the refurbishment of a simply supported structure*, Structural Engineering International, 17, 3, 228-234

Zordan, T., Briseghella, B. and Lan, C., (2011a), *Analytical Formulation for Limit Length of Integral Abutment Bridges*, Structural Engineering International, 21, 3, 304-310

Zordan, T., Briseghella, B. and Lan, C., (2011b), *Parametric and pushover analyses on integral abutment bridge*, Engineering Structures, 33, 2, 502-515

Zordan, T., Briseghella, B., Lan, C. and Xue, J. (2011c). *Long Term Behaviour of an Integral Abutment Bridge Designed for its Limit Length*. 35th International Symposium on Bridge and Structural Engineering, 52nd Annual Symposium of IASS, 6th International Conference on Space Structures. London, UK